

ISSN 2071-4726
2071-0305

Инженерно-строительный журнал

НАУЧНОЕ ИЗДАНИЕ

№8(84) 2018





ПОЛИТЕХ
Санкт-Петербургский
политехнический университет
Петра Великого

Инженерно-строительный институт
Центр дополнительных профессиональных программ
195251, г. Санкт-Петербург, Политехническая ул., 29,
тел/факс: 552-94-60, www.stroikursi.spbstu.ru,
stroikursi@mail.ru

**Приглашает специалистов организаций, вступающих в СРО,
на курсы повышения квалификации (72 часа)**

| Код | Наименование программы | Виды работ* |
|---------------------------------------|--|--|
| Курсы по строительству | | |
| БС-01-04 | «Безопасность и качество выполнения общестроительных работ» | п.1,2, 3, 5, 6, 7, 9, 10, 11, 12, 13, 14 |
| БС-01 | «Безопасность и качество выполнения геодезических, подготовительных и земляных работ, устройства оснований и фундаментов» | 1,2,3,5 |
| БС-02 | «Безопасность и качество возведения бетонных и железобетонных конструкций» | 6,7 |
| БС-03 | «Безопасность и качество возведения металлических, каменных и деревянных конструкций» | 9,10,11 |
| БС-04 | «Безопасность и качество выполнения фасадных работ, устройства кровель, защиты строительных конструкций, трубопроводов и оборудования» | 12,13,14 |
| БС-05 | «Безопасность и качество устройства инженерных сетей и систем» | 15,16,17,18,19 |
| БС-06 | «Безопасность и качество устройства электрических сетей и линий связи» | 20,21 |
| БС-08 | «Безопасность и качество выполнения монтажных и пусконаладочных работ» | 23,24 |
| БС-12 | «Безопасность и качество устройства мостов, эстакад и путепроводов» | 29 |
| БС-13 | «Безопасность и качество выполнения гидротехнических, водолазных работ» | 30 |
| БС-14 | «Безопасность и качество устройства промышленных печей и дымовых труб» | 31 |
| БС-15 | «Осуществление строительного контроля» | 32 |
| БС-16 | «Организация строительства, реконструкции и капитального ремонта. Выполнение функций технического заказчика и генерального подрядчика» | 33 |
| Курсы по проектированию | | |
| БП-01 | «Разработка схемы планировочной организации земельного участка, архитектурных решений, мероприятий по обеспечению доступа маломобильных групп населения» | 1,2,11 |
| БП-02 | «Разработка конструктивных и объемно-планировочных решений зданий и сооружений» | 3 |
| БП-03 | «Проектирование внутренних сетей инженерно-технического обеспечения» | 4 |
| БП-04 | «Проектирование наружных сетей инженерно-технического обеспечения» | 5 |
| БП-05 | «Разработка технологических решений при проектировании зданий и сооружений» | 6 |
| БП-06 | «Разработка специальных разделов проектной документации» | 7 |
| БП-07 | «Разработка проектов организации строительства» | 8 |
| БП-08 | «Проектные решения по охране окружающей среды» | 9 |
| БП-09 | «Проектные решения по обеспечению пожарной безопасности» | 10 |
| БП-10 | «Обследование строительных конструкций и грунтов основания зданий и сооружений» | 12 |
| БП-11 | «Организация проектных работ. Выполнение функций генерального проектировщика» | 13 |
| Э-01 | «Проведение энергетических обследований с целью повышения энергетической эффективности и энергосбережения» | |
| Курсы по инженерным изысканиям | | |
| И-01 | «Инженерно-геодезические изыскания в строительстве» | 1 |
| И-02 | «Инженерно-геологические изыскания в строительстве» | 2,5 |
| И-03 | «Инженерно-гидрометеорологические изыскания в строительстве» | 3 |
| И-04 | «Инженерно-экологические изыскания в строительстве» | 4 |
| И-05 | «Организация работ по инженерным изысканиям» | 7 |

*(согласно приказам Минрегионразвития РФ N 624 от 30 декабря 2009 г.)

**По окончании курса слушателю выдается удостоверение о краткосрочном повышении
квалификации установленного образца (72 ак. часа)**

Для регистрации на курс необходимо выслать заявку на участие, и копию диплома об образовании по телефону/факсу: 8(812) 552-94-60, 535-79-92, , e-mail: stroikursi@mail.ru.

Инженерно-строительный журнал

НАУЧНОЕ ИЗДАНИЕ

ISSN 2071-4726, 2071-0305

Свидетельство о государственной регистрации: ПИ №ФС77-38070, выдано Роскомнадзором

Специализированный научный журнал. Выходит с 09.2008.

Включен в Перечень ведущих периодических изданий ВАК РФ

Периодичность: 8 раз в год

Учредитель и издатель:

Санкт-Петербургский политехнический университет Петра Великого

Адрес редакции:

195251, СПб, ул. Политехническая, д. 29, Гидрокорпус-2, ауд. 245

Главный редактор:

Екатерина Александровна Линник

Научный редактор:

Николай Иванович Ватин

Выпускающий редактор:

Ксения Дмитриевна Борщева

Литературный редактор:

Крупина Анастасия

Редакционная коллегия:

д.ф.-м.н., доцент Р.А. Абдикаримов;
д.т.н., проф. В.В. Бабков;
к.т.н., проф. А.И. Боровков;
д.т.н., проф. Н.И. Ватин;
PhD, проф. М. Вельжкович;
д.т.н., проф. Э.К. Завадскас;
д.ф.-м.н., проф. М.Н. Кирсанов;
D.Sc., проф. М. Кнежевич;
д.т.н., проф. В.В. Лалин;
д.т.н., проф. Б.Е. Мельников;
д.т.н., академик М.М. Мирсаидов;
д.т.н., проф. Ф. Неправишта;
д.т.н., проф. Р.Б. Орлович;
Dr. Sc. Ing., professor
Л. Пакрастиньш;
Dr.-Ing. Habil., professor
Х. Пастернак;
д.т.н., проф. А.В. Перельмутер;
д.т.н., проф. М.Р. Петриченко;
д.т.н., проф. В.В. Сергеев;
д.ф.-м.н., проф. М.Х. Стрелец;
д.т.н., проф. О.В. Тараканов;
д.т.н., проф. В.И. Травуш;
д.т.н., проф. Д. Унгерман;
д.т.н., проф. С.В. Федосов

Дата выхода: 25.04.2019

Содержание

| | |
|---|-----|
| Бука-Вайваде К., Шлисерис Я., Сердюк Д.О., Пакрастиньш Л., Ватин Н.И. Возможность рационального использования HPSFRC в многоэтажном строительстве | 3 |
| Калдар-оол А.Б., Бабанов В.В., Аллахвердов Б.М., Саая С.С. Дополнительная нагрузка на коробовый свод в памятнике архитектуры | 15 |
| Калугин Ю.Б., Романов Р.С. Формирование календарных планов поточного строительства рассредоточенных объектов | 29 |
| Клюев С.В., Клюев А.В., Ватин Н.И. Фибробетон для строительной индустрии | 41 |
| Ерофеев В.Т., Родин А.И., Кравчук А.С., Казначеев С.В., Захарова Е.А. Биостойкие пеноситаллы на основе кремнеземосодержащих пород | 48 |
| Чжао Ц., Чен П., Ван Д., Вэй Ю. Модель для прогнозирования повреждений дорожного покрытия в районе сезонного промерзания | 57 |
| Сергеев В.В., Петриченко М.Р., Немова Д.В., Котов Е.В., Тарасова Д.С., Нефедова А.В., Бородинец А. Надстройка существующих зданий с применением легких стен по каркасной технологии | 67 |
| Гравит М.В., Голуб Е.В., Григорьев Д.М., Иванов И.О. Огнезащитные подвесные потолки с высокими пределами огнестойкости | 75 |
| Стешенко А.Б., Кудяков А.И. Цементный пенобетон с алюмосиликатной микросферой для монолитного домостроения | 86 |
| Славчева Г.С., Артамонова О.В. Критериальная оценка реологических характеристик цементных систем для строительной 3D-печати | 97 |
| Киянец А.В. Бетон с добавлением фибры из переработанного полиэтилентерефталата | 109 |
| Бокарев С.А., Жунев К.О., Усольцев А.М. Напряженное состояние сварных узлов железнодорожных пролетных строений | 119 |
| Земитис Ю., Бородинец А., Лаубертс А. Влияние вентиляции на концентрацию ЛОС, вызванных строительными материалами | 130 |
| Корнилов Т.А., Никифоров А.Я. Теплозащита малоэтажных зданий из легких стальных тонкостенных конструкций | 140 |
| Золина Т.В., Садчиков П.Н. Остаточный ресурс стального каркаса одноэтажного промышленного здания с мостовыми кранами | 150 |
| Коянкин А.А., Митасов В.М., Цхай Т.А. Совместность деформирования сборного тяжелого и монолитного легкого бетонов | 162 |
| Лам Т.В., Ву Д., Зиен В., Булгаков Б.И., Король Е.А. Свойства и теплоизоляционные эффективности легких бетонов | 173 |
| Фьюнг Н.Т.Х. Распределение яркости в условиях тропического неба | 192 |

© ФГАОУ ВО СПбПУ, 2018

© Иллюстрация на обложке: Илья Смагин

Контакты:

E-mail: mce@spbstu.ru

Web: <http://www.engstroy.spbstu.ru>

Magazine of Civil Engineering

SCHOLAR JOURNAL

ISSN 2071-4726, 2071-0305

Peer-reviewed scientific journal

Start date: 2008/09

8 issues per year

Publisher:Peter the Great St. Petersburg
Polytechnic University**Indexing:**Scopus, Russian Science Citation
Index (WoS), Compendex, DOAJ,
EBSCO, Google Academia, Index
Copernicus, ProQuest, Ulrich's Serials
Analysis System**Corresponding address:**245 Hydro Building, 29
Polytechnicheskaya st., Saint-
Petersburg, 195251, Russia**Editor-in-chief:**

Ekaterina A. Linnik

Science editor:

Nikolay I. Vatin

Technical editor:

Ksenia D. Borshcheva

Editorial board:R.A. Abdikarimov, D.Sc., associate
professor

V.V. Babkov, D.Sc., professor

A.I. Borovkov, PhD, professor

M. Veljkovic, PhD, professor

E.K. Zavadskas, D.Sc., professor

M.N. Kirsanov, D.Sc., professor

M. Knezevic, D.Sc., professor

V.V. Lalin, D.Sc., professor

B.E. Melnikov, D.Sc., professor

M.M. Mirsaidov, D.Sc., professor

F. Nepravishita, D.Sc., professor

R.B. Orlovich, D.Sc., professor

L. Pakrastinsh, Dr.Sc.Ing., professor

H. Pasternak, Dr.-Ing.habil.,
professor

A.V. Perelmuter, D.Sc., professor

M.R. Petrichenko, D.Sc., professor

V.V. Sergeev, D.Sc., professor

M.Kh. Strelets, D.Sc., professor

O.V. Tarakanov, D.Sc., professor

V.I. Travush, D.Sc., professor

S.V. Fedosov, D.Sc., professor

Date of issue: 25.04.2019

Contents

| | |
|---|-----|
| Buka-Vaivade, K., Sliseris, J., Serdjuks, D., Pakrastins, L., Vatin, N.I. Rational use of HPSFRC in multi-storey building | 3 |
| Kaldar-ool, A-Kh.B., Babanov, V.V., Allahverdov, B.M., Saaya, S.S. Additional load on barrel vaults of architectural monuments | 15 |
| Kalugin, Yu.B., Romanov, R.S. Scheduling workflows for scattered objects | 29 |
| Klyuev, S.V., Klyuev, A.V., Vatin, N.I. Fiber concrete for the construction industry | 41 |
| Erofeev, V.T., Rodin A.I., Kravchuk, A.S., Kaznacheev, S.V., Zaharova, E.A. Biostable silicic rock-based glass ceramic foams | 48 |
| Zhao, Q., Cheng, P., Wang, J., Wei, Y. Damage prediction model for concrete pavements in seasonally frozen regions | 57 |
| Sergeev, V.V., Petrichenko, M.R., Nemova, D.V., Kotov, E.V., Tarasova, D.S., Nefedova, A.V., Borodinecs, A.B. The building extension with energy efficiency light-weight building walls | 67 |
| Gravit, M.V., Golub, E.V., Grigoriev, D.M., Ivanov, I.O. Fireproof suspended ceilings with high fire resistance limits | 75 |
| Steshenko, A.B., Kudyakov, A.I. Cement based foam concrete with aluminosilicate microspheres for monolithic construction | 86 |
| Slavcheva, G.S., Artamonova, O.V. Rheological behavior of 3D printable cement paste: criterial evaluation | 97 |
| Kiyansets, A.V. Concrete with recycled polyethylene terephthalate fiber | 109 |
| Bokarev, S.A., Zhunev, K.O., Usol'tsev, A.M. Stress-strain behavior of welded joints in railway girders | 119 |
| Zemitis, J., Borodinecs, A.B., Lauberts, A. Ventilation impact on VOC concentration caused by building materials | 130 |
| Kornilov, T.A., Nikiforov, A.Y. Thermal protection of low-rise buildings from light steel thin-walled structures | 140 |
| Zolina, T.V., Sadchikov, P.N. Residual resource of a one-storey steel frame industrial building constructed with bridge cranes | 150 |
| Koyankin, A.A., Mitasov, V.M., Tskhay, T.A. Compatibility of precast heavy and monolithic lightweight concretes deforming | 162 |
| Lam, T.V., Vu, D.T., Dien, V.K., Bulgakov, B.I., Korol, E.A. Properties and thermal insulation performance of light-weight concrete | 173 |
| Phuong, N.T.K. Luminance distributions in the tropical sky conditions | 192 |

© Peter the Great St. Petersburg Polytechnic University. All rights reserved.

© Illustration – Ilya Smagin

E-mail: mce@spbstu.ruWeb: <http://www.engstroy.spbstu.ru/eng/index.html>

doi: 10.18720/MCE.84.1

Rational use of HPSFRC in multi-storey building

Возможность рационального использования HPSFRC
в многоэтажном строительстве

K. Buča-Vaivade,
J. Sliseris,
D. Serdjuks*,
L. Pakrastins,
Riga Technical University, Riga, Latvia
N.I. Vatin,
*Peter the Great St. Petersburg Polytechnic
University, St. Petersburg, Russia*

М.Сс., научный сотрудник К. Бука-Вайваде,
д-р техн. наук, ассоц. профессор
Я. Шлисери́с,
д-р техн. наук, профессор Д.О. Сердюк*,
д-р техн. наук, руководитель кафедры
Л. Пакрастиньш,
*Рижский технический университет, г. Рига,
Латвия*
д-р техн. наук, профессор Н.И. Ватин,
*Санкт-Петербургский политехнический
университет Петра Великого,
Санкт-Петербург, Россия*

Key words: high-performance concrete; high-performance steel fibre reinforced concrete; stress–strain curve; elements of multi-storey building

Ключевые слова: высокопрочный бетон; высокопрочный сталефибробетон; кривая напряжение-деформация; элементы многоэтажного здания

Abstract. Fibres improve concrete properties that can be used to solve the problem of limited resources. This research includes the numerical comparison of high-performance concrete (HPC) and high-performance steel fibre reinforced concrete (HPSFRC) behaviour. The numerical comparison is based on the analyse of stress-strain curves of considered materials. The limits of rational use of HPC and high-performance steel fibre reinforced concrete HPSFRC have been determined based on typical stress resultants values acting in the elements of multi-storey buildings. The values of stress resultants were determined by the numerical model, which was developed by the software ANSYS. Interaction diagrams of bending moments and axial forces $M-N$ for elements subjected to combined action of compression and bending with different cross-sections have been developed. Curves for slabs of two material types that describe the allowable values of distributed load at different spans of the slabs are created. The resulting curves are analysed together with the actual stress resultants of the elements concerned from the numerical model. Taking into account distribution of stress resultants in the elements of multi-storey buildings, it was stated that the elements subjected to flexure are preferable field of application for HPSFRC. Ultimate value of bending moment is higher for HPSFRC comparing to HPC with the same parameters of cross-section. It is found that it is more rational to use HPSFRC for columns in the first eight floors. HPSFRC should be preferred as a material of the lower and middle floors of multi-storey buildings and of the walls of all floors in the case of column spacing more than 8 m, and for the slabs with span interval 6–12 m.

Аннотация. Поскольку введение фибры приводит к улучшению свойств бетона, это может быть использовано для решения проблемы ограниченности ряда строительных материалов. Данное исследование включает в себя численное сравнение работы бетона высокой прочности (НПС) и бетона высокой прочности со стальной фиброй (HPSFRC). Сравнение основывается на анализе кривых «напряжения–деформации» данных материалов. Границы более рационального использования бетонов НПС и HPSFRC определяются на основе типовых значений внутренних усилий в конструкциях многоэтажных зданий, полученных на основе разработанной в среде ANSYS численной модели. Получены диаграммы взаимосвязи изгибающих моментов и осевых сил $M-N$ для внецентренно сжатых элементов с различными поперечными сечениями. Диаграммы, полученные для плит из двух исследуемых материалов, демонстрируют допустимые значения распределенной нагрузки для плит различных пролетов. Анализ полученных диаграмм проводится с учётом внутренних усилий соответствующих элементов из численной модели. В результате проведенной работы установлено, что при тех же параметрах поперечного сечения конструкции, выполненные из бетона HPSFRC, способны воспринимать более высокие значения изгибающего момента, чем конструкции на основе НПС. Выявлено, что наиболее рационально использовать HPSFRC для колонн первых восьми этажей. В качестве строительного материала для колонн

Бука-Вайваде К., Шлисери́с Я., Сердюк Д.О., Пакрастиньш Л., Ватин Н.И. Возможность рационального использования HPSFRC в многоэтажном строительстве // Инженерно-строительный журнал. 2018. № 8(84). С. 3–14.

нижних и средних этажей и всех стен ядра жесткости при шаге колонн более 8 м, а также для плит с пролетом в интервале от 6 до 12 м рекомендуется использовать HPSFRC.

1. Introduction

The number of people in the world is growing rapidly, according to the U.S. Census Bureau, every minute, the population of the planet is growing by an estimated 150 people, accounting for more than 80 million people per year. As a result, two issues remain: living space – there is a need for multi-storey buildings and availability of natural resources. The principle of sustainable development aims to preserve the environment and nature for future generations at least in the same quality as we have received. As stocks of non-renewable resources decrease every year, it is important to use these resources economically and rationally, with the greatest possible efficiency. This approach also applies to the construction industry.

The constructive solution of a multi-storey residential building with load-bearing structures from thin-walled high-performance concrete (HPC) or high-performance steel fibre reinforced concrete (HPSFRC) avoids the large vertical cross-sectional structure of the building on the lower floors [1–3]. This will allow us to reduce the self-weighting of structures, increase the useful area and save on non-renewable natural resources.

The use of fibres improves the properties of concrete especially in tension loads. This improvement depends on many factors: fibre shape, the ratio between fibre length and its equivalent diameter or aspect ratio l_f / d_f , fibre volume etc. [3–10]. Therefore, predicting the properties of fibre reinforced concrete is complicated. However, investigations have shown that the improvement of the strength of concrete from the use of fibres is usually negligible and not observed [11], while the fibres distribute localized stress, prevent the cracking of concrete, improve ductility of high-performance concrete and significantly improve the post-peak behaviour of the fibre reinforced concrete [8–19], as a result reduces the cost of maintenance and repair. When the first crack appears in concrete, fibres begin to work, fibre bridging effect affects the deformation properties of the concrete [3, 6, 9, 11].

There are many studies [3, 6, 9, 20–22] where stress-strain curves of the concrete with and without steel fibre reinforcement are experimentally obtained. The obtained stress-strain curves prove the significant increase in post-peak stage of permissible strain values, moreover, fibres can significantly reduce shrinkage of concrete. Dimensions of cross-sections and ratio of longitudinal reinforcement for load-bearing members of multi-storey building subjected to flexure and compression with the bending probably can be decreased due to this property of HPSFRC. As a consequence of this the use of HPSFRC can reduce the cost of labour and the delivery of bars. So, the aim of this investigation is to compare numerically the behaviour of HPC and HPSFRC with steel fibre dosage 25–35 kg/m³, and to evaluate the limits for effective use of HPSFRC. Distribution of the typical stress resultants acting in the elements of a multi-storey building with different column spacing should be analysed for this purpose. The task of the study is to determine the boundaries of the effective use of HPSFRC columns, walls and ribbed slabs. The field of application of the results obtained is the initial design stage, during which it is necessary to select the used structures and materials.

Load bearing capacity diagrams for combined bending and axial load for columns and walls of different sizes will be developed in this research. Curves characterizing the load-bearing capacity of ribbed slabs with different slab parameters and the parametric numerical model of the building for determining the typical work of the building will be created also.

2. Methods

2.1. Object of investigation

A multi-storey building (Figure 1) with a stiffness core walls in the centre and perimeter columns, providing self-supporting exterior walls and ribbed slabs, was considered as an object of this investigation. The columns cross-sections are selected as a box-type to provide the decreased consumption of materials and high stiffness of the element in the both planes. The box-type cross-section enables the integration of engineering communication inside or outside of columns.

2.2. Numerical model of the building

3D numerical model of the multi-storey building is developed by the ANSYS software. The parametric design language (APDL) of ANSYS software is used to automate the design process by defining geometry with relationships, variable parameters and criteria, and to create a parametric model.

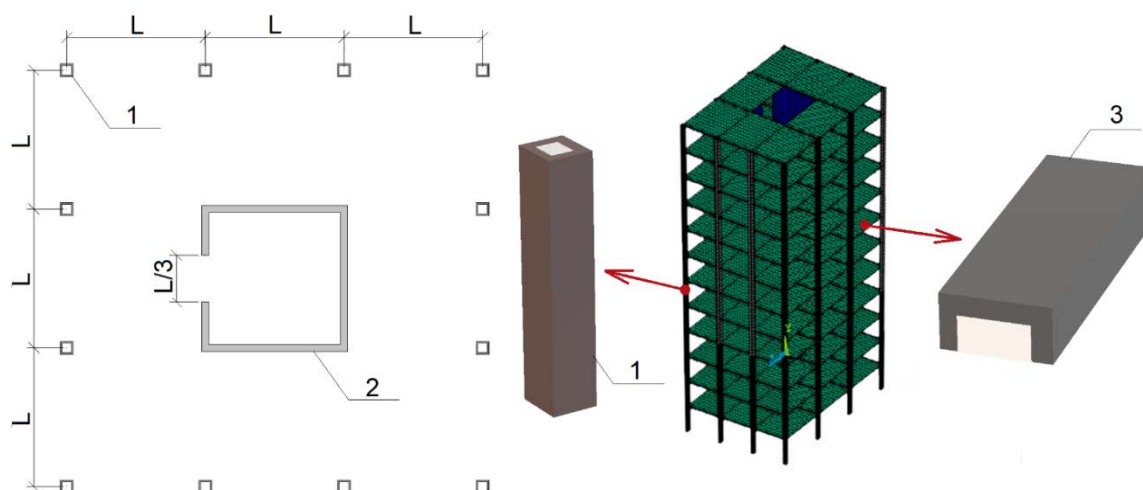


Figure 1. Structure of considered multi-storey building. 1 – columns, 2 – walls, 3 – ribbed slabs.

The building calculation model is developed with the ability to modify input data such as the column spacing (L), floor height (h), number of storeys (n), concrete strength and cross-sectional parameters of the elements. A building with twelve storeys is considered. The height of the storey is equal to 4 m and the column spacing changes within the limits from 6 to 13 m. The columns of the first storey are rigidly joined with the foundation as the supports of the model are considered as completely fixed from the linear displacements and rotations. A concrete core walls are created to ensure the rigidity of the building.

Structures of slabs and walls are modelled by the SHELL181 finite element type, while the columns and beams by the finite element type BEAM188. The transversal deformation is taken into account for both of considered type of elements [23].

Dimensions of the walls and columns cross-sections are defined parametrically. They are divided into three groups and changes for the storeys: from the 1st to the 4th storeys there is a first group, from 5th to 8th storey there is a second storey group and from the 9th to 12th storey there is a third storey group. Column cross-section is box-type, with constant external dimensions. It is 500×500 mm and variable wall thickness. Pinned support is modelled for the slabs by the degrees of freedom Coupling function, it allows rotation and prevent the translation movements.

The obtained model is analysed based on a constant load combination of permanent load, uniformly distributed imposed load 5 kN/m², which is applied to the all floors, including roof and wind load, which is applied as linear load to the columns of one of the facades. Openings are not taken into account. The created numerical model enables to determined forces of the building elements at different column spacing.

2.3. Modelling of structural materials

Three types of materials are used in the design model of the building, i.e. high-performance concrete, high-performance steel fibre reinforced concrete and steel. High-performance concrete is characterized as a brittle material. The structural members made of concrete have at least minimum reinforcement. High strength concrete of C80 / 95 class is used [24]. Improvement in peak strength due to the use of fibres is not respected, as it is usually negligible, while the improved of post-peak behaviour of the concrete is taken into account. For the high-performance steel fibre reinforced concrete are used steel fibres with length 50 mm, diameter 1 mm and dosage 25–35 kg/m³.

HPC and HPSFRC are approximated by using discrete lattice model to describe non-linear and discrete nature of concrete. Lattice model is obtained from standard tetrahedron finite element mesh, where each lattice member is edge of tetrahedron. The behaviour of non-linear material is characterized by degradation of Young's modulus cause of cracking. Damage variable is used for the prediction of behaviour of HPC and HPSFRC [25]:

$$E = E_{init} \cdot (1 - D),$$

where E_{init} – the initial material Young's modulus,

D – a damage variable (0 – undamaged, 1 – damaged material).

To obtain the dependences of the bending moments on the axial forces $M-N$, the axial load is applied in 10 steps from 0 to the maximum bearing capacity in compression. For each step, the maximum value of the bending moment, which can be additionally applied to an axial force, is determined iteratively. Numerical modelling approach in more detail is described in [25–29].

Used stress-strain curves of the materials [3, 4, 23, 30] are shown in Figures 2 and 3.

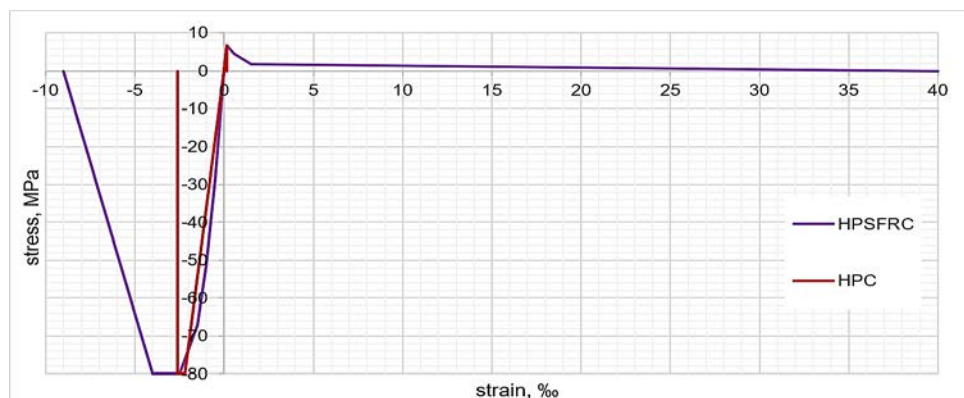


Figure 2. Stress-strain curve of high-performance concrete (HPC) and high-performance steel fibre reinforced concrete (HPSFRC).

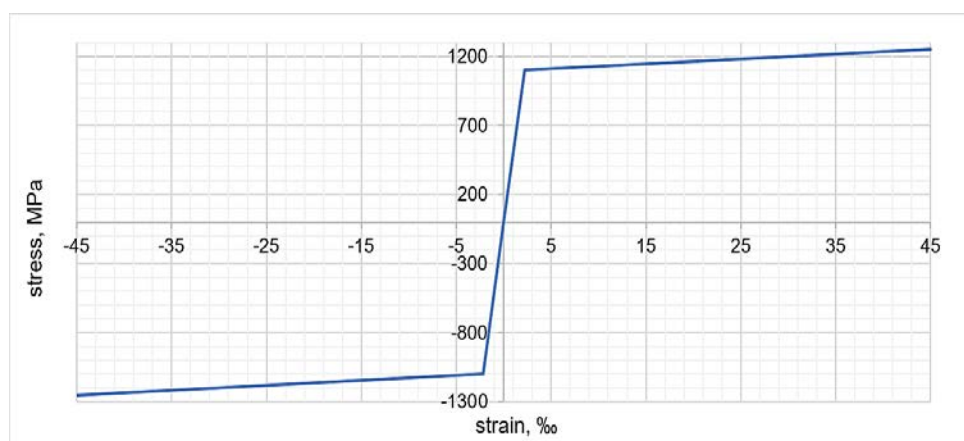


Figure 3. Stress-strain curve of high-strength steel.

Values of stress-strain curves of the HPC and HPSFRC are given in the Table 1.

Table 1. Stresses values of HPC and HPSFRC as a function from the strains.

| strain, ‰ | | -9.0 | -4.0 | -2.6 | -2.2 | -1.5 | 0.0 | 0.14 | 0.16 | 1.50 | 40.0 |
|-------------|--------|------|------|------|------|------|------|------|------|------|------|
| stress, MPa | HPC | 0 | 0.0 | 0.0 | 80.0 | 80.0 | 54.5 | 0.0 | 6.8 | 0.0 | 0.0 |
| | HPSFRC | 0 | 80.0 | 80.0 | 80.0 | 80.0 | 67.2 | 0.0 | 6.8 | 6.7 | 1.8 |

Values of stress-strain curves of the high-strength steel (HSS) are given in the Table 2.

Table 2. Stresses values of HSS as a function from the strains.

| strain, ‰ | -45.0 | -2.2 | 0.0 | 2.2 | 45.0 |
|-------------|-------|-------|-----|------|------|
| stress, MPa | -1250 | -1100 | 0.0 | 1100 | 1250 |

2.4. Analysis of elements behaviour

Interaction diagrams $M-N$ for columns and walls and load-bearing curves for slabs for different cross-sectional dimensions have been developed by the analysis of HPC and HPSFRC. The resulting diagrams include the maximum values of stress resultants obtained by the developed numerical buildings model. The diagrams enable to find out the limits for the rational use of HPC and HPSFRC.

The height of the building is divided into three groups, as it was mentioned in the Chapter 2. The thickness of the core walls and of the column box-type cross-section walls may vary for each group.

The ribbed slabs are analysed by using uniformly distributed load, which include permanent and imposed loads. The characteristic value of imposed load is 5 kN/m². The width of the ribbed slab, which is considered as a specimen used for comparison of HPC and HPSFRC, was equal to 1 m.

The minimum thickness of the concrete protective layer for reinforcement is $c_{nom,min} = 20 \text{ mm}$ [24]. Then the width of the rib of the slab (b_w) is:

$$b_w = \begin{cases} 2 \cdot c_{nom,min} + \varnothing = 2 \cdot 20 + \varnothing = 40 + \varnothing \text{ mm} - \text{pie } \varnothing \leq 10 \text{ mm}, \\ 2 \cdot (\varnothing + 10) + \varnothing = 20 + 3 \cdot \varnothing \text{ mm} - \text{pie } \varnothing > 10 \text{ mm}, \end{cases}$$

where \varnothing is diameter of longitudinal bar.

The width of the slab is rounded up by 10 mm in the calculations.

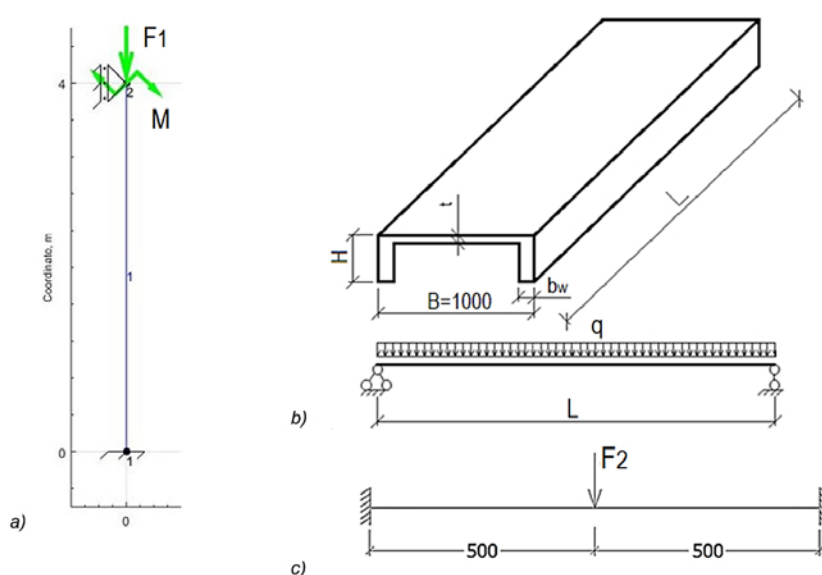


Figure 4. Design schemes of a) columns and walls elements subjected to compressive force; b) height (H) of the ribbed slabs and main geometric characteristics of ribbed slabs; c) thickness (t) of the slabs web.

The design schemes of the elements subjected to compression and the bending are shown in Figure 4. The thickness of the slab (t) is determined by loading the web of the slab with a concentrated force (Figure 4 (c)) for two cases – a slab of HPC and HPSFRC.

Comparison of load bearing capacity of the HPC and HPSFRC slabs was carried out. Calculations of slab deflections have been also done considering that the serviceability limit state is determinant for elements in bending. The deflection in the middle of the span of the ribbed slab is calculated by taking into account permanent and imposed loads and by using material stress-strain curves. The maximum available deflection is taken as 1/250 part of the span.

3. Results and Discussions

3.1. Columns behavior

The maximum axial forces and bending moments for the columns of all three groups with the distance between column centres equal to 8 m and for the columns of the first group with the spacings equal to 6 m are summarized in the Figure 5. The values of the axial forces and bending moments were obtained by the 3D model of the building, which was developed by the software ANSYS. Figure 5 include the interaction diagrams $M-N$ for combined bending and axial load for the HPC and HPSFRC columns with box-type cross-sections and wall thicknesses equal to 50 and 60 mm.

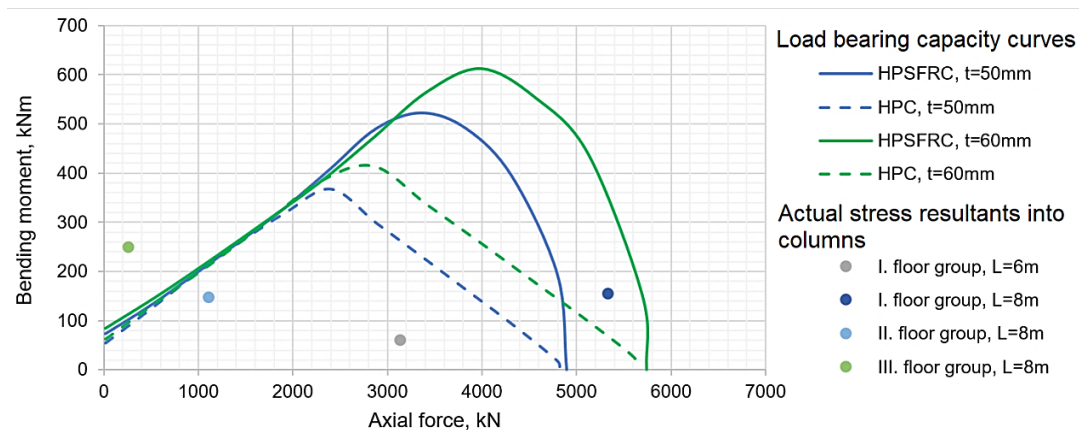


Figure 5. Dependences of the bending moments on the axial forces $M-N$ for the HPC and HPSFRC columns, with box-type cross-section and wall thicknesses equal to 50 and 60 mm.

As can be seen from Figure 5, the character of the dependences of the bending moments on the axial forces for HPC and HPSFRC are similar while the dependences for HPC reached its maximum bending moment. The maximal axial force in compression is also comparable for both materials. Behaviour of HPSFRC varies greatly with the growing of axial force and bending moment values. After reaching the peak bending moment of a HPC, this difference grows till 40–90 %.

Columns of the third storey group are characterized by a high bending moment value at low axial force, as a result, firstly, in order to ensure the load bearing capacity of the columns, these columns need an additional longitudinal reinforcement; secondly, considering that the character of behaviour of HPSFRC and HPC is not significantly different at low axial force values, it can be concluded that using of HPC for the columns of the third storey group enables to increase effectiveness of the structural materials use.

It is accepted that the thickness of the column box-type cross-section wall must be bigger than 50 mm due to the technological considerations. Then it can be seen that the material is not used rationally at the small column spacing, thereby HPC is sufficient to provide the bearing capacity of the columns.

The columns of the first group of the storeys for building with column spacing equal to 8 m are characterized by a relatively high bending moment value at a high axial force, resulting the load bearing capacity of the column with a uniform thickness of the box-type cross-section wall ($t = 60$ mm) can be provided by using of HPSFRC as the column material instead of HPC.

The maximum values of axial forces and bending moments for the columns of the first and second group of storeys are summarized in the Table 3 for columns spacings changing within the limits from 11 to 13 m.

Table 3. Maximum values of axial forces and bending moments for the different columns spacings.

| Storeys | $L = 11$ m | | $L = 12$ m | | $L = 13$ m | |
|---------|------------|-----------|------------|-----------|------------|-----------|
| | N , kN | M , kNm | N , kN | M , kNm | N , kN | M , kNm |
| 1–4 | 9874.8 | 613.6 | 11570 | 850.6 | 13454 | 1175 |
| | 9874 | 642.2 | | | 12429 | 1154.8 |
| 5–8 | 6534.4 | 32.3 | 7664.4 | 32.3 | 8929.4 | 5.8 |
| | 6011 | 387 | 7108.7 | 521.2 | 8426.3 | 722.4 |

The dependences of the bending moments on the axial forces $M-N$ for HPSFRC and HPC columns with box-type cross sections, which are differed by thicknesses of the walls so as amount and diameters of the longitudinal bars, is shown on the Figure 6. The values of stress resultants are obtained by the 3D numerical model of the building.

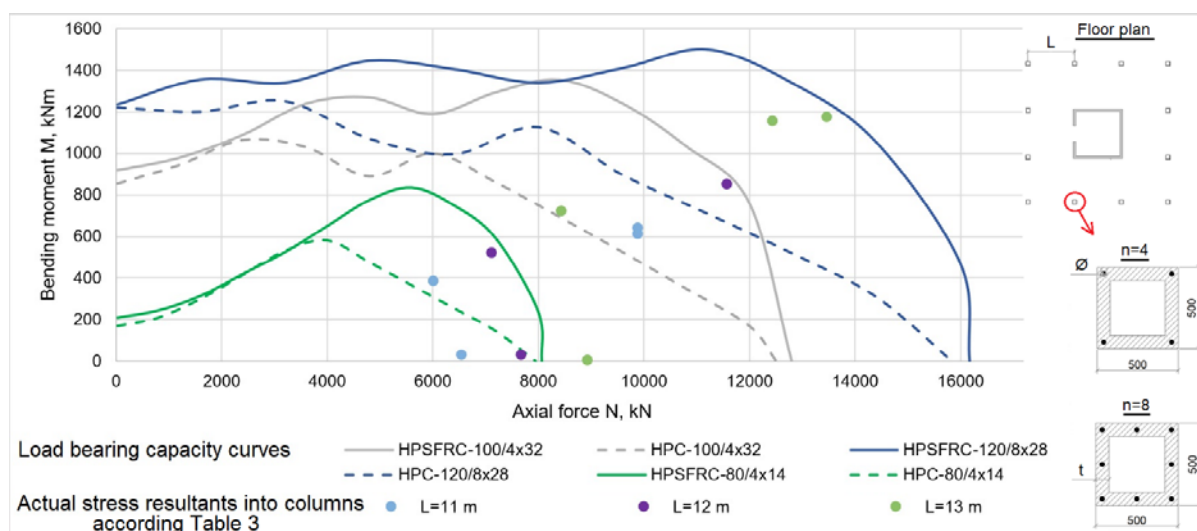


Figure 6. Dependences of the bending moments on the axial forces $M-N$ for HPSFRC and HPC columns for the first and second groups of storeys with box-type cross-sections. $t/n \times \varnothing$: t is box-type cross-section wall thickness, n is number of longitudinal bars in cross-section, \varnothing is diameter of longitudinal bars.

It can be concluded, that the use of HPSFRC as column material for the first and second storey group is justified. For example, maximum value of bending moment in the column of the first storey group is 851 kNm and of the second group is 521 kNm for building with column spacing equal to 12 m. HPSFRC columns with box-type cross-section 100/4×32 and 80/4×14, respectively, provide load bearing capacity, while 3.3 times smaller value of the bending moment can be taken up at the same parameters of cross-section HPC columns. As it shown in Figure 6, cross-section 100/4×32 of HPC column is needed to provide 521 kNm big bending moment. In this case, it means 25 % thicker wall of box-type cross-section or about 245 kg more concrete per one column and 2.28 times bigger diameter of bars or 0.13 tonnes more steel per one column. It means, that HPSFRC allows to considerably reduce cross-section size and diameter of longitudinal bars.

The required thicknesses of the walls so as amount and diameters of the longitudinal bars ($t/n \times \varnothing$) for cross sections of columns when the columns spacings changing within the limits from 11 to 13 m are summarized in the Table 4.

Table 4. HPSFRC column cross sections ($t/n \times \varnothing$) at different column spacing.

| L, m | 11 | 12 | 13 |
|------------------|----------|----------|----------|
| I. storey group | 100/4X32 | 100/4X32 | 120/8X28 |
| II. storey group | 80/4X14 | 80/4X14 | 100/4X32 |

3.2. Walls behavior

The dependences of the bending moments on the axial forces $M-N$ for HPSFRC and HPC walls with thickness 90 mm, with and without additional reinforcement, are shown on the Figure 7.

As can be seen, the stage in which the wall can take up both the axial force and the bending moment, for HPSFRC walls is significantly higher. The values of bending moment, which can be taken up by the wall, at corresponding values of axial forces, for HPSFRC are 20–100 % higher, than for HPC.

It can be seen from the Figure 7, that the minimum additional reinforcement significantly increases the value of the bending moment that can be applied to the wall unloaded by the axial force.

The maximum values of bending moments and axial forces, acting in the walls of the different storeys groups for buildings with column spacing of 8 and 12 m, according to 3D numerical model, is summarized in Table 5.

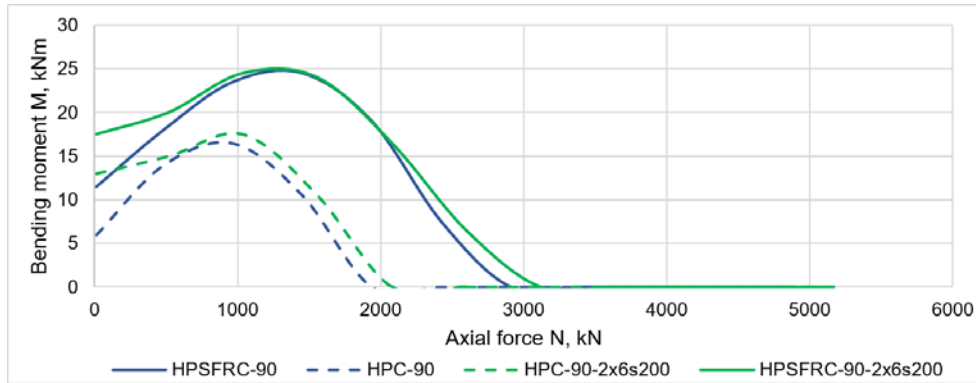


Figure 7. Dependences of the bending moments on the axial forces $M-N$ for walls with/without additional two-way reinforcement. HPSFRC is high-performance steel fibre reinforced concrete; HPC is high-performance concrete; -90 is wall thickness, 2×6s200 is two two-way slab reinforcement with bars spacing 200×200 and diameter 6 mm.

Table 5. Maximum values of bending moments and axial forces, in the walls of the different storeys groups.

| Storeys | $L = 8\text{ m}$ | | $L = 12\text{ m}$ | |
|---------|------------------|-----------|-------------------|-----------|
| | N , kN | M , kNm | N , kN | M , kNm |
| 1-4 | 2236.1 | 12.0 | 4666.9 | 36.6 |
| | 2024.6 | 13.1 | 2770.0 | 42.1 |
| 5-8 | 1950.2 | 13.4 | 4217.3 | 37.6 |
| | 1700.3 | 14.1 | 927.2 | 41.06 |
| 9-12 | 1609.0 | 13.9 | 3808.1 | 38.9 |
| | 1392.2 | 14.7 | 671.4 | 47.7 |

Maximal forces from the 3D numerical model of the building are plotted together with the dependences of the bending moments on the axial forces $M-N$ for walls with different thicknesses are shown on the Figure 8.

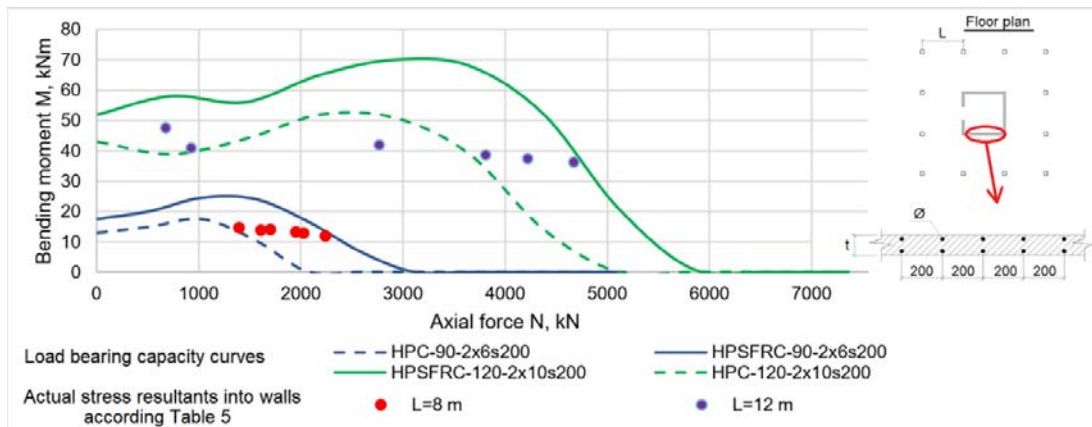


Figure 8. Dependences of the bending moments on the axial forces $M-N$ for walls. HPSFRC is high-performance steel fibre reinforced concrete; HPC is high-performance concrete; -90, -120 are wall thickness (t), 2×6s200 is two two-way slab reinforcement with bars spacing 200×200 and diameter $\varnothing = 6\text{ mm}$, 2×10s200 is two two-way slab reinforcement with bars spacing 200×200 and diameter $\varnothing = 10\text{ mm}$; $L = 8\text{ m}$, $L = 12\text{ m}$ are maximal forces in walls at the appropriate column spacing.

The maximum values of axial forces and bending moments in the walls does not have such a sharp difference in the storey groups. So, the use of HPSFRC is justified for the core walls of the buildings with various column spacing.

3.3. Slabs behavior

The dependence of the maximum bending moment, acting in the middle of the web span of the ribbed slab, from the thickness of the web is shown on the Figure 9. It can be seen from the Figure 9 that the bending moment that can be taken up by the HPSFRC slab web is 38 ... 41 % higher than that for slab web of HPC, with the same thickness of the slab web.

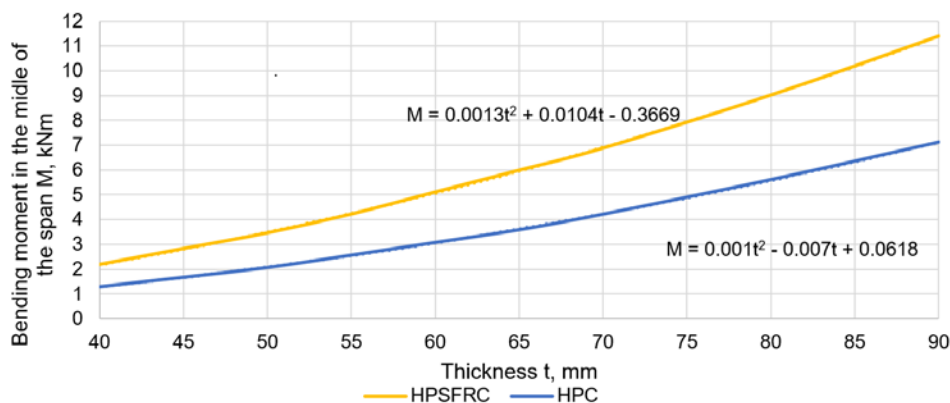


Figure 9. The dependence of the maximum bending moment, acting in the middle of the web span of the ribbed slab, from the thickness of the web (t), HPSFRC is high-performance steel fibre reinforced concrete; HPC is high-performance concrete.

Thickness of the slabs webs is rounded up by 5 mm due to technological limitations of manufacturing. Then the thickness of the web, which will provide a load bearing capacity of $F = 20$ kN ($M \approx 2.5$ kNm with web span 1 m), for HPSFRC is 45 mm, while for HPC it is 55 mm at the same load bearing capacity.

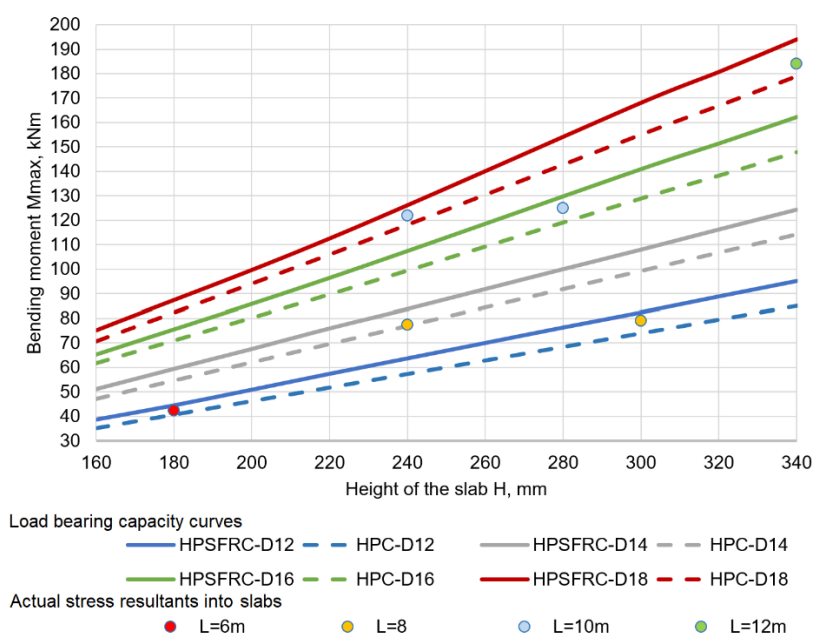


Figure 10. The dependence of bending moment in the middle of the span on the slab height with various bar diameter for HPC and HPSFRC. HPSFRC is high-performance steel fibre reinforced concrete; HPC is high-performance concrete, D is bar diameter.

Taking into account the obtained relationships for determining the width of the ribs and the thickness of the web, curves that describe the load bearing capacity of the slabs dependence of the slab height have been developed. Maximum bending moment in the middle of the slab is determined for the slabs with various heights and bars diameters of the ribs. The spans of the slabs are equal to 6, 8, 10 and 12 m (Figure 10).

It can be seen from the Figure 10 that differences between the load bearing capacities of the slabs of HPC and HPSFRC additionally longitudinally reinforced, is small. The load bearing capacities of the HPSFRC slabs are 5–10 % greater than that of HPC slabs.

The curves for HPC and HPSFRC slabs with 4 different cross-sections, which describes the value of the distributed load q , at which deflection (Δ) in the middle of the slab is equal to $L / 250$ for different slab spans, are summarized on the Figure 11.

The used values of distributed load (permanent and imposed loads) for slabs with span 6, 8, 10 and 12 m are shown on the Figure 11.

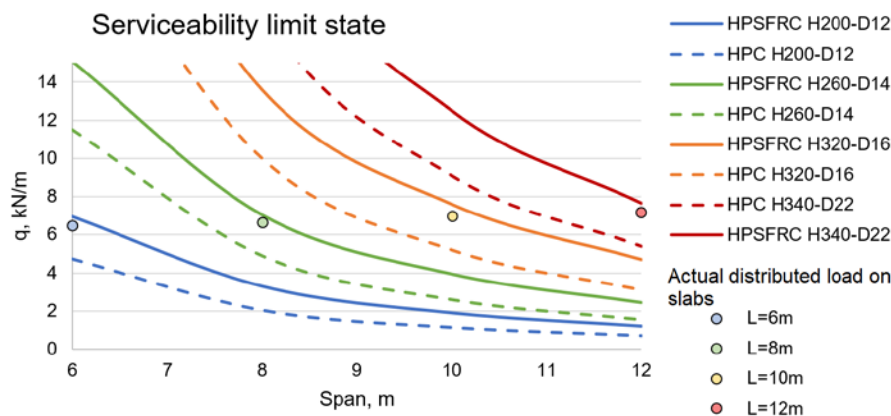


Figure 11. The dependences of uniformly distributed loads which satisfy the serviceability of the slabs on their spans for different slab height and reinforcement bars diameters for HPC and HPSFRC. HPSFRC is high-performance steel fibre reinforced concrete; HPC is high-performance concrete, H is slab height, D is bar diameter.

It can be concluded, that the slabs made of HPSFRC can take up load which is 42–46 % higher, than that for the slabs made of HPC. The serviceability limit state is determinant so as the intensity of the uniformly distributed load is such that cause the maximum vertical displacements equal to it maximum available value ($L / 250$).

4. Conclusions

Behaviour of HPSFRC and HPC load-bearing members of multi-storey building with columns spacings from 6 to 13 m was compared numerically. Preferable fields of application of high-performance steel fibre reinforced concrete for the load bearing members of considered twelve storey building were justified.

The results showed that:

- HPSFRC columns can take up 40–90 % higher bending moment in comparison with HPC columns at the same level of axial force and parameters of cross-sections, what can be applied for the first eight storeys of considered twelve storeys building with column spacing 8–13 m, where columns characterized by a relatively high bending moment value at a high axial force;
- The using of HPSFRC walls are effective for buildings with the columns spacings changing from 8 to 13 m;
- HPSFRC slab can carry 42–46 % more uniformly distributed load than HPC, for slabs with the same cross-sections and allowed deflection for the spans within limits from 6 to 12 m;
- Dimensions of cross-sections and ratio of longitudinal reinforcement for members subjected to flexure and compression with the bending can be decreased by 10–20 % by using high-performance steel fibre reinforced concrete.

References

1. Rigaud, S., Chanvillard, G., Chen, J. Characterization of bending and tensile behavior of ultra-high performance concrete containing glass fibers. RILEM Bookseries. 2012. Vol. 2. Pp. 373–380.
2. Song, P.S., Hwang, S. Mechanical properties of high-strength steel fiber-reinforced concrete. Construction and Building Materials. 2004. Vol.18. Pp. 669–673.

Литература

1. Rigaud S., Chanvillard G., Chen J. Characterization of bending and tensile behavior of ultra-high performance concrete containing glass fibers // RILEM Bookseries. 2012. Vol. 2. Pp. 373–380.
2. Song P.S., Hwang S. Mechanical properties of high-strength steel fiber-reinforced concrete // Construction and Building Materials. 2004. Vol. 18. Pp. 669–673.

3. Abdul-Razzak, A.A., Mohammed Ali, A.A. Modelling and numerical simulation of high strength fibre reinforced concrete corbels. *Applied Mathematical Modelling*. 2011. Vol. 35. No. 6. Pp. 2901–2915.
4. Jansson, A., Flansbjer, M., Löfgren, I., Lundgren, K., Gylltoft, K. Experimental investigation of surface crack initiation, propagation and tension stiffening in self-compacting steel-fibre-reinforced concrete. *Materials and Structures/Materiaux et Constructions*. 2012. Vol. 45. No. 8. Pp. 1127–1143.
5. Yusof, M.A., Nor, N.M., Zain, M.F.M., etc. Mechanical properties of hybrid steel fibre reinforced concrete with different aspect ratio. *Australian Journal of Basic and Applied Sciences*. 2011. Vol.5. No.7. Pp.159–166.
6. Bhargava, P., Sharma, U.K., Kaushik, S.K. Compressive stress-strain behaviour of small scale steel fibre reinforced high strength concrete cylinders. *Journal of Advanced Concrete Technology*. 2006. Vol.4. No.1. Pp. 109–121.
7. Klyuev, S.V., Klyuev, A.V., Abakarov, A.D., Shorstova, E.S., Gafarova, N.G. The effect of particulate reinforcement on strength and deformation characteristics of fine-grained concrete. *Magazine of Civil Engineering*. 2017. Vol.75. No. 7. Pp. 66–75.
8. Olivito, R.S., Zuccarello, F.A. An experimental study on the tensile strength of steel fiber reinforced concrete. *Composites: Part B*. 2010. Vol. 41. Pp. 246–255.
9. Keyvani Someh, A., Saeki, N. Prediction for the stress-strain curve of steel fiber reinforced concrete. *Transactions of the Japan Concrete Institute*. 1996. Vol.18. Pp. 175–182.
10. Aydin S. Effects of fiber strength on fracture characteristics of normal and high strength concrete. *Periodica Polytechnica Civil Engineering*. 2013. Vol. 57. No. 2. Pp. 191–200.
11. Singh, H. Steel fiber reinforced concrete – behavior, modelling and design. *Ludhiana: Springer*, 2017, 172 p.
12. Kazemi, M.T., Golsorkhtabar, H., Beygi, M.H.A., Gholamitabar, M. Fracture properties of steel fiber reinforced high strength concrete using work of fracture and size effect methods. *Construction and Building Materials*. 2017. Vol. 142. Pp. 482–489.
13. Ulas, M.A., Alyamac, K.E., Ulucan, Z.C. Effects of aggregate grading on the properties of steel fibre-reinforced concrete. *IOP Conference Series: Materials Science and Engineering*. 9th International Conference Fibre Concrete 2017, Prague, Czech Republic, September 13-16, 2017. Vol. 246, No. 1. Article No. 012015.
14. Nikolenko, S.D., Sushko, E.A., Sazonova, S.A., Odnolko, A.A., Manokhin, V.Ya. Behaviour of concrete with a disperse reinforcement under dynamic loads. *Magazine of Civil Engineering*. 2017. No. 7. Pp. 3–14.
15. Vougioukas, E., Papadatou, M. A model for the prediction of the tensile strength of fiber-reinforced concrete members, before and after cracking. *Fibers*. 2017. Vol. 5. No. 3. Article No. 27.
16. Simões, T., Octávio, C., Valença, J., Costa, H., Dias-da-Costa D., Júlio, E. Influence of concrete strength and steel fibre geometry on the fibre/matrix interface. *Composites Part B: Engineering*. 2017. Vol. 122. Pp. 156–164.
17. Balanji, E.K.Z., Sheikh, M.N., Hadi, M.N.S. Behavior of hybrid steel fiber reinforced high strength concrete. *Proceedings of the First European and Mediterranean Structural Engineering and Construction Conference EURO-MED-SEC-1, Istanbul, Turkey, May 24-29, 2016*. Pp. 29–34.
18. Travush, V.I., Konin, D.V., Krylov, A.S. Strength of reinforced concrete beams of high-performance concrete and fiber reinforced concrete. *Magazine of Civil Engineering*. 2018. No. 1. Pp. 90–100.
19. Savita, Shwetha S., Malanbi, Shweta, Saksheshwari, Manjunath K. Experimental study on strength parameters of steel fiber reinforced concrete using GI wire & fly ash. *International Research // Journal of Engineering and Technology*. 2018. Vol. 5. № 5. Pp. 3271–3277.
3. Abdul-Razzak A.A., Mohammed Ali A.A. Modelling and numerical simulation of high strength fibre reinforced concrete corbels // *Applied Mathematical Modelling*. 2011. Vol. 35. № 6. Pp. 2901–2915.
4. Jansson A., Flansbjer M., Löfgren I., Lundgren K., Gylltoft K. Experimental investigation of surface crack initiation, propagation and tension stiffening in self-compacting steel-fibre-reinforced concrete. *Materials and Structures/Materiaux et Constructions*. 2012. Vol. 45. № 8. Pp. 1127–1143.
5. Yusof M.A., Nor N.M., Zain, M.F.M., etc. Mechanical properties of hybrid steel fibre reinforced concrete with different aspect ratio // *Australian Journal of Basic and Applied Sciences*. 2011. Vol. 5. № 7. Pp.159–166.
6. Bhargava P., Sharma U.K., Kaushik S.K. Compressive stress-strain behaviour of small scale steel fibre reinforced high strength concrete cylinders // *Journal of Advanced Concrete Technology*. 2006. Vol. 4. № 1. Pp. 109–121.
7. Klyuev S.V., Klyuev A.V., Abakarov A.D., Shorstova E.S., Gafarova N.G. The effect of particulate reinforcement on strength and deformation characteristics of fine-grained concrete // *Magazine of Civil Engineering*. 2017. Vol. 75. № 7. Pp. 66–75.
8. Olivito R.S., Zuccarello F.A. An experimental study on the tensile strength of steel fiber reinforced concrete // *Composites: Part B*. 2010. Vol. 41. Pp. 246–255.
9. Keyvani Someh A., Saeki N. Prediction for the stress-strain curve of steel fiber reinforced concrete // *Transactions of the Japan Concrete Institute*. 1996. Vol. 18. Pp. 175–182.
10. Aydin S. Effects of fiber strength on fracture characteristics of normal and high strength concrete // *Periodica Polytechnica Civil Engineering*. 2013. Vol. 57. № 2. Pp. 191–200.
11. Singh H. Steel fiber reinforced concrete – behavior, modelling and design. *Ludhiana: Springer*, 2017, 172 p.
12. Kazemi M.T., Golsorkhtabar H., Beygi M.H.A., Gholamitabar M. Fracture properties of steel fiber reinforced high strength concrete using work of fracture and size effect methods // *Construction and Building Materials*. 2017. Vol. 142. Pp. 482–489.
13. Ulas M.A., Alyamac K.E., Ulucan, Z.C. Effects of aggregate grading on the properties of steel fibre-reinforced concrete // *IOP Conference Series: Materials Science and Engineering*. 9th International Conference Fibre Concrete 2017, Prague, Czech Republic, September 13–16, 2017. Vol. 246, № 1. Article № 012015.
14. Nikolenko S.D., Sushko E.A., Sazonova S.A., Odnolko A.A., Manokhin V.Ya. Behaviour of concrete with a disperse reinforcement under dynamic loads // *Magazine of Civil Engineering*. 2017. № 7. Pp. 3–14.
15. Vougioukas E., Papadatou M. A model for the prediction of the tensile strength of fiber-reinforced concrete members, before and after cracking // *Fibers*. 2017. Vol. 5. № 3. Article № 27.
16. Simões T., Octávio C., Valença J., Costa H., Dias-da-Costa D., Júlio, E. Influence of concrete strength and steel fibre geometry on the fibre/matrix interface // *Composites Part B: Engineering*. 2017. Vol. 122. Pp. 156–164.
17. Balanji E.K.Z., Sheikh M.N., Hadi M.N.S. Behavior of hybrid steel fiber reinforced high strength concrete // *Proceedings of the First European and Mediterranean Structural Engineering and Construction Conference EURO-MED-SEC-1, Istanbul, Turkey, May 24-29, 2016*. Pp. 29–34.
18. Travush V.I., Konin D.V., Krylov A.S. Strength of reinforced concrete beams of high-performance concrete and fiber reinforced concrete // *Magazine of Civil Engineering*. 2018. № 1. Pp. 90–100.
19. Savita, Shwetha S., Malanbi, Shweta, Saksheshwari, Manjunath K. Experimental study on strength parameters of steel fiber reinforced concrete using GI wire & fly ash. *International Research // Journal of Engineering and Technology*. 2018. Vol. 5. № 5. Pp. 3271–3277

Бука-Вайваде К., Шлисери Я., Сердок Д.О., Пакрастиныш Л., Ватин Н.И. Возможность рационального использования HPSFRC в многоэтажном строительстве // *Инженерно-строительный журнал*. 2018. № 8(84). С. 3–14.

- International Research Journal of Engineering and Technology. 2018. Vol. 5. No. 5. Pp. 3271–3277
20. Marara K., Erenb Ö., Yitmena İ. Compression specific toughness of normal strength steel fiber reinforced concrete (NSSFRC) and high strength steel fiber reinforced concrete (HSSFRC). *Materials Research*. 2011. Vol. 14. No. 2. Pp. 239–247.
 21. Neves R.D., De Fernandes Almeida J.C.O. Compressive behaviour of steel fibre reinforced concrete. *Structural Concrete*. 2005. Vol. 6. No. 1. Pp. 1–8.
 22. Li B., Xu L., Chi Y., Huang B., Li C. Experimental investigation on the stress-strain behavior of steel fiber reinforced concrete subjected to uniaxial cyclic compression. *Construction and Building Materials*. 2017. Vol. 140. Pp. 109–118.
 23. ANSYS 12.1 Mechanical APDL Manual. Ansys Inc., 2009.
 24. EN 1992-1-1: Eurocode 2: Design of concrete structures – Part 1-1: General rules and rules for buildings.
 25. Sliseris J. Numerical analysis of reinforced concrete structures with oriented steel fibers and re-bars // *Engineering Fracture Mechanics*. 2018. Vol. 194. Pp. 337-349.
 26. Sliseris J., Yan L., Kasal B. Numerical modelling of flax short fibre reinforced and flax fibre fabric reinforced polymer composites // *Composites Part B: Engineering*. 2016. Vol.89. Pp. 143–154.
 27. Sliseris J. Numerical estimation of the mechanical properties of a steel-fiber-reinforced geopolymer composite. *Mechanics of Composite Materials*, 2018. Vol. 54. No. 5. Pp. 1–18.
 28. Sliseris J., Rocens K. Rational structure of panel with curved plywood ribs. *World Academy of Science, Engineering and Technology: International Conference on Building Science and Engineering (ICBSE 2011)*, Italy, Venice, April 27-29, 2011. Pp. 317–323.
 29. Sliseris J., Rocens K. Optimal design of composite plates with discrete variable stiffness. *Composite Structures*. 2013. Vol. 98. Pp. 15–23.
 30. RILEM TC 162-TDF: 'Test and design methods for steel fibre reinforced concrete' σ - ϵ -design method. *Materials and Structures/Materiaux et Constructions*. 2003. Vol. 36. No. 262. Pp. 560–567.
 20. Marara K., Erenb Ö., Yitmena İ. Compression specific toughness of normal strength steel fiber reinforced concrete (NSSFRC) and high strength steel fiber reinforced concrete (HSSFRC) // *Materials Research*. 2011. Vol. 14. № 2. Pp. 239–247.
 21. Neves R.D., De Fernandes Almeida J.C.O. Compressive behaviour of steel fibre reinforced concrete // *Structural Concrete*. 2005. Vol. 6. № 1. Pp. 1–8.
 22. Li B., Xu L., Chi Y., Huang B., Li C. Experimental investigation on the stress-strain behavior of steel fiber reinforced concrete subjected to uniaxial cyclic compression // *Construction and Building Materials*. 2017. Vol. 140. Pp. 109–118.
 23. ANSYS 12.1 Mechanical APDL Manual. Ansys Inc., 2009.
 24. EN 1992-1-1: Eurocode 2: Design of concrete structures – Part 1-1: General rules and rules for buildings.
 25. Sliseris J. Numerical analysis of reinforced concrete structures with oriented steel fibers and re-bars // *Engineering Fracture Mechanics*. 2018. Vol. 194. Pp. 337-349.
 26. Sliseris J., Yan L., Kasal B. Numerical modelling of flax short fibre reinforced and flax fibre fabric reinforced polymer composites // *Composites Part B: Engineering*. 2016. Vol.89. Pp. 143–154.
 27. Sliseris J. Numerical estimation of the mechanical properties of a steel-fiber-reinforced geopolymer composite // *Mechanics of Composite Materials*, 2018. Vol. 54. № 5. Pp. 1–18.
 28. Sliseris J., Rocens K. Rational structure of panel with curved plywood ribs. *World Academy of Science // Engineering and Technology: International Conference on Building Science and Engineering (ICBSE 2011)*, Italy, Venice, April 27-29, 2011. Pp. 317–323.
 29. Sliseris J., Rocens K. Optimal design of composite plates with discrete variable stiffness // *Composite Structures*. 2013. Vol. 98. Pp. 15–23.
 30. RILEM TC 162-TDF: 'Test and design methods for steel fibre reinforced concrete' σ - ϵ -design method // *Materials and Structures/Materiaux et Constructions*. 2003. Vol. 36. № 262. Pp. 560–567.

Karina Buka-Vaivade,
+37126353082; *karina.buka.vaivade@gmail.com*

Карина Бука-Вайваде,
+37126353082;
эл. почта: *karina.buka.vaivade@gmail.com*

Janis Sliseris,
+37126214882; *janis.sliseris@rtu.lv*

Янис Шлисери́с,
+37126214882; эл. почта: *janis.sliseris@rtu.lv*

Dmitrijs Serdjuks,*
+37126353082; *Dmitrijs.Serdjuks@rtu.lv*

Дмитрий Олегович Сердюк,*
+37126353082;
эл. почта: *Dmitrijs.Serdjuks@rtu.lv*

Leonids Pakrastins,
+37129452138; *leonids.pakrastins@rtu.lv*

Леонид Пакрастиньш,
+37129452138; эл. почта: *leonids.pakrastins@rtu.lv*

Nikolai Vatin,
+79219643762; *vatin@mail.ru*

Николай Иванович Ватин,
+79219643762; эл. почта: *vatin@mail.ru*

© Buka-Vaivade, K., Sliseris, J., Serdjuks, D., Pakrastins, L., Vatin, N.I., 2018

doi: 10.18720/MCE.84.2

Additional load on barrel vaults of architectural monuments

Дополнительная нагрузка на коробовый свод
в памятнике архитектуры

A-Kh.B. Kaldar-ool*,
V.V. Babanov,
St. Petersburg State University of Architecture
and Civil Engineering, St. Petersburg, Russia

B.M. Allahverdov,
Petersburg State Transport University,
St. Petersburg, Russia

S.S. Saaya,
Tuvan State University, Kyzyl, Republic of Tuva,
Russia

Соискатель А.Б. Калдар-оол*,
канд. техн. наук, доцент В.В. Бабанов,
Санкт-Петербургский государственный
архитектурно-строительный университет,
Санкт-Петербург, Россия

**канд. техн. наук, доцент
Б.М. Аллахвердов**,
Петербургский государственный
университет путей сообщения Императора
Александра I, Санкт-Петербург, Россия
канд. техн. наук, доцент С.С. Саая,
Тувинский государственный университет,
г. Кызыл, Республика Тыва, Россия

Key words: barrel vault; method of forces;
strength; stresses; deformation; modulus of
elasticity; load

Ключевые слова: коробовый свод; метод сил;
прочность; напряжения; деформация; модуль
упругости; нагрузка

Abstract. In old buildings, which are architectural monuments, the stone three-centered barrel vaults and arches have been often used. In case of reconstruction of old buildings, it becomes necessary to increase the load on these elements. Calculation of additional load is based on instrumental examination of the vaults. While creating an analytical model of a barrel vault, it is necessary to use the experimental results of determination of the vault geometric parameters and material strength characteristics. The vault bearing capacity determined on base of analytical estimation is confirmed by similar calculations done by means of software packages, as well as by the data obtained by means of real loading of the vault. The proposed procedure for determination of additional load onto barrel vault may be also used in designing of similar architectural monuments.

Аннотация. В старинных зданиях, являющиеся памятниками архитектуры, часто в виде несущих элементов использовались каменные трехцентровые коробовые своды и арки. При реконструкции сооружений появляется необходимость увеличения нагрузки на эти элементы. Определение величины дополнительной нагрузки основано на результатах инструментального обследования сводов. При создании расчетной схемы модели коробового свода необходимо использовать результаты экспериментальных исследований: определение геометрических параметров свода и прочностных характеристик материалов. Несущая способность свода, определенная по результатам аналитического расчета, подтверждается аналогичными расчетами с использованием программных комплексов, а также данными, полученными при нагружении реального свода. Предложенная методика определения возможной дополнительной нагрузки на коробовый свод может быть использована при расчете аналогичных памятников архитектуры.

1. Introduction

Barrel vaults were widely used for construction of unique architectural buildings in XVIII to XIX century. They are often found in large-span inter-floor ceilings and covers of civil and industrial buildings, in church architecture, in the ceilings above basements, passages, corridors of low-rise residential and public buildings, as well as in the structures of stairwells and as span structures of bridges.

Cross-section of barrel vault has a shape of curve formed on base of several centers. There are three-centered, five-centered and multicentral barrel vaults. In this article, the symmetrical

three-centered barrel vaults consisting of three parts of circles of two different radii are described (Figure 1).

In contrast to elliptic vaults, the generatrix of barrel vaults is a curve consisting of several circular curve segments. These segments have common first-order derivative in their point of compound curvature; therefore, the centers of neighboring circles must be on the same line.

Until recently, axis plotting and approximate calculation of barrel vaults were carried out by various graphical methods.

The best-known works on calculation of arches and vaults of different shapes are [1–7] and experimental studies of stone vaults and arch structures are [8–20]. In these researches, methods of calculation of the stress-strain state for different shapes of stone arches and vaults have been developed, and behavior of vaults has been studied on base of numerical models.

Usually, methods of calculation have been worked out for parabolic vaults [21], but they are scantily suitable for designing of barrel vault axis configuration. These methods have just a historical value and have become the first attempt to solve the problem, but it has created a base for development of more perfect methods. In this case, the vault was represented as twice statically indeterminable single-hinged arch, which calculation is simplified due to symmetry properties [22].

Today the existing method of barrel vaults' calculation is usually based on graphic-analytical method for development of statically determined design model. No other methods were found in the cited literature.

In this regard, it is necessary to carry out more precise calculations, taking into account the specific geometry of barrel arches and the real extent of static indeterminacy of the vault analytical model.

It is obvious that development of methods permitting to estimate technical condition of the barrel vaults taking into account their construction technology and history of loading is of immediate interest.

The purpose of this article is to create a methodology for determination of the value of additional load on the vault during its further upkeeping.

To determine the value of the additional load it is necessary to solve several related tasks:

1. Creation of analytical expressions describing the barrel vault axis on base of the results of measuring the real vault geometry.
2. Static calculation of the vault taking into account all internal stresses.
3. Primary structure loading condition.
4. Obtaining the strength characteristics of the barrel vault brickwork on base of the results of experimental tests.
5. Determination of deformation characteristic (deformation modulus) of the vault brickwork taking into account changes in the material within the structure service period.
6. Determination of the additional load value. Experimental test.

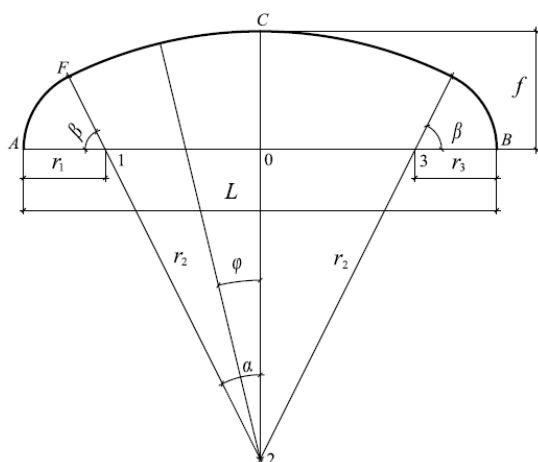


Figure 1. The axis of three-centered barrel vault, where L is the span of vault, f is the rise of vault, r_1 is small radius, r_2 is large radius.

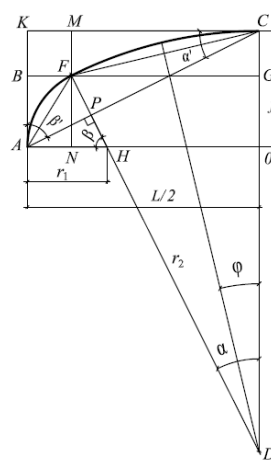


Figure 2. Method of constructing the three-centered barrel vault.

2. Methods

1. Creation of equations describing the shape of vault (arch) axis on base of the results of measuring the real span L and rise of vault f (Figure 2).

To design the shape of the arch axis, it is necessary to determine the values of small and large radii r_1 and r_2 . If $AO = L/2$, $CO = f$ the rectangle is build and angles are measured $\alpha' = \arctan\left(\frac{2f}{L}\right)$ and $\beta' = \arctan\left(\frac{L}{2f}\right)$. The triangles KCA , GDF and CDP are similar, as their sides are proportional and the angles between them are the same; in this case $\alpha = \alpha'$, $\beta = \beta'$ (Figure 2).

Let us make a system of equations:

$$\begin{cases} MF + FN = f = r_1 \cdot \sin \beta + (1 - \cos \alpha) \cdot r_2 \\ BF + FG = L/2 = (1 - \cos \beta) \cdot r_1 + \sin \alpha \cdot r_2. \end{cases} \quad (1)$$

Transformation matrix and output matrix are:

$$A = \begin{pmatrix} \sin \beta & 1 - \cos \alpha \\ 1 - \cos \beta & \sin \alpha \end{pmatrix}, \quad D = \begin{pmatrix} f \\ L/2 \end{pmatrix}. \quad (2)$$

Matrix equality of known radii is:

$$R = A^{-1} \cdot D = \begin{pmatrix} r_1 \\ r_2 \end{pmatrix}. \quad (3)$$

The equations of the vault axis as a function of current angle φ in the parametric form $y(\varphi) = f(x(\varphi))$ are:

$$x(\varphi) = \begin{cases} r_2 \cdot \sin(-\alpha) + r_1 \cdot \cos \beta - r_1 \cdot \cos\left(\frac{\pi}{2} + \varphi\right), \text{ if } -\frac{\pi}{2} < \varphi \leq -\alpha \\ r_2 \cdot \sin \varphi, \text{ if } \varphi \leq |\alpha| \\ r_2 \cdot \sin \alpha - r_1 \cdot \cos \beta + r_1 \cdot \cos\left(\frac{\pi}{2} - \varphi\right), \text{ if } \alpha < \varphi \leq \frac{\pi}{2} \end{cases} \quad (4)$$

$$y(\varphi) = \begin{cases} r_1 \cdot \sin\left(\varphi + \frac{\pi}{2}\right), \text{ if } -\frac{\pi}{2} \leq \varphi < -\alpha \\ \left[(r_2 \cdot (\cos \varphi - 1) + f) \right], \text{ if } -\alpha < \varphi \leq \alpha \\ r_1 \cdot \sin\left(\frac{\pi}{2} - \varphi\right), \text{ if } \alpha < \varphi \leq \frac{\pi}{2} \end{cases} \quad (5)$$

Thus, for analytical designing of the axis of spacial curve of symmetric vault, it is sufficient to know the span L and the rise f of the vault, as well as the design requirement: the point of contact of two curves composing the axis of the spacial curve should be located at the intersection of the bisectrices of the triangle formed by L and f values.

Each vault may be presented as a system of elementary arches forming the shape of the vault and bearing their load [24]. The vault analytic model may be approximately presented as a system of independent parallel arches. For these reasons, for the barrel vault calculation, we adopt a simplified calculation model in the form of no-hinged arch under the following boundary conditions:

if $z = -L/2$ (left abutment) $y(-L/2) = 0$; $\theta = y'(-L/2) = 0$;

if $z = L/2$ (right abutment) $y(L/2) = 0$; $\theta = y'(L/2) = 0$.

In the investigated three-centered arch on the segments with different radii there are gaps in the second derivative of the geometric axis of the arch. In this case, the internal forces (bending moment, etc.) have no breaks, since the moment is not associated with the second derivative of the geometry, but depends on the change in curvature.

First derivative:

$$y'(\phi) = \begin{cases} (-\tan(\phi)), & \text{if } -\pi/2 \leq \phi < -\alpha \\ (-\tan(\phi)), & \text{if } -\alpha < \phi \leq \alpha \\ (-\tan(\phi)), & \text{if } \alpha < \phi \leq \pi/2 \end{cases} \quad (6)$$

Second derivative:

$$y''(\phi) = \begin{cases} -\frac{1}{r_1 \cdot \cos(\phi)^3}, & \text{if } -\pi/2 \leq \phi < -\alpha \\ -\frac{1}{r_1 \cdot \cos(\phi)^3}, & \text{if } -\alpha < \phi \leq \alpha \\ -\frac{1}{r_1 \cdot \cos(\phi)^3}, & \text{if } \alpha < \phi \leq \pi/2 \end{cases} \quad (7)$$

Since the moment diagram has no gaps and the stresses in the arch are directly proportional to the change in the axis curvature, the stresses practically do not change on the butt sections with different radii of curvature.

For flat segments, the moment of inertia of the cross section may be determined by the general formula for the straight rod:

$$J = \frac{b \cdot h^3}{12}. \quad (8)$$

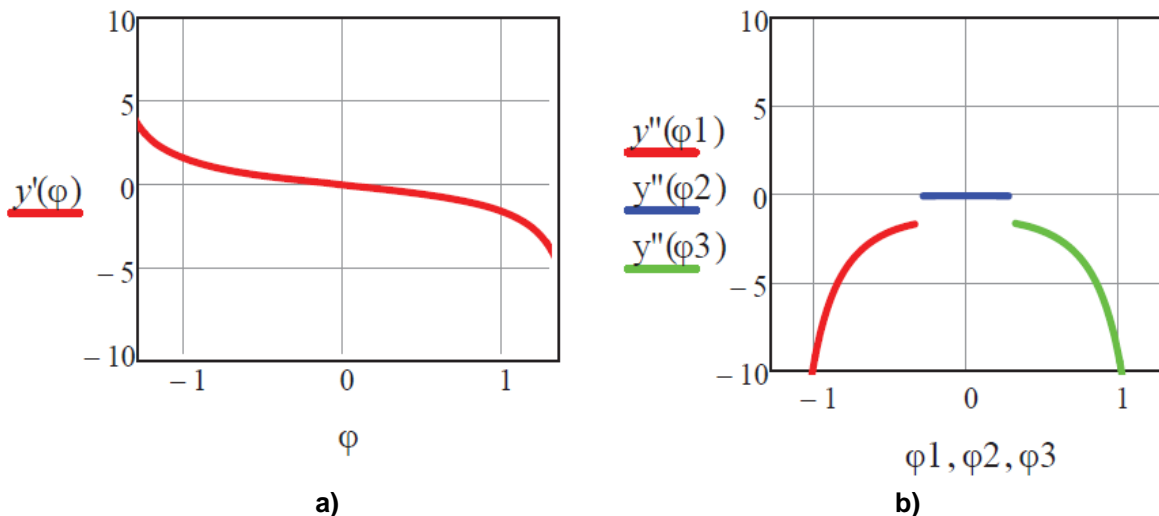


Figure 3. Diagrams of derivatives
a) diagram of the first derivative: function is continuous;
b) diagram of the second derivative: function has the gaps at $-\alpha$ and α .

In the steep part of the arches, where the neutral line is distinctly displaced, the moment of inertia of the section should be determined by the formula:

$$J' = \int_{-h/2}^{h/2} \frac{y^2 \cdot b}{1 + \frac{y}{r}} dy. \quad (9)$$

2. Static calculation.

The static calculation of triply statically indeterminate arch is performed by method of forces using Maxwell-Moore formula with a full set of internal forces for determining changes (bending moment, longitudinal and transverse forces) [24].

$$\delta_{ik} = \sum \int \frac{M_i(\varphi) \cdot M_k(\varphi) \cdot rd\varphi}{EA \cdot r^2} + \sum \int \frac{M_i(\varphi) \cdot M_k(\varphi) \cdot rd\varphi}{EJ_r} + \sum \int \frac{N_i(\varphi) \cdot N_k(\varphi) \cdot rd\varphi}{EA} + \mu \cdot \left[\sum \int \frac{Q_i(\varphi) \cdot Q_k(\varphi) \cdot rd\varphi}{GA} \right] + \sum \int \frac{M_k(\varphi) \cdot N_i(\varphi) \cdot r_1 d\varphi}{EA \cdot r_1} + \sum \int \frac{M_i(\varphi) \cdot N_k(\varphi) d\varphi}{EA}. \quad (10)$$

$$\Delta_{iq} = \sum \int \frac{M_i(\varphi) \cdot M_q(\varphi) \cdot rd\varphi}{EA \cdot r^2} + \sum \int \frac{M_i(\varphi) \cdot M_q(\varphi) \cdot rd\varphi}{EJ_r} + \sum \int \frac{N_i(\varphi) \cdot N_q(\varphi) \cdot rd\varphi}{EA} + \mu \cdot \left[\sum \int \frac{Q_i(\varphi) \cdot Q_q(\varphi) \cdot rd\varphi}{GA} \right] + \sum \int \frac{N_i(\varphi) \cdot M_q(\varphi) \cdot r_1 d\varphi}{EA \cdot r_1} + \sum \int \frac{M_i(\varphi) \cdot N_q(\varphi) d\varphi}{EA}. \quad (11)$$

3. General case of loading is described by four types of loads: self-weight of vault, brickwork back filling weight, evenly distributed load on top of the backfilling (weight of the floor), and different types of temporary loads F (weight of people and equipment) (Figure 4).

4. When examining the bearing capacity of the above-basement vaulted ceiling of Ethnographic Museum building in St. Petersburg, the question has arisen about the strength characteristics of the brickwork. More than 100 years have passed since its construction (the building was built in 1911). The vaulted ceiling has a three-centered arc shape.

Visual inspection of the above-basement vaulted ceiling has proved that the overall structure condition is satisfactory (usable) (Figure 5).

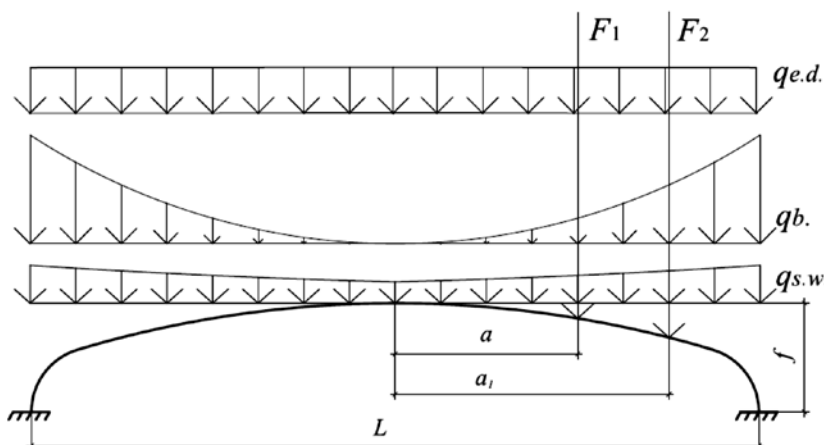


Figure 4. Actual loads on the vault; $q_{s.w}$ is the self-weight of vault; q_b is the brickwork back filling weight; $q_{e.d}$ is the load from structures on the top of vault; F – different types of temporary loads.

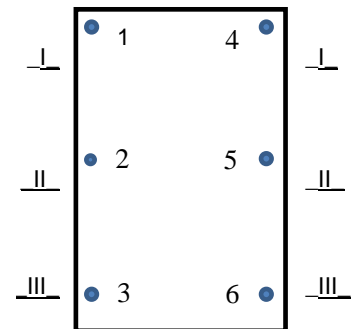


Figure 5. Location of vault materials testing points: UT test points on vault lower surface.

The arch bond strength was determined by the following methods:

- The strength of the brick and arch bond mortar on the upper surface of the vault according to Russian State Standards (GOST) 8462-85 [23] and 5802-86 [24] is determined by the destructive method. The selected samples have been tested in the laboratory of Saint Petersburg State University of Architecture and Civil Engineering.

- The strength of brickwork on the lower surface of the vault has been determined by means of ultrasonic method using UK-14P device.

Determination of the brickwork strength has been carried out by means of ultrasonic method using UK-14P device as follows:

1. brick strength limit (at the base on the surface of 100 mm)

$$R_1 = 7.5201 + 0.008 v_1 \text{ MPa};$$

2. the limit strength of the arch bond mortar (at the base of 40 mm)

$$R_2 = 7.3975 - 0.0068 v_2 \text{ MPa}.$$

The brickwork strength has been determined by the formula of Prof. L.I. Onishchik [25]:

$$R = 0.5R_u - 0.5AR_1(1 - a / (b + 0.5R_2 / R_1))\gamma.$$

in this case:

$$A = (9.81 + R_1) / (9.81 m + n R_1);$$

$$a = 0.2; b = 0.3; m = 1.25; n = 3.$$

The value of correction factor γ :

– according to the table: $R_{1,m} = 10.4 \text{ MPa}$, $R_{2,1} = 0.04R_{1,m} = 0.4 \text{ MPa} < R_{2,m} = 2.14 \text{ MPa}$,

thus $\gamma = 1$.

- In accordance with impact resilience using Schmidt hammer, according to Russian State Standard (GOST) 22690-88 [26].

To determine the brickwork load-carrying ability, the strength properties of brickwork have been examined. As a result of 12 tests, R_1, R_2, \dots, R_{12} sample data of brick and mortar of which the brickwork is made have been obtained.

Statistical processing of test results.

To estimate the mathematical expectation of normal distribution the following function (arithmetic mean of observed values of random variable) is used:

$$R_m = \frac{1}{n} (R_1 + R_2 + \dots + R_n),$$

where R_m is the mean value of the limit strength according to test results;

n is the number of the test sample;

RMS deviation of the observed values of R_i factor from their mean value R_m has been determined by the formula:

$$s = \sqrt{\frac{\sum_{i=1}^n (R_i - R_m)^2}{n}};$$

Using Student's distribution, the confidence interval of the brick and mortar strength has been determined:

$$R_{1,2} = R_m - t \frac{S_q}{\sqrt{n}};$$

where $t = 2.23$ is Student's coefficient at $n = 12$ and the confidence interval with a probability of 95 %.

5. Definition of the stiffness (deformation) characteristics of vault brickwork.

Before making calculations, it is necessary to determine the stiffness (deformation) characteristics of vault brickwork.

For this purpose, it is necessary to know the initial modulus of elasticity E_0 , the change of the modulus of deformation in time, taking into account the material plasticity, which in its turn results in a change in the initial modulus of deformation.

To determine the initial deformation modulus of the material, it is necessary to use the results presented in the work of N.S. Khamidzhanov. As a result of the step-by-step regression analysis, he has got an analytical dependence that relates the initial modulus of elasticity E_0 to the brick and mortar grade, which match with a probability of 0.99 the experimental data received by the author by F Fisher criterion and t Student's criterion. In our calculations, it is necessary to follow the linear model proposed by N.S. Khamidzhanov:

$$E_0 = 187R_{brick} + 173.2R_{mortar} + 5766, \quad (12)$$

To determine the value of the initial modulus of elasticity it is also possible to use the generally accepted formula of Professor L.I. Onishchik that is in force in normative documents and in the Russian Set of Rules SP 15.13330.2012 [27, 28]:

$$E_0 = \alpha_1 \cdot R_u, \quad (13)$$

where α_1 is brickwork elastic characteristic determined experimentally by L.I. Onishchik. The value of α_1 elastic characteristics for non-reinforced brickwork with the strength of the brick and mortar is accepted by means of interpolation.

$R_u = R \cdot k$ is temporary brickwork resistance (average strength limit);

R is calculated brickwork resistance;

k is the material safety factor, for brickwork it is 2.0.

Within the linear creeping, it is possible to use the concept of modulus of long-term deformation, which is determined by formula proposed by A.M. Rozenblyumas. It allows for validity of Hooke law for linear time-dependent deformations [29], but with a modified value of the initial deformation modulus:

$$E_t = \frac{E_0}{1 + \phi_t}, \quad (14)$$

where ϕ_t is the brickwork creep characteristic, which depends on time.

To determine the brickwork creep characteristic ϕ_t , we have adopted the exponential function in accordance with the data given in Eurocode 1992-1 [30]:

$$\phi_t = \varphi_0 \cdot \left(\frac{T}{T + \beta_n} \right)^{0.3}, \quad (15)$$

where $\varphi_0 = 1.5$ is theoretical creep factor adopted by Eurocode 1992-1-1 (how many times the deformation increases over the infinite duration of the load action).

$\beta_n = 657.82$ is a coefficient depending on relative humidity and theoretical size of the element (adopted for materials given in documentation of "Lira-9.6" software complex).

T is the number of days (the age of material), after which it is necessary to take into account the effect of creep.

To account for possible creep according to the Russian Set of Rules SP 15.13330.2012, the adopted coefficient of creep is $\nu = 2.2$ [28]. The deformation modulus in this case is determined by the formula

$$E_t = \frac{E_0}{2.2} \text{ [27, 28].}$$

In accordance with the Russian Set of Rules SP 15.13330.2012, when determining the deformation of masonry in case of stress calculation in statically indeterminate systems, the structures' stiffness characteristic is specified by the formula (accounting for material plastic properties) [27, 28]:

$$E = 0.8 \cdot E_t. \quad (16)$$

6. Determination of internal forces and stresses in barrel vault.

The barrel vault calculation was done using analytical method in "Mathcad 14" software system and for checking the finite element method was used in "Lira-Windows" software complex. In this case the vault surface deformations accumulated over the vault lifetime and found out by means of geodetic survey were taken into account.

There have been chosen the variants of elements that can provide triaxial calculation of the vault composed of 3D finite elements (Figure 6) and the shell (Figure 7), as well as the design in form of the arch composed of the rod-type finite elements (Figure 8). It is shown that the vault stressed state is described by the rod-type model without significant errors.

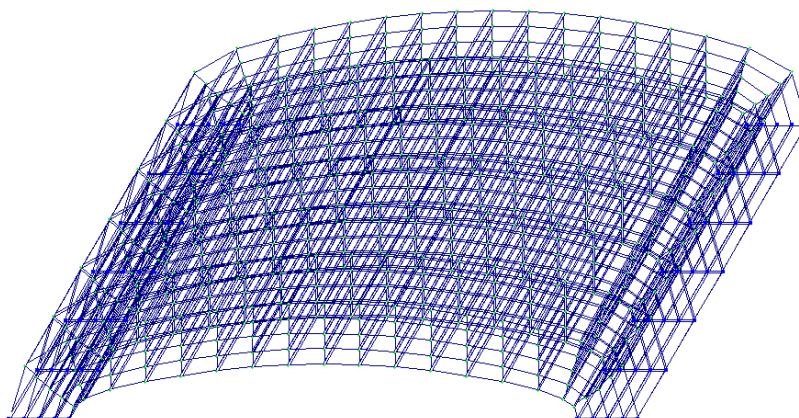


Figure 6. 3D Volumetric finite elements model of vault.

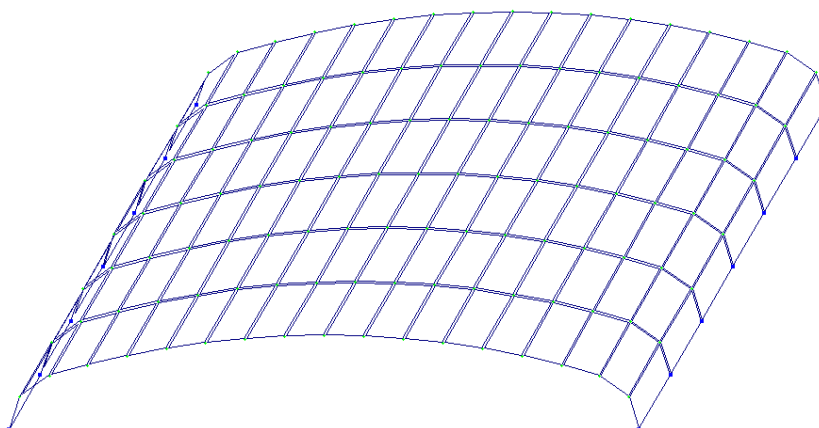


Figure 7. 3D Shell model of vault.

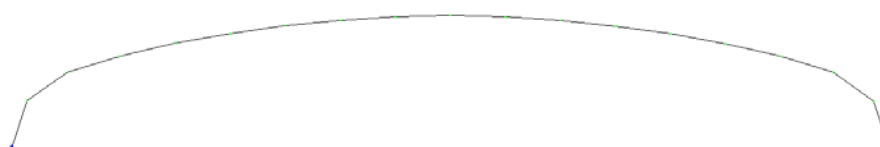


Figure 8. Flat arch design model of vault.

Determination of additional load onto vault is based on the results of calculations. Taking into account estimation of the value of the additional load onto the vault ($F_1 + F_2 = 10 \text{ kN/m}$), obtained by numerical calculation of the vault as an arch and spatial elements, it is possible to set this value $F_{\text{additional load}}$ for experimental research of the vault.

To identify the stressed state under load mechanical strain gauges with a base of 100 mm were used. Barrel vault vertical displacement was measured using deflectometer.

Loading was done using metal loads of 0.5 kN, placed on the vault to create a uniformly distributed load along a strip. For each stage of loading, the value of distributed load was taken to be equal to $\frac{1}{10} F^{\text{destroying}} \approx 2 \text{ kN/m}$. After five steps the maximum load of 10 kN/m was achieved. Loading was begun along the longitudinal section of the vault from both sides to the centre. At each stage after loading instrument readings were taken.

3. Results and Discussion

Table 1. The results of brick and mortar strength determination by means of nondestructive ultrasonic control method.

| Item No. | t_1 , microsecond | g_1 , m/s | R_1 , MPa | t_2 , microsecond | g_2 , m/s | R_2 , MPa | R_i , MPa | $p_i = \frac{R_i}{R_{min}}$ | $p_i R_i$ | $S_i = R_i - R_{\text{medium}}$ |
|----------|------------------------|----------------|----------------|------------------------|----------------|----------------|----------------|-----------------------------|-----------|---------------------------------|
| 1 | 32 | 3125 | 10 | 47 | 851 | 1.78 | 1.14 | 1.00 | 1.14 | -0.053 |
| 2 | 31 | 3226 | 10.1 | 54 | 741 | 2.51 | 1.25 | 1.10 | 1.37 | 0.056 |
| 3 | 36 | 2778 | 9.74 | 51 | 784 | 2.22 | 1.19 | 1.04 | 1.24 | -0.006 |
| 4 | 29 | 3448 | 10.3 | 48 | 833 | 1.90 | 1.17 | 1.03 | 1.21 | -0.019 |
| 5 | 30 | 3333 | 10.2 | 53 | 755 | 2.42 | 1.24 | 1.09 | 1.35 | 0.049 |
| 6 | 34 | 2941 | 9.87 | 49 | 816 | 2.01 | 1.17 | 1.02 | 1.19 | -0.028 |
| Σ | 6.28 | 7.50 | | | | | | | | |

$$R_{\text{med.}} = \sum p_i R_i / \sum p_i = 1.19 \text{ MPa.}$$

$$\Delta R = \sqrt{\frac{\sum p_i s_i^2}{(n-1) \sum p_i}} = 0.12 \text{ MPa.}$$

The brickwork design strength is:

$$R = R_{\text{medium}} - \Delta R = 1.07 \text{ MPa or } 10.92 \text{ kg/cm}^2;$$

at medium values:

$$\text{brick grade } M_{\text{brick}} = 102; R_{1, \text{medium}} = 10.03 \text{ MPa};$$

$$\text{mortar grade } M_{\text{mortar}} = 22; R_{2, \text{mortar}} = 2.14 \text{ MPa.}$$

Table 2. Results of tests of brick and mortar strength by means of rebound hammer method with the help of Schmidt hammer.

| Sample number | 1 | 2 | 3 | 4 | 5 | 6 | 7 | 8 | 9 | 10 | 11 | 12 |
|----------------------|-----|-----|-----|-----|------|-----|-----|------|-----|-----|------|------|
| Brick strength, MPa | 9.8 | 1.0 | 9.9 | 9.7 | 1.01 | 9.6 | 9.9 | 1.03 | 9.9 | 1.0 | 1.08 | 1.07 |
| Mortar strength, MPa | 2.1 | 2.7 | 1.9 | 1.8 | 2.2 | 3.1 | 3.0 | 2.6 | 2.2 | 2.9 | 1.8 | 2.9 |

Brick breaking strength is $R_1 = 9.8 \text{ MPa}$; mortar tensile strength is $R_2 = 2.1 \text{ MPa}$.

Table 3 compares the moments of inertia taking into account the effect of J axis curvature (formula (8)) and J' neutral axis of the vault according to the formula (9).

Table 3. Comparison of values of moments of inertia.

| Steep part of vault | | | Flat part of vault | | |
|---------------------|--------|----|--------------------|--------|---|
| J_1 | J'_1 | % | J_2 | J'_2 | % |
| 0.0629 | 0.0704 | 10 | 0.0486 | 0.0486 | 0 |

The difference between the results in the estimation of influence of the neutral axis shift in the flat part of the vault is 0 %, and in the steep part is 10 %. According to the results of the study it should be noted that the offset of neutral line may be neglected.

According to the obtained values of brick and mortar strength characteristics, the calculated brickwork resistance according to the Russian Set of Rules SP 15.13330.2012 is determined and compared with L.I. Onishchik formula (Table 4) [27, 28].

Table 4. Comparison of values of brickwork design strength.

| Brickwork design strength | According to the Russian Set of Rules SP 15.13330.2012 | According to L.I. Onishchik formula | | | % |
|---------------------------|--|-------------------------------------|------|--------------------|------|
| | | Rebound hammer method | % | Ultrasound control | |
| R (MPa) | 1.126 | 0.915 | 18.7 | 1.07 | 4.97 |

Evaluation of the design resistance of the brickwork by an elastic rebound according to the formula of Professor L.I. Onishchik and the Russian Set of Rules SP 15.13330.2012 differ by 18.7 %, in the ultrasonic inspection at 4.97 %. According to the Set of rules the strength of brickwork gets highest properties.

Table 5. Comparison of values of initial deformation modulus.

| Initial deformation modulus | According to the Russian Set of Rules SP 15.13330.2012 | According to N.S. Hamidzhanov formula | % |
|-----------------------------|--|---------------------------------------|-------|
| E_0 (MPa) | 2252 | 2883 | 21.88 |

The difference between the values of the initial modulus of elasticity according to N.S. Khamidzhanov formula and the Russian Set of Rules SP 15.13330.2012 is 21.88 % (Table 5). Taking into account that in the research [30] various correlations between brick and the mortar strength are close to those obtained in our tests, in further calculations we take into account the initial modulus of elasticity equal to $E_0 = 2883$ MPa.

Table 6. Estimation of values of modulus of long-term deformation.

| Modulus of long-term deformation | According to the Russian Set of Rules SP 15.13330.2012 | According to A.M. Rozenblyumas formula | % |
|----------------------------------|--|--|-------|
| E_t (MPa) | 1023.63 | 1156 | 11.45 |

Estimation of the values of modulus of long-term deformation calculated according to A.M. Rozenblyumas formula and according to the Russian Set of Rules SP 15.13330.2012 gives a difference of 11.45 %. In our calculation the adopted value of the modulus is taken according to A.M. Rozenblyumas data.

In accordance with the Russian Set of Rules SP 15.13330.2012, when determining the brickwork deformation in case of determining the strains in statically indeterminate systems, the stiffness properties of structures are taken in accordance with the formula:

$$E = 0.8 \cdot E_t.$$

Finally the modulus of deformation is adopted to be equal to $E = 925.55$ MPa.

According to the results of calculation, the normal stress and vertical displacement comparison was performed for E_0 initial modulus and E modulus of deformation in the Tables 7 and 8.

Table 7. Comparison of stresses at E_0 initial modulus of deformation and E modulus of deformation (coordinate $x = 3.342$ m).

| Stresses | E_0 vault (Lira) | E vault (Lira) | % | E_0 arch (Lira) | E arch (Lira) | % | E_0 Mathcad | E Mathcad | % |
|------------------|--------------------|------------------|---|-------------------|-----------------|---|---------------|-------------|------|
| σ , (MPa) | -0.4755 | -0.4755 | 0 | -0.5305 | -0.5305 | 0 | -0.53357 | -0.52316 | 1.95 |

Table 7 shows that the change in the modulus of deformation has almost no effect on the stress values.

Table 8. Comparison of displacements at different moduli of deformation (coordinate $x = 0$ m).

| Displacement | E_0 vault (Lira) | E vault (Lira) | % | E_0 arch (Lira) | E arch (Lira) | % | E_0 Mathcad | E Mathcad | % |
|--------------|--------------------|------------------|------|-------------------|-----------------|------|---------------|-------------|-------|
| f , (mm) | 0.9147 | 2.8494 | 67.9 | 0.9674 | 3.0136 | 67.9 | 1.19 | 3.71 | 67.92 |

From the Table 8 it is clear, that the change of modulus of deformation significantly affect the magnitude of displacements.

So for more than 100 years of service life of barrel vault structure, which description is given below, due to creep and plasticity, the deflections have grown by more than half.

Distribution of normal stresses in Mathcad and Lira:

The results of analytical and numerical methods of calculation are generally consistent.

Taking into account the spatial service of the vault analyzed by means of finite element method with volumetric elements, as well as in form of plates (compared to an arch analytic design), it proves that the calculated stress values are almost independent of the analytical solution.

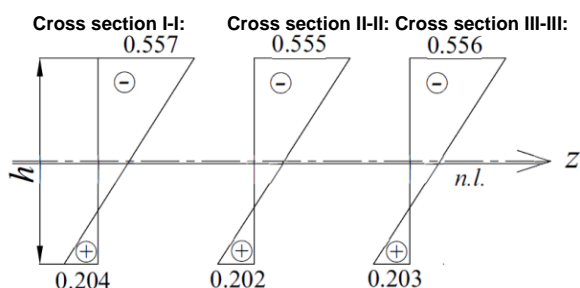


Figure 9. Distribution of normal stresses σ (MPa) in the cross-section near the vault skew-back ($x = 3.342$ m) under the action of constant loads in Mathcad.

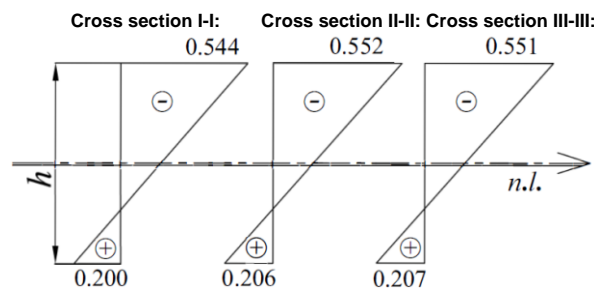


Figure 10. Distribution of normal stresses σ (MPa) in the cross-section near the vault skew-back ($x = 3.342$ m) under the action of constant loads in Lira.

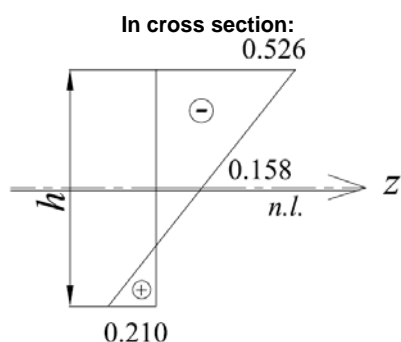


Figure 11. Distribution of normal stresses σ (MPa) in the cross-section near the vault skew-back ($x=3.342$ m) under the action of constant loads, three-dimensional analysis of vault in form of a shell in Lira.

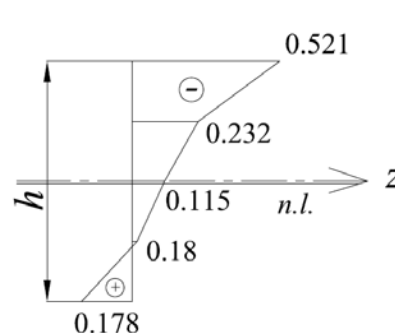


Figure 12. Distribution of normal stresses σ (MPa) in the cross-section near the vault skew-back ($x=3.342$ m) under the action of constant loads, three-dimensional analysis of vault according to the model with volumetric finite elements in Lira.

Based on the brickwork strength properties, the value of the additional load and the stressed state of the vault is determined. The analytical calculation, taking into account the displacement of the neutral layer of the vault, shows that the vault will withstand an additional load up to 10 kN/m under bending tensile stresses.

The dependence of displacements under specified load acting onto the test structure is shown in the Figure 13.

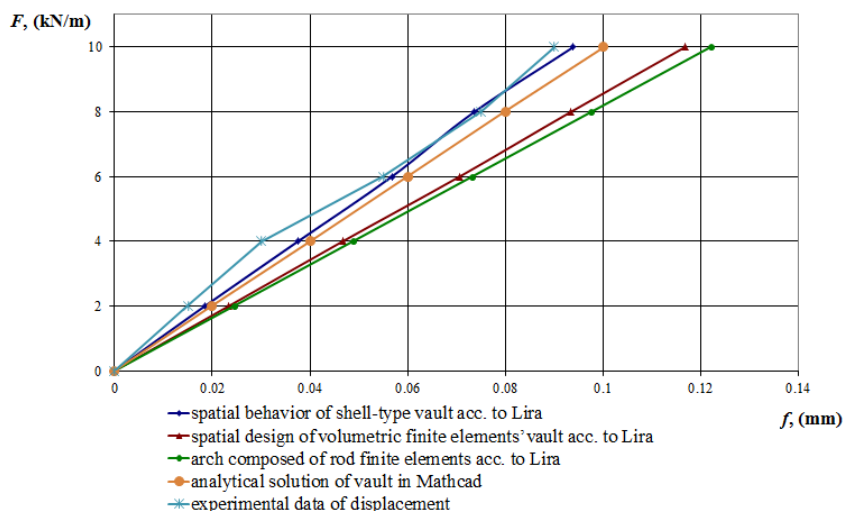


Figure 13. Dependence of vertical displacements in the crown of the vault.

Comparison of experimental and theoretical values of stresses and displacements of the structure shows that increase in stresses and displacements in case of load gradual increase is practically proportional to these loads. In this case, the modulus of deformation of object is approximately equal to the value taken in analytical calculations. It was the correct method of accounting for creep and plasticity in form of coefficients to the initial modulus of elasticity in the calculations.

To continue the comparison with the known works, this analytical solution is compared with the results of calculation of the arch outlined by the square parabola [21], which has been carried out for efficient selection of axis outline. Such arches are also often found in the ancient architectural components of the buildings.

The adopted outline of the arch axis is described by the expression:

$$y = f[\mu(x/d)^2 + (1-\mu)(x/d)^5],$$

where f is the rise of vault; $\mu = 0.966$.

Table 9. Comparison of stress values according to Kachurin and our data.

| Stress | According to Kachurin | According to our data | % |
|------------------|-----------------------|-----------------------|----|
| σ , (MPa) | 0.3997 | 0.2035 | 49 |

The difference between normal stresses in the results of design calculation of the arch defined by the parabolic law with the analytical solution for the arch as a three-centered compound curve is 49 %.

Thus, qualitatively, the experimental data completely confirm the derived analytical theory; but the calculation of the arch, described by the square parabola, has a noticeable discrepancy compared to the experiment results. It follows that calculation should be carried out with more accurate geometry and static uncertainty of the designed model of the vault.

4. Conclusions

1. The proposed herein a confirmatory method of calculation of barrel vaults of buildings constructed long ago (architectural monuments) allows to consider changes of physical and mechanical characteristics of the brickwork taking place in time. Modulus of initial deformation is taken from the works of N.S. Khamidzhanov, creep and plasticity are taken into account using A.M. Rozenblyumas formulas and adjustments to the Eurocode (material creep), as well as the nonlinearity of these characteristics (according to the Russian Set of Rules SP 15.13330.2012).

2. On the basis of analytical and numerical confirmatory calculations, the studies of the bearing capacity and the stressed state of the three-centered barrel vaults under the acting loads were carried out, which made

it possible to solve the task, i.e. to determine the amount of additional load that the considered barrel vault can withstand. The vault will be able to withstand the additional load up to 10 kN/m.

3. The experimental verification was carried out of the proposed method of studying the deformed state of the brickwork barrel vaults when loaded by short-term static load applied after a long period of time since the vault construction (more than 100 years).

4. The received test data and their comparison with the theoretical calculations of forces and displacements performed with the help of finite element method proved the proximity of the results.

5. The above calculations may be applied in the surveying and strength testing of barrel vaults used in architectural monuments.

References

1. Stefanou, I., Sab, K., Heck, J.V. Three dimensional homogenization of masonry structures with building blocks of finite strength: a closed form strength domain. *International Journal of Solids and Structures*. 2015. No. 54. Pp. 258–270.
2. Sab, K. Overall ultimate yield strength of a quasi-periodic masonry. *Comptes Rendus Mecanique*. 2009. No. 337. Pp. 603–609.
3. Skripchenko, I.V., Bepalov, V.V., Lukichev, S.Y., Zimin, S.S. Unconventional cases of the stone vaults. *Construction of Unique Buildings and Structures*. 2017. No. 2 (53). Pp. 87–95.
4. Basilio, I., Fedele, R., Lourenco, P.B., Milani, G. Assessment of curved FRP-reinforced masonry prisms: Experiments and modeling. *Construction and Building Materials*. 2014. No. 51. Pp. 492–505.
5. Milani, G. Upper bound sequential linear programming mesh adaptation scheme for collapse analysis of masonry vaults. *Advances in Engineering Software*. 2015. No. 79. Pp. 91–110.
6. Milani, G., Tralli, A. A simple meso-macro model based on SQP for the non-linear analysis of masonry double curvature structures. *International Journal of Solids and Structures*. 2012. No. 49. Pp. 808–834.
7. Kamal, O.A., Hamdy, G.A., El-Salakawy, T.S. Nonlinear analysis of historic and contemporary vaulted masonry assemblages. *HBRC Journal*. 2014. No. 10(3). Pp. 235–246.
8. Pottman, H., Eigensatz, M., Vaxman, A., Wallner, J. Architectural geometry. *Computers & Graphics*. 2015. No. 47. Pp. 145–164.
9. Cancelliere, I., Imbimbo, M., Sacco, E. Experimental tests and numerical modeling of reinforced masonry arches. *Engineering Structures*. 2010. No. 32. Pp. 776–792.
10. Ramaglia, G., Lignola, G.P., Prota, A. Collapse analysis of slender masonry barrel vaults. *Engineering Structures*. 2016. Vol. 117. Pp. 86–100.
11. Rizzi, E., Rusconia, F., Cocchetti, G. Analytical and numerical DDA analysis on the collapse mode of circular masonry arches. *Engineering Structures*. 2014. No. 60. Pp. 241–257.
12. Viola, E.L., Panzacci, F., Tornabene, F. General analysis and application to redundant arches under static loading. *Construction and Building Materials*. 2007. No. 21. Pp. 1129–1143.
13. De Santis, S., Tomor, A.K. Laboratory and field studies on the use of acoustic emission for masonry bridges. *NDT & E International*. 2013. No. 55. Pp. 64–74.
14. D'Ambrisi, A., Feo, L., Focacci, F. Masonry arches strengthened with composite unbundled tendons. *Composite Structures*. 2013. No. 98. Pp. 323–329.
15. Betti, M., Drosopoulos, G.A., Stavroulakis, G.E. Two non-linear finite element models developed for assessment of masonry arches. *Comptes Rendus Mecanique*. 2008. No. 336. Pp. 42–53.
16. Felice, G. Assessment of the load carrying capacity of multi span masonry arch bridges using fibre beam elements. *Engineering Structures*. 2009. No. 31. Pp. 1634–1647.

Литература

1. Stefanou I., Sab K., Heck J.V. Three dimensional homogenization of masonry structures with building blocks of finite strength: a closed form strength domain // *International Journal of Solids and Structures*. 2015. № 54. Pp. 258–270.
2. Sab K. Overall ultimate yield strength of a quasi-periodic masonry // *Comptes Rendus Mecanique*. 2009. № 337. Pp. 603–609.
3. Скрипченко И.В., Беспалов В.В., Лукичев С.Ю., Зимин С.С. Нетипичные случаи каменных сводов // *Строительство уникальных зданий и сооружений*. 2017. №2 (53). С. 87–95.
4. Basilio I., Fedele R., Lourenco P.B., Milani G. Assessment of curved FRP-reinforced masonry prisms: Experiments and modeling // *Construction and Building Materials*. 2014. № 51. Pp. 492–505.
5. Milani G. Upper bound sequential linear programming mesh adaptation scheme for collapse analysis of masonry vaults // *Advances in Engineering Software*. 2015. № 79. Pp. 91–110.
6. Milani G., Tralli A. A simple meso-macro model based on SQP for the non-linear analysis of masonry double curvature structures // *International Journal of Solids and Structures*. 2012. № 49. Pp. 808–834.
7. Kamal O.A., Hamdy G.A., El-Salakawy T.S. Nonlinear analysis of historic and contemporary vaulted masonry assemblages // *HBRC Journal*. 2014. № 10(3). Pp. 235–246.
8. Pottman H., Eigensatz M., Vaxman A., Wallner J. Architectural geometry // *Computers & Graphics*. 2015. № 47. Pp. 145–164.
9. Cancelliere I., Imbimbo M., Sacco E. Experimental tests and numerical modeling of reinforced masonry arches // *Engineering Structures*. 2010. № 32. Pp. 776–792.
10. Ramaglia G., Lignola G.P., Prota A. Collapse analysis of slender masonry barrel vaults // *Engineering Structures*. 2016. Vol. 117. Pp. 86–100.
11. Rizzi E., Rusconia F., Cocchetti G. Analytical and numerical DDA analysis on the collapse mode of circular masonry arches // *Engineering Structures*. 2014. № 60. Pp. 241–257.
12. Viola E.L., Panzacci F., Tornabene F. General analysis and application to redundant arches under static loading // *Construction and Building Materials*. 2007. № 21. Pp. 1129–1143.
13. De Santis S., Tomor A.K. Laboratory and field studies on the use of acoustic emission for masonry bridges // *NDT & E International*. 2013. № 55. Pp. 64–74.
14. D'Ambrisi A., Feo L., Focacci F. Masonry arches strengthened with composite unbundled tendons // *Composite Structures*. 2013. № 98. Pp. 323–329.
15. Betti M., Drosopoulos G.A., Stavroulakis G.E. Two non-linear finite element models developed for assessment of masonry arches // *Comptes Rendus Mecanique*. 2008. № 336. Pp. 42–53.
16. Felice G. Assessment of the load carrying capacity of multi span masonry arch bridges using fibre beam elements // *Engineering Structures*. 2009. № 31. Pp. 1634–1647.

Калдар-оол А.Б., Бабанов В.В., Аллахвердов Б.М., Саая С.С. Дополнительная нагрузка на коробовый свод в памятнике архитектуры // *Инженерно-строительный журнал*. 2018. № 8(84). С. 15–28.

17. Madani, K. A study of fiber deboning in circular composite arches. *Comptes Rendus Mecanique*. 2002. No. 330. Pp. 535–541.
18. Zhang, Y., Macorini, L., Izzuddin, B.A. Mesoscale partitioned analysis of brick-masonry arches. *Engineering Structures*. 2016. Vol. 124. Pp. 142–166.
19. Ramaglia, G., Lignola, G.P., Prota, A. Collapse analysis of slender masonry barrel vaults. *Engineering Structures*. 2016. Vol. 117. Pp. 86–100.
20. Felice, G. Assessment of the load-carrying capacity of multi span masonry arch bridges using fibre beam elements. *Engineering Structures*. 2009. No. 31. Pp. 1634–1647.
21. Zimin, S.S., Беспалов, В.В., Казиминова, А.С. Расчетная модель каменной арочной конструкции [The computational model stone arch] [online]. System requirements: Adobe Acrobat Reader. URL: [http://donna.sa.ru/publish_house/journals/vestnik/2015/vestnik_2015-3\(113\).pdf](http://donna.sa.ru/publish_house/journals/vestnik/2015/vestnik_2015-3(113).pdf). (assessed: 01 August 2018).
22. Zimin, S.S., Kokotkova, O.D., Беспалов, В.В. Vault structures of historical buildings. *Construction of Unique Buildings and Structures*. 2015. No. 2 (29). Pp. 57–72. (rus)
23. Russian State Standard GOST 8462-85. Materialy stenovyye. Metody opredeleniya predelov prochnosti pri szhatii i izgibe [Wall materials. Methods for determination of ultimate compressive and bending strength]. Moscow. Gosstandart Soyuz SSR, 1985. 10 p. (rus)
24. Russian State Standard GOST 5802-86 Rastvori stroitelnie. Metodi ispitaniya [Mortars. Test methods]. Moscow. Gosstandart Soyuz SSR, 1986. 22 p. (rus)
25. Zubkov, S.V., Ulybin, A.V., Fedotov, S.D. Assessment of mechanical properties of brick masonry by flat-jack method. *Magazine of Civil Engineering*. 2015. No. 8. Pp. 20–29. (rus)
26. Russian State Standard GOST 22690-88 Betony. Opredeleniye prochnosti mehanicheskimi metodami nerazrushayushchego kontrolya [Concretes. Determination of strength by mechanical methods of nondestructive testing]. Moscow. Gosstandart Rossii, 1988. 26 p. (rus)
27. Russian Construction Norms and Rules SNiP II-22-81. Kamennyye i armokamennyye konstruksii [Stone and reinforced structures]. Moscow: FGUP CPP, 2004. 40 p. (rus)
28. Russian Set of Rules SP 15.13330.2012. Svod pravil. Kamennyye i armokamennyye konstruksii. Aktualizirovannaya redaktsiya SNiP II-22-81* [Masonry and reinforced masonry structures. The actual formulation of Construction Norms and Regulations II-22-81*]. Moscow: FAU "FCS", 2012. 74 p. (rus)
29. EN 1996-1-1 (English). Eurocode 6: Design of masonry structures. Part 1-1: General rules for reinforced and unreinforced masonry structures. Management Centre: rue de Stassart. Brussels: 2005. Pp. 123.
30. EN 1992-1-1 (English). Eurocode 2: Design of concrete structures. Part 1-1: General rules and rules for buildings. Management Centre: rue de Stassart. Brussels: 2004. Pp. 226.
17. Madani K. A study of fiber deboning in circular composite arches // *Comptes Rendus Mecanique*. 2002. № 330. Pp. 535–541.
18. Zhang Y., Macorini L., Izzuddin B.A. Mesoscale partitioned analysis of brick-masonry arches // *Engineering Structures*. 2016. Vol. 124. Pp. 142–166.
19. Ramaglia G., Lignola G.P., Prota A. Collapse analysis of slender masonry barrel vaults // *Engineering Structures*. 2016. Vol. 117. Pp. 86–100.
20. Felice G. Assessment of the load-carrying capacity of multi span masonry arch bridges using fibre beam elements // *Engineering Structures*. 2009. № 31. Pp. 1634–1647.
21. Зимин С.С., Беспалов В.В., Казиминова А.С. Расчетная модель каменной арочной конструкции [Электронный ресурс]. Систем требования: Adobe Acrobat Reader. URL: [http://donna.sa.ru/publish_house/journals/vestnik/2015/vestnik_2015-3\(113\).pdf](http://donna.sa.ru/publish_house/journals/vestnik/2015/vestnik_2015-3(113).pdf) (дата обращения: 01.08.2018).
22. Зимин С.С., Кокоткова О.Д., Беспалов В.В. Сводчатые конструкции исторических зданий // *Строительство уникальных зданий и сооружений*. 2015. № 2(29). С. 57–72.
23. ГОСТ 8462-85. Материалы стеновые. Методы определения пределов прочности при сжатии и изгибе. М.: Госстандарт Союза ССР, 1985. 10 с.
24. ГОСТ 5802-86. Растворы строительные. Методы испытания. М.: Госстандарт Союза ССР, 1986. 22 с.
25. Зубков С.В., Улыбин А.В., Федотов С.Д. Исследование механических свойств кирпичной кладки методом плоских домкратов // *Инженерно-строительный журнал*. 2015. № 8. С. 20–29.
26. ГОСТ 22690-88. Бетоны. Определение прочности механическими методами неразрушающего контроля. М.: Госстандарт России, 1988. 26 с.
27. Строительные нормы и правила. Каменные и армокаменные конструкции: СНиП II-22-81*: нормативно-технический материал. Госстрой России. Офиц. изд. Взамен СНиП II-В.2-71; Введ. с 1 янв. 1983. М.: ФГУП ЦПП, 2004. 40 с.
28. СП 15.13330.2012. Каменные и армокаменные конструкции. Актуализированная редакция СНиП II-22-81. М.: ФАУ "ФЦС", 2012. 74 с.
29. EN 1996-1-1 (English). Eurocode 6: Design of masonry structures. Part 1-1: General rules for reinforced and unreinforced masonry structures. Management Centre: rue de Stassart. Brussels: 2005. Pp. 123.
30. EN 1992-1-1 (English). Eurocode 2: Design of concrete structures. Part 1-1: General rules and rules for buildings. Management Centre: rue de Stassart. Brussels: 2004. Pp. 226.

*Anay-Khaak Kaldar-ool**,
+7(981)801-26-87; oorzhaka-h@mail.ru

Vladimir Babanov,
+7(911)242-96-55; babanov_vladimir@mail.ru

Boris Allahverdiv,
+7(921)743-59-66; aborism@mail.ru

Svetlana Saaya,
+7(923)549-82-78; sedip@mail.ru

*Анай-Хаак Бугалдаевна Калдар-оол**.
+7(981)801-26-87; эл. почта: oorzhaka-h@mail.ru

Владимир Владимирович Бабанов,
+7(911)242-96-55;
эл. почта: babanov_vladimir@mail.ru

Борис Михайлович Аллахвердов,
+7(921)743-59-66; эл. почта: aborism@mail.ru

Светлана Сергеевна Саая,
+7(923)549-82-78; эл. почта: sedip@mail.ru

© Kaldar-ool, A-Kh.B., Babanov, V.V., Allahverdiv, B.M., Saaya, S.S., 2018

doi: 10.18720/MCE.84.3

Scheduling workflows for scattered objects

Формирование календарных планов поточного строительства рассредоточенных объектов

Yu.B. Kalugin,
R.S. Romanov,
Military Institute of rail transport troops and
military communications, St. Petersburg, Russia*

д-р техн. наук, профессор Ю.Б. Калугин,
адъютант Р.С. Романов,
Военный институт железнодорожных войск
и военных сообщений, Санкт-Петербург,
Россия*

Key words: civil engineering; construction management; project scheduling; flow shop scheduling problem for scattered objects.

Ключевые слова: календарное планирование и управление проектом; оптимизация календарных графиков по срокам; формирование минимальных расписаний для рассредоточенных объектов.

Abstract. As a rule, the task of optimal scheduling, including reducing the total duration of the project occurs when developing and adjusting schedules. The essence of flow shop scheduling problem on the scattered objects with the use methods and models calendar planning was presented. The branch and boundary method were proposed as an exact method for determining the optimal permutation including the scheme of branching and rules for determining the lower boundaries. Heuristic algorithms for determining the optimal sequence of work for scattered objects was substantiated. The general applicability of the algorithms was demonstrated with calculations including 30 variants from distinct flows. The performed studies show the possibility of reducing the planned time by about 15 %. The suggested methodology can be recommended for use by construction project managers.

Аннотация. Как правило, задача оптимального планирования, и в частности задача сокращения общей продолжительности проекта возникает при разработке и корректировке календарных графиков. Представлена сущность решения задачи выбора оптимальной последовательности поточного строительства рассредоточенных объектов. В качестве точного метода определения оптимальной перестановки предложен метод ветвей и границ, включающий схему ветвления и правила определения нижних границ. Обоснованы эвристические алгоритмы определения оптимальной последовательности работ для рассредоточенных объектов. Общая применимость алгоритмов продемонстрирована расчетами, включающими 30 вариантов различных потоков. Проведенные исследования показывают возможность сокращения запланированного времени примерно на 15 %. Предложенные методы могут быть рекомендованы для использования руководителями строительных проектов.

1. Introduction

A construction project is a complex process, which includes a large number of different tasks performed by different crews and displayed by calendar charts. When forming the schedules in case of exceeding the planned duration over deadlines requires a reduction in the total duration. In addition, with the operational management of the progress of work, it is also necessary to periodically adjust the schedule by dates [1–7].

One of the methods of reducing the planned duration of construction is the combinatorial optimization, and in particular, the formation of schedules of the minimum duration by finding the optimal sequence of work [8–11].

Numerous studies have been devoted to the problem of planning the flow organization of work (flow shop scheduling problem) [12–19]. A number of methods and algorithms (both exact and approximate) have been developed for the formation of minimum duration schedules.

The exact methods include, first of all, the method of directed search (branch and boundary method), which allows establish the optimal sequence in exponential time.

Widespread in practice are approximation algorithms [19–25], allowing to obtain a solution close to optimal in polynomial time.

The studies [8, 9, 11, 26, 27] have shown the effectiveness of using different methods of forming the optimal sequence for the flow organization of work on nearby objects.

However, the real conditions involve the operation of construction flows and in remote areas, the relocation time between which is commensurate with the duration of the work of each specialized crew. Under these conditions, combinatorial optimization problems arise, which reduce to finding the optimal sequence of work at the scattered objects.

The purpose of this paper is to substantiate methods and algorithms for determining the optimal sequencing of objects in the stream, providing a minimum duration for scattered objects.

Objectives of the study are:

1. The theoretical foundation of the method of directed enumeration (branch and bound) for finding the optimal sequence of flow shop of scattered objects;
2. Justification of heuristic approximate algorithms;
3. The calculations of variants of formation of flows of different methods and algorithms;
4. Comparison and selection of the most effective methods and algorithms for searching the optimal sequence.

2. Methods

The problem of finding the optimal (minimum total duration) sequence of objects included in the schedule, taking into account the time of moving crews from one object to another, can be formulated as follows.

On the scattered objects $1, 2, \dots, j \dots n$ in accordance with a given technology specialized crews perform various types of work $1, 2, \dots, i \dots m$.

The duration of the work i on the object $j - (t_{ij})$ is determined by known methods.

The works are organized by individual-flow method (critical path method) [8].

Each crew can simultaneously perform work only on one object.

Combining the work of crews on one object is not allowed.

The possible start time of i on object j (earliest start time – T_{ij}^{EST}) is defined by the following expression:

$$T_{ij}^{EST} = \max[(T_{(i-1),j}^{EFT}); (T_{i,(j-1)}^{EFT} + t_{(j-1),j}^{red})], \quad (1)$$

$T_{(i-1),j}^{EFT}$ is earliest finish time activity $(i - 1)$ on the j -th object;

$T_{i,(j-1)}^{EFT}$ is earliest finish time activity i on the $(j - 1)$ -th object;

$t_{(j-1),j}^{red}$ is the time for the redeployment of the team from the object $(j - 1)$ to an object j .

It is necessary to determine the optimal sequence of work P_{opt} , taking into account the time of relocation of crews from object to object, in which the total duration of the individual flow T_o will be minimal:

$$P_{opt} \subset Q, \quad (2)$$

Q is the set of all possible alternatives.

Along with this

$$Q: \left(\begin{array}{l} \forall i = 1 \div m \\ \forall j = 1 \div n \\ \forall P_{opt} = T_o \rightarrow \min \end{array} \right). \quad (3)$$

This type of problems can be solved by various optimization methods, the main of which is the branch and bound method [8, 14, 16, 28, 29]. Fundamental in this respect has been the work of Professor Afanasiev [8].

2.1. Using the branch and boundary method to find the optimal sequence for including scattered objects in a flow

The most important step of the branch and boundary method is to determine the prospects of further branching (in this case, the lower boundary).

The value of the lower boundary will be equivalent to the limit possible minimum duration of work (LPMD) [8].

The definition of the lower bounds for the considered sequence P is realized as follows:

1) Is determined for the sequence lower limit of the flow duration when passing the critical path through each type of work

$$g^P = \max g_i^P, (i = 1, \dots, m). \tag{4}$$

2) For a sequence P , the lower limit of the flow duration when passing a critical path through each object is determined

$$k^P = \max k_j^P, (j = 1, \dots, n). \tag{5}$$

3) As the lower bound (estimates of the prospects of the sequence P for further branching), the maximum of the obtained values is taken $g^P; k^P$ (taking into account the time for the redeployment of commands)

$$\eta_{S_j}^P = \max(g_i^P, k_j^P) + \sum t^{red}. \tag{6}$$

4) To further branching at the level S_j of the sequence is taken with a minimum value $\eta_{S_j}^P$.

The branching scheme and the order of implementation of the first stage of the algorithm (development of the tree to the level S_n) are shown in figures 1 and 2.

At the second stage of the algorithm (Figure 3) a comparison of estimates of the development prospects of the corresponding subsets with the flow duration calculated at the first stage is made T .

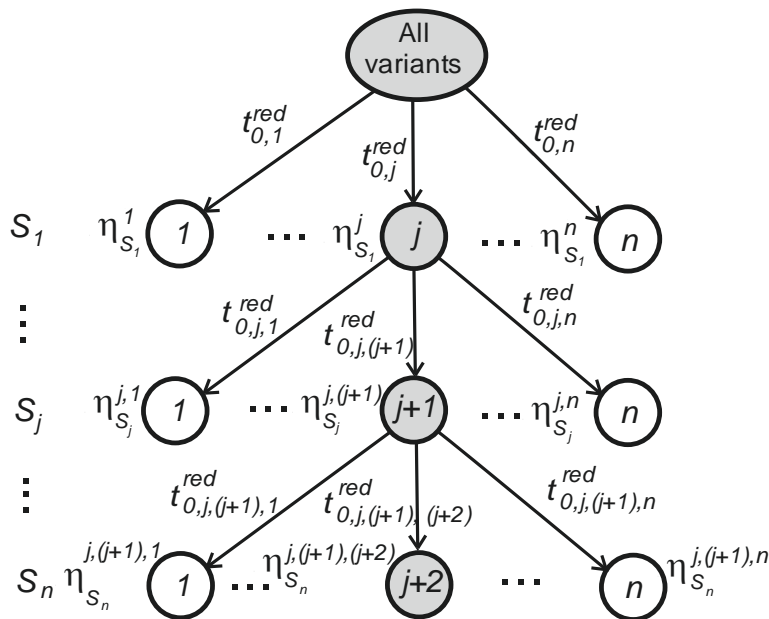


Figure 1. Branching scheme.

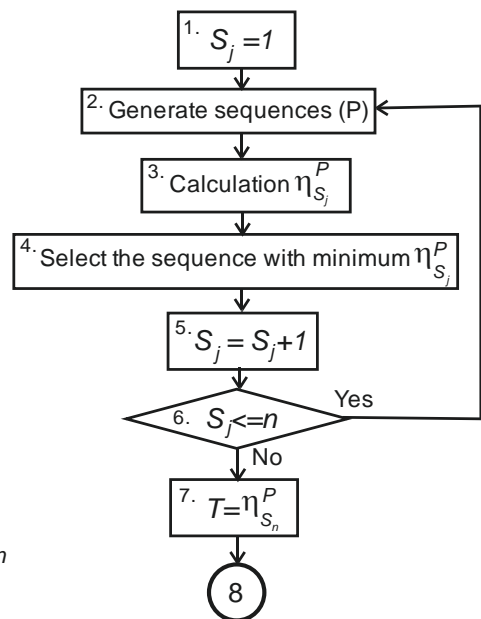


Figure 2. Implementation of the first stage of the algorithm.

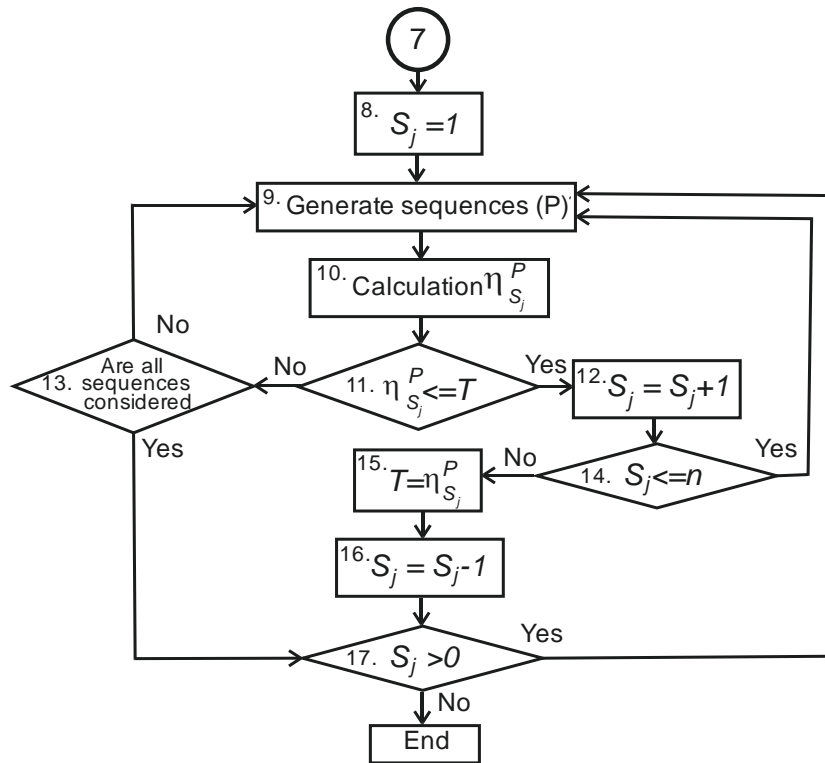


Figure 3. Implementation of the second stage of the algorithm.

Of particular importance is the calculation of the lower limits of the flow duration when passing the critical path through each type of work performed and each object [8].

The lower bound of the flow duration when passing the critical path through the *i*-th type of activity is determined by the mathematical expression (7):

$$g_i = T_{ir}^{EFT} + \sum_{j \in N \setminus \tilde{N}} t_{ij} + \min \sum_{j \in N \setminus \tilde{N}} t_{(i+1),j}, \quad (7)$$

T_{ir}^{EFT} is earliest finish time activity *i* on the *r*-th object; (earliest finish time activity *i* on objects already included in the subset \tilde{N} , ($r = |\tilde{N}|$));

$\sum_{j \in N \setminus \tilde{N}} t_{ij}$ is the duration activity of the *i* crew on the remaining objects;

$\min \sum_{j \in N \setminus \tilde{N}} t_{(i+1),j}$ is minimum from the sums activities of the remaining crews (starting from (*i* + 1))

on one of the remaining (not included in the subset \tilde{N}) object;

N is set of all objects.

The lower bound of the flow duration when passing the critical path through each object is defined as follows.

1. Calculation T_{1r}^{EFT} is earliest finish time activity 1 on the last (*r* – *th*) fixed object (from already included in the subset \tilde{N} , ($r = |\tilde{N}|$));

2. From a subset of loose objects one (*j*) is selected and taken as the considered object (the object through which the critical path can pass).

3. Loose objects are sorted as follows.

If the first type of activity on the j^* -th object is longer than the duration of the last type of activity ($i_{1j^*} > i_{mj^*}$), then this object falls below the considered (unfixed) and is included in the subset S (subsequent),

Otherwise ($i_{1j^*} < i_{mj^*}$), the object rises and is placed above the considered one, that is, it is included in the subset P (previous).

4. The total duration of the first crew on the objects preceding the considered ($j - th$) object, and the last crew – on the objects subsequent to the considered are determined.

5. From the condition of continuity of work of crews on the considered object (the object is not idle) the minimum possible duration of performance of all types of works is defined.

As a result, the lower bound of the duration of the flow during the passage of the critical path through the $j - th$ object is determined using the expression (8):

$$k_j = T_{1r}^{EFT} + \sum_{i=1}^m t_{ij} + \min \left(\sum_{p \in P; p \neq j} t_{1p}; \sum_{s \in S; s \neq j} t_{ms} \right); \quad (8)$$

T_{1r}^{EFT} is earliest finish time activity 1 on the last ($r - m$) fixed object (from already included in the subset \tilde{N});

$\sum_{i=1}^m t_{ij}$ is the minimum possible duration of all types of activity on the ($j - th$) object;

$\sum_{p \in P; p \neq j} t_{1p}$ is the total duration of the first crew on the objects preceding the considered ($j - th$) object;

$\sum_{s \in S; s \neq j} t_{ms}$ is total duration of the last crew on the objects subsequent to the considered ($j - th$) object.

The implementation of the presented approach using dependencies (4-8) and the corresponding branching scheme has shown its effectiveness for determining the optimal sequence of work on scattered objects.

At the same time, the development and improvement of heuristic methods of combinatorial optimization is of some interest.

2.2. Heuristic search algorithms for rational sequences of activities on scattered objects

For solve the problem of this type, heuristic algorithms are implemented, allowing for polynomial time to search for a rational sequence of work at scattered objects, taking into account the duration for the relocation of crews. The basis of these algorithms are methods and models of combinatorial optimization and integer programming [30, 31].

In this case, all objects are represented by a complete undirected graph consisting of n vertices connected by arcs, where $1, 2, \dots, j \dots n$ is the numbers of objects, and the arcs connecting the vertices show different sequences of work (routes of crews) (Figure 4).

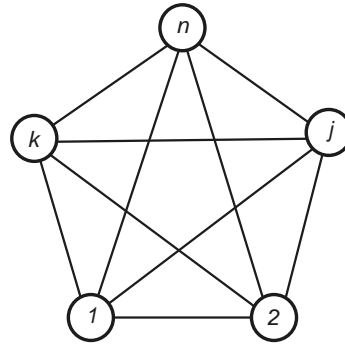


Figure 4. Complete undirected graph.

Algorithms with all their varieties are as follows.

2.3. An approach based on finding the shortest Hamiltonian contour

Step 1. For each pair of objects (j and k) is determined by the duration of the work in the forward and reverse direction (T_{jk} and T_{kj}).

Step 2. The ratio coefficient between the sum of pair durations of works and the true duration of the schedule is determined.

For a regular flow, it will be:

$$k_r = \frac{(m+1)(n-1)}{(m+n-1)}. \quad (9)$$

Calculations performed for 30 examples of non-rhythmic flow with random integer work durations from 1 to 5 with $m = 4$ and $n = 5$ showed that k_r it changed in the range from 1.87 to 2.85. The average value was 2.36. For a regular flow with $m = 4$ and $n = 5$, $k_r = 2.5$, which allows using expression (9) for the calculation k_r .

Step 3. For each pair of objects (j and k), the corrected duration of the work in the forward and reverse direction is determined – T_{jk}^* and T_{kj}^* :

$$T_{jk}^* = \frac{T_{jk}}{k_r}, \quad (10)$$

$$T_{kj}^* = \frac{T_{kj}}{k_r}, \quad (11)$$

Step 4. For each pair of objects (j and k) is determined by the corrected duration of the work in the forward and reverse direction, taking into account the duration of the redeployment from object to object (t_{jk}^{red}):

$$T_{jk}^{**} = T_{jk}^* + t_{jk}^{red}, \quad (12)$$

$$T_{kj}^{**} = T_{kj}^* + t_{kj}^{red}. \quad (13)$$

Step 5. On a graph with the lengths of arcs of equal T_{jk}^{**} and T_{kj}^{**} known methods are used to determine the shortest Hamiltonian circuit, which will determine the required sequence.

2.4. The approach based on the calculation of the potentials of the vertices of the graph

Steps 1–4 are similar to the steps above.

Step 5. For each pair of objects (j and k) the difference between the corrected durations of work T_{jk}^{**} and T_{kj}^{**} is determined. This distinction and constitute the so-called potential of vertex j on the edge jk and the potential of vertex k on the edge kj .

Step 6. After determining all vertex potentials on each edge of the graph, the total potentials of each vertex are calculated.

Step 7. The desired sequence of inclusion of objects in the flow is determined by increasing the potential of the vertices.

The combined approach is to determine the initial and final flow objects in the amount of 15–20 % of their total number (reference points) by the method of potentials.

For the remaining objects, the rational sequence is determined based on the shortest Hamiltonian contour.

3. Results and Discussion

The described methods and algorithms have been implemented for 30 different tasks of non-rhythmic flow with integer random duration of work from 1 to 5 and the duration of redeployment from 0.5 to 2.5 in increments of 0.25 ($m = 4$; $n = 5$).

The results of optimization using the above methods and approaches are presented in Table 1. Here 1 is the branch and bound method; 2 is the approach based on finding the shortest Hamiltonian contour; 3 is the approach based on calculating the vertex potentials of the graph; 4 is the combined approach.

Table 1. Optimization results by different methods.

| # task's | Average time for 120 variations | Method | P_{opt} | T_{opt} | $\Delta T(\%)$ | Undetermined variants (%) | Calculation time (h) |
|----------|---------------------------------|--------|-----------|-----------|----------------|---------------------------|----------------------|
| 1 | 32.56 | 1 | 45213 | 25.75 | 21 | 0 | 6.0 |
| | | 2 | 45213 | 25.75 | 21 | 0 | 2.0 |
| | | 3 | 25413 | 28.50 | 12 | 7 | 1.0 |
| | | 4 | 21543 | 28.0 | 14 | 3 | 1.5 |
| 2 | 36.40 | 1 | 21345 | 29.25 | 20 | 0 | 6.0 |
| | | 2 | 31254 | 30.75 | 16 | 2 | 2.0 |
| | | 3 | 23145 | 33.75 | 7 | 17 | 1.0 |
| | | 4 | 32145 | 33.25 | 9 | 11 | 1.0 |
| 3 | 37.50 | 1 | 21345 | 29.25 | 20 | 0 | 1.5 |
| | | 1 | 43521 | 31.0 | 17 | 0 | 6.0 |
| | | 2 | 34521 | 33.0 | 12 | 6 | 2.0 |
| | | 3 | 54321 | 31.25 | 17 | 1 | 1.0 |
| 4 | 36.23 | 4 | 54321 | 31.25 | 17 | 1 | 1.5 |
| | | 1 | 31254 | 30.75 | 15 | 0 | 6.0 |
| | | 2 | 52134 | 31.50 | 13 | 2 | 2.0 |
| | | 3 | 23154 | 36.25 | 0 | 48 | 1.0 |
| 5 | 36.06 | 4 | 23514 | 40.50 | -12 | 96 | 1.0 |
| | | 4 | 21354 | 34.50 | 5 | 18 | 1.5 |
| | | 1 | 43125 | 31.50 | 13 | 0 | 6.0 |
| | | 2 | 21345 | 33.25 | 8 | 6 | 2.0 |
| 6 | 35.50 | 3 | 32451 | 35.75 | 1 | 45 | 1.0 |
| | | 3 | 34251 | 32.25 | 10 | 2 | 1.0 |
| | | 4 | 34521 | 33.00 | 8 | 5 | 1.5 |
| | | 1 | 34521 | 30.00 | 15 | 0 | 6.0 |
| 7 | 38.18 | 2 | 54312 | 35.25 | 1 | 39 | 2.0 |
| | | 3 | 42531 | 31.75 | 11 | 7 | 1.0 |
| | | 4 | 43521 | 31.00 | 13 | 4 | 1.5 |
| | | 1 | 54312 | 32.25 | 16 | 0 | 6.0 |
| 8 | 34.76 | 2 | 31254 | 35.75 | 6 | 11 | 2.0 |
| | | 3 | 54321 | 33.25 | 13 | 1 | 1.0 |
| | | 4 | 54312 | 32.25 | 16 | 0 | 1.0 |
| | | 4 | 54312 | 32.25 | 16 | 0 | 1.5 |

| # task's | Average time for 120 variations | Method | P_{opt} | T_{opt} | $\Delta T(\%)$ | Undetermined variants (%) | Calculation time (h) |
|----------|---------------------------------|--------|-----------|-----------|----------------|---------------------------|--------------------------|
| | | 2 | 52134 | 29.50 | 15 | 0 | 2.0 |
| | | 3 | 15342 | 34.00 | 2 | 36 | 1.0 |
| | | | 15324 | 34.75 | 0 | 49 | 1.0 |
| | | 4 | 12534 | 31.00 | 11 | 3 | 1.5 |
| 9 | 35.33 | 1 | 52134 | 29.50 | 17 | 0 | 6.0 |
| | | 2 | 52134 | 29.50 | 17 | 0 | 2.0 |
| | | 3 | 53241 | 35.25 | 0.2 | 44 | 1.0 |
| | | 4 | 54321 | 31.25 | 12 | 2 | 1.5 |
| 10 | 33.73 | 1 | 52134 | 27.50 | 18 | 0 | 6.0 |
| | | 2 | 31254 | 32.75 | 3 | 31 | 2.0 |
| | | | 45213 | 33.75 | 0 | 50 | 2.0 |
| | | 3 | 51342 | 31.50 | 7 | 11 | 1.0 |
| | | 4 | 54312 | 29.25 | 13 | 1 | 1.5 |
| 11 | 32.62 | 1 | 54312 | 27.25 | 16 | 0 | 6.0 |
| | | 2 | 52134 | 27.50 | 16 | 1 | 2.0 |
| | | 3 | 53241 | 31.25 | 4 | 26 | 1.0 |
| | | 4 | 54321 | 28.25 | 13 | 2 | 1.5 |
| 12 | 34.00 | 1 | 21345 | 27.25 | 20 | 0 | 6.0 |
| | | 2 | 31254 | 27.75 | 18 | 1 | 2.0 |
| | | 3 | 23145 | 29.75 | 13 | 8 | 1.0 |
| | | 4 | 21345 | 27.25 | 20 | 0 | 1.5 |
| 13 | 32.84 | 1 | 52134 | 28.50 | 13 | 0 | 6.0 |
| | | 2 | 23451 | 31.50 | 4 | 21 | 2.0 |
| | | 3 | 23154 | 31.25 | 5 | 18 | 1.0 |
| | | 4 | 25134 | 28.75 | 12 | 1 | 1.5 |
| 14 | 34.05 | 1 | 52134 | 28.50 | 16 | 0 | 6.0 |
| | | 2 | 45213 | 30.75 | 7 | 10 | 2.0 |
| | | 3 | 51324 | 32.25 | 5 | 17 | 1.0 |
| | | | 51342 | 31.50 | 7 | 10 | 1.0 |
| | | 4 | 52134 | 28.50 | 16 | 0 | 1.5 |
| 15 | 31.50 | 1 | 43125 | 26.50 | 16 | 0 | 6.0 |
| | | 2 | 25431 | 29.50 | 6 | 9 | 2.0 |
| | | 3 | 41235 | 30.25 | 4 | 10 | 1.0 |
| | | | 41325 | 29.00 | 8 | 5 | 1.0 |
| | | 4 | 43125 | 26.50 | 16 | 0 | 1.5 |
| 16 | 33.48 | 1 | 45213 | 27.75 | 17 | 0 | 6.0 |
| | | 2 | 12543 | 31.00 | 7 | 12 | 2.0 |
| | | 3 | 51423 | 32.50 | 3 | 26 | 1.0 |
| | | | 54123 | 29.25 | 13 | 2 | 1.0 |
| | | 4 | 54213 | 29.50 | 12 | 4 | 1.5 |
| 17 | 32.43 | 1 | 21345 | 26.25 | 19 | 0 | 6.0 |
| | | 2 | 13452 | 29.50 | 9 | 11 | 2.0 |
| | | 3 | 21345 | 26.25 | 19 | 0 | 1.0 |
| | | | 21354 | 27.50 | 15 | 2 | 1.0 |
| | | 4 | 21345 | 26.25 | 19 | 0 | 1.5 |
| 18 | 29.49 | 1 | 12543 | 25.00 | 15 | 0 | 6.0 |
| | | 2 | 12543 | 25.00 | 15 | 0 | 2.0 |
| | | 3 | 12543 | 25.00 | 15 | 0 | 1.0 |
| | | 4 | 12543 | 25.00 | 15 | 0 | 1.5 |
| 19 | 31.85 | 1 | 52134 | 25.50 | 20 | 0 | 6.0 |
| | | 2 | 25134 | 27.75 | 13 | 2 | 2.0 |
| | | 3 | 35214 | 29.00 | 9 | 7 | 1.0 |
| | | 4 | 31524 | 26.75 | 16 | 1 | 1.5 |
| 20 | 34.21 | 1 | 43521 | 28.00 | 18 | 0 | 6.0 |
| | | 2 | 54321 | 29.25 | 14 | 4 | 2.0 |
| | | 3 | 45321 | 29.50 | 14 | 6 | 1.0 |
| | | 4 | 45231 | 28.25 | 17 | 1 | 1.5 |
| 21 | 38.54 | 1 | 52134 | 33.50 | 13 | 0 | 6.0 |
| | | 2 | 34521 | 36.00 | 7 | 7 | 2.0 |
| | | 3 | 35241 | 40.00 | -4 | 77 | 1.0 |
| | | | 53241 | 39.25 | -2 | 64 | 1.0 |
| | | 4 | 34521 | 36.00 | 7 | 7 | 1.5 |
| 22 | 30.46 | 1 | 45213 | 26.75 | 12 | 0 | 6.0 |
| | | 2 | 25431 | 27.50 | 10 | 2 | 2.0 |
| | | 3 | 42315 | 29.25 | 4 | 22 | 1.0 |
| | | 4 | 43125 | 27.50 | 10 | 2 | 1.5 |
| 23 | 33.98 | 1 | 52134 | 25.50 | 25 | 0 | 6.0 |
| | | 2 | 52134 | 25.50 | 25 | 0 | 2.0 |
| | | 3 | 51234 | 28.50 | 16 | 4 | 1.0 |
| | | 4 | 52134 | 25.50 | 25 | 0 | 1.5 |

| # task's | Average time for 120 variations | Method | P_{opt} | T_{opt} | $\Delta T(\%)$ | Undetermined variants (%) | Calculation time (h) |
|----------|---------------------------------|--------|-----------|-----------|----------------|---------------------------|--------------------------|
| 24 | 34.07 | 1 | 43125 | 28.50 | 16 | 0 | 6.0 |
| | | 2 | 43125 | 28.50 | 16 | 0 | 2.0 |
| | | 3 | 42135 | 30.50 | 10 | 2 | 1.0 |
| | | 4 | 43125 | 28.50 | 16 | 0 | 1.5 |
| 25 | 34.30 | 1 | 12543 | 30.00 | 13 | 0 | 6.0 |
| | | 2 | 12543 | 30.00 | 13 | 0 | 2.0 |
| | | 3 | 12534 | 31.00 | 10 | 6 | 1.0 |
| | | 4 | 15234 | 31.75 | 7 | 10 | 1.0 |
| 26 | 30.19 | 1 | 13452 | 25.50 | 16 | 0 | 6.0 |
| | | 2 | 31254 | 27.75 | 8 | 7 | 2.0 |
| | | 3 | 15342 | 29.00 | 4 | 26 | 1.0 |
| | | 4 | 15432 | 28.50 | 6 | 17 | 1.0 |
| 27 | 35.38 | 1 | 13452 | 25.50 | 16 | 0 | 6.0 |
| | | 2 | 31254 | 27.75 | 8 | 7 | 2.0 |
| | | 3 | 15342 | 29.00 | 4 | 26 | 1.0 |
| | | 4 | 15432 | 28.50 | 6 | 17 | 1.0 |
| 28 | 33.85 | 1 | 45213 | 27.75 | 18 | 0 | 6.0 |
| | | 2 | 43125 | 29.50 | 13 | 1 | 2.0 |
| | | 3 | 43521 | 31.00 | 8 | 9 | 1.0 |
| | | 4 | 45231 | 30.25 | 11 | 4 | 1.5 |
| 29 | 32.31 | 1 | 25431 | 27.5 | 15 | 0 | 6.0 |
| | | 2 | 52134 | 27.5 | 15 | 0 | 6.0 |
| | | 3 | 23451 | 28.50 | 12 | 5 | 2.0 |
| | | 4 | 24531 | 30.50 | 6 | 23 | 1.0 |
| 30 | 31.65 | 1 | 23451 | 28.50 | 12 | 5 | 1.5 |
| | | 2 | 23451 | 28.50 | 12 | 5 | 1.5 |
| | | 3 | 52134 | 24.50 | 23 | 0 | 6.0 |
| | | 4 | 23451 | 28.50 | 12 | 5 | 1.5 |

Based on the calculations, Table 2 was compiled.

Table 2. Parameters of compared methods.

| Average parameters for 30 tasks | Optimization method | | | |
|---------------------------------|----------------------|-------------------------|----------------------|-----------------------|
| | Branch and bound (1) | Hamiltonian circuit (2) | Potential method (3) | Combined approach (4) |
| $\Delta T(\%)$ | 17 | 11 | 8 | 14 |
| Undetermined variants (%) | 0 | 10 | 19 | 3 |
| Calculation time (h) | 6.0 | 2.0 | 1.0 | 1.5 |

The analysis of the parameters of the compared methods and approaches shows the following.

The directed search method (branch and bound method) established optimal sequences in all cases. The average value of schedule compression was 17 %.

The approach based on the combination of the method of potentials and the shortest Hamiltonian circuit allowed to achieve the average value of schedule compression – 14 %.

At the same time, undetermined sequences of shorter duration are only 3 %.

4. Conclusions

1. When forming the schedules in case of exceeding the planned duration over deadlines requires a reduction in the total duration. One of the methods of reducing the duration of the construction flow is to find the optimal sequence of work (flow shop scheduling problem).

2. This problem is solved for scattered objects. Methods and algorithms for determining the optimal sequence of work for dispersed objects are presented.

3. The branch and boundary method is proposed as an exact method for determining the optimal permutation. The scheme of branching and rules for determining the lower boundaries of the minimum are presented.

4. Heuristic algorithms for determining the optimal sequence of work for scattered objects are substantiated.

Калугин Ю.Б., Романов Р.С. Формирование календарных планов поточного строительства рассредоточенных объектов // Инженерно-строительный журнал. 2018. № 8(84). С. 29–40.

5. Calculations of 30 variants of flow formation by different methods and algorithms are presented. The performed calculations allow us to consider the method of branches and boundaries as a priority exact method of finding the optimal sequence in the formation of the schedule of construction of scattered objects. As an approximate method, the priority is a heuristic algorithm based on a combination of the potential method and the search for the shortest Hamiltonian circuit.

6. The performed studies show the possibility of reducing the planned time by 14–17 %, which shows the effectiveness of the proposed methods to reduce the duration of construction of scattered objects.

The suggested methods can be recommended for use by construction project managers to reduce project completion time.

References

1. Avdeev, Yu.A. Vyrabotka i analiz planovykh resheniy v slozhnykh proyektakh [Development and the analysis of planned decisions in complex projects]. Moscow. Economy. 1971. 96 p. (rus)
2. Mishakova, A.V., Vaxrushkina, A.V., Anishhenko, D.R., Tatarina Yu.A. Program Evaluation and Review Technique as the tool for time control. Magazine of Civil Engineering. 2017. No. 4 (77). Pp. 12–19 [Online]. URL: http://engstroy.spbstu.ru/index_2017_04/02.pdf
3. Bovteev, S.V., Kanyukova, S.V. Development of methodology for time management of construction projects. Magazine of Civil Engineering. 2016. No. 2 (62). Pp. 102–112 [Online]. URL: http://engstroy.spbstu.ru/index_2016_02/10.pdf
4. Kalugin, Yu. B. Reasons of delays in construction projects. Magazine of Civil Engineering. 2017. No. 6 (74). Pp. 61–69 [Online]. URL: http://engstroy.spbstu.ru/index_2017_06/06.pdf
5. Kalugin, Yu.B., Kaklauskas, A., Kazakov, Yu.N. Min-cut algorithm for network schedule by merging the vertices. Magazine of Civil Engineering. 2018. No. 4(80). Pp. 37–47 [Online]. URL: http://engstroy.spbstu.ru/index_2018_04/04.pdf
6. Sergeenkova, O.A. Kalendarnoe planirovanie stroitel'stva kompleksa obektov s uchetom osobennostey programmnykh sredstv [Scheduling of construction of a complex of objects taking into account features of software]. Construction of Unique Buildings and Structures. 2014. No. 7 (22). Pp. 176–193 [Online]. URL: http://unistroy.spbstu.ru/index_2014_22/14_sergeenkova_22.pdf (rus)
7. Bolotin, S.A., Gurieva, M.A., Chaxkiev, I.M. K voprosu obosnovaniya direktivnoy prodolzhitel'nosti stroitel'stva unikal'nykh ob'ektov [To the issue of substantiating the directive duration of unique objects construction]. Bulletin of civil engineers. 2014. No. 1 (42). Pp. 61–65 [Online]. URL: https://elibrary.ru/download/elibrary_21510011_41839425.pdf (rus)
8. Afanas'ev, V.A. Potochnaya organizatsiya stroitel'stva. [Flow organization of construction]. Leningrad. Stroyizdat, 1990. 303 p. (rus)
9. Bolotin, S.A., Nefedova, V.K., Kombinatornaya optimizatsiya v programmax upravleniya proektami [Combinatorial optimization in project management programs]. News of Higher Educational Institutions. Construction. 2003. No. 6. Pp. 47–51 [Online]. URL: <https://elibrary.ru/item.asp?id=18247890> (rus)
10. Bolotin, S.A., Meshhaninov, I.Yu. Metodika ocenki chuvstvitel'nosti sxemy realizatsii kombinatornoj optimizatsii ocherednosti osvoeniya ob'ektov [Method of estimation of sensitivity of the scheme of realization of combinatorial optimization of priority of development of objects]. Bulletin of civil engineers. 2009. No. 2. C. 20–24 [Online]. URL: https://elibrary.ru/download/elibrary_12795929_67530953.pdf (rus)
11. Chelnokova, V.M. Opredelenie racional'noj ocherednosti stroitel'stva ob'ektov pri kalendarnom planirovanii kompleksnogo osvoeniya territorii [Determination of rational priority of project construction in calendar planning of complex development of the territory]. Bulletin of civil engineers. 2015. No. 2 (49). Pp. 102–107 [Online]. URL:

Литература

1. Авдеев Ю.А. Выработка и анализ плановых решений в сложных проектах. М.: Экономика, 1971. 96 с.
2. Мишакова А.В., Вахрушкина А.В., Анищенко Д.Р., Татаркина Ю.А. Метод анализа и оценки программ как механизм контроля сроков // Инженерно-строительный журнал. 2017. № 4 (77). С. 12–19
3. Бовтеев С.В., Каныкова С.В. Развитие методики контроля сроков инвестиционно-строительного проекта // Инженерно-строительный журнал. 2016. № 2 (62). С. 102–112
4. Калугин Ю.Б. Причины отставаний строительных проектов // Инженерно-строительный журнал. 2017. № 6 (74). С. 61–69
5. Калугин Ю.Б., Каклаускас А., Казаков Ю.Н. Алгоритм поиска минимального разреза сетевой модели слиянием вершин // Инженерно-строительный журнал. 2018. № 4(80). С. 37–47
6. Сергеенкова О.А. Календарное планирование строительства комплекса объектов с учетом особенностей программных средств // Строительство уникальных зданий и сооружений. 2014. №7(22). С. 176–193
7. Болотин С.А., Гуриева М.А., Чакхкиев И.М. К вопросу обоснования директивной продолжительности строительства уникальных объектов // Вестник гражданских инженеров. 2014. № 1 (42). С. 61–65
8. Афанасьев В.А. Поточная организация строительства. Л.: Стройиздат, 1990. 303 с.
9. Болотин С.А., Нefeldова В.К., Комбинаторная оптимизация в программах управления проектами // Известия высших учебных заведений. Строительство. 2003. № 6. С. 47–51.
10. Болотин С.А., Мещанинов И.Ю. Методика оценки чувствительности схемы реализации комбинаторной оптимизации очередности освоения объектов // Вестник гражданских инженеров. 2009. № 2. С. 20–24
11. Челнокова В.М. Определение рациональной очередности строительства объектов при календарном планировании комплексного освоения территории // Вестник гражданских инженеров. 2015. № 2 (49). С. 102–107.
12. Johnson, S.M. Optimal two-and-three-stage production schedules with set-up times included. / S.M. Johnson // Naval Research Logistic Quarterly. 1954. Vol. 1. Pp. 61–68
13. Гере И., Кунош Л. Очередность строительства объектов // Экономика строительства. 1965. № 1. С. 57–59.
14. Спектор М.Д. Выбор оптимальной последовательности включения объектов в строительный поток // Известия высших учебных заведений. Строительство и архитектура. 1973. № 9. С. 89–92.
15. Соболев В.В. Математическое моделирование и оптимизация последовательности возведения объектов по критерию времени // Известия высших учебных заведений. Северо-Кавказский регион. Технические науки. 2011. № 3. С. 30–32.
16. Костенко В. А. Алгоритмы комбинаторной оптимизации, сочетающие жадные стратегии и ограниченный перебор //

- https://elibrary.ru/download/elibrary_23637272_80141885.pdf (rus)
12. Johnson, S.M. Optimal two-and-three-stage production schedules with set-up times included. S.M. Johnson. Naval Research Logistic Quarterly. 1954. Vol. 1. Pp. 61–68.
 13. Gere I., Kunosh L. Ocherednost' stroitel'stva ob'ektov [The order of construction of objects]. Construction economics. 1965. No.1. Pp. 57–59. (rus)
 14. Spektor, M.D. Vybor optimalnoy posledovatel'nosti vklyucheniya ob'ektov v stroitel'nyy potok [Selection of the optimal sequence of inclusion of objects in the construction stream]. News of Higher Educational Institutions. Construction and architecture. 1973. No. 9. Pp. 89–92. (rus)
 15. Sobolev, V.V. Matematicheskoe modelirovaniye i optimizatsiya posledovatel'nosti vozvedeniya ob'ektov po kriteriyu vremeni [Mathematical modeling and optimization of the sequence of erection of objects on the criterion of time]. News of Higher Educational Institutions. North Caucasus region. Technical Sciences. 2011. No. 3. Pp. 30–32 [Online]. URL: <https://cyberleninka.ru/article/v/matematicheskoe-modelirovaniye-i-optimizatsiya-posledovatel'nosti-vozvedeniya-ob'ektov-po-kriteriyu-vremeni> (rus)
 16. Kostenko, V.A. Combinatorial optimization algorithms combining greedy strategies with a limited search procedure. Journal of Computer and Systems Sciences International. 2017. Vol. 56, No. 2. Pp. 218–226 [Online]. URL: <https://doi.org/10.1134/S1064230717020137>
 17. Shen, L., Dauzere-Peres, S., Neufeld, J.S. Solving the flexible job shop scheduling problem with sequence-dependent setup times. European Journal of Operational Research. 2018. Vol. 265. No. 2. Pp. 503–516 [Online]. URL: <https://doi.org/10.1016/j.ejor.2017.08.021>
 18. Fernandez-Viagas, V., Dios, M., Jose, M. Framinana. Efficient constructive and composite heuristics for the Permutation Flow shop to minimize total earliness and tardiness. Computers & Operations Research. 2016. Vol. 75. November 2016. Pp. 38–48 [Online]. URL: <https://doi.org/10.1016/j.cor.2016.05.006>
 19. Azzouz, A., Ennigrou, M., Said, L.B. Flexible job-shop scheduling problem with sequence-dependent setup times using genetic algorithm. In ICEIS 2016 – Proceedings of the 18th International Conference on Enterprise Information Systems. 2016. Vol. 2 [Online] URL: <https://doi.org/10.5220/0005821900470053>
 20. Fernandez-Viagas, V., Ruiz, R., Jose, M. Framinana. A new vision of approximate methods for the permutation flow shop to minimize make span: State-of-the-art and computational evaluation. European Journal of Operational Research. 2017. Vol. 257. Pp. 707–721 [Online]. URL: <https://doi.org/10.1016/j.ejor.2016.09.055>
 21. Liu, W., Jin, Y., Price, M. A new improved NEH heuristic for permutation flow shop scheduling problems. International Journal of Production Economics. 2017. Vol. 193. November 2017. Pp. 21–30 [Online] URL: <https://doi.org/10.1016/j.ijpe.2017.06.026>
 22. Peng, K., Wen, L., Li R., Gao, L., Li, X. An Effective Hybrid Algorithm for Permutation Flow Shop Scheduling Problem with Setup Time. Procedia CIRP. 2018. Vol. 72. Pp. 1288–1292 [Online] URL: <https://doi.org/10.1016/j.procir.2018.03.258>
 23. Zobolas, G.I., Tarantilis, C.D., Ioannou G. Minimizing makespan in permutation flow shop scheduling problems using a hybrid metaheuristic algorithm. Computers & Operations Research. 2009. Vol. 36 (4). Pp. 1249–1267 [Online]. URL: <https://doi.org/10.1016/j.cor.2008.01.007>
 24. Allahverdi, A., Aydilek, H., Aydilek, A. No-wait flow shop scheduling problem with two criteria; total tardiness and makespan. European Journal of Operational Research. 2018. Vol. 269. Pp. 590–601 [Online]. URL: <https://doi.org/10.1016/j.ejor.2017.11.070>
 25. Singhal, E., Singh, S., Dayma, A. An Improved Heuristic for Permutation Flow Shop Scheduling (NEH ALGORITHM). International Journal Of Computational Engineering Research.
 26. Сиверикова А.И., Величкин В.З. Параллельно-поточный метод организации строительства // Строительство уникальных зданий и сооружений. 2015. № 4 (31). С. 135–162.
 27. Rossi F. L., Nagano M. S., Sagawa J. K. An effective constructive heuristic for permutation flow shop scheduling problem with total flow time criterion // The International Journal of Advanced Manufacturing Technology. 2017. Vol. 90 (1-4). Pp. 93–107.
 28. Silvestri S., Laporte G., Cerulli R. A branch-and-cut algorithm for the minimum branch vertices spanning tree problem // Computers and Operations Research. 2017. Vol. 81. Pp. 322–332.
 29. Crainic T.G. Parallel branch-and-bound algorithms. Montréal, 2006. 28 p.
 30. Greco F. Travelling Salesman Problem. Vienna, Austria. 2008. 202 p.
 31. Bryant K. Genetic Algorithms and the Traveling Salesman Problem. State of California. Department of Mathematics Harvey Mudd college, 2000. 34 p.

2012. Vol. 2(6). Pp. 95–100 [Online]. URL: <https://ru.scribd.com/document/112531906/International-Journal-of-Computational-Engineering-Research-IJCER>
26. Siverikova, A.I., Velichkin, V.Z. Parallel'no-potochny'j metod organizacii stroitel'stva [Parallel and stream methods of construction organization]. Construction of Unique Buildings and Structures. 2015. №4 (31). Pp. 135–162 [Online]. URL: http://unistroy.spbstu.ru/index_2015_31/9_siverikova_31.pdf
27. Rossi, F.L., Nagano, M.S., Sagawa, J.K. An effective constructive heuristic for permutation flow shop scheduling problem with total flow time criterion. The International Journal of Advanced Manufacturing Technology . 2017. Vol. 90 (1-4). Pp. 93–107 [Online]. URL: <https://doi.org/10.1007/s00170-016-9347-0>
28. Silvestri, S., Laporte, G., Cerulli, R. A branch-and-cut algorithm for the minimum branch vertices spanning tree problem. Computers and Operations Research. 2017. Vol. 81. Pp. 322–332 [Online]. URL: <https://doi.org/10.1016/j.cor.2016.11.010>
29. Crainic, T.G. Parallel branch-and-bound algorithms. Montréal, 2006. 28 p.
30. Greco, F. Travelling Salesman Problem. Vienna, Austria. 2008. 202 p. [Online]. URL: http://www.exatas.ufpr.br/portal/docs_degraf/paulo/TravellingSalesmanProblem.pdf
31. Bryant, K. Genetic Algorithms and the Traveling Salesman Problem. State of California. Department of Mathematics Harvey Mudd college, 2000. 34 p.

*Yuri Kalugin**,
+7(905)2162825; yuri_kalugin@inbox.ru

Roman Romanov,
+79675533507; sluzba2013@mail.ru

*Юрий Борисович Калугин**,
+7(905)2162825; эл. почта: yuri_kalugin@inbox.ru

Роман Станиславович Романов,
+79675533507; эл. почта: sluzba2013@mail.ru

© Kalugin, Yu.B., Romanov, R.S., 2018

doi: 10.18720/MCE.84.4

Fiber concrete for the construction industry

Фибробетон для строительной индустрии

S.V. Klyuev*,
A.V. Klyuev,
*Belgorod State technological University named
 after V.G. Shukhov, Belgorod, Russia*
N.I. Vatin,
*Peter the Great St. Petersburg Polytechnic
 University, St. Petersburg, Russia*

Канд. техн. наук, доцент С.В. Ключев,
 канд. техн. наук, старший преподаватель
 А.В. Ключев,
 Белгородский государственный
 технологический университет, г. Белгород,
 Россия*
д-р техн. наук, профессор Н.И. Ватин,
*Санкт-Петербургский политехнический
 университет Петра Великого,
 Санкт-Петербург, Россия*

Key words: composite binders; fibre concrete;
 blast furnace granulated slag; fiber; reinforcement

Ключевые слова: композиционные вяжущие;
 фибробетон; доменный гранулированный
 шлак; фибра; армирование

Abstract. The article considers the use of dispersed concrete reinforcement. The efficiency of reinforcing of concrete by a fiber is proved as its strength and deformative characteristics increase. For receiving composite binders were used: Portland cement of TsEM I 42.5H GOST 31108-2003 (Russian State Standard), blast furnace granulated slag with $M_o = 1.14$ and $M_a = 0.2$, mineral plasticizer Tricosal 181 softener in essence supplementing particle size distribution knitting, waste of wet magnetic separation of ferriferous quartzites (WMS). Different types of composite binders were developed and their physico-mechanical characteristics are defined. For disperse reinforcing alkaliproof glass fiber was chosen; it is produced in the form of a roving. The analysis of results showed positive influence of the composite binders on mixes strength characteristics. The microstructure of mixes on the basis of composite binders has significant effect on properties of a composite. The conducted researches showed that the most effective length of a glass fiber is 12 mm, percent of reinforcing – 4.5 % on weight at the relation of cement and sand equal 1:3. Optimum selection of filler and also use of fiber glass in an optimum dosage allowed to increase concrete durability by stretching at a bend for 172 % on a Portland cement and to 225 % on composite binders that allows to apply it to designs.

Аннотация. В статье рассмотрено применение дисперсного армирования бетонов. Доказана эффективность армирования бетонов фиброй, поскольку повышаются его прочностные и деформативные характеристики. Для получения композиционных вяжущих были использованы: портландцемент ЦЕМ I 42,5Н ГОСТ 31108–2003, доменный гранулированный шлак с $M_o = 1,14$ и $M_a = 0,2$, минеральный пластификатор Tricosal 181, по существу дополняющий гранулометрический состав вяжущего, отходы мокрой магнитной сепарации железистых кварцитов (ММС). Были разработаны различные виды композиционных вяжущих и определены их физико-механические характеристики. Для дисперсного армирования было выбрано щелочестойкое стекловолокно выпускается в виде ровинга. Анализ результатов показал положительное влияние композиционных вяжущих на прочностные характеристики смесей. Микроструктура смесей на основе композиционных вяжущих оказывает существенное влияние на свойства композита. Проведенные исследования показали, что наиболее эффективная длина стеклянной фибры 12 мм, процент армирования 4,5 по массе при отношении цемента и песка 1:3. Оптимальный подбор заполнителя и наполнителя, а также использование стекловолокна в оптимальной дозировке позволили увеличить прочности бетона на растяжение при изгибе на 172 % на портландцементе и до 225 % на композиционном вяжущем, что позволяет применять его для конструкций.

1. Introduction

A promising direction for the production of high-strength concrete is their micro-reinforcement. Dispersed reinforcement provides three-dimensional hardening of composites and allows changing fundamentally the properties of cement stone and other types of artificial composites, providing them with high crack resistance, increasing the resistance to shock and dynamic loads, etc. [1–5]

Ключев С.В., Ключев А.В., Ватин Н.И. Фибробетон для строительной индустрии // Инженерно-строительный журнал. 2018. № 8(84). С. 41–47.

The solution to the problem of reducing the cost of such materials is possible through the use of composite binders, the multicomponent composition of which allows not only to reduce the clinker component in the mixture, but also to manage effectively the processes of structure formation, providing high quality of the obtained concretes and products based on them [6–13].

The implementation of fillers, which can be represented as particles of the dispersed phase with other indicators of surface tension than the elementary structural elements of the binder, change the energy state of the dispersed system [14–18]. The choice and purpose of fillers mainly depend on their chemical activity. Effective fillers have a multifunctional value in the synthesis of materials with predetermined properties. In real conditions, there is a compaction of cement stone (reduction in the content of large capillary pores) not only by creating a denser packaging of the initial components, but also by changing the chemistry of the binder hardening [19–23].

2. Materials and methods of research

The research on the impact of the number and type of fillers on the activity of the composite binder, which was obtained by joint grinding of cement and additives, was carried out in the work. The specific surface area was 600 m²/kg.

To obtain composite binders, the following materials were used: Portland cement CEM I 42.5 N GOST 31108-2003 CJSC "Belgorod cement", Novolipetsk blast furnace granulated slag with Mo = 1.14 and Ma = 0.2, Tricosal 181 mineral plasticizer, essentially complementing the granulometric composition of the binder, wet magnetic separation waste of ferrous quartzites (WMS) (Tables 1–3).

Table 1. Chemical composition of the additive "TRICOSAL-181".

| Oxide | SiO ₂ | Al ₂ O ₃ | Fe ₂ O ₃ | CaO | MgO | SO ₃ | K ₂ O |
|-----------------|------------------|--------------------------------|--------------------------------|------|-------|-----------------|------------------|
| Tricosal-181, % | 1.55 | 1.66 | 0.283 | 89.1 | 0.629 | 6.37 | 0.23 |

Table 2. Chemical composition of mineral components of binder.

| Oxide | SiO ₂ | Al ₂ O ₃ | Fe ₂ O ₃ | FeO | CaO | MgO | SO ₃ | K ₂ O | Na ₂ O | MnO | CO ₂ |
|-------|------------------|--------------------------------|--------------------------------|------|------|------|-----------------|------------------|-------------------|------|-----------------|
| Slag | 37.1 | 7.3 | 0.65 | - | 41.4 | 9.4 | 1.83 | 0.59 | 0.35 | 1.02 | - |
| WMS | 77.8 | 0.57 | 6.58 | 7.12 | 1.5 | 2.26 | 0.128 | - | - | - | 3.63 |

Table 3. Physical properties of granulated blast furnace slag OJSC "NLMK".

| Parameters | Values |
|--|--------|
| Activity in the age, MPa | |
| 3 days | 0.11 |
| 7 days | 2.5 |
| 28 days | 19.1 |
| Bulk density in the dry state, kg/m ³ | 1090 |
| Real density, kg/m ³ | 2820 |
| Water demand, % | 15 |
| Fineness modulus | 2.71 |
| Basicity modulus | 1.14 |

The main experimental studies were conducted at the Center of high technologies of BSTU named after V.G. Shukhov, testing center "BSTU-sertis", in the laboratories of the departments of Architectural and Construction Institute and the Institute of Building Materials, Belgorod State Technological University named after V.G. Shukhov.

Studies of the structural-phase state were carried out using an X-ray diffractometer ARLX'TRA; X-ray fluorescence analysis of the elements-ARL9900 Intellipower Workstation.

High-resolution scanning electron microscope TESCAN MIRA 3 LMU including energy dispersive spectrometer (EMF) X-MAX 50 Oxford Instruments NanoAnalysis for electron-probe microanalysis was used to obtain micrographs of the surface, grain size, microstructure of hardened binders.

The alkali-resistant fiber used in experiments is produced in the form of roving RCR-15-190-2520-9. The figures indicate: the diameter of the elementary fiber in μm is 15; the linear density of the complex thread is 190; the linear density of the roving is 2520; the number of the oiler is 9. Breaking load of roving is 500 N; the limit of the tensile strength is 1600 MPa; the maximum deformation in tensile strength is 2.2 %; modulus of elasticity is 72 GPa; the shear modulus is 29.1 GPa.

The plasticizing additive "Polyplast PREMIUM" was used.

3. Results and Discussion

To detect the action of Tricosal 181 additive and Novolipetsk blast furnace granulated slag on composite binders, compositions with an additive in the amount of 0.5 % of the cement mass were prepared. Additive (AD) in Composition Binder (CB) was implemented from the milling of binders to specific surface area $600 \text{ m}^2/\text{kg}$. The compositions with different slag consumption: 10, 20 and 50 % were studied.

| Hardening time, day | 1 | 3 | 7 | 28 |
|------------------------------------|------|------|------|------|
| Cem. I 42.5 H, MPa | 20.8 | 43.8 | 53.3 | 62.8 |
| Cem. I 42.5 H+25g AD, MPa | 21.4 | 47.0 | 55.9 | 64.3 |
| Cem. I 42.5 H+10%SI +22.5g AD, MPa | 19.8 | 45.6 | 55.8 | 64.0 |
| Cem. I 42.5 H+20%SI +20g AD, MPa | 17.0 | 41.6 | 56.3 | 62.1 |
| Cem. I 42.5 H+50%SI +12.5g AD, MPa | 15.8 | 33.5 | 45.8 | 60.5 |

Figure 1. Kinetics of hardening of CB on the basis of slag.

When comparing the activity of binders, an increase in strength was observed for all compositions (Figure 1). In early terms, the slag slows down the hydration process, and by 28 days the strength indicators of all binders become equal to the strength of the clinker, and in some cases exceed it. The addition of slag 10 and 20 % does not reduce practically the strength parameters of the binders compared to the original clinker in all terms of hardening. CB with 50 % of slag reaches the values of the strength of the ground clinker to 28-day hardening period. This is due to the fact that the high plasticizing effect of the additive is determined by the high dispersion and mineral composition, so when it is mixed with water, it forms colloidal glue and physically binds a large amount of water, compacting the structure. At the same time, its particles, being priming, substrates and centers of crystallization of slag glass, have a catalytic effect on the processes of hydration and hardening of the binder. At the same time, after forming in the initial process of hydration, the particles of the additive adsorb a significant amount of water, thereby reducing the water-binding ratio, and this leads to the activation of the processes of structure formation and synthesis of smaller crystals of calcium hydrosilicates, which undoubtedly affects the optimization of the microstructure of the cement stone compared to the control samples (Figure 2).

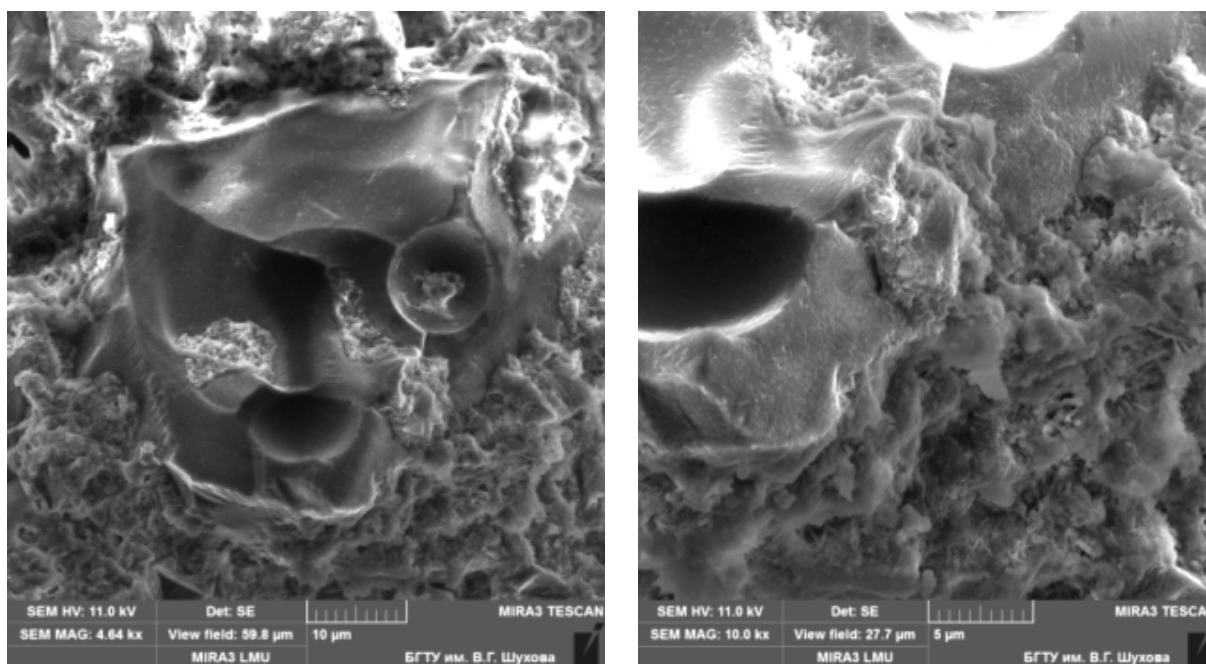


Figure 2. Microstructure of composite binder based on slag.

The study of the microstructure of samples with the addition of 0.5 % of clinker consumption and 50 % of slag showed that the resulting material is characterized by a dense matrix (Figure 2). Slag filler has good adhesion with cement stone. In this case, the additive particles, being the priming, substrates and crystallization centers of the slag glass, have a catalytic effect on the processes of hydration and hardening of the binder. In addition, the smallest particles of the filler, as well as non-hydrated cement grains, are also additional centers of crystallization, which is clearly visible in micrographs.

The hardened slag-portland cement stone is characterized by a lower content of crystalline portlandite, partially bound by slag grains and a denser hydrosilicate gel structure (Figure 2). These features of the structure explain the high water resistance and resistance to aggressive environments.

Also, various compositions of binders were obtained: fine cement (TMC 100) and composite binders consisting of cement and additives (CB 100 and CB 80 WMS). As a basis for obtaining such binders CEM I 42.5 N made at CJSC "Belgorod cement" (Belgorod) was chosen. The composite binder was obtained by grinding Portland cement with plasticizing additive "Polyplast PREMIUM" in a vibrator mill to a specific surface area of 600 m²/kg.

The main characteristics of the developed binders were determined (Table 4).

Table 4. Physical and mechanical characteristics of composite binders.

| Name of binder | Specific surface, m ² /kg | Beginning of setting, hours | Ending of setting, hours | Activity | |
|----------------|--------------------------------------|-----------------------------|--------------------------|-----------------|---------------------|
| | | | | In bending, MPa | In compression, MPa |
| CEM I 42.5N | 320 | 2.30 | 3.30 | 7.8 | 51.3 |
| TMC – 100 | 600 | 2.15 | 3.15 | 15.2 | 67.4 |
| CB-100 | 600 | 1.50 | 2.50 | 18.1 | 78.9 |
| CB-80 (WMS) | 600 | 2.05 | 3.00 | 10.9 | 56.9 |
| CB-80 (slag) | 600 | 3.20 | 4.00 | 15.7 | 62.1 |

As it can be seen from the results of studies, the binder CB-100 is characterized by a higher activity compared to cement CEM I 42.5 N and other binders.

Thus, the use of such composite binders allows improving the characteristics of concrete, compared with similar compositions based on cement. That is explained by more dense structure of a cement stone of composite binders, and consequently concretes on their basis, and also smaller porosity.

The interaction between the fibers and the matrix is a fundamental property that affects the quality of fibrous composite material based on the cement. Many factors are involved to understand the interaction between the fibers and the matrix and to predict the behavior of the composite. Here are the most important parameters that affect the interaction of fibers and matrix: matrix condition – without cracks or with cracks; the composition of the matrix; the characteristics of the type, geometry and fiber surface; the hardness of the fibers in comparison with the stiffness of the matrix; the orientation of the fibers; volume fraction of fibers; continuity of the fiber in the composite.

Production practice showed that the reinforcement of concrete with glass fiber, which has high chemical resistance to alkaline medium, became possible due to the directed development of fibers from glass of special compositions.

Available local materials were used to form the samples. The sand used for the manufacture of fine concrete was used. Its characteristics were determined by the methods of GOST 8835-88 "Sand for construction works. Test method". The fineness modulus of sand – 2.56; bulk density – 1700 kg/m³.

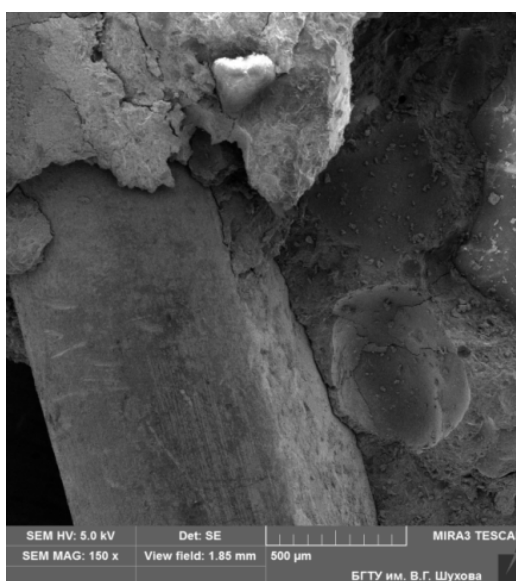
The practice of using optical fiber to dispersed reinforcement of concrete showed that from the point of view of duration of maintaining quality of reinforcing fiber with a diameter of 13-15 microns is acceptable, which is consistent with the used roving.

Studies showed that the most effective fiber length is 12 mm, the percentage of reinforcement is 4.5 by weight with a ratio of cement and sand 1:3. The output parameters were the average density of glass fibre concrete, tensile compressive strength, tensile strength in bending [24]. The results are presented in the Table 5.

Table 5. Test results of glass fibre concrete samples.

| Types of samples | fibers | | Density, kg/m ³ | σ_{bf} | | σ_t | |
|------------------|------------|-------------|----------------------------|---------------|-----------|------------|-----------|
| | length, mm | % by weight | | value, MPa | growth, % | value, MPa | growth, % |
| Without fiber | | | 2230 | 23.0 | | 3.6 | |
| CEM I 42.5 | 50 | 4.5 | 2140 | 17.0 | -26.1 | 10.0 | 172.8 |
| CB-80 WMS | 50 | 4.5 | 2180 | 23.0 | | 7.5 | 150 |
| CB-80 slag | 50 | 4.5 | 2240 | 25.5 | 10.8 | 11.5 | 219 |
| CB-100 | 50 | 4.5 | 2180 | 29.3 | 27.4 | 11.7 | 225 |

Analysis of the results showed a positive effect of composite binders on both compressive strength and tensile strength in bending. The microstructure of the composition based on CB has a significant effect on the composite properties. The solidified body contains pores of variable sizes. A significant change in volume occurs due to creep and shrinkage at temperature and humidity change (Figure 3).

**Figure 3. The contact area of fiber with composite binder CB100.**

4. Conclusion

1. Matrix and fibers form a microstructure, which is fundamentally different from the microstructure of the matrix. The interaction zone exists up to 50 microns deep into the fiber surface. This zone contains a double film with a thickness of about 1-2 microns, which surrounds the fiber, the area of large CH crystals, having a depth of up to 30 microns, and an area that has sufficient porosity. The contribution of the interaction zone to the mechanical properties of the composite is determined by the process of fiber binding and peeling.

2. Thus, the granulometric composition of mineral components of binders was optimized taking into account the genesis and morphology of the surface of the particles. It is found that the optimization of the structure formation of composite binders occurs due to the consistent growth of tumors during the hardening of the system "clinker minerals-filler-water-superplasticizer", determined by the different intensity and time of interaction of filler particles with the products of hydration of clinker minerals.

3. Rational selection of aggregate and filler, as well as the use of glass fiber in the optimal dosage allowed increasing the tensile strength of concrete in bending by 172 % on Portland cement and up to 225 % on the composite binder.

References

1. Wischers, G. Faserbewehrter Beton. Beton-Verlag. Düsseldorf 1975. Pp. 95–99.
2. Wörner, J.-D. Faserarten und – eigenschaften. Darmstädter Massivbau-Seminar. Darmstadt, 1990. Pp.75–81.
3. Alfes, Ch., Wiens, U. Stahlfaserbeton nach DAfStb-Richtlinie. Beton, Heft 4. 2010. Pp. 128–135.
4. Alfes, Ch. Qualitätssicherung von Stahlfaserbeton im Transportbetonwerk. BWI - Betonwerk International Heft 6. 2006. Pp. 212–218.
5. Grübl, P., Weigler, H., Karl, S. Beton. Art, Herstellung und Eigenschaften. Verlag Ernst & Sohn. 2001. Pp. 98–112.
6. Vatin, N.I., Barabanshchikov, Yu.G., Komarinskiy, M.V., Smirnov S.I. Modification of the cast concrete mixture by air-entraining agents. Magazine of Civil Engineering. 2015. 56(4). Pp. 1–10. (rus)
7. Dudin, M.O., Vatin, N.I., Barabanshchikov, Y.G. Modeling a set of concrete strength in the program ELCUT at warming of monolithic structures by wire. Magazine of Civil Engineering. 2015. 54(2). Pp. 33–45. (rus)
8. Dmitrieva, T.V., Strokova, V.V., Bezrodnykh, A.A. Influence of the genetic features of soils on the properties of soil-concretes on their basis. Construction Materials and Products. 2018. Vol. 1. No. 1. Pp. 69–77.
9. Klyuev, S.V., Klyuev, A.V., Abakarov, A.D., Shorstova, E.S., Gafarova, N.G. The effect of particulate reinforcement on strength and deformation characteristics of fine-grained concrete. Magazine of Civil Engineering. 2017. 75(7). Pp. 66–75.
10. Klyuyev, S.V., Klyuyev, A.V., Lesovik, R.V., Ntrebenko, A.V. High Strength Fiber Concrete for Industrial and Civil Engineering. World Applied Sciences Journal. 2013. 24(10). Pp. 1280–1285.
11. Lesovik, R.V., Klyuyev, S.V., Klyuyev, A.V., Ntrebenko, A.V., Kalashnikov, N.V. Fiber Concrete on Composite Knitting and Industrialsand KMA for Bent Designs. World Applied Sciences Journal. 2014. 30(8). Pp. 964–969.
12. Elistratkin, M.Yu., Kozhukhova, M.I. Analysis of the factors of increasing the strength of the non-autoclave aerated concrete. Construction Materials and Products. 2018. Vol. 1. No. 1. Pp. 59–68.
13. Morozov, V.I., Pukharenko, Yu.V., Yushin, A.V. The numerical investigations of double-span concrete beams strengthened with fiber reinforced plastics across the oblique section. Materials Physics and Mechanics. 2017. Vol. 31. No. 1-2. Pp. 40–43.
14. Zharikov, I.S., Laketich, A., Laketich, N. Impact of concrete quality works on concrete strength of monolithic constructions. Construction Materials and Products. 2018. Vol.1. No. 1. Po. 51–58.
15. Zagorodnyuk, L.Kh., Lesovik, V.S., Sumskey, D.A. Thermal insulation solutions of the reduced density. Construction Materials and Products. 2018. Vol. 1. No. 1. Pp. 40–50.
16. Klyuev, S.V., Klyuev, A.V., Vatin, N.I. Fine-grained concrete with combined reinforcement by different types of fibers. MATEC Web of Conferences. 2018. 245. 03006.
17. Klyuev, S.V., Khezhev, T.A., Pukharenko, Yu.V., Klyuev, A.V. The Fiber-Reinforced Concrete Constructions Experimental Research. Materials Science Forum. 2018. Vol. 931. Pp. 598–602.
18. Klyuev, S.V., Khezhev, T.A., Pukharenko, Yu.V., Klyuev, A.V. Fiber Concrete on the Basis of Composite Binder and Technogenic Raw Materials. Materials Science Forum. 2018. Vol. 931. Pp. 603–607.
19. Yu, R., Spiesz, P., Brouwers, H.J.H. Development of an ecofriendly Ultra-High Performance Concrete (UHPC) with efficient cement and mineral admixtures uses. Cement and Concrete Composites. 2015. Vol. 55. Pp. 383–394.

Литература

1. Wischers G. Faserbewehrter Beton // Beton-Verlag. Düsseldorf 1975. Pp. 95–99.
2. Wörner J.-D. Faserarten und – eigenschaften // Darmstädter Massivbau-Seminar. Darmstadt, 1990. Pp. 75–81.
3. Alfes Ch., Wiens U. Stahlfaserbeton nach DAfStb-Richtlinie // Beton, Heft 4. 2010. Pp. 128–135.
4. Alfes Ch. Qualitätssicherung von Stahlfaserbeton im Transportbetonwerk // BWI - Betonwerk International Heft 6. 2006. Pp. 212 – 218.
5. Grübl P., Weigler H., Karl S. Beton. Art, Herstellung und Eigenschaften // Verlag Ernst & Sohn. 2001. Pp. 98–112.
6. Ватин Н.И., Барабанщиков Ю.Г., Комаринский М.В., Смирнов С.И. Модификация литой бетонной смеси воздухововлекающей добавкой // Инженерно-строительный журнал. 2015. №4(56). С. 3–10.
7. Дудин М.О., Ватин Н.И., Барабанщиков Ю.Г. Моделирование набора прочности бетона в программе ELCUT при прогреве монолитных конструкций проводом // Инженерно-строительный журнал. 2015. №2(54). С. 33–45.
8. Dmitrieva T.V., Strokova V.V., Bezrodnykh A.A. Influence of the genetic features of soils on the properties of soil-concretes on their basis // Construction Materials and Products. 2018. Volume 1. Issue 1. Pp. 69–77.
9. Ключев С.В., Ключев А.В., Абакаров А.Д., Шорстова Е.С., Гафарова Н.Е. Влияние дисперсного армирования на прочностные и деформативные характеристики мелкозернистого бетона // Инженерно-строительный журнал. 2017. № 7(75). С. 66–75.
10. Klyuyev S.V., Klyuyev A.V., Lesovik R.V., Ntrebenko A.V. High Strength Fiber Concrete for Industrial and Civil Engineering // World Applied Sciences Journal. 2013. 24(10). Pp. 1280–1285.
11. Lesovik R.V., Klyuyev S.V., Klyuyev A.V., Ntrebenko A.V., Kalashnikov N.V. Fiber Concrete on Composite Knitting and Industrialsand KMA for Bent Designs // World Applied Sciences Journal. 2014. 30(8). Pp. 964–969.
12. Elistratkin M.Yu., Kozhukhova M.I. Analysis of the factors of increasing the strength of the non-autoclave aerated concrete // Construction Materials and Products. 2018. Vol. 1. № 1. Pp. 59–68.
13. Morozov V.I., Pukharenko Yu.V., Yushin A.V. The numerical investigations of double-span concrete beams strengthened with fiber reinforced plastics across the oblique section // Materials Physics and Mechanics. 2017. Т. 31. № 1-2. Pp. 40–43.
14. Zharikov I.S., Laketich A., Laketich N. Impact of concrete quality works on concrete strength of monolithic constructions // Construction Materials and Products. 2018. Vol. 1. № 1. Pp. 51 – 58.
15. Zagorodnyuk L.Kh., Lesovik V.S., Sumskey D.A. Thermal insulation solutions of the reduced density // Construction Materials and Products. 2018. Vol. 1. № 1. Pp. 40–50.
16. Klyuev S.V., Klyuev A.V., Vatin N.I. Fine-grained concrete with combined reinforcement by different types of fibers // MATEC Web of Conferences. 2018. 245. 03006.
17. Klyuev S.V., Khezhev T.A., Pukharenko Yu.V., Klyuev A.V. The Fiber-Reinforced Concrete Constructions Experimental Research // Materials Science Forum. 2018. Vol. 931. Pp. 598–602.
18. Klyuev S.V., Khezhev T.A., Pukharenko Yu.V., Klyuev A.V. Fiber Concrete on the Basis of Composite Binder and Technogenic Raw Materials // Materials Science Forum. 2018. Vol. 931. Pp. 603–607.
19. Yu R., Spiesz P., Brouwers, H.J.H. Development of an ecofriendly Ultra-High Performance Concrete (UHPC) with efficient cement and mineral admixtures uses // Cement and Concrete Composites. 2015. Vol. 55. Pp. 383–394.

20. Hezhev, T.A., Zhurtoov, A.V., Tsipinov, A.S., Klyuev, S.V. Fire resistant fibre reinforced vermiculite concrete with volcanic application. Magazine of Civil Engineering. 2018. 80(4). Pp. 181–194.
21. Khezhev, T.A., Pukharenko, Yu.V., Khezhev, Kh.A., Klyuev, S.V. Fiber Gypsum Concrete Composites with Using Volcanic Tuff Sawing Waste. ARPN Journal of Engineering and Applied Sciences. 2018. Vol. 13. No. 8. Pp. 2935–2946.
22. Sivakumar, N., Muthukumar, S., Sivakumar, V., Gowtham, D., Muthuraj, V. Experimental studies on High Strength Concrete by Using Recycled Coarse aggregate. Research Inveny: International Journal of Engineering and Science. 2014. Vol. 4. No. 1. Pp. 27–36.
23. Brouwers, H.J.H., Radix, H.J. Self-Compacting Concrete: Theoretical and experimental study. Cement and Concrete Research. 2005. Vol. 35. Pp. 2116–2136.
24. Klyuev, S.V., Klyuev, A.V., Khezhev, T.A., Pucharenko, Yu.V. Technogenic sands as effective filler for fine-grained fibre concrete. Journal of Physics: Conference Series. 2018. 1118. 012020.
20. Хежев Т.А., Журтов А.В., Ципинов А.С., Ключев С.В. Огнезащитные фибровермикулитобетоны с вулканическими добавками // Инженерно-строительный журнал. 2018. № 4(80). С. 181–194.
21. Khezhev T.A., Pukharenko Yu.V., Khezhev Kh.A., Klyuev S.V. Fiber Gypsum Concrete Composites with Using Volcanic Tuff Sawing Waste // ARPN Journal of Engineering and Applied Sciences. 2018. Vol. 13. № 8. Pp. 2935–2946.
22. Sivakumar N., Muthukumar S., Sivakumar V., Gowtham D., Muthuraj V. Experimental studies on High Strength Concrete by Using Recycled Coarse aggregate // Research Inveny: International Journal of Engineering and Science. 2014. Vol. 4. № 1. Pp. 27–36.
23. Brouwers H.J.H., Radix H.J. Self-Compacting Concrete: Theoretical and experimental study // Cement and Concrete Research. 2005. Vol. 35. Pp. 2116–2136.
24. Klyuev S.V., Klyuev A.V., Khezhev T.A., Pucharenko Yu.V. Technogenic sands as effective filler for fine-grained fibre concrete // Journal of Physics: Conference Series. 2018. 1118. 012020.

*Sergey Klyuev**,
+7(951)139-63-27; Klyuyev@yandex.ru

Alexander Klyuev,
+7(951)152-38-38; Klyuyev@yandex.ru

Nikolai Vatin,
+7(921)964-37-62; vatin@mail.ru

*Сергей Васильевич Ключев**,
+7(951)139-63-27; эл. почта: Klyuyev@yandex.ru

Александр Васильевич Ключев,
+7(951)152-38-38; эл. почта: Klyuyev@yandex.ru

Николай Иванович Ватин,
+7(921)964-37-62; эл. почта: vatin@mail.ru

© Klyuev, S.V., Klyuev, A.V., Vatin, N.I., 2018

doi: 10.18720/MCE.84.5

Biostable silicic rock-based glass ceramic foams

Биостойкие пеноситаллы
на основе кремнеземсодержащих пород

V.T. Erofeev,
A.I. Rodin*,
A.S. Kravchuk,
S.V. Kaznacheev,
Ogarev Mordovia State University, Saransk,
Respublika Mordoviya, Russia
E.A. Zaharova,
Lobachevsky State University of Nizhni
Novgorod, Nizhny Novgorod, Russia

д-р техн. наук, заведующий кафедрой
строительных материалов и технологий
В.Т. Ерофеев,
канд. техн. наук, доцент А.И. Родин,*
аспирант А.С. Кравчук,
канд. техн. наук, доцент С.В. Казначеев,
Мордовский государственный университет
им. Н.П. Огарёва, г. Саранск, Республика
Мордовия, Россия
научный сотрудник Е.А. Захарова,
Нижегородский государственный
университет им Н.И. Лобачевского,
г. Нижний Новгород, Россия

Key words: glass ceramic foams; thermal insulation material; biostability; silicic rock

Ключевые слова: пеноситалл; теплоизоляционный материал; биологическая стойкость; кремнеземсодержащая порода

Abstract. The search for the possibility of expanding the resource base through the use of local rocks, as well as reducing the cost of final product, is one of the scientific research areas in the field of obtaining foam glass-based building materials. The aim of the research is the development of compositions and recommendations for the production of silicic rock-based glass ceramic foams. These studies will allow to create strong and durable building materials with low density and thermal conductivity, as well as increased biological stability. The results of studying the phase transformations occurring in the charge (tripoli : soda ash) during heating, obtained by thermal analysis methods are presented as well as the production technology, physico-mechanical and thermophysical properties of the developed glass ceramic foams. As a result, construction materials resistant to aggressive media with a density of 200 to 600 kg/m³, thermal conductivity from 0.053 to 0.115 W/m·°C, compressive strength from 1.2 to 9.8 MPa, have been developed. Due to its properties, developed glass ceramic foams will be used primarily as insulants for the construction of nuclear power plants, in the gas and oil industries, industrial and civil engineering.

Аннотация. Расширение сырьевой базы за счёт применения местных горных пород, а также снижение стоимости готовой продукции, является одним из научных направлений исследования в области получения строительных материалов из пеностекла. Целью исследований является разработка составов и рекомендаций по получению пеноситаллов на основе кремнеземсодержащих пород. Данные исследования позволят создать прочные и долговечные строительные материалы с низкой плотностью и теплопроводностью, повышенной биологической стойкостью. Представлены результаты исследований фазовых превращений, происходящих в шихте (трепел : кальцинированная сода) при нагревании, полученные методами термического анализа; а также технология получения, физико-механические и теплофизические свойства разработанных пеноситаллов. В результате разработаны строительные материалы плотностью от 200 до 600 кг/м³, теплопроводностью от 0,053 до 0,115 Вт/м·°С, прочностью при сжатии от 1,2 до 9,8 МПа, стойкие в условиях агрессивного воздействия биологических сред. Разработанные пеноситаллы благодаря своим свойствам найдут достойное применение в первую очередь в качестве утеплителя при строительстве АЭС, в газо- и нефтепромышленности, промышленном и гражданском строительстве.

1. Introduction

Foam glass is a unique building material, which consists of glass cells for almost 100 %. Foam glass-based materials are light, have very low thermal conductivity, sufficient operational durability, do not shrink and do not change the geometric dimensions over time under the influence of operational loads, withstand high temperatures during operation, corrosion-resistant. All this ensures the reliability and quality of the final

Ерофеев В.Т., Родин А.И., Кравчук А.С., Казначеев С.В., Захарова Е.А. Биостойкие пеноситаллы на основе кремнеземсодержащих пород // Инженерно-строительный журнал. 2018. № 8(84). С. 48–56.

product, which allows us to recommend this material primarily as an insulant for the construction of nuclear power plants, in the gas and oil industries, industrial and civil construction [1]. The tightening of thermotechnical requirements for enclosing structures became an additional reason for the massive use of this material in the reconstruction of existing building projects and the construction of new ones [2–4].

Modern world scientific research in the field of producing the foam glass-based building materials has the following directions: search for not material-intensive production methods of foam glass [5–7]; low-temperature synthesis of glass mass without the use of glass-melting furnaces [7–9]; foaming of the charge mixture while bypassing the process of high-temperature melting glass [7–11]; expansion of the resource base through the use of various types of glass, cullet and local rocks, which allows to significantly increase the availability of raw materials and, at the same time, reduce its cost [5, 7, 9–19]; use of various gasifiers [6, 20–25]; optimization of foaming and annealing thermal modes [26].

The production technology of foam glass is quite complex. The first step is melting the glass. Then, the cooled glass is grounded with gas-forming additives and reheated, followed by annealing of the material obtained. The line of scientific research we offer implies the abandonment of the first stage (glass melting), the founding and foaming of the charge mixture should be carried out for one heating, which will allow to significantly reduce production costs. In addition, this technology allows the use of cheap components in the production, which are available in Russia in large quantities, (diatomite, tripoli, flask, etc.).

Physical-chemical bloating processes of zeolites, clay and perlitic rocks, slag and glass are well studied. These mechanisms cannot be correlated with the processes occurring during the bloating of silica-containing rocks, such as diatomite, tripoli and flask. However, science knows cases of foaming of tripoli with the addition of alumina to its composition, as well as foaming of diatomites with the addition of NaOH or KOH aqueous solutions [7, 10, 11].

Suggested foaming method of silica-containing rock is based on the uniqueness of its natural composition, or on rationally selected one during the production. The chemical composition of diatomite, tripoli and flask does not contain a sufficient amount of elements included in the composition of fluxes flows (Na, K, etc.), which are required in order to obtain low-temperature eutectics, to reduce the viscosity of the glass phase, etc. The main rock component is cristobalite (SiO_2), which, in the presence of calcite (CaCO_3) microcrystalline structure (regulates the melting temperature, viscosity, improves the mechanical and chemical properties of the future material), as well as of soda ash (Na_2CO_3) (reduces the melting temperature) begins to react when heated to a temperature of about 400 °C with the formation of silicates. The silication rate is the higher, the higher is the activity of the charge mixture components, and it also depends on the amount of alkaline and alkaline-earth components in the composition. Silication also accelerates in the presence of moisture in the composition, especially hydrate one, as well as it depends on the fineness degree of the charge mixture. It is known that the formation of devitrite-type ternary compounds is already finished at a temperature of 600–650 °C in mixtures consisting of silica, soda ash and a sufficient amount of alumina. The eutectics formed by these compounds and sodium silicates melt already at a temperature of 710–760 °C [27]. There are no bloating components in many silica-containing rocks. The rock presented in this work has at least two components that can be classified as bloating ones: muscovite, which releases structural water at a temperature of about 700 °C (Figure 1, Differential thermogravimetric analysis (DTG) curve 2) and heylandite, which is characterized by stepwise dehydration up to 700 °C temperature [28]. Therefore, it can be assumed that the charge mixture consisting of silica-containing rock and soda ash, which is presented in this paper, will foam when heated to a 750–800 °C temperature.

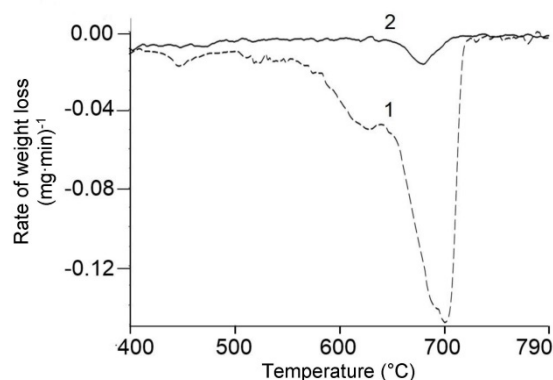


Figure 1. DTG curves of the rock (1) and muscovite (2).

The conducted researches are aimed to the development of the compositions and recommendations for the production of silicic rock-based glass ceramic foams. The following problems were solved:

– the phase transformations occurring in the charge mixture during heating, as well as the phase composition of glass ceramic foams were studied;

– the physical, mechanical and thermophysical properties of the glass ceramic foams, as well as their biological resistance were studied.

2. Methods

The following materials were used as raw materials for the production of highly biostable glass ceramic foams:

– silica-bearing rock (tripoli), which deposit is near the Engalychevo village, Dubensky District, Republic of Mordovia, chemical composition: SiO_2 – 71.00 %, CaO – 9.01 %, Al_2O_3 – 8.90 %, Fe_2O_3 – 2.86 %, K_2O – 2.06 %, MgO – 1.61 %, TiO_2 – 0.444 %, Na_2O – 0.252 %, P_2O_5 – 0.171 %, SrO – 0.064 %, BaO – 0.029 %, SO_3 – 0.027 %, ZrO_2 – 0.017 %, V_2O_5 – 0.012 %, MnO – 0.012 %, Cr_2O_3 – 0.009 %, Rb_2O – 0.010 %, CuO – 0.008 %, ZnO – 0.005 %, other impurities – 3.50 %, mineralogical composition: cristobalite (SiO_2) – 42.1 %, heylandite ($(\text{Ca}, \text{Sr}, \text{K}_2, \text{Na}_2)[\text{Al}_2\text{Si}_6\text{O}_{16}] \cdot 5\text{H}_2\text{O}$) – 17.7 %, muscovite ($\text{KAl}_2[\text{AlSi}_3\text{O}_{10}](\text{OH})_2$) – 14.4 %, calcite (CaCO_3) – 13.9 %, quartz (SiO_2) – 11.2 %, tridymite (SiO_2) – 0.7 %. DTG of the rock is presented in Figure 1, curve 1.

– first grade industrial soda ash, which meets the requirements of all-Union State Standard 5100-85. Its chemical formula is Na_2CO_3 .

The charge mixture for the manufacture of glass ceramic foam was obtained by mixed grinding of the above-mentioned rock dried to constant weight at $t = 105$ °C, and soda ash until the specific surface was equal to 1000–1100 m^2/kg . The obtained mixture was then poured into a metal mold, pre-treated with kaolin coating and compacted. The form with the mixture was set in a muffle furnace and heated at a speed from 1.5 to 4.5 °C/min to a temperature from 750 to 950 °C with soaking for 30 minutes at the maximum temperature. After cooling the mold with the obtained material and the furnace to 40 °C, it was disassembled, and the material was removed for further testing.

Phase transformations occurring in the charge mixture during heating were studied using the TGA/DSC1 device. 0.15–0.16 g of the mixture was weighed to the accuracy of 0.0001 g and poured into an alundum thimble with a volume of 150 mcl. The sample was compacted by tapping the thimble on the table. Next, the thimble was placed on the holder and then in an oven. The sample was heated from 30 to 900 °C at a rate of 10 °C/min.

The phase composition of glass ceramic foams was determined by X-ray phase analysis (XRD) using an ARL X'tra diffractometer (Switzerland). Diffractograms were recorded on $\text{CuK}\alpha_{1+2}$ radiation in the angle range $2\theta = 4$ –70° at a speed of 2 °C/min. During shooting, the sample was rotating at a speed of 60 revolutions/min. Qualitative phase analysis was performed according to the Hanavalt method using the ICDD PDF-2 database. Quantitative X-ray phase analysis was performed according to the Rietveld method using the software Siroquant 3 Sietronics Pty Ltd.

The physical and mechanical properties of the developed material were determined in accordance with all-Union State Standard 33949-2016.

The thermal conductivity index was determined by the probe method in accordance with all-Union State Standard 30256-94.

The mold fungi treeing of glass ceramic foams obtained from charge mixtures with different compositions was determined using beam samples of 10×10×30 mm in size according to all-Union State Standard 9.049-91. Methods 1 (without additional sources of carbon and mineral nutrition) and 3 (using solid Czapek's nutrient medium) were used, the funginertness and fungicity were determined.

3. Results and Discussion

In order to approve the above-mentioned statement, thermal analysis methods (differential thermal analysis (DTA) and differential thermogravimetric analysis (DTG)) were used to study phase transformations of the charge mixture that was ground to a specific surface area of 1000–1100 m^2/kg (a mixture of tripoli and soda ash in the ratio from 85:15 to 76:24). The methodology of the experiment is described above. The compositions and research results are presented in Figure 2.

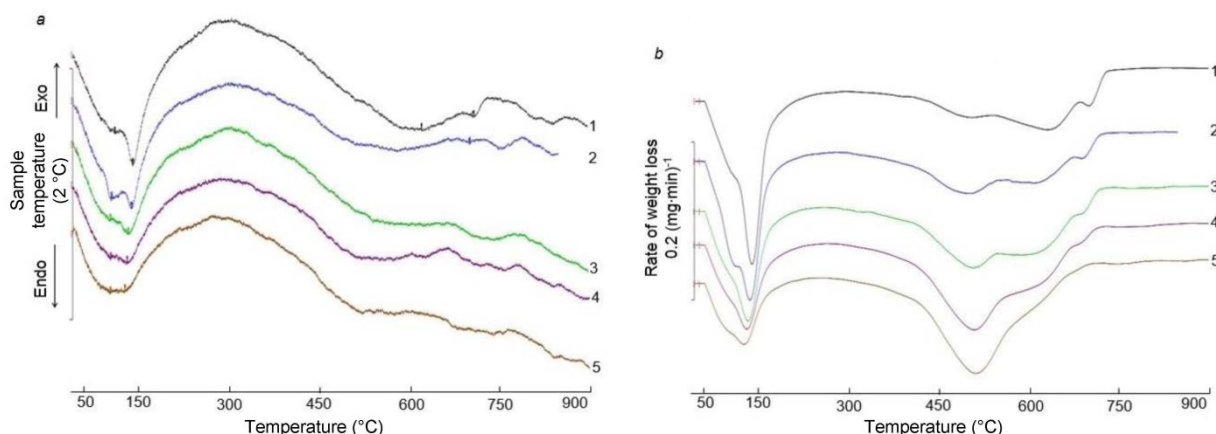


Figure 2. DTA (a) and DTG (b) curves of the mixture of tripoli and Na_2CO_3 with ratios: 1, 2, 3, 4, 5 – 85:15; 82.5:17.5; 80:20; 78:22; 76:24 respectively.

According to the data presented in Figure 2, the following main phase transformations were identified as a result of heating the mixture. The first peak in the 25 to 100 °C temperature range (endoeffect) corresponds to the dissociation of crystalline unbound water. The second peak at a temperature near 150 °C corresponds to the dissociation of the NaHCO_3 formed due to the presence of an insignificant moisture amount in the charge mixture. The third and fourth endoeffects at temperatures of 240 and 350 °C correspond to the dehydration of heylandite in the rock. The following endothermic effect and a significant mass loss in the 400 to 550 °C temperature range corresponds to the formation of sodium silicates, the intensity of which increases with an increase of Na_2CO_3 content in the mixture. The endothermic effect in the 550 to 700 °C temperature range corresponds to the decarbonization of unreacted calcite, as well as to the dehydration of structurally bound water in the rock. The intensity of this peak decreases with an increase of soda ash content in the mixture. The last peak (endoeffect) and mass loss in the 700 to 720 °C temperature range corresponds to the release of structural water from muscovite. Melting of the charge mixture, according to the data in Figure 2, a, begins at a temperature of about 650 °C. All the foregoing confirms the assumption that obtaining foam material from silica-containing rock during one mixture heating is possible.

After heating the charge mixture (consisting of tripoli and soda ash at a 80:20 ratio, respectively) to a maximum temperature of 750 °C, the composition of the calcine consisted of 60 % amorphous phase and 40 % quartz according to the result of the XRD (Figure 3). With an increase of the maximum temperature by 100 °C, the calcine consisted of 55 % of amorphous phase, 26 % of wollastonite, albite and devitrite of 6.5 % each, and 6 % of quartz. When the maximum temperature was increased by 100 °C more, the composition of the material was represented by the 60 % of amorphous phase and 40 % of wollastonite. According to the data obtained, the developing material was named as glass ceramic foam. The photo of the experimental sample of glass ceramic foam is exposed in Figure 4.

Studies of the physical, mechanical and thermophysical properties of the developed materials were carried out in order to confirm the foregoing. The compositions and research results are presented in Table 1.

The research was conducted in order to determine the correlations between the changes in average density as well as compressive strength of the obtained material and the quantitative content of soda ash in the composition (Table 1, C1-C3). The mixture was heated to 850 °C at a rate of 4.5 °C/min. According to the data obtained, the average density of glass ceramic foam reduced slightly from 600 to 570 kg/m^3 with an increase in the content of soda ash in the mixture from 15 to 17.5 %. A further increase of the soda content up to 20 % leads to a directly proportional material density decrease to 220 kg/m^3 .

The compressive strength of the obtained material has a similar correlation regarding the above-mentioned factors. With an increase of the Na_2CO_3 content in the mixture from 15 to 17.5 %, the compressive strength decreases slightly from 9.8 to 8.2 MPa. With an increase of the quantitative content of soda up to 20 %, the compressive strength decreases to 1.2 MPa.

According to the conducted research, the rational content of the soda ash should be in the range of 15 to 20 % during the production of glass ceramic foam based on a mixture of silica-containing rock (tripoli) and soda ash. A further increase of Na_2CO_3 will lead to a significant increase in the liquid phase, as well as in the cost of the final product.

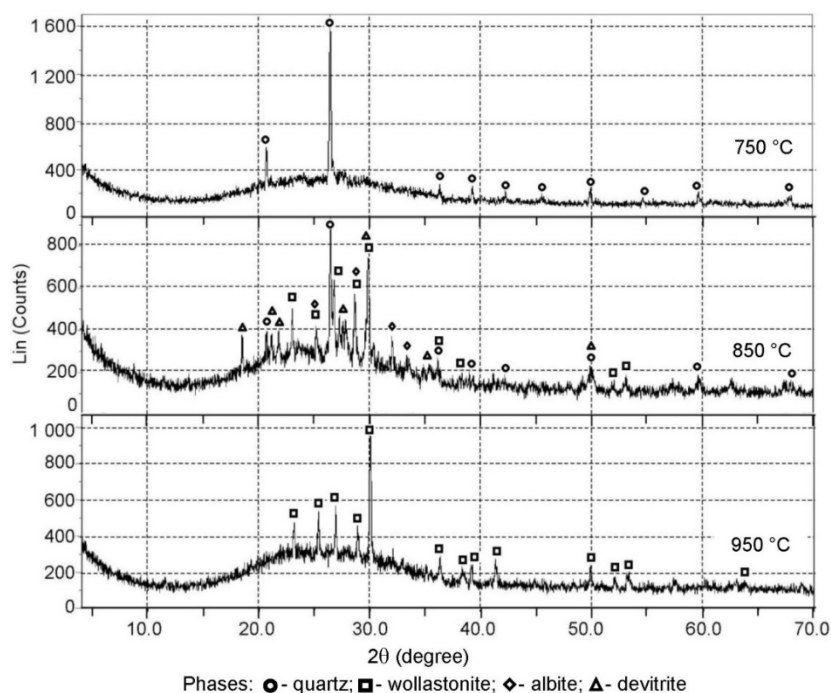


Figure 3. XRD of glass ceramic foams obtained with various maximum heating temperatures of the mixture.



Figure 4. Experimental glass ceramic foam sample.

Table 1. The compositions and properties of the developed materials.

| The compositions and properties | | Indicators for compositions | | | | | | | | | | |
|--|---------------------------------|-----------------------------|-------|-------|-------|-------|-------|-------|-------|-------|-------|--|
| | | C1 | C2 | C3 | C4 | C5 | C6 | C7 | C8 | C9 | C10 | |
| Composition (%) | tripoli | 85 | 82.5 | 80 | | | | | | | | |
| | Na ₂ CO ₃ | 15 | 17.5 | 20 | | | | | | | | |
| Maximum mixture heating temperature (°C) | | 850 | | | | 750 | 800 | 820 | 850 | 900 | | |
| Heating rate (°C/min) | | 4.5 | | 3 | 1.5 | 4 | | | | | | |
| Properties | | | | | | | | | | | | |
| Average density (kg/m ³) | | 600 | 570 | 220 | 240 | 285 | 305 | 250 | 200 | 230 | 260 | |
| Compression strength (MPa) | | 9.8 | 8.2 | 1.2 | 1.5 | 1.9 | 1.8 | 1.42 | 1.28 | 1.25 | 1.2 | |
| Water absorption (%) | | – | – | 20 | 22.5 | 34 | 5.1 | 10.3 | 15.9 | 20 | 7 | |
| Thermal conductivity (W/m·°C) | | 0.115 | 0.104 | 0.053 | 0.054 | 0.068 | 0.063 | 0.055 | 0.053 | 0.054 | 0.061 | |

Further studies were devoted to determining the correlations between the change in the average density, as well as water absorption and compressive strength of the obtained material, and the heating rate of the charge mixture (Table 1, C3-C5). In this regard, the mixture containing 20 % soda ash was heated in a muffle furnace to a temperature of 850 °C at a 1.5 to 4.5 °C/min rate with a soaking at the maximum temperature for 30 minutes. According to the data obtained, the average density of glass ceramic

foam increases almost positively associated from 220 to 285 kg/m³ while the heating rate decreases from 4.5 to 1.5 °C/min.

The water absorption of the obtained material after 1 day of soaking in water was slightly increased from 20 to 22.5 % by volume while reducing the heating rate from 4.5 to 3 °C/min. A further decreasing the heating rate to 1.5 °C/min leads to a water absorption increase up to 34 %.

According to the obtained data, the compressive strength of the developed material in the dry state increases from 1.2 to 1.5 MPa with a decrease in the heating rate from 4.5 to 3 °C/min. A further decreasing the heating rate to 1.5 °C/min leads to an increase in compressive strength of glass ceramic foam to 1.9 MPa. The compressive strength of a material in a water-saturated state slightly decreases regardless of the heating rate of the charge mixture.

According to the conducted research, the heating rate should vary from 3 to 4.5 °C/min during the production of glass ceramic foams based on a mixture of silica-containing rock (tripoli) and soda ash.

Studies aimed at determining the correlations between changes in the average density, water absorption, compressive strength of the developed materials, and the maximum heating temperature of the mixture are important (Table 1, C6-C10). For this purpose, the mixture containing 20 % of soda ash was heated in a muffle furnace at a rate of 4 °C/min to a 750 to 900 °C temperature with 30 minutes soaking time. According to the obtained data, the average density of the developed material decreases from 305 to 200 kg/m³ with an increase in the maximum mixture heating temperature from 750 to 820 °C. A further increasing the heating temperature up to 900 °C leads to the average density increase up to 260 kg/m³.

The water absorption of the material by volume after 1 day of soaking in water increases from 5.1 to 20 % with an increase in the heating temperature from 750 to 850 °C, and its increase from 850 to 900 °C leads to a decrease in water absorption to 7 %.

The compressive strength of the obtained material in the dry state decreases from 1.8 to 1.2 MPa with an increase in the maximum mixture heating temperature from 750 to 900 °C. The compressive strength of glass ceramic foam in a water-saturated state, reached at the mixture maximum heating temperature of 750 °C, is almost 20 % more than the strength of the material in the dry state. This can be explained by the ability of this material to interact with water as a result of its insufficient heat treatment. At the maximum heating temperature of the charge mixture from 800 to 900 °C, the compressive strength of a water-saturated glass ceramic foam is almost equal to the compressive strength in a dry state.

According to the conducted research, the production of glass ceramic foam based on a mixture of silica-containing rock (tripoli) and soda ash requires the maximum heating temperature from 800 to 850 °C.

The studies of the correlation between thermal conductivity change of the obtained material and the temperature as well as the heating rate of the mixture are set out below (Table 1).

According to the obtained data, the thermal conductivity of the developed material decreases from 0.063 to 0.053 W/m·°C with an increase of the maximum mixture heating temperature from 750 to 820 °C. With a further increasing the maximum temperature up to 900 °C, the thermal conductivity increases to 0.061 W/m·°C.

The thermal conductivity of glass ceramic foam is decreasing from 0.068 to 0.054 W/m·°C with an increase in the heating rate of the mixture (maximum heating temperature equals 850 °C) from 1.5 to 3 °C/min. A further increase of the heating rate to 4.5 °C/min does not have a significant effect on the thermal conductivity of the obtained material.

It was determined that in order to obtain the lowest thermal conductivity of the developed material, the heating rate of the charge mixture should vary from 3 to 4.5 °C/min, and the maximum heating temperature from 800 to 850 °C.

Recently, the problem of biological corrosion of materials has become especially urgent. The corrosion increases with high humidity, cyclically operating temperatures and other environmental factors. The world annual economic damage from biodeterioration reaches tens of billions of dollars. The appearance of buildings and the indoor ecological situation are getting worse, and the list of human diseases caused by microscopic organisms is expanding [29–31]. Further research results (Table 2) are devoted to studying the impact of the mixture composition on treeing and the dominant microorganism species on the glass ceramic foam sample.

According to the research results, the developed glass ceramic foams with a density of 200 to 600 kg/m³ are funginert, i.e. they are not a nutrient source for mold fungi, and after a month of testing in a standard filamentous fungi environment, 2 types of micromycetes of the genus *Penicillium* (*Penicillium cyclopium* and *Penicillium chrysogenum*) were identified on their surface as well as 1 species of the genus *Trichoderma* (*Trichoderma viride*). It was determined that the fungi on the samples develop very slowly, which indicates the antifungal properties of the obtained material.

Table 2. The impact of the mixture composition on treeing and dominant microbial species on glass ceramic foam sample.

| No. | Mixture composition, % | | Characteristic according to all-Union State Standard 9.049-91 | | Dominant microorganism species on the sample |
|-----|------------------------|-------------------|---|----------|--|
| | Tripoli | NaCO ₃ | Method 1 | Method 3 | |
| 1 | 85 | 15 | 0 | 5 | Penicillium cyclopium, Penicillium chrysogenum, Trichoderma viride |
| 2 | 82.5 | 17.5 | 0 | 4 | Penicillium cyclopium, Penicillium chrysogenum, Trichoderma viride |
| 3 | 80 | 20 | 0 | 4 | Penicillium cyclopium, Penicillium chrysogenum, Trichoderma viride |

4. Conclusions

1. Thermal insulating materials based on tripoli and soda ash were developed using only one charge mixture heating with a glass-ceramic structure and 200 to 600 kg/m³ density, 0.053 to 0.115 W/m·°C thermal conductivity, compressive strength from 1.2 to 9.8 MPa, as well as increased biological resistance.

2. The phase transformations occurring in the mixture (tripoli : soda ash) during heating were determined using the thermal analysis. The silicate formation in the mixture begins at a temperature of about 400 °C, and melting mixture is at about 650 °C. The foaming process is carried out due to separating the structural water from muscovite, which is a part of the tripoli, at a temperature of about 700 °C.

3. The phase composition of the crushed baked material was determined using the XRD method, which consists of crystalline phases by 40–45 % and of amorphous phases by 55–60 %. The obtained material was named as glass ceramic foam.

4. It was determined that the production of glass ceramic foam based on a mixture of silica-containing rock (tripoli) and soda ash requires the rational content of the soda ash in ranges from 15 to 20 %, the heating rate of the mixture is about 4 °C/min, and the maximum heating temperature is about 820 °C.

5. The developed glass ceramic foams are funginert, which makes it possible to recommend their use in buildings and structures with aggressive biological media.

Acknowledgement

The study was conducted using research grant from the Russian Science Foundation (project No. 18-73-00213).

References

- Manevich, V.E., Subbotin, K.Yu. Foam glass and problems of energy conservation. Glass and Ceramics (English translation of Steklo i Keramika). 2008. Vol. 65. No. 3-4. Pp. 105–108. DOI: 10.1007/s10717-008-9026-1.
- Danilevsky, L.N., Danilevsky, S.L. The algorithm and accuracy of definition of heattechnical indicators of buildings. Magazine of Civil Engineering. 2017. 73(5). Pp. 49–61. DOI: 10.18720/MCE.73.5.
- Korniyenko, S.V., Vatin, N.I., Gorshkov, A.S. Thermophysical field testing of residential buildings made of autoclaved aerated concrete blocks. Magazine of Civil Engineering. 2016. 64(4). Pp. 10–25. DOI: 10.5862/MCE.64.2.
- Portnyagin, D.G. Improving the thermal performance of the building envelopes with the use of foam glass-ceramics. Magazine of Civil Engineering. 2015. 60(8). Pp. 56–67. DOI: 10.5862/MCE.60.7.
- Ivanov, K.S., Radaev, S.S., Selezneva O.I. Diatomites in Granular Foam-Glass Technology. Glass and Ceramics (English translation of Steklo i Keramika). 2014. Vol. 71. No. 5-6. Pp. 157–161. DOI: 10.1007/s10717-014-9641-y.
- Vaisman, I., Ketov, A., Ketov, I. Cellular glass obtained from non-powder preforms by foaming with steam. Ceramics International. 2016. Vol. 42. No. 14. Pp. 15261–15268. DOI: 10.1016/j.ceramint.2016.06.165.
- Orlov, A.D. Optimizirovannaya odnostadijnaya tekhnologiya granulirovannogo penostekla na osnove nizkotemperaturnogo sinteza steklofazy [Optimized single-stage technology of granulated foam glass based on low-

Литература

- Manevich V.E., Subbotin K.Yu. Foam glass and problems of energy conservation // Glass and Ceramics (English translation of Steklo i Keramika). 2008. Vol. 65. № 3-4. Pp. 105–108. DOI: 10.1007/s10717-008-9026-1.
- Данилевский Л.Н., Данилевский С.Л. Алгоритм и точность определения теплотехнических показателей зданий // Инженерно-строительный журнал. 2017. № 5(73). С. 49–61. DOI: 10.18720/MCE.73.5.
- Корниенко С.В., Ватин Н.И., Горшков А.С. Натурные теплофизические испытания жилых зданий из газобетонных блоков // Инженерно-строительный журнал. 2016. №4(64). С. 10–25. DOI: 10.5862/MCE.64.2.
- Портнягин Д.Г. Повышение теплозащиты узлов ограждающих конструкций зданий с применением пеностеклокристаллического материала // Инженерно-строительный журнал. 2015. №8(60). С. 56–67. DOI: 10.5862/MCE.60.7.
- Ivanov K.S., Radaev S.S., Selezneva O.I. Diatomites in Granular Foam-Glass Technology // Glass and Ceramics (English translation of Steklo i Keramika). 2014. Vol. 71. № 5-6. Pp. 157–161. DOI: 10.1007/s10717-014-9641-y.
- Vaisman I., Ketov A., Ketov I. Cellular glass obtained from non-powder preforms by foaming with steam // Ceramics International. 2016. Vol. 42. № 14. Pp. 15261–15268. DOI: 10.1016/j.ceramint.2016.06.165.
- Орлов А.Д. Оптимизированная одностадийная технология гранулированного пеностекла на основе низкотемпературного синтеза стеклофазы // Строительные материалы. 2015. № 1. С. 24–26.

Ерофеев В.Т., Родин А.И., Кравчук А.С., Казначеев С.В., Захарова Е.А. Биостойкие пеноситаллы на основе кремнеземсодержащих пород // Инженерно-строительный журнал. 2018. № 8(84). С. 48–56.

- temperature synthesis of glass phase] *Stroitel'nye Materialy*. 2015. No. 1. Pp. 24–26. (rus)
8. Qu, Y.-N., Xu, J., Su, Z.-G., Ma, N., Zhang, X.-Y., Xi, X.-Q., Yang, J.-L. Lightweight and high-strength glass foams prepared by a novel green spheres hollowing technique. *Ceramics International*. 2016. Vol. 42. No. 2. Pp. 2370–2377. DOI: 10.1016/j.ceramint.2015.10.034.
 9. Manevich, V.E., Subbotin, R.K., Nikiforov, E.A., Senik, N.A., Meshkov, A.V. Diatomite – Siliceous material for the glass industry. *Glass and Ceramics* (English translation of *Steklo i Keramika*). 2012. Vol. 69. No. 5-6. Pp. 168–172. DOI: 10.1007/s10717-012-9438-9.
 10. Kazantseva, L.K. Particulars of foam glass manufacture from zeolite-alkali batch. *Glass and Ceramics* (English translation of *Steklo i Keramika*). 2013. Vol. 70. No. 7-8. Pp. 277–281. DOI: 10.1007/s10717-013-9560-3.
 11. Nikitin, A.I., Storozhenko, G.I., Kazanceva, L.K., Vereshchagin, V.I. Teploizolyacionnye materialy i izdeliya na osnove trepelov Potaninskogo mestorozhdeniya [Heat-insulating materials and products on the basis of Tripoli of the Potaninsky field]. *Stroitel'nye Materialy*. 2014. No. 8. Pp. 34–37. (rus)
 12. Bernardo, E., Albertini, F. Glass foams from dismantled cathode ray tubes. *Ceramics International*. 2006. Vol. 32. No. 6. Pp. 603–608. DOI: 10.1016/j.ceramint.2005.04.019.
 13. Chen, M., Zhang, F.-S., Zhu, J. Lead recovery and the feasibility of foam glass production from funnel glass of dismantled cathode ray tube through pyrovacuum process. *Journal of Hazardous Materials*. 2009. Vol. 161. No. 2-3. Pp. 1109–1113. DOI: 10.1016/j.jhazmat.2008.04.084.
 14. Fernandes, H.R., Tulyaganov, D.U., Ferreira, J.M.F. Preparation and characterization of foams from sheet glass and fly ash using carbonates as foaming agents. *Ceramics International*. 2009. Vol. 35. No. 1. Pp. 229–235. DOI: 10.1016/j.ceramint.2007.10.019.
 15. Guo, Y., Zhang, Y., Huang, H., Meng, X., Liu, Y., Tu, S., Li, B. Novel glass ceramic foams materials based on polishing porcelain waste using the carbon ash waste as foaming agent. *Construction and Building Materials*. 2016. Vol. 125. Pp. 1093–1100. DOI: 10.1016/j.conbuildmat.2016.08.134.
 16. Li, Z., Luo, Z., Li, X., Liu, T., Guan, L., Wu, T., Lu, A. Preparation and characterization of glass–ceramic foams with waste quartz sand and coal gangue in different proportions. *Journal of Porous Materials*. 2016. Vol. 23. No. 1. Pp. 231–238. DOI: 10.1007/s10934-015-0074-y.
 17. Rincón, A., Giacomello, G., Pasetto, M., Bernardo, E. Novel 'inorganic gel casting' process for the manufacturing of glass foams. *Journal of the European Ceramic Society*. 2017. Vol. 37. No. 5. Pp. 2227–2234. DOI: 10.1016/j.jeurceramsoc.2017.01.012.
 18. Yin, H., Ma, M., Bai, J., Li, Y., Zhang, S., Wang, F. Fabrication of foam glass from iron tailings. *Materials Letters*. 2016. Vol. 185. Pp. 511–513. DOI: 10.1016/j.matlet.2016.09.034.
 19. Zhang, Q., He, F., Shu, H., Qiao, Y., Mei, S., Jin, M., Xie, J. Preparation of high strength glass ceramic foams from waste cathode ray tube and germanium tailings. *Construction and Building Materials*. 2016. Vol. 111. Pp. 105–110. DOI: 10.1016/j.conbuildmat.2016.01.036.
 20. Fang, X., Li, Q., Yang, T., Li, Z., Zhu, Y. Preparation and characterization of glass foams for artificial floating island from waste glass and Li₂CO₃. *Construction and Building Materials*. 2017. Vol. 134. Pp. 358–363. DOI: 10.1016/j.conbuildmat.2016.12.048.
 21. Hesky, D., Aneziris, C.G., Groß, U., Horn, A. Water and waterglass mixtures for foam glass production. *Ceramics International*. 2015. Vol. 41. No. 10. Pp. 12604–12613. DOI: 10.1016/j.ceramint.2015.06.088.
 22. König, J., Petersen, R.R., Yue, Y., Suvorov, D. Gas-releasing reactions in foam-glass formation using carbon and Mn_xO_y as the foaming agents. *Ceramics International*. 2017. Vol. 43. No. 5. Pp. 4638–4646. DOI: 10.1016/j.ceramint.2016.12.133.
 23. Østergaard, M.B., Petersen, R.R., König, J., Johra, H., Yue, Y. Influence of foaming agents on solid thermal conductivity of foam glasses prepared from CRT panel
 8. Qu, Y.-N., Xu, J., Su, Z.-G., Ma, N., Zhang, X.-Y., Xi, X.-Q., Yang, J.-L. Lightweight and high-strength glass foams prepared by a novel green spheres hollowing technique // *Ceramics International*. 2016. Vol. 42. No. 2. Pp. 2370–2377. DOI: 10.1016/j.ceramint.2015.10.034.
 9. Manevich V.E., Subbotin R.K., Nikiforov E.A., Senik N.A., Meshkov A.V. Diatomite – Siliceous material for the glass industry // *Glass and Ceramics* (English translation of *Steklo i Keramika*). 2012. Vol. 69. No. 5-6. Pp. 168–172. DOI: 10.1007/s10717-012-9438-9.
 10. Kazantseva L.K. Particulars of foam glass manufacture from zeolite-alkali batch // *Glass and Ceramics* (English translation of *Steklo i Keramika*). 2013. Vol. 70. No. 7-8. Pp. 277–281. DOI: 10.1007/s10717-013-9560-3.
 11. Никитин А.И., Storozhenko Г.И., Kazanceva Л.К., Vereshchagin В.И. Теплоизоляционные материалы и изделия на основе трепелов Потанинского месторождения // *Строительные материалы*. 2014. № 8. С. 34–37.
 12. Bernardo E., Albertini F. Glass foams from dismantled cathode ray tubes // *Ceramics International*. 2006. Vol. 32. No. 6. Pp. 603–608. DOI: 10.1016/j.ceramint.2005.04.019.
 13. Chen M., Zhang F.-S., Zhu J. Lead recovery and the feasibility of foam glass production from funnel glass of dismantled cathode ray tube through pyrovacuum process // *Journal of Hazardous Materials*. 2009. Vol. 161. No. 2-3. Pp. 1109–1113. DOI: 10.1016/j.jhazmat.2008.04.084.
 14. Fernandes H.R., Tulyaganov D.U., Ferreira J.M.F. Preparation and characterization of foams from sheet glass and fly ash using carbonates as foaming agents // *Ceramics International*. 2009. Vol. 35. No. 1. Pp. 229–235. DOI: 10.1016/j.ceramint.2007.10.019.
 15. Guo Y., Zhang Y., Huang H., Meng X., Liu Y., Tu S., Li B. Novel glass ceramic foams materials based on polishing porcelain waste using the carbon ash waste as foaming agent // *Construction and Building Materials*. 2016. Vol. 125. Pp. 1093–1100. DOI: 10.1016/j.conbuildmat.2016.08.134.
 16. Li Z., Luo Z., Li X., Liu T., Guan L., Wu T., Lu A. Preparation and characterization of glass–ceramic foams with waste quartz sand and coal gangue in different proportions // *Journal of Porous Materials*. 2016. Vol. 23. No. 1. Pp. 231–238. DOI: 10.1007/s10934-015-0074-y.
 17. Rincón A., Giacomello G., Pasetto M., Bernardo E. Novel 'inorganic gel casting' process for the manufacturing of glass foams. *Journal of the European Ceramic Society*. 2017. Vol. 37. No. 5. Pp. 2227–2234. DOI: 10.1016/j.jeurceramsoc.2017.01.012.
 18. Yin H., Ma M., Bai J., Li Y., Zhang S., Wang F. Fabrication of foam glass from iron tailings. *Materials Letters*. 2016. Vol. 185. Pp. 511–513. DOI: 10.1016/j.matlet.2016.09.034.
 19. Zhang Q., He F., Shu H., Qiao Y., Mei S., Jin M., Xie J. Preparation of high strength glass ceramic foams from waste cathode ray tube and germanium tailings. *Construction and Building Materials*. 2016. Vol. 111. Pp. 105–110. DOI: 10.1016/j.conbuildmat.2016.01.036.
 20. Fang X., Li Q., Yang T., Li Z., Zhu Y. Preparation and characterization of glass foams for artificial floating island from waste glass and Li₂CO₃. *Construction and Building Materials*. 2017. Vol. 134. Pp. 358–363. DOI: 10.1016/j.conbuildmat.2016.12.048.
 21. Hesky D., Aneziris C.G., Groß U., Horn A. Water and waterglass mixtures for foam glass production // *Ceramics International*. 2015. Vol. 41. No. 10. Pp. 12604–12613. DOI: 10.1016/j.ceramint.2015.06.088.
 22. König J., Petersen R.R., Yue Y., Suvorov D. Gas-releasing reactions in foam-glass formation using carbon and Mn_xO_y as the foaming agents // *Ceramics International*. 2017. Vol. 43. No. 5. Pp. 4638–4646. DOI: 10.1016/j.ceramint.2016.12.133.
 23. Østergaard M.B., Petersen R.R., König J., Johra H., Yue Y. Influence of foaming agents on solid thermal conductivity of foam glasses prepared from CRT panel

- glass. Journal of Non-Crystalline Solids. 2017. Vol. 465. Pp. 59–64. DOI: 10.1016/j.jnoncrysol.2017.03.035.
24. Petersen R.R., König J., Yue Y. The viscosity window of the silicate glass foam production. Journal of Non-Crystalline Solids. 2017. Vol. 456. Pp. 49–54. DOI: 10.1016/j.jnoncrysol.2016.10.041.
 25. Souza M.T., Maia B.G.O., Teixeira L.B., de Oliveira K.G., Teixeira A.H.B., Novaes de Oliveira A.P. Glass foams produced from glass bottles and eggshell wastes. Process Safety and Environmental Protection. 2017. Vol. 111. Pp. 60–64. DOI: 10.1016/j.psep.2017.06.011.
 26. Méar F., Yot P., Ribes M. Effects of temperature, reaction time and reducing agent content on the synthesis of macroporous foam glasses from waste funnel glasses. Materials Letters. 2006. Vol. 60. No. 7. Pp. 929–934. DOI: 10.1016/j.matlet.2005.10.046.
 27. Pak V.N., Gavronskaya Y.Y., Burkat T.M. Porous glass and nanostructured materials. Nova. New York, 2015. 113 p.
 28. Xu R., Pang W., Yu J., Huo Q., Chen J. Chemistry of Zeolites and Related Porous Materials: Synthesis and Structure. John Wiley & Sons (Asia) Pte Ltd, 2007. 696 p.
 29. Erofeev V., Rodin A., Rodina N., Kalashnikov V., Irina, E. Biocidal Binders for the Concretes of Unerground Constructions // Procedia Engineering. 2016. Vol. 165. Pp. 1448–1454. DOI: 10.1016/j.proeng.2016.11.878.
 30. Erofeev V.T., Bogatov A.D., Smirnov V.F., Bogatova S.N., Rimshin V.I., Kurbatov V.L. Bioresistant building composites on the basis of glass wastes. Biosciences Biotechnology Research Asia. 2015. Vol. 12. No. 1. Pp. 661–669. DOI: 10.13005/bbra/1710.
 31. Travush V.I., Karpenko N.I., Erofeev V.T., Rodin A.I., Smirnov V.F., Rodina N.G. Development of Biocidal Cements for Buildings and Structures with Biologically Active Environments. Power Technology and Engineering. 2017. Vol. 51. No. 4. Pp. 377–384. DOI: 10.1007/s10749-017-0842-8.
 24. Petersen R.R., König J., Yue Y. The viscosity window of the silicate glass foam production // Journal of Non-Crystalline Solids. 2017. Vol. 456. Pp. 49–54. DOI: 10.1016/j.jnoncrysol.2016.10.041.
 25. Souza M.T., Maia B.G.O., Teixeira L.B., de Oliveira K.G., Teixeira A.H.B., Novaes de Oliveira A.P. Glass foams produced from glass bottles and eggshell wastes // Process Safety and Environmental Protection. 2017. Vol. 111. Pp. 60–64. DOI: 10.1016/j.psep.2017.06.011.
 26. Méar F., Yot P., Ribes M. Effects of temperature, reaction time and reducing agent content on the synthesis of macroporous foam glasses from waste funnel glasses // Materials Letters. 2006. Vol. 60. No. 7. Pp. 929–934. DOI: 10.1016/j.matlet.2005.10.046.
 27. Pak V.N., Gavronskaya Y.Y., Burkat T.M. Porous glass and nanostructured materials. Nova. New York, 2015. 113 p.
 28. Xu R., Pang W., Yu J., Huo Q., Chen J. Chemistry of Zeolites and Related Porous Materials: Synthesis and Structure. John Wiley & Sons (Asia) Pte Ltd, 2007. 696 p.
 29. Erofeev V., Rodin A., Rodina N., Kalashnikov V., Irina, E. Biocidal Binders for the Concretes of Unerground Constructions // Procedia Engineering. 2016. Vol. 165. Pp. 1448–1454. DOI: 10.1016/j.proeng.2016.11.878.
 30. Erofeev V.T., Bogatov A.D., Smirnov V.F., Bogatova S.N., Rimshin V.I., Kurbatov V.L. Bioresistant building composites on the basis of glass wastes // Biosciences Biotechnology Research Asia. 2015. Vol. 12. No. 1. Pp. 661–669. DOI: 10.13005/bbra/1710.
 31. Travush V.I., Karpenko N.I., Erofeev V.T., Rodin A.I., Smirnov V.F., Rodina N.G. Development of Biocidal Cements for Buildings and Structures with Biologically Active Environments // Power Technology and Engineering. 2017. Vol. 51. No. 4. Pp. 377–384. DOI: 10.1007/s10749-017-0842-8.

Vladimir Erofeev,
(8342)47-40-19; al_rodin@mail.ru

Alexander Rodin,*
+79510514528; al_rodin@mail.ru

Aleksej Kravchuk,
+79991501555; a.kravchuk.s@yandex.ru

Sergej Kaznacheev,
+79176954146; kaznacheevsv@rambler.ru

Elena Zaharova,
+7(960)1840546;
zaharova_elena_aleksandrovna@mail.ru

Владимир Трофимович Ерофеев,
(8342)47-40-19; эл. почта: al_rodin@mail.ru

Александр Иванович Родин,*
+79510514528; эл. почта: al_rodin@mail.ru

Алексей Сергеевич Кравчук,
+79991501555; эл. почта:
a.kravchuk.s@yandex.ru

Сергей Валерьевич Казначеев,
+79176954146;
эл. почта: kaznacheevsv@rambler.ru

Елена Александровна Захарова,
+7(960)1840546;
эл. почта:
zaharova_elena_aleksandrovna@mail.ru

© Erofeev, V.T., Rodin, A.I., Kravchuk, A.S., Kaznacheev, S.V., Zaharova, E.A., 2018

doi: 10.18720/MCE.84.6

Damage prediction model for concrete pavements in seasonally frozen regions

Модель для прогнозирования повреждений дорожного покрытия в районе сезонного промерзания

Q. Zhao,
P. Cheng*,
Northeast Forestry University, Harbin,
Heilongjiang, China

J. Wang,
Harbin Dongan Automobile Engine Manufacturing
Co.,Ltd., Harbin, Heilongjiang, China

Y. Wei,
Yellow River Survey Planning and Design Co.,
Ltd., Zhengzhou City, Henan Province, China

PhD Ц. Чжао,
PhD П. Чен*,
Northeast Forestry University, Харбин, Кумай,
д-р техн. наук Д. Ван,
Harbin Dongan Automobile Engine Manufacturing
Co.,Ltd., Харбин, Кумай,
д-р техн. наук Ю. Вэй,
Yellow River Survey Planning and Design Co.,
Ltd., г. Чжэнчжоу, Кумай

Key words: concrete pavement; damage prediction environmental factor; statistical product and service solution

Ключевые слова: цементно-бетонное покрытие; прогноз состояния повреждения; фактор воздействия на окружающую среду

Abstract. Vehicle loads and environmental differences are the key technical factors in the model construction of concrete pavement damage prediction. According to the data of the 168-month actual number of actions of different vehicle axle types, average temperature, average wind speed, rainfall, snowfall and days below 0 °C collected from the Mudanjiang-provincial section of the He-da highway in China, the broken slab ratio of cement concrete (DBL) was calculated. Cracking rate(CRK) and environmental factor(SF) were introduced into the model. This paper uses SPSS analysis method to carry out correlation analysis and partial correlation analysis by introducing SF to the model of DBL and CRK, so that the concrete pavement damage prediction model in seasonally frozen regions can be constructed and tested. Results show that CRK and SF both have positive linear relationship with DBL; Concrete pavement damage in seasonally frozen regions can be predicted by analyzing parameters like actual number of actions of different vehicle axle types, road service time and freezing index, etc. No multiple collinearity exists in the parameters of the model and the construction of model for concrete pavement damage prediction in seasonally frozen regions is of great theoretical significance for timely and effective pavement maintenance. The model has achieved good results in damage prediction accuracy and efficiency.

1. Introduction

After the opening of concrete pavement to withstand the repeated loading of vehicles, under the influence of the climate and material characteristics, the road will gradually appear all kinds of damage. Pavement damage will aggravate or produce derivative diseases over time. The relationship between the prediction of road surface service performance and the prediction of the road damage status established by the law of the development of road disease change is the prediction model of road damage [1–3]. The model can effectively and accurately analyze and evaluate the damage status of pavement in the future. The model can choose and determine the best maintenance plan to prolong the service life of pavement. Therefore, the study on the prediction of pavement damage can provide the theoretical basis and scientific basis for pavement maintenance and decision.

Since the 1950s, domestic and foreign scholars began to study the condition of pavement damage. The obtained research results include deterministic model, probabilistic model [4–6], neural network model [7–9] and so on. In the probabilistic model, various probabilistic models need to rely on experts to score, the subjectivity is strong. The prediction of pavement damage status based on the gray theory model [10–11] can well solve the index problem of complex and fuzzy, but its whitening weight function, the exponent of the evaluation index and the gray clustering coefficient all depend on the empirical range of each index, there are also some subjective experiences. Neural network prediction model has a strong nonlinear fitting ability, and the learning rules are simple, but there are some shortcomings of the model

Чжао Ц., Чен П., Ван Д., Вэй Ю. Модель для прогнозирования повреждений дорожного покрытия в районе сезонного промерзания // Инженерно-строительный журнал. 2018. № 8(84). С. 57–66.

itself, which requires sufficient data support, and the reasoning process and reasoning basis are very strict. Zeng Qingxia [12] of Changsha Polytechnic University predicted the damage condition of concrete pavement based on vector machine. The model used machine learning and statistical learning theory and method, the evaluation speed is fast, but there is a lack of consider in diversification and uncertainty of evaluation index influencing factors. Guangdong Province [13] established the PCI deterministic model of pavement condition index by sorting out, analyzing and using empirical methods based on years of accumulated traffic data. However, this model is only an implicit equation of regression coefficient and road age with no consideration of environmental factors. The above results were obtained in the non-seasonally frozen regions, due to the vast territory of our country, the provinces in terms of the number of vehicle axle load, the average temperature, rainfall, snowfall and so on are different, and the road damage status vulnerable to environmental, and traffic and other factors. Combining with the characteristics of climatic environment in seasonally frozen regions, this paper starts with the traffic conditions and environmental factors and establishes a scientific predicting model of the damage condition of concrete pavement.

Based on the field survey data of pavement cracks, environmental factors and the number of vehicle axle loads in He-da highway in China from Mudanjiang to provincial boundary, the paper analyzes the model of pavement cracks and environmental factors in MEPDG, analyzes the model by using SPSS software. SPSS is a "statistical product and service solution" software, the outstanding feature is the use of regression analysis to solve the statistical relationship between a variable and its influencing factors. The relationship between the prediction model of concrete pavement damage in frozen area [14, 15] and the crack model of concrete pavement and the model of environmental factors are also presented to predict the long-term damage of concrete pavement in seasonally frozen regions.

2. Methods

"The Technical Code for Road Maintenance" divides the forms of concrete pavement into the following four types: seams, vertical displacements, cracks and surface damages, and uses the concrete pavement breaking rate (*DBL*) as the evaluation of pavement damage index. The use of RTM intelligent road test car pavement section of the survey to detect the status of damage. The test car through the image acquisition equipment put the damaged image into high-performance computer, the computer image processing real-time road surface treatment, detection, identification, analysis, and to find out the location and size of cracks in the image on the road, the road crack width measurement accuracy is greater than 1.5 mm, Length measurement accuracy is less than 5%. In Figure 1, the road age and climatic conditions of Mudanjiang to provincial boundary in He-da highway are the same, but the difference between the survey results of pavement damage on the up and down directions is quite large. The traffic in the up and down directions is different at different sections. When the difference of traffic volume accounts for 3.45% ~ 6.23% of the total traffic volume in the surveyed interval, the impact width of pavement cracks is between 8.067 m and 55.681 m. In Figure 2, the traffic volume and road structure of Xu-chang Section National Highway 107 (K759~K775) and Mudanjiang to provincial boundary (K143~K159) in He-da highway are similar. The annual average temperature of the location of He-da highway and Xu-chang Section in National Highway 107 is 6.1 °C and 14.5 °C, and the width of the pavement cracks is between 64.795 m and 248.937 m.

The above shows that the *DBL* of concrete pavement shows obvious differences with the traffic load and environmental factors, which provides an important basis for constructing the damage prediction model of traffic and climate impact factors, and makes the model more reasonable.

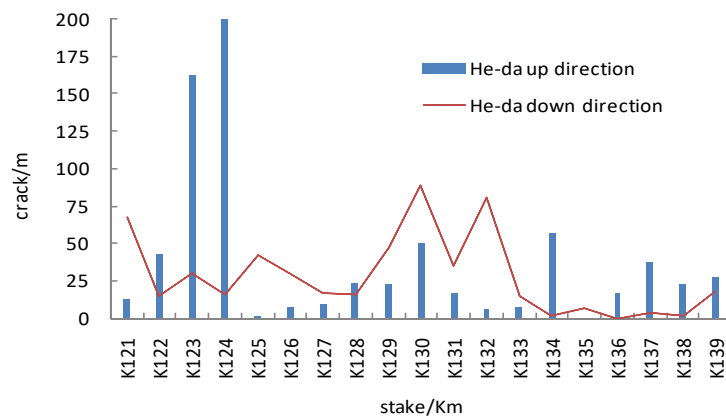


Figure 1. Cracks distribution with mileage in the same section.

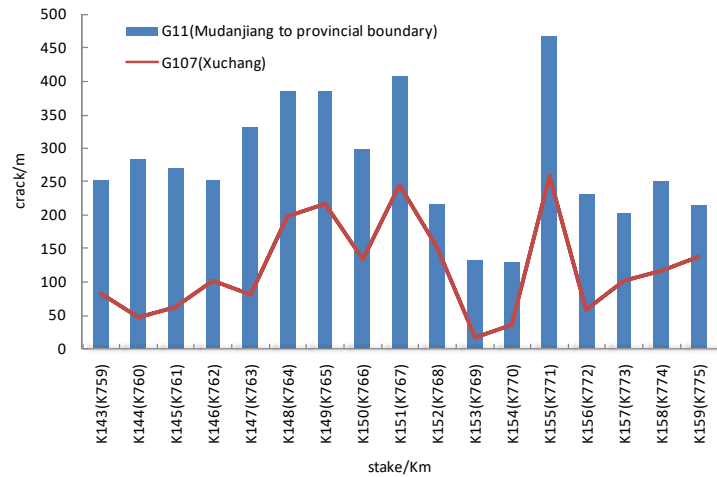


Figure 2. Cracks distribution with mileage in different sections.

Traffic data are obtained by perennial observation of traffic volume, that is, the annual observation time is 365 days and the daily observation time is 24 hours. Because it is difficult to adopt the method of setting up traffic survey stations on the highway to manually calculate the traffic volume of the road sections. Therefore, the use of highway toll stations for road traffic statistics.

The actual number of actions of different vehicle axle types of the survey carried out using the HDS-1-type culvert axle, coal checkpoint, SM2000S axle load automatic detection system and other weight measurement equipment on the actual axle load on the road for 24 hours of full monitoring, classification recorded Survey sections of different shaft weight axis, for summary. Figure 3 shows the traffic volume survey of He-da highway from Mudanjiang to provincial boundary Figure 4 shows the Type I (single shaft, single wheel), type II shaft (single shaft, double wheel on each side), type III shaft (double shaft, double wheel on each side) and IV Type shaft (triple shaft, double wheel on each side) the actual number of times.



Figure 3. He-da highway from Mudanjiang to provincial boundary.

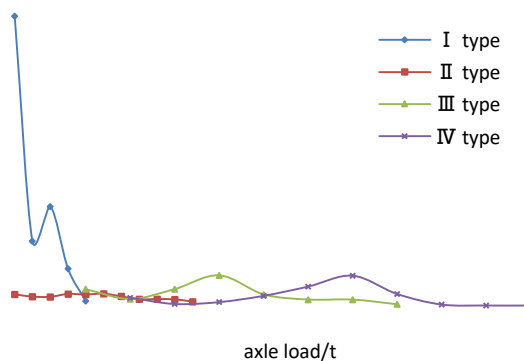


Figure 4. Actual loading times of different vehicles.

He-da highway where the location of the climate has obvious characteristics of seasonally frozen regions, the climate data comes from 80 meteorological observation stations, and the data of temperature has a total of 168 months from 2003 to 2016. Table 1 shows the survey results of some surveys Data include the temperature of the area under investigation, average wind speed, rainfall, snowfall and the number of days below 0 °C.

Table 1. Road section climate.

| year/ month | The highest temperature/°C | Lowest temperature/°C | average temperature/°C | average wind speed /km·h ⁻¹ | Rainfall /mm | Snowfall /mm | Less than 0 °C days /d |
|----------------|-------------------------------|--------------------------|---------------------------|--|-----------------|-----------------|---------------------------|
| 2012/1 | - 3 °C | - 33 °C | - 20.5 °C | 16.05 | 0 | 8 | 31 |
| 2012/2 | 0 °C | - 29 °C | - 16.5 °C | 16.75 | 0 | 9 | 28 |
| 2012/3 | 5 °C | - 21 °C | - 7.5 °C | 17.15 | 0 | 7 | 31 |

3. Results and Discussion

Mechanistic-Empirical Pavement Design Guide [16–20] is a research project of AASHTO and the National Highway of America, which calculates the stress and strain of pavement structures using traditional mechanics, supplemented by experience Methods to make up for the gap between the indoor test and field test, fully taking into account the characteristics of the pavement materials, pavement traffic conditions and climatic conditions.

CRK (Crack) and *SF* (Site Factor) are two prediction models based on MEPDG. *CRK* indicates the proportion of cracks in cement concrete slab. The cracks include horizontal, vertical and diagonal cracks, corner fractures and cross fractures. *CRK* is a composite function based on *DI_F* (fatigue damage). Prediction of *DI_F* is based on Miner's principle of damage accumulation. It is expressed by the ratio of the number of repetitions of traffic load to the number of repetitions of allowed load, as shown in the following formula 1; *SF* represents environmental impact prediction model, which is a composite function of the age of the material, the freezing index and the passing rate of the roadbed material when the mesh size is 0.075 mm, as shown in Equation 2 below; *FI* denotes the freezing index, as shown in Equation 3 below.

$$CRK = \frac{1}{1 + DI_F^{-1.98}} \quad (1)$$

$$SF = AGE(1 + 0.5556 * FI)(1 + P_{200}) * 10^{-6} \quad (2)$$

$$FI = \sum_{i=0}^n (0 - T_i) \quad (3)$$

Where: *DI_F* means fatigue damage, *AGE* means the service life of the road, *FI* means the freezing index; *P₂₀₀* means the passing rate of roadbed material when the mesh size is 0.075 mm; *n* means the number of days below 0 °C and *T_i* means the average daily temperature.

To characterize the impact of *FI* on *DBL* in the environmental impact models of seasonal and non-seasonally frozen regions, the *SF* comparison between the Mudanjiang to provincial boundary in He-da highway and Xu-chang section in the national highway 107 shown in Figure 5. Seasonal frost-free period throughout the year between 100 to 150 days in seasonally frozen regions, the annual average temperature between -5 °C~9 °C, the climate is significant. From 2003 to 2016, the *SF* of Mudanjiang to the provincial boundary in He-da highway was $6.13 \times 10^{-3} \sim 86.80 \times 10^{-3}$. From 2003 to 2016, the *SF* of National Highway107 was $0.48 \times 10^{-3} \sim 6.07 \times 10^{-3}$, the *SF* of Mudanjiang to the provincial boundary in He-da highway was larger than the *SF* of Xu-chang Section in national highway 107 10.60 times to 17.84 times, the difference was significant.

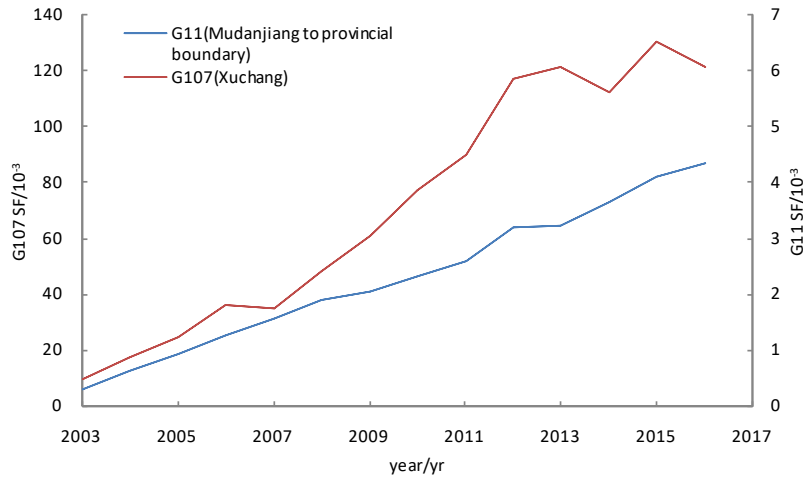


Figure 5. Comparison of *SF*.

Predictive models include two forms. The first type of prediction model is called the direct prediction model, that is, *DBL* and *CRK*, *DBL* and *SF* directly construct the corresponding functional relationship. The second prediction model is to use the *SF* index as a parameter in the *DBL* and *CRK* prediction models. The data model prediction process mainly includes: without introducing other parameter items, fitting the *DBL* and *CRK*, *DBL* and *SF* respectively according to the distribution of scatter plot to determine the linear or nonlinear relationship; In order to accurately characterize the impact of road age on pavement damage, also in order to reflect the difference caused by the same traffic load but different environmental parameters, introduce *SF* into *DBL* and *CRK* models as a parameter; According to the above results of the fitting hypothesis testing and analysis of model validity and verification, and come to accurate and reasonable prediction model.

Based on the 168-month observation data of traffic volume and environmental parameters collected from the site of Mudanjiang to the provincial boundary in He-da highway and the *CRK* model under MEPDG theory, the cumulative *CRK* of 168-month surveyed road sections was obtained. The *DBL* and the *CRK* of the initial scatter plot fitted to a linear relationship, the logarithmic relationship and the exponential relationship in Figure 6.

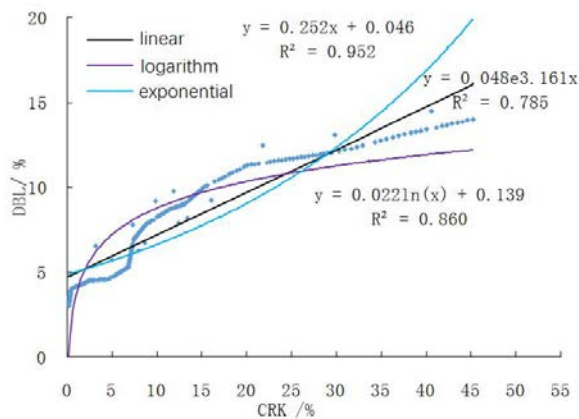


Figure 6. *DBL* and *CRK* fitted curves.

As can be seen from the three regression models in Figure 6, the correlation coefficients of the linear regression, logarithmic regression and exponential regression are 0.952, 0.860 and 0.785, respectively, and the three correlation coefficient values are large, *CRK* and *DBL* is strongly correlated with the previously analyzed. When *CRK* tends to 0, the initial *DBL* value in the linear regression is 0.046, which is obviously smaller than the initial *DBL* values of logarithmic regression and exponential regression, which is consistent with the analysis that basically no cracks occur in concrete pavement. Therefore, considering only the deterministic coefficients obtained from the above regression equations and the reasonableness of fitting results, there should be a linear relationship between *DBL* and *CRK*.

Чжао Ц., Чен П., Ван Д., Вэй Ю. Модель для прогнозирования повреждений дорожного покрытия в районе сезонного промерзания // Инженерно-строительный журнал. 2018. № 8(84). С. 57–66.

It can be seen from the above analysis that when the same repeated load caused by traffic is present, there is a big difference in pavement damage due to different environmental factors. Therefore, in order to characterize the effect of same traffic load but different environmental factors on the prediction model, the environmental impact factors need to be considered in order to enhance the environmental factors on the damage of pavement. According to the results of fitting, the more reasonable forecasting relation model is obtained. Based on the above mentioned climatic data of the location of He-da Highway, a total of 168 survey data are collected in monthly. Combined with the *SF* prediction model under MEPDG, the cumulative *SF* value of 168 months was obtained. The scatter plot between *DBL* and *SF* in field survey was initially fitted to a linear, logarithmic and exponential relationship is shown in Figure7.

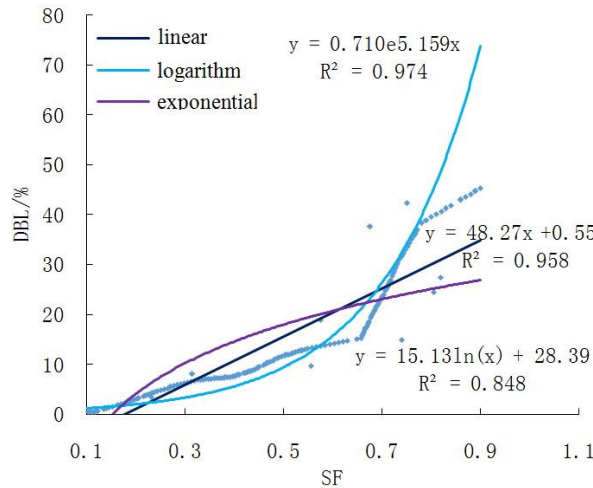


Figure 7. *DBL* and *SF* fitted curves.

As can be seen from the three regression models in Figure 7, the correlation coefficients of linear regression, logarithmic regression and exponential regression were 0.958, 0.848 and 0.974, respectively. Among the three correlation coefficient, the regression coefficient of the exponential model has the largest correlation, indicating that the exponential regression has the strongest correlation. When the *SF* tends to 0, the minimum initial *DBL* is 0.551, with just completed the opened concrete pavement basically no crack analysis is also consistent. Therefore, only from the above regression equation can be drawn from the coefficient of determination and reasonable consideration, the linear regression appears to be relatively reasonable.

In order to further verify the correlation among *DBL*, *CRK* and *SF*, SPSS software was used to analyze the correlation between *DBL* and *CRK* (Table 2); *DBL*, *CRK* and *SF* (Table 3) were analyzed for partial correlation. In Table 2, *CRK* and *DBL* correlation coefficient was 0.944, the significance level was 0.000, less than 0.05, indicating that *CRK*, *DBL* correlation was positive, and strong correlation. In Table 3, when *DBL* was not controlled, the correlation coefficient of *CRK* and *SF* was 0.990, the significance level was 0.000 and less than 0.01. When *DBL* was controlled, the correlation coefficient of *CRK* and *SF* was 0.935 and the significance level was 0.000, so *CRK*, *SF* and *DBL* is positive and highly correlated.

Table 2. Correlation of *DBL* and *CRK*.

| Control variables | | <i>DBL</i> /month | <i>CRK</i> /month |
|-------------------|--------------------------|-------------------|-------------------|
| <i>DBL</i> /month | Pearson Correlation | 1.000 | 0.944 |
| | Significance (Bilateral) | — | 0.000 |
| | N | 168.000 | 168.000 |
| <i>CRK</i> /month | Pearson Correlation | 0.944 | 1.000 |
| | Significance (Bilateral) | 0.000 | — |
| | N | 168.000 | 168.000 |

Table 3. Partial Correlation of DBL, CRK and SF.

| Control variables | | CRK/Month | SF/Month | DBL/Month |
|-------------------|--------------------------|-----------|----------|-----------|
| CRK/Month | Pearson Correlation | 1.000 | 0.990 | 0.944 |
| | Significance (Bilateral) | — | 0.000 | 0.000 |
| | df | 0.000 | 166.000 | 166.000 |
| SF/Month | Pearson Correlation | 0.990 | 1.000 | 0.924 |
| | Significance (Bilateral) | 0.000 | — | 0.000 |
| | df | 166.000 | 0.000 | 166.000 |
| DBL/Month | Pearson Correlation | 0.944 | 0.924 | 1.000 |
| | Significance (Bilateral) | 0.000 | 0.000 | — |
| | df | 166.000 | 166.000 | 0.000 |
| CRK/Month | Pearson Correlation | 1.000 | 0.935 | — |
| | Significance (Bilateral) | — | 0.000 | — |
| | df | 0.000 | 165.000 | — |
| SF/Month | Pearson Correlation | 0.935 | 1.000 | — |
| | Significance (Bilateral) | 0.000 | — | — |
| | df | 165.000 | 0.000 | — |

3.1. Selection and determination of model parameters

According to the above *DBL* and *CRK*, *DBL* and *SF* respectively regression model and various forms of model try to comparison analysis, that *DBL* as dependent variable and *CRK*, *SF* as an independent variable closer to the linear relationship. For further verification, *CRK* and *SF* data accumulated 168 months were imported into the SPSS software. Multiple linear regression and multivariate nonlinear regression were performed respectively. The constant items and Variable coefficients are seen in Tables 4 and 5.

Table 4. SPSS multiple linear regression coefficient.

| model | Non-standardized coefficient | | Standard factor | t Sig. | |
|------------|------------------------------|----------------|-----------------|--------|-------|
| | B | Standard error | trial version | | |
| (constant) | 0.181 | 0.013 | — | 14.099 | 0.000 |
| CRK/Month | 5.701 | 0.663 | 1.523 | 8.601 | 0.000 |
| SF/Month | 0.309 | 0.094 | 0.585 | 3.300 | 0.001 |

Table 5. SPSS non-linear regression parameter estimates.

| parameter | Estimate | Standard error | 95% Confidence interval | |
|-----------|----------|----------------|-------------------------|--------|
| | | | Lower limit | Capped |
| a | -0.336 | 0.028 | -0.390 | -0.281 |
| b | 4.949 | 0.218 | 4.520 | 5.379 |
| c | 0.077 | 0.011 | 0.055 | 0.099 |

As can be seen from Table 4, the coefficients of *CRK* and *SF* in regression equation are 5.701 and 0.309. When the two indexes of *CRK* and *SF* tend to 0, the constant term is 0.181. The initial *DBL* in multivariate linear regression is also relatively small, and the evaluation result is reasonable. In table 5, the confidence intervals of the three parameters of the nonlinear equation do not contain 0, which proves that all three parameters are statistically significant. However, when the *CRK* and *SF* tend to be 0, *DBL* is negative. As an index to evaluate the damage status of concrete pavement, *DBL* can not have a negative value, which is inconsistent with the actual project situation and inconsistent with the positive correlation in the above correlation analysis. In addition, though the SPSS software for multiple linear regression, use

the stepwise regression method, the correlation coefficient R^2 from 0.892 to 0.899. In summary, the prediction model for the damage of *concrete* pavement in seasonally frozen regions is:

$$DBL = 0.181 + 5.701CRK + 0.309SF \quad (4)$$

In order to validate the effectiveness of the predictive model for predicting the damage of concrete pavement in seasonally frozen regions, SPSS software was used for statistical analysis. CRK and SF were all considered as independent variables, and global analysis was conducted by stepwise regression. The order of entry was CRK , SF , and no variables were removed, the results of stepwise regression analysis in Table 6. From the analysis of the model, all the variables and constant items passed the parameter test, and all are positive, which is consistent with the actual situation. From the Table 6, the contribution rate of variance is more than 90 % from itself, Eigen values are only 2.887 and less than 10 (SPSS parameters are considered to be collinearity when the default number of states is greater than 10); the maximum value of conditional index is 24.03 and less than 30 (SPSS parameters are considered to be collinearity when the default number of states is greater than 30) There is no multicollinearity. The above analysis validates the stability of the prediction model for the damage of concrete pavement in seasonally frozen regions.

Table 6. Collinearity diagnosis.

| model | dimension | Eigen values | Conditional index | Variance ratio | | |
|-------|-----------|--------------|-------------------|----------------|--------------|-------------|
| | | | | constant | CRK /Month | SF /Month |
| 1 | 1 | 1.932 | 1.000 | 0.030 | 0.030 | — |
| | 2 | 0.068 | 5.324 | 0.970 | 0.970 | — |
| 2 | 1 | 2.887 | 1.000 | 0.010 | 0.000 | 0.000 |
| | 2 | 0.111 | 5.090 | 0.330 | 0.000 | 0.010 |
| | 3 | 0.001 | 24.030 | 0.660 | 1.000 | 0.990 |

In order to verify the accuracy of the predictive model for predicting the damage of concrete pavement in seasonally frozen regions, the prediction data of the prediction model of concrete pavement damage in seasonally frozen regions are derived from the measured data of Mudanjiang to provincial boundary in He-da highway as shown in Figure 8: The predicted value of the transitional model in the region from 2012 to 2016 is closer to the measured value of DBL than the predicted value of the traditional model of Sun Lijun, which shows that the accuracy of the prediction model is guaranteed.

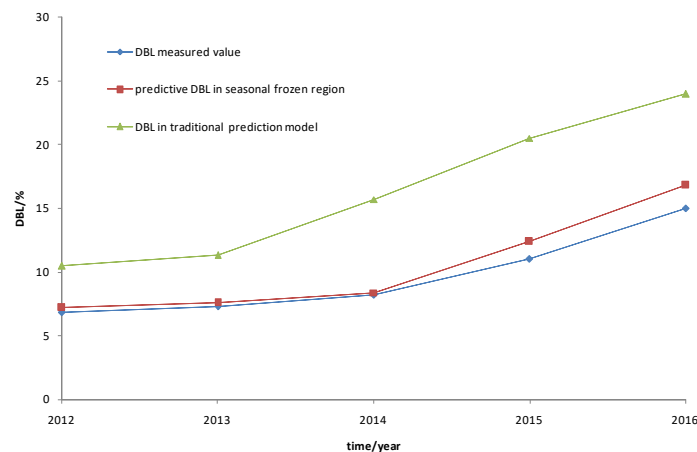


Figure 8. DBL predicted and measured values contrast.

4. Conclusion

1. DBL showed obvious differences with different traffic load and environmental factors. When the road age and climate status of the survey section are consistent, the difference in traffic volume accounts for 3.45 % ~ 6.23 % of the total traffic volume in the survey interval. The difference in the width of the pavement crack is between 8.067 and 55.681 m. When the quantity and the road structure are consistent,

the annual average temperature is 6.1 °C and 14.5 °C, respectively, and the width of the road surface crack caused by the climate difference is between 64.795 and 248.937 m.

2. There was a large difference in SF between seasonally frozen and non-seasonally frozen regions. When the annual average temperature between the seasonally and non-seasonally frozen areas differs by 8.4 ~ 10.2 °C, the SF of the surveyed section of the seasonally frozen area is 10.6 ~ 17.84 times larger than that of the non-seasonally frozen area.

3. Indicator CRK and SF have a strong positive correlation with DBL , which ensures the correctness of the linear correlation of the model. The correlation coefficient between DBL and CRK is 0.944, while the correlation coefficient between DBL and SF is 0.924, with significance level being 0, less than 0.05, and the correlation between CRK and SF and DBL is positive and strong.

4. The predictive model for the damage of concrete pavement in seasonally frozen regions can predict the damage condition of the concrete pavement through the parameters of traffic load, road age, freezing index and so on. In the collinearity diagnosis of the model, more than 90 % of the variance comes from itself. The maximum eigenvalue is only 2.887, less than 10. The maximum value of the conditional index is 24.03, which is less than 30, which proves that there is no multicollinearity problem at this time.

5. The predicted value of the model is closer to the measured value of DBL than the predicted value of traditional model, which ensures the accuracy of the model prediction.

References

1. Zhou, L. Research on performance evaluation and prediction of expressway asphalt pavement. Nanjing: Southeast University, 2015.
2. Liu, B., Yao, Z. Asphalt pavement performance prediction. Journal of China Highway, 1991. No. 4(02). Pp. 5–15.
3. Zhang, Z., Wang, X. Service performance prediction model of asphalt pavement with two corrected parameters. Journal of Traffic and Transportation Engineering, 2007. No. 7(05). Pp. 54–57.
4. He, D. Study on the Prediction of Highway Asphalt Pavement Performance Based on Combination Forecasting Model [J]. Journal of Highway Engineering. 2015. Vol. 40. No. 06. Pp. 264–270.
5. Wu, J., Liu, D., Li, F., Wang, X. Performance prediction of asphalt pavement maintenance based on time series analysis. Journal of Chang'an University (Natural Science Edition). 2015. 35(03). Pp. 1–7.
6. Tang, X., Dai, J., Jia, Q. Research on predicting expressway pavement performance by parameter adaptive tracking method. Journal of Chang'an University (Natural Science Edition). 2007. 27(03). Pp. 31–33.
7. Guo, Z., Tan, Y., Ma, G., Pan, Y., Chen, C. Measurement of driving spirit fatigue based on BP neural network. Journal of Harbin Institute of Technology. 2014. 46(08). Pp. 118–121.
8. Chen, J., You, W., Tian, J. Improvement of Economic Forecasting Method Based on Neural Network. Journal of Harbin Institute of Technology. 2006. No. 38(06). Pp. 897–898.
9. Ni, F., Fang, Y., Xue, Z. Application of time series in prediction of road roughness [J]. Journal of Southeast University (Natural Science Edition). 2006. No. 36(04). Pp. 634–637.
10. Wang, G., An, J., Chen, R. Application of gray theory in pavement performance prediction. Journal of Highway and Transportation Research and Development. 2002. No. 19(03). Pp. 16–19.
11. Du, E., Ma, S., Jing, H. Asphalt pavement performance prediction model based on gray system theory. Journal of Tongji University (Natural Science Edition). 2010. No. 38(08). Pp. 1161–1164.
12. Zeng, Q. Study on performance evaluation and prediction of cement pavement based on support vector machine.

Литература

1. Zhou L. Research on performance evaluation and prediction of expressway asphalt pavement. Nanjing: Southeast University, 2015.
2. Liu B., Yao Z. Asphalt pavement performance prediction // Journal of China Highway, 1991. No. 4(02). Pp. 5–15.
3. Zhang Z., Wang X. Service performance prediction model of asphalt pavement with two corrected parameters // Journal of Traffic and Transportation Engineering, 2007. No. 7(05). Pp. 54–57.
4. He D. Study on the Prediction of Highway Asphalt Pavement Performance Based on Combination Forecasting Model [J] // Journal of Highway Engineering. 2015. Vol. 40. № 06. Pp. 264–270.
5. Wu J., Liu D., Li F., Wang X. Performance prediction of asphalt pavement maintenance based on time series analysis // Journal of Chang'an University (Natural Science Edition). 2015. № 35(03). Pp. 1–7.
6. Tang X., Dai J., Jia Q. Research on predicting expressway pavement performance by parameter adaptive tracking method // Journal of Chang'an University (Natural Science Edition). 2007. № 27(03). Pp. 31–33.
7. Guo Z., Tan Y., Ma G., Pan Y., Chen C. Measurement of driving spirit fatigue based on BP neural network // Journal of Harbin Institute of Technology. 2014. № 46(08). Pp. 118–121.
8. Chen J., You W., Tian J. Improvement of Economic Forecasting Method Based on Neural Network // Journal of Harbin Institute of Technology. 2006. № 38(06). Pp. 897–898.
9. Ni F., Fang Y., Xue Z. Application of time series in prediction of road roughness [J] // Journal of Southeast University (Natural Science Edition). 2006. № 36(04). Pp. 634–637.
10. Wang G., An J., Chen R. Application of gray theory in pavement performance prediction // Journal of Highway and Transportation Research and Development. 2002. № 19(03). Pp. 16–19.
11. Du E., Ma S., Jing H. Asphalt pavement performance prediction model based on gray system theory // Journal of Tongji University (Natural Science Edition). 2010. № 38(08). Pp. 1161–1164.
12. Zeng Q. Study on performance evaluation and prediction of cement pavement based on support vector machine. Changsha: Changsha University of Science and Technology, 2008.

Чжао Ц., Чен П., Ван Д., Вэй Ю. Модель для прогнозирования повреждений дорожного покрытия в районе сезонного промерзания // Инженерно-строительный журнал. 2018. № 8(84). С. 57–66.

- Changsha: Changsha University of Science and Technology, 2008.
13. Zhang, T. Purpose performance prediction of pavement based on artificial neural network. Harbin: Harbin Institute of Technology, 2009.
 14. Zhang, F., Lin, B., Feng, D., Ling, X. Construction of permanent deformation of highway subgrade under long-term traffic load in seasonal frozen soil area. Journal of Harbin Institute of Technology. 2017. No. 49(03). Pp. 120–126.
 15. Tan, Y., Xu, H., Zhou, C., et al. Space field distribution law of subgrade in seasonal frozen area. Journal of Harbin Institute of Technology. 2011. No. 43(08). Pp. 98–102.
 16. Kim, S., Ceylan, H., Ma, D., Gopalakrishnan, K. Calibration of Pavement ME Design and Mechanistic-Empirical Pavement Design Guide Performance Prediction Models for Iowa Pavement Systems. Journal of Transportation Engineering. 2014. No. 140(10). Pp. 348–360.
 17. Karavaşin, M., Terzi, S. Performance model for asphalt concrete pavement based on the fuzzy logic approach // Transport. 2014. No. 29(1). Pp. 18–27.
 18. Abaza, K.A. Deterministic Performance Prediction Model for Rehabilitation and Management of Flexible Pavement // International Journal of Pavement Engineering. 2004. No. 5(2). No. 111–121.
 19. Peng, T., Wang, X.L., Chen, S.F. Pavement Performance Prediction Model Based on Weibull Distribution. Applied Mechanics and Materials. 2013. No. 2578(378). Pp. 61–64.
 20. Wang, H., Zhang, C., You, Z., et al. Calibration of rutting prediction model in MEPDG based on mathematical statistics method [J]. Journal of Chang'an University (Natural Science Edition). 2013. No. 33(06). Pp. 1–7.
 21. Zhang, T. Purpose performance prediction of pavement based on artificial neural network. Harbin: Harbin Institute of Technology, 2009.
 22. Zhang, F., Lin, B., Feng, D., Ling, X. Construction of permanent deformation of highway subgrade under long-term traffic load in seasonal frozen soil area // Journal of Harbin Institute of Technology. 2017. No. 49(03). Pp. 120–126.
 23. Tan, Y., Xu, H., Zhou, C., et al. Space field distribution law of subgrade in seasonal frozen area // Journal of Harbin Institute of Technology. 2011. No. 43(08). Pp. 98–102.
 24. Kim, S., Ceylan, H., Ma, D., Gopalakrishnan, K. Calibration of Pavement ME Design and Mechanistic-Empirical Pavement Design Guide Performance Prediction Models for Iowa Pavement Systems // Journal of Transportation Engineering. 2014. No. 140(10). Pp. 348–360.
 25. Karavaşin, M., Terzi, S. Performance model for asphalt concrete pavement based on the fuzzy logic approach // Transport. 2014. No. 29(1). Pp. 18–27.
 26. Abaza, K.A. Deterministic Performance Prediction Model for Rehabilitation and Management of Flexible Pavement // International Journal of Pavement Engineering. 2004. No. 5(2). No. 111–121.
 27. Peng, T., Wang, X.L., Chen, S.F. Pavement Performance Prediction Model Based on Weibull Distribution // Applied Mechanics and Materials. 2013. No. 2578(378). Pp. 61–64.
 28. Wang, H., Zhang, C., You, Z., et al. Calibration of rutting prediction model in MEPDG based on mathematical statistics method [J] // Journal of Chang'an University (Natural Science Edition). 2013. No. 33(06). Pp. 1–7.

Qianqian Zhao,
045188028393; 492954791@qq.com

Peifeng Cheng,*
13946139402; chengpeifeng@126.com

Jianwu Wang,
13603625185; nihaone@163.com

Yuwei Wei,
13783869126; weiyuwei1991@qq.com

Цяньцянь Чжао,
045188028393; эл. почта: 492954791@qq.com

Пифэнг Чен,*
13946139402;
эл. почта: chengpeifeng@126.com

Дзеньу Ван,
13603625185; эл. почта: nihaone@163.com

Юйвэй Вэй,
13783869126;
эл. почта: weiyuwei1991@qq.com

© Zhao, Q., Cheng, P., Wang, J., Wei, Y., 2018

doi: 10.18720/MCE.84.7

The building extension with energy efficiency light-weight building walls

Надстройка существующих зданий с применением легких стен по каркасной технологии

V.V. Sergeev,
M.R. Petrichenko,
D.V. Nemova,
E.V. Kotov,
D.S. Tarasova*,
A.V. Nefedova,
Peter the Great St. Petersburg Polytechnic University, St. Petersburg, Russia
A.B Borodinecs,
Riga Technical University, Riga, Latvia

д-р техн. наук, профессор,
член-корреспондент РАН, проректор по научной работе В.В. Сергеев,
д-р техн. наук, заведующий кафедрой М.Р. Петриченко,
канд. техн. наук, доцент, директор центра Д.В. Немова,
аспирант Е.В. Котов,
ассистент Д.С. Тарасова,*
студентка А.В. Нефедова,
Санкт-Петербургский политехнический университет Петра Великого,
Санкт-Петербург, Россия
д-р техн. наук, профессор А. Бородинец,
Рижский технический университет, г. Рига, Латвия

Key words: light wall; light steel thin-walled structures; energy efficiency; civil engineering; buildings; construction

Ключевые слова: каркасные ограждающие конструкции; легкие стены по каркасной технологии; тонкостенные конструкции; надстройка; энергоэффективность

Abstract. The effective use of plan area is more crucial in high-rise buildings, since they are mostly narrow compared to the conventional buildings. The measurement of the overall thermal transmittance of lightweight steel-framed walls, including the effect of thermal bridges due to metal structure, is a challenge for designers, engineers and energy audits. In this paper the energy efficiency light-weight wall technology for over story of buildings was considered. In this work was developed a mathematical model of non-stationary heat transfer through the enclosing wall using the lightweight wall technology and evaluated the efficiency of various designs of lightweight wall. In this model, the profile perforation is taken into account due to the results of the solution of the test problem while maintaining the possibility of using structured grids with the number of elements not exceeding 1 million, which allowed to obtain more accurate results.

Аннотация. Вопрос об увеличении площади зданий становится все более актуальным. В данной статье рассмотрено решение по устройству легких стен по каркасной технологии. Сделан вывод об экономической и энергетической эффективности использования данной технологии для жилого и общественного строительства. Были построены математические модели фрагментов тонкостенного профиля и термокаркаса. Сделан вывод об эффективности работы термопрофиля только в совокупности с утеплителем. Исследовано влияние анизотропных включений в конструкцию, посредством построения математической модели в ПК ANSYS для фрагментов термопрофиля и легких стен по каркасной технологии. В рассматриваемой модели перфорация профиля учтена за счет результатов решения тестовой задачи при сохранении возможности использования структурированных сеток с числом элементов не превышающих 1 млн, что позволило получить более точные результаты.

1. Introduction

Construction becomes dependent on climatic parameters, seasons, transport accessibility. Low temperatures, high wind speed and heavy rainfall make us care not about the architectural appearance of buildings, but about their energy and economic component.

Сергеев В.В., Петриченко М.Р., Немова Д.В., Котов Е.В., Тарасова Д.С., Нефедова А.В., Бородинец А. Надстройка существующих зданий с применением легких стен по каркасной технологии // Инженерно-строительный журнал. 2018. № 8(84). С. 67–74.

In recent decades, the issue of increasing the buildings area due to overstory is becoming increasingly important. The desire of investors to use the already built-up area more effectively is justified [1–5].

The purpose of this work is to determine the effectiveness of the use of energy efficiency lightweight building walls for high-rise construction.

Work tasks that need to be solved to achieve the goal:

- 1) Development of a mathematical model of non-stationary heat transfer through the enclosing wall using the lightweight wall technology.
- 2) Evaluation of efficiency of various designs of lightweight wall.

The purpose of the simulation is to determine the presence and location of cold bridges, in the presence of which, expensive heat out of the room; such a building can not be called energy efficient. Heat loss can also occur because of heterogeneity of enclosing structures, including the presence of heat-stressed elements.

With the development of computer technology it became possible to create mathematical models of various types of structures, including enclosing, using all kinds of domestic and foreign software systems. The use of the software allows for rapid thermal diagnostics of external heterogeneous multilayer enclosing structures with different geometric characteristics and thermal properties of the materials used in real operating conditions [6–10].

In work [11-18] because of the conducted research of mathematical model of the protecting design in the ANSYS PC recommendations on creation of a humidity mode indoors are given.

Thus, in this paper, for the construction of a mathematical model of the enclosing structure and the study of the heat transfer process, we will use the ANSYS software package based on the finite element method [19–27].

2. Materials and Methods

The rectangular region of the enclosure structure excluding cladding is selected for research of the nonstationary heat transfer lightweight wall. However, the most interesting is the steady-state operation of lightweight wall at specified climatic parameters and temperature at the inner boundary of the frame.

The structure of the wall consists of the main frame: rack and guide Ists profiles of galvanized steel with perforation. The width of the guide profile is 154 mm, the width of the rack profile is 150 mm. Inside the profile is a mineral wool insulation based on basalt fiber with a thickness of 150 mm, a density not more than 35 kg/m³. Outside, the insulation is closed with a layer of hydro-windproof membrane, installed overlap, which eliminates moisture from the outside on the surface of the insulation, and prevents weathering of low density insulation fibers. On the opposite side of the frame are installed guides of Z-profile, between which is placed a layer of insulation thickness of 50 mm, a density not less than 90 kg/m³. From the room side is arranged the base for the interior finish of two layers of plasterboard, insulation between layers. All materials are fastened together by exhaust rivets or stainless steel screws. The lightweight wall is fixed on the floor slabs through the bearing brackets. A paronite gasket is installed between the bracket and the floor slab.

The light-weight wall structure is presented at Figure 1. Value of heat transfer resistance of enclosing walls is 5.06 [m²·C/W]

The enclosing structure consist of: ceramic granite 10 mm; air gap 40 mm, windscreens, insulation in the thermal profile 150 mm; insulation 50 mm; gypsum wallboard 25 mm.

The following conditions were accepted as assumptions in the construction of a mathematical model:

- 1) thermal characteristics of the materials in the lightweight wall do not depend on the humidity and temperature of the material and are taken under normal conditions;
- 2) heat transfer is carried out only due to the thermal conductivity of the material;
- 3) do not take into account in the design of such elements as: slopes, tides, fire cut-offs, elements of ventilated facade;
- 4) take account of the perforation of the walls of the thermal profile is carried out using the input correction coefficient obtained when comparing the fragment profiles with and without perforation.

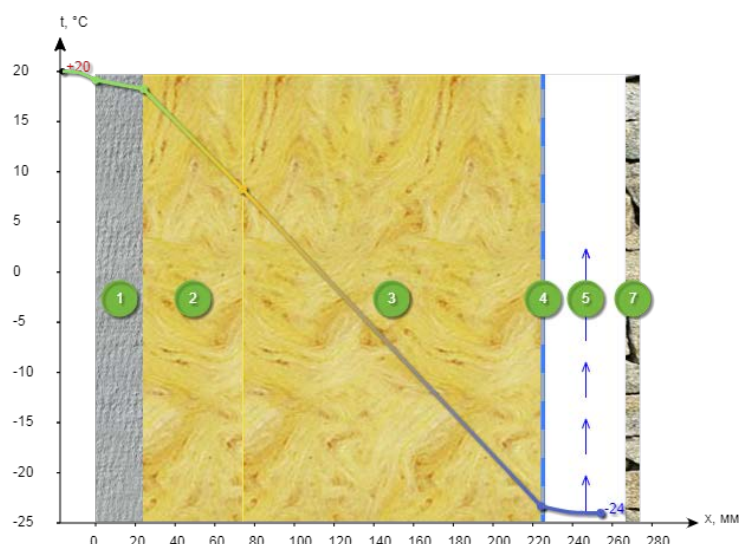


Figure 1. The light-weight wall structure.

For the mathematical formulation of the problem are given the geometric parameters of structures and thermal characteristics. Heat transfer in a multilayer enclosing structure is reduced to the solution of the direct heat transfer problem, in which it is required to obtain a temperature field under specified boundary conditions.

The solution of the direct heat transfer problem is reduced to the solution of the differential equation of thermal conductivity at the given thermal conductivity coefficients λ (1).

$$\frac{\partial t}{\partial \tau} = \lambda \left(\frac{\partial^2 T}{\partial x^2} + \frac{\partial^2 T}{\partial y^2} + \frac{\partial^2 T}{\partial z^2} \right), \quad (1)$$

where T – temperature, τ – time, x, y, z – coordinates of the temperature function, λ – coefficient of thermal conductivity.

To calculate the problem of conjugate heat transfer at the interface of two materials, the conditions of equality of temperatures and heat fluxes are set.

Boundary conditions of the first kind, in which the temperature distribution on the surface of the body for each moment of time is given: $T_m = f(y)$, the special case $T_m = \text{const}$;

Boundary conditions of the second kind, in which the heat flux for each point of the surface of the body and for any point in time $q_c = f(y, \tau)$, the special case $q_c = \text{const}$;

Boundary conditions of the third kind, in which the ambient temperature is set TSR and the law of heat transfer between the surface of the body and the environment in the cooling and heating process, which is described by Newton-Richman's law: the heat flux density q is proportional to the temperature difference between the surface of the body and the environment.

$$q = \alpha (T_{cp} - T_m), \quad (3)$$

where is the heat transfer coefficient.

In our case, there are boundary conditions of the third kind, as we have information about the ambient temperature outside the structure (indoor temperature of the building and outdoor temperature). However, since the value of the heat transfer coefficient (3) is unknown for the solution search, the boundary conditions of the first kind shifted for the walls (boundaries) by 1 m from the calculated region of the solid structure were applied.

On the walls of the calculated areas are given boundary conditions of constant temperature (conditions of the first kind): the temperature of the hot wall $T_h = 293$ K (20 °C); the temperature of the cold

wall $T_C = 233 \text{ K}$ ($-40 \text{ }^\circ\text{C}$). Symmetry conditions are set for the walls: $dV/dy = 0$. The temperature on the surface of the solid is obtained convective, and the center of the heat conduction.

For a solid according to Fourier law: the amount of heat transferred is proportional to temperature, time and cross-sectional area.

The amount of heat transferred to the unit area and the unit of time pattern is as follows:

$$q = -\lambda \text{grad}T, \tag{4}$$

Fourier law for the case of heat transfer through a homogeneous layer (wall):

$$q = -\lambda \frac{dT}{dx}, \tag{5}$$

When solving the temperature problem for a wall consisting of several homogeneous layers with different properties, it is necessary to take into account the conditions at the boundaries of the regions: according to the law of energy conservation, the heat flow must be constant and for all layers the same. Therefore, for each layer we have:

$$\frac{\lambda_i}{\delta_i} \frac{dT_i(x)}{dx} = \frac{\lambda_{i+1}}{\delta_{i+1}} \frac{dT_{i+1}(x)}{dx}, \tag{6}$$

where λ_i, λ_{i+1} – thermal conductivity coefficients, δ_i, δ_{i+1} – thicknesses.

It is assumed that the boundaries of the regions are close to each other and have a common temperature, i.e. $T_{(x-0)} = T_{(x+0)}$.

The temperature difference between the cold and hot walls is 44 K. Mathematically, natural convection is described by a system of equations (7)–(9), the process of heat transfer in a solid roof structure consisting of homogeneous layers is represented by equations (1)–(6).

3. Results

First of all, it is necessary to analyze the results of modeling the temperature field for the profile fragments without leaks, and thermal profile with leaks. The boundary conditions of the 1st kind related to the distance of 1 m from the structure on both sides were used in the construction. The simulation results are shown in Figure 2 for continuous profile (1, a) and for thermal profile (2, b).

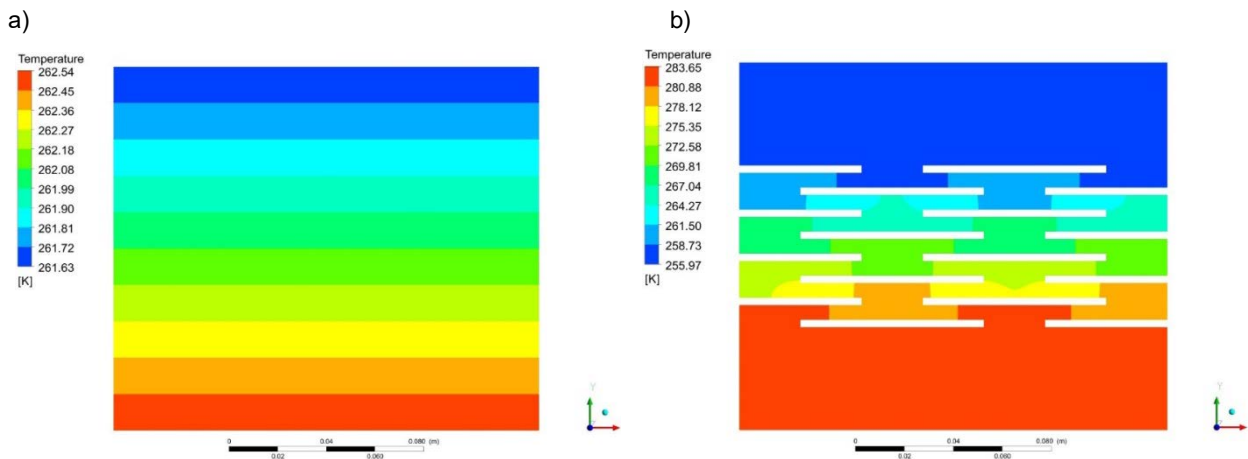


Figure 2. Temperature fields of a) continuous profile, b) thermal profile.

It is also worth noting that all results are obtained on structured grids that provide grid independence of the obtained solutions.

According to the obtained data of temperature fields, it is obvious that the thermal profile with gaps does not give a significant gain in thermal conductivity. Because of the lightweight wall works as a whole, and the insulation in the cavities has a margin of 100 mm on each side, it is obvious that the thermal profile with the gaps works only in conjunction with the mineral wool insulation, which fills the gaps. So the

consideration of an independent thermal profile is an incorrect solution. Thus it is necessary to research an additional model with thermal insulation in the cavities (Figure 3).

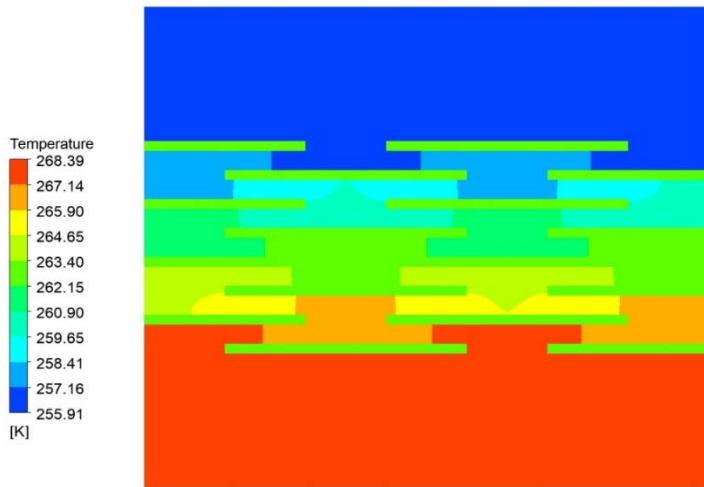


Figure 3. Temperature fields in the thermal profile with insulation in the gaps

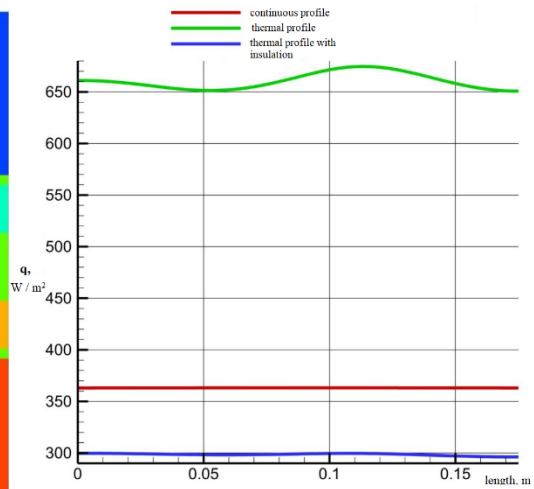


Figure 4. The distribution of the thermal flow q along the length of the structure

On the schedule (Figure 4) the heat flow on the surface of the metal profile and thermal profile with different filling of the gaps is presented. The heat flow through the thermal profile without filling is much larger than the same solid profile (Figure 4). For a uniform profile, the value of the thermal averaged over the length is 363 W/m^2 . The value for the average heat flux through the thermal profile with mineral wool insulation filling is 18 % less. Thus it is possible to formulate the main conclusion about the effectiveness of the thermal profile only in conjunction with the insulation.

The next step is to analyze the results of mathematical modeling of the lightweight wall construction fragment.

The problem was solved in 3D formulation for a continuous profile. From the temperature distribution can be seen (Figure 5), that the greatest heat losses occur through the profile due to its high heat capacity.

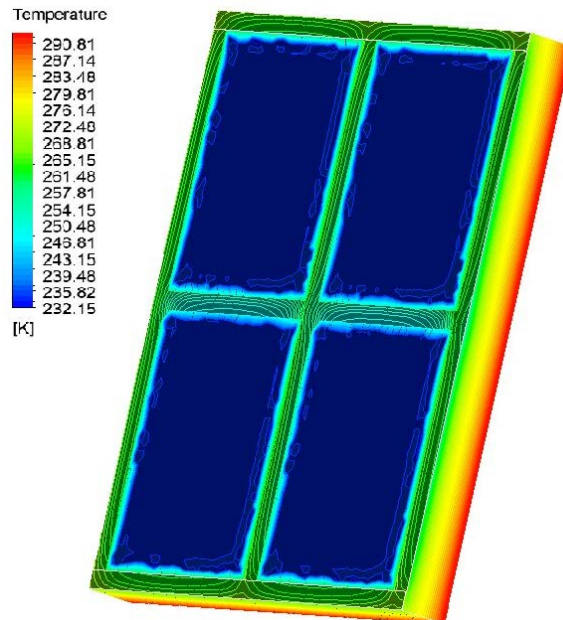


Figure 5. Temperature field of three-dimensional fragment lightweight wall.

Figure 6 presents the simulation results of the same fragment in a 2D configuration (horizontal slit insulation and mullion profile).

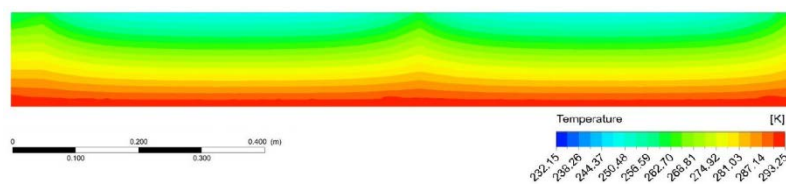


Figure 6. The temperature field of a two-dimensional fragment of the thermal frame structure.

Thus when used in this model thermal profile in tandem with mineral wool insulation, which fills the cavity leaks, local heat loss can be reduced by 18 %, thereby improving the quality of the entire structure.

Many researchers have approached the experimental calculation of the Uoverall for lightweight walls in laboratory conditions [28–33]. The authors [28] combined experimental measurements and numerical simulations in order to calculate the Uoverall of a LSF wall. Another researchers [29] calculated the Uoverall of a LSF wall based on the Zone Method of ASHRAE [31], which is a simplified and accurate numerical method [32]. The difference between the theoretical and experimental values of Uoverall was approximately 9 %.

4. Conclusion

The mathematical models of fragments of thin-walled profile and lightweight wall were constructed. The mathematical model of the profile was made in three configurations: solid steel profile, profile with perforation, and profile with perforation and filling with mineral wool insulation.

The main conclusion on the analysis of the results of the temperature fields of the profile is the efficiency of the thermal profile with perforation only in conjunction with the insulation. Thermal profile without insulation is the least effective of the three selected profile configurations. A profile with filling is 18% more efficient than a solid profile.

Analysis of the results of the temperature fields of the lightweight wall fragment showed obvious results that the greatest heat losses are in areas with the inclusion of a continuous profile. Thus, when using an effective thermal profile in tandem with the insulation, an excellent thermal insulation ability of the entire enclosing structure will be achieved.

References

1. López-Ordóñez, C.F., Roset, J., Rojas-Cortorreal, G. Analysis of the direct solar radiation in the streets of barcelona, based on the relation between its morphology and vegetation [Análisis de la radiación solar directa en las calles de barcelona, en base a la relación entre su morfología y vegetación]. Architecture, City and Environment. 2017. No. 12 (34). Pp. 45–68.
2. de Gracia, A., Navarro, L., Castell, A., Cabeza, L.F. Energy performance of a ventilated double skin facade with PCM under different climates. Energy and Buildings. 2015. No. 91. Pp. 37–42.
3. Cianfrini, C., Corcione, M., Habib, E., Quintino, A. Energy performance of a lightweight opaque ventilated facade integrated with the HVAC system using saturated exhaust indoor air. Energy and Buildings. 2012. No. 20. Pp. 26–34
4. Mohammed, Z.S., Alibaba, H.Z. Integration of Double Skin Facade with HVAC Systems: The State of the Art on Building Energy Efficiency. International Journal of Recent Research in Civil and Mechanical Engineering. 2016. No. 2. Pp. 37–50.
5. Manca, O., Nardini, S. Thermal design of uniformly heated inclined channels in natural convection with and without radiative effects. Heat Transfer Engineering. 2001. No. 22(2). Pp. 13–28.
6. Auletta, A., Manca, O. Heat and Fluid Flow Resulting from the Chimney Effect in a Symmetrically Heated Vertical Channel with Adiabatic Extensions. International Journal of Thermal Sciences. 2002. No. 41. Pp. 1101–1111.
7. Colla, L., Fedele, L., Manca, O., Marinelli, L., Nardini, S. Experimental and numerical investigation on forced convection in circular tubes with nanofluids. Heat Transfer Engineering. 2016. No. 37. Pp. 1201–1210.

Литература

1. López-Ordóñez C.F., Roset J., Rojas-Cortorreal G. Analysis of the direct solar radiation in the streets of barcelona, based on the relation between its morphology and vegetation [Análisis de la radiación solar directa en las calles de barcelona, en base a la relación entre su morfología y vegetación] // Architecture, City and Environment. 2017. № 12 (34). Pp. 45–68.
2. de Gracia A., Navarro L., Castell A., Cabeza L.F. Energy performance of a ventilated double skin facade with PCM under different climates // Energy and Buildings. 2015. № 91. Pp. 37–42.
3. Cianfrini C., Corcione M., Habib E., Quintino A. Energy performance of a lightweight opaque ventilated facade integrated with the HVAC system using saturated exhaust indoor air // Energy and Buildings. 2012. № 20. Pp. 26–34.
4. Mohammed Saleh Z., Alibaba H.Z. Integration of Double Skin Facade with HVAC Systems: The State of the Art on Building Energy Efficiency // International Journal of Recent Research in Civil and Mechanical Engineering. 2016. № 2. Pp. 37–50.
5. Manca O., Nardini S. Thermal design of uniformly heated inclined channels in natural convection with and without radiative effects // Heat Transfer Engineering. 2001. № 22(2). Pp. 13–28.
6. Auletta A., Manca O. Heat and Fluid Flow Resulting from the Chimney Effect in a Symmetrically Heated Vertical Channel with Adiabatic Extensions // International Journal of Thermal Sciences. 2002. № 41. Pp. 1101–1111.
7. Colla L., Fedele L., Manca O., Marinelli L., Nardini S. Experimental and numerical investigation on forced

8. Manca, O., Ricci, D., Nardini, S., Lorenzo, G. Di. Thermal and fluid dynamic behaviors of confined laminar impinging slot jets with nanofluids. *International Communications in Heat and Mass Transfer*. 2016. No. 70. Pp. 15–26.
9. Corral, R., Crespo, J. A hybrid unstructured/spectral method for the resolution of Navier-Stokes equations. *Proceedings of the ASME Turbo Expo*. 2009.
10. Corral, R., Crespo, J. A harmonic balance method in graphics processing units for vibrating blades. *11th European Conference on Turbomachinery Fluid Dynamics and Thermodynamics, ETC*. 2015.
11. Minea, A.A. Uncertainties in modeling thermal conductivity of laminar forced convection heat transfer with water alumina nanofluids. *International Journal of Heat and Mass Transfer*. 2014. No. 68. Pp. 78–84.
12. Minea, A.A. Challenges in hybrid nanofluids behavior in turbulent flow: recent research and numerical comparison. *Renewable and Sustainable Energy Reviews*. 2017. No. 7. Pp. 426–434.
13. Kharkov, N.S. Nonstationary heat and mass transfer in the multilayer building construction with ventilation channels. *Journal of Physics: Conference Series*. 2017. No. 891.
14. Statsenko, E.A., Ostrovaia, A.F., Olshevskiy, V.Y., Petrichenko, M.R. Temperature and velocity conditions in vertical channel of ventilated facade. *Magazine of Civil Engineering*. 2018. 80(4). Pp. 119–127. DOI: 10.18720/MCE.80.11
15. Gorshkov, A.S., Vatin, N.I., Rymkevich, P.P., Kydrevich, O.O. Payback period of investments in energy saving. *Magazine of Civil Engineering*. 2018. 78(2). Pp. 65–75. DOI: 10.18720/MCE.78.5.
16. Titkov, V.V., Bekbayev, A.B., Munsyzbai, T.M., Shakenov, K.B. Construction of autonomous buildings with wind power plants. *Magazine of Civil Engineering*. 2018. 80(4). Pp. 171–180. DOI: 10.18720/MCE.80.15.
17. Vedishcheva, I.S., Ananin, M.Y., Al Ali, M., Vatin, N.I. Influence of heat conducting inclusions on reliability of the system «sandwich panel -metal frame». *Magazine of Civil Engineering*. 2018. 78(2). Pp. 116–127. DOI: 10.18720/MCE.78.9.
18. Khrapunov, E.F., Potechin, I.V., Chumakov, Y.S. Structure of a free convective flow over a horizontal heated surface under conditions of conjugate heat transfer. *Journal of Physics: Conference Series*. 2017. No. 891(1).
19. Kharkov, N.S. Nonstationary heat and mass transfer in the multilayer building construction with ventilation channels. *Journal of Physics: Conference Series*. 2017. No. 891(1).
20. Korotkov, A.S., Gravit, M. 3D-map modelling for the melting points prediction of intumescent flame-retardant coatings, SAR and QSAR in Environmental Research. 2017. 28(8). Pp. 677–689.
21. Mityakov, A., Babich, A., Bashkatov, A., Gusakov, A., Dymkin, A., Zainullina, E., Sapozhnikov, S., Mityakov, V., Seroshtanov, V. Investigating heat transfer augmentation using gradient heat flux measurement and PIV method. *MATEC Web of Conferences*. 2017. No. 115.
22. Statsenko, E.A., Musorina, T.A., Ostrovaia, A.F., Olshevskiy, V.Ya., Antuskov, A.L. Moisture transport in the ventilated channel with heating by coil. *Magazine of Civil Engineering*. 2017. 70(2). Pp. 11–17. DOI: 10.18720/MCE.70.2
23. Starkov, V., Ovchinnikov, P., Dzampaev, T. Optimization of energy performance of windows by applying self-adjustable shadings. *MATEC Web of Conferences*. 2016. No. 73.
24. Babenkov, M.B. Temperature of rock formation and fracturing fluid during the hydraulic fracturing process. *IOP Conference Series: Earth and Environmental Science*. 2018. No. 93 (1).
- convection in circular tubes with nanofluids // *Heat Transfer Engineering*. 2016. № 37. Pp. 1201–1210.
8. Manca O., Ricci D., Nardini S., Lorenzo G. Di. Thermal and fluid dynamic behaviors of confined laminar impinging slot jets with nanofluids // *International Communications in Heat and Mass Transfer*. 2016. № 70. Pp. 15–26.
9. Corral R., Crespo J. A hybrid unstructured/spectral method for the resolution of Navier-Stokes equations // *Proceedings of the ASME Turbo Expo*. 2009.
10. Corral R., Crespo J. A harmonic balance method in graphics processing units for vibrating blades // *11th European Conference on Turbomachinery Fluid Dynamics and Thermodynamics, ETC*. 2015.
11. Minea A.A. Uncertainties in modeling thermal conductivity of laminar forced convection heat transfer with water alumina nanofluids // *International Journal of Heat and Mass Transfer*. 2014. № 68. Pp. 78–84.
12. Minea A.A. Challenges in hybrid nanofluids behavior in turbulent flow: recent research and numerical comparison // *Renewable and Sustainable Energy Reviews*. 2017. № 7. Pp. 426–434.
13. Kharkov N.S. Nonstationary heat and mass transfer in the multilayer building construction with ventilation channels // *Journal of Physics: Conference Series*. 2017. № 891.
14. Стаценко Е.А., Островая А.Ф., Ольшевский В.Я., Петриченко М.Р. Температурный и скоростной режимы в вертикальном канале вентилируемого фасада // *Инженерно-строительный журнал*. 2018. № 4(80). С. 119–127.
15. Горшков А.С., Ватин Н.И., Рымкевич П.П., Кудревич О.О. Период возврата инвестиций в энергосбережение // *Инженерно-строительный журнал*. 2018. № 2(78). С. 65–75.
16. Титков В.В., Бекбаев А.Б., Мунсызбай Т.М., Шакенов К.Б. Строительство автономных зданий с ветроэнергетическими установками // *Инженерно-строительный журнал*. 2018. № 4(80). С. 171–180.
17. Ведищева Ю.С., Ананьин М.Ю., Ал Али М., Ватин Н.И. Влияние теплопроводных включений на надежность системы «сэндвич-панель – каркас здания» // *Инженерно-строительный журнал*. 2018. № 2(78). С. 116–127.
18. Khrapunov E.F., Potechin I.V., Chumakov Y.S. Structure of a free convective flow over a horizontal heated surface under conditions of conjugate heat transfer // *Journal of Physics: Conference Series*. 2017. № 891(1).
19. Kharkov N.S. Nonstationary heat and mass transfer in the multilayer building construction with ventilation channels. *Journal of Physics: Conference Series*. 2017. № 891 (1)
20. Korotkov A.S., Gravit M. 3D-map modelling for the melting points prediction of intumescent flame-retardant coatings, SAR and QSAR in Environmental Research. 2017. 28(8). Pp. 677–689.
21. Mityakov A., Babich A., Bashkatov A., Gusakov A., Dymkin A., Zainullina E., Sapozhnikov S., Mityakov V., Seroshtanov V. Investigating heat transfer augmentation using gradient heat flux measurement and PIV method // *MATEC Web of Conferences*. 2017. № 115.
22. Стаценко Е.А., Мусорина Т.А., Островая А.Ф., Ольшевский В.Я., Антуськов А.Л. Влагоперенос в вентилируемом канале с нагревательным элементом // *Инженерно-строительный журнал*. 2017. № 2(70). С. 11–17.
23. Starkov V., Ovchinnikov P., Dzampaev T. Optimization of Energy Performance of Windows by Applying Self-Adjustable Shadings // *MATEC Web of Conferences*. 2016. № 73.
24. Babenkov M.B. Temperature of rock formation and fracturing fluid during the hydraulic fracturing process // *IOP*

Сергеев В.В., Петриченко М.Р., Немова Д.В., Котов Е.В., Тарасова Д.С., Нефедова А.В., Бородинец А. Надстройка существующих зданий с применением легких стен по каркасной технологии // *Инженерно-строительный журнал*. 2018. № 8(84). С. 67–74.

25. Khrapunov, E.F., Chumakov, Y.S. Unsteady processes in a natural convective plume. Journal of Physics: Conference Series. 2018. No. 1038(1).
26. Zaborova, D., Vieira, G., Musorina, T., Butyrin, A. Experimental Study of Thermal Stability of Building Materials. 2018. Advances in Intelligent Systems and Computing. No. 692. Pp. 482–489.
27. Davydov, V.V. Some specific features of the NMR study of fluid flows. Optics and Spectroscopy (English translation of Optika i Spektroskopiya). 2016. 121(1). Pp. 18–24.
28. Santos, P., Martins, C., da Silva, L.S., Bragança, L. Thermal performance of lightweight steel framed wall: the importance of flanking thermal losses. J. Build. Phys. 2013. 38(1). Pp. 81–98.
29. Gorgolewski, M. Developing a simplified method of calculating U-values in light steel framing Build. Environ., 42 (1) (2007). Pp. 230–236.
30. Thorsell, T., Bomberg, M. Integrated methodology for evaluation of energy performance of the building enclosures: part 3 – uncertainty in thermal measurements. J. Build. Phys. 2011. No. 35 (1). Pp. 83–96.
31. Roque, E., Santos, P. The effectiveness of thermal insulation in lightweight steel-framed walls with respect to its position. Buildings. 2017. No. 7 (13). Pp. 1–18.
32. Santos, P. Energy efficiency of lightweight steel-framed buildings. Energy Effic. Build. (2017). Pp. 35–60.
33. Atsonios, I.A., Mandilaras, I.D., Kontogeorgos, D.A., Founti, M.A. Two new methods for the in-situ measurement of the overall thermal transmittance of cold frame lightweight steel-framed walls. Energy and Buildings. 2018. Vol. 170. Pp. 183–194.
- Conference Series: Earth and Environmental Science. 2018. № 93(1).
25. Khrapunov E.F., Chumakov Y.S. Unsteady processes in a natural convective plume. 2018 // Journal of Physics: Conference Series, № 1038(1).
26. Zaborova D., Vieira G., Musorina T., Butyrin A. Experimental Study of Thermal Stability of Building Materials. 2018. Advances in Intelligent // Systems and Computing. № 692. Pp. 482–489.
27. Davydov V.V. Some specific features of the NMR study of fluid flows // Optics and Spectroscopy (English translation of Optika i Spektroskopiya). 2016. № 121(1). Pp. 18–24.
28. Santos P., Martins C., da Silva L.S., Bragança L. Thermal performance of lightweight steel framed wall: the importance of flanking thermal losses // J. Build. Phys. 2013. № 38 (1). Pp. 81–98.
29. M. Gorgolewski. Developing a simplified method of calculating U-values in light steel framing Build. Environ., 42 (1) (2007). Pp. 230–236.
30. Thorsell T., Bomberg M. Integrated methodology for evaluation of energy performance of the building enclosures: part 3 – uncertainty in thermal measurements // J. Build. Phys. 2011. № 35 (1). Pp. 83–96.
31. Roque E., Santos P. The effectiveness of thermal insulation in lightweight steel-framed walls with respect to its position // Buildings. 2017. № 7 (13). Pp. 1–18.
32. Santos P. Energy efficiency of lightweight steel-framed buildings // Energy Effic. Build. 2017. Pp. 35–60.
33. Ioannis A. Atsonios, Ioannis D. Mandilaras, Dimos A. Kontogeorgos, Maria A. Founti. Two new methods for the in-situ measurement of the overall thermal transmittance of cold frame lightweight steel-framed walls // Energy and Buildings. 2018. Vol. 170. Pp. 183–194.

Vitaly Sergeev,
+7(921)9805437; sergeev_vitaly@mail.ru

Виталий Владимирович Сергеев,
+7(921)9805437;
эл. почта: sergeev_vitaly@mail.ru

Mikhail Petrichenko,
+7(921)3300429; fonpetrich@mail.ru

Михаил Романович Петриченко,
+7(921)3300429; эл. почта: fonpetrich@mail.ru

Darya Nemova,
+79218900267; nemova_dv@spbstu.ru

Дарья Викторовна Немова,
+79218900267;
эл. почта: nemova_dv@spbstu.ru

Evgeny Kotov,
+79213461312; ekotov.cfd@gmail.com

Евгений Владимирович Котов,
+79213461312;
эл. почта: ekotov.cfd@gmail.com

Darya Tarasova*,
+7(931)2564594; tarasovads@gmail.com

Дарья Сергеевна Тарасова*,
+7(931)2564594;
эл. почта: tarasovads@gmail.com

Anna Nefedova,
+7(931)36-93-893; anyanefedova94@mail.ru

Анна Владимировна Нефедова,
+7(931)36-93-893;
эл. почта: anyanefedova94@mail.ru

Anatolijs Borodinecs,
+37126079655; anatolijs.borodinecs@rtu.lv

Анатолий Бородинец,
+37126079655;
эл. почта: anatolijs.borodinecs@rtu.lv

© Sergeev, V.S., Petrichenko, M.R., Nemova, D, Kotov, E.V., Tarasova, D.S., Nefedova, A.V., Borodinecs, A.B, 2018

doi: 10.18720/MCE.84.8

Fireproof suspended ceilings with high fire resistance limits

Огнезащитные подвесные потолки с высокими пределами огнестойкости

M.V. Gravit,
E.V. Golub*,
*Peter the Great St. Petersburg Polytechnic
University, St. Petersburg, Russia*
D.M. Grigoriev,
I.O. Ivanov,
*LLC «Fire Safety Technology», St. Petersburg,
Russia*

*Канд. техн. наук, доцент М.В. Гравит,
студент Е.В. Голуб*,
Санкт-Петербургский политехнический
университет Петра Великого,
Санкт-Петербург, Россия*
**Технический директор Д.М. Григорьев,
Генеральный директор И.О. Иванов,
ООО «Противопожарные технологии»,
Санкт-Петербург, Россия**

Key words: oil and gas complex; building structure; steel construction; fire resistance; hydrocarbon fire; standard fire; suspended ceiling

Ключевые слова: нефтегазовый комплекс; строительная конструкция; стальная конструкция; огнестойкость; углеводородный пожар; стандартный пожар; подвесной потолок

Abstract. Suspended ceiling is an effective way to fire protection of horizontal structures with steel beams due to its lightness, reliability and functionality. Three designs of fireproof suspended ceiling with silicate plates on cement binder are considered. A detailed description of the tested structures is given. Experiments were carried out to determine the fire resistance of the samples. The results of fire tests on suspended ceilings under standard fire temperature regime are presented in this study. It was found that the structures that have shown their effectiveness under the standard regime cannot satisfy the conditions of the hydrocarbon temperature regime. For the purpose of efficiency in the hydrocarbon regime and isolating the beams from the fire, in addition to fire-retardant plates, non-combustible heat insulation was used in the construction of the ceiling. The results of testing the ceiling with fire-retardant plates and rock wool when creating a hydrocarbon fire regime are given. It is shown that at the end of the fire exposure, the limiting state of the loss of bearing capacity and the loss of integrity was not fixed, visible changes during the test period was not found.

Аннотация. Подвесной потолок является эффективным способом огнезащиты горизонтальных конструкций перекрытий со стальными балками за счет своей легкости, надежности и функциональности. Рассмотрены три конструкции огнезащитного подвесного потолка с силикатными плитами на цементном вяжущем. Дано подробное описание испытываемых конструкций. Проведены эксперименты с целью определения огнестойкости образцов. Приведены результаты огневых испытаний подвесных потолков при создании стандартного температурного режима пожара. Получено, что конструкции, показавшие свою эффективность при стандартном режиме, не могут удовлетворить условиям углеводородного температурного режима. С целью эффективности при углеводородном режиме и изолирования балок от огня, кроме огнезащитных плит использована в конструкции потолка негорючая теплоизоляция. Приведены результаты испытания потолка с огнезащитными плитами и каменной ватой при создании углеводородного режима пожара. Показано, что на момент окончания огневого воздействия предельное состояние по потере несущей способности и по потере целостности не зафиксировано, видимых изменений в течение времени проведения испытания не обнаружено.

1. Introduction

Fires have a big impact on buildings and structures as directly when the fire is located on the site itself, and indirectly [1]. Therefore, the number of emergency actions [2] should include fire impacts arising from a fire, as well as the choice of space planning solutions [3] should be determined taking into account the requirements of fire safety. For example, the fire effect significantly changes the rigidity of steel beam-to-column connections [4], welded tubular joints are very defenseless without fire protection [5], and the

aluminum parts of the structures are most exposed to melting during combustion [6]. In this way, the design of fire protection is a mandatory requirement in the design of structures [7, 8].

Protection of buildings and structures, equipment, structures of tankers and offshore platforms in the conditions of combustion of fire-hazardous and explosive substances at oil and gas facilities is an actual problem [9–11].

Until recently, in Russia, all tests of structures and materials were carried out only under conditions of a standard temperature regime, otherwise known as cellulose, whose combustion materials are wood, cloth, paper [12–14]. Fires resulting from the burning of petroleum products, as a rule, can be attributed to the so-called hydrocarbon fire, which is characterized by a rapid temperature rise, and is accompanied by a shock wave of flame on structures, fireproof coatings, combustible finishing and building materials [15, 16]. Materials and structures that have proven effective under standard conditions, as a rule, cannot provide the required level of protection under conditions of hydrocarbon fire [17].

The range of materials, burning of which refers to a hydrocarbon fire, is very wide. They can act not only pure hydrocarbons (gasoline and natural gases – methane, ethane, propane, butane, etc.), but also their organic derivative (alcohols, phenols, ketones), virtually all oil products, lubricants and varnishes, many plastics with a low oxygen index.

A detailed review of international standards for determining the fire resistance of structures under a hydrocarbon fire, as well as an analysis of technical regulations in the field of fire protection for ships and offshore platforms is given in [18].

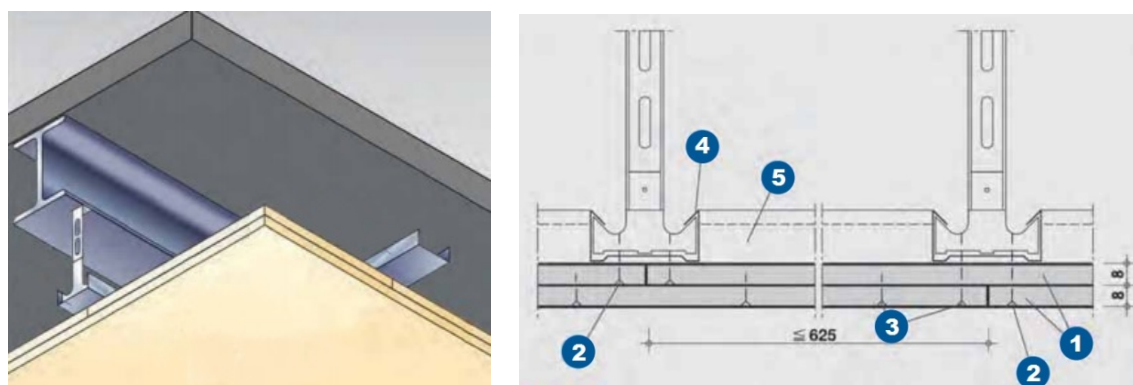
At present, there is a tendency to simulate a hydrocarbon fire in different software complexes in order to determine the effect of fire on various structures [19–23].

One of the important approaches for ensuring fire safety of buildings and structures is the use of a method for analyzing, assessing and managing the risk of an accident. This method allows to develop the most safe and at the same time economical design solution [24, 25].

The principle of passive fire protection in a hydrocarbon fire is to isolate the protected structure from fire. The insulation provides a thermal barrier, slowing the rate of heating of the steel and providing the required time for the fire extinguishing prior to the destruction of structures [26, 27].

One way to protect horizontal structural elements from the effects of a hydrocarbon fire is the fireproof suspended ceilings, which relate to constructive fire protection. The use of constructive fire protection is considered to be the most effective method, from the number used today to protect the structures of buildings and structures from the effects of fire and high temperatures in fires. In addition, when using this type of fire protection there are no wet processes and work can be carried out at any ambient temperature.

Suspended ceilings are used to protect horizontal structures of coatings and slabs with steel beams and are structural and functional elements. Important advantages of such fire protection are the ease of the suspended ceiling, as well as the reliability of the structure due to the formation of an air gap, which additionally increases the fire resistance limit [28].



1 – PROMATECT-H $t = 10$ mm plates in 2 layers; 2 – screws 4.2×25 pitch 150–200 mm;
3 – screws 4.2×35 pitch 200 mm; 4 – C-profile of floor structure CD 60×27×0.6 with anchoring;
5 – profile above the cross joint

Figure 1. The design of the fireproof suspended ceiling PROMATECT-H on metal I-beams (left) and a cross-section (right).

Also, fireproof suspended ceilings serve to protect against fire engineering communications systems, such as ventilation and air conditioning systems, electricity supply. By installing this type of ceiling, an independent fire compartment is created for communications, protecting them in the inter-ceiling space and ensuring their fire safety.

In addition to protecting structures with steel beams, fireproof suspended ceilings are also used to protect coatings from profiled sheets. In work [29], the influence of the gap size of the air layer on the fire resistance of the structure as a whole was investigated. Most of the studies are devoted to the development of either thin-layer fire retardant coatings [13, 30, 31], or constructive fire protection in the form of separate plate elements [26, 27], and holistic elements, such as a fireproof suspended ceiling, are given little attention.

In this work the designs of the suspended ceiling with fire resistant plates PROMATECT-H and PROMATECT-T were investigated. They are insensitive to moisture, large format and self-supporting. The difference in the name determines the possibility of using the hydrocarbon regime (PROMATECT-T). PROMATECT-T plates are used as cladding of elements and structures of tunnels, underground transport structures and any objects with increased requirements to heat load and resistance to aggressive environment, can be used both indoors and outdoors with increased wind load (including in the Arctic). PROMATECT-H plates serve as constructive fire protection of buildings and structures, are used indoors and can be an additional decorative element.

The fire retardant plates used in work belong to the class of fireproof plates on cement binder. Table 1 shows the characteristics of plates of other producers belonging to this class.

Table 1. The main properties of the plates on cement binder.

| Producer | Promat | Promat | Knauf | PROZASK | PROZASK |
|--|--|----------------------------------|---|---|------------------------------------|
| Plate | PROMATECT-H | PROMATECT-T | AQUAPANEL Cement Board Outdoor | Firepanel | PYRO-SAFE AESTUVER-T |
| Composition (main components) | silicate plates on cement binder | silicate plates on cement binder | Portland cement, expanded clay sand, perlite, hydrophobic and other additives | Cement binder with light mineral filler | Cement binder, fiberglass, perlite |
| Density, kg/m ³ | 870 | 900 | 1100-1200 | 1100-1200 | 980 |
| Moisture content, % | 6 | 5 | - | - | 7 |
| Alkalinity, pH | 12 | 10 | 12 | 12 | 12 |
| Thermal conductivity, W/m ² K | 0.175 | 0.212 | 0.350 | 0.350 | 0.185 |
| Moisture diffusion resistance, μ | 20 | 5 | 66 | 66 | - |
| Flexural strength, MPa | 7.6 | 5 | >10 | 5.4 | 7.5 |
| Tensile strength, MPa | 4.8 | 1.2 | - | - | 7.5 |
| Compressive strength, MPa | 9.3 | 4 | - | - | - |
| Elastic modulus, MPa | 4200 (longitudinal) 2900 (transverse) | 1400 | 4000 | - | 4500 |
| Combustibility | Non combustible | Non combustible | Non combustible | Non combustible | Non combustible |
| Fire temperature regime | standard | hydrocarbon | standard | hydrocarbon | hydrocarbon |

* "-" there is no information on the producer's website

PROMATECT-T plates are a product of Etex Building Performance, owner of Promat – the world's largest producer of flame retardant materials and high-temperature insulation. Thanks to their work, fire safety projects around the world have been implemented in civil and industrial construction, petrochemical, gas, nuclear and power engineering. In addition, the company is engaged in testing and certification of fire protection systems for steel, reinforced concrete, wooden structures and utilities. The assortment of fire resistant coatings Promat is presented by compositions of different type and purpose. This allows you to provide comprehensive protection for any object. The proposed fire retardant coatings are of high quality and at the same time cost-effective.

The work carried out tests of three systems of designs with fireproof ceilings:

- under standard temperature conditions, the ceiling was tested with a PROMATECT-H plate with a thickness of 8 mm in two layers ($2 \times 8 = 16$ mm);
- under standard temperature conditions, the ceiling was tested with a PROMATECT-H plate with a thickness of 10 mm in two layers ($10 \times 2 = 20$ mm);
- under hydrocarbon temperature conditions, the ceiling was tested with a 15 mm thick PROMATECT-T plate, fixed to the steel substructure in two layers ($2 \times 15 = 30$ mm), with a thermal insulation layer of stone wool 200 mm thick with a density of 60 kg/m³.

The aim of the work was to select the thickness of the thermal insulation and the thickness of the fireproof ceiling slabs to obtain the test results for the fire resistance parameters in the hydrocarbon fire for at least 150 minutes.

2. Methods

Tests of prototypes of the construction of a fireproof suspended ceiling were carried out to determine the flame retardant efficiency of the samples presented in accordance with Russian State Standards GOST 30247.0-94 "Elements of building constructions. Fire-resistance test methods. General requirements" and GOST R 53298-2009 "Suspended ceilings. Fire-resistance test method".

The duration of the test was determined by the onset of the limit state by loss of integrity (E) and the loss of bearing capacity (R), depending on which of the limit states occurs earlier.

Initially, tests were carried out on a standard temperature regime to determine the limiting possibilities for the fire resistance of panels on cement binder

2.1. Fireproof ceiling test with standard temperature regime

Samples of the ceiling with a size of 2800×3000 mm consist of 8 mm thick plates on cement binder in 2 layers (2 samples) and 10 mm thick in 2 layers (2 samples) mounted on a frame of steel profiles. The frame with the help of suspensions attached to the bearing I-beams No. 20 and reinforced concrete floor slabs. The distance from the bottom of the beam to the ceiling is 160 mm.

In the fire chamber of the furnace, the standard temperature regime was maintained, characterized by the following relationship:

$$T - T_0 = 345 \cdot \lg(8t + 1), \quad (1)$$

where T is the temperature in the furnace, corresponding to the time t , °C;

T_0 is the temperature in the furnace before the onset of heat exposure (ambient temperature), °C;

t is the time calculated from the beginning of the test, min.

For the design of the ceiling with fire resistant panels 8 mm thick in 2 layers, the ambient temperature and relative humidity of the air during the first test were 25 °C and 69 %, respectively, in the second test these readings were equal to 26 °C and 64 %.

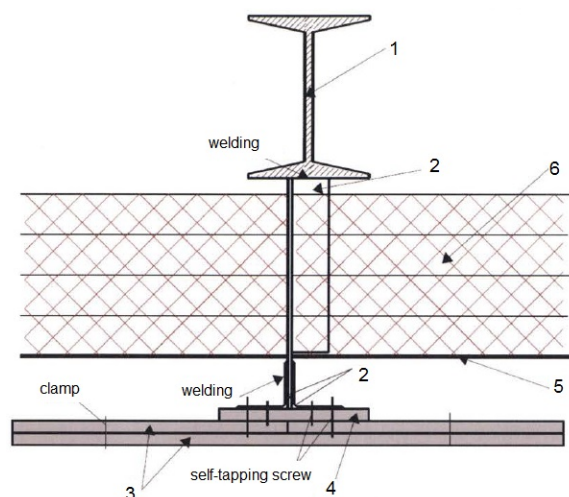
For the design of the ceiling with 10 mm thick flame retardant plates, the ambient temperature and relative air humidity in the first test were 15 °C and 66 %, respectively, in the second these readings were 14 °C and 65 %.

The temperature in the fire chamber of the furnace and on the test samples is measured using furnace thermocouples, and the vertical deformations of the samples during the test are measured with a deflectometer.

2.2. Fireproof ceiling test with hydrocarbon temperature regime

For the tests, 2 samples of the design of the fireproof suspended ceiling with dimensions of 5000×3000×545 mm were presented. The height is indicated taking into account the metal prefabricated substructure made of the rolling profiles of the angular and I-section sections.

A schematic diagram of the design of a prototype of a fireproof suspended ceiling is shown in Figure 2.



1 – beam 20B1; 2 – corner L 40×4; 3 – plate PROMATECT-T $t = 15$ mm;
4 – strip from the plate PROMATECT-T $t = 15$ mm, width 160 mm; 5 – metal mesh 100×100 wire
diameter 5 mm; 6 – rock wool slabs $t = 50$ mm, 4 layers

Figure 2. Schematic diagram of the design of a prototype of a fireproof suspended ceiling.

The metal frame of the suspended ceiling was made by installing vertical supports welded to the beams of the I-section profile No. 20B1 in accordance with Russian State Standard GOST 26020-83 (reduced thickness of metal – 3.4 mm), set in the number of 5 pieces. To these supports longitudinal guides were welded from the double angle 40×4 mm in accordance with Russian State Standard GOST 8509-93, and in the transverse direction the guides were connected by double angles 40×4 mm welded to the side by side elements. Thus, the nominal pitch of the metal elements of the framework of the fireproof suspended ceiling, forming a flat welded cage for fixing the plate materials of the enclosing part, was 626–1250 mm.

At the bottom of the flat welded cage of the metal frame of the suspended ceiling, strips of width 160 mm, made of plates on cement binder 15 mm thick, fastened to the metal sub-structure with self-tapping screws, were fastened. After that, over the metal elements of the frame, a two-layer covering was made with plates on cement binder 15 mm thick ($2 \times 15 = 30$ mm), fasteners of which were made with self-tapping screws and staples installed with a pitch (300 ± 10) mm.

At the end of the assembly of the enclosing part of the suspended ceiling from panels on cement binder, a metal grid with a cell of 100×100 mm made of a wire of 5 mm and 4 layers of heat insulation boards made of rock wool 50 mm thick and with a density of 60 kg/m^3 was laid along the top of the steel angles. The total thickness of the thermal insulation layer was 200 mm.

To prevent the penetration of the flame around the perimeter of the sample, the insulation was laid, covering the cracks between the lining of the furnace and the plates of the enclosing part of the suspended ceiling.

In order to simulate the construction of the ceiling and ensure the thermal regime of heating the metal structures of the suspended ceiling protected by the enclosure, the steel I-beam beams were laid with reinforced concrete covering plates. On the perimeter, the sides of the prototype were covered with slabs of incombustible mineral wool insulation. To simulate the mode of movement of air in the allocated space above the fence of the fireproof suspended ceiling, along the end parts of the samples, a device of openings 300×500 mm in size was provided.

The ambient temperature and the relative humidity of the air during the first test were 21 °C and 50 %, respectively, in the second, these readings were equal to 23 °C and 52 %. The speed of air movement in both tests did not exceed 0.5 m/sec.

2.3. Test procedure

The experimental samples were placed on an experimental setup and subjected to unilateral thermal action.

In the fire chamber of the furnace, a hydrocarbon temperature regime was created in accordance with Russian State Standard GOST R EN 1363-2-2014, characterized by the following relationship:

$$T = 1080 \cdot \left(1 - 0.325e^{-0.167t} - 0.675e^{-2.5t} \right) + 20, \quad (2)$$

where T is the temperature in the furnace, corresponding to the time t , °C;
 t is time, calculated from the beginning of the test, min.

The temperature in the fire chamber of the furnace was measured by furnace thermocouples, evenly distributed along the length of the sample at six locations.

On the experimental samples, the temperature was measured by thermocouples installed in an amount of 9 pieces on the I-beams of the metal skeleton of the suspended ceiling in the middle of their spans (with the exception of the two outer beams), in accordance with the requirements set out in 5.4.4 Russian State Standard GOST R 53295-2009.

3. Results and Discussion

3.1. Ceiling test results at a standard temperature regime

Curves of temperature changes in the controlled points when creating a standard temperature regime are shown in Figure 3.

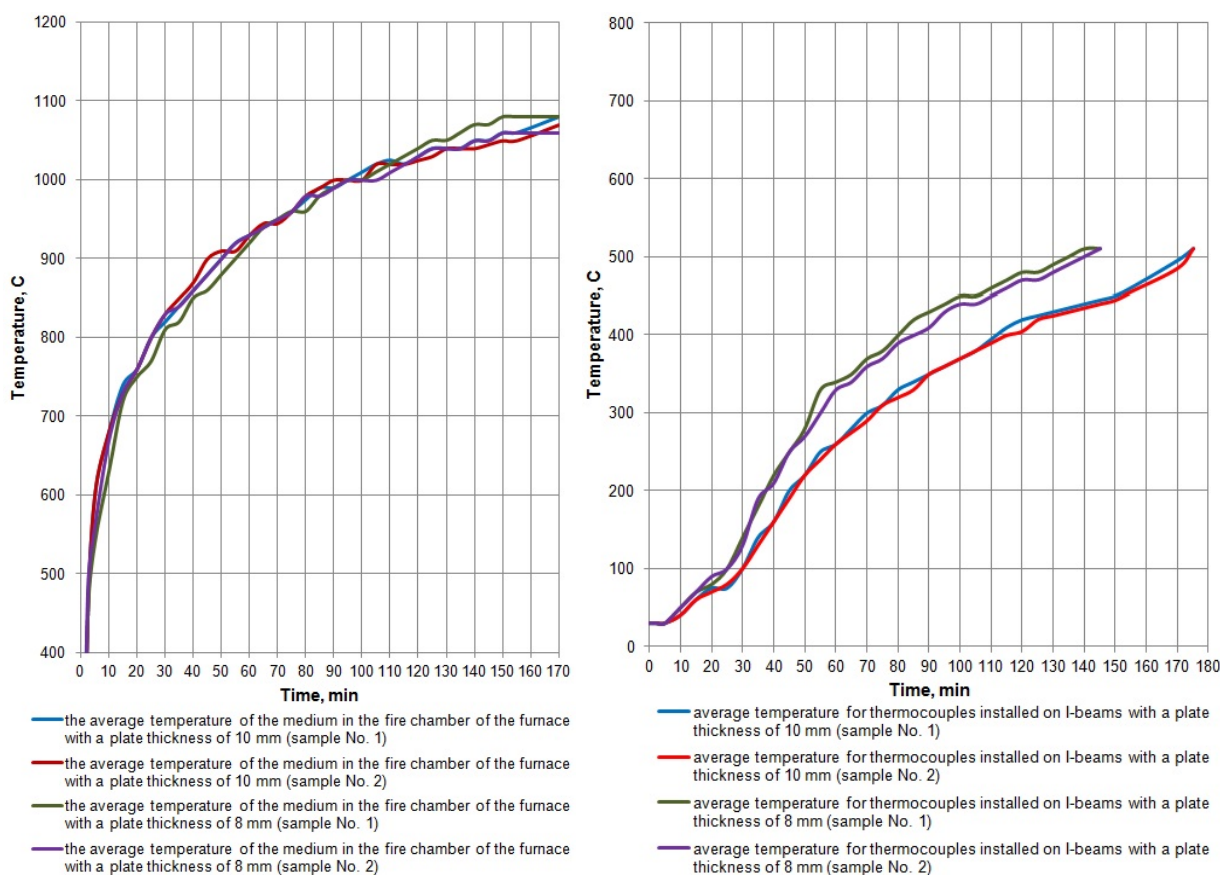


Figure 3. Temperature curves in the fire chamber of the furnace (left) and on I-beams of steel frames (right) in standard regime.

Table 2. The results of monitoring the tests for the construction with a plate thickness of 8 mm.

| Sample 1 | | Sample 2 | |
|----------|---|----------|-----------------------------------|
| Time | The results of monitoring | Time | The results of monitoring |
| 0' | The beginning of the test | 0' | The beginning of the test |
| 5' | Strong emission of steam from the structure | 15' | Steam emission from the structure |
| 30' | Deflection 0 mm | 45' | Deflection 0 mm |
| 45' | Steam emission decreased | 50' | Steam emission decreased |
| 90' | Deflection 2 mm | 95' | Deflection 2 mm |
| 135' | Deflection 4 mm | 140' | Deflection 4 mm |
| 148' | The test is over | 146' | The test is over |

As a result, the limit state was achieved by loss of bearing capacity and amounted to 136 minutes for sample 1, 142 minutes for sample 2.

Table 3. The results of monitoring the tests for the construction with a plate thickness of 10 mm.

| Sample 1 | | Sample 2 | |
|----------|---|----------|---|
| Time | The results of monitoring | Time | The results of monitoring |
| 0' | The beginning of the test | 0' | The beginning of the test |
| 16' | Smoke emission from the junction of reinforced concrete slabs | 17' | Smoke emission from the junction of reinforced concrete slabs |
| 40' | Deflection 5 mm | 45' | Deflection 5mm |
| 61' | Deflection 10 mm | 65' | Deflection 15 mm |
| 110' | Deflection 15 mm | 95' | Deflection 18 mm |
| 166' | Deflection 18 mm | 140' | Deflection 19 mm |
| 175' | The test is over | 176' | The test is over |

As a result, the limit state was reached by loss of bearing capacity and amounted to 172 minutes for sample 1, 175 minutes for sample 2.

3.2. Ceiling test results at a hydrocarbon temperature regime

Curves of temperature changes in the controlled points when creating a hydrocarbon temperature regime are shown in Figure 4.

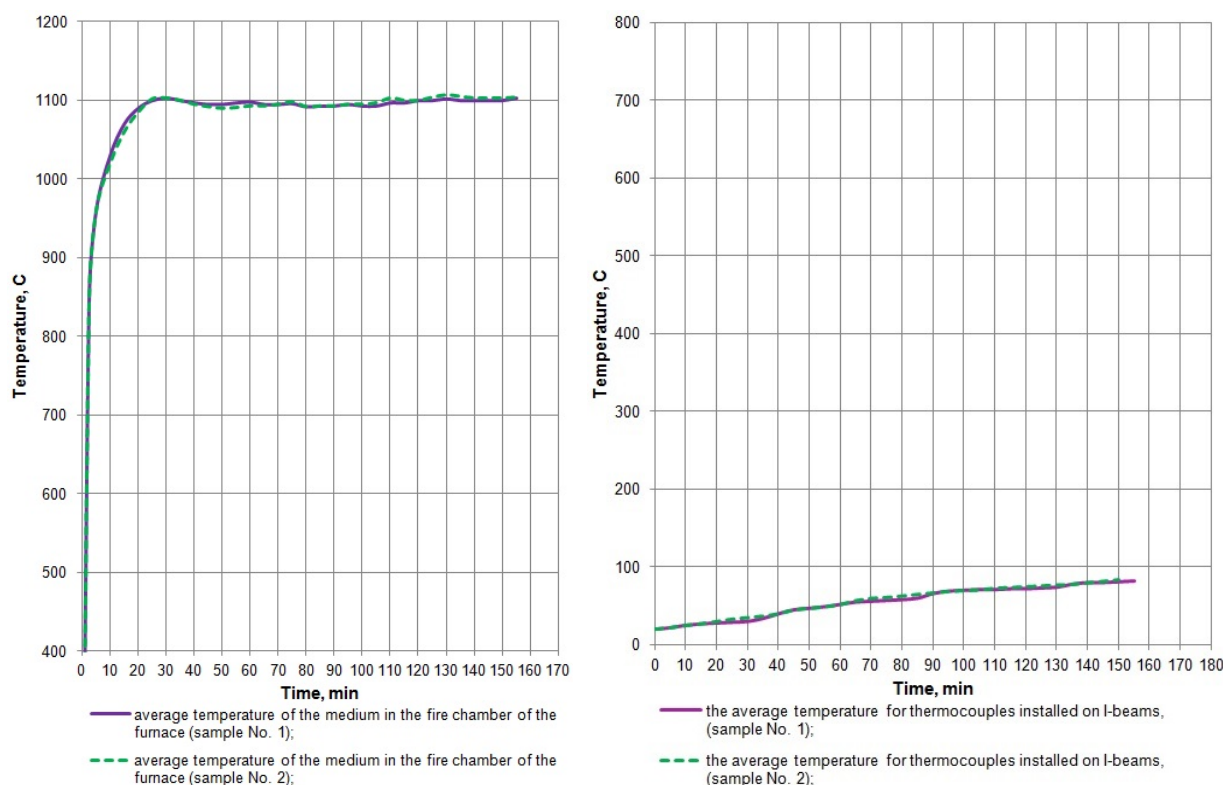


Figure 4. Temperature curves in the fire chamber of the furnace (left) and on I-beams of steel frames (right) in hydrocarbon regime.

According to agreement with the producer, the tests were stopped at the 155th minute. During the testing of the prototypes of the fireproof suspended ceiling, no visible changes were observed in the state of the protecting parts of the plates on cement binder.

At the time of the end of the fire impact (155 min), the wall part of the plates on cement binder did not collapse. Displacements and violations of the integrity of the layer of insulation from rock wool were not fixed. The deformation of the steel elements of the skeleton of the suspended ceiling has not been observed.

At the time of the end of the fire action, the average temperature for the thermocouples installed on the steel I-beams of the frame was 75 °C and 82 °C for the 1st and 2nd samples, respectively.

Thus, none of the limiting states for which the tests were conducted was achieved during the time of fire tests.

Partial collapse of the plates of the fencing part of the suspended ceiling was recorded after the cooling of the prototypes.



Figure 5. A sample of the ceiling design before the test (left) and partial collapse of the enclosing part of the suspended ceiling during cooling (right)

The tests of the fireproof suspended ceiling showed that the design of the ceiling, tested in the standard regime, will not be able to satisfy the conditions of hydrocarbon combustion, with a stronger effect of the hydrocarbon regime, the critical temperature of 500 °C will be reached much earlier. In order to be effective in the hydrocarbon regime and isolate the beams from the fire, it is necessary, in addition to fire-retardant plates, to use non-combustible heat insulation in the ceiling design and increase the own thickness of the plates on cement binder, which made it possible to ensure the required fire resistance of the structure.

The fireproof suspended ceiling showed its effectiveness not only under standard conditions [28, 29], but also under conditions of hydrocarbon fire. Therefore, testing this design under different conditions is necessary to create a complete picture of the behavior of the suspended ceiling, which will allow more extensive use this type of passive fire protection for horizontal structures of ceilings and slabs. Most of the studies are devoted to the development of either thin-layer fire retardant coatings [13, 30, 31], or constructive fire protection in the form of separate plate elements [26, 27], and holistic elements, such as a fireproof suspended ceiling, are given little attention.

4. Conclusions

The study leads to the following conclusions:

- 1) Testing of samples of a flame-retardant suspended ceiling made of PROMATECT-H plates 16 mm thick, provided that a standard regime was created in the fire chamber of the furnace, was completed by reaching the limit state for loss of bearing capacity after 136 min and 142 min for samples 1 and 2;
- 2) Testing of samples of a flame-retardant suspended ceiling made of PROMATECT-H plates with a thickness of 20 mm, provided that a standard regime was created in the fire chamber of the furnace, ended with reaching the limit state of loss of bearing capacity after 172 min and 175 min for sample 1 and 2;
- 3) Testing of samples of a flame-retardant suspended ceiling made of PROMATECT-T plates with a thickness of 30 mm, with an insulating layer of rock wool, provided that a hydrocarbon temperature regime was created in the fire chamber of the furnace did not end with reaching the limit state of loss of bearing capacity of the structure and the occurrence of ultimate strains at the time the end of fire exposure (155 min). The critical temperature of 500 °C during the tests (155 min) on the steel I-beams of the samples was not reached (the average temperature for thermocouples at the time of ending of the fire exposure was 75 °C and 82 °C, for the 1st and 2nd sample, respectively);
- 4) The designs of the fireproof ceiling using plates on cement binder have proven their effectiveness under standard temperature regime;
- 5) To achieve the required degree of fire protection in hydrocarbon fire conditions, it is necessary to use plates on cement binder with a greater thickness compared to structures that have proven to be effective in a standard regime, as well as to use non-combustible insulation.

References

1. Fryanova, K.O., Perminov, V.A. Impact of forest fires on buildings and structures. *Magazine of Civil Engineering*. 2017. 75(7). Pp. 15–22. DOI: 10.18720/MCE.75.2.
2. Alekseytsev, A.V., Kurchenko, N.S. Deformations of steel roof trusses under shock emergency action. *Magazine of Civil Engineering*. 2017. 73(5). Pp. 3–13. DOI: 10.5862/MCE.73.1.
3. Gusakova, N.V., Filyushina, K.E., Gusakov, A.M., Minaev, N.N. Selection criteria of space planning and structural solutions of low-rise buildings. *Magazine of Civil Engineering*. 2017. 75(7). Pp. 84–93. DOI: 10.18720/MCE.75.8.
4. Tusnina, V.M. Semi-rigid steel beam-to-column connections. *Magazine of Civil Engineering*. 2017. 73(5). Pp. 25–39. DOI: 10.18720/MCE.73.3.
5. Garifullin, M.R., Barabash, A.V., Naumova, E.A., Zhuvak, O.V., Jokinen, T., Heinisuo, M. Surrogate modeling for initial rotational stiffness of welded tubular joints. *Magazine of Civil Engineering*. 2016. 63(3). Pp. 53–76. DOI: 10.5862/MCE.63.4
6. Hirkovskis, A., Serdjus, D., Goremikins, V., Pakrastins, L., Vatin, N.I. Behaviour analysis of load-bearing aluminium members. *Magazine of Civil Engineering*. 2015. 57(5). Pp. 86–96. DOI: 10.5862/MCE.57.8
7. Saknite, T., Serdjus, D., Goremikins, V., Pakrastins, L., Vatin, N.I. Fire design of arch-type timber roof. *Magazine of Civil Engineering*. 2016. 64(4). Pp. 26–39. DOI: 10.5862/MCE.64.3
8. Priadko, I.N., Mushchanov, V.P., Bartolo, E., Vatin, N.I., Rudnieva, I.N. Improved numerical methods in reliability analysis of suspension roof joints. *Magazine of Civil Engineering*. 2016. 65(5). Pp. 27–41. DOI: 10.5862/MCE.65.3
9. Imran, M., Liew, M.S., Nasif, M.S. Experimental Studies on Fire for Offshore Structures and its Limitation: A Review. *Chemical Engineering Transactions*. 2015. Vol. 45. Pp. 1951–1956.
10. Imran, M., Liew, M.S., Nasif, M.S., Niazi, U.M., Yasreen, A. Hazard assessment studies on hydrocarbon fire and blast: An overview. *Advanced Science Letters*. 2017. Vol. 23. Pp. 1243–1247.
11. Gravit, M.V., Golub, E.V., Antonov, S.P. Fire protective dry plaster composition for structures in hydrocarbon fire. *Magazine of Civil Engineering*. 2018. 79(3). Pp. 86–94. DOI: 10.18720/MCE.79.9.
12. Gravit, M.V., Nedviga, Y.S., Vinogradova, N.A., Teplova, Z.S. Ognestoykost sborno-monolitnykh chastorebristyykh plit po balkam so stalnym profilom [Fireproof of prefabricated monolithic multi-ribbed plate with rolled steel beam]. *Construction of Unique Buildings and Structures*. 2016. 51(12). Pp. 73–83. (rus)
13. Schaumann, P., Kirsch, T. Protected Steel and Composite Connections: Simulation of the mechanical behaviour of steel and composite connections protected by intumescent coating in fire. *Journal of Structural Fire Engineering*. 2015. No. 1(6). Pp. 41–48.
14. Kraus, P., Mensinger, M., Tabeling, F., Schaumann, P. Experimental and Numerical Investigations of Steel Profiles with Intumescent Coating Adjacent to Space-Enclosing Elements in Fire. *Journal of Structural Fire Engineering*. 2015. No. 4(6). Pp. 237–246.
15. Bronzova, M.K., Garifullin, M.R. Fire resistance of thin-walled cold-formed steel structures Article history. *Construction of Unique Buildings and Structures*. 2016. No. 3(42). Pp. 61–78.
16. Shvyrkov, S.A., Yuryev, Y.I. Temperaturnyy rezhim pozhara dlya opredeleniya predela ognestoykosti ograždnykh sten neftnykh rezervuarov [The temperature regime of the fire for determination of the fire resistance of the enclosing walls of oil tanks]. *Technology of technosphere safety*. 2016.

Литература

1. Фрянова К.О., Перминов В.А. Воздействие лесных пожаров на здания и сооружения // *Инженерно-строительный журнал*. 2017. № 7. С. 15–22.
2. Алексейцев А.В., Курченко Н.С. Деформации стальных стропильных ферм при ударных аварийных воздействиях // *Инженерно-строительный журнал*. 2017. № 5(73). С. 3–13.
3. Гусакова Н.В., Филюшина К.Э., Гусаков А.М., Минаев Н.Н. Критерии выбора объемно-планировочных и конструктивных решений малозэтажных зданий // *Инженерно-строительный журнал*. 2017. № 7(75). С. 84–93.
4. Туснина В.М. Податливые соединения стальных балок с колоннами // *Инженерно-строительный журнал*. 2017. № 5(73). С. 25–39.
5. Гарифуллин М.Р., Барабаш А.В., Наумова Е.А., Жувак О.В., Йокинен Т., Хейнисуо М. Суррогатное моделирование для определения начальной жесткости вращения сварных трубчатых соединений // *Инженерно-строительный журнал*. 2016. № 3(63). С. 53–76.
6. Хирковский А., Сердюк Д.О., Горемыкин В.В., Пакрастиньш Л., Ватин Н.И. Анализ работы несущих элементов из алюминиевых сплавов // *Инженерно-строительный журнал*. 2015. № 5(57). С. 86–96.
7. Сакните Т., Сердюк Д.О., Горемыкин В.В., Пакрастиньш Л., Ватин Н.И. Проектирование огнестойких арочных деревянных покрытий // *Инженерно-строительный журнал*. 2016. № 4(64). С. 26–39.
8. Прядко Ю.Н., Муцанов В.Ф., Бартоло Х., Ватин Н.И., Руднева И.Н. Усовершенствование численных методов расчета надежности узлов висячих покрытий // *Инженерно-строительный журнал*. 2016. № 5(65). С. 27–41.
9. Imran M., Liew M.S., Nasif M.S. Experimental Studies on Fire for Offshore Structures and its Limitation: A Review // *Chemical Engineering Transactions*. 2015. Vol. 45. Pp. 1951–1956.
10. Imran M., Liew M.S., Nasif M.S., Niazi U.M., Yasreen A. Hazard assessment studies on hydrocarbon fire and blast: An overview // *Advanced Science Letters*. 2017. Vol. 23. Pp. 1243–1247.
11. Гравит М.В., Голуб Е.В., Антонов С.П. Огнезащитный штукатурный состав для конструкций в условиях углеводородного горения // *Инженерно-строительный журнал*. 2018. № 3(79). С. 86–94.
12. Гравит М.В., Недвига Е.С., Виноградова Н.А., Теплова Ж.С. Огнестойкость сборно-монолитных часторебристых плит по балкам со стальным профилем // *Строительство уникальных зданий и сооружений*. 2016. № 12 (51). С. 73–83.
13. Schaumann P., Kirsch T. Protected Steel and Composite Connections: Simulation of the mechanical behaviour of steel and composite connections protected by intumescent coating in fire // *Journal of Structural Fire Engineering*. 2015. № 1(6). Pp. 41–48.
14. Kraus P., Mensinger M., Tabeling F., Schaumann P. Experimental and Numerical Investigations of Steel Profiles with Intumescent Coating Adjacent to Space-Enclosing Elements in Fire // *Journal of Structural Fire Engineering*. 2015. № 4(6). Pp. 237–246.
15. Bronzova M.K., Garifullin M.R. Fire resistance of thin-walled cold-formed steel structures Article history // *Construction of Unique Buildings and Structures*. 2016. № 3(42). Pp. 61–78.
16. Швырков С.А., Юрьев Я.И. Температурный режим пожара для определения предела огнестойкости ограждающих стен нефтяных резервуаров // *Технологии техносферной безопасности*. 2016. № 4(68). С. 50–56 [Электронный ресурс]. Систем. требования: AdobeAcrobatReader. URL: <http://agps-2006.narod.ru/ttb/2016-4/20-04-16.ttb.pdf> (дата обращения: 02.12.2018).

Гравит М.В., Голуб Е.В., Григорьев Д.М., Иванов И.О. Огнезащитные подвесные потолки с высокими пределами огнестойкости // *Инженерно-строительный журнал*. 2018. № 8(84). С. 75–85.

- No. 4(68). Pp. 50–56 [Electronic resource]. System requirements: Adobe Acrobat Reader. URL: <http://agps-2006.narod.ru/ttb/2016-4/20-04-16.ttb.pdf> (date of application: 02.12.2018). (rus)
17. Golovanov, V., Pekhotikov, A., Pavlov, V. Raschet ognestoykosti konstruksiy iz stali s povyshennymi pokazatelyami ognestoykosti dlya obyektov neftegazovoy promyshlennosti [Calculation of the fire resistance of steel structures with increased fire resistance for oil and gas industry facilities]. Territoriya «Neftegaz». 2007. No. 4. Pp. 72–77. [Electronic resource]. System requirements: Adobe Acrobat Reader. URL: <http://neftegas.info/upload/uf/ff0ff0fa86672e368d8c93aeef1e6b8cc51.pdf> (date of application: 02.12.2018). (rus)
 18. Khasanov, I., Gravit, M.V., Kosachev, A.A., Pekhotikov, A.V., Pavlov, B.V. Garmonizatsiya yevropeyskikh i rossiyskikh normativnykh dokumentov, ustanavlivayushchikh obshchiye trebovaniya k metodam ispytaniy na ognestoykost stroitelnykh konstruksiy i primeneniyu temperaturnykh rezhimov, uchityvayushchikh realnyye usloviya pozhara [Harmonization of European and Russian regulatory documents that establish general requirements for fire test methods of building structures and the use of temperature regimes that take into account the actual fire conditions]. Fire and Explosion Safety. 2014. No. 3(23). Pp. 49–57. (rus)
 19. Gravit, M., Gumerova, E., Bardin, A., Lukinov, V. Increase of Fire Resistance Limits of Building Structures of Oil-and-Gas Complex Under Hydrocarbon Fire. Springer, Cham: International Scientific Conference Energy Management of Municipal Transportation Facilities and Transport. 2018. Pp. 818–829.
 20. Palazzi, E., Fabiano, B. Analytical modelling of hydrocarbon pool fires: Conservative evaluation of flame temperature and thermal power. Process Safety and Environmental Protection. 2012. No. 2(90). Pp. 121–128.
 21. Shebeko, A., Shebeko, Y., Gordiyenko, D. Raschetnaya otsenka ekvivalentnoy prodolzhitel'nosti pozhara dlya stalnykh konstruksiy tekhnologicheskoy estakady neftepererabatyvayushchego predpriyatiya [A settlement assessment of equivalent fire duration for steel structures of pipe rack of a refinery]. Pozharnaya bezopasnost. 2017. No. 1. Pp. 25–29 [Electronic resource]. System requirements: Internet Explorer. URL: <https://elibrary.ru/item.asp?id=28844556> (date of application: 02.12.2018). (rus)
 22. Shebeko, A., Shebeko, Y. Vzaimosvyaz velichin temperatury stroitelnykh konstruksiy pri standartnom i uglevodorodnom temperaturnykh rezhimakh pozhara [Relationship of temperatures of building structures at the standard and hydrocarbon regimes of fires]. Pozharnaya bezopasnost. 2017. No. 2. Pp. 46–49 [Electronic resource]. System requirements: Internet Explorer. URL: <https://elibrary.ru/item.asp?id=29328068> (date of application: 02.12.2018). (rus)
 23. Payá-Zaforteza, I., Garlock, M.E.M. A 3D numerical analysis of a typical steel highway overpass bridge under a hydrocarbon fire. Structures in Fire – Proceedings of the Sixth International Conference, SiF'10. 2010. Pp. 11–18.
 24. Gimranov, F. Prognozirovaniye stseneriyev razvitiya avari na neftekhimicheskikh proizvodstvakh [Prediction accident scenarios in the petrochemical industry]. Vestnik Kazanskogo tekhnologicheskogo universiteta. 2010. No. 5. Pp. 158–161 [Electronic resource]. System requirements: Internet Explorer. URL: <https://cyberleninka.ru/article/n/prognozirovanie-stsenariyev-razvitiya-avariy-na-neftekhimicheskikh-proizvodstvakh> (date of application: 02.12.2018). (rus)
 25. Paik, J.K., Czujko, J. Engineering and design disciplines associated with management of hydrocarbon explosion and fire risks in offshore oil and gas Facilities. Transactions – Society of Naval Architects and Marine Engineers. 2013. Vol. 120. Pp. 167–197.
 26. Paik, J.K., Czujko, J. Assessment of hydrocarbon explosion and fire risks in offshore installations: Recent advances and future trends // IES Journal Part A: Civil and Structural Engineering. 2016. Vol. 4. Pp. 167–179.
 27. Дыбаль Д.А., Шишилов О.Н., Гарустович И.В. Пассивная огнезащита в условиях углеводородного пожара // Лакокрасочные материалы и их применение. 2017. № 6. С. 16–19 [Электронный ресурс]. Систем. требования: Adobe Acrobat Reader. URL: https://o3.com/pdf/LKM-17-6_view-18-20.pdf (дата обращения: 02.12.2018).
 28. Шабалин С. Методы пассивной огнезащиты // Газовая промышленность. 2017. № 9. С. 122–125 [Электронный ресурс]. Систем. требования: Internet Explorer. URL: <https://elibrary.ru/item.asp?id=30006385> (дата обращения: 02.12.2018).
 29. Голованов В.И., Кузнецова Е.В. Эффективные средства огнезащиты для стальных и железобетонных конструкций
 17. Голованов В., Пехотиков А., Павлов В. Расчет огнестойкости конструкций из стали с повышенными показателями огнестойкости для объектов нефтегазовой промышленности // Территория «Нефтегаз». 2007. № 4. С. 72–77 [Электронный ресурс]. Систем. требования: Adobe Acrobat Reader. URL: <http://neftegas.info/upload/uf/ff0ff0fa86672e368d8c93aeef1e6b8cc51.pdf> (дата обращения: 02.12.2018).
 18. Хасанов И., Гравит М.В., Косачев А.А., Пехотиков А.В., Павлов В.В. Гармонизация европейских и российских нормативных документов, устанавливающих общие требования к методам испытаний на огнестойкость строительных конструкций и применению температурных режимов, учитывающих реальные условия пожара // Пожаровзрывобезопасность. 2014. № 3(23). С. 49–57.
 19. Gravit M., Gumerova E., Bardin A., Lukinov V. Increase of Fire Resistance Limits of Building Structures of Oil-and-Gas Complex Under Hydrocarbon Fire // Springer, Cham: International Scientific Conference Energy Management of Municipal Transportation Facilities and Transport. 2018. Pp. 818–829.
 20. Palazzi E., Fabiano B. Analytical modelling of hydrocarbon pool fires: Conservative evaluation of flame temperature and thermal power // Process Safety and Environmental Protection. 2012. № 2(90). Pp. 121–128.
 21. Шебеко А., Шебеко Ю., Гордиенко Д. Расчетная оценка эквивалентной продолжительности пожара для стальных конструкций технологической эстакады нефтеперерабатывающего предприятия // Пожарная безопасность. 2017. № 1. С. 25–29 [Электронный ресурс]. Систем. требования: Internet Explorer. URL: <https://elibrary.ru/item.asp?id=28844556> (дата обращения: 02.12.2018).
 22. Шебеко А., Шебеко Ю. Взаимосвязь величин температуры строительных конструкций при стандартном и углеводородном температурных режимах пожара // Пожарная безопасность. 2017. № 2. С. 46–49. Систем. требования: Internet Explorer. URL: <https://elibrary.ru/item.asp?id=29328068> (дата обращения: 02.12.2018).
 23. Payá-Zaforteza I., Garlock M.E.M. A 3D numerical analysis of a typical steel highway overpass bridge under a hydrocarbon fire // Structures in Fire – Proceedings of the Sixth International Conference, SiF'10. 2010. Pp. 11–18.
 24. Гимранов Ф. Прогнозирование сценариев развития аварий на нефтехимических производствах // Вестник Казанского технологического университета. 2010. № 5. С. 158–161 [Электронный ресурс]. Систем. требования: Internet Explorer. URL: <https://cyberleninka.ru/article/n/prognozirovanie-stsenariyev-razvitiya-avariy-na-neftekhimicheskikh-proizvodstvakh> (дата обращения: 02.12.2018).
 25. Paik J.K., Czujko J. Engineering and design disciplines associated with management of hydrocarbon explosion and fire risks in offshore oil and gas Facilities // Transactions – Society of Naval Architects and Marine Engineers. 2013. Vol. 120. Pp. 167–197.
 26. Paik J.K., Czujko J. Assessment of hydrocarbon explosion and fire risks in offshore installations: Recent advances and future trends // IES Journal Part A: Civil and Structural Engineering. 2016. Vol. 4. Pp. 167–179.
 27. Дыбаль Д.А., Шишилов О.Н., Гарустович И.В. Пассивная огнезащита в условиях углеводородного пожара // Лакокрасочные материалы и их применение. 2017. № 6. С. 16–19 [Электронный ресурс]. Систем. требования: Adobe Acrobat Reader. URL: https://o3.com/pdf/LKM-17-6_view-18-20.pdf (дата обращения: 02.12.2018).
 28. Шабалин С. Методы пассивной огнезащиты // Газовая промышленность. 2017. № 9. С. 122–125 [Электронный ресурс]. Систем. требования: Internet Explorer. URL: <https://elibrary.ru/item.asp?id=30006385> (дата обращения: 02.12.2018).
 29. Голованов В.И., Кузнецова Е.В. Эффективные средства огнезащиты для стальных и железобетонных конструкций

- future trends. IES Journal Part A: Civil and Structural Engineering. 2016. Vol. 4. Pp. 167–179.
27. Dybal, D.A., Shishilov, O.N., Garustovich I.V. Passivnaya ognезashchita v usloviyakh uglevodorodnogo pozhara [Passive fire protection in hydrocarbon fire]. Lakokrasochnyye materialy i ikh primeneniye. 2017. No. 6. Pp. 16–19 [Electronic resource]. System requirements: AdobeAcrobatReader. URL: https://o3.com/pdf/LKM-17-6_view-18-20.pdf (date of application: 02.12.2018). (rus)
28. Shabalin, S. Metody passivnoy ognезashchity [Methods of passive fire protection]. Gas Industry. 2017. No. 9. Pp. 122–125 [Electronic resource]. System requirements: Internet Explorer. URL: <https://elibrary.ru/item.asp?id=30006385> (date of application: 02.12.2018). (rus)
29. Golovanov, V.I., Kuznetsova, Y.V. Effektivnyye sredstva ognезashchity dlya stalnykh i zhelezobetonnykh konstruksiy [Effective Means of Fire Protection for Steel and Concrete Structures]. Industrial and civil engineering. 2015. No. 9. Pp. 82–90. (rus)
30. Zharkov, A.F., Zharkov, F.A., Chesnokova, O.G. Ognestoykost pokrytiy iz proflistov s podvesnymi potolkami s vozduшной прослойкой // Интернет-вестник ВолгГАСУ. 2015. № 4(40). С. 10 [Электронный ресурс]. Систем. требования: AdobeAcrobatReader. URL: <http://vestnik.vg.asu.ru/attachments/10ZharkovZharkovChesnokova.pdf> (дата обращения: 02.12.2018).

Marina Gravit,
+7(912)9126407; marina.gravit@mail.ru

Марина Викторовна Гравит,
+7(912)9126407; эл. почта: marina.gravit@mail.ru

Elena Golub,*
+7(911)9722466; alen-go@bk.ru

Елена Владимировна Голуб,*
+7(911)9722466; эл. почта: alen-go@bk.ru

Denis Grigoriev,
+7(911)2236078; gdm@pptech.ru

Денис Михайлович Григорьев,
+7(911)2236078; эл. почта: gdm@pptech.ru

Igor Ivanov,
+7(812)6407353; info@pptech.ru

Игорь Олегович Иванов,
+7(812)6407353; эл. почта: info@pptech.ru

© Gravit, M.V., Golub, E.V., Grigoriev, D.M., Ivanov, I.O., 2018

doi: 10.18720/MCE.84.9

Cement based foam concrete with aluminosilicate microspheres for monolithic construction

Цементный пенобетон с алюмосиликатной микросферой для монолитного домостроения

A.B. Steshenko*,
A.I. Kudyakov,
Tomsk State University of Architecture
and Building, Tomsk, Russia

Канд. техн. наук, доцент А.Б. Стешенко*,
д-р техн. наук, профессор А.И. Кудяков,
Томский государственный архитектурно-
строительный университет, г. Томск,
Россия

Key words: foam concrete mixture; microsphere; plastic shrinkage; average density; porosity; strength; softening coefficient; thermal conductivity; monolithic construction

Ключевые слова: пенобетонная смесь; микросфера; пластическая усадка; средняя плотность; пористость; прочность; коэффициент размягчения; теплопроводность; монолитное домостроение

Abstract. The present paper investigates cement foam concrete of natural hardening with aluminosilicate microsphere made from bottom ash waste from Seversk Heat and Power Station in Tomsk Region. The relevance of the given study is conditioned by the necessity to provide the required process parameters of mixture for transportation and laying the formwork, as well as providing strength and thermal and physical characteristics of wall structures for economy-class housing construction. Porous microsphere from bottom ash wastes applied within the technology of cement foam concrete of natural hardening contributes to ensuring increased microporosity and strength of inter-pore partitions of foam concrete. The study was conducted in the Laboratory of Tomsk State University of Architecture and Building which is accredited in accordance with the national standards requirements. The optimal content of microsphere in the cement foam concrete mixture was 5–10 % of the cement weight. Foam concrete mixture with microsphere possesses higher flowability and concrete has reduced plastic shrinkage by 40 %. The average pores diameter in foam concrete with microspheres is reduced from 308 to 210.2 μm , mean square deviation of the pores diameter is reduced from 23.6 to 14.2 μm . The maximum effect of reducing thermal conductivity coefficient up to the value of 33 % is observed with 5 % microsphere content of the cement weight. Inclusion of microsphere within the process of mixture formation enables to increase concrete strength at the age of 28 days by 40 % and its softening coefficient by 15 %. The elaborated composition and technology of foam concrete production with aluminosilicate microsphere is intended for use in the walls structures in monolithic construction.

Аннотация. Приведены результаты исследований цементного пенобетона естественного твердения с алюмосиликатной микросферой из золошлаковых отходов Северной ТЭЦ Томской области. Актуальность исследования обусловлена необходимостью обеспечения требуемых технологических параметров смесей для транспортирования и укладки в опалубку, а также прочностных и теплофизических характеристик стеновых конструкций для строительства комфортного жилья эконом класса. Путем применения пористой микросферы из золошлаковых отходов ТЭЦ в технологии цементного пенобетона естественного твердения достигается повышенная микропористость и прочность межпоровых перегородок пенобетона. Исследование пенобетонной смеси и пенобетона проводилось в аккредитованной лаборатории ТГАСУ в соответствии с требованиями национальных стандартов. Оптимальное содержание микросферы в цементной пенобетонной смеси – 5–10 % от массы цемента. В пенобетонной смеси с микросферой повышается растекаемость смеси и снижается пластическая усадка пенобетона в среднем на 40 %. В пенобетоне с микросферой уменьшаются средний диаметр пор с 308 до 210 мкм, среднее квадратичное отклонение среднего диаметра – с 23.6 до 14.2 мкм. Максимальный эффект снижения коэффициента теплопроводности наблюдается при дозировке микросферы 5 % от массы цемента и составляет 33 %. При введении микросферы в смесь в процессе ее приготовления повышается прочность пенобетона в 28 суточном возрасте на 40 % и коэффициент размягчения в среднем на

15 %. Разработанный состав пенобетона с алюмосиликатной микросферой предназначен для устройства стеновых конструкций малоэтажных домов в монолитном домостроении.

1. Introduction

Great attention is paid to the construction of monolithic low-rise buildings using effective wall materials from local raw materials that provide the required thermal protection, comfortable conditions and ecological safety along with affordable pricing for the people in implementing the national program "Provision with available and comfortable housing and utilities of the Russian citizens" [1].

Cement based foam concrete of natural hardening is recommended to be used while construction of wall structures in individual housing [2–6]. Foam concrete has good thermal insulation properties and adequate strength for wall structures thus providing energy efficiency and durability of a residential building during operation.

Monolithic construction of low-rise buildings using foam concrete requires ensuring the necessary process parameters of mixtures for transportation and placement, as well as the strength and thermal and physical characteristics of wall structures.

It is necessary to use a system approach during the whole lifecycle of a wall structure when managing the process of structure formation of cement based foam concrete. Also it is necessary to take into account many factors starting from selection of initial components up to maintaining the given quality parameters subjected to environmental impacts during building operation [7–10]. Proper selection of a number of processing methods for establishing high quality foam concrete production is possible due to comprehension of physical and chemical processes of structure formation, particularly at the early stage. Based on the analysis of the known processing methods [3, 5–8] the authors have recommended two effective directions to form the rational structure of foam concrete and to ensure better thermal properties and maintain or increase its strength:

- strengthening of the frame (interpore partitions);
- enhancing of porous structure (type, size and pores volume).

Effective ways to increase the quality of foam concrete mixtures and foam concrete along with reduction of cement consumption and its cost is inclusion of fine-grained active mineral additives (FAMA) into the mixture [11–13].

Improving the properties of foam concrete mixture while FAMA inclusion are attributed to the chemical interaction with the minerals of hardened cement paste [12, 14–16]. Moreover, fine-grained particles of micro-filler of colloidal size could be crystallization centers of cement newgrowths the structural elements of hardened cement are clustering around, forming mixed-type clusters of a "binder-filler" type [11, 17].

The following peculiar features of FAMA's influence on the structure formation and physical and mechanical properties of foam concrete should be specified:

- reacting with calcium hydrated of crystalhydrate cement matrix which results in enlarging the volume of hydrosilicate binder [12];
- acceleration of the initial stage of structure formation of cement composition;
- strengthening of the contact zone between the hardened cement paste and fillers in concrete;
- alteration of differential porosity of foam concrete mixture with decreasing pore size (placement of filler particles between the cement particles), which contributes to the formation of cement paste with smaller size of capillary pores and strengthening of foam concretes.

To increase the microporosity and strength of interpore partitions of foam concrete, it is recommended to introduce porous FAMA into the foam concrete mixture, given as thermo-modified peat, hollow glass microspheres and ceramic microspheres [16, 18–20].

Manufacture of glass, ceramic microspheres and thermo-modified peat requires significant energy consumption thus resulting in rising prices for the ready foam concrete products.

Therefore, in the present work authors suggest using aluminosilicate microsphere as porous FAMA made from bottom ash waste, the local silica-containing raw, from Seversk Heat and Power Station (Tomsk Region, Russia) [21–24].

After burning of coals of various deposits at the temperature of 1400–1800 °C bottom ash wastes are formed; they are washed out by the water and transported along the pipeline into ash-disposal area.

Steshenko, A.B., Kudyakov, A.I. Cement based foam concrete with aluminosilicate microspheres for monolithic construction. Magazine of Civil Engineering. 2018. 84(8). Pp. 86–96. doi: 10.18720/MCE.84.9.

Annual outlet of bottom ash wastes in Russia composes 25–30 million tons, and there are 1.2–1.5 billion tons of wastes in disposal areas. Only 8–12 % of bottom ash wastes in Russia are being used, mostly in building materials production, construction of buildings, structures and automobile roads [25]. Moreover, currently there are some difficulties with allocation of additional spaces for bottom ash wastes storage.

Microspheres have low thermal conductivity of $0.1 \text{ W/m}\cdot\text{C}$. In this regards, they are used as the initial material for production of thermal insulation ceramic products, special cements, finishing and plastering mortars for thermal insulation of external building walls [17–24]. The use of aluminosilicate microspheres, the product of the processing of ash and slag waste, in the production of foam concrete is important.

When microspheres are incremented into the foam concrete mixture, the cement matrix acquires uniformly distributed cellular structure while in inter-pore partitions microspheres originate micropores [19, 20]. Applying of microspheres almost does not complicate the technology of concrete mixture production, its cohesion is improved and closed porosity stable in time is provided making it possible to increase significantly frost resistance of foam concretes.

During assembling of walls from foam concrete mixture in monolithic construction shrinkage deformations of foam concrete occur, particularly at an early stage of structure formation due to physical-chemical interaction of cement particles with water. This complicates providing of the given geometrical sizes of wall structures and causes crack formation.

In the present work, on the ground of research results analysis authors made an assumption on possible reduction of foam concrete mixture plastic shrinkage and increase of its flowability, as well as improved properties of foam concrete by inclusion of porous additive given as microsphere.

The given research aims to elaborate scientifically-justified compositions and establish peculiar features of structure formation, and to determine the properties of foam concrete with mineral porous additive microsphere made from ash bottom wastes for its further application in wall structures of monolithic low-rise buildings.

2. Materials and Methods

In the present research FAMA given as aluminosilicate microsphere of bottom ash wastes from Seversk Heat and Power Station in Tomsk Region (Russia) were used. The picture of microsphere and its elemental and chemical compositions are given in Figures 1, 2 and Table 1. The basic elements of microsphere are Si and Al (silicon oxide and aluminium oxide). Physical properties and grain composition of microsphere are given in Tables 2, 3. Effective specific activity of natural radioactive nuclides was determined in the Accredited Laboratory of Radiation Survey of Regional Committee for Environmental Protection and Nature in Tomsk, its value is 300 Bq that makes it possible to use it in new built and reconstructed residential and public buildings.

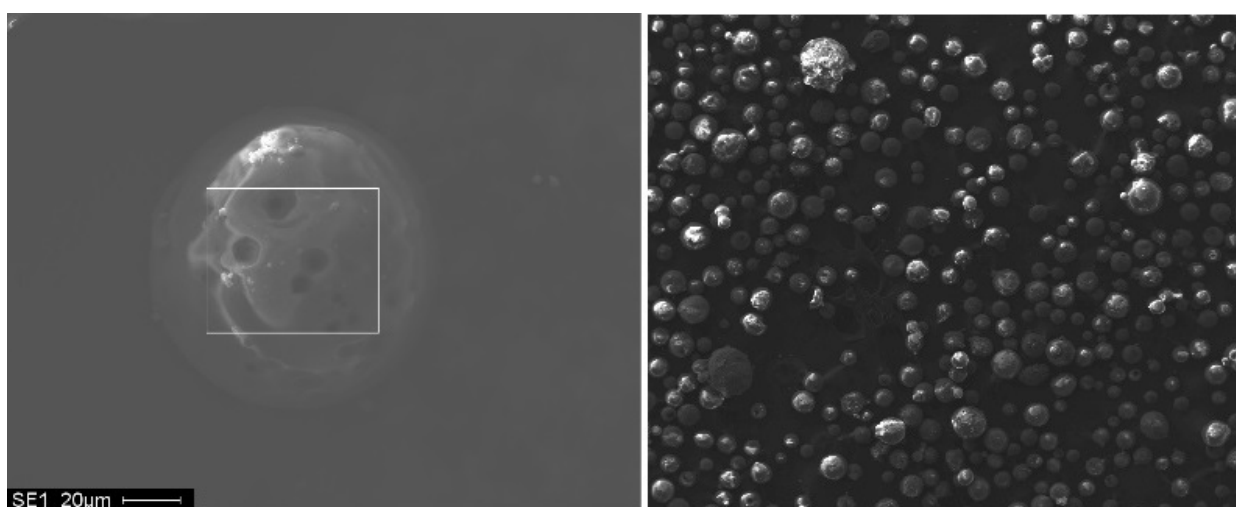


Figure 1. Microsphere (on the left – zoom x1500, on the right – zoom x100).

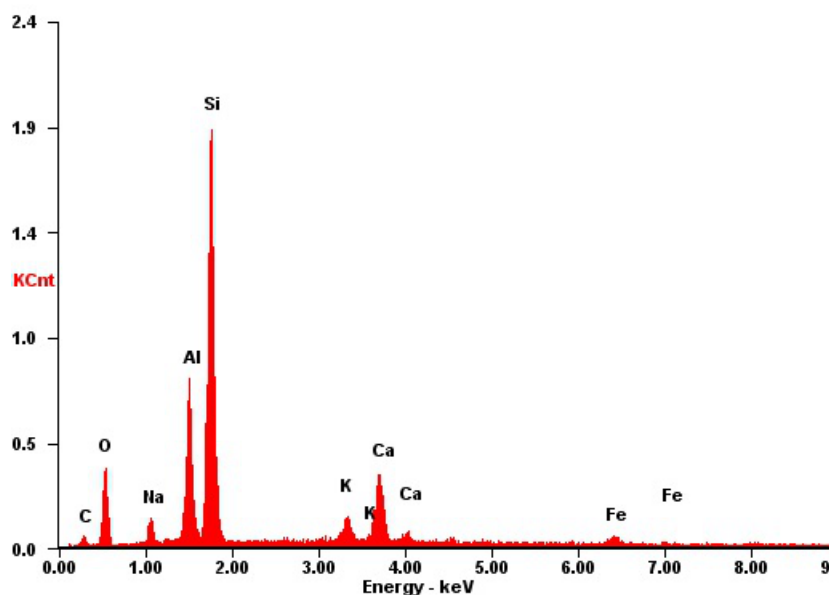


Figure 2. Elemental composition of microsphere of Seversk Heat and Power Station (Tomsk Region, Russia).

Table 1. Chemical composition of microsphere of Seversk Heat and Power Station (Tomsk Region, Russia).

| Oxides content, % | | | | | | | | | |
|-------------------|------------------|--------------------------------|--------------------------------|------|------|-----|-------------------|------------------|-----------------|
| SiO ₂ | TiO ₂ | Al ₂ O ₃ | Fe ₂ O ₃ | CaO | MgO | Mn | Na ₂ O | K ₂ O | SO ₃ |
| 47.06 | 1.17 | 22.67 | 12.44 | 4.34 | 1.49 | 0.3 | 0.94 | 0.61 | 1.25 |

Table 2. Physical properties of aluminosilicate microsphere.

| Colour | Bulk density, kg/m ³ | Apparent density, kg/m ³ | Mass humidity, % | Content of floating precipitate by weight, % |
|--------|---------------------------------|-------------------------------------|------------------|--|
| Grey | 750-800 | 1800 | 0.2 | 0.1 |

Table 3. Grain composition of aluminosilicate microsphere.

| Partial/complete residuals, % by weight on the sieves size, mm | | | | | External blinding admixtures |
|--|-------|------|------|--------|------------------------------|
| 0.5 | 0.315 | 0.16 | 0.08 | < 0.08 | |
| 0.0 | 0.0 | 0.4 | 23.1 | 23.56 | Absent |
| 0.0 | 0.0 | 0.4 | | 76,5 | |

Fractional composition of aluminosilicate microsphere corresponds to the requirements of Specifications 5712-089-00884306-2016.

As binders Portland cement of Topki Cement Factory (Kemerovo Region, Russia) CEM I 42.5H (Russian State Standard GOST 30515-2013) was used, sand of Kudrovskoe deposit of Tomsk Region (Russia) with fineness modulus 1.86 (Russian State Standards GOST 8736-2014 and GOST 26633-2012), water (Russian State Standard GOST 23732-2011) and foam agent PB-2000.

Foam concrete mixture formation was performed in one stage using laboratory foam concrete mixer. Physical and mechanical properties of foam concrete were defined in accordance with Russian State Standards requirements: compressive strength (GOST 10180-2012); average density (GOST 12730.1-78); water adsorption (GOST 12730.3-78). Thermal conductivity coefficient was determined using ITS-1 Thermal Conductivity Meter (Russian State Standard GOST 7076-99). Plastic shrinkage was determined within the first three hours from the moment of foam concrete mixture placement into the mould according to methodology described in [26]. The structure of pore volume of foam concretes was investigated using Quanta 200 3D Two-beam Scanning Electron Microscope. The images were obtained within the low vacuum mode at the stable accelerating voltage up to 20 kV. The images were further processed using computer program. The microscope is equipped with X-ray spectrometer to conduct element microanalysis (EDAX). In order to study porous structure of foam concrete mercury injection method was applied using

Quantachrome 33 Porosimeter. It allows obtaining the information on porous structure within the wide range of pores sizes.

Basic composition of foam concrete was selected in accordance with Russian Standard SN 277-80 "Instructions for the production of cellular concrete products" and given taking into account the actual average density of the concrete mix (Table 4) [8, 26].

Table 4. Basic composition of foam concrete per 1 m³.

| Content of microsphere in foam concrete | Components consumption | | | | |
|---|------------------------|----------|-----------------|-----------|---------------|
| | cement, kg | sand, kg | microsphere, kg | water, kg | foam agent, l |
| Basic (reference) | 288.0 | 144.0 | - | 216.0 | 1.7 |
| 5% | 289.6 | 146.3 | 14.8 | 217.0 | 1.7 |
| 10% | 282.5 | 144.0 | 28.8 | 218.0 | 1.7 |
| 15% | 338.0 | 149.0 | 50.2 | 219.0 | 1.7 |

During the research the content of microsphere in foam concrete mixture was changing from 5 to 25 % of the cement weight. For the freshly mixed foam concrete mixture that can be transported and laid in the formwork it is required to provide good flowability along the length of the molded wall structure. It also requires conducting rheological properties assessment within the process technology of building structures production, particularly in the process of early structure formation of foam concrete.

In order to establish the ways microsphere influences the volume changes of mixture within the first hours of structure formation the studies of plastic shrinkage of foam concrete mixtures were carried out. Plastic shrinkage has a negative influence on the formation of porous structure, it causes crack formation and complicates provision of a close contact with the elements of wall structure, for instance with window and door frames [27–29].

3. Results and Discussion

It was established experimentally (Figure 3) that along with inclusion of aluminosilicate microsphere into the mixture it gets more plastic. The spread diameter of foam concrete mixture with additive was determined using Suttard's Viscosity Analyzer and its value increased from 10 to 15.5 cm, which can be explained by decrease in the sizes of entrained air bubbles in foam concrete mixture, as well as glass-covered surface, and by the less surface area of microspheres [30]. We should also note the significant difference of the apparent density of microspheres (1800 kg/m³) and cement paste 1750 kg/m³ in foam concrete mixture.

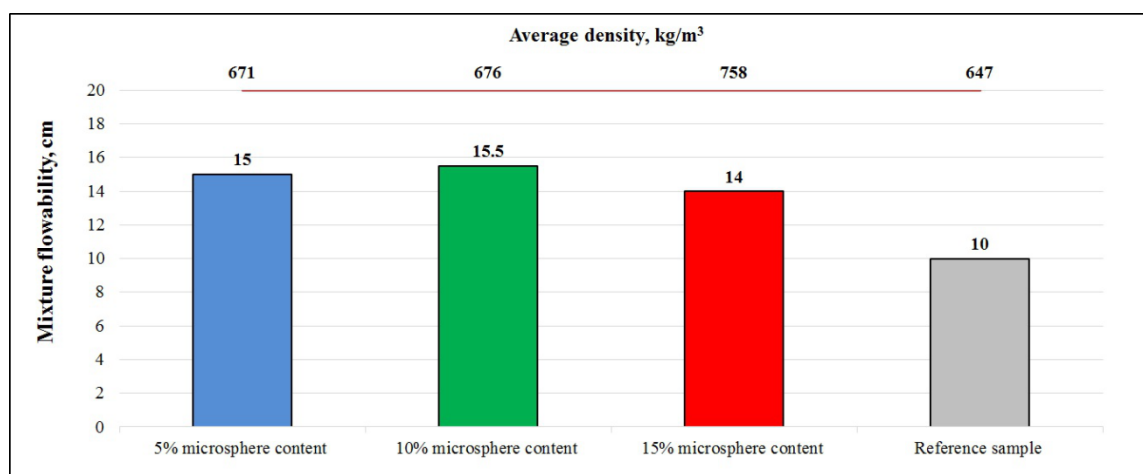


Figure 3. The influence of aluminosilicate microsphere on the flowability and average density of foam concrete mixture.

In case the content of aluminosilicate microsphere is 15 % of the cement weight, the process of foam formation deteriorates and results in reduction of volume and enlargement of the average density of the obtained foam concrete mixture by 111 kg/m³ (up to 758 kg/m³). Resulting from the conducted studies it was concluded to use microspheres in the amount of 5 and 10 % of the cement weight in further studies of foam concrete mixture and foam concrete.

Results of studies in plastic shrinkage of foam concrete mixtures are given in Figure 4. The assumption made by authors was proved experimentally. When aluminosilicate microsphere is applied in foam concrete mixtures in the amount of 5 % of the cement weight shrinkage decreases by 28.8 %, and in the amount of 10 % it decreases by 52.3 %. Thanks to the ideal shape and small size of microsphere particles effective filling of inter-pore partitions is provided. Along with that acceleration of early structure formation process occurs, homogenous fine-grained structure is formed with even distribution of pores along the whole volume; this contributes to the reduction of plastic deformation at the early stages of structure formation.

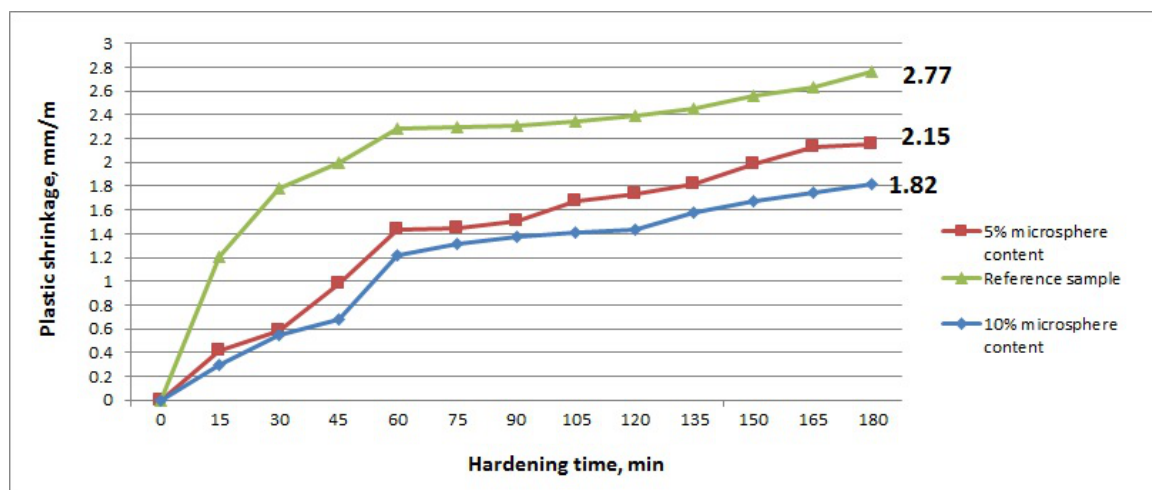


Figure 4. Plastic shrinkage of foam concrete mixture with microsphere.

The largest interest in controlling the quality of foam concrete with microsphere is taken by the studies of parameters of porous structure, namely the type, size and volume of the pores using Quanta 200 3D scanning electron microscope. Results of studies of 28-days foam concrete samples after mechanical compressive tests are given in Figure 5 and Table 5. It is seen from the images that the basic feature of foam concrete samples with aluminosilicate microsphere is more homogenous structure; the pores are evenly distributed along the whole volume. In foam concrete without additives perforated inter-pore partitions are observed.

Improvement of the structure of foam concrete hardening system occurs by interaction of aluminosilicate microsphere with the cement matrix. The cluster "binder-filler" is formed due to high surface energy of filler particles which compacts the structure of inter-pore space of foam concrete (Figure 5, b–c). Microsphere inclusion contributed to the formation of large amount of closed pores. At the same time, general porosity of foam concrete almost does not change. Redistribution of the type and pores volume takes place.

By means of computer research the average pores diameter of a sample of cellular structure was determined, and average square deviation (δ) was defined. The average square deviation of the average pore diameter characterizes polydispersity of cellular pores, i.e. their quantity distribution by sizes. After inclusion of microsphere into foam concrete mixture in the amount of 5 and 10 % the average diameter of foam concrete pores decreases from 308 to 210 and 242 μm , the average square deviation of the average pores diameter is reduced from 23.6 to 15.5 and 8.2, the volume of open capillary pores is reduced from 20.40 % to 12.47 and 12.34 %, porosity of conventionally closed pores is increased from 22.93 % to 29.77 and 38.48 %, microporosity of foam concrete decreases from 0.05 to 0.04 and sorption humidity decreases by 16 %, accordingly. The average density of foam concrete with microspheres decreases by 1–3 %, i.e. almost does not change.

Based on test results provided in Table 6, the strength of foam concrete with 5 % microsphere content at the age of 28 days increased by 40 %. Water adsorption by weight decreases significantly in foam concrete with 5 % microsphere content from 40.0 to 25.2 % and further with microsphere content of 10 % it almost does not decrease. The values of water adsorption correlate well with the defined porosity parameters, i.e. to the content of closed pores in the foam concrete samples with microspheres. By full immersion of samples about one third of the pores volume and capillaries remain unfilled with water.

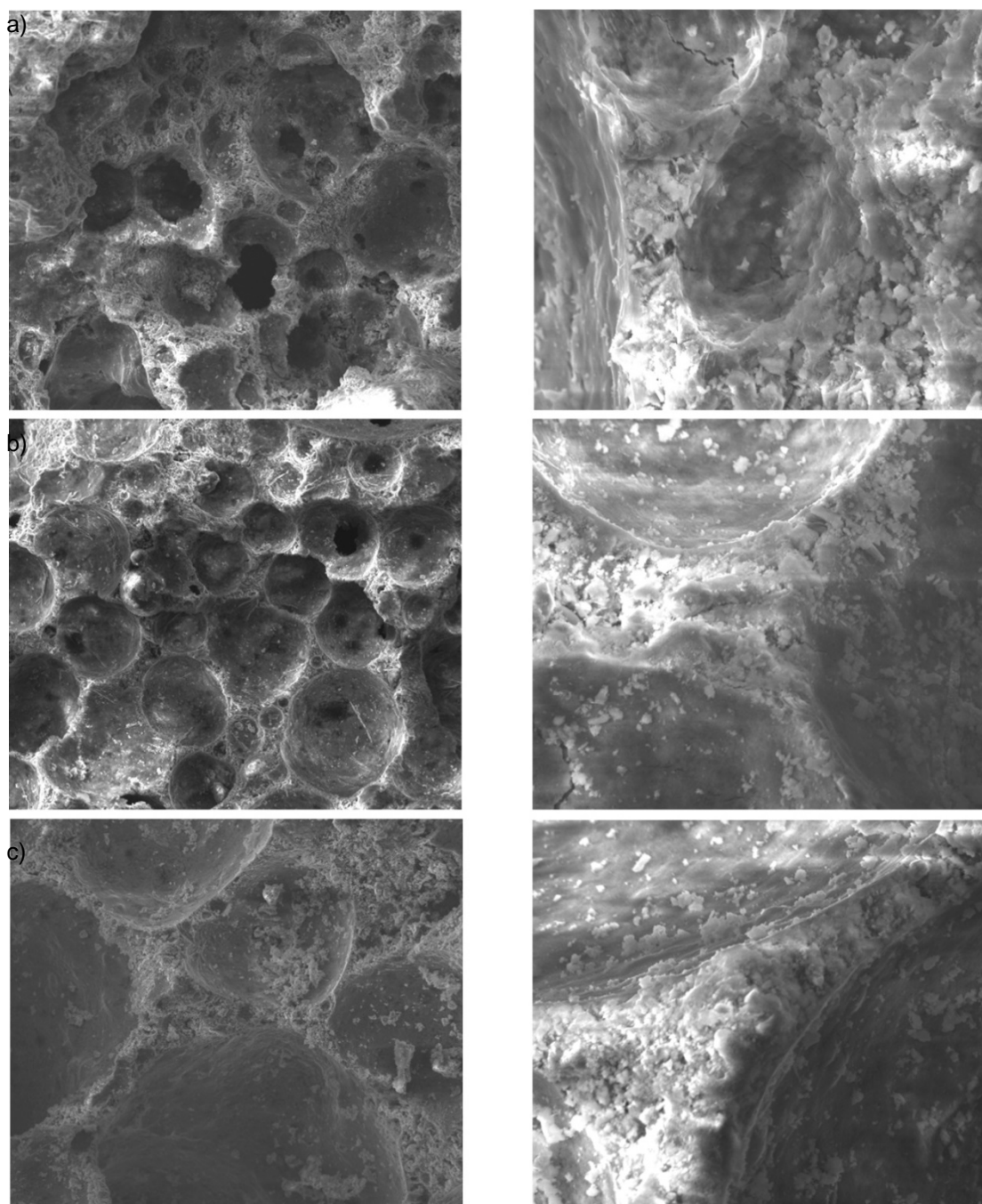


Figure 5. Structure of cement based foam concrete. On the left – zoom x250, on the right – zoom x2000: a) without additives b) with 5 % microsphere content c) with 10 % microsphere content.

Table 5. The influence of microsphere on the changing parameters of foam concrete porous structure.

| Foam concrete with additives | Average density, kg/m ³ | Average pores diameter, μm | δ of pores diameter | General porosity, % | The volume of open capillary pores, % | Porosity of conventionally closed pores, % | Microporosity index | Sorption humidity % |
|------------------------------|------------------------------------|----------------------------|---------------------|---------------------|---------------------------------------|--|---------------------|---------------------|
| Without additive | 510 | 308 | 23.6 | 77.83 | 20.40 | 22.93 | 0.05 | 5.8 |
| 5 % Microsphere content | 495 | 210 | 14.2 | 78.24 | 12.47 | 29.77 | 0.04 | 4.99 |
| 10 % Microsphere content | 505 | 242 | 16.3 | 77.46 | 12.34 | 38.48 | 0.04 | 5.2 |

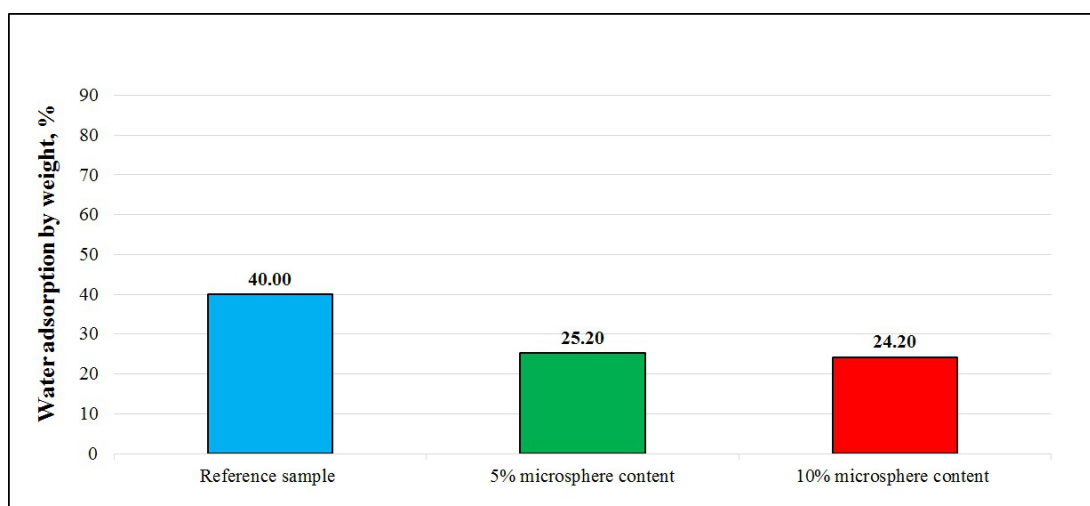


Figure 6. Influence of microsphere on water adsorption by foam concrete weight.

Table 6. Softening coefficients of foam concrete with microsphere.

| Composition | Ultimate compressive strength, MPa | | Softening coefficient |
|--------------------------|------------------------------------|------------------------|-----------------------|
| | prior to water saturation | after water saturation | |
| 5 % microsphere content | 1.26 | 1.1 | 0.86 |
| 10 % microsphere content | 1.55 | 1.4 | 0.90 |
| Reference sample | 0.9 | 0.7 | 0.77 |

The capacity of porous materials to moisten while they contact with water due to capillary suction and saturate with water mainly define further operation properties of building products: strength and frost resistance. The ability of foam concrete to keep compressive strength in humid conditions is estimated by the softening coefficient. Table 6 shows softening coefficients of foam concrete samples with microspheres.

Softening coefficient of foam concretes with aluminosilicate microsphere is 13–17 % higher compared to the reference sample. This is explained by the fact that these samples acquire optimal structure with the least amount of contact pores which do not let water inside foam concrete.

The data on thermal conductivity of foam concrete samples are given in Figure 7.

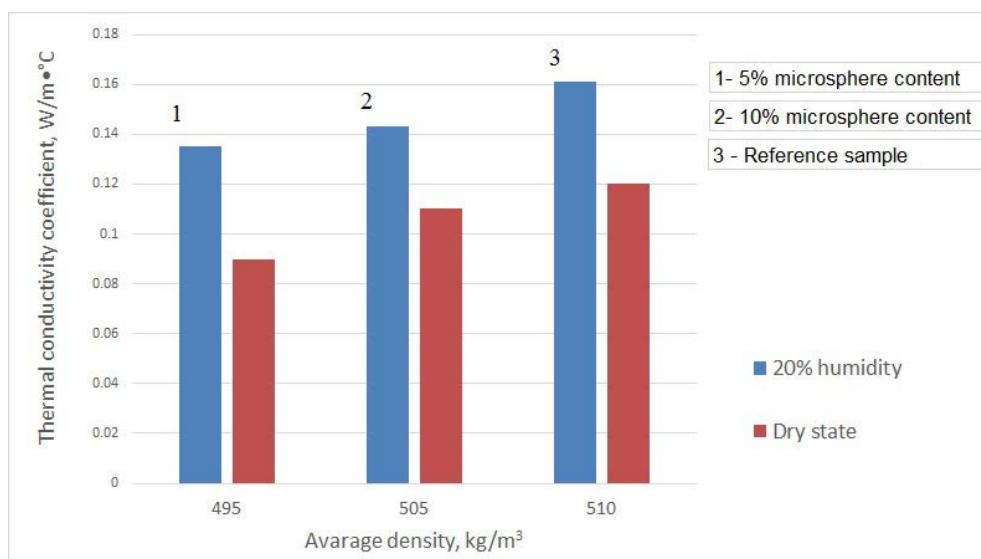


Figure 7. Thermal conductivity of cement based foam concrete samples.

Having analyzed the obtained results, it can be concluded that thermal conductivity coefficient of foam concrete in dry state with 5 % aluminosilicate microsphere content was reduced by almost 33 % and with 10 % content by 8 % compared to the reference sample. The obtained results correspond to the

requirements of Russian State Standard GOST 25485-89 "Cellular concretes. Specifications" in terms of average density of the elaborated foam concrete composition.

Using the received research results authors developed actual compositions to establish resource-saving technology for production of porous cement building compositions with regulated volume changes using porous mineral additives from bottom ash wastes for their further use in wall structures of monolithic construction.

4. Conclusions

1. Optimal content of aluminosilicate microsphere made from bottom ash wastes from Seversk Heat and Power Station is 5–10 % of the cement weight in foam concrete mixture based on Portland cement, sand, water and a foaming agent. Foam concrete mixture with aluminosilicate microsphere has better flowability of mixture from 10 to 15.5 cm and reduced plastic shrinkage of natural hardening foam concrete by 28.8–52.3 %.

2. Foam concrete mixture with aluminosilicate microsphere has its average pores diameter decreased from 308 to 210 μm , average square error decreased from 23.6 to 14.2, microporosity decreased from 0.05 to 0.04, and sorption humidity decreased by 16 %. The maximum effect in reduction of thermal conductivity coefficient was observed by 5 % microsphere content of the cement weight and its value is 33 %.

3. Inclusion of microsphere into foam concrete mixture enables to increase foam concrete strength at the age of 28 days by 40 % and softening coefficient by 13–17 %.

4. Good agreement of the experimental results obtained by the authors was established while elaboration of scientifically-justified compositions of foam concrete with application of aluminosilicate microspheres made from bottom ash wastes, and that agrees with the other private research results of other authors obtained during application of glassceramic and ceramic microspheres and given in independent sources.

5. Resulting from studies recommendations were formulated on compositions of foam concrete with aluminosilicate microspheres for monolithic construction of wall structures in low-rise housing.

5. Acknowledgement

The research was conducted with the financial support of Russian Foundation for Basic Research and administration of Tomsk Region within the research project No. 18-48-703042.

References

- Gusakova, N.V., Filyushina, K.E., Gusakov, A.M., Minaev, N.N. Selection criteria of space planning and structural solutions of low-rise buildings. *Magazine of Civil Engineering*. 2017. 75(7). Pp. 84–93. DOI: 10.18720/MCE.75.8.
- Vytchikov, Y., Saparev, M., Golikov, V. Application of monolithic foam concrete in building envelopes of a cottage, used in conditions of intermittent heating. *MATEC Web of Conferences*. Vol. 196. № 04015. Pp. 1–5. DOI: 10.1051/mateconf/201819604015
- Mestnikov, A. Thermal highly porous insulation materials made of mineral raw materials. *IOP Conf. Ser.: Mater. Sci. Eng.* 2015. Vol. 71. No. 012014. Pp. 1–4. DOI: 10.1088/1757 899X/71/1/012014
- Gola, L., Václavík, V., Valíček, J., Harničárová, M., Kušnerová, M., Dvorský, T. Drainage concrete based on cement composite and industrial waste. *Mechanical and Materials Engineering of Modern Structure and Component Design. Advanced Structured Materials*. 2015. Vol. 70. Pp. 155–165. DOI: 10.1007/978-3-319-19443-1_12
- Dunn, T., van Zijl, G., van Rooyen, A.S. Investigating a reinforced lightweight foamed concrete walling system for low-rise residential buildings in moderate seismic regions. *Journal of Building Engineering*. 2018. Vol. 20. Pp. 663–670. DOI: 10.1016/j.jobbe.2018.09.011
- Morgun, V.N., Morgun, L.V. The effect of the ratio between water and foam concentrate at the desired density in the foam concrete mixes. *Materials Science Forum*. 2018. Vol. 931. Pp. 573–577. DOI: 10.4028/www.scientific.net/MSF.931.573

Литература

- Гусакова Н.В., Филюшина К.Э., Гусаков А.М., Минаев Н.Н. Критерии выбора объемно-планировочных и конструктивных решений малоэтажных зданий // *Инженерно-строительный журнал*. 2017. № 7(75). С. 84–93. DOI: 10.18720/MCE.75.8
- Vytchikov Y., Saparev M., Golikov V. Application of monolithic foam concrete in building envelopes of a cottage, used in conditions of intermittent heating // *MATEC Web of Conferences*. Vol. 196. № 04015. Pp. 1–5. DOI: 10.1051/mateconf/201819604015
- Mestnikov A. Thermal highly porous insulation materials made of mineral raw materials // *IOP Conf. Ser.: Mater. Sci. Eng.* 2015. Vol. 71. № 012014. Pp. 1–4. DOI: 10.1088/1757 899X/71/1/012014
- Gola L., Václavík V., Valíček J., Harničárová M., Kušnerová M., Dvorský T. Drainage concrete based on cement composite and industrial waste // *Mechanical and Materials Engineering of Modern Structure and Component Design. Advanced Structured Materials*. 2015. Vol. 70. Pp. 155–165. DOI: 10.1007/978-3-319-19443-1_12
- Dunn T., van Zijl G., van Rooyen A.S. Investigating a reinforced lightweight foamed concrete walling system for low-rise residential buildings in moderate seismic regions // *Journal of Building Engineering*. 2018. Vol. 20. Pp. 663–670. DOI: 10.1016/j.jobbe.2018.09.011
- Morgun V.N., Morgun L.V. The effect of the ratio between water and foam concentrate at the desired density in the foam concrete mixes // *Materials Science Forum*. 2018. Vol. 931.

Стешенко А.Б., Кудяков А.И. Цементный пенобетон с алюмосиликатной микросферой для монолитного домостроения // *Инженерно-строительный журнал*. 2018. № 8(84). С. 86–96.

7. Namsonea, E., Šahmenkoa, G., Korjakin, A. Durability properties of high performance foamed concrete. *Procedia Engineering*. 2017. Vol. 172. Pp. 760–767. DOI: 10.1016/j.proeng.2017.02.120
8. Kudryakov, A.I., Steshenko, A.B. Investigation of the influence of the crystalline glyoxal on properties of air hardened cement based foam concrete. *Lett. Mater.* 2015. 5(1). Pp. 3–6. DOI: 10.22226/2410-3535-2015-1-3-6. (rus)
9. Ghazy, M.F., Abd, El Hameed, M.F. Optimization of lightweight concrete process by Gray-Taguchi method. *ACI Mater. J.* 2015. Vol. 112. Pp. 365–373. DOI: 10.14359/51687235
10. Kozłowski, M., Kadela, M. Mechanical characterization of lightweight foamed concrete. *Advances in Materials Science and Engineering*. 2018. Vol. 2018. № 6801258. Pp. 1–8. DOI: 10.1155/2018/6801258
11. Kunhanandan Nambiar, E.K. Influence of filler type on the properties of foam concrete. *Cem. Concr. Compos.* 2006. Vol. 28. Pp. 475–480. DOI: 10.1016/j.cemconcomp.2005.12.001
12. Gökçe, H.S., Hatungimana, D., Ramyar, K. Effect of fly ash and silica fume on hardened properties of foam concrete. *Constr. Build. Mater.* 2019. Vol. 194. Pp. 1–11. DOI: 10.1016/j.conbuildmat.2018.11.036
13. Chen, B., Wu, Z., Liu, N. Experimental research on properties of high-strength foamed concrete. *J. Mater. Civ. Eng.* 2012. Vol. 24. Pp. 113–118. DOI: 10.1061/(ASCE)MT.1943-5533.0000353
14. Onprom, P., Chaimoon, K., Cheerarot, R. Influence of bottom ash replacements as fine aggregate on the property of cellular concrete with various foam contents. *Advances in Materials Science and Engineering*. 2015. Vol. 2015. Pp. 1–11. DOI: 10.1155/2015/381704
15. Abdulrahman Hilal, A., Thom, N., Dawson, A. The use of additives to enhance properties of pre-formed foamed concrete. *International Journal of Engineering and Technology*. 2015. Vol. 7. № 4. Pp. 286–293. DOI: 10.7763/IJET.2015.V7.806
16. Kudryakov, A.I. et al. Foam concrete of increased strength with the thermomodified peat additives. *IOP Conf. Ser.: Mater. Sci. Eng.* Vol. 71. № 012012. Pp. 1–7. DOI: 10.1088/1757-899X/71/1/012012
17. Inozemtsev, A.S., Korolev, E.V. Osobennosti reologicheskikh svoystv vysokoprochnykh legkikh betonov na polykh mikrosferakh [Peculiar Rheological Properties of Highstrength Lightweight Concretes Having Hollow Microspheres]. *Vestnik MGSU*. 2013. No. 6. Pp. 100–108. DOI: 10.22227/1997-0935.2013.6.100-108. (rus)
18. Inozemtcev, A.S., Korolev, E.V. A method for the reduction of deformation of high-strength lightweight cement concrete. *Advances in Cement Research*. 2016. Vol. 28. Pp. 92–98. DOI: 10.1680/jadcr.15.00049
19. Oreshkin, D.V., Semenov, V.S., Belyayev, K.V., Rozovskaya, T.A. Syryevaya smes dlya polucheniya penobetona [Raw mix for foam concrete]. Patent Russia no. 2507182, 2012. (rus)
20. Kotlyarevskaya, A.V. Penofibrobetony s primeneniym mikrouprochniteley i modifitsiruyushchikh dobavok [Foam-fiber concrete with the use of micro-strength and modifying additives]. PhD Thesis. Volgograd, 2013. 161 p. (rus)
21. Sokol, E.V. et al. Hollow silicate microspheres from fly ashes of the Chelyabinsk brown coals (South Urals, Russia). *Fuel Processing Technology*. 2000. Vol. 67. Pp. 35–52. DOI: 10.1016/S0378-3820(00)00084-9
22. Semenov, V. Properties of dry masonry mixtures based on hollow aluminosilicate microspheres. *MATEC Web of Conferences*. 2017. Vol. 117. No. 00149. Pp. 1–7. DOI: 10.1051/mateconf/20171170014900149.
23. Bubnov, A.S., Khorev, V.S., Boyko, I.A. The effect of lightweight agents on the density of cement slurry applied during oil and gas well drilling. *IOP Conf. Series: Earth and Pp.* 573–577. DOI: 10.4028/www.scientific.net/MSF.931.573
7. Namsonea E., Šahmenkoa G., Korjakin A. Durability properties of high performance foamed concrete // *Procedia Engineering*. 2017. Vol. 172. Pp. 760–767. DOI: 10.1016/j.proeng.2017.02.120
8. Кудряков А.И., Стешенко А.Б. Исследование влияния кристаллического глиоксала на свойства цементного пенобетона естественного твердения // *Письма о материалах*. 2015. Т. 5. № 1. С. 3–6. DOI: 10.22226/2410-3535-2015-1-3-6
9. Ghazy M.F., Abd El Hameed M.F. Optimization of lightweight concrete process by Gray-Taguchi method // *ACI Mater. J.* 2015. Vol. 112. Pp. 365–373. DOI: 10.14359/51687235
10. Kozłowski M., Kadela M. Mechanical characterization of lightweight foamed concrete // *Advances in Materials Science and Engineering*. 2018. Vol. 2018. № 6801258. Pp. 1–8. DOI: 10.1155/2018/6801258
11. Kunhanandan Nambiar E.K. Influence of filler type on the properties of foam concrete // *Cem. Concr. Compos.* 2006. Vol. 28. Pp. 475–480. DOI: 10.1016/j.cemconcomp.2005.12.001
12. Gökçe H.S., Hatungimana D., Ramyar K. Effect of fly ash and silica fume on hardened properties of foam concrete // *Constr. Build. Mater.* 2019. Vol. 194. Pp. 1–11. DOI: 10.1016/j.conbuildmat.2018.11.036
13. Chen B., Wu Z., Liu N. Experimental research on properties of high-strength foamed concrete // *J. Mater. Civ. Eng.* 2012. Vol. 24. Pp. 113–118. DOI: 10.1061/(ASCE)MT.1943-5533.0000353
14. Onprom P., Chaimoon K., Cheerarot R. Influence of bottom ash replacements as fine aggregate on the property of cellular concrete with various foam contents // *Advances in Materials Science and Engineering*. 2015. Vol. 2015. Pp. 1–11. DOI: 10.1155/2015/381704
15. Abdulrahman Hilal A., Thom N., Dawson A. The use of additives to enhance properties of pre-formed foamed concrete // *International Journal of Engineering and Technology*. 2015. Vol. 7. № 4. Pp. 286–293. DOI: 10.7763/IJET.2015.V7.806
16. Kudryakov A.I. et al. Foam concrete of increased strength with the thermomodified peat additives // *IOP Conf. Ser.: Mater. Sci. Eng.* Vol. 71. № 012012. Pp. 1–7. DOI: 10.1088/1757-899X/71/1/012012
17. Иноземцев А.С., Королев Е.В. Особенности реологических свойств высокопрочных легких бетонов на полых микросферах // *Вестник МГСУ*. 2013. № 6. С. 100–108. DOI: 10.22227/1997-0935.2013.6.100-108
18. Inozemtcev A.S., Korolev E.V. A method for the reduction of deformation of high-strength lightweight cement concrete // *Advances in Cement Research*. 2016. Vol. 28. Pp. 92–98. DOI: 10.1680/jadcr.15.00049
19. Патент 2507182 С1 Российская Федерация, МПК С04В 38/10. Сырьевая смесь для получения пенобетона / Орешкин Д.В., Семёнов В.С., Беляев К.В., Розовская Т.А., 2012.
20. Котляревская А.В. Пенофибробетоны с применением микропрочнителей и модифицирующих добавок: дис ... канд. техн. наук: спец. 05.23.05. Волгоград, 2013. 161 с.
21. Sokol E.V. et al. Hollow silicate microspheres from fly ashes of the Chelyabinsk brown coals (South Urals, Russia) // *Fuel Processing Technology*. 2000. Vol. 67. Pp. 35–52. DOI: 10.1016/S0378-3820(00)00084-9
22. Semenov V. Properties of dry masonry mixtures based on hollow aluminosilicate microspheres // *MATEC Web of Conferences*. 2017. Vol. 117. №. 00149. Pp. 1–7. DOI: 10.1051/mateconf/20171170014900149.
23. Bubnov A.S., Khorev V.S., Boyko I.A. The effect of lightweight agents on the density of cement slurry applied during oil and gas well drilling // *IOP Conf. Series: Earth and*

- Environmental Science. 2015. Vol. 24. № 012008. Pp. 1-5. DOI: 10.1088/1755-1315/24/1/012008
24. Inozemtcev, A.S. Srednyaya plotnost i poristost vysokoprochnykh legkikh betonov [Average density and porosity of high-strength lightweight concrete]. Magazine of Civil Engineering. 2014. No. 7(51). Pp. 31–37 DOI: 10.5862/MCE.51.4. (rus)
 25. Sirotyuk, V.V., Lunev, A.A. Strength and deformation characteristics of ash and slag mixture. Magazine of Civil Engineering. 2017. 74(6). Pp. 3–16. DOI: 10.18720/MCE.74.1.
 26. Steshenko, A.B., Kudyakov, A.I. Ranneye strukturoobrazovaniye penobetonnoy smesi s modifitsiruyushchey dobavkoy [Early structure formation of foam concrete mix containing modifying admixture]. Magazine of Civil Engineering. 2015. 54(2). Pp. 56–62. DOI: 10.5862/MCE.54.6.
 27. Ghourchian, S., Wyrzykowski, M., Plamondon, M., Lura, P. On the mechanism of plastic shrinkage cracking in fresh cementitious materials. Cem. Concr. Res. 2019. Vol. 115. Pp. 251–263. DOI: 10.1016/j.cemconres.2018.04.013
 28. Kudyakov, A.I., Steshenko, A.B. Shrinkage deformation of cement foam concrete. IOP Conf. Ser.: Mater. Sci. Eng. 2015. Vol. 71. No. 012019. Pp. 1–5. DOI: 10.1088/1757-899X/71/1/012019
 29. Steshenko, A.B., Kudyakov, A.I., Konusheva, V.V., Syrkin, O.O. Structure formation control of foam concrete. AIP Conf. Proc. 2017. Vol. 1800. No. 020001. Pp. 1–8. DOI: 10.1063/1.4973017
 30. Sagradyan, A.A., Zimakova, G.A. Izucheniye svoystv tyazhelogo betona, modifitsirovannogo organomineralnoy dobavkoy, vklyuchayushchey zolnyye mikrosfery [The study of the properties of heavy concrete, modified organo-mineral additive, including ash microspheres]. Izvestiya vysshikh uchebnykh zavedeniy. Stroitelstvo. 2012. No. 4. Pp. 26–31. (rus)
- Environmental Science. 2015. Vol. 24. № 012008. Pp. 1–5. DOI: 10.1088/1755-1315/24/1/012008
24. Иноземцев А.С. Средняя плотность и пористость легких бетонов // Инженерно-строительный журнал. 2014. № 7. С. 31–37. DOI: 10.5862/MCE.51.4
 25. Сиротюк В.В., Лунёв А.А. Прочностные и деформационные характеристики золошлаковой смеси // Инженерно-строительный журнал. 2017. № 6(74). С. 3–16. DOI: 10.18720/MCE.74.1
 26. Стешенко А.Б., Кудяков А.И. Раннее структурообразование пенобетонной смеси с модифицирующей добавкой // Инженерно-строительный журнал. 2015. № 2(54). С. 56–62. DOI: 10.5862/MCE.54.6
 27. Ghourchian S., Wyrzykowski M., Plamondon M., Lura P. On the mechanism of plastic shrinkage cracking in fresh cementitious materials // Cem. Concr. Res. 2019. Vol. 115. Pp. 251-263. DOI: 10.1016/j.cemconres.2018.04.013
 28. Kudyakov A.I., Steshenko A.B. Shrinkage deformation of cement foam concrete // IOP Conf. Ser.: Mater. Sci. Eng. 2015. Vol. 71. № 012019. Pp. 1–5. DOI: 10.1088/1757-899X/71/1/012019
 29. Steshenko A.B., Kudyakov A.I., Konusheva V.V., Syrkin O.O. Structure formation control of foam concrete // AIP Conf. Proc. 2017. Vol. 1800. № 020001. Pp. 1–8. DOI: 10.1063/1.4973017
 30. Саградян А.А., Зимакова Г.А. Изучение свойств тяжелого бетона, модифицированного органоминеральной добавкой, включающей золыные микросферы // Известия высших учебных заведений. Строительство. 2012. № 4. С. 26–31.

*Aleksei Steshenko**,
+7(909)5396643; steshenko.alexey@gmail.com

Aleksandr Kudyakov,
+7(913)8208554; kudyakow@mail.tomsknet.ru

*Алексей Борисович Стешенко**,
+7(909)5396643;
эл. почта: steshenko.alexey@gmail.com

Александр Иванович Кудяков,
+7(913)8208554;
эл. почта: kudyakow@mail.tomsknet.ru

© Steshenko, A.B., Kudyakov, A.I., 2018

doi: 10.18720/MCE.84.10

Rheological behavior of 3D printable cement paste: critical evaluation

Критериальная оценка реологических характеристик цементных систем для строительной 3D-печати

G.S. Slavcheva*,
O.V. Artamonova,
Voronezh State Technical University, Voronezh,
Russia

Д-р техн. наук, профессор Г.С. Славчева*,
канд. хим. наук, доцент О.В. Артамонова,
Воронежский государственный технический
университет, г. Воронеж, Россия

Key words: 3D build printing; cement paste;
rheology; squeezing test; extrudability; buildability

Ключевые слова: строительная 3D-печать;
цементные смеси; реология; сдвигающий
тест; экструдированность; формоустойчивость

Abstract. The extrudability and firm stability are the critical rheological characteristics of building 3D printable mixtures. From the point of view of classical rheology of disperse systems, the theoretical analysis of the rheological behavior of a cement paste has been analyzed for all stages of 3D printing process. Apparently both the theoretical analysis criteria and technological tools to control rheological behavior of a 3D printable mixture have been justified. The squeezing test is used in the experimental research as a rheological behavior identification tool of cement-based materials, in order to evaluate the extrudability and buildability. The squeezing test, with constant plate speed, is determining plastic yield value and elasticity criterion of a cement paste as criteria of the extrudability. The squeezing test, with constant strain rate, is determining structural and plastic strength, plastic deformations as a criteria for the ability of a cement paste to hold shape during multi-layer casting. It is shown that these properties are significantly controlled by the W/C-ratio, concentration of plasticizer additives as factors of changes in the concentration of the dispersed phase and properties of the dispersion liquid in a system «cement + water» as matrix for printing concrete.

Аннотация. С позиций классической структурной реологии дисперсных систем произведен теоретический анализ реологического поведения смесей в процессе 3D-печати. Обоснованы технологические факторы регулирования экструдированности и формоустойчивости как критериальных реологических характеристик смесей. Представлены результаты экспериментальных исследований экструдированности и формоустойчивости модельных цементных систем как матриц смесей для 3D-печати. Для оценки экструдированности использован сдвигающий тест с постоянной скоростью деформирования, по результатам которого найдены критериальные значения пределов ползучести, текучести и эластичности цементных систем. Для оценки формоустойчивости использован сдвигающий тест с постоянной скоростью нагружения, по результатам которого найдены значения структурной и пластической прочности, пластических деформаций цементных систем, характеризующие их способность сохранять форму при действии возрастающих сжимающих напряжений в процессе печати. Получены количественные данные о влиянии В/Ц-отношения и концентрации суперпластификатора на комплекс реологических характеристик цементных систем. Установлено, что В/Ц-отношение, определяющее концентрацию частиц дисперсной фазы в системе «цемент + вода», является главным фактором структурирования и упрочнения цементных систем. Введение пластификатора как фактора изменения свойств дисперсионной среды является средством не только регулирования пластичности, но повышения формоустойчивости.

1. Introduction

3D-building printing is an innovative process of robotized creation of minor architecture forms, single structural elements of buildings and low storey houses by multilayer casting of viscoplastic materials [1]. Potential advantages of this process include ability to receive materials of different functionality directly at the construction site, to print freeform constructions without mould, to reduce materials consumption and labor input of construction [2, 3]. One of the top priority problems defining the ability to introduce this

innovative method of constructing building sites into building practice is the problem of creating nomenclature of mixtures ensuring the implementation of this process. Efficiency and manufacturability of 3D-building printing depend on the adjustability of parameters of the mixtures at all stages of the process. To ensure the required quality and construction time, management of rheological behaviour of mixtures must be done according to the conditions securing fluidity for their transfer, plasticity for extrusion, integrity of surface shape after laying, structural durability for load accommodation of the upper layers. The processes of preparation and transportation of the mixture to the extruder are maximally adapted to the existing building machinery, therefore the issue of adjusting technical parameters of mixtures at these stages of the technological process has been studied quite well. However, at other stages of the process rheological behaviour has to be significantly different from traditional properties of building mixtures and composites. Fundamental possibility and efficiency of their implementation are defined by extrudability, buildability, structural build up of mixtures and composites.

Currently, the studies being conducted can be divided in two categories. In the first one, researchers focus their attention on the issues of optimization of mixture compositions [4–13]. As a result of collecting an array of experimental information, quite a big nomenclature of mixture has been received and tested. The obtained mixtures are multi-component, their compositions include superplasticizers, viscosity modifying additives, structural build-up regulators, fillers and filling materials of various chemical-mineral composition and dispersibility. Still, there is no systemized information and common approaches to explanation of the role of each of formula factors for guided regulation of extrudability, buildability and structural build up of mixtures. Only the influence of dosage of superplasticizer on the parameters of fluidity of mixtures has been definitely established (for instance, in studies [9–10]).

The second category of research is aimed at the study and modelling of rheological behavior of disperse systems in the processes of 3D printing [14–22]. Approaches to implementation of the studies are based on squeeze flow theory, key points of which are summarized in the study [14]. As a result, methods of squeeze flow rheometry as a tool of identifying 3D printable building materials rheological behaviour under compression stress typical for extrusion and multi-layer casting have been formed and have become widely spread. One of the most effective methods of squeeze flow rheometry is grounded in the works of N. Roussel [15–16] who developed the squeezing test with constant plate speed. The constant plate speed may vary within the range of 0.1–5 mm/s depending on the properties of the studied materials. Plastic yield value of viscoplastic materials is determined as quantitative criterion of extrudability based on the results of squeezing test. The second option of evaluation of 3D-printability of building mixtures under compression is grounded and implemented in the works of A. Perrot [17]. This option presupposes modelling the parameters of loading on the first poured layer from consistently growing pressure of the upper poured layers. During the test a sample is gradually loaded until cracks appear in its side faces. Based on the results of the experiment, structural strength and time of the beginning of destruction are determined as quantitative criteria of buildability. The developed approaches of squeeze flow rheometry and methods of squeezing tests should be accepted as maximally adapted to the conditions of 3D-building printing.

Problem statement of the studies is conditioned by the need to form common approaches to the parameters of mixtures optimization by the criteria of extrudability, buildability and structural build up. Formation of such approaches, acquisition of quantitative data on the influence of different formula factors on rheological behavior will allow unambiguously substantiating the requirements for their compositional analysis in accordance with the specified functionality. Therefore, it is necessary to conduct system research allowing to identify and quantitatively evaluate the influence on the set of rheological parameters of mixtures of each single formula factor used today in order to obtain them.

Two groups of mixtures are used to implement 3D-printing in building: coarsely disperse (size of particles $d > 100 \mu\text{m}$) and microdisperse (size of particles $d \sim 1 \div 100 \mu\text{m}$) systems. According to the classic structural rheology of disperse systems main factors of stability of these systems were identified in our work [23]. There are kinetic, electrostatic, molecular-adsorptive, hydrodynamic factors. Behavior of the disperse systems in dynamic (during transfer and extrusion) and static (during multi-layer casting) conditions of 3D-printing is limited by interaction of these factors. Effectiveness of their influence on stability of the systems is evaluated by criteria of aggregation and strength. Priority of theoretical justification of the criteria belongs to the classic fundamental works of the Soviet physico-chemical mechanic [24–28].

Concerning the mixtures for 3D-printing such as high-concentration pastes belong to heterogeneous disperse systems with close coagulation of particles, spontaneous formation of coagulation structures is possible in dispersions with the size of particles of about $50 \div 500 \mu\text{m}$. Strength criterion defines the functional strength dependence of disperse system structure on the size of particles, strength of individual contacts and concentration of solid phase in liquid phase determining the amount

of contacts in a unit of structure volume. It has been proved [24] that critical concentration of particles of solid phase under the formation of coagulation structure and its strengthening for each pair “solid phase – liquid phase” depend on the parameters of particles of solid phase and properties of liquid phase.

On that basis, in the work [23] we have justified basic means of management of rheological behavior of disperse system under the conditions of 3D-printing. In connection with solid phase, they include its concentration, size of particles and their morphology, chemical-mineralogical composition, physicochemical characteristics of the surface of particles defining the contribution of kinetic, electrostatic and molecular-adsorptive factors in the stability. In connection with liquid phase, they include its ionic composition, viscosity, density, defining the contribution of electrostatic, molecular-adsorptive and hydrodynamic factors in the stability. According to these means of management, a set of formula technological factors has been suggested for management of rheological characteristics of 3D printable concrete. They include the type of binding agent, type and granulometry of fillers and filling agents, types and dosages of additives of electrolytes, plastisizers, viscosity modifying additives, etc.

It should be stressed that in accordance with strength criterion of heterogeneous disperse systems, concentration of solid phase is the defining factor of its stability. Its optimal values for each specific disperse system are also defined by properties of its particles and characteristics of liquid phase. For this reason, it can be stated that the factors studied in this research are the main technological means of regulating rheological behavior of mixtures for solution of practical tasks. They include:

- water/cement ratio as a factor defining the concentration of solid phase in the disperse system,
- concentration of plasticizers as a factor defining the properties of liquid phase.

This article is dedicated to the results of the initial stage of comprehensive studies conducted by the authors on this issue. Presented are the data of system experimental evaluation of the influence of water/cement ratio and concentration of plasticizer for model cement pastes as matrixes of 3D printable concrete on the set of rheological parameters criterial for extrusion and multi-layer casting of the 3D-printing.

2. Methods

Three types of cement pastes were studied (Table 1). Portland cement CEM I 42.5 (EN 197 – 1 : 2011), plasticizer of Sika trademark based on polycarboxylic ethers, manufacturing water were used as initial components of the system.

Table 1. Mix composition.

| Systems | System's specimen | Plasticizer, mass/mass cement (%) | Water/cement ratio |
|----------------------------------|-------------------|-----------------------------------|--------------------|
| “cement + water” | $C - W$ | - | 0.24 |
| | | | 0.25 |
| | | | 0.26 |
| | | | 0.27 |
| | | | 0.28 |
| “cement + water + plasticizer 1” | $C - W - P1$ | 0.1 | 0.23 |
| | | | 0.24 |
| | | | 0.25 |
| | | | 0.26 |
| | | | 0.27 |
| “cement + water + plasticizer 2” | $C - W - P2$ | 0.2 | 0.22 |
| | | | 0.23 |
| | | | 0.24 |
| | | | 0.25 |
| | | | 0.26 |

Cylindrical samples of fresh cement paste with radius R equal to their height $h_0 = 25$ mm were used for the implementation of the experiment. For squeezing test, the sample was put between two smooth plates diameter of which corresponded to the size of the sample and was loaded into a universal floor hydraulic testing system “INSTRON Sates 1500 HDS”.

To evaluate the plasticity of cement pastes, defining their extrudability, the squeezing test with constant plate speed was used in accordance with the methodology developed in the works of N. Roussel [15–16]. The test was conducted on a fresh sample for all compositions of cement paste directly after their manufacture. High compression speed test using constant plate speed $\nu = 5$ mm/sec was implemented as the behavior of the system in the process of extrusion is most adequately modelled with this speed. The curves “compression force N – displacement Δ ” obtained during the experiments were interpreted as influence curves of reduced compression load F^* from relative change of height of the sample h_i/R .

$$F_i^* = \frac{Ph_i}{\rho R^2}, \quad (1)$$

where $h_i = (h_0 - \Delta)$, h_0 is initial height of the sample, Δ is transfer in the i point of time, value R was taken as constant and equal to the radius of the sample at the beginning of the experiment.

According to the results of the analysis of the received experimental curves for the studied systems values K_i , called plastic yield value by N. Roussel [15], were calculated:

$$K_i \left(\frac{h}{R} \right) = \frac{\sqrt{3}F^*}{2}. \quad (2)$$

For compositions of cement paste the samples of which visually kept their form, the squeezing test with constant strain rate was conducted. Methodology of its implementation corresponds to the approaches of A. Perrot [13] to evaluation of buildability of the 3D printable mixtures. The squeezing test was conducted with constant strain rate $\nu = 0.5$ N/c which conforms to the average speed of load increase during multi-layer casting of building sites by industrial printers. Thus, the load on the first poured layer from gradually increasing pressure of upper layers during 3D-printing was simulated.

The squeezing test with constant strain rate was conducted for the samples: 1) directly after molding, 2) after curing during 30 min, 3) after curing during 60 min. Squeezing was conducted until the rupture of the samples, during the experiments the curves “displacement Δ – time t ”, “compression force N – displacement Δ ” were recorded. Based on the obtained experimental curves, values of structural strength of cement pastes were calculated for the moments corresponding to the start of deformation and the start of cracking in the samples by the formula:

$$\sigma = \frac{P}{\pi R^2}. \quad (3)$$

Thus, rheological behavior of cement pastes and their stability under the conditions simulating the influence of compression stress during extrusion and multi-layer casting was evaluated by the following criteria:

- plastic yield value K_i ,
- structural strength σ_0 at the beginning of the deformation,
- plastic strength σ_{pl} and value of plastic deformations Δ_{pl} which were evaluated at the beginning of cracking.

3. Results

3.1. F^* vs. h_i/R experimental curves and plastic behavior

As a result of interpretation of the squeezing test with constant plate speed we received experimental curves $F^* = f(h_i/R)$ (Figure 1) which correspond to the similar curves of N. Roussel [15]. Analysis of experimental curves $F^* = f(h_i/R)$ for description of rheological behavior of cement paste during squeezing was conducted on the basis of approaches of fundamental structural rheology of disperse systems priority of theoretical justification of which belongs to P.A. Rehbinder [27].

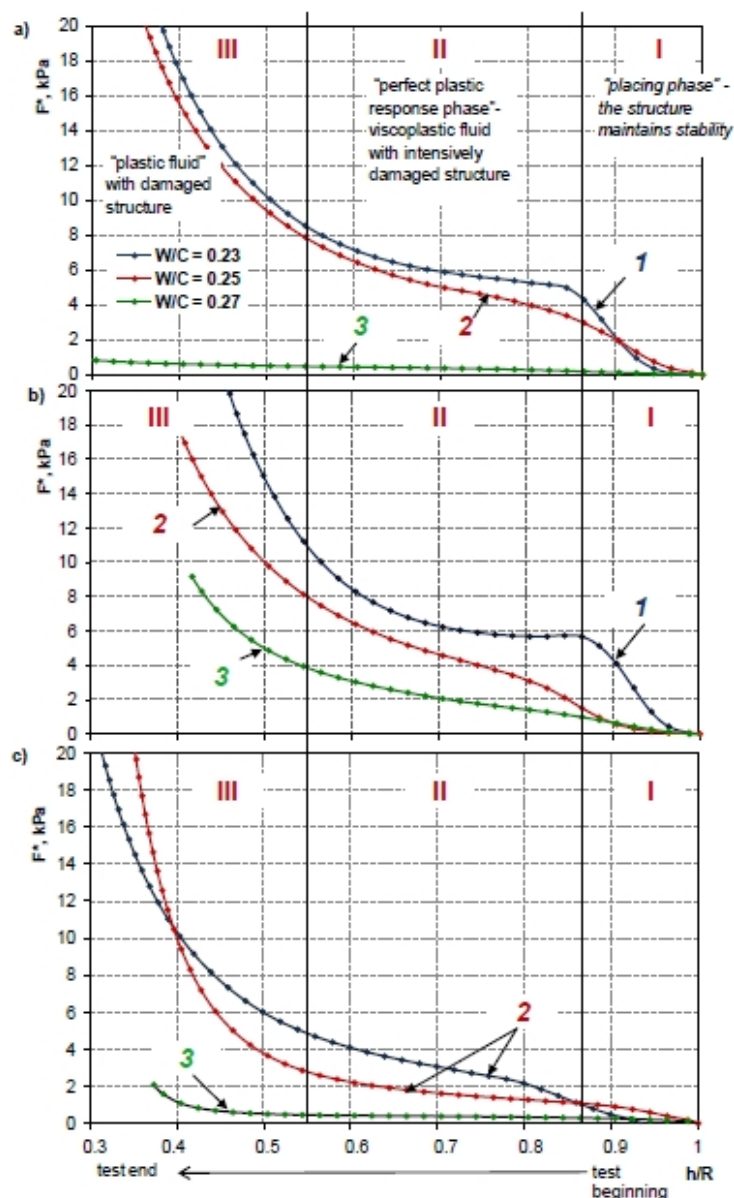


Figure 1. Typical tested cement pastes $F^*(h_i/R)$ curves.
a) system C – W; b) system C – W – P1; c) system C – W – P2.

Under the action of low compression stress on the first section of the curve within deformation range $\sim 0.8 < h_i/R < 1$ the structure maintains stability («placing phase» according to terminology of N. Roussel). Comparison $F^* = f(h_i/R)$ with classic rheological curve first obtained in the works of P.A. Rehbinder [27] allows correlating this section of «placing phase» with the section of viscoplastic fluid of disperse system with undisturbed structure on the curve of P.A. Rehbinder (Shvedov's model). When the stress on the second section increases with $0.5 < h_i/R < 0.8$, the system is plastically deformed while its structure loses its stability («perfect plastic response phase» according to N. Roussel). This section can be correlated with the section of viscoplastic fluid with intensively damaged structure on the curve of P.A. Rehbinder (Bingham's model). Sudden increase of load and intensification of fluid on the third section $h_i/R < 0.5$ are related to full destruction of cement paste structure.

On this basis, it is suggested to evaluate the following criterial rheological characteristics by experimental $F^*(h/R)$ curves.

Value K_i suggested by N. Roussel for the identification of the material plastic properties is suggested to be calculated in two inflection points of $F^*(h/R)$ curves. In this case, value K_i corresponds to Shvedov's plastic yield stress (hereafter plastic yield value $K_i(I)$) in the first inflection point and to Bingham's yield stress (hereafter yield value $K_i(II)$) in the second inflection point.

It appears effective to use elasticity criterion λ first suggested by N.N. Kruglitsky [28] as a comprehensive parameter of evaluation of plasto-elastic properties to evaluate stability and durability of viscoplastic heterogeneous disperse systems

$$\lambda = \frac{E_1}{E_1 + E_2}, \quad (4)$$

characterizing the ratio of moduli of elasticity E_1 and E_2 corresponding to the developments of deformations at different stages of viscoplastic flow of disperse system.

Concerning the conditions of the implementation of squeezing test, the calculation of their values was conducted according to ratios

$$E_1 = \frac{K_i(I) \cdot h_0}{\varepsilon_0}, \quad (5)$$

$$E_2 = \frac{K_i(II) \cdot h_0}{\varepsilon_2}, \quad (6)$$

where h_0 is thickness of the deformed layer corresponding to the initial height of the sample, ε_0 is fast elastic deformation in the first inflection point of the curve $F^* = f(h_i/R)$, ε_2 is slow plastic deformation at the arrival to the second inflection point of the curve $F^* = f(h_i/R)$.

According to the approach the experimental results show three kinds of $F^*(h/R)$ curves. The first kind has expressed horizontal section of plastic deformation between the two points of inflection (No 1, Figure 1, a, b). For the systems rheological behavior of which corresponds to this kind the value of reduced load F^* required for the transfer from stable condition to plastic flow accounts for ~ 6 kPa, transfer into the condition of the flow with damaged structure happens with $F^* = \sim 9$ kPa. For such systems the values of plastic yield value $K_i(I)$ are within the range of $3.5 \div 5$ kPa, yield value $K_i(II) - 5.5 \div 8.5$ kPa (Table 2). These systems do not possess sufficient extrudability due to insufficient plasticity.

Table 2. Change of structural-mechanical characteristics of cement pastes depending on W/C-ratio and dosage of plasticizer.

| System's specimen | Plasticizer, mass/mass cement (%) | W/C-ratio | plastic yield value $K_i(I)$, kPa | yield value $K_i(II)$, kPa | Elasticity λ |
|-------------------|-----------------------------------|-----------|------------------------------------|---|----------------------|
| C – W | - | 0.23 | 4.02 | 7.98 | 0.59 |
| | | 0.24 | 3.98 | 7.49 | |
| | | 0.25 | 2.38 | 5.96 | |
| | | 0.26 | 2.06 | 4.39 | |
| | | 0.27 | 0.26 | The system loses elastic-viscoplastic properties and stability while acquiring fluidity at the initial moment of loading at $F^* < 0.3$ kPa | |
| | | 0.28 | 0.24 | | |
| C – W – P1 | 0.1 | 0.23 | 4.93 | 8.31 | 0.74 |
| | | 0.24 | 2.66 | 5.54 | 0.69 |
| | | 0.25 | 1.12 | 2.64 | 0.66 |
| | | 0.26 | 0.61 | The system loses elastic-viscoplastic properties and stability while acquiring fluidity at the initial moment of loading at $F^* < 0.3$ kPa | |
| | | 0.27 | 0.44 | | |
| C – W – P2 | 0.2 | 0.22 | 4.07 | 4.23 | 0.78 |
| | | 0.23 | 2.08 | 3.22 | 0.59 |
| | | 0.24 | 1.06 | 2.79 | 0.49 |
| | | 0.25 | 0.43 | The system loses elastic-viscoplastic properties and stability while acquiring fluidity at the initial moment of loading at $F^* < 0.3$ kPa | |
| | | 0.26 | 0.24 | | |
| | | 0.27 | 0.18 | | |

For the second type of curves there are no expressed transitions between the section of the curve recorded (No 2, Figure 1 a, b; c). Value F^* corresponding to the start of plastic flow accounts for ~ 3 kPa, values of plastic yield value $Ki(I)$ are within the range of $1.0 \div 1.5$ kPa, yield value $Ki(II) - 2.5 \div 3.0$ kPa. Such systems possess best extrusion ability exactly due to their sufficient plasticity and capacity for viscoplastic flow without the damage of the structure.

The third type of the curve is typical for systems the structure of which is inevitably destroyed at the starting moment of loading with $F^* < 0.3$ kPa (No 3, Figure 1 a, b, c). As a result, they lose stability and acquire fluidity. Such systems do not possess the required elastic-viscoplastic properties and stability for extrusion ability.

3.2. The squeezing test with constant strain rate and firm stability

Potential of resistance of cement paste to deformations and destruction under the increasing load was evaluated by the example of three mixtures, one for each of the systems C – W, C – W – P2, C – W – P2. The mixtures were chosen by the criterion of required plasticity (comparable to values of plastic yield value $Ki(I) \cong 2.0 \div 2.5$ kPa) and capacity for visually holding the shape (Figure 2). Analysis of the received experimental data of the curves “displacement Δ – time τ ” (Figure 3) shows that 3 typical sections can be distinguished on them.



Figure 2. Photo of the cement paste samples having firm stability.

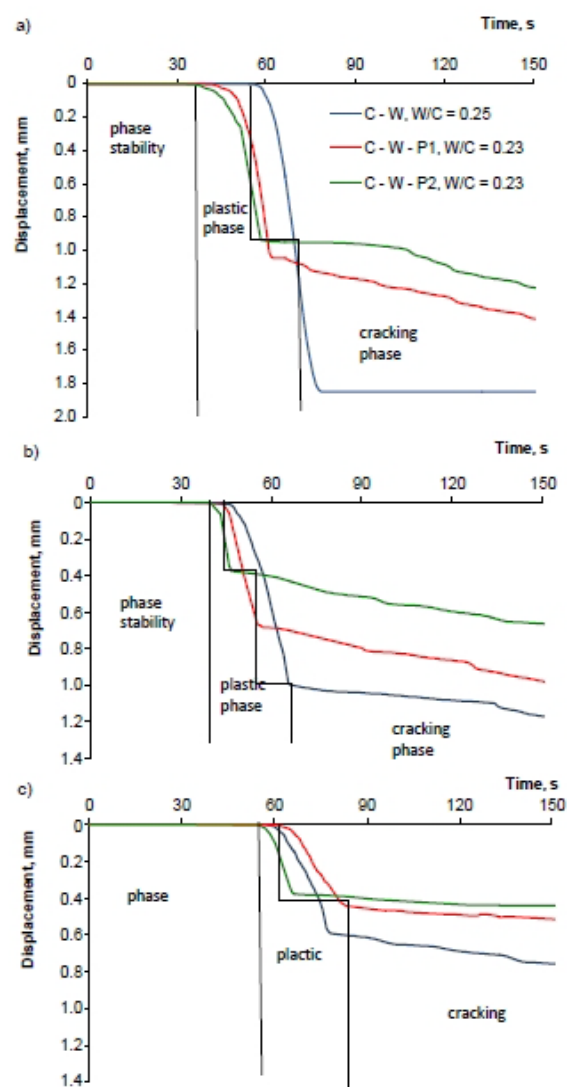


Figure 3. Tested cement pastes «displacement Δ – time τ » experimental results a) fresh cement paste; b) after 30 minutes from the beginning of cement paste hardening; c) after 60 minutes from the beginning of cement paste hardening.

The first section is characterized by the lack of deformations under the influence of load. The quantity of structural strength σ_0 calculated on the basis of the quantity load N at the start of deformation can be considered as the main criterion of buildability (Table 3). This is condition by the fact that structural strength σ_0 characterizes the ability of the system to maintain stability and resist to deformation when loaded.

Table 3. Change of strength and deformation of cement systems during setting time.

| Setting time | Structural strength σ_0 , kPa | Plastic strength σ_{pl} , kPa | Plastic deformation Δ_{pl} , mm |
|-------------------------|--------------------------------------|--------------------------------------|--|
| C – W (W/C = 0.25) | | | |
| ~5 min | 0.87 | 45.22 | 1.85 |
| 30 min | 4.72 | 33.82 | 0.99 |
| 60 min | 9.92 | 21.02 | 0.43 |
| C – W – P1 (W/C = 0.24) | | | |
| ~5 min | 1.92 | 41.40 | 1.42 |
| 30 min | 5.38 | 39.00 | 0.68 |
| 60 min | 12.18 | 33.12 | 0.59 |
| C – W – P2 (W/C = 0.23) | | | |
| ~5 min | 2.86 | 38.84 | 0.93 |
| 30 min | 14.11 | 29.33 | 0.37 |
| 60 min | 16.15 | 23.43 | 0.24 |

The second section is a section of plastic deformation. The system's ability to deform without destruction is evaluated by the quantity plastic strength σ_{pl} calculated on the basis of the quantity load N at the beginning of cracking. To characterize buildability, it seems reasonable to evaluate the quantity of plastic deformations on this section Δ_{pl} , which have to be minimized for 3D printable materials.

The third section is a section of crack formation and irreversibly destruction of the structure. On the experimental curves "compression force N – displacement Δ " the moment of the beginning of crack formation is definitely fixed by the peak of sudden drop of load (Figure 4).

4. Discussion

The transition between three test curves $F^* = f(h/R)$ types is linked to W/C-ratio and dosage of plasticizer.

W/C-ratio defining the concentration of particles in solid phase in the system is the main factor of structuring and strengthening of cement paste. This is why plastic yield value $Ki(I)$ as evaluation of structural stability for all systems naturally decreases with the increase of W/C (Table 2). When critical values are reached, W/C systems lose stability. These values of W/C in their turn depend on the properties of liquid phase in the system "cement + water".

Introduction of plasticizer into disperse system "cement + water" is a regulating factor of liquid phase properties changing surface developments on the border of the division of phases and molecular interactions between solid particles. When high-concentration disperse systems solid particle are formed under the influence of polar molecules of water, dispersion of solid phase particles takes place and its specific surface is increased. At the same time, adsorption of plasticizer molecules takes place on the surface of cement particles. Their monomolecular layer on the surface of particles suddenly lowers the level of free interfacial energy on the border of the division of phases, reduces the interaction force in the contacts between the particles by several digits. As a result, plasticity of the system increases and its flow under stresses becomes easier. Therefore, when plasticizer is introduced and its dosage is increased, the value of load required for the transfer of systems with the same concentration of disperse phase (W/C = const) from the state of stability to the state of viscoplastic flow reduces. For instance, for cement paste with W/C = 0.24 viscoplastic flow of systems C – W, C – W – P1 starts at $F^* \sim 6$ kPa and systems C – W – P2 at $F^* \sim 2.5$ kPa. Thus, the introduction of plasticizer is a regulating factor for plasticity of cement paste.

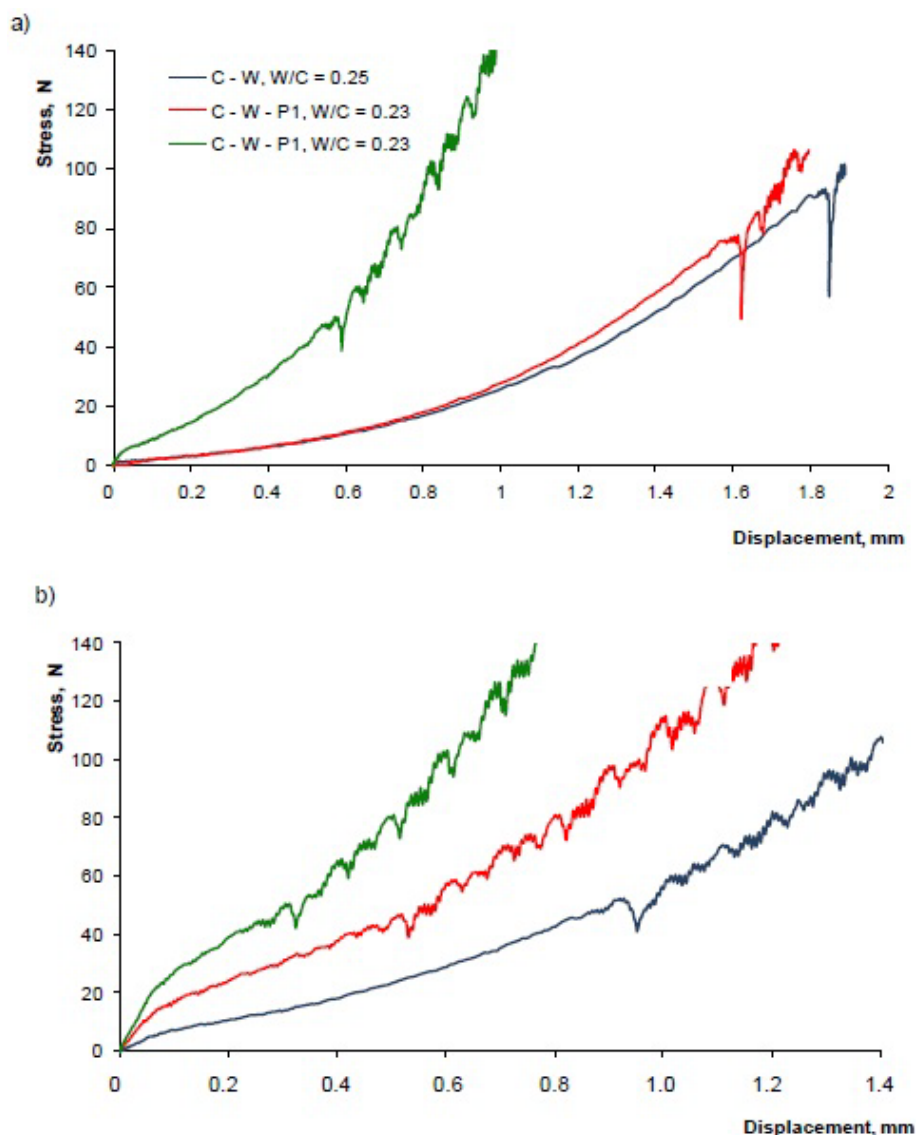


Figure 4. Tested cement pastes “compression force N – displacement Δ ” experimental results a) fresh cement paste; b) after 30 minutes from the beginning of cement paste hardening.

Thus, the extrudability is defined by stability of cement pastes and their capacity for plastic flow with undisturbed structure under the influence of compression stress. To ensure this, the values of plastic yield value $Ki(I) \cong 1.0 \div 2.5$ kPa and elasticity criterion $\lambda \cong 0.5$ should be considered critical. With values $Ki(I) > 2.5$ kPa cement-based materials are not plastic enough for extrusion. With values $Ki(I) < 1$ kPa, $\lambda < 0.5$ the systems lose stability almost immediately after load application, their structure is irreversibly destroyed, the flow begins. The obtained values of quantities $\lambda = 0.51 \div 0.59$ for cement pastes possessing stability fully correspond to the data of N.N. Kruglitsky [28] according to which the value of elasticity criterion of at least $\lambda = 0.5$ corresponds to the stable state of disperse systems.

Analysis of the received curves “ $\Delta - \tau$ ” for the samples tested right after their manufacture shows that system C – W displays the least values of structural σ_0 and plastic σ_{pl} strength and the largest values of plastic deformations Δ_{pl} (Table 3, Figure 3). At the same time, the curves “ $N - \Delta$ ” show that complete destruction of the structure for this system happens right after the first cracks appear (Figure 4).

When plasticizer is introduced into the system, values of structural and plastic strength increase by 2–3 times and value of plastic deformations Δ_{pl} decreases by 1.5–2 times in the systems C – W – P1, C – W – P2. The nature of destruction changes: after the beginning of crack formation, it is typical for the samples of systems C – W – P1, C – W – P2 that multiple peaks of load fluctuation appear on the curves

“ $N - \Delta$ ” indicating the appearance of microcracks. As a result, the interval between the moment when first cracks appear and destruction becomes longer, which is a sign of increased system stability to the influence of the load.

This effect of increased stability of cement paste is logically related to the influence of plasticizer. During adsorption of molecules of plasticizer on the surface of cement particles, functional groups of their radical (for example, OH^- , ONa^- , etc.) are directed to the dipolar medium due to their polarity and likeness to the liquid phase (water). The liquid phase lyophilic in respect to the radical will be drawn into the gap between cement particles, the thickness of adsorption-combined water layer will exceed the double length of the radical. As a result, the presence of adsorbed polar molecules of plasticizer in the system allows structuring the water in the interlayers between cement particles. Such structuring of disperse medium in cement pastes ensures the increase of their firm stability and consequently buildability. According to the experimental data, system C – W – P2 with the largest content of plasticizer is characterized by the maximum value of structural strength σ_0 and minimal plastic deformations Δ_{pl} . The nature of deformation and destruction of the studied cement systems logically changes in the process of their setting and hardening (Figure 4 b). As coagulation-crystallization phase contacts are formed in the structure during setting, the value of structural strength σ_0 grows for all the studied systems with increased time of hardening. At the same time, the ability of the system to plastically deform without destruction is reduced. Correspondingly, plastic strength σ_{pl} is reduced, too. The nature of destruction changes: after the beginning of crack formation, prolongation of the period of formation and accumulation of microcracks preceding the destruction is typical for all samples of the studied systems hardening during 60 min. According to the experimental data, system C – W – P2 with the largest content of plasticizer is characterized by the maximum value of structural strength σ_0 and minimal plastic deformations Δ_{pl} not only right after the manufacture but also after hardening during 30 and 60 minutes.

Therefore, introduction of plasticizer into cement paste allows increasing the stability of cement systems also during flocculation and hardening.

5. Conclusions

An effective method of evaluation of rheological behavior of viscoplastic 3D printable building materials is squeeze flow rheometry determining quantitative values of rheological parameters criterial for extrudability and buildability. Analysis of the study results shows that the use of the squeezing test with constant plate speed is effective for evaluation of extrudability. Interpretation of the results of this test from the positions of structural rheology of disperse systems allows categorizing the parameters of plastic yield value $K_i(I)$ and yield value $K_i(II)$, elasticity criterion λ as criteria defining the ability of 3D printable materials to plastically deform without structure destruction and maintain stability during extrusion. To ensure this, values of plastic yield value $K_i(I) \cong 1.0 \div 2.5$ kPa and elasticity criterion $\lambda \cong 0.5 \div 0.6$ should be considered criterial.

The squeezing test with constant strain rate is effective for the evaluation of buildability. The values of structural and plastic strength, plastic deformations defined by the results of this test characterize the system's ability to hold its form, resist the influence of increasing compressions stresses during multi-layer casting.

It has been established that W/C-ratio defining the concentration of solid phase particles in the system is the main factor of structuring and strengthening of cement paste. Structural stability of cement paste can be changed by 3–4 times by regulating W/C. Introduction of plasticizer as a factor changing the properties of liquid phase in the system “cement + water” is an effective method not only for plasticity regulation but also for increasing the resistance of 3D printable cement-based materials to the influence of load during the printing of constructions.

Development of the studies is related to the identification of effectiveness of the influence of viscosity modifying additives, fillers and filling agents of different chemical-mineralogical composition and dispersion on parameters of extrudability and buildability of 3D-cement based materials. Optimization of compositions and effective regulation of the properties of mixtures at all stages of 3D printing process requires quantitative evaluation and determination of criterial values of the specified set of their rheological parameters.

6. Acknowledgement

This research work has been carried out in the frame of the 7.10781.2018/11.12 Project, financed by the Russian government in order to obtain initial scientific results broadening the participation of subordinate educational organisations in the implementation of the National Technological Initiative.

References

1. Tay, Y., Panda, B., Paul, S., Noor, M., Tan, M., Leong, K. 3D printing trends in building and construction industry: a re-view. *Virtual and Physical Prototyping*. 2017. No. 12(3). Pp. 261–276. doi.org/10.1080/17452759.2017.1326724
2. Marijnissen, M., van Der Zee, A. 3D Concrete Printing in Architecture. A research on the potential benefits of 3D Concrete Printing in Architecture. *Material Studies – Methodologies*. 2017. No. 2. Pp. 299–308.
3. Bos, F., Wolfs, R., Ahmed, Z., Salet, T. Additive manufacturing of concrete in construction: potentials and challenges of 3D concrete printing. *Virtual and Physical Prototyping*. 2016. No. 11(3). Pp. 209–225. dx.doi.org/10.1080/17452759.2016.1209867
4. Feng, P., Meng, X., Chen, J., Ye, L. Mechanical properties of structures 3D printed with cementitious powders. *Construction and Building Materials*. 2015. No. 93. Pp. 486–497. dx.doi.org/10.1016/j.conbuildmat.2015.05.132
5. Wolfs, R., Bos, F., Salet, T. Early age mechanical behaviour of 3D printed concrete: Numerical modelling and experimental testing. *Cement and Concrete Research*. 2018. No. 106. Pp. 103–116. doi.org/10.1016/j.cemconres.2018.02.001
6. Shakor, P., Sanjayan, J., Nazari, A., Nejadi, S. Modified 3D printed powder to cement-based material and mechanical properties of cement scaffold used in 3D printing. *Construction and Building Materials*. 2017. No. 138. Pp. 398–409. dx.doi.org/10.1016/j.conbuildmat.2017.02.037
7. Tay, Y.W., Panda, B., Paul, S.C., Tan, M.J., Qian, S.Z., Leong, K.F., Chua, C.K. Processing and Properties of Construction Materials for 3D Printing. *Materials Science Forum*. 2016. Vol. 861. Pp. 177–181. dx.doi.org/10.4028/www.scientific.net/MSF.861.177
8. Paul, S.C., Tay, Y.W.D., Panda, B., Tan, M.J. Fresh and hardened properties of 3D printable cementitious materials for building and construction. *Archives of Civil and Mechanical Engineering*. 2018. No. 18(1). Pp. 311–319. dx.doi.org/j.acme.2017.02.008
9. Ngo, T.D., Kashani, A., Imbalzano, G., Nguyen, K., Hui, D. Additive manufacturing (3D printing): A review of materials, methods, applications and challenges // *Composites Part B: Engineering*. Vol. 143. 103 p. dx.doi.org/10.1016/j.compositesb.2018.02.012
10. Lin, J.C., Wu, X., Yang, W., et al. Application of P.O and R-SAC mortar for 3D printing in construction. *IOP Conference Series: Materials Science and Engineering*. 2017. Vol. 292. No. 1. Pp. 1–7. dx.doi.org/10.1088/1757-899X/292/1/012070
11. Malaeb, Z., Hachem, H., Tourbah, A., et al. 3D Concrete Printing: Machine and Mix Design. *International Journal of Civil Engineering and Technology*. 2015. Vol. 6(4). Pp. 14–22.
12. Kazemian, A., Yuan, X., Cochran, E., Khoshnevis, B. Cementitious materials for construction-scale 3D printing: Laboratory testing of fresh printing mixture. *Construction and Building Materials*. 2017. Vol. 145. Pp. 639–647. 10.1016/j.conbuildmat.2017.04.015
13. Le, T.T., Austin, S.A., Lim, S., Buswell, R.A., Gibb, A.G.F., Thorpe, T. Mix design and fresh properties for high-performance printing concrete. *Materials and Structures*. 2012. No. 45(8). Pp. 1221–1232. dx.doi.org/10.1617/s11527-012-9828-z
14. Engmann, J., Servais, C., Burbidge, A.S. Squeeze flow theory and applications to rheometry: A review. *Journal of Non-Newtonian Fluid Mechanics*. 2005. No. 132(1–3). Pp. 1–27. dx.doi.org/10.1016/j.jnnfm.2005.08.007
15. Toutou, Z., Roussel, N., Lanos, C. The squeezing test: A tool to identify firm cement-based material's rheological behaviour and evaluate their extrusion ability. *Cement and Concrete Research*. 2005. No. 35(10). Pp. 1891–1899. dx.doi.org/10.1016/j.cemconres.2004.09.007

Литература

1. Tay Y., Panda B., Paul S., Noor M., Tan M. Leong K. 3D printing trends in building and construction industry: a re-view // *Virtual and Physical Prototyping*. 2017. № 12(3). Pp. 261–276. doi.org/10.1080/17452759.2017.1326724
2. Marijnissen M., Van Der Zee A. 3D Concrete Printing in Architecture // A research on the potential benefits of 3D Concrete Printing in Architecture. *Material Studies – Methodologies*. 2017. № 2. Pp. 299–308.
3. Bos, F., Wolfs, R., Ahmed, Z., Salet, T. Additive manufacturing of concrete in construction: potentials and challenges of 3D concrete printing // *Virtual and Physical Prototyping*. 2016. № 11(3). Pp. 209–225. dx.doi.org/10.1080/17452759.2016.1209867
4. Feng P., Meng X., Chen J., Ye L. Mechanical properties of structures 3D printed with cementitious powders // *Construction and Building Materials*. 2015. № 93. Pp. 486–497. dx.doi.org/10.1016/j.conbuildmat.2015.05.132
5. Wolfs R., Bos F., Salet T. Early age mechanical behaviour of 3D printed concrete: Numerical modelling and experimental testing // *Cement and Concrete Research*. 2018. № 106. Pp. 103–116. doi.org/10.1016/j.cemconres.2018.02.001
6. Shakor P., Sanjayan J., Nazari A., Nejadi S. Modified 3D printed powder to cement-based material and mechanical properties of cement scaffold used in 3D printing // *Construction and Building Materials*. 2017. № 138. Pp. 398–409. dx.doi.org/10.1016/j.conbuildmat.2017.02.037
7. Tay Y.W., Panda B., Paul S.C., Tan M.J., Qian S.Z., Leong K.F., Chua C.K. Processing and Properties of Construction Materials for 3D Printing // *Materials Science Forum*. 2016. Vol. 861. Pp. 177–181. dx.doi.org/10.4028/www.scientific.net/MSF.861.177
8. Paul S.C., Tay Y.W.D., Panda, B., Tan M.J. Fresh and hardened properties of 3D printable cementitious materials for building and construction // *Archives of Civil and Mechanical Engineering*. 2018. № 18(1). Pp. 311–319. dx.doi.org/j.acme.2017.02.008
9. Ngo T.D. Kashani A., Imbalzano G., Nguyen K., Hui D. Additive manufacturing (3D printing): A review of materials, methods, applications and challenges // *Composites Part B: Engineering*. Vol. 143. 103 p. dx.doi.org/10.1016/j.compositesb.2018.02.012
10. Lin J.C., Wu X., Yang W., et al. Application of P.O and R-SAC mortar for 3D printing in construction // *IOP Conference Series: Materials Science and Engineering*. 2017. Vol. 292. № 1. Pp. 1–7. dx.doi.org/10.1088/1757-899X/292/1/012070
11. Malaeb Z., Hachem H., Tourbah A., et al. 3D Concrete Printing: Machine and Mix Design // *International Journal of Civil Engineering and Technology*. 2015. Vol. 6(4). Pp. 14 – 22.
12. Kazemian A., Yuan X., Cochran E., Khoshnevis B. Cementitious materials for construction-scale 3D printing: Laboratory testing of fresh printing mixture // *Construction and Building Materials*. 2017. Vol. 145. Pp. 639–647. 10.1016/j.conbuildmat.2017.04.015
13. Le T.T., Austin S.A., Lim S., Buswell R.A., Gibb A.G.F., Thorpe T. Mix design and fresh properties for high-performance printing concrete. *Materials and Structures*. 2012. № 45(8). Pp. 1221–1232. dx.doi.org/10.1617/s11527-012-9828-z
14. Engmann J., Servais C., Burbidge A.S. Squeeze flow theory and applications to rheometry: A review // *Journal of Non-Newtonian Fluid Mechanics*. 2005. № 132(1–3). Pp. 1–27. dx.doi.org/10.1016/j.jnnfm.2005.08.007
15. Toutou Z., Roussel N., Lanos C. The squeezing test: A tool to identify firm cement-based material's rheological behaviour and evaluate their extrusion ability // *Cement and*

16. Russel, N., Lanos, C. Plastic Fluid Flow Parameters Identification Using a Simple Squeezing Test. *Applied Rheology*. 2003. No. 13(3). Pp. 3–5.
17. Perrot, A., Rangeard, D., Pierre, A. Structural built-up of cement-based materials used for 3D-printing extrusion techniques. *Materials and Structures*. 2016. No.49. Pp. 1213–1220. dx.doi.org/10.1617/s11527-015-0571-0
18. Perrot, A., Mélinge, Y., Estellé, P., Lanos, C. Vibro-extrusion: a new forming process for cement-based materials. *Advances in Cement Research*. 2009. No. 21(3). Pp. 125–133. dx.doi.org/10.1680/adcr.2008.00030
19. Perrot, A., Rangeard, D., Mélinge, Y., Estellé, P., Lanos, C. Extrusion Criterion for Firm Cement-Based Materials. *Applied Rheology*. 2009. No. 19. Pp. 111–127. dx.doi.org/10.3933/ApplRheol-19-53042
20. Perrot, A., Mélinge, Y., Rangeard, D., Micaelli, F., Estellé, P., Lanos, C., Estellé, P. Use of ram extruder as a combined rheo-tribometer to study the behaviour of high yield stress fluids at low strain rate. *Rheologica Acta*. Springer Verlag. 2012. No. 51(8). Pp. 743–754.
21. Ma, S., Qian, Y., Kawashima S. Experimental and modeling study on the non-linear structural build-up of fresh cement pastes incorporating viscosity modifying admixtures. *Cement and Concrete Research*. 2018. No. 108. Pp. 1–9. dx.doi.org/10.1016/j.cemconres.2018.02.022
22. Lecompte, T., Perrot A. Non-linear modeling of yield stress increase due to SCC structural build-up at rest. *Cement and Concrete Research*. 2017. No. 92. Pp. 92–97. dx.doi.org/10.1016/j.cemconres.2016.11.020
23. Slavcheva, G.S., Artamonova, O.V. The rheological behavior of disperse systems for 3d printing in construction: the problem of control and possibility of «nano» tools application. 2018. Internet-journal «nanotechnologies in construction» Vol. 10. No. 3. Pp. 107–122. dx.doi.org/10.15828/2075-8545-2018-10-3-107-122. (rus)
24. Urieв, N.B. Fizikohimicheskaya dinamika strukturirovannykh nanodispersnykh sistem i nanodispersnykh kompozitsionnykh materialov. Chast 1 [Physico-chemical dynamics of structured nanodispersed systems and nanodispersed composite materials. Part 1]. *Fizikohimiya poverhnosti i zashchita materialov*. 2010. Vol. 46. No 1. Pp. 3–23. (rus)
25. Urieв, N.B. Vysokokontsentrirrovannye dispersnye sistemy [Highly concentrated disperse systems]. *Moskow: Chemistry*, 1980. 319 p. (rus)
26. Yaminskij, V.V., Pchelin, V.A., Amelina, E.A., Shchukin, E.D. Koagulyacionnye kontakty v dispersnykh sistemah [Coagulation contacts in dispersed systems]. *Moskow: Chemistry*, 1982. 185 p. (rus)
27. Rebindер, P.A. Izbrannye trudy. Poverhnostnye yavleniya v dispersnykh sistemah. Fiziko-himicheskaya mekhanika [Selected Works. Surface phenomena in dispersed systems. Physico-chemical mechanics]. *Moskow: Science*, 1979. 384 p. (rus)
28. Kruglickij, N.N. Oчерki po fiziko-himicheskoy mekhanike [Feature article about physicochemical mechanics]. *Kiev: Scientific thought*, 1988. 224 p. (rus)
- Concrete Research. 2005. № 35(10). Pp. 1891–1899. dx.doi.org/10.1016/j.cemconres.2004.09.007
16. Russel N., Lanos C. Plastic Fluid Flow Parameters Identification Using a Simple Squeezing Test // *Applied Rheology*. 2003. № 13(3). Pp. 3–5.
17. Perrot A., Rangeard D., Pierre A. Structural built-up of cement-based materials used for 3D-printing extrusion techniques // *Materials and Structures*. 2016. № 49. Pp. 1213–1220. dx.doi.org/10.1617/s11527-015-0571-0
18. Perrot A., Mélinge Y., Estellé P., Lanos, C. Vibro-extrusion: a new forming process for cement-based materials // *Advances in Cement Research*. 2009. № 21(3). Pp. 125–133. dx.doi.org/10.1680/adcr.2008.00030
19. Perrot A., Rangeard D., Mélinge Y., Estellé P., Lanos C. Extrusion Criterion for Firm Cement-Based Materials // *Applied Rheology*. 2009. № 19. Pp. 111–127. dx.doi.org/10.3933/ApplRheol-19-53042
20. Perrot A., Mélinge Y., Rangeard D., Micaelli F., Estellé P., Lanos C., Estellé P. Use of ram extruder as a combined rheo-tribometer to study the behaviour of high yield stress fluids at low strain rate // *Rheologica Acta*. Springer Verlag. 2012. № 51(8). Pp. 743–754.
21. Ma S., Qian Y., Kawashima S. Experimental and modeling study on the non-linear structural build-up of fresh cement pastes incorporating viscosity modifying admixtures // *Cement and Concrete Research*. 2018. № 108. Pp. 1–9. dx.doi.org/10.1016/j.cemconres.2018.02.022
22. Lecompte T., Perrot A. Non-linear modeling of yield stress increase due to SCC structural build-up at rest. *Cement and Concrete Research*. 2017. № 92. Pp. 92–97. dx.doi.org/10.1016/j.cemconres.2016.11.020
23. Славчева Г.С., Артамонова О.В. Реологическое поведение дисперсных систем для строительной 3d-печати: проблема управления и возможности арсенала «нано» // *Нанотехнологии в строительстве*. 2018. Том 10, № 3. С. 107–122. dx.doi.org/10.15828/2075-8545-2018-10-3-107-122.
24. Урьев Н.Б. Физико-химическая динамика структурированных нанодисперсных систем и нанодисперсных композиционных материалов. Часть 1 // *Физикохимия поверхности и защита материалов*. 2010. Т. 46. № 1. С. 3 – 23.
25. Урьев Н.Б. Высококонтцентрированные дисперсные системы. М.: Изд. Химия, 1980. 319 с.
26. Яминский В.В., Пчелин В.А., Амелина Е.А., Щукин Е.Д. Коагуляционные контакты в дисперсных системах. М.: Изд-во «Химия», 1982. 185 с.
27. Ребиндер П.А. Избранные труды. Поверхностные явления в дисперсных системах. Физико-химическая механика. М.: Наука, 1979. 384 с.
28. Круглицкий Н.Н. Очерки по физико-химической механике. Киев: Наукова думка, 1988. 224 с.

*Galina Slavcheva**,
+79601329475; gslavcheva@yandex.ru

Olga Artamonova,
+79202180330; ol_artam@rambler.ru

*Галина Станиславовна Славчева**,
+79601329475;
эл. почта: gslavcheva@yandex.ru

Ольга Владимировна Артамонова,
+79202180330; эл. почта: ol_artam@rambler.ru

© Slavcheva, G.S., Artamonova, O.V., 2018

doi: 10.18720/MCE.84.11

Concrete with recycled polyethylene terephthalate fiber

Бетон с добавлением фибры из переработанного полиэтилентерефталата

A.V. Kiyaneets,
South Ural State University, Chelyabinsk, Russia

канд. техн. наук, доцент А.В. Киянец,
Южно-Уральский государственный
университет, Челябинск, Россия

Key words: polyethylene terephthalate; PET; PET recycling; fiber; flex; PET fiber-reinforced concrete; fiber concrete

Ключевые слова: полиэтилентерефталат; ПЭТ; переработка ПЭТ; фибра; флекс; фибробетон

Abstract. The purpose of this study was to obtain the data on the influence of fiber from the products of recycled polyethylene terephthalate (PET) on the strength properties of fiber-reinforced concrete. In the experiments, used the direct product of industrial recycling of plastic bottles (flex), as well as specially prepared smooth and ribbed fiber from the same raw material. The influence factors were chosen fiber length from 1 to 5 cm and the amount of fiber-from 1 to 3 % by weight of cement. It has been found that the use of PET fibers provides a gain in the concrete tensile strength of up to 66 %. The compressive strength of the studied samples of fiber-reinforced concrete within the limits of the varying factors decreased by 3–25 %. The most favorable ratio of the increase in the bending tensile strength and the decrease in the compressive strength was obtained in concrete with the addition of smooth 4cm long fiber with the smallest reinforcement value. The abrasion capacity (abrasive wear) of the samples decreased with the addition of 3 % of smooth and ribbed 4 cm long fiber. The research resulted in the experimental determination of the effective fiber length (critical fiber length) providing the most reliable fastening of the fiber in the concrete matrix.

Аннотация. Целью данного исследования было получение данных о влиянии фибры из продуктов вторичной переработки полиэтилентерефталата (ПЭТ) на прочностные свойства фибробетона. В экспериментах применялись прямой продукт промышленной переработки пластиковых бутылок (флекс), а также специально подготовленная фибра гладкой и ребристой формы из того же сырья. Варьируемыми факторами, кроме типа фибры, были выбраны длина волокон от 1 до 5 см и количество вводимой фибры – от 1 до 3 % от массы цемента. Было выяснено, что применение ПЭТ фибры обеспечивает прирост прочности бетона на растяжение до 66 %. Прочность на сжатие исследуемых образцов фибробетона в границах варьируемых факторов снизилась на 3–25 %. Наиболее благоприятное соотношение увеличения показателя прочности на растяжения при изгибе и понижения показателя прочности на сжатие, получилось в бетоне с добавлением гладкой фибры длиной 4 см при наименьшей величине армирования. Истираемость (абразивный износ) образцов снизилась при добавке 3 % гладкой и ребристой фибры длиной 4 см. В результате исследований экспериментальным путем была определена эффективная длина фибры (критическая длина фибры), обеспечивающая наиболее надежное закрепление волокна в матрице бетона.

1. Introduction

The problem of a sustainable development of the civilization and the global construction complex is inextricably linked with the environmental management and the use of modern construction materials with enhanced physical and mechanical characteristics. Such materials include fiber-reinforced concrete [1–3].

Dispersed reinforcement of concrete with different types of fiber, as opposed to discrete reinforcement with reinforcement rods, grids and frameworks, has a number of advantages noted by many scientists [4–8]. Fiber-reinforced concrete also has technological advantages: labor expenditures for reinforcement of structures are significantly lowered or completely eliminated, loads on the vertical formwork are reduced [9, 10].

There are developed regulatory documents on the design engineering and production technology for steel fiber concrete and specialized equipment allowing to use it safely [11–13]. This makes it possible to state the perspective development of the concrete technology with the addition of various types of fiber based on other materials: fiberglass, basalt, polypropylene, etc.

Recently, the use of the products of recycled polyethylene terephthalate (PET) has been studied intensively. Numerous types of water and beverage bottles and various types of containers and packaging are made of this plastic. The output of this product worldwide is many millions of tons. Waste (secondary raw materials), which is formed after the use of the products, is actively recycled [14]. However, as far as the use increases significantly throughout the world, collection and recycling efforts are insufficient. Therefore, the issue of using recycled PET containers in other industries, including construction, as a concrete reinforcing additive (fiber) has become increasingly important [15].

A number of studies dealing with this topic have already been conducted worldwide. Scientists from Japan have noted the safety of using PET fibers in concrete, as well as improving the physical and mechanical characteristics of concrete. There are two successful examples of using structures made of this material [16]. In general, there is a proven positive influence of PET fibers on the strength of concrete samples, which is shown in the works of researchers from the universities in Italy and Malta [17]. They studied various types of straight and deformed milled recycled PET fibers, alongside with different fiber lengths: 30 mm and 50 mm. They evaluated various options of percentage concrete additives and determined tensile properties and stretching characteristics of fibers. Then, they evaluated the effects of the fibers for soothing of plastic cracking and drying shrinkage, and finally, determined the compressive and bending strength of fiber-reinforced concrete. The cracking potential of thin plates of a fiber-reinforced mortar was also evaluated.

A Portuguese article reports on the strength behavior of concrete containing three types of recycled polyethylene terephthalate (PET) [18]. The results are also analyzed to determine the influence of the PET aggregate on the bending, splitting and compressive strength.

Three types of PET aggregates were used in the experiment. Samples were made with a 5 %, 10 % and 15 % content of the PET aggregate. The samples were tested after 7, 28 and 91 days. It is shown that the introduction of any type of the PET aggregate significantly reduces the compressive strength of the resulting concrete. However, the introduction of the PET aggregate improves the stiffness of the resulting concrete. This behavior depends on the shape of the PET aggregate and is maximized for concrete containing a rough, peeling PET aggregate. The tensile and bending strengths are proportional to the decrease in the compressive strength of concrete containing plastic aggregates.

Employees of the Warsaw University of Technology published an article on the use of PET in concrete. The research results have shown that the introduction of PET fibers does not worsen the mechanical strength of the concrete composite. However, the presence of polymer fibers worsens the slump of the concrete mix cone, which can cause difficulty in mixing or laying of the concrete mix [19].

Researchers from Malaysia worked with concrete containing PET fiber in the volume of 0.5 %, 1.0 % and 1.5 % of the fraction. They noted a slight increase in strength [20].

Employees of Baba Ghulam Shah Badshah University (India) also studied the behavior of various types of concrete of grades B20, B25 and B30, with the addition of a certain amount of PET fibers (2 %, 3 %, 4 % and 5 %). They noted that the environmental pollution from various non-biodegradable waste does not only pose an environment risk, but can also entail serious consequences for the human life. The use of these materials instead of a fine aggregate in concrete allows to partially solve this problem.

Then, the mechanical properties, such as compressive strength, were compared with ordinary concrete. The optimum compressive strength of concrete was achieved with the addition of 3 % of PET fibers [21].

Employees of another Indian university also noted that polyethylene terephthalate (PET) is an outstanding material, which is widely used as a raw material for the production of containers. The purpose of the research was to determine the reusability of PET as a replacement of aggregates in Portland cement. In this research, they used concrete with 0 %, 5 %, 10 %, 15 % and 20 % of PET waste.

In their conclusions they noted that a solid substance (concrete) with PET waste significantly reduces the consumption of cement, and this helps in the preparation of a concrete mix with an increased specific gravity. Concrete with the addition of PET also had an increased compressive strength and bending strength as compared to PET-free concrete [22].

Several directions can be outlined in the latest published works dealing with the use of PET recycling waste for concrete additives:

- use of various types of PET reinforcement, for example, grids [23];
- study of the influence of the shape of PET fibers introduced into concrete, for example, ring-shaped fibers [24];
- complex use of PET fibers and other reinforcing materials (other types of plastics, rubber) also obtained by waste recycling, and additives in the form of ash and silica fume [25, 26].

Thus, till present, the overall efficiency of using polyethylene terephthalate fiber in a concrete matrix has been proven for the purpose of recycling plastic waste, facilitating concrete structures, saving cement consumption and improving the strength characteristics of concrete. In most studies, researchers use PET fiber obtained by extrusion and remelting from PET waste. Or apply PET granules heat-treated. Therefore, the question of the effectiveness of the use of industrial Flex (Flex – raw material obtained by recycling waste from PET, serving for the production of plastic bottles, containers, etc.), without additional processing as an additive to concrete remains relevant. This method would significantly reduce the cost of production of fiber concrete with PET-fiber.

But the researchers did not come to a consensus on the effective consumption of fiber in reinforcement, the influence of the shape of the fibers used on the properties of fiber concrete, as well as the areas of application of this material.

Therefore, the problem of this study is the effectiveness of the use of fiber in concrete from waste PET materials (obtained by mechanical grinding), and not subjected to heat treatment. The aim of this study is to assess the effect of PET fiber on the properties of fiber concrete.

For this purpose, it is necessary to solve a number of research problems. To check usability of industrial flex (a direct product of PET waste recycling, without any special treatment) as an additive to concrete. To assess the influence of the shape of specially produced fibers on the characteristics of fiber-reinforced concrete. To study the dependence of the strength characteristics of fiber-reinforced concrete on the amount of the added PET fiber. To obtain the value of the “critical length” of fiber, the indicator determining the degree of anchoring (fastening strength) of the fiber in the concrete matrix, which, in its turn, determines the strength of the fiber concrete structure.

2. Methods

The properties of concrete mixes with the use of fibers from the materials of recycled PET bottles were studied in several stages:

- creation and testing of PET fiber-free concrete samples;
- creation and testing of concrete samples with the addition of industrial PET fiber (flex);
- creation and testing of concrete with the addition of various amounts of smooth PET fiber;
- creation and testing of concrete with the addition of various amounts of ribbed PET fiber;
- analysis of the obtained results;
- conclusions.

The fiber was added in the amount of 1.2 and 3 % of the cement weight. In absolute values it is 4.42 kg/m³, 8.84 kg/m³, 13.26 kg/m³, respectively. The fiber length was: for industrial flex – 1 cm (the standard length of this type of raw material), for the specially prepared smooth and ribbed fiber – 3.4 and 5 cm (Figure 1).

Standard methods were used for the studies (EN 12390 Testing hardened concrete). We used B30 concrete of the following composition: M400 cement – 442 kg; sand – 446 kg; 5–20 mm crushed stone – 1254 kg; water – 207 liters.

Series of samples were made for various tests. 28-day old samples were tested in a dry state.

The compressive strength was tested on 100×100×100 mm cube samples, while the bending tensile strength was determined on 100×100×400 mm samples.

The abrasion capacity of fiber concrete is studied according to the procedure of Russian State Standard GOST 13087-81 (Concretes. Methods of determination of abrasion) on the LKI-3 abrasive disc. The abrasion

capacity of the 70×70×70 cube samples was estimated by the weight loss per unit area (kg/cm²) during the abrasive wear.

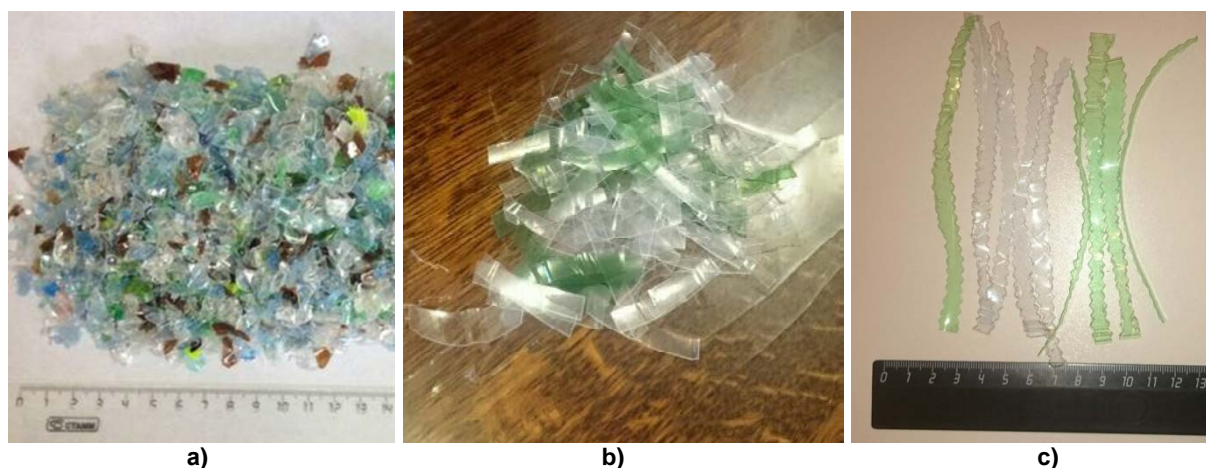


Figure 1. Different types of PET fiber used in the study: a) flex; b) smooth fiber; c) ribbed fiber.

The samples are placed in special sockets of the abrasive disc. A concentrated vertical force of (300±5) N is applied to each sample (center-wise), which corresponds to the pressure of (60±1) kPa (Figure 2). The total abrasion path is 600 m.



Figure 2. Testing the fiber samples for abrasive capacity (abrasive wear).

As it is known, the joint work of the fiber and the matrix under load has been the subject of numerous studies. In some of them, experimental and theoretical models of fiber-reinforced concrete systems are based on the assumptions that the fiber and the matrix have some elasticity before the destruction, and the fiber-matrix contact area is solid and uniform. At the same time, it is assumed that stresses are distributed linearly in the fiber from the zero values at the ends of the fiber to the maximum values at some distance from them, while shear stresses are considered constant at the same sections.

Let us consider the phenomenon that occurs when of the matrix interacts with short straight fibers in the process of stretching with the effort P of the fiber concrete sample. For this purpose, we will outline an elementary region consisting of a single fiber and the volume of the matrix adjacent to it from the stretchable sample.

The fiber with the length l_f and the cross section area S adheres to the matrix. Under the influence of the force P , there appear shear stresses with respect to the fiber in the contact area of the fiber-matrix system. With increasing load there is tearing of fibers of concrete or rupture of the fibers. In any event, the fiber stops working in the concrete.

Thus, we define the “critical length” of the fiber as the minimum allowable length, which provides a reliable fixation of the fiber in the concrete by the tangential stresses (reaction to the force) under the influence of the tensile force.

15 cm long fibers were cut for testing (Figure 3). We also prepared casting molds. After all the fibers were laid in the mold, we prepared a cement-sand mortar and poured it into the mold. Then, they were compacted on the platform vibrator. After the samples gained the necessary strength, they were subject to stretching (Figure 4).



Figure 3. A sample for testing the fiber adhesion strength with the concrete matrix (determination of the critical length of the fiber).

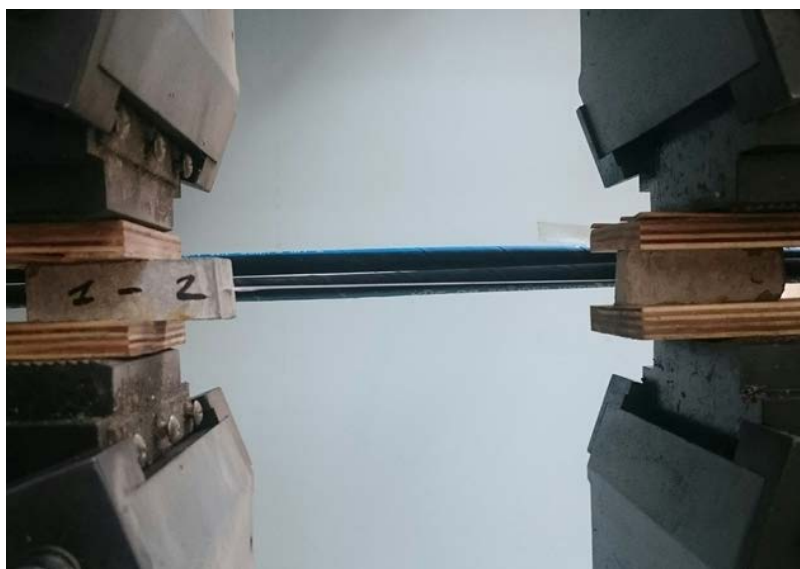


Figure 4. Testing of the fiber adhesion strength with the concrete matrix (determination of the critical length of the fiber).

The test results are as follows: the fiber broke (was destroyed) under the load $P_1 = 200$ N; the fiber came out of the concrete body without destruction under the load of $P_2 = 110$ N.

Then, we make calculations using the formulas:

$$P_1 = \sigma \cdot S, \quad (1)$$

where S is the cross-section area of the fiber, mm^2 ($S = 0.1 \text{ mm}^2$);

$$P_2 = \tau \cdot u \cdot l, \quad (2)$$

where: τ is shear stresses, N/mm^2 ;

u is the perimeter of the fiber cross section, mm , ($u = 11.04 \text{ mm}$);

l is the length of the fiber, which is in concrete, mm , ($l = 23 \text{ mm}$).

From formula (1) we will find the rupture strength of the fiber:

$$\sigma = P_1 / S. \quad (3)$$

From formula (2) we will find the shear stresses:

$$\tau = P_2 / u \cdot l. \quad (4)$$

So that the fiber did not leave the concrete body, but broke, we will equate formulas (1) and (2) and find the critical length of a half of the fiber.

$$l = \sigma \cdot S / \tau \cdot u. \quad (5)$$

Then, the length of the whole fiber will be:

$$l_f = 2 \cdot l. \quad (6)$$

Thus, the fiber will not be pulled out of the matrix contact area if the fiber is not shorter than 8.426 cm. The critical length of the fiber is $l_f = 8.426$ cm.

3. Results and Discussion

Based on the obtained experimental data, we will build diagrams of the dependence of the compressive and bending tensile strength of concrete on various factors.

As it is shown by the experiment results, if we add the PET fiber, the compressive strength of all types of samples decreases. This is consistent with a number of studies [15–17], but contradicts other publications [19, 20]. The compressive strength is 49.3 MPa for the control samples with 0 % of the PET fiber. The maximum strength loss is observed in the samples with the addition of the industrial flex. At the maximum amount of fiber added (3 %), the strength is reduced by 25 % (37.1 MPa). The maximum strength loss was 20 % (39.5 MPa) for the samples with smooth fiber. The compressive strength reduced by 15 % (42.3 MPa) for the samples with ribbed fiber. The decrease in the compressive strength can be explained by a low adhesion between the surface of the PET fiber and the concrete matrix. Therefore, when the volume of injected fiber increases, the compressive strength decreases. When using longer fibers, the strength decreases less. This is due to the larger surface area, and higher adhesion forces. As well as the effect of mechanical engagement of fiber in concrete. That allows you to resist the load when the sample is destroyed. The best effect is achieved by ribbed fiber. This material has the best strength characteristics, due to the better engagement of the fiber in the concrete matrix.

The values of the tensile strength of the studied compounds have a different nature. The addition of PET fiber to concrete provides an increase in tensile strength, which is confirmed by the work of other researchers [21–23]. The tensile strength of additive-free concrete is 3.6 MPa. The strength of the flex samples increases to 122 % (4.4 MPa) with the addition of 1 % of fiber. The strength of the samples with smooth fiber reaches 166 % (5.8 MPa), with a 1 % reinforcement with 3 cm long fiber. It is up to 153 % (5.5 MPa) in the samples with ribbed fiber. This confirms the effectiveness of the use of PET fiber

It is also worth noting that when testing prism samples with the addition of 400×100×100 mm smooth and ribbed fiber for tensile bending, it was noted that when the sample lost its strength, it almost did not lose its stability indicators and kept its shape under its own weight, after there was no load.

A generalized concrete strength indicator R was introduced in the diagrams to eliminate the ambiguity of the influence of various factors and facilitate the determination of the dependence of the strength characteristics on the parameters of the used fiber

$$R = R_{bt} / R_b, \quad (7)$$

where R_{bt} is the tensile strength of concrete, R_b is the compressive strength of concrete.

After evaluating the influence of the type of fiber used on the strength of concrete (Figure 5), we can conclude that the most optimal is ribbed (uneven) fiber. Such a shape allows the fiber to be more firmly fixed in concrete and ensures the transfer of tensile stresses from concrete to PET fiber. This contributes to an increase in the strength characteristics.

An increase in the amount of introduced fiber also predetermines an improvement of strength characteristics (Figure 6). It should be noted that this dependence is changeable (within the experiment), but is best described by a straight line.

The strength increases with an increase in the length of the fiber used (Figure 7). This can be explained by an increase in the effective adhesion area of the fiber and the concrete matrix with an increase in the size of the PET fiber used. This effect was noted in the works of other researchers who studied PET fiber reinforcement grids.

The abrasion capacity of fiber-reinforced concrete with PET fibers increases slightly with an increasing strength. This is not typical for concrete. Usually, the wear resistance increases with an increasing strength. This property can be explained by a poor adhesion of the fiber and the concrete matrix, especially in the area of the sample wear, which leads to spalling (separation) of the fine aggregate during the test. The abrasion capacity of fiber-free concrete was 0.52 g/cm². The abrasion capacity of the concrete with the addition of different amounts of PET fibers of various shapes and lengths ranges from 0.44 g/cm²

to 0.62 g/cm². In general, we can speak about a neutral influence of PET fibers on the durability of fiber-reinforced concrete. This confirms the effectiveness of the use of PET fiber (Figure 8).

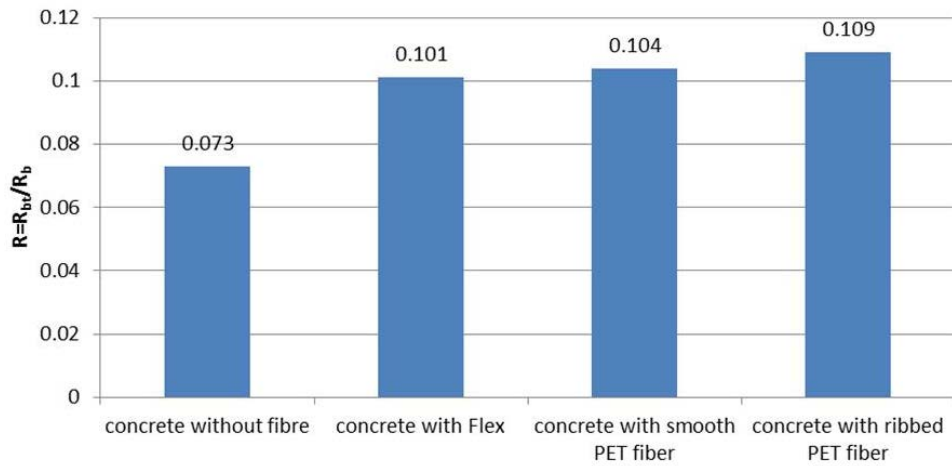


Figure 5. The dependence of the fiber concrete strength on the type of the PET fiber used.

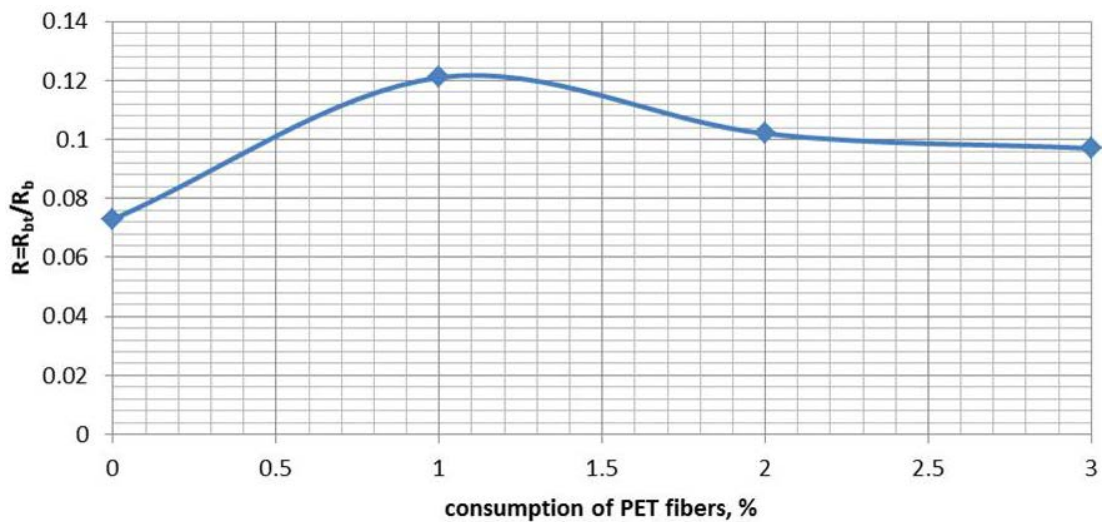


Figure 6. The dependence of the fiber concrete strength on the amount of introduced PET fibers.

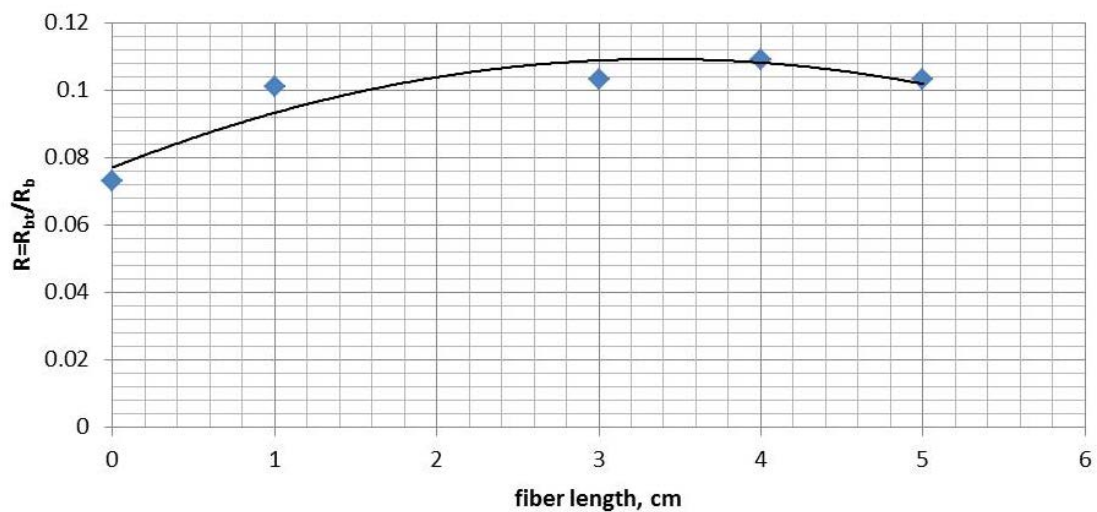


Figure 7. The dependence of the fiber concrete strength on the length of the fiber used.

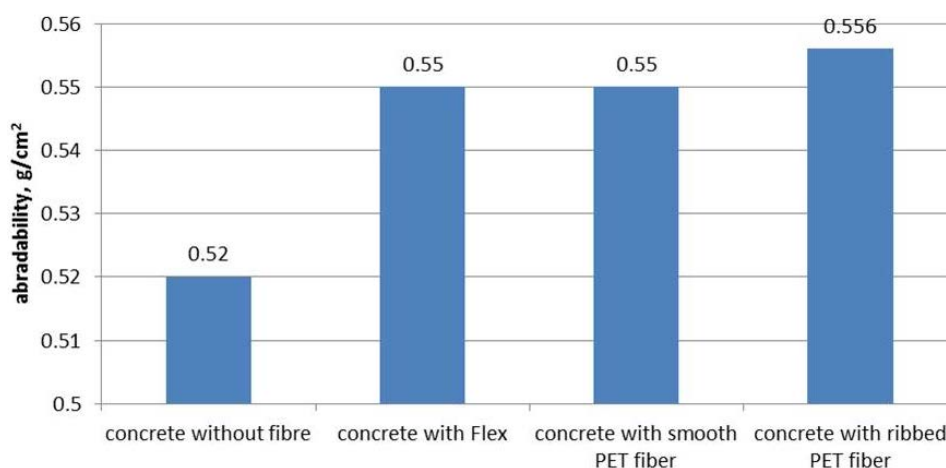


Figure 8. The dependence of fiber concrete abrasion on the type of fiber used.

4. Conclusions

With an obvious increase in the bending tensile strength indicator, which reaches 22–66 %, was obtained a decrease in the compressive strength indicator, which reaches 3–25 %. The most favorable ratio of the increase in the bending tensile strength indicator and the decrease in the compressive strength was obtained in the concrete with the addition of a smooth 4 cm long fiber with the lowest amount of reinforcement, 66 % increase in the bending tensile strength and 3 % decrease in the compressive strength. The most unfavorable ratio is in the concrete with the addition of the industrial PET flex with the highest reinforcement, where we obtained a decrease in strength in both tests, 13 % decrease in the bending tensile strength, and 25 % decrease in the compressive strength.

A decrease in the concrete abrasion capacity indicator was shown only by the samples with smooth and ribbed fiber, cut manually, with the largest value of concrete reinforcement (15 % and 7 %, respectively). The use of Flex leads to an increase in abrasion.

We calculated the critical fiber length (l_f) equal to 8.426 cm, at which the fiber would not be pulled out from the contact area of the matrix. This fiber length is in conflict with the procedure of introducing fibers into concrete, its preparation, transportation and laying in structures. Therefore, the variant of the ribbed fiber concrete, which is almost not inferior in strength to the smooth fiber concrete, is more favorable because of the possibility to reduce the fiber length due to various shapes of anchors on the lateral surface.

In general, the use of fiber in concrete from waste PET materials (obtained by mechanical grinding), and not subjected to heat treatment can increase the tensile strength. Compressive strength is reduced.

Industrial Flex is not recommended as a fiber (additive) in concrete, as it leads to a decrease in strength characteristics. Increased tensile strength is provided by the use of specially prepared PET fiber.

The study proved the possibility of using in concrete pet fiber from waste PET materials (obtained by mechanical grinding), and not subjected to heat treatment. PET fiber is recommended for use in concrete structures to increase tensile strength. This will make it possible to dispose of some plastic waste and preserve the environment.

5. Acknowledgment

The work was supported by Act 211 Government of the Russian Federation, contract № 02.A03.21.0011.

References

1. Weizsacker, E., Karlson, H., Smith, M. Faktor, 5. Formula ustojchivogo rosta [Factor 5 Formula for sustainable growth]. Moscow: AST-Press Kniga, 2013. 368 p. (rus)
2. Kornienko, S.V., Popova, E.D. «Green» construction in Russia and other countries Construction of Unique Buildings and Structures. 2017. 55(4). Pp. 68–83. (rus) DOI: 10.18720/CUBS.55.5
3. Golovnev, S.G. Sovremennye stroitel'nye tekhnologii: Monografiya [Modern Construction Technologies:

Литература

1. Вайцеккер Э., Харгроуз К., Смит М. Фактор пять. Формула устойчивого роста. М.:АСТ-ПРЕСС КНИГА, 2013. 368 с.
2. Корниенко С.В., Попова Е.Д. «Зеленое» строительство в России и за рубежом // Строительство уникальных зданий и сооружений. 2017. № 4. С. 68–83. DOI: 10.18720/CUBS.55.5

- monograph]. Chelyabinsk: South Ural State University Publishing Center, 2010. 268 p. (rus)
4. Rabinovich, F.N. Kompozity na osnove dispersno armirovannyh betonov. Voprosy teorii i proektirovaniya, tekhnologiya, konstrukcii: Monografiya [Composites based on disperse reinforced concretes. Questions of theory and design, technology, constructions: Monograph]. Moscow, Publishing house ASV, 2004. 560 p. (rus)
 5. Kiyanev, A.V. Technological Parameters of Magnesia Mortars // ICIE 2017 Procedia Engineering. 2017. Vol. 206. Pp. 826–830.
 6. Rudnov, V., Belyakov, V., Moskovsky, S. Properties and Design Characteristics of the Fiber Concrete. ICIE 2016 Procedia Engineering. 2016. Vol. 150. Pp. 1536–1540.
 7. Klyuev, S.V., Klyuev, A.V., Abakarov, A.D., Shorstova, E.S., Gafarova, N.G. The effect of particulate reinforcement on strength and deformation characteristics of fine-grained concrete. Magazine of Civil Engineering. 2017. 75(7). Pp. 66–75. DOI: 10.18720/MCE.75.6
 8. Nizina, T.A., Balykov, A.S., Volodin, V.V., Korovkin, D.I. Fiber fine-grained concretes with polyfunctional modifying additive. Magazine of Civil Engineering. 2017. 72(4). Pp. 73–83. DOI: 10.18720/MCE.72.9.
 9. Nikolenko, S.D., Sushko, E.A., Sazonova, S.A., Odnolko, A.A., Manokhin, V.Ya. Behaviour of concrete with a disperse reinforcement under dynamic loads. Magazine of Civil Engineering. 2017. 75(7). Pp. 3–14. DOI: 10.18720/MCE.75.1.
 10. Pikus, G.A., Manzhosov, I.V. Pressure of Fiber Reinforced Concrete Mixtures on Vertical Formwork Panels. ICIE 2017 Procedia Engineering. 2017. Vol. 206. Pp. 836–841.
 11. Gao, J., Sun, W., Morino, K. Mechanical properties of steel fiber-reinforced, high-strength, lightweight concrete. Cement and Concrete Composites. 1997. Vol. 19. Pp. 307–313.
 12. Mohammadi, Y., Singh, S.P., Kaushik, S.K. Properties of steel fibrous concrete containing mixed fibres in fresh and hardened state. Construction and Building Materials. 2008. Vol. 22. Pp. 956–965.
 13. Pikus, G.A. Steel Fiber Concrete Mixture Workability. ICIE 2016 Procedia Engineering. 2016. Vol. 150. Pp. 2119–2123.
 14. Malik, N., Kumar, P., Shrivastava, S., Ghosh, S.B. An overview on PET waste recycling for application in packaging. International Journal of Plastics Technology. 2017. Vol. 1. No. 1. Pp. 156–165.
 15. Sharma, R., Bansal, P.P. Use of different forms of waste plastic in concrete. Journal of Cleaner Production. 2016. Vol. 112. Pp. 473–482.
 16. Ochi, T., Okubo, S., Fukui, K. Development of recycled PET fiber and its applications as concrete-reinforcing fiber. Cement and Concrete Composites. 2007. Vol. 29. Pp. 448–455.
 17. Borg, R.P., Baldacchino, O., Ferrara, L. Early age performance and mechanical characteristics of recycled PET fibre reinforced concrete. Construction and Building Materials. 2016. Vol. 108. Pp. 29–47.
 18. Saikia, N., De Brito, J. Waste Polyethylene Terephthalate as an Aggregate in Concrete. Materials Research. 2013. Vol. 16. No. 2. Pp. 341–350.
 19. Wilinska, D., Lukowska, P., Rokickib G.. Application of fibres from recycled PET bottles for concrete reinforcement. Journal of Building Chemistry. 2016. Vol. 1. Pp. 1–9.
 20. Irwan, J.M., Asyraf, R.M., Othman, N., Koh, H.B., Annas, M.M.K., Faisal, S.K. The mechanical properties of PET fiber reinforced concrete from recycled bottle wastes. Advanced Materials Research. 2013. Vol. 795. Pp. 347–351.
 21. Maqbool, S., Sood, H. Effect of PET fibers on the mechanical properties of concrete. SSRG International Journal of Civil Engineering. 2016. Vol. 3. No. 12. Pp. 25–30.
 3. Головнев С.Г. Современные строительные технологии: монография. Челябинск: Издательский центр ЮУрГУ, 2010. 268 с.
 4. Рабинович Ф.Н. Композиты на основе дисперсно-армированных бетонов. Вопросы теории и проектирования, технология, конструкции: Монография. М.: Издательство АСВ, 2004. 560 с.
 5. Kiyanev A.V. Technological Parameters of Magnesia Mortars // ICIE 2017 Procedia Engineering. 2017. Vol. 206. Pp. 826–830.
 6. Rudnov V., Belyakov V., Moskovsky S. Properties and Design Characteristics of the Fiber Concrete // ICIE 2016 Procedia Engineering. 2016. Vol. 150. Pp. 1536–1540.
 7. Ключев А.В., Абакаров А.Д., Шорстова Е.С., Гафарова Н.Е. Влияние дисперсного армирования на прочностные и деформативные характеристики мелкозернистого бетона // Инженерно-строительный журнал. 2017. № 7(75). С. 66–75. DOI: 10.18720/MCE.75.6
 8. Низина Т.А., Бальков А.С., Володин В.В., Коровкин Д.И. Дисперсно-армированные мелкозернистые бетоны с полифункциональными модифицирующими добавками // Инженерно-строительный журнал. 2017. № 4(72). С. 73–83. DOI: 10.18720/MCE.72.9.
 9. Николенко С.Д., Сушко Е.А., Сазонова С.А., Однолько А.А., Манокhin В.Я. Поведение бетона с дисперсным армированием при динамических воздействиях // Инженерно-строительный журнал. 2017. № 7(75). С. 3–14. DOI: 10.18720/MCE.75.1.
 10. Pikus G.A., Manzhosov I.V. Pressure of Fiber Reinforced Concrete Mixtures on Vertical Formwork Panels. ICIE 2017 Procedia Engineering. 2017. Vol. 206. Pp. 836–841.
 11. Gao J., Sun W., Morino K. 1997 Mechanical properties of steel fiber-reinforced, high-strength, lightweight concrete // Cement and Concrete Composites. Vol. 19. Pp. 307–313.
 12. Mohammadi Y., Singh S.P., Kaushik S.K. Properties of steel fibrous concrete containing mixed fibres in fresh and hardened state // Construction and Building Materials. 2008. Vol. 22. Pp. 956–965.
 13. Pikus G.A. Steel Fiber Concrete Mixture Workability // ICIE 2016 Procedia Engineering. 2016. Vol. 150. Pp. 2119–2123.
 14. Malik N., Kumar P., Shrivastava S., Ghosh, S.B. An overview on PET waste recycling for application in packaging // International Journal of Plastics Technology. 2017. Vol. 1. No. 1. Pp. 156–165.
 15. Sharma R., Bansal P.P. Use of different forms of waste plastic in concrete // Journal of Cleaner Production. 2016. Vol. 112. Pp. 473–482.
 16. Ochi T., Okubo S., Fukui K. Development of recycled PET fiber and its applications as concrete-reinforcing fiber // Cement and Concrete Composites. 2007. Vol. 29. Pp. 448–455.
 17. Borg R.P., Baldacchino O., Ferrara L. Early age performance and mechanical characteristics of recycled PET fibre reinforced concrete // Construction and Building Materials. 2016. Vol. 108. Pp. 29–47.
 18. Saikia N., De Brito J. Waste Polyethylene Terephthalate as an Aggregate in Concrete // Materials Research. 2013. Vol. 16. No. 2. Pp. 341–350.
 19. Wilinska D., Lukowska P., Rokickib G.. Application of fibres from recycled PET bottles for concrete reinforcement // Journal of Building Chemistry. 2016. Vol. 1. Pp. 1–9.
 20. Irwan J.M., Asyraf R.M., Othman N., Koh H.B., Annas M.M.K., Faisal S.K. The mechanical properties of PET fiber reinforced concrete from recycled bottle wastes // Advanced Materials Research. 2013. Vol. 795. Pp. 347–351.
 21. Maqbool S., Sood H. Effect of PET fibers on the mechanical properties of concrete // SSRG International Journal of Civil Engineering. 2016. Vol. 3. No. 12. Pp. 25–30.

22. Mastan Vali, N., Asadi, S.S. Pet bottle waste as a supplement to concrete fine aggregate. *International Journal of Civil Engineering and Technology*. 2017. Vol. 8. No. 1. Pp. 558–568.
23. Vishnu, A., Mohana, V., Manasi, S., Ponmalar, V. Use of polyethylene terephthalate in concrete. *International Journal of Civil Engineering and Technology*. 2017. Vol. 8. No. 7. Pp. 1171–1176.
24. Khalid, F.S., Irwan, J.M., Ibrahim, M.H.W., Othman N., Shahidan S. Performance of plastic wastes in fiber-reinforced concrete beams. *Construction and Building Materials*. 2018. Vol. 183. Pp. 451–464.
25. Bui, N.K., Satomi, T., Takahashi, H. Recycling woven plastic sack waste and PET bottle waste as fiber in recycled aggregate concrete: An experimental study. *Waste Management*. 2018. Vol. 78. Pp. 79–93.
26. Sakulneya, A., Wattanachai, P. A comparison study on elasticity of rubberized concrete with and without poly (Ethylen eterephthalate) fibre. *Songklanakarin Journal of Science and Technology*. 2018. Vol. 40. No. 3. Pp. 492–497.
22. Mastan Vali N., Asadi S.S. Pet bottle waste as a supplement to concrete fine aggregate // *International Journal of Civil Engineering and Technology*. 2017. Vol. 8. № 1. Pp. 558–568.
23. Vishnu A., Mohana V., Manasi S., Ponmalar V. Use of polyethylene terephthalate in concrete // *International Journal of Civil Engineering and Technology*. 2017. Vol. 8. № 7. Pp. 1171–1176.
24. Khalid F.S., Irwan, J.M., Ibrahim M.H.W., Othman N., Shahidan S. Performance of plastic wastes in fiber-reinforced concrete beams // *Construction and Building Materials*. 2018. Vol. 183. Pp. 451–464.
25. Bui N.K., Satomi T., Takahashi H. Recycling woven plastic sack waste and PET bottle waste as fiber in recycled aggregate concrete: An experimental study // *Waste Management*. 2018. Vol. 78. Pp. 79–93.
26. Sakulneya A., Wattanachai P. A comparison study on elasticity of rubberized concrete with and without poly (Ethylen eterephthalate) fibre. *Songklanakarin // Journal of Science and Technology*. 2018. Vol. 40. № 3. Pp. 492–497.

Aleksandr Kiyanets,
+7(905)8305181; *kiyanets2007@mail.ru*

Александр Валерьевич Киянец,
+7(905)8305181;
эл. почта: kiyanets2007@mail.ru

© Kiyanets. A.V., 2018

doi: 10.18720/MCE.84.12

Stress-strain behavior of welded joints in railway girders

Напряженное состояние сварных узлов
железнодорожных пролетных строений

S.A. Bokarev,
Siberian State University of Railway Engineering,
K.O. Zhunev*,
A.M. Usol'tsev,
Siberian State University of Railway Engineering,
Novosibirsk, Russia

*Д-р техн. наук, проректор по научной
работе С.А. Бокарев,
инженер К.О. Жунев*,
инженер А.М. Усольцев,
Сибирский Государственный Университет
Путей Сообщения, г. Новосибирск, Россия*

Key words: railway bridge; welded span; fatigue crack; finite element method; residual stresses; reinforcement

Ключевые слова: железнодорожный мост; сварное пролетное строение; усталостная трещина; метод конечных элементов; остаточные напряжения; усиление

Abstract. A metal construction with welded joints often fails under repeated loads by fatigue. Fatigue cracks at welded joints occur because real stress-strain behavior of welded joints is not taken into consideration by standard design. The article is devoted to the stress behavior determination of welded joints in railway girders under external loads and residual stresses. Design deficiencies and technological features of welded girders were identified. These features may increase stresses at welded joints and decrease fatigue life. As a result of studying the existing methods for determining stresses in welded joints, authors used a method, that takes into account the residual welding stresses and design features of welded girder. In this study, the stresses were determined in a cracking area of a girder with the help of finite element modeling. It was shown the correspondence of the stresses in the finite element model and the real girder, tested under the moving load. Retrofitting of stiffeners in welded girders with fatigue cracks was carried out using corner plate connected tightly stiffener and beam flange. Strain measurements under the moving load before and after the retrofitting near cut ribs were taken. The dependence of the stresses at the beam webs was demonstrated near the upper welded ends of stiffeners on the stiffness of rib connections to beam flanges. These findings can be useful at the fatigue life design of the welded elements at building constructions.

Аннотация. Металлические конструкции со сварными узлами подвержены частым отказам при воздействии на них переменных нагрузок. Усталостные трещины в сварных узлах образуются из-за того, что еще на этапе проектирования конструкции не учитывают действительное напряженно-деформированное состояние этих элементов. Статья посвящена определению напряженного состояния сварных узлов железнодорожных пролетных строений от внешних нагрузок. Перечислены технологические и конструктивные особенности сварных пролетных строений, повышающие напряжения в сварных узлах и снижающие их усталостную долговечность. В результате изучения существующих методов определения напряжений в сварных узлах использован метод, учитывающий остаточные сварочные напряжения и конструктивные особенности сварных пролетных строений. Приведены результаты определения напряжений в трещинопасном узле пролетного строения при помощи конечно-элементного моделирования. Показано соответствие напряжений в конечно-элементной модели и реальном пролетном строении, испытанном под обрабатываемой нагрузкой. Приведены данные по результатам усиления вертикальных ребер жесткости пролетного строения уголковыми накладками, увеличивающими жесткость крепления ребер к поясу балки. Измерения деформаций стенки балки под обрабатываемой нагрузкой, выполненные до усиления и после, доказывают на практике наличие зависимости напряжений, возникающих в стенке балки у верхних концов сварных швов прикрепления ребра жесткости, от жесткости прикрепления ребра жесткости к поясу главной балки. Полученные результаты исследований могут быть полезны при проектировании усталостной долговечности сварных элементов строительных конструкций.

1. Introduction

The railway system of Russia comprises more than 11300 metal girders. Half of these girders are welded girders. At such structures, the connections of longitudinal stringers and transverse beams are implemented with high-strength bolts, whereas the connections of stiffeners to the longitudinal stringers and butt joints are accomplished using the machine welding. The bridges in Russia have been employing welding connections instead of riveting ones since the 1970s. However, the short-term operation of welded structures has unveiled their unexpected vulnerability to fatigue cracks forming in weld toes. Nowadays, about 15 % of all welded girders are operated with fatigue cracks.

Fatigue fracture of metals is a result of the action of varied or repeated loads whose value is less than the ultimate static load. Practically, most metal structures fail by fatigue and relatively few by static loads [1]. Fatigue cracks are encountered at mechanical engineering, at aviation, at shipbuilding, and at building structures. It is well known that the fatigue resistance is largely affected by such factors as the magnitude of stresses, the stress cycle asymmetry, the presence of stress concentrators, the residual stresses, and the surface roughness.

In Russia, studies of the fatigue life of welded railway girders were initiated in the 1980s. Large-scale inspections of welded girders were carried out, typical crack formation cases were described, a classification of typical cracks was given, and recommendations on the maintenance and repair of girders with cracks were delivered [2]. By now, it is known more than twenty types of fatigue cracks encountered in metal girders. As a rule, fatigue cracks are located near the welded ends of stiffeners of the main beams or the floor beams. Statistics of welded girders failure shows that the most negative consequences for the strength and for the service life of structures come as a result of the cracking in the beam web (cracks T-9 and T-10) [3]. Such cracks, under development, reduce the load-bearing capacity of longitudinal stringers and transverse beams. Location of such cracks at welded girder is demonstrated at Figure 1.

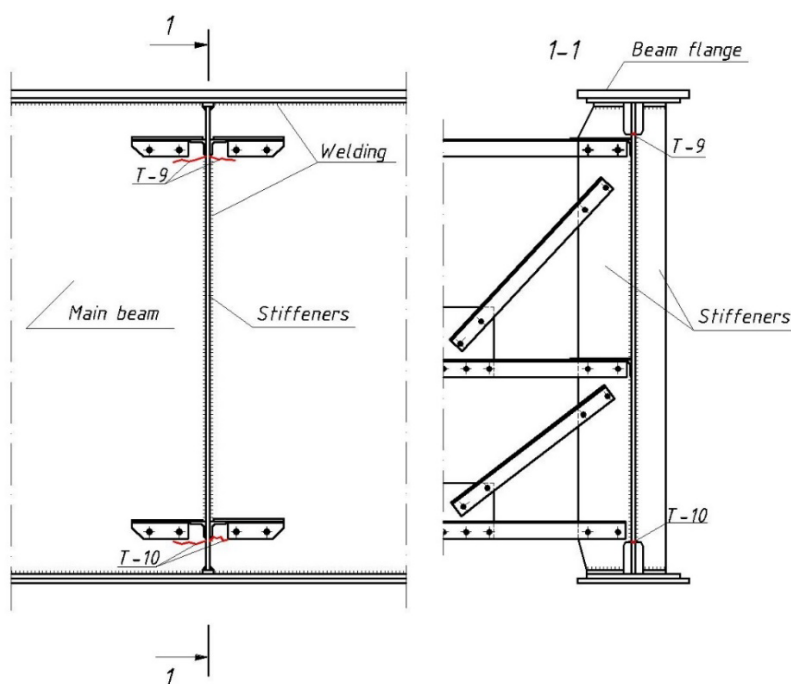


Figure 1. Location of fatigue cracks in welded girders.

In the course of inspections of welded girders, it was found that possible reason for the formation of such fatigue cracks was the loose fit of stiffeners to beam flanges and the off-center action of moving load. As a result, the beam flanges have additional vertical displacements and twisting motions under the load. The beam web experiences bending deformations along stiffener cuts; the latter circumstance led to a substantial growth of stresses at the ends of stiffener welds. An analysis of results gained while performing annual inspections of welded girders shows that, initially, fatigue cracks develop at stiffeners located near supports [2]. It has allowed us to advance a hypothesis about a substantial influence of shear stresses on the fatigue resistance.

In the same years, staff members of several Russian universities have carried out studies on the evaluation of the fatigue life of welded girders. Those studies have shown that, typically, welded joints have a very short fatigue life due to some features of the welding process [4]. A sharp local increase and

Bokarev, S.A., Zhunev, K.O., Usol'tsev, A.M. Stress-strain behavior of welded joints in railway girders. Magazine of Civil Engineering. 2018. 84(8). Pp. 119–129. doi: 10.18720/MCE.84.12.

decrease of temperature induced by the welding process led to the generation of tensile residual stresses, which, according to research data [5–8], could reach a value of 0.5–0.6 yield strength. Various internal flaws form in the weld due to the violation of the welding process. Such flaws as slug inclusions, weld undercutting, lack of penetration and other flaws act as additional stress concentrators.

The impact of the climatic factor on the crack formation processes in welded girders was analyzed according to the database of the Automated Control System for Artificial Structures (ACS ASs) and the annual inspections data of welded girders. Author has performed the grouping of Russian railways based on climatic-zoning data contained in the Russian Building Rules “Construction Climatology” [9]. All the climatic zones were divided into two groups, those with favorable climatic conditions (average monthly temperature – 0 to -14 °C in January and +12 to +28 °C in July); and those with unfavorable climatic conditions (average monthly temperature below -14 °C in January and 0 to +20 °C in July) [10]. The distribution of welded girders with fatigue cracks of the railway system is shown in Figure 2.

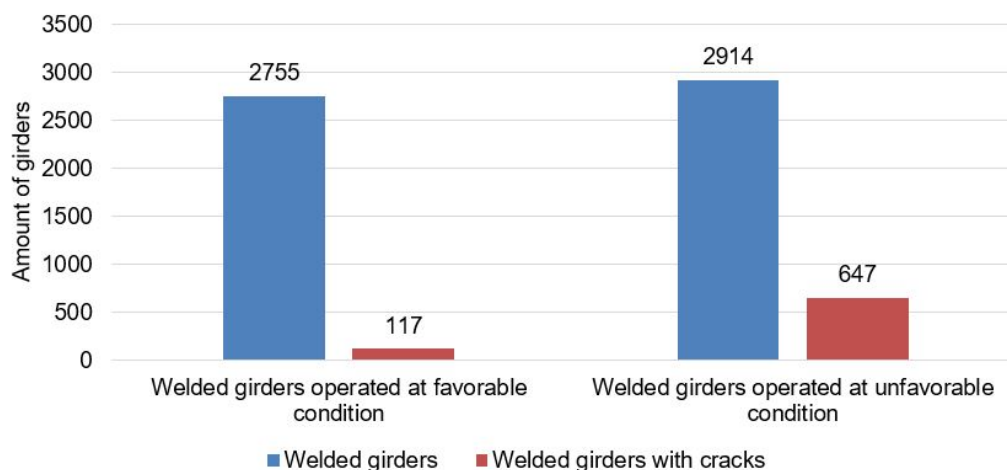


Figure 2. Amount of welded girders with fatigue cracks.

It was established that in the railways with unfavorable climatic conditions the number of welded girders with cracks was six times as much that in the railways with favorable one. Total numbers of welded girders in both groups are equal.

Scientific publications [11–14], engaged in the fatigue life evaluation of welded joints, show that the formation of fatigue cracks in welded beams was a consequence of inaccurate evaluation of the stress-strain behavior near the welded ends of stiffeners. The increase of stresses near the welded ends of stiffeners was a consequence of some specific features of the operation of these structures and the action of the moving loads. Evaluating the stress-strain behavior with all features can be taken into consideration by the finite element method (FEM). It enables to determinate the stress-strain behavior of the structure with allowance for its 3D operation and specific design features.

Different approaches of stress determination were designed using FEM such as nominal stress, hot spot stress and effective notch stress [15]. Nominal stress approach based on huge numbers of laboratory fatigue test results for different weld details with different geometries, a number of design S-N curves that represent a 97.7 % survival probability for the details that are associated with each curve have been provided in the design codes [16, 17].

The hot spot stress approach was originally developed for welded joints of circular and rectangular hollow sections. The structural hot spot stress can be determined using reference points and extrapolation to the weld toe at the hot spot in consideration. The method has been later applied successfully to welded plate structures [18–20]. Evaluation of hot spot structural stress from the finite element analysis was updated by Radaj et al. [21].

The effective notch stress approach is mainly based on the computed highest elastic stress at the critical points, i.e. crack initiation points. This method was proposed by Radaj et al. [22] who took account of stress averaging in the micro-support theory according to the Neuber’s rule with a fictitious radius of 1 mm for plate thicknesses of 5 mm and above. For smaller plate thicknesses, Zhang and Richter [23] have proposed the use of a fictitious radius of 0.05 mm, which is based on the relationship between the stress-intensity factor and the notch stress.

However, these researches do not take into consideration welding residual stresses. To accurately analyze crack behavior in fusion welded components Citirik et al. [24] used two finite element softwares (HEAT2D and FRAC2D_WELD). In Li [25] prediction of welding residual stress was performed by using two finite element softwares SYSWELD and FRAC3D. 3D welding simulations were carried out in order to determine the residual stresses which are transported to the 3D fracture analyses.

Also strain-life approach is widely used for fatigue analyses of welded structures. After the strain-life approach was applied the cyclic elastic-plastic strain has to be assessed at the place where damage is expected to develop in the structure. The local strain range is recommended to be determined based on Neuber's heuristic formula [26]. The modified strain criterion-based method for fatigue assessment of structures is discussed in the article [27].

The article [28] shows a method for estimating the reliability of railway girders. A solution describes the probability of failure-free operation at the level of 0.97–0.98. Such solution is relevant for railways of normal traffic conditions with the possibility of providing high-speed rail traffic. This technical method for rapid assessment of the reliability of railway bridges girders can be used as a basis for harmonizing the Russian National Standard and for the further evolution of the codes for high-speed railway.

An analysis of the fatigue studies of welded girders has shown that the formation of fatigue cracks in structural elements in operation is related with a number of factors involving:

- weld residual stresses;
- specific features of the moving loads action and features of the external loads transfer by the bridge deck;
- insufficiently rigid fastening of stiffeners to the flanges;
- bending deformations of beam webs over the stiffener cut length;
- impact of the high range of minimal and maximal temperatures in the region where the girder is operated.

The totality of these factors substantially increases the stresses at cracking area in comparison with design calculations and leads to a shorter fatigue life of welded joints. The most important factor for crack formation is residual stresses after welding, because the welded part is most likely to be identified as the initial location of fracture. Consequently, an accurate and efficient technique for the determination of the weld residual stress distribution is the required starting point for an accurate fracture prediction methodology for welded structures. Fatigue analyses of welded structures should be performed by using FEM.

The purpose of the present study is the determination of the stress-strain behavior of welded joints in railway girders.

In this study the following problems are being solved:

- the determination of the residual stresses value after welding of stiffener by finite element method;
- the evaluation of stresses at the beam web under moving loads;
- the evaluation of the influence of stiffeners' rigid fastening to the flanges over stresses at the beam web.

2. Methods

The finite element model of the metal railway bridge girder was generated in Midas Civil software [29] for determining the girder stress induced by the moving loads action. The model of the girder was approximated with plate elements to model the stiffeners and to take into consideration the bending of the beam webs in two planes. The finite elements were located on the middle surface of the profile [30]. The reinforced concrete slabs of the ballastless bridge deck were also modeled with plate elements. The fastening of plates to the beams was modeled with rigid bonds. Cross bracing was modeled with beam elements. The model view illustration is shown in Figure 3. Moving load was assumed as the heaviest operating electric locomotive with 24.5-tons/axle load. Load displacement on the model of the girder was modeled with nodal forces moving along the model. Application of the moving load in transverse direction is illustrated in Figure 4.

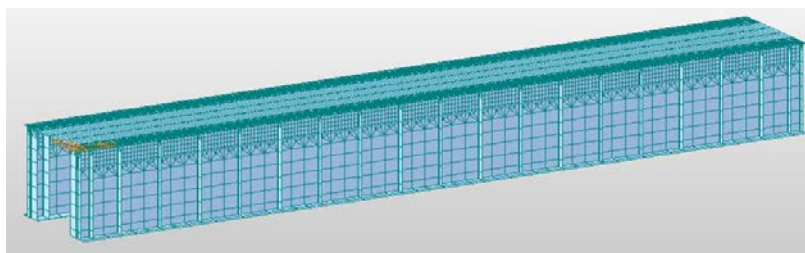


Figure 3. General view of the girder model.

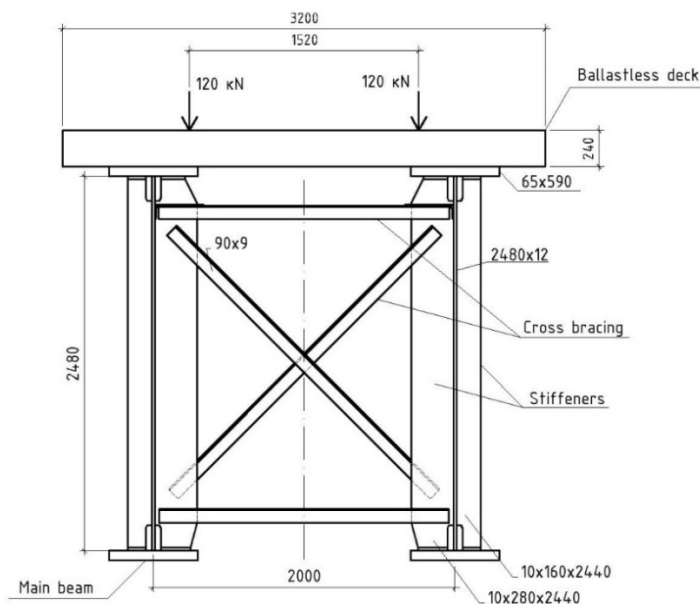


Figure 4. Application of the moving load.

The welding residual stresses were simulated using Sysweld software [31] for performing thermal calculations. Sysweld solves the problem for the non-stationary statement, thus the software is allowed to take into consideration all thermomechanical phenomena and metallurgical effects. The initial dates for the model are shown in Table 1.

Table 1. The initial dates for the model in Sysweld.

| Heat energy, J/mm | Welding speed, mm/sec | Leg of weld, mm | Yield strength, MPa | Young's modulus, MPa | Poisson's ratio |
|-------------------|-----------------------|-----------------|---------------------|----------------------|-----------------|
| 1300 | 3 | 7 | 250 | $2 \cdot 10^5$ | 0.3 |

Thermomechanical properties were assigned as for low-alloyed steel from the programming library. The solution took into account constitutional change of steel. The Goldak's double ellipsoidal heat source model [32] was used for heat source simulating of arc welding procedures. This model takes into consideration the formation of a recess in the weld pool.

Sysweld evaluated the residual stresses as equivalent stresses defined by the formula:

$$\sigma_{eqv} = \frac{1}{\sqrt{2}} \sqrt{(\sigma_1 \sigma_2)^2 + (\sigma_2 \sigma_3)^2 + (\sigma_1 \sigma_3)^2}, \quad (1)$$

where σ_1 , σ_2 , σ_3 are respectively the first, the second, and the third principal stresses of the stress behavior, MPa.

The stress-strain behavior of welded joint is determined by using Ansys software [33]. Computed residual stresses from Sysweld were imported into Ansys as pressure. It was possible because the same finite element model was used at Ansys and Sysweld. For this reason, a part of beam model 1 m in length was modeled at Ansys and Sysweld by solid elements SOLID 185. The part of beam model at Ansys was loaded by the computed external forces from Midas Civil and residual stresses from Sysweld. Moreover,

Ansys software is capable to solve contact problems; as a result, software obtains a possibility to model the loose support beam flange on the stiffeners.

The obtained stresses in the finite element model were verified on a real girder under a moving load. The strains in the beam web were measured using the Tensor-MS electronic measuring complex [34]. The complex involves strain gauges and data collector, which are located on the beam web. Also the influence of stiffeners' reinforcement on the stresses at the beam web was studied. The reinforcement was implemented using angel bar connected tightly to the stiffener and the beam flange resulting in fixity of beam flanges. The scheme of reinforcement stiffener is shown in Figure 5. The reinforcement effectiveness was evaluated from the beam web deformations under the moving load before and after the reinforcement. Measurements were conducted under the heaviest operating electric locomotive with 24.5-tons/axle load. The installation of the measuring gauges before and after the reinforcement is shown in Figure 6.

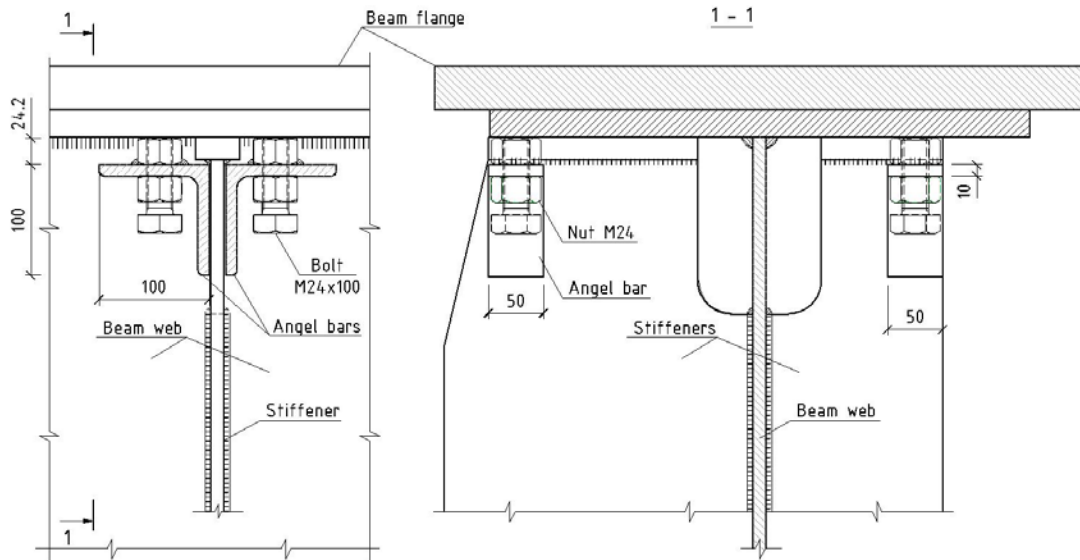


Figure 5. The scheme of reinforcement stiffener.

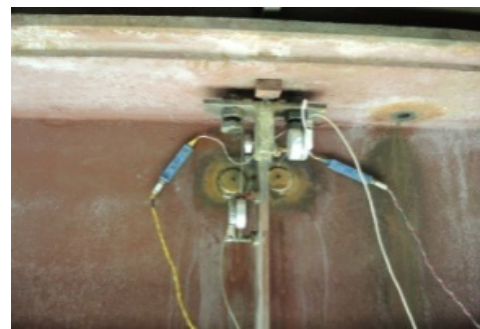
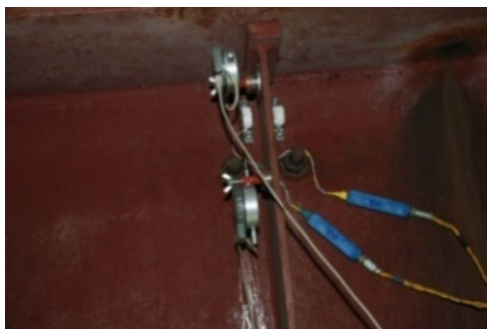
Before reinforcement

After reinforcement



outer beam surface

outer beam surface



inner beam surface

inner beam surface

Figure 6. Installation of strain gauges.

3. Results and Discussion

3.1. Residual stresses after welding

During the modeling of the welding processes in Sysweld, the temperature reached 1500 °C. A sharp increase of stresses to 120 MPa was observed at the upper and lower edges of weld after cooling to 20 °C. Figure 7 shows the residual stresses after welding simulation.

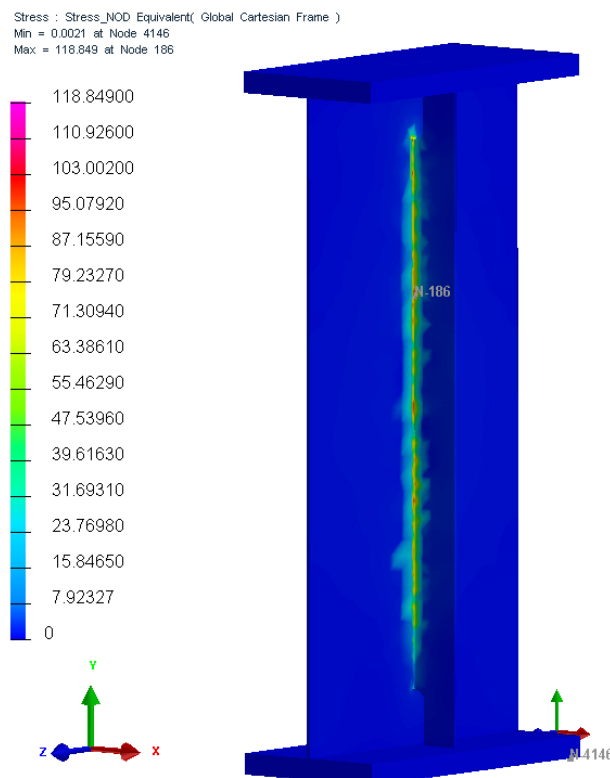


Figure 7. Distribution of residual equivalent stresses after cooling, MPa.

During the experiment residual stress of the weld toe was measured via $\sin 2\psi$ method by using XRD with Cr-K α radiation [35]. The surface tensile residual stress approximately corresponded to 100 MPa. Dexter et al. [36, 37] measured residual stresses in welded stiffened panel specimens after fatigue tests. It was demonstrated that these stresses can be idealized by the triangular distribution [36] or the rectangular distribution [37], with peak residual tensile stress equal to the yield strength of the steel under consideration. Tensile regions around the stiffeners are idealized as rectangular or triangular shapes with a base width equal to 10 mm, where the stress level reaches the yield strength of the considered material, $\sigma_o = 235$ MPa [38].

3.2. Stresses at the beam web under external loads

As a result of the modeling of the entire girder structure under moving load, it was found that equivalent stresses near the stiffeners reach 15 MPa. The equivalent stresses of the girder model under moving loads in Midas Civil is detailed in Figure 8. In the study [39], finite modelling of truss girder with a length of 55 m under the same load showed that equivalent stresses near the stiffeners reach 30 MPa. However, such stresses are insufficient for the formation of fatigue cracks. Low values of stresses in the model are the reason why the model ignores the residual stresses and the loose support of beam flange on the stiffeners.

Studying the impact of the rigidity of stiffener fixation to beam flanges on the stress behavior near stiffener weld ends, we have modeled four specimens with clearances between the stiffener and the beam flange. Those clearances were equal to 0 mm (no clearance), 0.5 mm, 1 mm and 2 mm. Based on the result, it was plotted the graphs illustrating the variation of equivalent stresses over the beam height. Graphs that illustrate the variation of equivalent stresses over the beam height at near the weld toe on both the outer and inner sides of the beam web are shown in Figures 9 and 10.

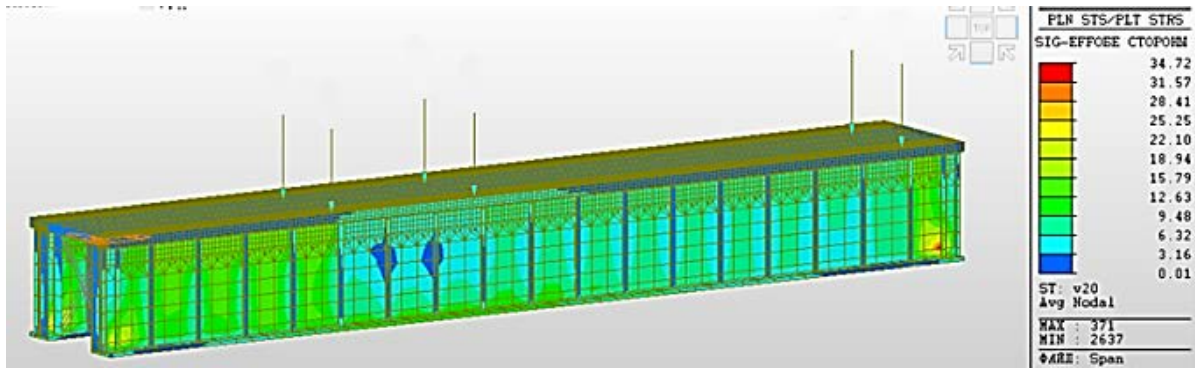


Figure 8. Equivalent stresses due to the action of the moving loads, MPa.

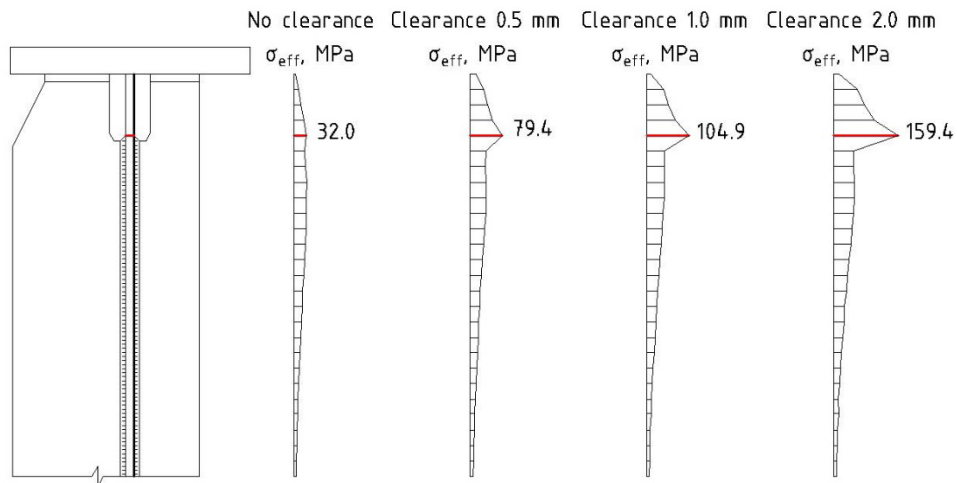


Figure 9. Variation of stresses over the height on the outer surface of the beam web near the weld toe.

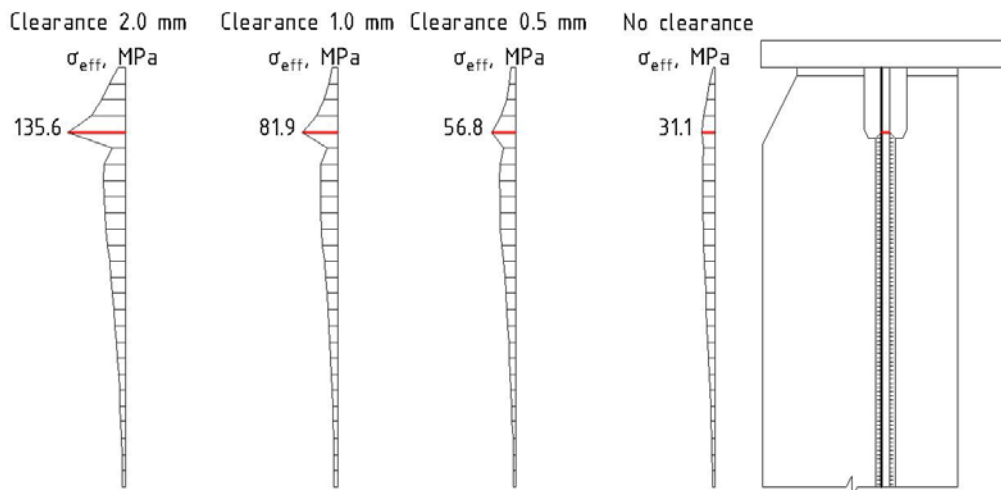


Figure 10. Variation of stresses over the height on the inner surface of the beam web near the weld toe.

The graphs clearly demonstrate the increase of stresses at the weld end and, also, a considerable increase of the stresses in the case of clearance between the stiffener end and the beam flange. In the case of tight fixation of stiffener there are no flexural-torsional deformations of beam web over the stiffener cut length. The latter fact substantially reduces the stresses and prolongs the fatigue life of such joints.

Measurements of strains in the beam web under the moving load showed a good convergence with the finite element model. The effectiveness of the stiffeners reinforcement with angel bar has been demonstrated. The measured stress values are summarized in Table 2.

Table 2. Stresses at the beam web.

| | Stresses, MPa | |
|----------------------|--------------------|--------------------|
| | inner beam surface | outer beam surface |
| Before reinforcement | 50.0 | 53.5 |
| After reinforcement | 23.4 | 22.0 |

The same reinforcement of stiffeners was applied in Seto-Ohashi Bridges in Japan [40]. The stress distributions around the fatigue cracks were measured before and after the repair works by the TSA technique when live loading acted on the bridge and the effectiveness of the severity reduction using these repair methods was investigated [40]. Stresses at connection of stiffener and beam flange under loading were reduced from 186 MPa to 137 MPa after reinforcement. The thermoelastic stress measurement was conducted using an infrared camera with a QVGA InSb array detector [41].

4. Conclusions

1. The numerical simulation has confirmed the influence of service conditions, design and technological features on the fatigue life of welded girders.

2. It was shown that residual stress over the height on the surface of the beam web near the weld toe reach 0.4–0.6 of the yield strength of steel (100–150 MPa).

3. It was shown that stress on the surface of the beam web near the weld toe depends on the rigidity of stiffener fixation to beam flanges. In case of clearance equal to 0.5 mm, stress on the surface of the beam web near the weld toe doubled and reached 60–70 MPa.

4. In practice, the effectiveness of stiffener fixation was proven for reducing the stresses on the surface of the beam web near the weld toe. Rigid fixation of the stiffener led to decrease in stresses near the weld toe in half.

5. It was shown that a combination of several factors increased stresses at the stiffener cuts, and the elimination of one of these factors could decrease the stresses arising due to external load. It should to prolong the fatigue life of the welded joint.

References

- Forrest, P. Fatigue of metals. London, 1962. 354 p.
- Ukazaniya po osmotru i usileniyu ekspluatiruyemykh svarynykh proletrykh stroyeniy [Guidelines for inspecting and reinforcing operated welded girders]. Moscow: MPS, 1990. 19 p. (rus)
- Bokarev, S.A., Zhunev, K.O. Osobennosti i perspektivy otsenki ostatochnogo resursa svarynykh metallicheskih proletrykh stroyeniy zheleznodorozhnykh mostov [Features and prospects of residual fatigue life estimation of welded metal spans of railway bridges]. The Siberian Transport University Bulletin. 2017. Vol. 1. Pp. 30–35. (rus).
- Bokarev, S.A., Murovanny, Yu.N., Pribytkov, S.S., Usoltsev A.M. Usloviya obespecheniya dvizheniya tyazhelovesnykh poyezdov po iskusstvennym sooruzheniyam [Conditions for heavy trains' movement on bridges]. Railway Transport. 2017. Vol. 7. Pp. 64–67. (rus).
- Nurguzhin, M.R., Danenova, G.T., Reytarov, O.V., Nurpiisova, G.D. Kompyuternoye modelirovaniye vliyaniya mekhanicheskogo vozdeystviya na ostatochnyye svarochnyye napryazheniya i deformatsii [Computer modeling of influence of mechanical impact on residual welding stresses and strains]. International journal of experimental education. 2014. Vol. 3. Pp. 114–118. (rus).
- Genchev, G., Doynov, N., Ossenbrink R., Michailov V., Bokuchava, G., Petrov, P. Residual stresses formation in multi-pass weldment: A numerical and experimental study. Journal of constructional steel research. 2017. Vol. 138. Pp. 633–641.
- Brar, G.S., Singh, C.S. FEA of residual stress in cruciform welded joint of hollow sectional tubes. Journal of Constructional Steel Research. 2014. Vol. 102. Pp. 44–58.
- Garifullin, M., Launert, B., Heinisuo, M., Pasternak, H., Mela, K., Pajunen, S. Effect of welding residual stresses on local behavior of rectangular hollow section joints. Part 1 –

Литература

- Forrest P. Fatigue of metals. London, 1962. 354 p.
- Указания по осмотру и усилению эксплуатируемых сварных пролетных строений. М.: МПС, 1990. 19 с.
- Бокарев С.А., Жунев К.О. Особенности и перспективы оценки остаточного ресурса сварных металлических пролетных строений железнодорожных мостов // Вестник Сибирского государственного университета путей сообщения. 2017. № 1. С. 30–35.
- Бокарев С.А., Мурованный Ю.Н., Прибытков С.С., Усольцев А.М. Условия обеспечения движения тяжеловесных поездов по искусственным сооружениям // Железнодорожный транспорт. 2017. № 7. С. 64–67.
- Нургужин М.Р., Даненова Г.Т., Рейтаров О.В., Нурпиисова Г.Д. Компьютерное моделирование влияния механического воздействия на остаточные сварочные напряжения и деформации // Международный журнал экспериментального образования. 2014. №3. С. 114–118.
- Genchev G., Doynov N., Ossenbrink R., Michailov V., Bokuchava G., Petrov P. Residual stresses formation in multi-pass weldment: A numerical and experimental study // Journal of constructional steel research. 2017. Vol. 138. Pp. 633–641.
- Brar G.S., Singh C.S. FEA of residual stress in cruciform welded joint of hollow sectional tubes // Journal of Constructional Steel Research. 2014. Vol. 102. Pp. 44–58.
- Garifullin M., Launert B., Heinisuo M., Pasternak H., Mela K., Pajunen S. Effect of welding residual stresses on local behavior of rectangular hollow section joints. Part 1 – Development of numerical model // Bauingenieur. 2018. Vol. 93, № April. Pp. 152–159.
- СП 131.13330.2012 Актуализированная версия СНиП 23-01-99* «Строительная климатология». М.: Минрегион, 2012. 109 с.

Бокарев С.А., Жунев К.О., Усольцев А.М. Напряженное состояние сварных узлов железнодорожных пролетных строений // Инженерно-строительный журнал. 2018. № 8(84). С. 119–129.

- Development of numerical model. Bauingenieur. 2018. Vol. 93, No. April. Pp. 152–159.
9. Russian Building Rules SP 131.13330.2012 Aktualizirovannaya versiya SNiP 23-01-99* «Stroitel'naya klimatologiya» [Construction Climatology]. Moscow. 2012. 109 p. (rus).
 10. Zhunev, K.O. Statisticheskiy analiz faktorov treshchinoobrazovaniya v svarnykh proletnykh stroeniyakh [Statistical analysis of the crack formation factors in welded spans]. Transportnaya infrastruktura Sibirskogo regiona: materialy VIII mezhdunarodnoy nauchno-prakticheskoy konferentsii. Irkutsk: IrGUPS, 2017. Pp. 455–460. (rus).
 11. Hobbacher, A. The new IIW recommendations for fatigue assessment of welded joints and components – A comprehensive code recently updated. International Journal of Fatigue. 2009. Vol. 31. Pp. 50–58.
 12. Bowman, M., Fu, G., Zhou, E., Connor, R., Godbole, A. Fatigue evaluation of steel bridges. Washington, 2012. 124 p.
 13. Melaku, A.F., Jung, K.S. Evaluation of welded joints of vertical stiffener to web under fatigue load by hotspot stress method. International journal of steel structures. 2017. Vol. 17(1). Pp. 271–278.
 14. Heinsen, C. Fatigue life assessment of a critical field welded connection on a temporary railway bridge span: Master's Thesis. Arlington, 2015. 143 p.
 15. Aygul M. Fatigue analysis of welded structures using the finite element method: Master's Thesis. Gothenburg, 2012. 56 p.
 16. Eurocode 3: Design of steel structures – Part 1-9: Fatigue. The European Union Per Regulation, 2004. 37 p.
 17. AASHTO LRFD. Bridge Design Specifications – 6th Edition. Washington, 2012. 1661 p.
 18. Fricke, W. Fatigue analysis of welded joints: State of development. Marine structures. 2003. Vol. 16. Pp. 185–200.
 19. Niemi, E., Marquis, G. Structural hot spot stress method for fatigue analysis of welded components. International Conference on Metal Structures. 2003. Pp. 39–44.
 20. Eriksson, A., Lignell, A., Olsson, C., Spennare, H. Weld evaluation using FEM – A guide to fatigue-loaded structures. Gothenburg, 2003. 288 p.
 21. Radaj, D., Sonsino, C., Fricke, W. Fatigue Assessment of Welded Joints by Local Approaches (Second Edition). Cambridge, 2006. 639 p.
 22. Radaj, D., Sonsino, C.M., Fricke, W. Recent developments in local concepts of fatigue assessment of welded joints. International Journal of Fatigue. 2009. Vol. 31. Pp. 2–11.
 23. Zhang, G., Richter, B. New approach to the numerical fatigue-life prediction of spot-welded structures. Fatigue and Fracture of Engineering Materials and Structures. 2000. Vol. 23. Pp. 499–508.
 24. Citirik, E., Ozkan, U., Nied, H. Three dimensional fracture analysis of I-beams with fillet welds. Journal of Terraspace Science and Engineering. 2009. Vol. 1. Pp. 89–97.
 25. Li, Z. Fracture analysis using enriched finite elements for tree-dimensional welded structures: Master's Thesis. Bathlehem, 2011. 129 p.
 26. Neuber* H. Theory of Stress Concentration for Shear Strained Prismatic Bodies with Arbitrary Non-Linear Stress Strain Law. Journal of Applied Mechanics. 1961. Vol. 28. Pp. 544–550.
 27. Petinov, S.P., Guchinsky, R.V., Sidorenko, V.G. Damage identity in fatigue assessment of structures. Magazine of Civil Engineering. 2016. 61(1). Pp. 82–88. DOI: 10.5862/MCE.61.8
 28. Indeykin, A.V., Chizhov, S.V., Shestakova, E.B., Antonyuk, A.A., Kulagin, N.I., Smirnov, V.N., Karpov, V.V., Golitsynsky, D.M. Approximated methods of estimation of the reliability of framed railway structures of railway bridges. 10. Жунев К.О. Статистический анализ факторов трещинообразования в сварных пролетных строениях. Транспортная инфраструктура Сибирского региона: материалы VIII международной научно-практической конференции. Иркутск: ИрГУПС, 2017. С. 455–460.
 11. Hobbacher A. The new IIW recommendations for fatigue assessment of welded joints and components – A comprehensive code recently updated // International Journal of Fatigue. 2009. Vol. 31. Pp. 50–58.
 12. Bowman M., Fu G., Zhou E., Connor R., Godbole A. Fatigue evaluation of steel bridges. Washington, 2012. 124 p.
 13. Melaku A. F., Jung K.S. Evaluation of welded joints of vertical stiffener to web under fatigue load by hotspot stress method // International journal of steel structures. 2017. Vol. 17(1). Pp. 271–278.
 14. Heinsen C. Fatigue life assessment of a critical field welded connection on a temporary railway bridge span: Master's Thesis. Arlington, 2015. 143 p.
 15. Aygul M. Fatigue analysis of welded structures using the finite element method: Master's Thesis. Gothenburg, 2012. 56 p.
 16. Eurocode 3: Design of steel structures – Part 1-9: Fatigue. The European Union Per Regulation, 2004. 37 p.
 17. AASHTO LRFD. Bridge Design Specifications – 6th Edition. Washington, 2012. 1661 p.
 18. Fricke W. Fatigue analysis of welded joints: State of development // Marine structures. 2003. Vol. 16. Pp. 185–200.
 19. Niemi E., Marquis G. Structural hot spot stress method for fatigue analysis of welded components. International Conference on Metal Structures. 2003. Pp. 39–44.
 20. Eriksson A., Lignell A., Olsson C., Spennare H. Weld evaluation using FEM – A guide to fatigue-loaded structures. Gothenburg, 2003. 288 p.
 21. Radaj D., Sonsino C., Fricke W. Fatigue Assessment of Welded Joints by Local Approaches (Second Edition). Cambridge, 2006. 639 p.
 22. Radaj D., Sonsino C.M., Fricke W. Recent developments in local concepts of fatigue assessment of welded joints // International Journal of Fatigue. 2009. Vol. 31. Pp. 2–11.
 23. Zhang G., Richter B. New approach to the numerical fatigue-life prediction of spot-welded structures // Fatigue and Fracture of Engineering Materials and Structures. 2000. Vol. 23. Pp. 499–508.
 24. Citirik E., Ozkan U., Nied H. Three dimensional fracture analysis of I-beams with fillet welds // Journal of Terraspace Science and Engineering. 2009. Vol. 1. Pp. 89–97.
 25. Li Z. Fracture analysis using enriched finite elements for tree-dimensional welded structures: Master's Thesis. Bathlehem, 2011. 129 p.
 26. Neuber H. Theory of Stress Concentration for Shear Strained Prismatic Bodies with Arbitrary Non-Linear StressStrain Law // Journal of Applied Mechanics. 1961. Vol. 28. Pp. 544–550.
 27. Петинoв С.В., Гучинский Р.В., Сидоренко В.Г. Идентичность повреждения в расчете ресурса конструкций // Инженерно-строительный журнал. 2016. №1(61). С. 82–88. DOI: 10.5862/MCE.61.8
 28. Индейкин А.В., Чижов С.В., Шестакова Е.Б., Кулагин Н.И., Смирнов В.Н., Карпов В.В., Голицынский Д.М. Приближенные методы оценки надежности балочных пролетных строений железнодорожных мостов // Инженерно-строительный журнал. 2017. № 7(75). С. 150–160. DOI: 10.18720/MCE.75.15.
 29. Midas Civil. Getting Started. MIDAS IT, 2015. 240 p.
 30. Туснина О.А., Данилов А.И. Жесткость рамных узлов сопряжения ригеля с колонной коробчатого сечения // Инженерно-строительный журнал. 2016. № 4(64). С. 40–51. DOI: 10.5862/MCE.64.4
 31. SYSWELD. Reference Manual. ESI Group, 2015. 392 p.

- Magazine of Civil Engineering. 2017. 75(7). Pp. 150–160. DOI: 10.18720/MCE.75.15.
29. Midas, Civil. Getting Started. MIDAS IT, 2015. 240 p.
 30. Tusnina, O.A., Danilov, A.I. The stiffness of rigid joints of beam with hollow section column. Magazine of Civil Engineering. 2016. 64(4). Pp. 40–51. DOI: 10.5862/MCE.64.4
 31. SYSWELD. Reference Manual. ESI Group, 2015. 392 p.
 32. Goldak, J., Chakravarti, A., Bibby, M. A new finite element model for welding heat sources. Metallurgical Transactions B. 1984. Vol. 15. Pp. 299–305.
 33. ANSYS guide. ANSYS release 16.2. Canonsburg, 2017. 1286 p.
 34. Bokarev, S.A., Yashnov, A.N., Snezhkov, I.I., Slyusar, A.V. Malogabaritnyye avtomatizirovannyye sistemy dlya diagnostiki ISSO [Small-sized automated systems for the diagnosis of engineering structures]. Railway Track and Facilities. 2007. Vol. 9. Pp. 25–26. (rus).
 35. Mikheyev, G.V., Lysikov, N.N., Pogorelov, D.Yu., Krugovova, Ye.A., Kiryan, V.I., Malgin, M.G. Raschet dinamicheskoy nagruzhenosti i ustalostnoy dolgovечности zheleznodorozhnykh mostov metodami kompyuternogo modelirovaniya [Calculation of dynamic loading and durability of railway bridges by computer simulation]. East Ukrainian Volodymyr Dahl National University. 2013. Vol. 18. Pp. 184–191. (rus).
 36. Fueki, R., Takahashi, K. Prediction of fatigue limit improvement in needle peened welded joints containing crack-like defects. International Journal of Structural Integrity. 2018. Vol. 9. Pp. 50–64.
 37. Dexter R.J., Pilarski P.J., Mahmoud H.N. Analysis of crack propagation in welded stiffened panels // International Journal of Fatigue. 2003. Vol. 25. Pp. 1169–1174.
 38. Mahmoud H.N., Dexter R.J. Propagation rate of large cracks in stiffened panels under tension loading // Marine structures. 2005. Vol. 18. Pp. 265–288.
 39. Bozic, Z., Schmauder, S., Wolf, H. The effect of residual stresses on fatigue crack propagation in welded stiffened panels. Engineering Failure Analysis. 2018. Vol. 84. Pp. 346–357.
 40. Sakagami, T., Mizokami, Y., Shiozawa, D., Fujimoto, T., Izumi, Y., Hanai, T., Moriyama, A. Verification of the repair effect for fatigue cracks in members of steel bridges based on thermoelastic stress measurement. Engineering Fracture Mechanics. 2017. Vol. 183. Pp. 1–12.
 41. Sakagami, T., Mizokami, Y., Shiozawa, D., Izumi, Y., Moriyama, A. TSA based evaluation of fatigue crack propagation in steel bridge members. Procedia Structural Integrity. 2017. Vol. 5. Pp. 1370–1376.
 42. Goldak J., Chakravarti A., Bibby M. A new finite element model for welding heat sources // Metallurgical Transactions B. 1984. Vol. 15. Pp. 299–305.
 43. ANSYS guide. ANSYS release 16.2. Canonsburg, 2017. 1286 p.
 44. Бокарев С.А., Яшнов А.Н., Снежков И.И., Слюсарь А.В. Малогабаритные автоматизированные системы для диагностики ИССО // Путь и путевое хозяйство. 2007. № 9. С. 25–26.
 45. Михеев Г.В., Лысиков Н.Н., Погорелов Д.Ю., Круговова Е.А., Кирьян В.И., Мальгин М.Г. Расчет динамической нагруженности и усталостной долговечности железнодорожных мостов методами компьютерного моделирования // Вестник восточноевропейского национального университета имени Владимира Даля. 2013. №18. С. 184–191.
 46. Fueki R., Takahashi K. Prediction of fatigue limit improvement in needle peened welded joints containing crack-like defects // International Journal of Structural Integrity. 2018. Vol. 9. Pp. 50–64.
 47. Dexter R.J., Pilarski P.J., Mahmoud H.N. Analysis of crack propagation in welded stiffened panels // International Journal of Fatigue. 2003. Vol. 25. Pp. 1169–1174.
 48. Mahmoud H.N., Dexter R.J. Propagation rate of large cracks in stiffened panels under tension loading // Marine structures. 2005. Vol. 18. Pp. 265–288.
 49. Bozic Z., Schmauder S., Wolf H. The effect of residual stresses on fatigue crack propagation in welded stiffened panels // Engineering Failure Analysis. 2018. Vol. 84. Pp. 346–357.
 50. Sakagami T., Mizokami Y., Shiozawa D., Fujimoto T., Izumi Y., Hanai T., Moriyama A. Verification of the repair effect for fatigue cracks in members of steel bridges based on thermoelastic stress measurement // Engineering Fracture Mechanics. 2017. Vol. 183. Pp. 1–12.
 51. Sakagami T., Mizokami Y., Shiozawa D., Izumi Y., Moriyama A. TSA based evaluation of fatigue crack propagation in steel bridge members // Procedia Structural Integrity. 2017. Vol. 5. Pp. 1370–1376.

Sergey Bokarev,
+7(913)9175594; bokarevsa@stu.ru

Kirill Zhunev,*
+7(913)9110991; junev.kirill@yandex.ru

Andrey Usol'tsev,
+7(903)9016405; uam@stu.ru

Сергей Александрович Бокарев,
+7(913)9175594; эл. почта: bokarevsa@stu.ru

Кирилл Олегович Жунев,*
+7(913)9110991; эл. почта: junev.kirill@yandex.ru

Андрей Михайлович Усольцев,
+7(903)9016405; эл. почта: uam@stu.ru

© Bokarev, S.A., Zhunev, K.O., Usol'tsev, A.M., 2018

doi: 10.18720/MCE.84.13

Ventilation impact on VOC concentration caused by building materials

Влияние вентиляции на концентрацию ЛОС, вызванных строительными материалами

J. Zemitis,
A. Borodinecs,
A. Lauberts,
Riga Technical University, Riga, Latvia*

D.Sc., доцент Ю. Земитис,
д-р техн. наук, профессор А. Бородинец,
М.С., инженер А. Лаубертс,
Рижский технический университет, г. Рига,
Латвия*

Key words: VOC; ventilation; buildings; climatic chamber; indoor climate; acryl-based paint; solvent based paint; acrylic based hermetic sealant

Ключевые слова: ЛОС; вентиляция; здания; климатическая камера; краска; герметик; спрей

Abstract. Many of building products emit volatile organic compounds (VOCs) therefore reducing the indoor air quality. The emitted amount and pollution type depends on each specific source. This paper analyses the VOC concentration change caused by such sources as sprayable window cleaner, aroma candles, sprayable air refresher, waterborne acryl-based paint, solvent based paint and acrylic based hermetic sealant. The tests are done at both closed and ventilated climatic chamber conditions. The results show that three different types of VOC concentration change dynamics can be separated depending on the pollution source. If the room is ventilated according to the local regulations the threshold level which indicates hazardous environment for persons is exceeded for 12 hours after applying the pain at given conditions. The obtained data can be used for future studies and to develop high precision methods of VOC concentration prediction and serve as an information source for future ventilation standard development.

Аннотация. Многие строительные изделия выделяют летучие органические соединения (ЛОС), в результате чего снижается качество воздуха в помещении. Величина и тип загрязнения зависят от конкретного источника. В данной статье анализируется изменение концентрации ЛОС, вызванное такими источниками, как распыляемый очиститель для окон, ароматические свечи, распыляемый освежитель воздуха, акриловая краска на водной основе, краска на основе растворителя и герметик на акриловой основе. Испытания проведены в климатической камере как в герметичных, так и в вентилируемых условиях. Результаты показывают, что в зависимости от источника загрязнения могут быть выделены три разных типа динамики изменения концентрации ЛОС. Если помещение вентилируется в соответствии с местными нормами, то пороговый уровень превышает в течение 12 часов, следовательно возникает опасная среда для людей. Полученные данные могут быть использованы для будущих исследований и разработки высокоточных методов прогнозирования концентрации ЛОС, а также могут служить источником информации для разработки новых стандартов вентиляции.

1. Introduction

Volatile organic compounds are carbon-base compounds with a vapor pressure high enough to evaporate and enter the atmosphere under atmospheric pressure and participate in atmospheric photochemical reactions. Many different types of VOCs can be found in the air, such as alkanes, halogenated hydrocarbons, aromatic hydrocarbons, terpenes, aldehydes, ketones and alcohols. Some of these compounds are toxic or cancerogenic therefore have limited values for airborne concentrations in order to avoid harmful effects on human health. Depending on the boiling point of the VOCs they are divided in several subgroups – very volatile (VVOC), volatile and semi-volatile organic compounds (SVOC). The VVOCs are so volatile that they are almost entirely found in the gas state while SVOC, although found in indoor air, will be mostly in solid or liquid form on surfaces of building materials, furniture and dust. Also, according to study [1] the VOC pollution can be divided in two types – primary and secondary. The primary

emission is defined as the physical release of VOCs from new products, while the secondary emission is released after the chemical reactions with existing indoor substances and surfaces.

VOCs found in buildings are exceptionally dangerous to humans, because we spend the largest part of the day indoors where the concentration can reach 10 times higher amount than compared to the outside. A wide range of consumer products and personal hygiene products release a significant amount of VOCs during their use. The main sources of VOCs are building materials, decoration materials, furniture, cleaning products, dry cleaners, paints, varnishes, solvents, glues, aerosols, refrigerants, fungicides, bactericides, cosmetics and textiles, household appliances, air fresheners, clothing, tobacco smoke and visible mold [2]. Insufficient indoor air exchange can result in an accumulation of VOCs and serving as a potential risk for human health [3]. VOCs emitted from many building materials are taken as the major sources causing poor indoor air quality, which negatively affect people's comfort, health and productivity [4; 5]. This can be especially notable in countries where large amount of old buildings is present and high potential of renovation projects are possible with feasible payback period [6]. As for example in case of schools and kindergartens the renovation usually occurs during the summer period and is finished only couple of days before the start of next semester when all children return to the premises [7].

One of the most common VOCs found in buildings is formaldehyde which is used to produce phenolic, urea, melamine and polyacetyl resin adhesives and binders for wood products, paper and synthetic fiber products. Its application in wood products, carpets, paints and varnishes causes it to be the main source of formaldehyde in the premises. As a study of energy efficient houses in Lithuania shows, formaldehyde was the only pollutant that exceeded the limit values for this chemical in all studied homes [8]. The formaldehyde also is generated by particleboards and plywood, and the studies show how the amount of emitted VOCs depends on room temperature and moisture content [9; 10]. This could be linked to a study that shows the change of indoor air depending on building characteristic and outside parameters [11]. Different study [12] showed that the toluene was the most abundant indoor VOC and that the indoor concentrations of certain VOCs were significantly higher for the one-month post-occupancy stage than the pre-occupancy stage, which was likely attributable to emissions from furniture and household products used by inhabitants after moving in, as well as building finishing materials.

In general, it is necessary to determine the TVOC value to judge if the indoor air quality is appropriate for long term stay. According to a study [13] it is suggested that the upper limit of TVOC should not exceed $300 \mu\text{g}/\text{m}^3$. This value is based on the data collected from a study in German residential houses. At the same time, the same study stresses that the concentration level of different VOC classes, like alkanes, aromatic hydrocarbons, terpenes, halogens, esters, should also be regulated.

To make predictions and to understand how the VOC level changes due to different common household pollution sources it is necessary to perform experiments in controlled environment. Such experiments have already been performed by various authors focusing on different pollutants. For example, a study [14] analyzed how seven most commonly occurring compounds discovered (benzene, toluene, methylethylketone, styrene, methyl group, ethyl alcohol and terpenoid) increase the VOC concentration at three different volumes of 0.1, 0.5 and 1.0 ml in 5 m^3 large space without air exchange. The results showed that most of the products seem to have very little short-term effect. However, if exposed over certain durations, this can lead to enhanced health risks. Interesting measurements regarding the VOC emissions from various aroma candles was performed in a study [15] providing results that indicate the high amount of released formaldehyde especially when the candles are lit. This must be taken into account, for example, in historic buildings like churches, where a high number of candles can be simultaneously lit to choose the necessary minimal amount of ventilation [16; 17]. In study [18] VOC emissions from several consumer and commercial products like body wash, dishwashing detergent, air freshener, windshield washer fluid, lubricant, hair spray, and insecticide, were studied and compared. The spray products were found to emit the highest amount of VOCs while the body wash products showed the lowest VOC contents.

The paints are one of the most common and noticeable sources of VOC in indoor environment. In near past almost all paint was solvent based. Such paints contain higher levels of VOCs compared to water-based paints and they evaporate and release VOCs into the atmosphere resulting in a strong odor and toxic impact on the environment. Nowadays due to local regulations and environmental protection directives the use of solvent based paints is noticeably reduced. Measurements in a study [19] regarding the VOC concentration increase caused by solvent paints in ventilated chamber was performed. The results showed that it takes about 12 h for the chamber to be ventilated if the air exchange rate is about 9 times and a method of concentration prediction was developed. In different study [20] low-VOC and zero-VOC paints was analyzed. The data showed that in these type of paints, part of the VOCs is replaced by SVOCs. Chemical compounds, which are often used as solvents in the usual colors still remain in the "green" colors, albeit to a lesser extent. At the same time, during the 72 hours test period the tested paints still released a

high concentration of pollutants. Based on this result, the differences between traditional colors and the low-VOC and zero-VOC paints are less significant than expected.

This paper focuses on widening the existing information regarding the VOC emissions from various common pollution sources. In most cases the only notice written on commonly used building materials is that they should be used in well ventilated rooms. However, no additional information what is meant by this is given. Therefore, one of the objectives of this study is to measure the VOC level caused by using different type of paints in environment that simulates the ventilation rate according to local regulations. The obtained information can serve as a future data source to develop methodology on how to predict the VOC concentration after applying some of the sources. During the tests the comparison between solvent and acrylic based paints will also be performed. The experiments will be done in controlled environment in climatic chamber. At first the chamber will be unventilated while in second set of measurements it will be ventilated according to local regulations [21] to study if under such conditions the environment is not harmful for human health.

2. Methods

The experiments were carried out at a climatic chamber with dimensions of 3 by 4 m and ceiling height of 2.3 m, thus the total volume of chamber is 27.6 m³. The climatic chamber was tightly sealed therefore making it almost perfectly air tight. The climatic chamber was equipped with VOC measuring sensor, ILH with VOC measuring range of 450–2000 ppm. The VOC sensor detects wide variety of hydrocarbons such as cigarette smoke, exhaled breathing air, solvent vapours, building material emissions and cleaning agent vapours. The data was continuously logged during the time of experiment and the measured values were noted after each 15 seconds. Information regarding air temperature, relative humidity and CO₂ levels also was measured. To ensure that the pollution is equally spread in the chamber a small fan was placed in the middle of the room.

The experiment was divided into two phases. During the first phase various VOC sources and sources with different concentration were introduced in the unventilated climatic chamber one by one to. Afterwards the climatic chamber was shut, and measurements of VOC concentration changes were performed until the steady state was reached. Therefore, it was possible to determine the strength of different pollution sources and the time it takes to reach steady state depending on the introduced concentration of each pollution source. After each measuring series the climatic chamber was fully ventilated until VOC reached the background level.

During the second phase the climatic chamber was equipped with ventilator ensuring stable flow of 36 m³/h which is the minimal necessary amount determined by the local Latvian building norm LBN 211-15 "Residential buildings" that require air flow of 3 m³/m². Afterwards pollution sources of VOC were introduced in the climatic chamber and measurements were started. During this phase it was possible to determine whether and for how long the VOC level exceeds the one stated in the regulations regarding human safety.

The tested pollution sources were as follows: sprayable window cleaner, aroma candles, sprayable air refresher, waterborne acryl-based paint, solvent based paint and acrylic based hermetic sealant. For each of the pollution sources the composition was analysed and the main and most hazardous VOC emitting substance determined. This was done to determine the various danger thresholds levels which are different for each substance. The information regarding the immediate danger threshold, 15 min danger threshold and limit allowed for 8h period per day was obtained after studying international standards [22–24].

For the sprayable window cleaner, the main VOC is ethanol and its compounds. The immediate limit of life hazard of ethanol is 3300 ppm, but for 8h a day period the concentration the limit is 1000 ppm. The composition of the sprayable air refresher with the citrus scent is not given but comparing to a similar product data sheet it is determined that the main VOC emitting substance is limonene. This contaminant poses an immediate risk to human health if the concentration level of 20 ppm is exceeded. Aromatic candles contain cinnamon aldehyde, eugenol and benzyl benzoate. These substances do not indicate any immediate danger to humans according to available sources.

The solvent-based paint compound contains mostly white spirit (90–100 % aliphatic and alicyclic hydrocarbons; < 10 % terpenes and terpenoids; < 0.1 % benzene), which is thought to be the main volatile organic compound. The solvent-based paint contamination immediate danger threshold limit is 750 ppm, but the concentration limit for 15 minutes period is 440 ppm while a concentration limit for 8 hr working day is 85 ppm.

The composition of acrylic based paint was not specified, but comparing to a similar product data sheet, diuron and ammonia are taken as the main pollutants. From acrylic pollutants, only ammonia has an immediate hazard limit for life – 500 ppm, but the total concentration limit allowed for 8h working day is 35 ppm (diuron -10 ppm + ammonia 25 ppm).

The composition of the acrylic based hermetic sealant indicates that it contains propylene and butylene groups which are accepted as the main VOC elements. The immediate hazard limit for life of acrylic based hermetic sealant contamination is determined to be 20 000 ppm (2-propane-12 000 ppm + n-butane 8 000 ppm) while a concentration limit of 500 ppm (2-propane-400 ppm + n-butane 100 ppm) is allowed for 8h per day.



Figure 1. Pictures showing how the pollution sources - acrylic based hermetic sealant (left side); waterborne acrylic-based paint (middle) and solvent based paint (right side), were applied.

3. Results and Discussions

3.1. Sprayable window cleaner

The first measurements were performed with the sprayable window cleaner. It was sprayed directly into the middle of the chamber and for comparison, two different volumes were sprayed. For measurements number one and two the sprayed amount was equal to two full spray presses while for measurements three and four the spray was pressed four times therefore doubling the introduced amount of pollutant.

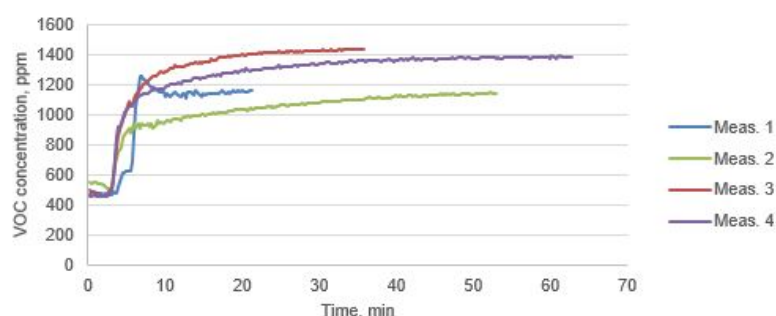


Figure 2. VOC concentration change in time caused by spraying of window cleaner.

To analyze the results, it is necessary to determine the influence of each pollution source therefore it is needed to subtract the background VOC level which is caused by the emissions from existing elements in climatic chamber. As seen from the figures presented in the results section, this background level is not equal for all cases as the VOC level varies during the different experiments. This could be explained due to fact that although after each experiment the rooms were fully ventilated, some of the VOCs could settle to the walls and be released in the air as a secondary pollutant.

As seen from the Figure 2 the total VOC level after the use of a window cleaner if it is sprayed two times is about 1100–1150 ppm, while if the introduced amount of pollution source is doubled then the concentration of total VOCs reaches about 1400 ppm. If we subtract the background VOC concentration, which in specific case is about 500 ppm, then the VOC level increase caused directly by applied window cleaner is 650 ppm and 900 ppm respectively. It means that the VOC has increased by approximately half of the expected rate if double amount is introduced in the room. Therefore, it can be concluded that doubling the pollution source amount does not necessarily mean that the VOC level will also double. This could be explained by the fact that the spray product stays on the surface and does not immediately evaporate into the room and gets released in prolonged period of time. The results obtained in the experiment indicate that the contamination level of VOCs caused by using window washer agent in enclosed space does not pose immediate hazard to human life at given amount as the danger limit for ethanol, which is considered

low toxicity, is relatively high – 3000 ppm for immediate risk and 1000 ppm for 8h period. However, it must be noted that under realistic conditions the sprayed amount would be a lot higher and could cause health risk if working indoors in unvented space. If the VOC increase of one spray is adjusted for 1 m³ of the room than the results show that the window cleaner is causes the VOC level to rise by 7 590 ppm.

3.2. Acrylic based hermetic sealant

The second analysed substance was acrylic based hermetic sealant. It is acrylic polymer based on water which ensures resistance against UV and moisture. Used for filling cracks, repairing surface defects before painting and for indoor window and door sealing. A total of 5 meters of acrylic sealant was applied on a laminated particleboard (older scrap that would not significantly affect the concentration of VOC in the room).

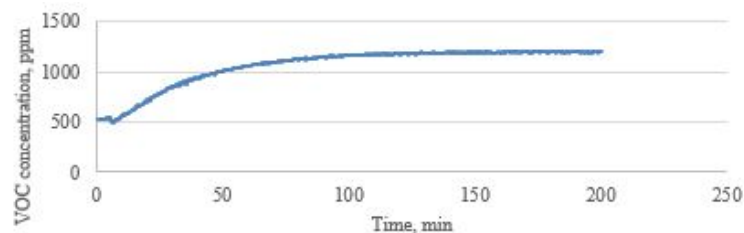


Figure 3. VOC concentration change in time caused by acrylic based hermetic sealant.

By analyzing the Figure 3 which represents the results regarding the VOC emission from acrylic based hermetic sealant it can be seen that the VOC level rapidly rises during the first two hours and then settles at a constant level of 1200 ppm. If the background VOC concentration is subtracted, then it can be estimated that the pollution directly from the sealant is about 700 ppm. It means that the concentration is much lower compared to the one that causes immediate health risk (20 000 ppm) but is slightly above the allowed 8h per day (500 ppm). By knowing that 5 m of sealant was introduced into the room and that the room volume is 27.6 m³ it can be calculated that 1 m of such sealant gives about 3860 ppm if located 1 m³ large room.

3.3. Air refresher

Regarding the sources that are used to improve the scent of air, two substances were tested – sprayable air refresher and aroma candles. The air refresher was sprayed in the middle of the room by pressing the spray button for 3 seconds. As for the aroma candles three candles were introduced in the room, but due to fire safety requirements the candles were not lit.

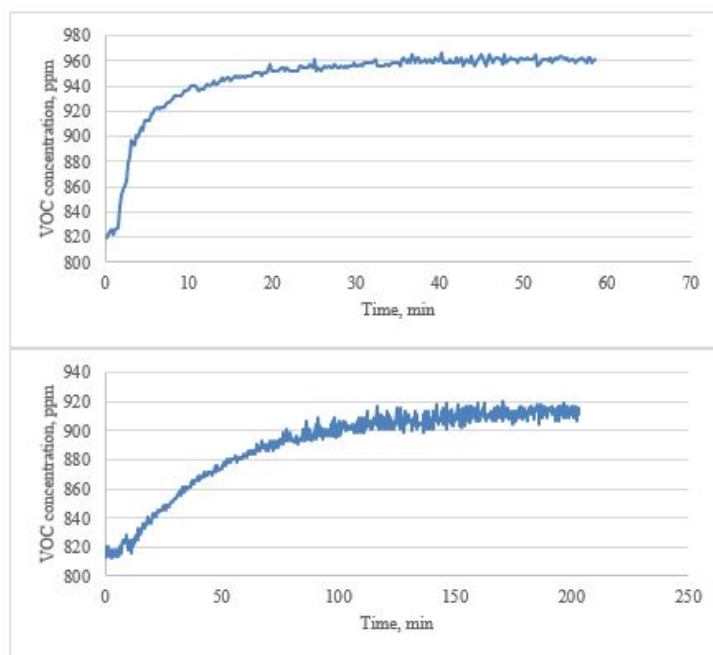


Figure 4. VOC concentration change in time caused by sprayable air refresher (left side) and aroma candles (right side).

The Figure 4 shows how the VOC level rises after air refresher and aroma candles are applied in closed room. It can be seen that in case of air refresher the VOC sensor immediately responds and the maximal level, which is 980 ppm, is reached in about 3 minutes. While for aroma candle the VOC increases noticeably slower and reaches steady state in 2 hours, which is 910 ppm. In both cases the absolute value of VOC increase taking into account the background pollution is similar – 140 and 90 ppm respectively. Although this seems a low number it exceeds the immediate hazard risk of 20 ppm of limonene. However not all of the measured VOC is necessarily linked to this substance as the limonene is only half of the composition of sprayable air refresher. Adjusting the results for 1 m³ large room and 1 second long spray of air refresher it can be calculated that the VOC would rise by 1288 ppm, while for one aroma candle it would rise by 828 ppm.

3.4. Acryl-based and solvent based paint

To compare how different types of paint emit VOCs waterborne acryl-based paint and solvent based paint was tested. In the first experiment the acryl-based paint was put on 4 m² of laminated particleboard. In the second experiment the solvent based paint was first put on 2 m² of laminated particleboard, but afterwards also on 0.25 m² because of the limitations of measuring device as in case when the paint was put on 2 m² the VOC concentration reached 2000 ppm.

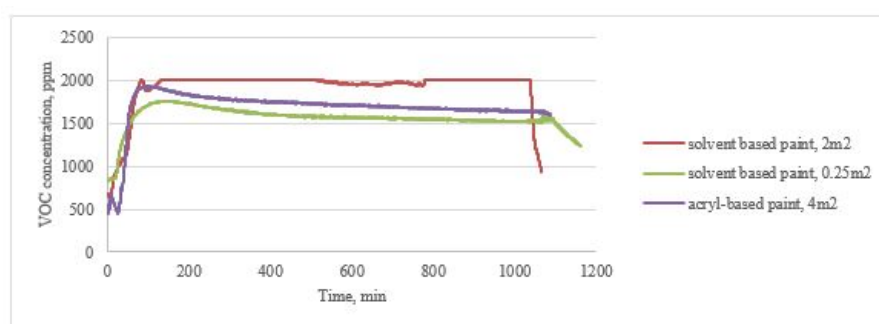


Figure 5. VOC concentration change in time caused by waterborne acryl-based and solvent based paints.

In Figure 5 the comparison between waterborne acryl-based and solvent based paints can be seen. The results show that the VOC emissions from waterborne acryl-based paint is a lot lower than from solvent based paints. In all experiments the maximal VOC level was reached in 1.5 h but then started to slightly decline until reached the steady state level in about 5 hours. For solvent based paint with area of 0.25 m² the VOC level stabilizes out at 1550 ppm, while for acryl-based with area of 4 m² this level is 1680 ppm. In the absolute values the VOC emissions from acryl-based paint reaches 1450 ppm and stabilizes at 1200 ppm, while from solvent based paint the values are 900 ppm and 700 ppm respectively. If these numbers are adjusted for 1 m² of paint at 1 m³ room, then they read 8 280 ppm for acryl-based paint and 77 280 ppm for solvent based paint. This means that the emission level from solvent based paint is approximately 9 times higher. For both paints the danger threshold for immediate and 8 h period was exceeded. In case of acryl-based paint the immediate hazard level of 500 ppm was exceeded 3 times, while for solvent based paint the threshold level of 750 ppm was exceeded for the first 7 hours.

Afterwards the climatic chamber was equipped with ventilator and the measurements performed on how VOC concentration changes during longer periods if some elements in the room are painted. First the simulation with waterborne acryl-based paint was performed. A total of 3 m² of waterborne acryl-based painted surface was introduced into the climatic chamber and the VOC data was logged for almost 3 days.

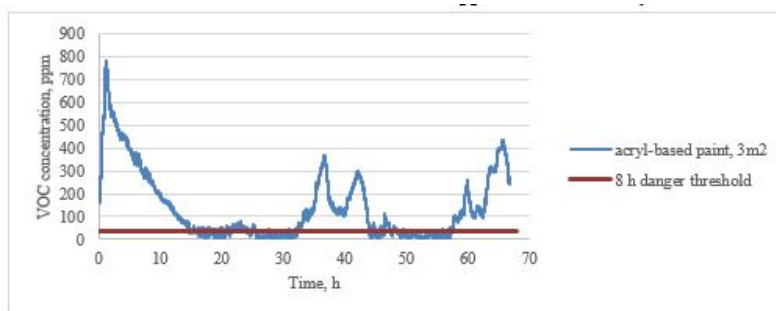


Figure 6. VOC concentration change in ventilated test chamber caused by acryl-based paint.

The second tested substance was solvent based paint. For this test only 0.25 m² of painted surfaces were introduced into the climatic chamber as the experience from previous experiments showed that VOC emission from it are a lot more intense. The test was run for 60 hours to see how the day cycle influences the VOC values.

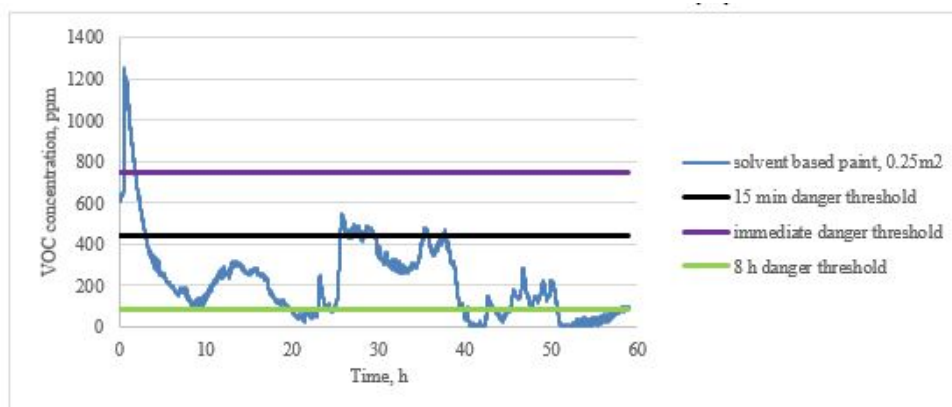


Figure 7. VOC concentration change in ventilated test chamber caused by solvent-based paint.

The Figures 6 and 7 present the results of VOC emissions from waterborne acryl-based and solvent based paints located in ventilated room. They both show that the ventilation does not affect the immediate spike in VOC concentration that reaches the maximum in 1.5 h, the same as in unventilated room. However, the maximal value is slightly decreased if compared to unventilated room. For acryl-based paint it reaches 780 ppm, while for solvent based paint 1200 ppm. The calculated decrease therefore is about 33 %. The further influence of ventilation is also noticeable as the VOC level gets decreased to minimum at around 10-hour time. However, the results also show that there is a periodical increase in the VOC levels during the next days of experiment. This could be explained by the increase in the room temperature during the daytime, which possibly stimulates the reaction of the paint and release of additional VOCs. Also, the graphs show that the room where acryl-based paint is introduced the air quality is mostly harmless for human health if it is ventilated according to local regulations. In case of solvent based paint, the situation is different and even if only 0.25 m² of such paint is introduced in the room the air quality is not adequate and persons should not be present for more than 15 minutes.

The results also showed that three different types of VOC concentration increase can be defined. The first one is the rapid increase of VOC level if the pollution source is sprayed as aerosol in the air. In such case the maximal VOC level is reached in around 10 minutes. The second type is the slow and stable release of VOCs in the air that occur from materials, like hermetic sealants or aroma candles, that are introduced into the room. In this case the concentration rises following logarithmic scale for about 1.5 h and then achieves the stable state or keeps slowly increasing. The third type is similar to the second one, when the maximal VOC level is achieved after 1.5 h but then a slow fall of concentration occurs. This is a typical case for paints, which can be explained because at the first moment the paints are rapidly drying and therefore releasing large amount of VOCs, but after the initial process the drying slows down and some of the VOCs settle on the surface of the room.

It is relatively difficult to compare the obtained results with other authors' works due to the specifics of used materials and how the emitted VOCs can vary depending on the source. Also, the measuring devices, their working principle and experimental setup varies between the authors. However, if comparing the results how VOC concentration changes in ventilated chamber if solvent-based paint is introduced into it with the results presented by previous paper [19] then it can be noted that the VOC change dynamic is quite similar. By knowing that in other experiment the ventilation rate was nine exchange rate per hour while in our experiment only one, then the expected results would be even more comparable as the VOC level would decrease in shorter time period.

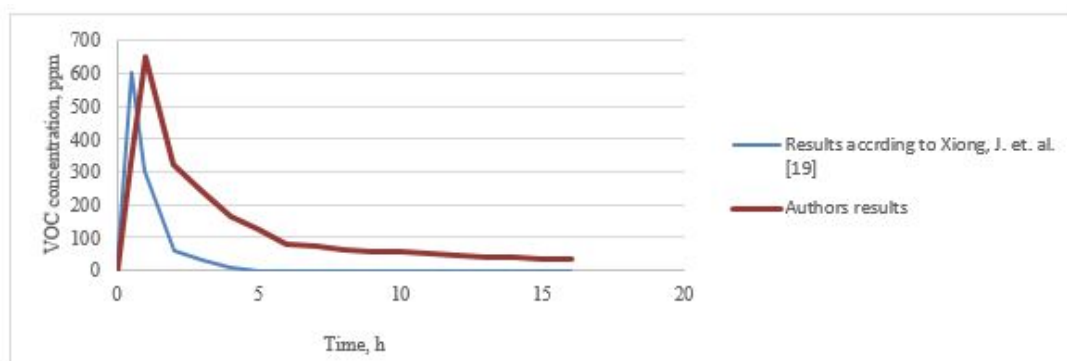


Figure 8. Comparison of authors and other researchers results of VOC concentration change in ventilated test chamber caused by solvent-based paint.

For future experiments additional tests should be made where the same pollution source is introduced in the room in various amounts to determine the relation between the pollution amount, the measured VOC level and room volume. Also, different types of the same pollution sources should be analyzed to determine whether they differ and for some of the sources full analysis of the actual compounds that make up the total VOC concentration should be specified.

4. Conclusions

During the experiment following VOC pollution sources were tested in a closed climatic chamber-sprayable window cleaner, aroma candles, sprayable air refresher, waterborne acryl-based paint, solvent based paint and acrylic based hermetic sealant. The results showed that for each pollutant type the VOC level differs depending on the content and amount of the pollutant, but in all cases the pollution level exceeded the threshold limit which is not harmful for human health.

By testing different amounts of sprayable window cleaner it was concluded that by doubling the pollution source the measured VOC level is not doubled but increases only by 50 %.

Three different types VOC concentration increase profiles were determined - rapid increase, slow release and slow release with small backdrop of VOC concentration. This is dependent on the type of pollution source, whether it is directly deployed in the air as an aerosol or laid on the surface.

In case the chamber is ventilated with an air exchange rate according to local regulations of $3 \text{ m}^3/\text{h}/\text{m}^2$ the maximum concentration of VOC is reached approximately at the same time as in unventilated chamber, but the maximal concentration is lower by 33 % than in an unventilated room. However, the study confirms that if a room is ventilated according to the local Latvian building code LBN 211-15 the premise will be fully ventilated and harmless for people health only after 15–20 h after the introduction of the pollution source.

Acknowledgements

This work has been supported by the European Regional Development Fund within the Activity 1.1.1.2 "Post-doctoral Research Aid" of the Specific Aid Objective 1.1.1 "To increase the research and innovative capacity of scientific institutions of Latvia and the ability to attract external financing, investing in human resources and infrastructure" of the Operational Programme "Growth and Employment" (No. 1.1.1.2/VIAA/1/16/033).

References

1. Uhde, E., Salthammer, T. Impact of reaction products from building materials and furnishings on indoor air quality-A review of recent advances in indoor chemistry. *Atmospheric Environment*. 2007. No. 41 (15). Pp. 3111–3128. DOI: 10.1016/j.atmosenv.2006.05.082.
2. Sarigiannis, D.A., Karakitsios, S.P., Gotti, A., Liakos, I.L., Exposure to major volatile organic compounds and carbonyls in European indoor environments and associated health risk. *Environment International*, 2011. No. 37 (4). Pp. 743–765. DOI: 10.1016/j.envint.2011.01.005.
3. Dimitroulopoulou, C. Ventilation in European dwellings: A review. *Building and Environment*. 2012. No. 47 (1). Pp. 109–125. DOI: 10.1016/j.buildenv.2011.07.016.

Литература

1. Uhde E., Salthammer T. Impact of reaction products from building materials and furnishings on indoor air quality-A review of recent advances in indoor chemistry // *Atmospheric Environment*. 2007. № 41(15). Pp. 3111–3128. DOI: 10.1016/j.atmosenv.2006.05.082.
2. Sarigiannis D.A., Karakitsios S.P., Gotti A., Liakos I.L., Exposure to major volatile organic compounds and carbonyls in European indoor environments and associated health risk // *Environment International*, 2011. № 37(4). Pp. 743–765. DOI: 10.1016/j.envint.2011.01.005.
3. Dimitroulopoulou C. Ventilation in European dwellings: A review // *Building and Environment*. 2012. № 47(1). Pp. 109–125. DOI: 10.1016/j.buildenv.2011.07.016.

4. Kim, Y.M., Harrad, S., Harrison, R.M. Concentrations and sources of VOCs in urban domestic and public microenvironments. *Environmental Science & Technology*. 2001. Vol. 35. Pp. 997–1004. DOI: 10.1021/es000192y.
5. WHO. 1989. World Health Organization. Indoor air quality: organic pollutants. Copenhagen: WHO Regional Office for Europe; EURO Report and Studies 1111.
6. Gorshkov, A.S., Vatin, N.I., Rymkevich, P.P., Kydrevich, O.O. Payback period of investments in energy saving. *Magazine of Civil Engineering*. 2018. 68(2). Pp. 65–75. DOI: 10.18720/MCE.78.5.
7. Borodinecs, A., Zemitis, J., Sorokins, J., Baranova, D.V., Sovetnikov, D.O. Renovation need for apartment buildings in Latvia. *Magazine of Civil Engineering*. 2016. 68(8). Pp. 58–64. DOI: 10.5862/MCE.68.6
8. Kaunelienė, V., Prasauskas, T., Krugly E., Stasiulaitienė I., et al. Indoor air quality in low energy residential buildings in Lithuania. *Building and Environment*. 2006. Vol. 108. Pp 63–72. DOI: 10.1016/j.buildenv.2016.08.018.
9. Jiang, C., Li, D., Zhang, P., Li, J., et al. Formaldehyde and volatile organic compound (VOC) emissions from particleboard: Identification of odorous compounds and effects of heat treatment. *Building and Environment*. 2017. Vol. 117. Pp. 118–126. DOI: 10.7764/RDLC.16.3.527.
10. Aydin, I., Colakoglu, G., Colak, S., Demirkir, C. Effects of moisture content on formaldehyde emission and mechanical properties of plywood. *Building and Environment*. 2006. Vol. 41. No. 10. Pp. 1311–1316. DOI: 10.1016/j.buildenv.2005.05.011
11. Bilous, I.Yu., Dешко, V.I., Sukhodub, I.O. Building inside air temperature parametric study. *Magazine of Civil Engineering*. 2016. 68(8). Pp. 65–75. DOI: 10.5862/MCE.68.7.
12. Seung-Ho, S. Wan-Kuen, J. Volatile organic compound concentrations in newly built apartment buildings during pre- and post-occupancy stages. *International Journal of Environmental Analytical Chemistry*. 2013. Vol. 94. Pp. 356–369. DOI: 10.1080/03067319.2013.814125.
13. Berglund, B., Clausen, G., De Ceaurriz, J., Kettrup, A., Total Volatile Organic Compounds (TVOC) in Indoor Air Quality Investigations. Report No 19. Luxembourg: Indoor Air Quality Investigations, 1997. Pp. 48. DOI: http://www.inive.org/medias/ECA/ECA_Report19.pdf
14. Rahman, M.M., Kim, K.H. Potential hazard of volatile organic compounds contained in household spray products. *Atmospheric Environment*. 2014. Vol. 85. Pp. 266–274. DOI: 10.1016/j.atmosenv.2013.12.001.
15. Ahn, J., Kim, K., Kim, Y., Kim, B. Characterization of hazardous and odorous volatiles emitted from scented candles before lighting and when lit. *Journal of Hazardous Materials*. 2015. Vol. 286. Pp. 242–251. DOI: <http://dx.doi.org/10.1016/j.jhazmat.2014.12.040>.
16. Pukhkal, V., Vatin, N., Murgul, V. Central Ventilation System with Heat Recovery as One of the Measures to Upgrade Energy Efficiency of Historic Buildings. *Applied Mechanics and Materials*. 2014. Vols. 633-634. Pp. 1077–1081. DOI: 10.4028/www.scientific.net/AMM.633-634.1077.
17. Murgul, V., Vuksanovic, D., Vatin, N., Pukhkal, V. The Use of Decentralized Ventilation Systems with Heat Recovery in the Historical Buildings of St. Petersburg. *Applied Mechanics and Materials*. 2014. Vols. 635-637. Pp. 370–376. DOI: 10.4028/www.scientific.net/AMM.635-637.370.
18. Dinh, T.V., Kim, S.Y., Son, Y.S. et al. Emission characteristics of VOCs emitted from consumer and commercial products and their ozone formation potential. *Environmental Science and Pollution Research*. 2015. Vol. 22. Pp. 9345–9355. DOI: 10.1007/s11356-015-4092-8
19. Xiong, J., Wang, L., Bai, Y., Zhang, Y. Measuring the characteristic parameters of VOC emission from paints.
4. Kim Y.M., Harrad S., Harrison R.M. Concentrations and sources of VOCs in urban domestic and public microenvironments // *Environmental Science & Technology*. 2001. Vol. 35. Pp. 997–1004. DOI: 10.1021/es000192y.
5. WHO. 1989. World Health Organization. Indoor air quality: organic pollutants. Copenhagen: WHO Regional Office for Europe; EURO Report and Studies 1111.
6. Горшков А.С., Ватин Н.И., Рымкевич П.П., Кудревич О.О. Период возврата инвестиций в энергосбережение // *Инженерно-строительный журнал*. 2018. № 2(78). С. 65–75. DOI: 10.18720/MCE.78.5.
7. Бородинец А., Земитис Ю., Сорокин Ю., Баранова Д.В., Советников Д.О. Необходимость реновации жилых зданий в Латвии // *Инженерно-строительный журнал*. 2016. № 8(68). С. 58–64. DOI: 10.5862/MCE.68.6
8. Kaunelienė V., Prasauskas T., Krugly E., Stasiulaitienė I., et al. Indoor air quality in low energy residential buildings in Lithuania // *Building and Environment*. 2006. Vol. 108. Pp 63–72. DOI: 10.1016/j.buildenv.2016.08.018.
9. Jiang C., Li D., Zhang P., Li J., et al. Formaldehyde and volatile organic compound (VOC) emissions from particleboard: Identification of odorous compounds and effects of heat treatment // *Building and Environment*. 2017. Vol. 117. Pp. 118–126. ISSN 0360-1323, Available from DOI: 10.7764/RDLC.16.3.527.
10. Aydin I., Colakoglu G., Colak S., Demirkir C. Effects of moisture content on formaldehyde emission and mechanical properties of plywood // *Building and Environment*. 2006. Vol. 41. № 10. Pp. 1311–1316. DOI: 10.1016/j.buildenv.2005.05.011
11. Белоус И.Ю., Дешко В.И., Сухогуб И.О. Параметрический анализ внутренней температуры воздуха здания // *Инженерно-строительный журнал*. 2016. № 8(68). С. 65–75. DOI: 10.5862/MCE.68.7.
12. Seung-Ho S. Wan-Kuen J. Volatile organic compound concentrations in newly built apartment buildings during pre- and post-occupancy stages // *International Journal of Environmental Analytical Chemistry*. 2013. Vol. 94. Pp. 356–369. DOI: 10.1080/03067319.2013.814125.
13. Berglund B., Clausen G., De Ceaurriz J., Kettrup A., Total Volatile Organic Compounds (TVOC) in Indoor Air Quality Investigations. Report No 19. Luxembourg: Indoor Air Quality Investigations, 1997. Pp. 48. DOI: http://www.inive.org/medias/ECA/ECA_Report19.pdf
14. Rahman M.M., Kim K.H. Potential hazard of volatile organic compounds contained in household spray products. *Atmospheric Environment*. 2014. Vol. 85. Pp. 266–274. DOI: 10.1016/j.atmosenv.2013.12.001.
15. Ahn J., Kim K., Kim Y., Kim B. Characterization of hazardous and odorous volatiles emitted from scented candles before lighting and when lit // *Journal of Hazardous Materials*. 2015. Vol. 286. Elsevier. Pp. 242–251. DOI: <http://dx.doi.org/10.1016/j.jhazmat.2014.12.040>.
16. Pukhkal V., Vatin N., Murgul V. Central Ventilation System with Heat Recovery as One of the Measures to Upgrade Energy Efficiency of Historic Buildings // *Applied Mechanics and Materials*. 2014. Vols. 633-634. Pp. 1077–1081. DOI: 10.4028/www.scientific.net/AMM.633-634.1077.
17. Murgul V., Vuksanovic D., Vatin N., Pukhkal V. The Use of Decentralized Ventilation Systems with Heat Recovery in the Historical Buildings of St. Petersburg // *Applied Mechanics and Materials*. 2014. Vols. 635-637. Pp. 370–376. DOI: 10.4028/www.scientific.net/AMM.635-637.370.
18. Dinh T.V., Kim S.Y., Son Y.S. et al. Emission characteristics of VOCs emitted from consumer and commercial products and their ozone formation potential // *Environmental Science and Pollution Research*. 2015. Vol. 22. Pp. 9345–9355. Available from DOI: 10.1007/s11356-015-4092-8

- Building and Environment. 2013. Vol. 66. Pp. 65–71. DOI: 10.1016/j.buildenv.2013.04.025.
20. Schieweck, A, Bock, M.C Emissions from low-VOC and zero-VOC paints – Valuable alternatives to conventional formulations also for use in sensitive environments? Building and Environment. 2015. Vol. 85. Pp. 243–252. DOI: 10.1016/j.buildenv.2014.12.001.
 21. LBN 211-15: 2015. Dzivojamas ekas [Residential buildings]. Latvian building code.
 22. OSHA. 2018. OSHA Occupational Chemical Database [online], [cited 5 June 2018]. Occupational Safety and Health Administration. Available from Internet: <https://www.osha.gov/chemicaldata/>
 23. NIOSHA. 2018. NIOSHA The National Institute for Occupational Safety and Health [online], [cited 5 June 2018]. The National Institute for Occupational Safety and Health. Available from Internet: <https://www.cdc.gov/niosh/index.htm>
 24. ACGIH. 2018. ACGIH Association Advancing Occupational and Environmental Health [online], [cited 5 June 2018]. Association Advancing Occupational and Environmental Health. Available from Internet: <https://www.acgih.org/>
 19. Xiong J., Wang L., Bai Y., Zhang Y. Measuring the characteristic parameters of VOC emission from paints // Building and Environment. 2013. Vol. 66. Pp. 65–71. ISSN: 03601323. Available from DOI: 10.1016/j.buildenv.2013.04.025.
 20. Schieweck A, Bock M.C Emissions from low-VOC and zero-VOC paints – Valuable alternatives to conventional formulations also for use in sensitive environments? // Building and Environment. 2015. Vol. 85. Pp. 243–252. DOI: 10.1016/j.buildenv.2014.12.001.
 21. LBN 211-15: 2015. Dzivojamas ekas [Residential buildings]. Latvian building code.
 22. OSHA. 2018. OSHA Occupational Chemical Database [online], [cited 5 June 2018]. Occupational Safety and Health Administration. Available from Internet: <https://www.osha.gov/chemicaldata/>
 23. NIOSHA. 2018. NIOSHA The National Institute for Occupational Safety and Health [online], [cited 5 June 2018]. The National Institute for Occupational Safety and Health. Available from Internet: <https://www.cdc.gov/niosh/index.htm>
 24. ACGIH. 2018. ACGIH Association Advancing Occupational and Environmental Health [online], [cited 5 June 2018]. Association Advancing Occupational and Environmental Health. Available from Internet: <https://www.acgih.org/>

*Jurgis Zemitis**,
+37128369940; jurgis.zemitis@rtu.lv

Anatolijs Borodinecs,
+37126079655; anatolijs.borodinecs@rtu.lv

Austris Lauberts,
+37126362273; austris.lauberts@gmail.com

*Юргис Земитис**,
+37128369940; эл. почта: jurgis.zemitis@rtu.lv

Анатолий Бородинец,
+37126079655;
эл. почта: anatolijs.borodinecs@rtu.lv

Аустрис Лаубертс,
+37126362273;
эл. почта: austris.lauberts@gmail.com

© Zemitis, J., Borodinecs, A.B, Lauberts, A., 2018

doi: 10.18720/MCE.84.14

Thermal protection of low-rise buildings from light steel thin-walled structures

Теплозащита малоэтажных зданий из легких стальных тонкостенных конструкций

T.A. Kornilov,
A.Y. Nikiforov,
North-Eastern Federal University named after
M.K. Ammosov, Yakutsk, Russia*

Д-р техн. наук, директор Т.А. Корнилов,
аспирант А.Я. Никифоров,
Северо-Восточный федеральный
университет имени М.К. Аммосова,
г. Якутск, Россия*

Key words: thermal protection; infiltration; temperature; light steel thin-walled structures; cold bridges; wall structures; basement floor

Ключевые слова: тепловая защита; инфильтрация; температура; легкие стальные тонкостенные конструкции; мостики холода; стеновые конструкции; цокольное перекрытие

Abstract. Thermal protection providing of frame buildings in the extreme conditions of the Far North depends on air infiltration. Elements of buildings frame on light steel thin-walled structures (LSTS below) technology – lightweight, thin-walled steel profiles make up multiple thermal bridges. The basic principles of designing the exterior walling of low-rise buildings from LSTS in the Far North are developed with taking into account the increased air infiltration and the heat transfer components and assemblies. The construction with double insulation layer and the intermediate airtight barrier of particleboard, the indicative panels (OSB below) are proposed as the exterior walls. The concrete ground slab and thermofiller using of lightweight concrete blocks are recommended in buildings with pile foundation. The two-stage disposition of blocks between the steel frame elements and the basement ceiling allow to overlap joints of thermal insulation materials with other structural elements which reduces the impact of air infiltration. The specific heat loss values for a multilayer wall construction and assembly of its coupling with a ground overlap, depending on various parameters are obtained with the calculating program application of three-dimensional temperature fields.

Аннотация. Обеспечение тепловой защиты каркасных зданий в экстремальных условиях Крайнего Севера во многом зависит от инфильтрации воздуха. Элементы каркаса зданий по технологии ЛСТК – легкие стальные тонкостенные профили создают многочисленные мостики холода. Разработаны основные принципы проектирования наружных ограждающих конструкций малоэтажных зданий из ЛСТК в условиях Крайнего Севера, учитывающие повышенную инфильтрацию воздуха и наличие теплопроводных элементов и узлов. В качестве наружных стен предложены конструкции с двухслойным теплоизоляционным слоем и промежуточным воздухонепроницаемым барьером из стружечно-ориентировочных плит (OSB). В зданиях со свайными фундаментами рекомендовано устройство железобетонного цокольного перекрытия и применение термовкладышей из легких бетонных блоков. Двухступенчатое расположение блоков между стальными элементами каркаса и цокольным перекрытием позволяет перекрывать стыки теплоизоляционных материалов с другими конструктивными элементами, что снижает влияние инфильтрации воздуха. С применением программы расчета трехмерных температурных полей получены значения удельных потерь теплоты для многослойной стеновой конструкции и узла ее сопряжения с цокольным перекрытием в зависимости от различных параметров.

1. Introduction

The Sakha (Yakutia) Republic is the largest federal subject of Russia located in the North-East of the country. Almost half of the region is located in the Arctic Circle. The territory of the Yakutia is characterized by extreme climate conditions for the construction of buildings and structures. Almost the entire territory located in the permafrost zone, which is the most powerful in the world. Subarctic climate of Yakutia is sharply continental. The period with negative daily temperatures has no analogues in the world and varies from 312 days in the distant Arctic islands to 202 days in South Yakutia. In winter, the outdoor

temperature in the central part of Yakutia during 50–60 days, and in the Arctic regions 60–80 days is below $-40\text{ }^{\circ}\text{C}$. The calculated air parameters for regions of Yakutia include: outdoor temperature in the coldest period from $-40\text{ }^{\circ}\text{C}$ to $-59\text{ }^{\circ}\text{C}$; during the heating period average temperature is from $-13.6\text{ }^{\circ}\text{C}$ to $-25.0\text{ }^{\circ}\text{C}$; duration of the heating period from 239 to 308 days. In such climate, the energy efficiency of buildings has special urgency.

In recent years construction of low-rise buildings in the Yakutia actively applied frame housing technology of light steel thin-walled structures. The main advantage of this technology is simplicity and convenience of assembly elements, combining functions of bearing and protecting thin-walled profiles. In permafrost conditions, lightweight buildings of such structures allows using surface foundations or screw piles. LSTS technology is an important advantage for isolated locations and remote regions by prefabricated buildings and high transportability, thereby decreasing the cost of transportation materials [1]. At the same time, this constructing technology is based on using cold carcass profiles from thin sheet galvanized steel with high thermal conductivity and accordingly it creates “cold bridges”, which is very confusing the provision of thermal protection buildings in the extreme conditions of the Far North.

Basic design and construction principles of energy efficient buildings are in using the external enclosing structures with a high level of thermal protection, the rational choice of architectural and planning decisions, the application of modern heating and ventilation systems, renewable energy [2–3]. The most important question in the design of buildings thermal protection is calculation of the filler structures transfer resistance considering heat-conducting inclusions [4–5]. In the frame structure buildings from LSTS in terms of thermal protection, the most vulnerable point are “cold bridges” – thin-walled steel profiles and their connections [6–8]. Thermal performance of lightweight steel-framed walls of various constructions and insulation materials considered in [9–14]. In the result of thermal calculations P. Santos [9] found, that the position of thermal insulation in LSF facade walls plays a major role in its thermal performance effectiveness. Most manufacturers offer for use thermo-profiles with special perforation on a wall. In [15, 17] presented the results of researches about effect of the thin steel profiles perforation on the thermal characteristics of filler structures. The results of researches about heat keeping properties various filler structures with application of steel profiles are in [18–21]. In [22] based on theoretical and experimental researches are expediency to use polystyrene-concrete as a filler for walling of steel profiles. In [23] presented the results of a natural experiment in the Leningrad region about determination of thermal characteristics of light frame structures using steel thermo-profiles and thermal insulation material efficiency. A review of work showed that in the previous researches were considered a filler structures by thin-walled steel profiles with a single insulating layer of mineral wool or other effective materials in temperate climates.

Experience in the construction and operation of buildings in the Far North shows that the one of the main reasons for decreasing of buildings thermal protection is a high air infiltration. Specific for the Yakutia outdoor temperature is for $-40\text{ }^{\circ}\text{C}$ to $-59\text{ }^{\circ}\text{C}$ the difference of indoor and outdoor air pressure on the first floor of a two-storey house with a wind speed about 1 m/s is from 5.9 Pa to 10.5 Pa, which is ten times higher than if outdoor temperature is $-10\text{ }^{\circ}\text{C}$. For the Arctic regions, the average wind speed in the coldest months reaches up to 5–6 m/s. Consequently, the air infiltration in these areas even higher and reaches 23–26 Pa. In such climatic conditions and the presence of ventilated underground using pile foundation the negative impact of air infiltration is particularly evident in low-rise frame houses using LSTS. Any violation of the outer shell of buildings, for example, the poor performance of joints different structural elements or junction leakage of thermal insulation materials, produces in winter to cold air infiltration and to disruption of the buildings thermal protection. By V.G. Gagarin etc. [24–26] carried out the researches of air infiltration impact on heat-shielding properties enclosing structures and showed the reduce of heat-shielding properties of external fences.

The purpose of research is to increase the thermal protection of low-rise LSTS houses, taking into account the climatic conditions of the Far North. To achieve that purpose were delivered the following tasks:

- development of the basic design principles of LSTS buildings taking into account high air infiltration and the presence of numerous heat transfer elements;
- calculation and analysis of thermal fields of wall fences and nodes and their contiguity to the ground overlap.

2. Methods

With the aim of identifying the reasons for the breach of the thermal protection carried out on-site inspections of low-rise LSTS buildings of, built on the territory of the Republic of Sakha (Yakutia) in 2012–2016. The objects are two-storey buildings with an area of 120–1350 m²: kindergartens and schools, apartment buildings. The outer walls of buildings were a frame of thin-walled steel profiles 150 mm wide, usually,

arranged in increments of 600 mm and filled with mineral wool plates with a density of 50–75 kg/m³. The inner and outer sides of the outer walls are provided with additional thermal insulation layers each 50 mm thick and the covering. The frame of the LSTS house is established on bearing rolling steel beams on screw piles.

On-site surveys of objects included instrumental monitoring of the temperature and humidity conditions of the interior of buildings and thermal imaging of the surface of the external enclosing structures. In the beginning, for the formation of the general characteristics of the object, an overview thermography of the external and internal surfaces of the enclosing structures was carried out, then on the identified problem areas – detailed thermography of the internal surfaces with the preservation of thermograms. To measure temperature, humidity and speed of movement of interior air in buildings used instrument Testo 435-4 with the trifunctional probe, to conduct thermal imaging – a thermographic camera SATG-90. Thermal imaging measurements are made at an ambient temperature below –30 °C, i.e. at a temperature difference between outside and inside air exceeding the minimum permissible difference. On each object the report on thermal imaging inspection is made.

Calculations of temperature fields and thermal characteristics according to the certified program “Shaddan 3D ST” were performed for the numerical analysis of external walling structures and units of LSTS buildings. This program allows you to determine the spatial temperature fields of structures of any complex configuration, bordering environments with different parameters. The problem is solved by the method of grids with the help of a difference scheme of the second order of accuracy on spatial variables on an uneven rectangular grid. Testing of the program is carried out with application of earlier developed programs of calculation of two-dimensional and three-dimensional temperature fields [27, 28].

3. Results and Discussion

Thermal imaging survey of low-rise houses, built for the first time on the territory of Yakutia by LSTS technology, revealed the presence of numerous sites with heat leakage. From thermograms presented on Figure 1, you can clearly see the impact of heat-conducting inclusions in the form of steel profiles, joints of separate wall panels and insulating materials. The most problematic areas of low-rise LSTS houses is the connection of the outer wall fence with a basement ceiling. In most cases, the heat losses occur in abutting the steel rack profiles for horizontal track.

The main causes of violations of the thermal protection LSTS houses more thoroughly analyzed in [29] and are as follows:

- designing covering constructions performed without taking into account the increased air infiltration in the northern conditions and the presence of numerous thermal bridges in the form of light steel profiles and rolled steel beams on screw piles;
- allowance on the construction of buildings low quality insulation work and thermal insulation materials are used having a low elasticity;
- thermofiller and sealing tape between steel elements do not perform their functions;
- violated the integrity of the building airtight envelope in the joints, in areas abutting the wall fencing in the basement and attic floors, in the areas around the perimeter of window and door openings.

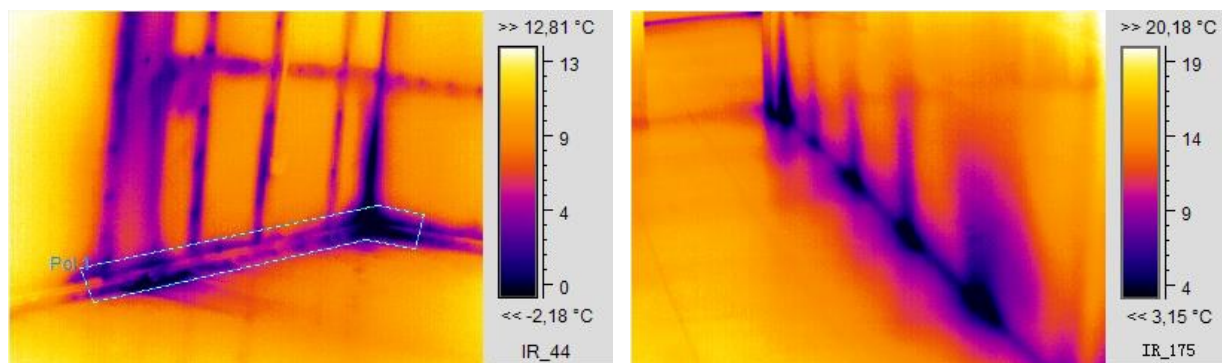


Figure 1. Thermograms wall surfaces of LSTS at an air temperature of $t_o = -42$ °C and $t_i = +25$ °C.

In traditional solutions of buildings from LSTS is a single-layer wall construction with a frame made of thin-walled steel profiles (Figure 2). To fill the wall fencing used fiberglass material density of 10–20 kg/m³ or mineral wool density of 50–75 kg/m³. These materials are breathable materials. When performing installation

work on the construction site it is difficult to provide high-quality thermal insulation materials laying between the profiles due to the presence of bends rack shelves profiles, projections self-tapping screws.



Figure 2. Typical design solution for low-rise home of LSTS for temperate climate.

The main provisions of the design heat protection of external covering constructions are regulated by the updated Construction norms and regulations SNIP 23-02-2003 “Thermal protection of buildings” – Code of Practice SP 50.13330.2012. According to the regulations, in the first place need to comply with thermal performance of external walling normalized values based thermally conductive inclusions depending on the area of building industry. In addition to these requirements, taking into account the increased air infiltration and the presence of numerous thermal bridges are offered to consider the following basic principles for the design of low-rise buildings walling from LSTS in the Far North:

- multilayer external walling airtight;
- in the compounds of the wall fence with a ground location of the overlap frame of steel profiles in a warm area of the building;
- use in conjunction with a ground wall protections overlapping multi thermofiller of materials with low thermal conductivity.

When the multi-layer wall structures decision with LSTS decreases influence of thermal bridges and improves the heat-shielding properties of the fence. The joints between the insulation boards and rack-mount profiles overlap the separate layers. Unlike traditional solutions offered below constructive decisions of walls from LSTS to decrease the impact of air infiltration in the northern regions should be placed OSB boards with mandatory sizing joints airtight tape between the separate layers of thermal insulation wall. The outer insulating layer framing walls are encouraged to take out at least 100 kg/m³ density mineral wool slabs, which will also help reduce the impact of air infiltration. In the inner layers of the insulating panels must have a certain elasticity in order to facilitate the installation of the material in the construction of a metal frame.

The article [30] various options multilayer walls of houses from LSTS were considered for the averaged calculated parameters to ensure the heat protection of buildings in the Arctic: the design outdoor air temperature $t_o = -54$ °C; rated value reduced thermal resistance of the wall at least $R_o = 5.25$ (m²·°C)/W; indoor air temperature $t_i = +21$ °C. The analysis of temperature fields and thermal performance, the unit cost for the installation of wall structures found that the best solution is two-layered fencing wall (Figure 3). The two-layer construction of the walls LSTS line with zero temperature in place of steel profiles rack arrangement is located in the outer insulating layer, and on the wall portion between the steel profiles placed in the middle of the inner layer. This fact is particularly important to ensure that the rated values of the temperature on the inner wall surface. It should be noted that the first facility built on the territory of Yakutia, were applied three-layer wall construction with mineral wool insulation thickness of 50 mm on the inside, which led to a breach of the temperature regime of buildings. One of the reasons for such a breach is offset line with the zero point at the inner side in the locations of rack profiles [30].

The specific heat loss, which can be widely used by designers is determined to unify the calculations reduced heat transfer resistance of double-layer wall fencing with LSTS. In the design of low-rise buildings of LSTS step rack mountable steel profiles take in most cases mineral wool slabs with the width of 600 mm. Therefore, to determine the specific heat losses, taking into account the characteristic step rack mountable profiles examined the wall fencing portion of width 0.6 m and height 0.6 m in the space scheme (Figure 3).

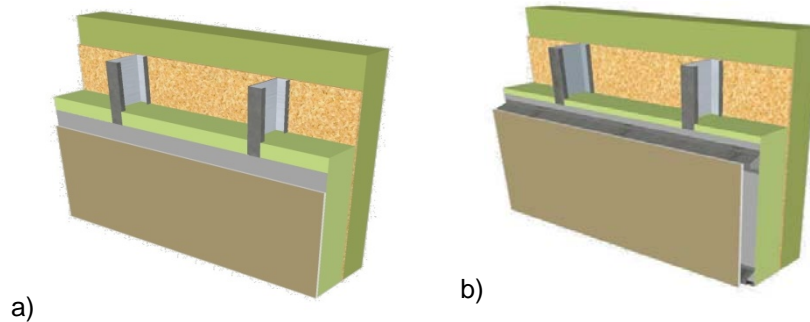


Figure 3. The proposed designs of external walls of buildings from LSTS: (a) double-layer wall fence, (b) double-layer wall fence with an air gap.

On the heat loss through the double-layer wall fencing with LSTS following parameters affect: the thermal conductivity of applied materials; the thickness of the outer and inner layers; the thickness and size of steel profiles; the presence of plate dowels; the presence of a steel bracket. As a heat-insulating material considered mineral wool slabs having a density of 40 kg/m³ in the inner layer ($\lambda = 0.041$ W/(m·°C) and density of 125 kg/m³ in the outer layer with ($\lambda = 0.042$ W/(m·°C). Thermal characteristics of other materials are given in Table 1. The thickness of the steel profiles, plate dowels and bracket are not taken into account in the calculations of specific losses wall fences.

Specific heat loss calculation results are shown in Table 1.

Table 1. Specific heat losses Ψ , W/(m²·°C) for a double-layer wall fencing with thin-walled steel profiles.

| Sketch of wall fencing and thermal characteristics | δ_1 (mm) | δ_2 (mm) | Specific heat losses Ψ (W/(m ² ·°C)) |
|---|-----------------|-----------------|--|
| <p>(1) mineral wool P125 mark slabs ($\lambda = 0.042$ W/(m·°C)), (2) rack mountable steel profile thickness of 1.8 mm and step of 600 mm ($\lambda = 58$ W/(m·°C)), (3) mineral wool P40 mark slabs ($\lambda = 0.041$ W/(m·°C)), (4) gypsum plasterboard ($\lambda = 0.21$ W/(m·°C)), (5) roughly strand slabs OSB ($\lambda = 0.34$ W/(m·°C)), (6) wind-hydroprotective membrane, (7) vapor barrier membrane.</p> | 150 | 100 | 0.22 |
| | | 150 | 0.175 |
| | | 200 | 0.146 |
| | 200 | 50 | 0.272 |
| | | 100 | 0.203 |
| | | 150 | 0.164 |
| | 250 | 50 | 0.251 |
| | | 100 | 0.191 |
| | | 150 | 0.156 |
| <p>(1) mineral wool P125 mark slabs ($\lambda = 0.042$ W/(m·°C)), (2) rack mountable steel profile thickness of 1.8 mm and step of 600 mm ($\lambda = 58$ W/(m·°C)), (3) mineral wool P40 mark slabs ($\lambda = 0.041$ W/(m·°C)), (4) gypsum plasterboard ($\lambda = 0.21$ W/(m·°C)), (5) roughly strand slabs OSB ($\lambda = 0.34$ W/(m·°C)), (6) layer of air ($\lambda = 0.357$ W/(m·°C)), (7) hatter steel profile thickness of 1.8 mm and step of 600 mm ($\lambda = 58$ W/(m·°C)), (8) wind-hydroprotective membrane, (9) vapor barrier membrane.</p> | 150 | 100 | 0.216 |
| | | 150 | 0.173 |
| | | 200 | 0.145 |
| | 200 | 50 | 0.267 |
| | | 100 | 0.2 |
| | | 150 | 0.162 |
| | 250 | 50 | 0.248 |
| | | 100 | 0.189 |
| | | 150 | 0.154 |

Steel profiles used for the frame thickness generally of 0.8 to 1.8 mm. The analysis shows that changes in the thickness of the steel profiles within the specified limits has little effect on the values of specific heat loss through the wall fence considered. In this case, profiles adopted maximum thickness of 1.8 mm, which will create some margin for evaluation thermal performance walling with using smaller thickness of steel profiles. As a result, thermal calculations that sets the plate dowel for fastening heat-insulating slabs made of fiberglass plays a minor role in the formation of the temperature field for wall fencing and steel bracket has a local effect on the temperature distribution. The temperature is leveled at the area in the middle of the inner heat-insulating layer and does not differ from areas on the inner surface of the wall section in the bracket. This situation is due to the presence of an intermediate barrier OSB slabs with a lower thermal conductivity. Therefore, the presence of plate dowels and steel bracket do not considered when determining the specific heat loss wall fencing.

From a comparison of the specific heat loss values with the same total thickness of the walls it is seen that the most effective to take a smaller thickness of the inner layer and vary the thickness of the outer layer to provide normalized values of the wall fencing reduced thermal resistance. For example, the specific heat loss through the building wall structure of the total thickness of 330 mm:

$$- \Psi = 0.175 \text{ W}/(\text{m}^2 \cdot ^\circ\text{C}) \text{ if } \delta_1 = 150 \text{ mm и } \delta_2 = 150 \text{ mm};$$

$$- \Psi = 0.203 \text{ W}/(\text{m}^2 \cdot ^\circ\text{C}) \text{ if } \delta_1 = 200 \text{ mm и } \delta_2 = 100 \text{ mm};$$

$$- \Psi = 0.251 \text{ W}/(\text{m}^2 \cdot ^\circ\text{C}) \text{ if } \delta_1 = 250 \text{ mm и } \delta_2 = 50 \text{ mm}.$$

Heat loss through the wall fencing from LSTS in the presence of an air layer is somewhat reduced as compared to the first option (Table 1). Also previously [11], it was established that the inner surface temperature of steel profiles location areas is increased by 1.1°C in the presence of an air layer.

In the previous works considered fundamentally different structural solution panels from LSTS, mainly intended for a temperate climate [6–23]. Comparison of the results obtained on proposed solutions panels with data of other authors obtained several incorrect. Double-layer wall fence with an intermediate layer of roughly strand slabs OSB effectively reduces the impact of thermal bridges and increased infiltration of air at very low outside temperature during winter.

Under the conditions of permafrost lightweight buildings from LSTS allows the use of screw piles. As a rule, on steel screw piles installed rolled I-beams, in which is being built from LSTS frame house. With this solution (Figure 4) in this frame section there is a plurality cold bridges. As the experience of operation buildings, this design solution is not suitable for the construction of buildings in the northern climate zone. Therefore, based on the above design principles of the buildings from LSTS offered to create airtight layer from the lower side of the building by device of reinforced concrete basement ceiling. The thermofiller can be used in the form of masonry materials such as autoclaved aerated concrete blocks, with a lower coefficient thermal conductivity $\lambda \leq 0.16 \text{ W}/(\text{m} \cdot ^\circ\text{C})$ (Table 2) to reduce the influence of cold bridges. The configuration of the masonry rater to take a stage that allows overlap the joints of lower heat-insulation layer by the upper heat-insulating layer. With such a design solution as the calculations of temperature fields, steel elements are located in a zone with a positive temperature (Figure 5).

To evaluate the thermal performance and determine the specific heat loss calculated the three-dimensional temperature field fragments nodes conjugation double-layer wall fencing from LSTS with a basement ceiling. Angle conjugation considered in three-dimensional variations with the following parameters: the height of the wall fencing of 1.2 m, the length and width of track of 0.6 m, taking the step profiles.

On the heat loss through the node interface wall fencing with a basement ceiling influenced by the following parameters: the thermal conductivity of using materials; the thickness of the basement ceiling, heat insulating thickness of the basement ceiling, the thickness of the outer and inner layers. Thermal characteristics of the materials shown in Table 2. The thickness of the steel profiles taken closer to the maximum of 1.8 mm and a reinforced concrete slab – 200 mm. Components of the floor in the calculations not considered that will create some stock of heat-shielding properties for under conjugation.

In under consideration conjugations of the walls with a basement ceiling the line of zero temperature is located below the placement areas of steel profiles in sections of both steel rack mountable profile and section heat-insulation, i.e., all steel profiles are in the warm zone. The lowest temperature of the inner surface ($t_{s,min}$) is observed in the corner zones of location rack mountable profiles. For example, for the variant $\delta_1 = 150 \text{ mm}$, $\delta_2 = 130 \text{ mm}$ and $\delta_3 = 300 \text{ mm}$ is $t_{s,min} = +14.4 \text{ }^\circ\text{C}$ at the design outdoor air temperature $t_o = -54 \text{ }^\circ\text{C}$ and indoor air temperature $t_i = +21 \text{ }^\circ\text{C}$. The average temperature on the inner surface of the conjugation under consideration is $t_{s,a} = +18.3 \text{ }^\circ\text{C}$.

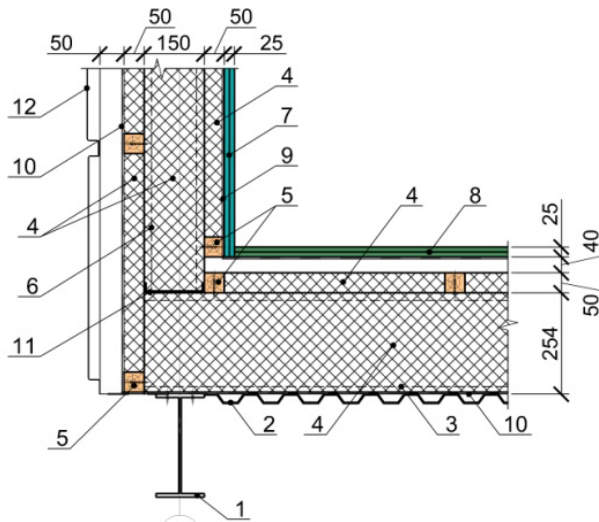


Figure 4. Typical solution of the conjugation of the outer wall with a basement ceiling; (1) foundation I-beam, (2) profiled decking, (3) thin-walled steel profile, (4) rock wool density 75 kg/m³, (5) block of wood, (6) rack mountable steel profile, (7) gypsum plasterboard, (8) glass-magnesium sheets, (9) vapor barrier membrane, (10) wind-water-proof membrane, (11) thin-walled steel guide profile and sealing tape Knauf- Dihntungsband, (12) front sheet.

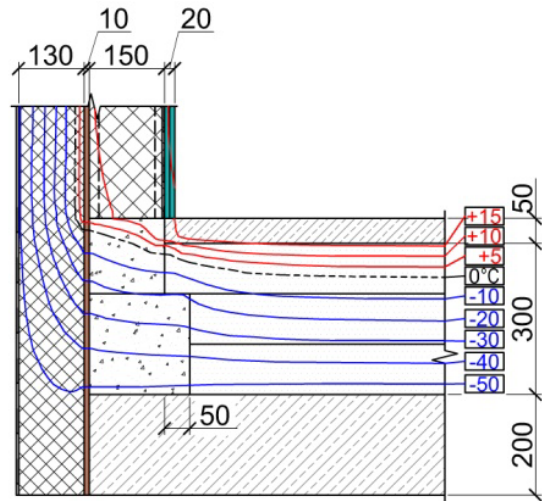


Figure 5. The distribution of temperature in the corner joints in the vertical section at the location of the rack mountable steel profile with an air temperature $t_o = -54\text{ °C}$ and $t_i = +21\text{ °C}$.

Table 2. Specific heat losses Ψ , W/(m²•°C) for a double-layer wall fencing conjugation with a basement ceiling.

| Sketch of wall fencing and thermal characteristics | δ_o (mm) | δ_1 (mm) | δ_2 (mm) | Specific heat losses Ψ (W/(m ² •°C)) |
|---|-----------------|-----------------|-----------------|--|
| <p>(1) mineral wool P125 mark slabs ($\lambda = 0.042\text{ W/(m}\cdot\text{°C)}$), (2) roughly strand slab OSB ($\lambda = 0.34\text{ W/(m}\cdot\text{°C)}$), (3) mineral wool P40 mark slabs ($\lambda = 0.041\text{ W/(m}\cdot\text{°C)}$) between the rack mountable steel profiles thickness of 1.8 mm and a step of 600 mm ($\lambda = 58\text{ W/(m}\cdot\text{°C)}$), (4) gypsum plasterboard ($\lambda = 0.21\text{ W/(m}\cdot\text{°C)}$), (5) vapor barrier membrane, (6) cement-sand screed M150 ($\lambda = 0.76\text{ W/(m}\cdot\text{°C)}$), (7) polystyrene slab PSB-S-35 ($\lambda = 0.04\text{ W/(m}\cdot\text{°C)}$), (8) thermal break of lightweight concrete ($\lambda = 0.16\text{ W/(m}\cdot\text{°C)}$), (9) monolithic reinforced concrete slab ($\lambda = 1.92\text{ W/(m}\cdot\text{°C)}$), (10) wind-hydroprotective membrane.</p> | 300 | 150 | 100 | 0.341 |
| | | | 150 | 0.304 |
| | | | 200 | 0.282 |
| | | 200 | 50 | 0.423 |
| | | | 100 | 0.353 |
| | | | 150 | 0.32 |
| | 250 | 50 | 0.426 | |
| | | 100 | 0.365 | |
| | | 150 | 0.335 | |
| | 400 | 150 | 100 | 0.315 |
| | | | 150 | 0.275 |
| | | | 200 | 0.252 |
| 200 | | 50 | 0.399 | |
| | | 100 | 0.324 | |
| | | 150 | 0.287 | |
| 250 | 50 | 0.399 | | |
| | 100 | 0.332 | | |
| | | 150 | 0.299 | |

As a result of analysis of the specific heat loss values through the conjugation wall fencing with a basement ceiling found less heat loss with a smaller thickness of the internal layer of heat insulating wall fencing is installed of LSTS. By increasing the thickness of the heat insulation layer basement ceiling from 300 mm to 400 mm, the specific heat loss through the considered conjugation is reduced from 5.6 to 10.7 %.

4. Conclusion

The basic principles proposed for the design of wall fencing from thin-walled steel profiles in the Far North. Designed for low-rise buildings of LSTS multi-layer wall fencing and node conjugations with a basement ceiling consider for increased air infiltration in the northern climatic zone with a stable very low temperature of the outside air in the winter and the presence plentifully cold bridges in the form of thin-walled steel profiles. The values of specific heat loss depending on various parameters are calculated for the double-layer wall fencing and node conjugation with a basement ceiling. From the analysis of the specific heat loss values determined that the proposed solutions for wall fencing of LSTS most efficient to take a smaller thickness of the inner layer and vary the thickness of the outer heat-insulating layer. Proposed solutions for node conjugation of wall fencing with a basement ceiling allow dispose positioning steel profiles in the area with positive temperature by thermofiller and their echelon allow overlap joints of the lower insulation layer by a top layer.

References

1. Mezentseva, Ye.A., Lushnikov, S.D. Bystrovozvodimyye zdaniya iz legkikh stalnykh konstruksiy [Lightweight steel buildings]. Vestnik MGSU. Spetsvypusk. 2009. No. 1. Pp. 62–64.
2. Gorshkov, A.S. Energoeffektivnost v stroitelstve: voprosy normirovaniya i mery po snizheniyu energopotrebleniya zdaniy [The energy efficiency in the field of construction: questions of norms and standards and solutions for the reduction of energy consumption at buildings]. Magazine of Civil Engineering. 2010. No. 1. Pp. 9–13. (rus)
3. Vatin N.I., Nemova D.V., Rymkevich P.P., Gorshkov A.S. Influence of building envelope thermal protection on heat loss value in the building. Magazine of Civil Engineering. 2012. No. 8(34). Pp. 4–14. (rus)
4. Krivoshein, A.D., Fedorov, S.V. K voprosu o raschete privedenogo soprotivleniya teploperedache [About the calculation of reduced total thermal resistance of walling]. Magazine of Civil Engineering. 2010. No. 8(18). Pp. 21–27. (rus)
5. Gagarin, V.G., Kozlov, V.V. O normirovanii teplozashchity i trebovaniya raskhoda energii na otopeniye i ventilyatsiyu v proyekte aktualizirovannoy redaktsii SNIiP «Teplovaya zashchita zdaniy [On the regulation of thermal protection and energy consumption requirements for heating and ventilation in the draft updated version of SNIiP "Thermal protection of buildings]. Vestnik Volgogradskogo gosudarstvennogo arkhitekturno-stroitel'nogo universiteta. Seriya: Stroitelstvo i arkhitektura. 2013. No. 31-2(50). Pp. 468–474. (rus)
6. Tenpierik, M.J., Van der Spoel, W.H., Cauber, J.M. Analytical model for computing thermal bridge effects in high performance building panels [Online]. URL: http://www.researchgate.net/publication/242269808_Analytical_Model_for_Computing_Thermal_Bridge_Effects_in_High_Performance_Building_Panels (date of application: 11.12.2017)
7. Garay, R., Uriarte, A., Apraiz, I. Performance assessment of thermal bridge elements into a full scale experimental study of a building façade. Energy and buildings, 2014. No. 85. Pp. 579–591.
8. Mao, G., Johannesson, G. Dynamic calculation of thermal bridges. Energy and Buildings. 1997. Vol. 26. No. 3. Pp. 233–240.
9. Santos, P. Energy efficiency of lightweight steel-framed buildings [Online]. URL <https://www.intechopen.com/books/energy-efficient-buildings/energy-efficiency-of-lightweight-steel-framed-buildings> (date of application: 11.12.2017).
10. Santos, P., Martins, C., Sim es da Silva, L. Thermal performance of lightweight steel-framed construction systems. Metall Res Technol. 2014. No. 111(6). Pp. 329–338.

Литература

1. Мезенцева Е.А., Лушников С.Д. Быстровозводимые здания из легких стальных конструкций // Вестник МГСУ. Спецвыпуск. 2009. № 1. С. 62–64.
2. Горшков А.С. Энергоэффективность в строительстве: вопросы нормирования и меры по снижению энергопотребления зданий // Инженерно-строительный журнал. 2010. № 1. С. 9–13.
3. Ватин Н.И., Немова Д.В., Рымкевич П.П., Горшков А.С., Влияние уровня тепловой защиты ограждающих конструкций на величину потерь тепловой энергии в здании // Инженерно-строительный журнал. 2012. № 8(34). С. 21–27.
4. Кривошеин А.Д., Федоров С.В. К вопросу о расчете приведенного сопротивления теплопередаче // Инженерно-строительный журнал. 2010. № 8 (18). С. 21–27.
5. Гагарин В.Г., Козлов В.В. О нормировании теплозащиты и требования расхода энергии на отопление и вентиляцию в проекте актуализированной редакции СНиП «Тепловая защита зданий» // Вестник Волгоградского государственного архитектурно-строительного университета. Серия: Строительство и архитектура. 2013. № 31-2 (50). С. 468–474.
6. Tenpierik M.J., Van der Spoel W.H., Cauber J.M. Analytical model for computing thermal bridge effects in high performance building panels [Электронный ресурс]. URL:http://www.researchgate.net/publication/242269808_Analytical_Model_for_Computing_Thermal_Bridge_Effects_in_High_Performance_Building_Panels (дата обращения: 11.12.2017)
7. Garay R., Uriarte A, Apraiz I. Performance assessment of thermal bridge elements into a full scale experimental study of a building façade // Energy and buildings, 2014. № 85. Pp. 579–591.
8. Mao G., Johannesson G. Dynamic calculation of thermal bridges // Energy and Buildings. 1997. Vol. 26. № 3. Pp. 233–240.
9. Santos P, Energy efficiency of lightweight steel-framed buildings [Электронный ресурс]. URL <https://www.intechopen.com/books/energy-efficient-buildings/energy-efficiency-of-lightweight-steel-framed-buildings> (дата обращения 11.12.2017).
10. Santos P, Martins C, Sim es da Silva L. Thermal performance of lightweight steel-framed construction systems // Metall Res Technol. 2014. № 111(6). Pp. 329–338.
11. Roque E, Santos P. The effectiveness of thermal insulation in lightweight steel-framed walls with respect to its position [Электронный ресурс]. URL: https://www.researchgate.net/publication/313813336_The_Effectiveness_of_Thermal_In

11. Roque, E., Santos, P. The effectiveness of thermal insulation in lightweight steel-framed walls with respect to its position [Online]. URL: https://www.researchgate.net/publication/313813336_The_Effectiveness_of_Thermal_Insulation_in_Lightweight_Steel-Framed_Walls_with_Respect_to_Its_Position (date of application: 11.12.2017).
12. Enrico de Angelis, Ermanno Serraa. Light steel-frame walls: thermal insulation performances and thermal bridges// Energy Procedia. 2014. No. 45. Pp. 362–371.
13. Santos, P., Martins, C., Simo es da Silva, L. Thermal performance of lightweight steel framed wall: the importance of flanking thermal losses. Journal of Building Physics. 2014. No. 38(1). Pp. 81–98.
14. Naji, S., Çelik, O.C., Alengaram, U.J., Jumaat, M.Z., Shamshirband S. Structure, energy and cost efficiency evaluation of three different lightweight construction systems used in low-rise residential buildings. Energy and buildings, 2014. No. 84. Pp. 727–739.
15. Chernyavskiy, V.V., Semko, V.O., Yurin, O.I., Prokhorenko, D.A. Vliyaniye perforatsii legkikh stalnykh tonkostennykh profiley na teplofizicheskiye kharakteristiki ograzhdayushchikh konstruktsiy [The effect of perforation of light steel thin-walled profiles on the thermophysical characteristics of enclosing structures]. Otrasl'evoye mashinostroyeniye, stroitelstvo. Sb. nauch. trudov. Poltava: PolNTU. 2011. No. 1(29). Pp. 194–199.
16. Semko, V.O., Leshchenko, M.V., Kotko, N.O. Issledovaniya vliyaniya konstruktivnykh parametrov na teploprovodnost legkikh stalnykh ograzhdayushchikh konstruktsiy [Studies of the influence of design parameters on the thermal conductivity of light steel enclosing structures]. Stroitelstvo, materialovedeniye, mashinostroyeniye. Sb. nauchn.trudov. Dnepropetrovsk: PGASA. 2012. No. 65. Pp. 567–571.
17. Veljkovic, M., Johansson, B. Light steel framing for residential buildings. Thin-Walled Structures. 2006. Vol. 44. No. 12. Pp. 1272–1279.
18. Semko, V.O., Leshchenko, M.V., Filippovich, L.M., Reznikov, A.A. Eksperimentalnyye issledovaniya teploprovodnosti ograzhdayushchikh konstruktsiy iz stalnykh tonkostennykh profiley [Experimental studies of the thermal conductivity of enclosing structures made of steel thin-walled profiles]. Resursosberegayushchiye materialy, konstruktsii, zdaniya i sooruzheniya. Sb.nauchn.trudov. Rovno. 2013. No. 25. Pp. 606–611.
19. Kuzmenko, D.V. Ograzhdayushchaya termopanel s karkasom iz termoprofiley [Enclosing thermopanel with a frame made of thermoprofiles]. Zhilishchnoye stroitelstvo. 2009. No. 4. Pp. 2–4. (rus)
20. Kuzmenko, D.V., Vatin, N.I. Ograzhdayushchiye konstruktsii «nulevoy» tolshchiny dlya karkasnykh zdaniy [Zero thickness fencing structures for frame buildings]. Magazine of Civil engineering. 2008. No. 1. Pp. 13–21. (rus)
21. Davies, J.M. Light gauge steel cassette wall construction – theory and practice. Journal of Constructional Steel Research. 2006. Vol. 62. No. 11. Pp. 1077–1086.
22. Leshchenko, M.V., Semko, V. Thermal characteristics of the external walling made of cold-formed steel studs and polystyrene concrete. Magazine of Civil Engineering. 2015. No. 8. Pp. 44–55. (rus)
23. Petrosova, D.V., Kuzmenko, N.M., Petrosov, D.V. Eksperimentalnoye issledovaniye teplovogo rezhima legkoy ograzhdayushchey konstruktsii v naturnykh usloviyakh [A field experimental investigation of the thermal regime of lightweight building envelope construction]. Magazine of Civil Engineering. 2013. No. 8(43). Pp. 31–37. (rus)
24. Gagarin, V.G., Kozlov, V.V., Sadchikov, A.V., Mekhnetsov, I.A. Prodolnaya filtratsiya vozdukha v sovremennykh ograzhdayushchikh konstruktsiyakh [Accounting for longitudinal air filtration in the evaluation of thermal protection of the wall with a ventilated facade]. AVOK. 2005. No. 8. Pp. 60–70. (rus)
25. sulation_in_Lightweight_Steel-Framed_Walls_with_Respect_to_Its_Position (дата обращения: 11.12.2017).
12. Enrico de Angelis, Ermanno Serraa. Light steel-frame walls: thermal insulation performances and thermal bridges// Energy Procedia. 2014. № 45. Pp. 362–371.
13. Santos P., Martins C., Simo es da Silva L. Thermal performance of lightweight steel framed wall: the importance of flanking thermal losses // Journal of Building Physics. 2014. № 38 (1). Pp. 81–98.
14. Naji S., Çelik O.C., Alengaram U. J., Jumaat M.Z., Shamshirband S. Structure, energy and cost efficiency evaluation of three different lightweight construction systems used in low-rise residential buildings// Energy and buildings, 2014. № 84. Pp. 727–739.
15. Чернявский В.В., Семко В.О., Юрин О.И., Прохоренко Д.А. Влияние перфорации легких стальных тонкостенных профилей на теплофизические характеристики ограждающих конструкций // Отраслевое машиностроение, строительство. Сб. науч. трудов. Полтава: ПолНТУ. 2011. №1(29). С. 194–199. URL: http://lib.pntu.edu.ua/?module=elilib*id*7879
16. Семко В.О., Лещенко М.В., Котко Н.О. Исследования влияния конструктивных параметров на теплопроводность легких стальных ограждающих конструкций // Строительство, материаловедение, машиностроение. Сб. науч. трудов. Днепропетровск: ПГАСА. 2012. № 65. С. 567–571.
17. Veljkovic M., Johansson B. Light steel framing for residential buildings // Thin-Walled Structures. 2006. Vol 44. № 12. Pp. 1272–1279.
18. Семко В.О., Лещенко М.В., Филиппович Л.М., Резников А.А. Экспериментальные исследования теплопроводности ограждающих конструкций из стальных тонкостенных профилей // Ресурсосберегающие материалы, конструкции, здания и сооружения. Сб.научн.трудов. Ровно, 2013. № 25. С. 606–611.
19. Кузьменко Д.В. Ограждающая термopанель с каркасом из термопрофилей // Жилищное строительство. 2009. № 4. С. 2–4.
20. Кузьменко Д.В., Ватин Н.И. Ограждающие конструкции «нулевой» толщины для каркасных зданий // Инженерно-строительный журнал. 2008. № 1. С. 13–21.
21. Davies J.M. Light gauge steel cassette wall construction – theory and practice // Journal of Constructional Steel Research. 2006. Vol. 62. № 11. С. 1077–1086.
22. Лещенко М.В., Семко В.А. Теплотехнические свойства стеновых ограждающих конструкций из стальных тонкостенных профилей и полистиролбетона // Инженерно-строительный журнал. 2015. № 8. С. 44–55.
23. Петросова Д.В., Кузьменко Н.М., Петросов Д.В. Экспериментальные исследования теплового режима легкой ограждающей конструкции в натуральных условиях // Инженерно-строительный журнал. 2013. № 8. С. 31–37.
24. Гагарин В.Г., Козлов В.В., Садчиков А.В., Мехнецов И.А. Продольная фильтрация воздуха в современных ограждающих конструкциях // АВOK. 2005. № 8. С. 60–70.
25. Гагарин В.Г., Козлов В.В., Садчиков А.В. Учет продольной фильтрации воздуха при оценке теплозащиты стены с вентилируемым фасадом // Промышленное и гражданское строительство. 2005. № 6. С. 42–45.
26. Петриченко М.Р., Петросова Д.В., Петроченко М.В. Фильтрационный процесс воздухом консервативной примеси (температуры и теплоты) сквозь стену // Научно-технические ведомости СПбГПУ. 2012. № 4(159). С. 221–226.
27. Данилов Н.Д., Шадрин В.Ю., Павлов Н.Н. Прогнозирование температурного режима угловых соединений наружных ограждающих конструкций //

Корнилов Т.А., Никифоров А.А. Теплозащита малоэтажных зданий из легких стальных тонкостенных конструкций // Инженерно-строительный журнал. 2018. № 8(84). С. 140–149.

25. Gagarin, V.G., Kozlov, V.V., Sadchikov, A.V. Uchet prodolnoy filtratsii vozdukhа pri otsenke teplozashchity steny s ventiliruyemyм fasadom [Accounting for longitudinal air filtration in the evaluation of thermal protection of the wall with a ventilated facade]. *Promyshlennoye i grazhdanskoye stroitelstvo*. 2005. No. 6. Pp. 42–45.
26. Petrichenko, M.R., Petrosova, D.V., Petrochenko, M.V. Filtratsionnyy protsess vozdukhom konservativnoy primesi (temperatury i teploty) skvoz stenu [Air filtration process of a conservative impurity (temperature and heat) through the wall]. *Nauchno-tekhnicheskiye vedomosti SPbGPU*. 2012. No. 4(159). Pp. 221–226.
27. Danilov, N.D., Shadrin, V.Yu., Pavlov, N.N. Prognozirovaniye temperaturnogo rezhima uglovykh soyedineniy naruzhnykh ograzhdayushchikh konstruksiy [Prediction of the temperature regime of the corner joints of external enclosing structures]. *Promyshlennoye i grazhdanskoye stroitelstvo*. 2010. No. 4. Pp. 20–22.
28. Danilov, N.D., Sobakin, A.A., Slobodchikov, Ye.G., Fedotov, P.A., Prokopyev, V.V. Analiz formirovaniya temperaturnogo polya naruzhnoy steny s fasadnoy zhelezobetonnoy panelyu [Analysis of the formation of the temperature field of the outer wall with the facade reinforced concrete panel]. *Zhilishchnoye stroitelstvo*. 2013. No. 11. Pp. 46–49.
29. Kornilov, T.A., Gerasimov, G.N. O nekotorykh oshibkakh proyektirovaniya i stroitelstva maloetazhnykh domov iz LSTK v usloviyakh Kraynego Severa [On some mistakes in the design and construction of low-rise houses from LSTK in the conditions of the Far North]. *Promyshlennoye i grazhdanskoye stroitelstvo*. 2015. No. 3. Pp. 42–46.
30. Kornilov, T.A., Gerasimov, G.N. Naruzhnyye steny maloetazhnykh domov iz legkikh stalnykh tonkostennykh konstruksiy dlya usloviy Kraynego Severa [External walls of low-rise houses from light steel thin-walled structures for the conditions of the Far North]. *Zhilishchnoye stroitelstvo*. 2016. No. 6. Pp. 20–24.
- Промышленное и гражданское строительство. 2010. № 4. С. 20–22.
28. Данилов Н.Д., Собакин А.А., Слободчиков Е.Г., Федотов П.А., Прокопьев В.В. Анализ формирования температурного поля наружной стены с фасадной железобетонной панелью // *Жилищное строительство*. 2013. № 11. С. 46–49.
29. Корнилов Т.А., Герасимов Г.Н. О некоторых ошибках проектирования и строительства малоэтажных домов из ЛСТК в условиях Крайнего Севера // *Промышленное и гражданское строительство*. 2015. № 3. С. 42–46.
30. Корнилов Т.А., Герасимов Г.Н. Наружные стены малоэтажных домов из легких стальных тонкостенных конструкций для условий Крайнего Севера // *Жилищное строительство*. 2016. № 6. С. 20–24.

*Terentii Kornilov**,
+7(914)2735260; kornt@mail.ru

Alexsandr Nikiforov,
+7(914)1000304; nialyk@mail.ru

*Терентий Афанасьевич Корнилов**,
+7(914)2735260; эл. почта: kornt@mail.ru

Александр Яковлевич Никифоров,
+7(914)1000304; эл. почта: nialyk@mail.ru

© Kornilov, K.T., Nikiforov, A.Y., 2018

doi: 10.18720/MCE.84.15

Residual resource of a one-storey steel frame industrial building constructed with bridge cranes

Остаточный ресурс стального каркаса одноэтажного промышленного здания с мостовыми кранами

*T.V. Zolina,
P.N. Sadchikov*,
Astrakhan State Architectural and Construction
University, Astrakhan, Russia*

*Д-р техн. наук, помощник ректора
по развитию профессионального
образования Т.В. Золина,
канд. техн. наук, доцент П.Н. Садчиков*,
Астраханский государственный
архитектурно-строительный университет,
г. Астрахань, Россия*

Key words: industrial building; Residual resource; probabilistic model; system of reliability coefficients; stress-strain state; matrix of rigidity

Ключевые слова: промышленное здание; остаточный ресурс; вероятностная модель; система коэффициентов надежности; напряженно-деформированное состояние; матрица жесткости

Abstract. The scheme of an integrated approach to the study of changes in the stress-strain state of the frame one-story industrial building constructed with bridge cranes, caused by accumulation of damage caused during the operation. The algorithm has been developed for estimating and predicting the residual resource of a production facility on the basis of processing the results of a series of surveys. It allows to obtain the values of reliability indicators in the correlation approximation using probabilistic models of disturbing influences. This approach is based on the assessment of the reserve strength of the framework structures, determined by the difference between their bearing capacity and the largest value of the generalized load. The article demonstrates the numerical implementation of the algorithm on the example of calculating the building of the shipbuilding shop of a marine shipbuilding plant. Consistent solution positive, negative and predictive tasks enabled by analyzing the dynamics of natural frequencies building frame under the action of the aggregate load estimate time reaches the maximum allowable state. The results allow to regulate the timing and direction of the actions of the repair work at lower 4...8 times the intensity of the survey.

Аннотация. Построена схема комплексного подхода к исследованию изменений напряженно-деформированного состояния каркаса одноэтажного промышленного здания с мостовыми кранами, вызванных накоплением повреждений, возникших в процессе эксплуатации. Разработан алгоритм оценки и прогнозирования остаточного ресурса производственного объекта на основе обработки результатов серии обследований. Он позволяет получить значения показателей надежности в корреляционном приближении с использованием вероятностных моделей возмущающих воздействий. Данный подход построен на оценке резерва прочности конструкций каркаса, определяемым разностью между их несущей способностью и наибольшим значением обобщенной нагрузки. Приведена демонстрация численной реализации предложенного алгоритма на примере расчета здания судокорпусного цеха морского судостроительного завода. Последовательное решение прямой, обратной и прогнозной задач позволило посредством анализа динамики частот собственных колебаний каркаса здания под действием совокупности нагрузок оценить период времени достижения им предельно допустимого состояния. Полученные результаты позволяют регламентировать сроки и направленность действия ремонтно-восстановительных работ при снижении в 4...8 раз интенсивности проведения обследований.

1. Introduction

Continuous growth of production capacity and introduction of modern technologies speaks about the need for technical re-equipment of industrial buildings already in operation. In this case, the problem of estimating and predicting their residual resource comes to the forefront. Special urgency its decision to

acquire in the case of buildings, equipped with overhead cranes, because as the first option for Reconstruction acts replacing the existing crane equipment to increase its capacity. Such buildings are widely used in the organization of the technological process of machine-building, ship-repairing, metallurgical and ore-dressing plants.

The current practice of assessing the residual technical resource is mainly based on a deterministic approach, which is associated with the need for full-scale inspection of the building frame at a certain time [1–4]. The corresponding algorithm is reduced to an estimate of the safety factor based on the comparison of the results of the verification calculation of the actual characteristics of the stress-strain state obtained during the inspection of the building with the corresponding normative values.

The random character of the time variation of the stiffness characteristics of the structural elements, as well as the duration and direction of the disturbing effects, implies the determination of the time period for the safe operation of the building in a probabilistic setting. The analysis of the scientific literature made it possible to classify the problems of studying the changes in the behavior of the frame of a building into two types. The greatest interest is shown in the formulation of two types of problems. The first of these is the definition of the properties of the output parameters of the system with known probabilistic characteristics of the input combinations of loads [5-8]. The solution of the problem in this formulation is realized by finding the mathematical expectation and the standard of ordinates of the random function, and the search for the values of the required parameters reduces to an analysis of the correlation dependencies. This technique does not take into account the dynamics of changes in the physical parameters of materials and the static scheme as a result of force and non-force impacts on the object of investigation, corrosion of metal structures and destruction of bolted connections. The second type is aimed at solving a boundary value problem formalized through a system of nonlinear differential equations, the coefficients for unknowns and the load in which are random functions [9, 10]. The search for a solution is reduced to the implementation of a direct method for estimating the reliability of a building, the random character of which is determined by the spread of the properties of the geometric and rigidity parameters of the structure. This method has not yet found wide application in engineering practice, which is caused by the lack of a sufficient number of developed probabilistic calculation methods for spatial models of buildings and the complexity of computational nature.

In this situation, the problem of estimating the residual resource becomes particularly urgent, since its solution allows us to predict the kinetics of the change in the stress-strain state with allowance for damages arising during the operation of the technical system and determine the time of its repair ability outcome. The timeliness of the work required to restore the identified structural elements with a high degree of accumulated deformation can lead to a significant extension of the further operation of the facility as a whole.

In the course of work on the topic, the results of numerous theoretical and applied studies of domestic and foreign scientists that have made a significant contribution to the development and improvement of methods of the theory of the reliability of building structures are studied [9, 11–15]. Methods for assessing changes in the stress-strain state of steel structures as components of the frame of an industrial building are considered when they perceive beyond design-fire [16], impact [17] and crane [18] effects. Based on the analysis of the sources studied, issues that require substantial refinement for the possibility of constructing a generalized method for probabilistic estimation and forecasting the resource of an industrial building in operation are identified. At the same time, proposals for the construction and implementation of algorithms for the complex optimal design of structural elements of the framework with a view to making the most effective decisions [19–22] are taken into account. The accents of the strategic line of further studies of the kinetics of the change in the stiffness characteristics of the framework of the production facility are placed with the random nature of the impacts and the numerical realization of their results in application to engineering practice.

The approach proposed by the authors of the article is radically different from the ones currently used in conducting the examination. It is based on an estimate of the strength reserve of carcass structures [23], determined by the difference between their bearing capacity and the largest value of the generalized load.

As an objective of the research implementing this approach, it is an increase in the service life of buildings and structures by carrying out repair and restoration works at the sites of the construction complex during the estimated periods of their operation. For achieve this goal, the authors resolved the following questions:

- development of an analytical apparatus for predicting the stress-strain state of the frame of an industrial building, taking into account random factors of impacts and adjusting the stiffness matrix, depending on the change in the displacements at fixed points of the design scheme;
- definition of functions of fictitious loading and working capacity of the building, taking into account the dynamics of changes in stresses in the individual structural elements of the framework, arising under the influence of a combination of factors;
- development of a methodology for assessing the residual life of an operational condition of industrial building structures, relying on a system of reliability coefficients;
- carrying out numerical studies and comparative analysis of the calculated results with experimental data and known computational solutions presented in the scientific and regulatory literature.

2. Methods

Analyzing the advantages and disadvantages of existing methods, the most suitable for ensuring the required reliability of the obtained numerical estimation results is a method based on the correlation of the levels of time series of stress values at individual points in the design scheme of the object. For the possibility of its implementation, it is required to develop an integrated approach to the study of changes in the rigidity characteristics of the framework under the action of a load factor aimed at solving the general problem of estimating the resource of an industrial building at any fixed time of its operation. As a defining criterion, a 10 % reduction in the frequency of the first forms of natural oscillations appears.

In the construction of the space frame design scheme research facility are taken into account such factors as:

- a variant of a layout of plates and quality of an embedding of seams in a covering;
- the effect of longitudinal vertical bonds on the torsional stiffness;
- split bracing structures;
- way of representing the overhead crane.

The general form of spatial computational schemes storey industrial buildings with equal height spans equipped constructed with bridge cranes, is shown in Figure 1.

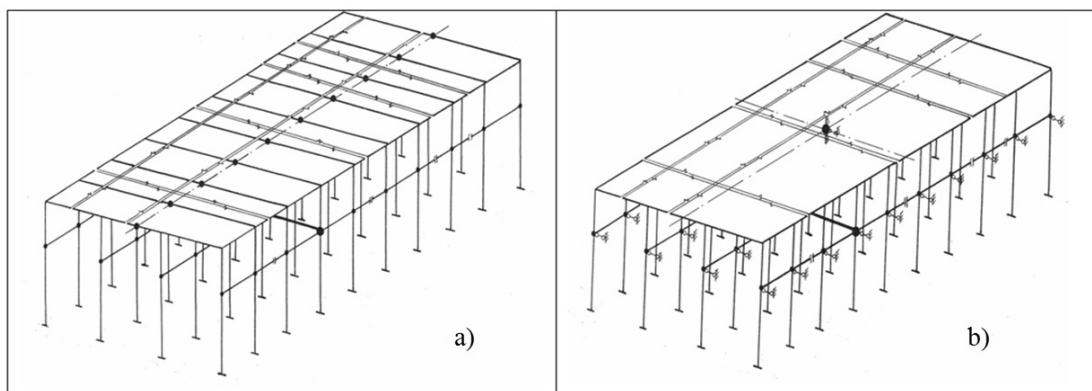


Figure 1. Generalized calculation scheme of a single-storey industrial building: a) with a compliant coating in its plane, b) with a rigid coating in its plane.

The design scheme in general form defines the geometry of an industrial facility, including n longitudinal rows of columns and p transverse frames. In the cross-sections of the transverse frames there are constructed with bridge cranes. The masses of crane and brake structures, constructed with bridge cranes, parts of columns and wall fences are concentrated in the level of crane structures. The masses in the level of crane structures are determined by the weight of the structures and the time load. They are concentrated between two horizontal planes, passing in the middle of the heights of the crane and crane parts of the columns. Points of intersection of the frames and the longitudinal axis of the coating, columns and brake structures are taken for the calculated points. Each calculated point of the beam-column system receives one degree of freedom – horizontal displacement in the plane of the transverse frame [24], and on the cover two degrees – the horizontal displacement in the same plane and the angle of rotation in the plane of the coating.

Taking as a basis presented generalized calculation schemes, considered various options for building and ways to influence the implementation of such structural elements of the framework, such as: brake system designs; transverse end diaphragm; links imposed on the disk cover. The results of the research on the influence of crane equipment to the building frame work [25] made valid conclusions that the crane bridge is a component of the lateral frame. Redistributing the loads between opposite rows of columns, the bridge crane is taken into account as an absolutely rigid link in the level of the upper belt of the crane beams in the cross-section of the transverse frame.

According to the results to identify the most significant factors determining the calculation model of an industrial building equipped with overhead cranes, built a conceptual study scheme of its stress-strain state (Figure 2). It regulates the sequence of actions of the performer, starting with the organization of the collection of data on the object of the survey, until the deadlines for reaching the limit states in the work of its structural elements are established.

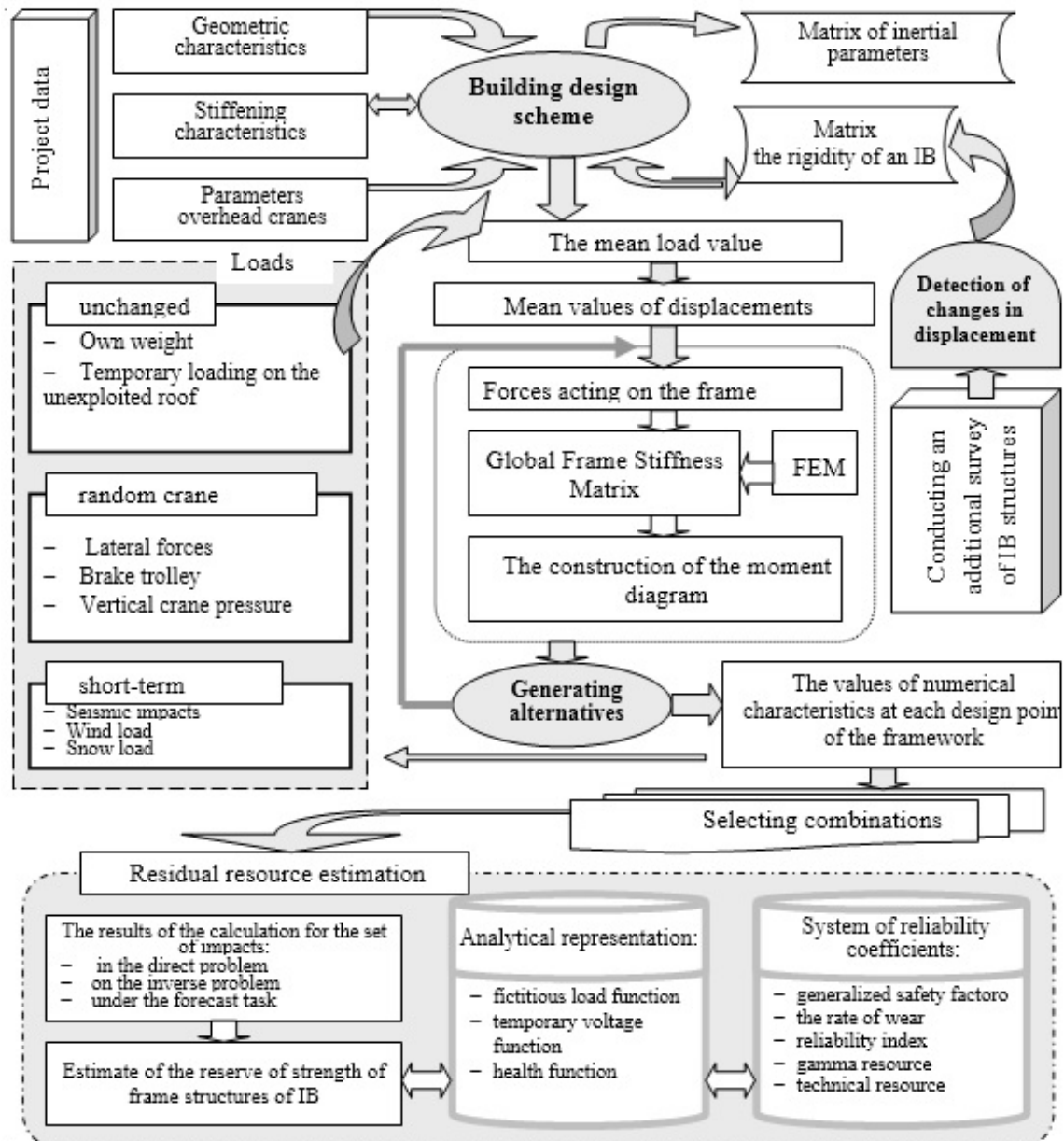


Figure 2. Scheme of an integrated approach to the study of the stress-strain state of an industrial building.

The presented scheme assumes on the part of the performer the wide variation in the formation of the loading of the design scheme of the object of investigation. However, as the most unfavorable combination of disturbing influences on the frame of a building, the authors justified accept a combined, including:

- constant loads from the own weight of the enclosing and load-bearing frame structures;

Zolina, T.V., Sadchikov, P.N. Residual resource of a one-storey steel frame industrial building constructed with bridge cranes. Magazine of Civil Engineering. 2018. 84(8). Pp. 150–161. doi: 10.18720/MCE.84.15.

- vertical pressure from two closely spaced constructed with bridge cranes;
- lateral force when moving with a skew of one overhead crane, the highest carrying capacity;
- snow load;
- wind load.

This combination is formed both with the participation and absence of a short-term component of the generalized load presented in the form of a seismic action [15, 26–28].

Carrying out calculations for assessing the reliability and durability of the structure of the building frame is made possible through the use of the limit state method. The algorithm for processing the information obtained is based on an estimate of the strength reserve for the structure of the building frame \tilde{S} , determined by the difference between their bearing capacity \tilde{R}_S and the highest value of the generalized load \tilde{F} , the mathematical expectation of which is found by the formula:

$$m_{\tilde{S}} = m_{\tilde{R}_S} - m_{\tilde{F}}. \quad (1)$$

Value $m_{\tilde{R}_S}$ is represented in the form of the average value of the standard resistance of the frame by the known maximum permissible value of the standard resistance \bar{R}_{Sn} at a given level of significance α

$$m_{\tilde{R}_S} = \frac{\bar{R}_{Sn}}{1 - t_{\alpha} f_s}, \quad (2)$$

where f_s – coefficient of variation of the strength properties of the material of the structure.

The mathematical expectation of the random value of the load factor $m_{\tilde{F}}$ is represented as a sum of all stresses from the action of both static and dynamic loads considered in various combinations.

At repeated carrying out of inspection of constructive elements of a building by the electric measuring devices shifting's in concrete points of the accepted settlement scheme are fixed. The dynamics of changes in the obtained displacements characterizes the changes in the rigidity characteristics of the structure as a whole [29–32]. The stiffness matrix of the building from known displacements in the design points of the framework is determined by solving the inverse problem of structural mechanics using software and hardware [33, 34].

Having a corrected stiffness matrix taking into account the wear of the structures, and knowing the direction and magnitude of the acting load, the numerical characteristics of the bending moments and stresses are determined. The accumulated results obtained during the processing of the data of the conducted building surveys allow the generation of time series of stress dynamics at individual points in the calculation scheme. Correlating the levels of each of them, it is possible to construct the corresponding regression. The normalization of the analytical dependence of the generalized load on the time factor makes it possible to construct the function of a fictitious load $g(t)$. Then the time functions of the mathematical expectation of the generalized load at the individual points of the design scheme for a known value $m_{\tilde{F}}$ at the initial time t_0 take the form:

$$m_F(t) = m_{\tilde{F}(t_0)} g(t), \quad (3)$$

The values of the generalized safety factor, which assesses the risk factor for further exploitation of building structures at different times, are described by the function:

$$\xi(t) = \frac{m_{\tilde{R}_S}}{m_F(t)} \quad (4)$$

Taking into account the values of mathematical expectations of the bearing capacity of an industrial building (2) and the generalized load $m_F(t)$ (3), determine the rate of wear:

$$\bar{V}_S(t) = \frac{d}{dt} m_{\tilde{S}}(t), \quad (5)$$

Then, the health functions $S(t)$ and reliability index $\beta_S(t)$ taking into account the wear become:

$$S(t) = m_{\tilde{S}(t_0)} - t \bar{V}_S(t), \quad (6)$$

$$\beta_S(t) = \frac{m_{\tilde{S}(t_0)} - t \bar{V}_S(t)}{\sqrt{\sigma_{\tilde{R}_S}^2 - t^2 \sigma_{V_S}^2}}, \quad (7)$$

where $m_{\tilde{S}(t_0)}$ is the mathematical expectation of the reserve strength at the first inspection,

$$\sigma_{\tilde{R}_S} = m_{\tilde{R}_S} f_S \text{ is standard carrier capacity of construct,}$$

$$\sigma_{V_S} = \bar{V}_S f_{V_S} \text{ is standard wear rate, } f_{V_S} \text{ is wear rate coefficient of variation.}$$

Reliability index, which allows to evaluate the durability of a building and the maintenance of its operability before the onset of the limit state since the last survey, is a gamma resource. For a given confidence level of results, it is defined as:

$$T_\gamma(t_n) = \frac{2m_{\tilde{S}(t_0)} \bar{V}_S(t_n) - \sqrt{4m_{\tilde{S}(t_0)}^2 \bar{V}_S^2(t_n) - 4(\bar{V}_S^2 - \beta_S^2(t_n) \sigma_{V_S}^2) (m_{\tilde{S}(t_0)}^2 - \beta_S^2(t_n) \sigma_{m_{\tilde{S}}}^2)}}}{2(\bar{V}_S^2(t_n) - \beta_S^2(t_n) \sigma_{V_S}^2)}. \quad (8)$$

where t_n is the time interval from the commissioning of the facility until the last survey.

As a final indicator of the assessment of the total period of operation of the facility from the moment of construction to reaching the limit state, a technical resource is adopted:

$$T = t_n + T_\gamma(t_n). \quad (9)$$

A practice in which, based on the results of only one field test, conclusions are drawn about the magnitude of the wear rate, should be considered erroneous. In this case, the obtained calculated values of the strength reserve, corresponding to the stress-strain state at the time of the survey, are compared with similar design indicators. With such a formulation of the problem, the researcher initially comes to unreliable results, since the actual values of the displacements at fixed points of the frame under the action of a generalized load when the building is started may differ significantly from the calculated ones. It should be concluded that it is necessary to conduct at least two full field tests of the object being examined. Moreover, for greater reliability of the results obtained, the first of them should take place at the initial stage when the industrial building is commissioned.

3. Results and Discussion

The reliability of the results of the numerical implementation of the developed algorithm is ensured by good convergence with the experimental data obtained during surveys of industrial buildings of the "Red Barricades" ship hull and naval shipbuilding plant, the diesel ceremonial workshop of the Lenin shipbuilding and shiprepair plant, the main building of the "Promstroimaterialy" plant of reinforced concrete structures operating on the territory of the Astrakhan region of the Russian Federation.

As an example, we present an analysis of the results of calculating the building of the shipbuilding shop of the Astrakhan Marine Shipbuilding Plant. Its spatial design scheme corresponds to that presented in Figure 1(b), and is refined taking into account the factors that significantly affect the work of the framework [25, 35].

In the course of implementing the algorithm, three problems were solved successively: direct, inverse and predictive (Figure 3). Based on the results of measuring dynamic parameters during the first survey at the initial stage of building operation in 1986, the direct task of assessing the technical state of the facility was solved. Its formulation is aimed at determining the stress-strain state of an object at a particular time, starting from the initial data and the known patterns of its behavior. For determine them in the level of the crane beam

Zolina. T.V., Sadchikov. P.N. Residual resource of a one-storey steel frame industrial building constructed with bridge cranes. Magazine of Civil Engineering. 2018. 84(8). Pp. 150–161. doi: 10.18720/MCE.84.15.

and the cover, movements from the loads acting on the frame of the building are fixed. The initial data for solving direct problems: the geometric dimensions of buildings and its main load-bearing structures, complete information on the cranes used, external and internal loads, stiffness matrix and mass matrix. In 1996 the movements in the same control points were re-determined, which made it possible to implement the inverse problem algorithm. It boils down to the search for new values of stiffness characteristics when establishing the design points of the framework, in which there was a change in the displacements associated with a decrease in rigidity of the carcass after several years of operation. The received corrected matrix is used in further studies in solving problems of assessing the performance of structures under the influence of external influences. The forecast task is aimed at finding a time point when the frequency of the building's fluctuation will decrease by 10 % relative to the initial one. Algorithm for its solution allows to determine the time period for the object to reach a state that requires an unscheduled survey.

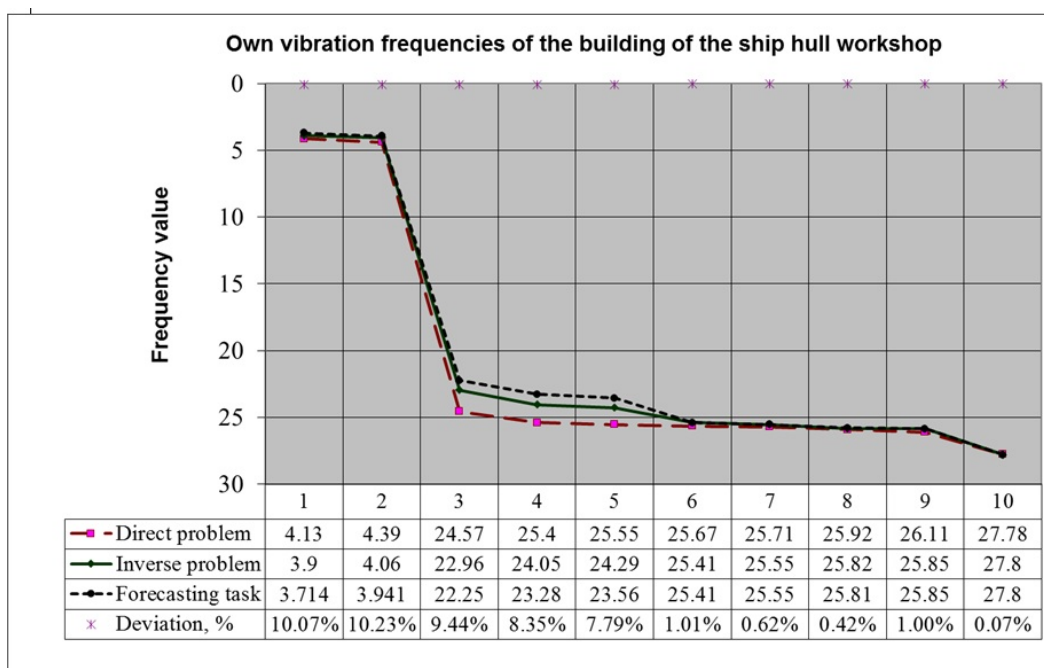


Figure 3. Dynamics of frequency distribution for the first 10 forms of vibration.

At the initial stage, the oscillation frequency in the first form was 4.15 sek^{-1} , and after 10 years of operation 3.90 sek^{-1} . The change in the dynamic characteristic was 5.5 %, which does not exceed 10 %, established by standards. With a 10% change in the initial frequency, its value in the first waveform will be 3.714 sek^{-1} .

The performed calculations in the probabilistic setting, taking into account the lower stiffness characteristics, can be used to assess the hazard of the action of the established loads after a specific service life of the object. During the analysis of the calculation results, the largest stress values were recorded at the monitored points of the most loaded transverse frame, in which the bridge crane functions. Realizing the proposed algorithm for assessing the reliability and durability of the object (1)–(9), it becomes possible to construct correlation dependencies of the considered indicators. The basis of the dependencies put the wear rate of the structural element and the planned number of t years of operation of the research object.

The values of the numerical characteristics of the generalized load, voltage, reserve, operability and reliability obtained during the processing of the results of the two surveys made it possible to establish a compliance with the time factor (Figures 4–8). The graphs are plotted for the worst values of the indices calculated for each of the monitored points of the model of the object with and without taking into account the seismic component. Rationing the analytical representation of the value of the generalized load made it possible to perform the construction of the corresponding function (Figure 4).

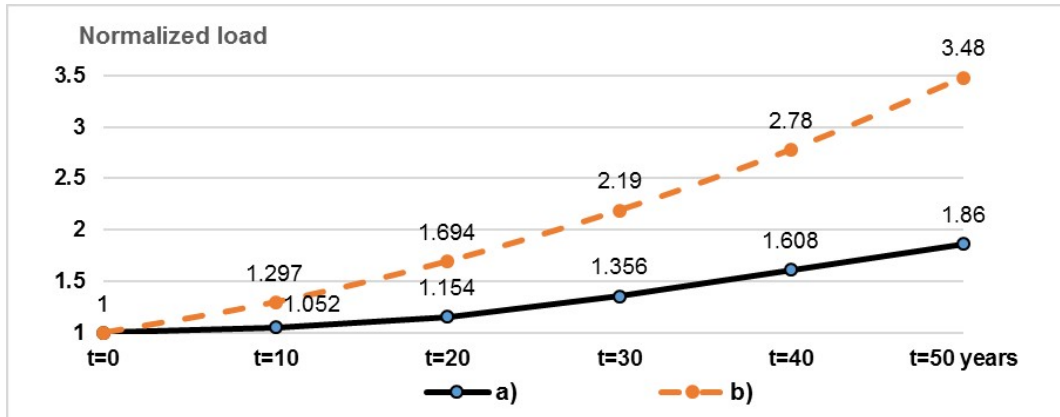


Figure 4. Fictitious load function: a) without seismic actions, b) taking into account seismic actions.

Fictitiousness lies in the fact that, in accordance with the statement of the problem, the load factor remains unchanged. Therefore, this function displays the magnitude of the effects applied to the framework with the initial stiffness characteristics that would allow to achieve the displacements predicted after 10, 20, ... years of operation.

Then the dynamics of the change in the maximum stresses at the node points of the design scheme during long-term operation of the shipbuilding shop can be traced by analyzing the behavior of the corresponding time function (Figure 5).

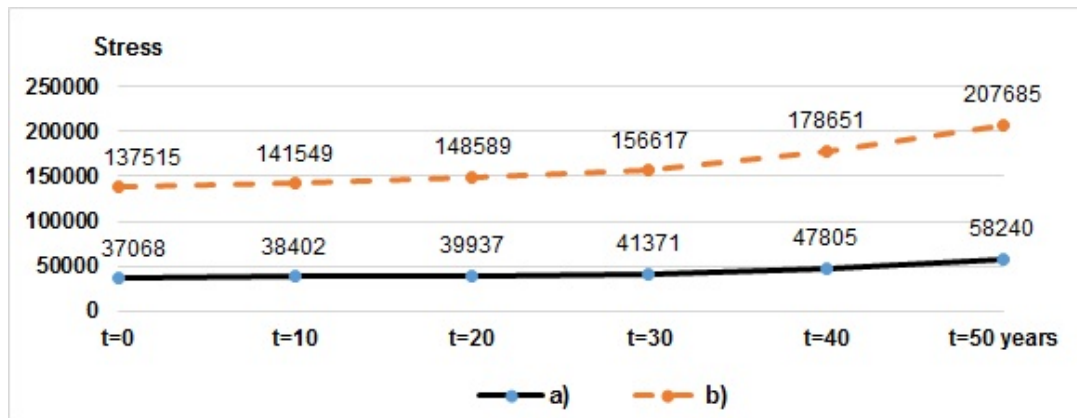


Figure 5. Time function of stress: a) without seismic actions, b) taking into account seismic actions.

The generalized safety factor, which assesses the risk factor for further exploitation of building structures at different times, is described by the function graphically presented in Figure 6.

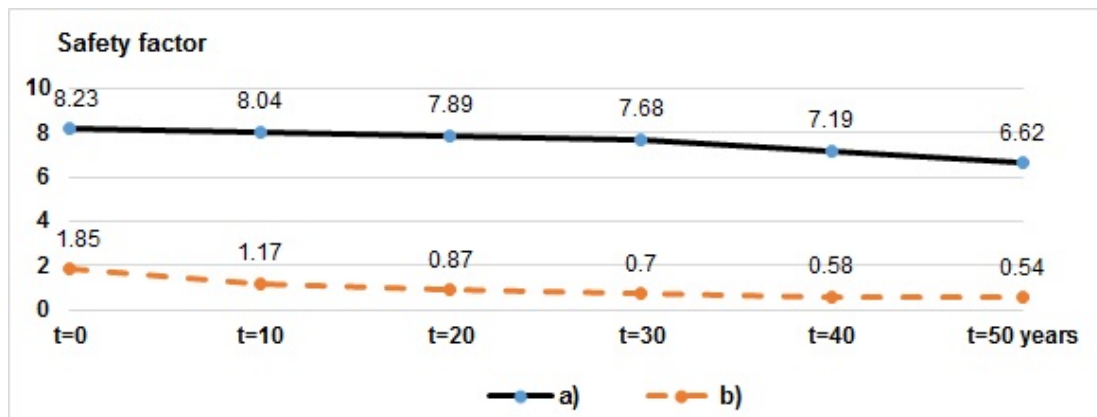


Figure 6. The function of the generalized safety factor: a) without seismic actions, b) taking into account seismic actions.

For the possibility of predicting the reliability indicators under consideration, proceeding from the difference in the sums of the mathematical expectations of all stresses from the action of the unchanged load factor based on the results of the two surveys, the average annual wear rate was determined. Taking into account this value, construction of operability functions (Figure 7) and reliability index (Figure 8), describing the reduction of the system's carrying capacity during the operation of the facility, was carried out.

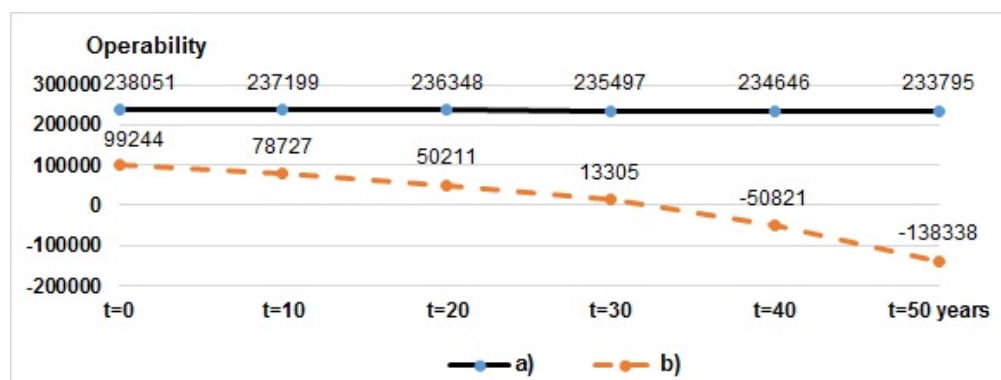


Figure 7. Operability function: a) without seismic actions, b) taking into account seismic actions.

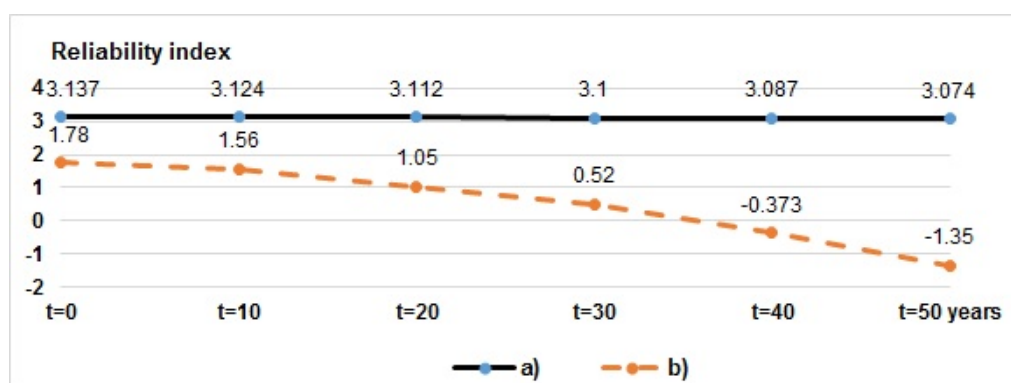


Figure 8. Reliability index function: a) without seismic actions, b) taking into account seismic actions.

Judging by the graphs of the functions shown in Figures 6, 7 and 8, the reliability of structural elements of the building frame is significantly reduced during operation. This fact is a consequence of a gradual decrease in horizontal rigidity and accumulation of damages in the mating interfaces of load-carrying structures of the frame.

Under the action of a combined combination of loads, taking into account seismic actions, significant increments in all the considered dynamic indices are fixed in the level of the completion of the columns, which is explained by the motions of the soil at the base of the frame. For the possibility of conducting a comparative analysis, Table 1 presents the average annual growth rates for each of them.

Table 1. Average annual growth rates of indicators.

| Indicators | Fictitious load | Temporary voltage function | The generalized safety factor | Operability function | Reliability index |
|-------------------------------------|-----------------|----------------------------|-------------------------------|----------------------|-------------------|
| without seismic actions | 1.76% | 1.04% | -0.38% | -0.04% | -0.04% |
| taking into account seismic actions | 4.96% | 0.98% | -1.31% | -4.65% | -3.53% |

Table 2 shows the results of an assessment of the safety of operation of the shop building according to the spectrum of the most unfavorable values of these indicators, determined for all nodes of the design scheme at the time of the second survey.

Table 2. Extreme values of indicators.

| Combined combination of loads | The generalized coefficient of reserve | Reliability index | Wear rate (kPa/year) | Residual resource (years) |
|-------------------------------------|--|-------------------|----------------------|---------------------------|
| without seismic actions | 8.04 | 3.12 | 97 | 17 |
| taking into account seismic actions | 1.17 | 1.56 | 4751 | 0.43 |

Analysis of the results of calculations for a specific research object allowed the following conclusions:

- the value of the reliability index is provided for all positions only under the action of the generalized load without taking into account seismic disturbances;
- the smallest generalized safety factor excluding the seismic action is 8.04, which is within the range of the recommended design practice [6; 9];
- the smallest generalized safety factor taking into account the action of seismic load drops to 1.17, due to the 50-fold increase in the wear rate structures;
- the predicted service life, after which the frequency of natural oscillations of the carcass structures will change by 10 %, decreases with taking into account the seismic load from 17 years to 0.43 years.

These parameters are the basis for deciding whether to implement structural measures to strengthen the framework.

4. Conclusions

Thus, the implementation of the developed mathematical apparatus allows not only to assess the technical condition of the building at the time of the survey, but also to predict the timing of the onset of a dangerous state on the basis of an analysis of changes in its dynamic characteristics. The forecasting of the dynamics of the stress-strain state changes allows planning the timing and direction of the repair of load-bearing structures in order to increase their service life.

The reliability of the obtained results is provided by taking into account the entire range of possible deviations of the input parameters of the calculation model and the loads with respect to the corresponding mathematical expectations.

The presented algorithm for estimating the residual life of an industrial building in operation allows:

1. to formalize the concept of a probabilistic approach to the study of changes in the stress-strain state of the framework of a production facility in the process of its operation, taking into account the variability of impacts through the sequential solution of direct, inverse and predictive problems;
2. to orient the formulation and search for the solution of the research tasks to assess the resource by analyzing the dynamics of the natural oscillation frequencies at the controlled points of the framework when constructing in the correlation approximation the functions of fictitious load and the performance of the building;
3. to carry out calculations to assess the reliability and durability of the steel frame structures of an industrial building using the limit state method, taking into account the random nature of the existing loads and the strength properties of building materials based on the results of surveys using a probabilistic model.

References

1. Patrikeyev, A.V., Salatov, Ye.K. Osnovy metodiki dinamicheskogo monitoringa deformatsionnykh kharakteristik zdaniy i sooruzheniy [Bases of a technique of dynamic monitoring of deformation characteristics of buildings and constructions]. Vestnik MGSU. 2013. No. 1. Pp. 133–138.
2. Ulybin, A.V., Vatin, N.I. Quality of visual inspection of buildings and constructions and technique of his performance. Construction of Unique Buildings and Structures. 2014. No. 10(25). Pp. 134–146. (rus)
3. Braila, N.V., Khazieva, K.L., Staritsyna, A.A. Results of technical inspection monitoring of the operation object. Magazine of Civil Engineering. 2017. 74(6). Pp. 70–77. DOI: 10.18720/MCE.74.7
4. Mushchanov, V.P., Orzhekhovskii, A.N., Zubenko, A.V., Fomenko S.A. Refined methods for calculating and designing engineering structures. Magazine of Civil Engineering. 2018. 78(2). Pp. 101–115. DOI: 10.18720/MCE.78.8
5. Brownjohn, J.M., Pan, T.C., Deng, X. Correlating dynamic characteristics from field measurements and numerical analysis of a high rise building. Earthquake Engineering & Structural Dynamics. 2000. No. 29(4). Pp. 523–543.
6. Danilov, A.I. Kontseptsiya upravleniya protsessom razrusheniya stroitel'nogo obyektu [The concept of controlling

Литература

1. Патрикеев А.В., Салатов Е.К. Основы методики динамического мониторинга деформационных характеристик зданий и сооружений // Вестник МГСУ, 2013. № 1. С. 133–138 [Электронный ресурс]. URL: <http://vestnikmgsu.ru/index.php/ru/archive/article/display/45/16>
2. Улыбин А.В., Ватин Н.И. Качество визуального обследования зданий и сооружений и методика его выполнения // Строительство уникальных зданий и сооружений. 2014. № 10(25). С. 134–146.
3. Брайла Н.В., Хазиева Л.Ф., Старицына А.А. Результаты мониторинга технического обследования объекта эксплуатации // Инженерно-строительный журнал. 2017. № 6(74). С. 70–77. DOI: 10.18720/MCE.74.7
4. Мушанов В.Ф., Оржеховский А.Н., Зубенко А.В., Фоменко С.А. Уточненные методы расчета и проектирования инженерных сооружений // Инженерно-строительный журнал. 2018. № 2(78). С. 101–115. DOI: 10.18720/MCE.78.8
5. Brownjohn J.M., Pan T.C., Deng X. Correlating dynamic characteristics from field measurements and numerical analysis of a high rise building // Earthquake Engineering & Structural Dynamics. 2000. № 29(4). Pp. 523–543.

Zolina, T.V., Sadchikov, P.N. Residual resource of a one-storey steel frame industrial building constructed with bridge cranes. Magazine of Civil Engineering. 2018. 84(8). Pp. 150–161. doi: 10.18720/MCE.84.15.

- the process of destruction of a building object]. *Industrial and Civil Engineering*. 2014. No. 8. Pp. 74–77. [Online]. URL: <http://www.pgs1923.ru/russian/2014/14i08r.htm>. (rus)
7. Kaewkulchai, G., Williamson, E.B. Beam element formulation and solution procedure for dynamic progressive collapse analysis. *Computers & Structures*. 2004. Vol. 82, issues 7-8. Pp. 639–651.
 8. Wang, L., Chu, J., Mao, W. A condition-based replacement and spare provisioning policy for deteriorating systems with uncertain deterioration to failure. *European Journal of Operational Research*. 2009. Vol. 194. Issue 1. Pp. 184–205.
 9. Bolotin, V.V. Stochastic models of fracture with applications to the reliability theory. In: *Structural safety and reliability*. Amsterdam, Oxford, New York: Elsevier, 1981. Pp. 31–56.
 10. Yu, H., Izzuddin, B.A., Zha, X.-X. Progressive collapse of steel-framed buildings: influence of modelling approach. *Advanced Steel Construction*. 2010. Vol. 6. No. 4. Pp. 932–948.
 11. Belostotsky, A.M., Akimov, P.A., Negrozov, O.A., Petryashev, N.O., Petryashev, S.O., Sherbina, S.V., Kalichava, D.K., Kaytukov, T.B. Adaptive finite-element models in structural health monitoring systems. *Magazine of Civil Engineering*. 2018. 78(2). Pp. 169–178. DOI: 10.18720/MCE.78.14
 12. Nethercot, D.A. Design of building structures to improve their resistance to progressive collapse. *The Twelfth East Asia-Pacific Conference on Structural Engineering and Construction*. Procedia Engineering. 2011. No. 14. Pp. 1–13.
 13. Hoef, N.P. Risk and Safety Considerations at Different Project Phases. *Safety, risk and reliability – trends in engineering*. International Conference. Malta. 2001. Pp. 1–8.
 14. Holicky, M., Ostlund, L. Vagueness of Serviceability Requirements. *Proceeding the International Conference «Design and Assessment of Building Structures»*. Prague. 1996. Vol. 2. Pp. 81–89.
 15. Chopra, A.K. *Dynamic of structures. Theory and Applications to Earthquake Engineering*. New Jersey: Prentice-Hall, 2006. 794 p.
 16. Rybakov, V.A., Ananeva, I.A., Rodicheva, A.O., Ogidan, O.T. Stress-strain state of composite reinforced concrete slab elements under fire activity. *Magazine of Civil Engineering*. 2017. 74(6). Pp. 161–174. DOI: 10.18720/MCE.74.13
 17. Alekseytsev, A.V., Kurchenko, N.S. Deformations of steel roof trusses under shock emergency action. *Magazine of Civil Engineering*. 2017. 73(5). Pp. 3–13. DOI: 10.18720/MCE.73.1
 18. Tushnina, O.A. Finite element analysis of crane secondary truss. *Magazine of Civil Engineering*. 2018. No. 1. Pp. 68–89. DOI: 10.18720/MCE.77.7
 19. Serpik, I.N., Alekseytsev, A.V. Optimization of flat steel frame and foundation posts system. *Magazine of Civil Engineering*. 2016. 61(1). Pp. 14–24. DOI: 10.5862/MCE.61.2
 20. Serpik, I.N., Alekseytsev, A.V., Balabin, P.Yu., Kurchenko, N.S. Flat rod systems: optimization with overall stability control. *Magazine of Civil Engineering*. 2017. 76(8). Pp. 181–192. DOI: 10.18720/MCE.76.16
 21. Alekseytsev, A.V. Evolutionary optimization of steel trusses with the nodal joints of rods. *Magazine of Civil Engineering*. 2013. 40(5). Pp. 28–37. DOI: 10.5862/MCE.40.3
 22. Rybakov, V.A., Al Ali, M., Panteleev, A.P., Fedotova, K.A., Smirnov, A.V. Bearing capacity of rafter systems made of steel thin-walled structures in attic roofs. *Magazine of Civil Engineering*. 2017. 76(8). Pp. 28–39. DOI: 10.18720/MCE.76.3
 23. Zolina, T.V., Sadchikov, P.N. Revisiting the Reliability Assessment of frame constructions of Industrial Building. *Applied Mechanics and Materials*. 2015. Vols. 752–753. Pp. 1218–1223.
 6. Данилов А.И. Концепция управления процессом разрушения строительного объекта // *Промышленное и гражданское строительство*. 2014. № 8. С. 74–77.
 7. Kaewkulchai G., Williamson E.B. Beam element formulation and solution procedure for dynamic progressive collapse analysis // *Computers & Structures*. 2004. Vol. 82. № 7-8. Pp. 639–651.
 8. Wang L., Chu J., Mao W. A condition-based replacement and spare provisioning policy for deteriorating systems with uncertain deterioration to failure // *European Journal of Operational Research*. 2009. Vol. 194. Issue 1. Pp. 184–205.
 9. Bolotin, V.V. Stochastic models of fracture with applications to the reliability theory. In: *Structural safety and reliability*. Amsterdam, Oxford, New York: Elsevier, 1981. Pp. 31–56.
 10. Yu H., Izzuddin B.A., Zha X.-X. Progressive collapse of steel-framed buildings: influence of modelling approach // *Advanced Steel Construction*. 2010. Vol. 6. No. 4. Pp. 932–948.
 11. Белостоцкий А.М., Акимов П.А., Негрозов О.А., Петряшев Н.О., Петряшев С.О., Щербина С.В., Каличава Д.К., Кайтуков Т.Б. Адаптивные конечноэлементные модели в системах мониторинга зданий и сооружений // *Инженерно-строительный журнал*. 2018. № 2(78). С. 169–178. DOI: 10.18720/MCE.78.14
 12. Nethercot D.A. Design of building structures to improve their resistance to progressive collapse // *The Twelfth East Asia-Pacific Conference on Structural Engineering and Construction*. Procedia Engineering. 2011. № 14. Pp. 1–13.
 13. Hoef, N.P. Risk and Safety Considerations at Different Project Phases // *Safety, risk and reliability – trends in engineering*. International Conference. Malta. 2001. Pp. 1–8.
 14. Holicky M., Ostlund L. Vagueness of Serviceability Requirements // *Proceeding the International Conference «Design and Assessment of Building Structures»*. Prague: 1996. Vol. 2. Pp. 81–89.
 15. Chopra A.K. *Dynamic of structures. Theory and Applications to Earthquake Engineering*. New Jersey: Prentice-Hall, 2006. 794 p.
 16. Рыбаков В.А., Ананьева И.А., Родичева А.О., Огидан О.Т. Напряженно-деформированное состояние фрагмента сталежелезобетонного перекрытия в условиях огневого воздействия // *Инженерно-строительный журнал*. 2017. № 6(74). С. 161–174. DOI: 10.18720/MCE.74.13
 17. Алексейцев А.В., Курченко Н.С. Деформации стальных стропильных ферм при ударных аварийных воздействиях // *Инженерно-строительный журнал*. 2017. № 5(73). С. 3–13. DOI: 10.18720/MCE.73.1
 18. Туснина О.А. Конечно-элементное моделирование и расчёт подкраново-подстропильной фермы // *Инженерно-строительный журнал*. 2018. № 1(77). С. 68–89. DOI: 10.18720/MCE.77.7
 19. Серпик И.Н., Алексейцев А.В. Оптимизация системы стальной плоской рамы и столбчатых фундаментов // *Инженерно-строительный журнал*. 2016. №1(61). С. 14–24. DOI: 10.5862/MCE.61.2
 20. Серпик И.Н., Алексейцев А.В., Балабин П.Ю., Курченко Н.С. Плоские стержневые системы: оптимизация с контролем общей устойчивости // *Инженерно-строительный журнал*. 2017. № 8(76). С. 181–192. DOI: 10.18720/MCE.76.16
 21. Алексейцев А.В. Эволюционная оптимизация стальных ферм с учетом узловых соединений стержней // *Инженерно-строительный журнал*. 2013. №5. С. 28–37. DOI: 10.5862/MCE.40.3
 22. Рыбаков В.А., Ал Али М., Пантелеев А.П., Федотова К.А., Смирнов А.В. Несущая способность стропильных систем из стальных тонкостенных конструкций в чердачных крышах // *Инженерно-строительный журнал*. 2017. № 8(76). С. 28–39. DOI: 10.18720/MCE.76.3
 23. Zolina T.V., Sadchikov P.N. Revisiting the Reliability Assessment of frame constructions of Industrial Building //

Золина Т.В., Садчиков П.Н. Остаточный ресурс стального каркаса одноэтажного промышленного здания с мостовыми кранами // *Инженерно-строительный журнал*. 2018. № 8(84). С. 150–161.

24. Tushina, O.A., Danilov, A.I. The stiffness of rigid joints of beam with hollow section column. Magazine of Civil Engineering. 2016. 64(4). Pp. 40–51. DOI: 10.5862/MCE.64.4
25. Zolina, T.V., Sadchikov, P.N. Modelirovanie raboty konstruksiy promyshlennogo zdaniya s uchetom izmeneniya zhestkosti v protsesse ekspluatatsii [Modeling the work of industrial building structures taking into account changes in rigidity during operation]. Vestnik MGSU. 2012. No. 10. Pp. 69–76.
26. Lin, Y.K., Shih, T.Y. Column response to horizontal and vertical earthquakes. Journal of Engineering Mechanics Division. ASCE. 1980. vol. 106. No EM-6. Pp. 1099–1109.
27. Sosnin, A.V. Ob utochnenii koeffitsiyenta dopuskayemykh povrezhdeniy K1 i yego soglasovannosti s kontseptsiyey reduksii seysmicheskikh sil v postanovke spektralnogo metoda (v poryadke obsuzhdeniya) [About specification of seismic force reduction factor K1 and its coherence with response modification technique to the spectrum method formulation (in order of discussion)]. Vestnik grazhdanskikh inzhenerov. 2017. No. 1(60). Pp. 92–114. (rus)
28. Albert, Y.U., Dolgaya, A.A., Ivanova, T.V., Nesterova, O.P., Uzdin, A.M., Guan, J., Ivashintzov, D.A., Voronkov, O.K., Shtilman, S.G., Shulman, V.B., Khrapkov, A.A. Seismic input models for tuned mass damper designing. Magazine of Civil Engineering. 2017. 76(8). Pp. 98–105. DOI: 10.18720/MCE.76.9
29. Perelmuter, A.V., Kabantsev, O.V. Accounting for the elements stiffness change in the course of erection and operation. Magazine of Civil Engineering. 2015. 53(1). Pp. 6–14. DOI: 10.5862/MCE.53.1
30. Zolina, T.V., Sadchikov, P.N. Modelirovanie izmeneniy matritsy zhestkosti promyshlennogo zdaniya v protsesse ego ekspluatatsii [Modeling of changes in the stiffness matrix of an industrial building during its operation]. Industrial and Civil Engineering. 2012. No. 8. Pp. 19–20. (rus)
31. Eremin, K.I., Shulga, S.N. Napryazhenno-deformirovannoe sostoyaniye uzlov podkranovo-podstropilnykh ferm [Stressed-strained state of crane-rafter trusses joints]. Industrial and Civil Engineering. 2012. No. 7. Pp. 52–55. (rus)
32. Novikov, P.I. Identifying Real Stiffness Properties of Structural Elements of Adapted Finite-Element Models of Buildings and Structures. Part 1: Problem Setting. Applied Mechanics and Materials. 2014. No. 670-671. Pp. 732–735.
33. Zolina, T.V., Sadchikov, P.N. Evaluation of software realization algorithms of industrial building operation life. Advances in Energy, Environment and Materials Science Proceedings of the International Conference on Energy, Environment and Materials Science (EEMS 2015). CRC Press. 2016. Pp. 777–780.
34. Krinitsky, E.V. Information model of the building (BIM). Magazine of Civil Engineering. No. 2. 2010. Pp. 16–18.
35. Zolina, T.V. Poryadok provedeniya obsledovaniy zdaniya s tselyu posleduyushchey otsenki yego ostatochnogo resursa [Order of carrying out inspections of the building for the purpose of the subsequent assessment of his residual resource]. Vestnik MGSU. 2014. No. 11. Pp. 98–108.)
- Applied Mechanics and Materials. 2015. Vols. 752-753. Pp. 1218–1223.
24. Туснина О.А., Данилов А.И. Жесткость рамных узлов сопряжения ригеля с колонной коробчатого сечения // Инженерно-строительный журнал. 2016. № 4(64). С. 40–51. DOI: 10.5862/MCE.64.4
25. Золина Т.В., Садчиков П.Н. Моделирование работы конструкций промышленного здания с учетом изменения жесткости в процессе эксплуатации // Вестник МГСУ. 2012. № 10. С. 69–76.
26. Lin, Y.K. Column response to horizontal and vertical earthquakes / Y.K. Lin, T.Y. Shih // Journal of Engineering Mechanics Division. ASCE. 1980. Vol. 106. No EM-6. Pp. 1099–1109.
27. Соснин А.В. Об уточнении коэффициента допускаемых повреждений K1 и его согласованности с концепцией редукции сейсмических сил в постановке спектрального метода (в порядке обсуждения) // Вестник гражданских инженеров. 2017. № 1(60). С. 92–114.
28. Альберт И.У., Долгая А.А., Иванова Т.В., Нестерова О.П., Уздин А.М., Гуань Ю., Ивашинцов Д.А., Воронков О.К., Штильман В.Б., Шульман С.Г., Храпов А.А. Расчетное сейсмическое воздействие для сооружения с динамическим гасителем колебаний // Инженерно-строительный журнал. 2017. № 8(76). С. 98–105. DOI: 10.18720/MCE.76.9
29. Перельмутер А.В., Кабанцев О.В. Учет изменения жесткостей элементов в процессе монтажа и эксплуатации // Инженерно-строительный журнал. 2015. №1. С. 6–14. DOI: 10.5862/MCE.53.1
30. Золина Т.В., Садчиков П.Н. Моделирование изменений матрицы жесткости промышленного здания в процессе его эксплуатации // Промышленное и гражданское строительство. 2012. № 8. С. 19–20.
31. Еремин К.И., Шульга С.Н. Напряженно-деформированное состояние узлов подкраново-подстропильных ферм // Промышленное и гражданское строительство. 2012. № 7. С. 52–55.
32. Novikov P.I. Identifying Real Stiffness Properties of Structural Elements of Adapted Finite-Element Models of Buildings and Structures – Part 1: Problem Setting // Applied Mechanics and Materials. 2014. № 670-671. Pp. 732–735.
33. Zolina T.V., Sadchikov P.N. Evaluation of software realization algorithms of industrial building operation life // Advances in Energy, Environment and Materials Science Proceedings of the International Conference on Energy, Environment and Materials Science (EEMS 2015). CRC Press. 2016. Pp. 777–780.
34. Криницкий Е.В. Информационная модель здания (BIM) // Инженерно-строительный журнал. №2. 2010. С. 16–18.
35. Золина Т.В. Порядок проведения обследований здания с целью последующей оценки его остаточного ресурса // Вестник МГСУ. 2014. № 11. С. 98–108.

Tatiana Zolina,
+7(905)3645858; zolintv@yandex.ru

Pavel Sadchikov*,
+7(902)1119067; pn_sadchikov@mail.ru

Татьяна Владимировна Золина,
+7(905)3645858; эл. почта: zolintv@yandex.ru

Павел Николаевич Садчиков*,
+7(902)1119067; эл. почта:
pn_sadchikov@mail.ru

© Zolina T.V., Sadchikov P.N., 2018

doi: 10.18720/MCE.84.16

Compatibility of precast heavy and monolithic lightweight concretes deforming

Совместность деформирования сборного тяжёлого и монолитного лёгкого бетонов

A.A. Koyankin*,
V.M. Mitasov,

*Novosibirsk state University of architecture
and construction, Novosibirsk-8, Russia*

T.A. Tskhay,

Siberian Federal University, Krasnoyarsk, Russia

Канд. техн. наук, доцент А.А. Коянкин*,
д-р техн. наук, профессор В.М. Митасов,
*Новосибирский государственный
архитектурно-строительный университет,
г. Новосибирск-8, Россия*

магистрант Т.А. Цхай,

*Сибирский федеральный университет,
г. Красноярск, Россия*

Key words: reinforced concrete structures; precast and monolithic structures; lightweight concrete; connection of monolithic and precast concrete; keyed connection of concretes; shear strength

Ключевые слова: железобетонные конструкции; сборно-монолитные конструкции; лёгкий бетон; сопряжение монолитного и сборного бетонов; шпоночное сопряжение бетонов; сопротивление на сдвиг

Abstract. Safe performance of connecting joint applied to different concrete ages is highly important when joints is placed in composite structures since joint is involved in mutual deformation of precast and monolithic concretes. This experimental study was carried out to determine how type of joint influence on it bearing capacity when perceiving shearing forces. The tests were carried out on a specially manufactured horizontal bench and a vertical press, which provided a shear force in the samples of different ages and with different concrete strength (light monolithic and heavy precast concretes). The following options of the joint were considered: a smooth surface, where the connection is done only by the forces of adhesion and friction; a joint with keys, the spacing of which varied; and a joint with the use of cross reinforcement. This paper determines nuances of the load-bearing capacity exhaustion in a composite structure at shear depending on the type of joint of lightweight monolithic and heavy precast concrete. A comparative analysis of the results obtained in the experimental studies and the data of previous studies has been carried out. The highest bearing capacity under shearing loads was determined in the joint with the cross reinforcement. Moreover, it was noted that keyed connection of concretes let guarantee sufficiently safe performance of connection.

Аннотация. Надёжная работа шва сопряжения бетонов разного возраста наиболее важна, когда он расположен в сборно-монолитных конструкциях, поскольку шов обеспечивает совместное деформирование сборного и монолитного бетонов. С целью изучения влияния вида шва сопряжения на его несущую способность при восприятии сдвигающих усилий авторами проведены экспериментальные исследования. Исследования были выполнены на специально изготовленном горизонтальном стенде и вертикальном прессе, которые обеспечивали создание сдвигающего усилия в образцах с разновозрастными и разно прочными бетонами (лёгкий монолитный и тяжёлый сборный). Были рассмотрены следующие варианты устройства шва сопряжения: гладкая поверхность, где сопряжение обеспечивается только за счёт сил адгезии и трения; шов сопряжения выполняемый со шпонками, шаг которых варьировался; сопряжение, выполняемое с использованием поперечной арматуры. Определены нюансы характера истощения несущей способности сборно-монолитной конструкции при сдвиге в зависимости от вида шва сопряжения лёгкого монолитного и тяжёлого сборного стержня. Проведён сопоставительный анализ полученных при экспериментальных исследованиях результатов с данными ранее выполненных исследований. Наибольшую несущую способность на восприятие сдвигающего усилия показал шов сопряжения, усиленный поперечной арматурой. Вместе с тем, шпоночное сопряжение также позволяет обеспечить достаточную надёжность сопряжения.

1. Introduction

At present, precast and monolithic building is becoming more and more popular, which is manifested by a significant increase in a specific share of this type of construction against the background of the total mass of erected buildings. Such a phenomenon is quite logical and expected because the precast-monolithic frame of a building is deemed as a more flexible construction system. Indeed, the disadvantages, which are well-known and sometimes are quite a challenge, of separately precast or monolithic building systems can be solved easily enough by erecting buildings and structures made from precast and monolithic reinforced concrete. An intensive growth of popularity of such system inevitably led to the need of developing optimal constructive precast and monolithic frameworks and a simultaneous interest in obtaining new experimental data which take into account all the innovations proposed by modern builders. Many researchers conducted various surveys to study the features of the stress-strain behaviour of precast and monolithic structures, moreover, such studies were carried out either on buildings or fragments of buildings and considered the features of deformation of a building as a whole [1, 10, 11, 21, 23–27], and on its individual structural elements [2–4, 9, 12, 13, 20, 29]. In particular, the authors in [1, 9] carried out experimental studies on full-scale samples of the composite monolithic frame of BelNIIS (Belarusian Scientific and Research Institute for Construction) suggested by the Belarusian builders. Moreover, in [9], they tested a single frame floor member which showed its sufficient reliability. When studying the precast and monolithic structures and the structures reinforced by extending their sections with monolithic concrete, in [2], they took into account the loading background of the precast (or reinforced) part of the structure, which is an important factor for the above structures. The influence of the factor of the sequence of assembling and loading the precast-monolithic structure was analysed in the course of numerical studies in [27], and the performance of the precast-monolithic structure exposed to elevated temperatures was studied by the author of [13]. Besides, engineers and scientists are actively developing more and more efficient building systems of precast and monolithic framed buildings [1, 10, 14–17, 19, 20, 28]. The engineering solutions suggesting using lightweight concrete [18, 27] seem to be interesting, because it enables reducing the mass of the structure significantly, and hence, the constant loads. The authors of this paper also carried out surveys (experimental, numerical) to study the stress-strain behaviour of precast and monolithic structures [5, 6, 27], and in addition, proposed various constructive solutions to improve them [7, 8].

After the performed surveys of structures with a precast and monolithic frame, as well as having studied the practices of this type of construction, we concluded that there are relatively few surveys devoted to joint deformation of precast heavy and monolithic lightweight concretes. At the same time, such combination of concretes is quite promising for arranging floors where a precast part of a slab acts as a form until monolithic concrete develops the necessary strength, and after maturing both the parts jointly begin taking the forces caused by external loads. Based on the above, we conceived the purpose of this research as identifying the features of joint deformation of precast heavy and monolithic lightweight concretes depending on the type of their connection surface.

2. Methods

The models were made and tested in two stages to achieve this stated goal: first, precast parts from the heavy concrete of grade B25 were made, which were then poured with lightweight concrete (constructional LECA concrete of grade B12.5). The final overall dimensions were 300×100×140 (h) mm. The samples were divided into 4 series (P1 ... P6), with 5 pieces of identical samples in each series (Figure 1), according to the constructive design of the joint of precast and monolithic concretes:

- P1 is a smooth surface connection;
- P2 is a surface with two keys (the key has a width of 30 mm, depth 10 mm), which corresponds to 150 mm spacing;
- P3 is a surface with 3 keys (the width of 30 mm, the depth of 10 mm), which corresponds to 100 mm spacing;
- P4 is a connection surface with 2 rows of rebars ($\varnothing 6A240$), which corresponds to 150 mm spacing;
- P5 is a connection surface with 3 rows of rebars ($\varnothing 6A240$), 100 mm spacing;
- P6 is a connection surface with 5 rows of rebars ($\varnothing 6A240$), 50 mm spacing.

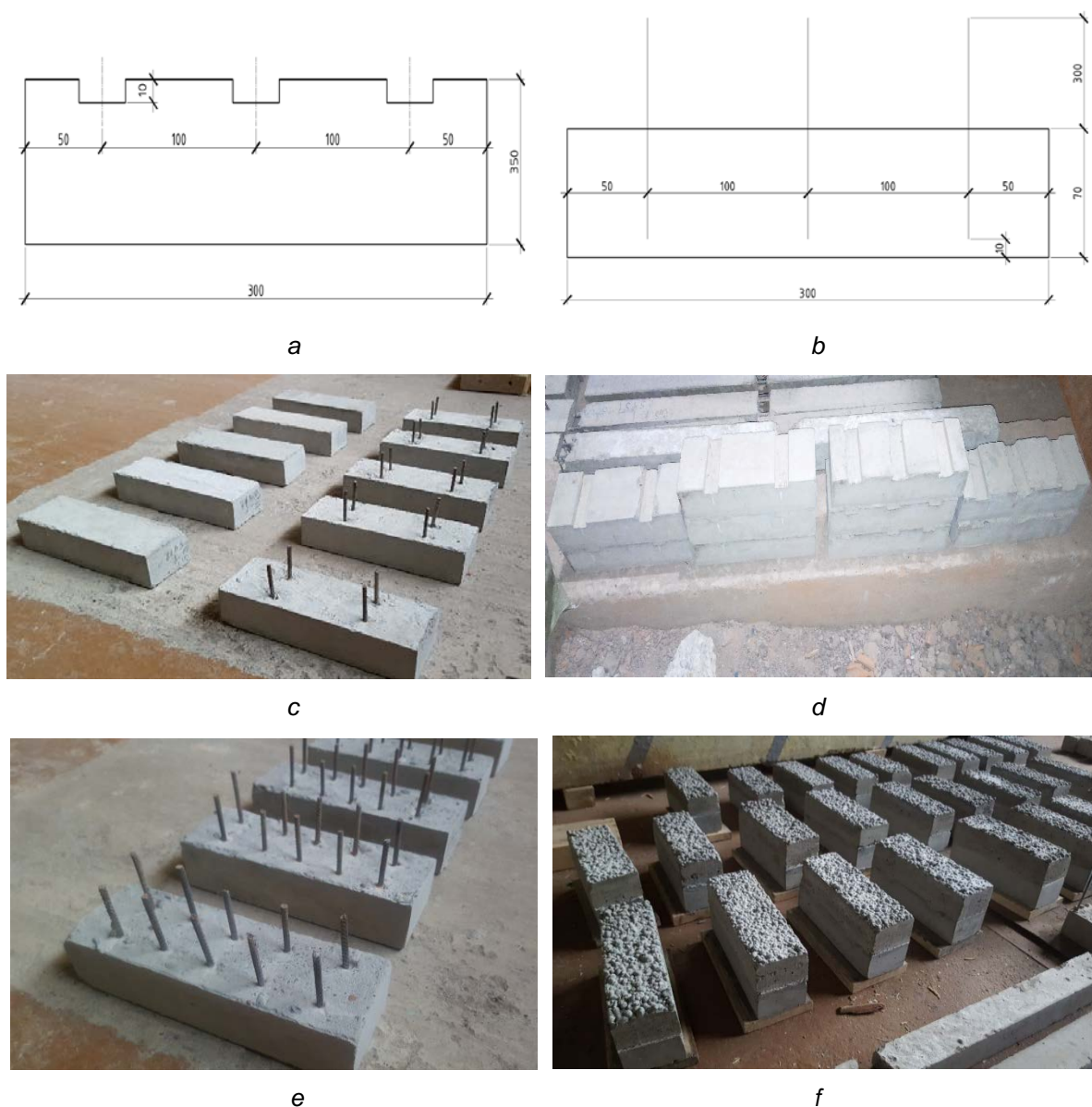
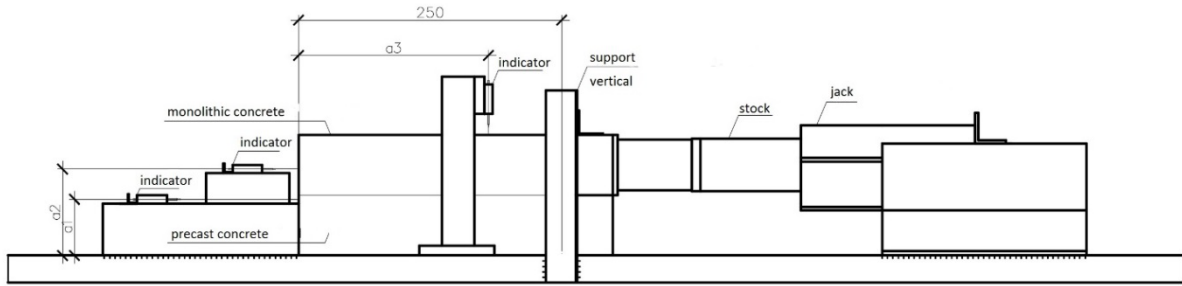


Figure 1. Experimental samples: a, b – drawings of the assembly parts of P3, and P5 samples; c, d – general view of the assembly parts of the samples of P1, P4 and P2, P3 series; e – general view of the assembly parts of the samples of P6 series; f – general view of the ready samples.

The tests of the samples for P1...P4 were carried out on an experimental bench which enables creating a shearing force of 150 kN (Figure 2), where a precast part laid against a rigid stop of the bench, and the force was applied horizontally to a monolithic section of the sample. Deformations and displacements were recorded by means of horizontally and vertically positioned dial indicators (Dial Indicator 10). The P5 and P6 samples were tested on a powered vertical press (Figure 2).

3. Results and Discussion

Getting ahead of the detailed analysis, we ascertain that in all the experimental samples there was no mutual move of monolithic and precast concretes observed before the moment of fracturing. Also until this moment, there was no local fracturing of separate sections of precast and monolithic concretes (cracks, crushes, splitting, etc.). At the time of exhaustion of the load-bearing capacity, an abrupt sudden fracturing of the samples occurred without any noticeable increase in deformations at the previous phases. At the same time, the patterns of the samples failure we observed were different and depended on the type of jointing.



a



b



c

Figure 2. Experimental tests: a – a layout of the horizontal experimental bench; b – a photo of the horizontal experimental bench; c – a photo of the powered vertical press.

A more detailed analysis of the research results shows that a uniform pattern of fracturing is observed in the P1 samples, namely, a sudden shear of the monolithic concrete section relatively to the precast one along the smooth joint (Figure 3). However, we did not observe any significant damage to the integrity of individual sections of the samples (at best, we noted splitting of small fragments of precast or monolithic concretes at the time of failure, and partial minor shearing of monolithic concrete). The experimental samples fractured at the following load values: P1-1 – 49.2 kN; P1-2 – 34.5 kN; P1-3 – 29.5 kN; P1-4 – 49.2 kN; P1-5 – 64.0 kN. The average value of the breaking load was 45.28 kN.



a



b



c



d

Figure 3. The photos of fracture of the P1 series samples: a, b, c, d – respectively, the photos of the fractured samples P1-1, P1-2, P1-3 and P1-4.

The fracture patterns which were obtained during the tests of the P1 samples clearly indicate that in the case of using a smooth joint of two concretes of different age, the sections mutually move due to the shear forces exceeding the adhesion and friction forces. Thus, it is absolutely obvious that it is not enough to confine oneself to these forces to ensure a joint deformation, but it is necessary to provide additional technical solutions capable of ensuring a joint load resistance by precast and monolithic concretes.

The fracture pattern is more complex in the samples of P2 series. Due to the use of keys, the joint's load-bearing capacity increased because the existing bearing capacity of the forces of adhesion and friction in the smooth joint was added by the strength of the keyed joint, so there was no clear fracturing along the joint. We observed both exhaustion of the bearing capacity along the smooth part of the joint, a shift in the monolithic part, cutoff of the keys and partial fracture of the individual sections of the P2 series samples. In particular, the pattern of load-bearing capacity exhaustion basically looks as follows: on the part of the element, the shear occurs in the body of the monolithic section (approximately at the level of 0.5 ... 1.0 cm from the joint), while in the smooth joint, a shear along the joint surface or cleavage of precast concrete with cutoff of its keys in the rest of the joint (Figure 4). The ultimate load in the samples of P2 series was: P2-1 – 51.7 kN; P2-2 – 61.5 kN; P2-3 – 71.4 kN; P2-4 – 56.6 kN; P2-5 – 83.7 kN. The average value of the breaking load was 64.98 kN.

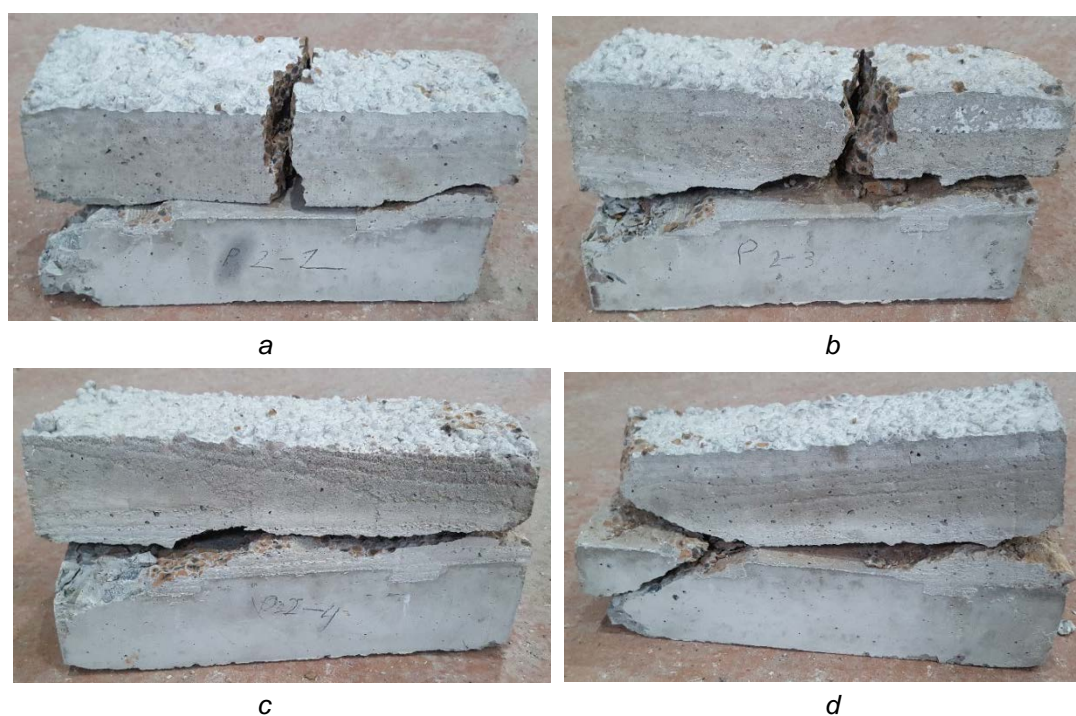


Figure 4. The fracture photos of the P2 series samples: a, b, c, d – respectively, the photos of the fractured samples P2-2, P2-3, P2-4 and P2-5.

We noted a greater precision of the testing results for the samples with two keys in contrast to the samples with a smooth joint. More specifically, the range of divergence in the ultimate loads is 53.8 % in regard to the maximum value of the force in the P1 samples, while in the P2 samples this divergence amounts to 38.2 %. This signifies that the adhesion and friction factor is scantily predictable, and as a result of the inclusion of a more stable (in terms of providing the shear capacity) technical solution (application of the keys), the specific share of instability reduces, resulting in a greater predictability of the joint performance. In addition, the average ultimate load of the P2 samples exceeded the P1 samples by 43.5 %, which also indicates a significant positive effect of the keys on the bearing capacity of the contact joint.

The testing results for the P3 samples showed that a more dense spacing between the keys makes it possible to significantly increase the load-bearing capacity of the joint of monolithic concrete with precast one. In particular, the ultimate loads ranged from 71.4 kN to 150 kN with an average one of 99.1 kN. At the same time, the load-bearing capacity exhausted due to reaching of the limit of the ultimate compression strength of monolithic lightweight concrete with the joint remained integral (no mutual movement of the samples sections relative to each other was recorded). Thus, it can be summarized that if a certain spacing between the keys is observed, it is possible to secure the required load-bearing capacity, which can guarantee joint deformation of concretes of different age (Figure 5).

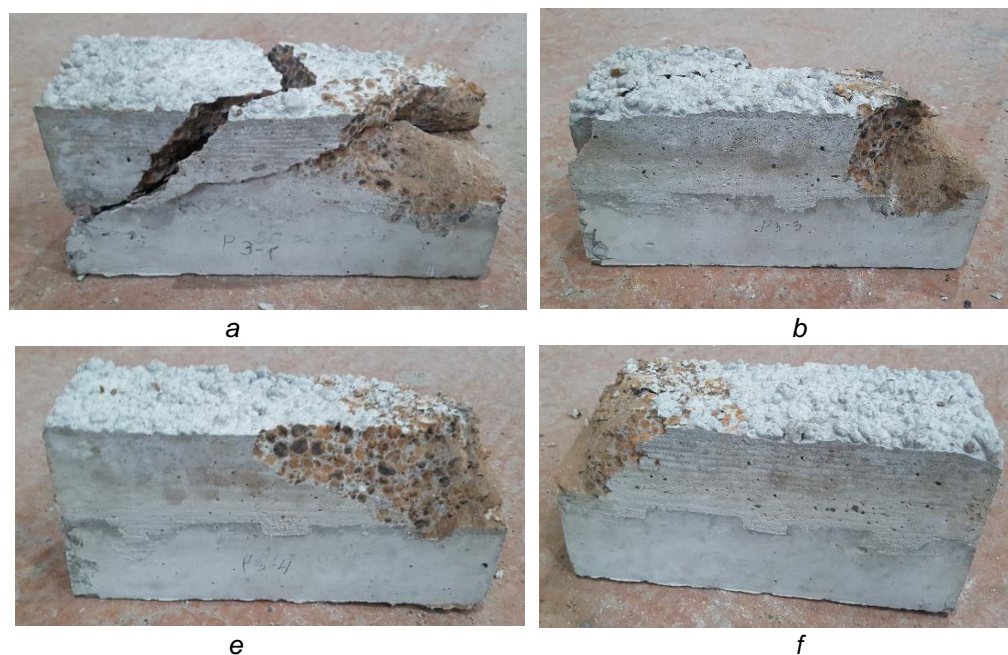


Figure 5. The fracture photos of the P3 series samples: a, b, c, d – respectively, the photos of the fractured samples P3-1, P3-3, P3-4 and P3-5.

Testing the samples with three keys resulted in a precision similar to that of the samples with two keys, which, unlike when using the smooth one, also clearly indicates a more stable joint deformation in the keyed joint. The average ultimate load of P3 samples 2 times exceeded the value of the same load in P1.

The fracture pattern in the P4 samples with transverse reinforcement rebars spaced at intervals of 150 mm is comparable with the general fracturing pattern for the P2 samples, i.e. we see some balancing between the joint's shear strength and compression strength of the materials (precast and monolithic concretes), and, at the same time, there is no clear fracturing along the joint only. However, unlike in P2 series, the P4 samples showed exhaustion of load-bearing capacity resulted from both a shear along the smooth part of the joint and a shear inside the body of the monolithic part with a partial breaking of the separate sections of the samples. Notice that the fracture load here is higher and lies in the range from 81.2 kN to 103.4 kN (Figure 6), with the average of 94.4 kN, which is 2 times higher than the similar value in those samples without any keys and rebars.

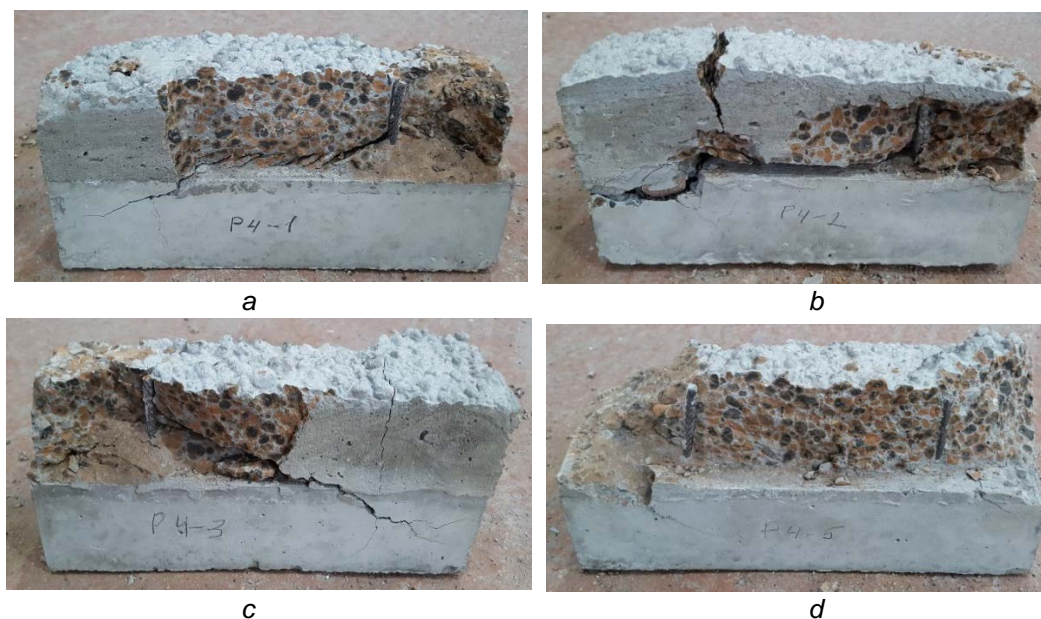


Figure 6. The fracture photos of the P4 series samples: a, b, c, d – respectively, the photos of the fractured samples P4-1, P4-2, P4-3 and P4-5.

When testing the samples with two rows of rebars, we noted that the difference between the maximum and minimum results did not exceed 22 %, which manifests a sufficient stability of these results in contrast to the connection at the expense of the adhesion and friction forces, and even compared to the elements where concrete keys were embedded as a reliable joint. It should be pointed out additionally that any noticeable damage (such as rupture, shear or any movements) of the rebars was not detected; we observed only a small incline of the traverse rebars, which is quite natural.

A more dense spacing of the transverse reinforcement bars in the P5 and P6 series samples allowed ensuring the compatibility of deformation of monolithic light and precast heavy concretes, which is manifested in their destruction pattern, precisely, the destruction of monolithic concrete as a compressed element from transverse stretching strains. It should be noted additionally that if previously in the P1 ... P4 samples, we occasionally observed a boundary state in the fracture pattern between the destruction of monolithic concrete and the mutual displacement of parts, but in case of the P5 and P6 samples, a clear picture of their fracture due to exhaustion of the carrying compression capacity of monolithic light (less durable) concrete.

At the same time, we noted an increase in the carrying capacity of samples with transverse reinforcement (series P4 ... P6) on resisting the compression load as the number of rebars increase in the reinforcement, which drove us to the conclusion that traverse reinforcement had a positive effect on the strength of the compressed concrete. This is explained by the fact that the reinforcement bars, located across the compressive load applied, act as an indirect reinforcement and quite effectively perceive the transverse stretching strains occurring in the compressed concrete.

The bearing capacity of the P5 samples was exhausted within the range of loads from 112.5 kN to 128.0 kN (124.6 kN average) due to the fracturing of monolithic concrete; at the same time, there were no significant signs of fracturing, except for small local chips in the precast part (Figure 7). The transverse reinforcement bars slightly deflected. We observe a significant 3-fold exceedance of the average ultimate fracturing value over the samples of P1 series.

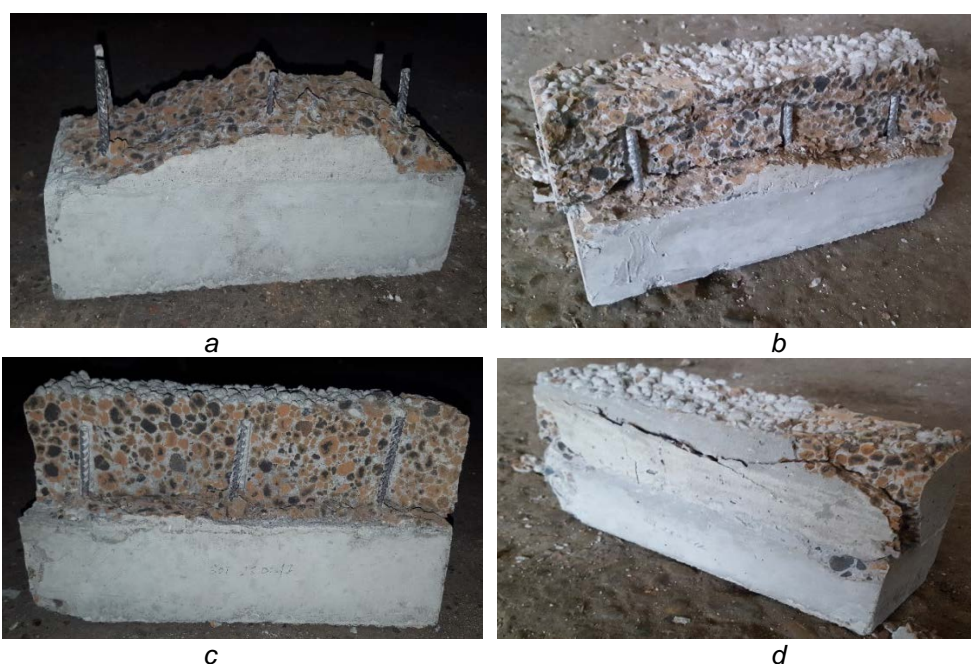


Figure 7. The fracture photos of the P5 series samples: a, b, c, d – respectively, the photos of the fractured samples P5-1, P5-2, P5-3 and P5-4.

When testing the samples with three rows of rebars, the discrepancy between the maximum and minimum results did not exceed 12%, which indicated the stability of the results compared to the P1 ... P4 samples.

The most typical fracture patterns are in Figure 8.

The carrying capacity of the P6 samples was generally greater than that of the P5 samples, which is, actually, expected, keeping in mind the earlier conclusion about the positive effect of the transverse reinforcement (confinement reinforcement) on the strength of the compressed concrete. The critical load ranged from 178.5 kN to 196 kN. In such case, as it was previously noted, the fracturing occurred due to achieving the ultimate compression strength of monolithic light (less strong) concrete. In four samples of

the P6 series, precast concrete retained its integrity, regardless of minor chips, but in one sample, simultaneous fracture of both monolithic and precast concrete occurred. The traverse reinforcement rebars got bare as a result of the fracture of monolithic concrete and slightly inclined, and the rebars that remained in the body of monolithic concrete remained intact.

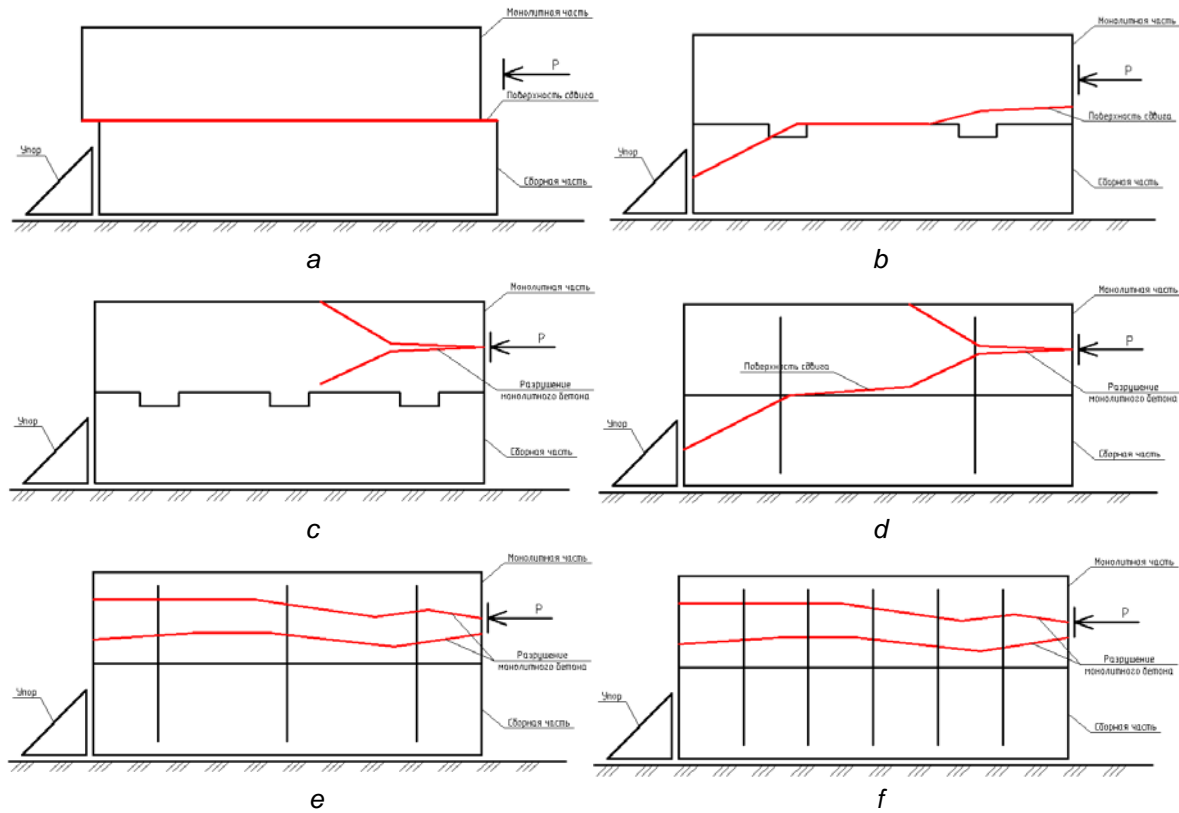


Figure 8. The typical fracture patterns: a – P1 samples; b – P2 samples; c – P3 samples; d – P4 samples.

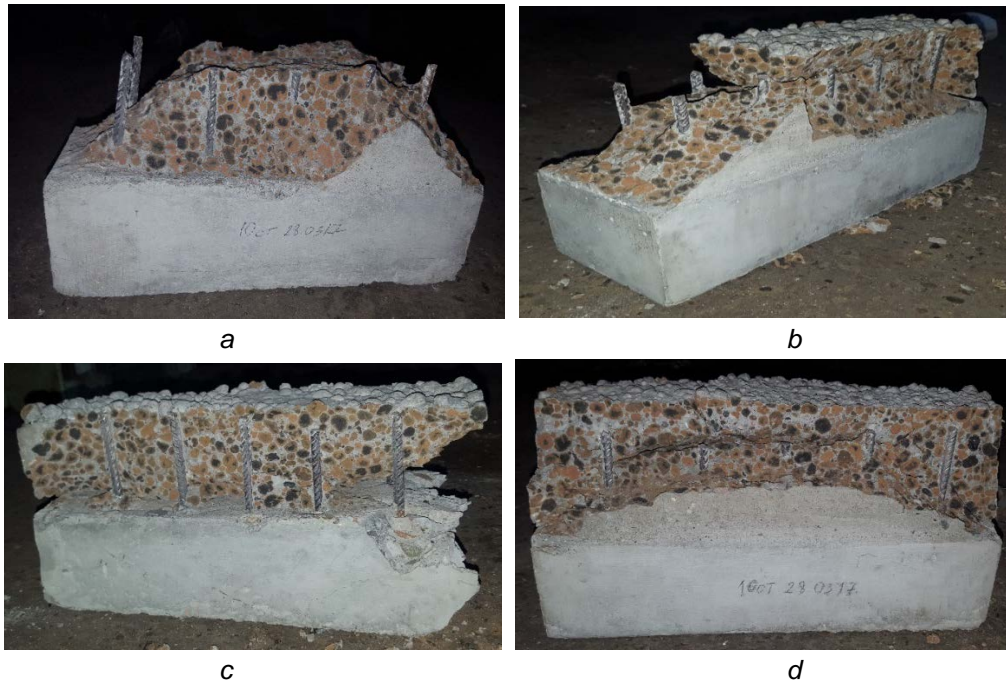


Figure 8. The fracture photos of the P6 series samples: a, b, c, d – respectively, the photos of the fractured samples P6-1, P6-2, P6-3 and P6-4.

The results provided by this paper are in good correlation with the data obtained in earlier surveys conducted by various authors, including the authors of this paper. Particularly, the results of bending tests on precast and monolithic beams in [2] showed a high shear rigidity in the case when transverse reinforcement was used in the joint. Previous works by the authors [5, 6] where, among other things, they tested bendable precast and monolithic transversely reinforced beams showed no mutual movement of the sections of monolithic and precast concrete relative to each other. A similar result was in [1–4, 9–13].

4. Conclusions:

1. The pattern of concrete failure – along the connection joint or along concrete – depends on the type of concretion of the concrete;

2. A smooth surface connection of monolithic light and precast heavy concretes, that provides adhesion only due to the adhesion and friction forces, is inefficient to ensure a joint deformation of two conjugated concretes; the fracturing occurs as a result of mutual displacement of the sections;

3. An efficient and at the same time low-cost method for ensuring a joint deformation of adjacent concretes along the joint is either a keyed joint or a joint with transverse reinforcement;

4. The most reliable is the connection between monolithic and precast concretes with the use of transverse reinforcement which along with increasing the joint's strength also ensures a more reliable result. In addition, this type of joint is simpler when manufacturing precast elements, as well as the subsequent construction and assembly operations on installation of monolithic concrete;

5. Adding transverse reinforcement indirectly increases the compression strength of concrete.

References

1. Mordich, A.I., Belevich, V.N., Simbirkin, V.N., Navoy, D.I. Opyt prakticheskogo primeneniya i osnovnyye rezultaty naturnykh ispytaniy sborno-monolitnogo karkasa BelNIIS [Experience of practical application and the main results of field tests of precast-monolithic frame BelNIIS]. Byulleten stroitelnoy tekhniki. 2004. No. 8. Pp. 8–12. (rus)
2. Povetkin, M.S. Napryazhenno-deformirovannoye sostoyaniye usilennykh pod nagruzkoy zhelezobetonnykh izgibayemykh prednapryazhennykh elementov [Stress-deformed state of reinforced reinforced concrete bent prestressed elements under load]. PhD Thesis. Kursk, 2009. 187 p. (rus)
3. Nikonorov, R.M. Sovmestnaya soprotivlyayemost, deformativnost zhelezobetonnykh elementov perekrytiya sborno-monolitnykh karkasov s ploskimi plitami i skrytymi rigelyami [Joint resistance, deformability of reinforced concrete elements of prefabricated prefabricated monolithic frames with flat plates and hidden bolts]. PhD Thesis. Moscow, 2008. 219 p. (rus)
4. Skobeleva, Ye.A. Deformirovaniye prednapryazhennykh zhelezobetonnykh izgibayemykh elementov sostavnogo secheniya [Deformation of prestressed reinforced concrete bent elements of composite section]. PhD Thesis. Orel, 2008. 208 p. (rus)
5. Koyankin, A.A., Mitasov V.M. Ispytaniya sborno-monolitnogo perekrytiya na stroyashchemsya zhilom dome [Tests of precast-monolithic overlap on a residential house under construction]. Beton i zhelezobeton. 2016. No. 3. Pp. 20–22.
6. Koyankin, A.A., Mitasov, V.M. Nekotoryye rezultaty naturnykh ispytaniy fragmenta karkasnogo zdaniya v sborno-monolitnom ispolnenii [Some results of field tests of a fragment of a frame building in a composite monolithic execution]. Beton i zhelezobeton. 2015. No. 5. Pp. 18–20. (rus)
7. Koyankin, A.A., Mitasov, V.M., Bokova, Ye.K. Sbornomonolitnoye zhelezobetonnoye perekrytiye [Precast monolithic reinforced concrete floor]. Patent Russia no. 169084, 2017. (rus)
8. Koyankin, A.A., Mitasov, V.M. Sbornomonolitnoye zhelezobetonnoye perekrytiye [Precast monolithic reinforced concrete floor]. Patent Russia no. 149440, 2015. (rus)
9. Mordich, A.I., Galkin, S.L. Rezultaty ispytaniya sborno-monolitnogo perekrytiya karkasnogo zdaniya vertikalnoy

Литература

1. Мордич А.И., Белевич В.Н., Симбиркин В.Н., Навой Д.И. Опыт практического применения и основные результаты натурных испытаний сборно-монолитного каркаса БелНИИС // Бюллетень строительной техники. 2004. № 8. С. 8–12.
2. Поветкин М.С. Напряжённо-деформированное состояние усиленных под нагрузкой железобетонных изгибаемых преднапряжённых элементов: Дис. ... канд. техн. Наук: 05.23.01 /Поветкин Максим Сергеевич. Курск, 2009. 187 с.
3. Никоноров Р.М. Совместная сопротивляемость, деформативность железобетонных элементов перекрытия сборно-монолитных каркасов с плоскими плитами и скрытыми ригелями: Дис. ... канд. техн. Наук: 05.23.01 /Никоноров Руслан Михайлович. Москва, 2008. 219 с.
4. Скобелева Е.А. Деформирование преднапряжённых железобетонных изгибаемых элементов составного сечения: Дис. ... канд. техн. Наук: 05.23.01 /Скобелева Елена Анатольевна. Орёл, 2008. 208 с.
5. Коянкин А.А., Митасов В.М. Испытания сборно-монолитного перекрытия на строящемся жилом доме // Бетон и железобетон. 2016. № 3. С. 20–22.
6. Коянкин А.А., Митасов В.М. Некоторые результаты натурных испытаний фрагмента каркасного здания в сборно-монолитном исполнении // Бетон и железобетон. 2015. №5. С. 18–20.
7. Пат. 169084 RU, МПК E04C2/06. Сборно-монолитное железобетонное перекрытие /А.А. Коянкин, В.М. Митасов, Е.К. Бокова (RU). – № 2016134363; заявл. 22.08.2016; опубл. 02.03.2017.
8. Пат. 149440 RU, МПК E04B5/16. Сборно-монолитное железобетонное перекрытие /А.А. Коянкин, В.М. Митасов (RU). – № 2014131676; заявл. 30.07.2014; опубл. 10.01.2015.
9. Мордич А.И., Галкин С.Л. Результаты испытания сборно-монолитного перекрытия каркасного здания вертикальной нагрузкой // Строительная наука и техника. 2011. № 3. С. 33–42.
10. Семченков А.С., Хавкин А.К., Соколов Б.С. Испытание натурального фрагмента каркаса «РАДИУСС» с

Коянкин А.А., Митасов В.М., Цхай Т.А. Совместность деформирования сборного тяжёлого и монолитного лёгкого бетонов // Инженерно-строительный журнал. 2018. № 8(84). С. 162–172.

- nagruzkoj [The test results of precast-monolithic overlap of the frame building with a vertical load]. *Stroitel'naya nauka i tekhnika*. 2011. No. 3. Pp. 33–42. (rus)
10. Semchenkov, A.S., Khavkin, A.K., Sokolov B.S. Ispytaniye naturnogo fragmenta karkasa «RADIUSS» s primeneniym kruglopustotnykh plit [Testing the full-scale fragment of the frame "RADIUSS" using round hollow core slabs]. *Beton i zhelezobeton*. 2008. No. 6. Pp. 2–5. (rus)
 11. Semchenkov, A.S. Ispytaniye naturnogo fragmenta karkasa «RADIUSS NPU» s plitami sploshnogo secheniya [Test of a full-scale fragment of the frame "RADIUSS NPU" with plates of continuous section]. *Beton i zhelezobeton*. 2009. No. 1. Pp. 2–5. (rus)
 12. Medvedev, V.N., Semeniuk, S.D. Durability and deformability of braced bending elements with external sheet reinforcement. *Magazine of Civil Engineering*. 2016. 63(3). Pp. 3–15. DOI: 10.5862/MCE.63.1.
 13. Nedviga, E., Beresneva, N., Gravit, M., Blagodatskaya, A. Fire Resistance of Prefabricated Monolithic Reinforced Concrete Slabs of «Marko» Technology. *Advances in Intelligent Systems and Computing*, 692. 2018. Pp. 739–749.
 14. Yan J.B., Wang J.Y., Liew J.Y.R., Qian X.D., Zhang W. Reinforced ultra-lightweight cement composite flat slabs: Experiments and analysis. *Materials and Design*. 2016. № 95. Pp. 148–158.
 15. Cho Y.S., Lee S., Bae J.S. Reinforcement Placement in a Concrete Slab Object Using Structural Building Information Modeling. *Computer-Aided Civil and Infrastructure Engineering*. 2014. No. 29. Pp. 47–59.
 16. Шембаков В.А. Сборно-молитное каркасное домостроение. Руководство к принятию решения. Чебоксары: ООО «Чебоксарская типография № 1», 2005. 119 с.
 17. Шаленный В.Т., Паперник Р.Б. Повышение технологичности проектных решений монолитных и сборно-молитных зданий и сооружений // *Промышленное и гражданское строительство*. 2010. №2. С. 19–21.
 18. Коянкин А.А. Облегчённое сборно-молитное перекрытие // *Вестник МГСУ*. 2017. № 6(105). С. 636–641.
 19. Breccolotti M., Gentile S., Tommasini M., Materazzi A.L., Bonfigli M.F., Pasqualini B., Colone V., Giancesini M. Beam-column joints in continuous RC frames: Comparison between cast-in-situ and precast solutions // *Engineering Structures*. 2016. № 127. Pp. 129–144.
 20. Prior R.C. Identification and preliminary assessment of existing precast concrete floor framing systems // *Theses and Dissertations*, 2003. 213 p.
 21. Ключева Н.В., Колчунов В.И., Рыпаков Д.А., Бухтиярова А.С. Прочность и деформативность сборно-молитных каркасов жилых зданий пониженной материалоемкости при запроектных воздействиях // *Промышленное и гражданское строительство*. 2015. № 1. С. 5–9.
 22. Теплова Ж.С., Виноградова Н.А. Сборно-молитные перекрытия системы «МАРКО» // *Строительство уникальных зданий и сооружений*. 2015. №8. С. 48–59.
 23. Olmati P., Sagaseta J., Cormie D., Jones AEK. Simplified reliability analysis of punching in reinforced concrete flat slabbuildings under accidental actions // *Engineering Structures*. 2017. № 130. Pp. 83–98.
 24. Qian K., Li B. Resilience of Flat Slab Structures in Different Phases of Progressive Collapse // *ACI Structural Journal*. 2016. № 113. Pp. 537–548.
 25. Drakatos I.S., Muttoni A., Beyer K. Internal slab-column connections under monotonic and cyclic imposed rotations // *Engineering Structures*. 2016. № 123. Pp. 501–516.
 26. Micallef K., Sagaseta J., Fernandez Ruiz M., Muttoni A. Assessing Punching Shear Failure in Reinforced Concrete Flat Slabs Subjected to Localized Impact Loading // *International Journal of Impact Engineering*, № 71. 2014. Pp. 17–33.
 27. Коянкин А.А., Митасов В.М. Напряжённо-деформированное состояние сборно-молитного здания // *Инженерно-строительный журнал*. 2017. № 6(74). С. 175–184. DOI: 10.18720/MCE.74.14.
 28. Парашенко Н.А., Горшков А.С., Ватин Н.И. Частично-ребристые сборно-молитные перекрытия с

25. Drakatos, I.S., Muttoni, A., Beyer, K. Internal slab-column connections under monotonic and cyclic imposed rotations. *Engineering Structures*. 2016. No. 123. Pp. 501-516.
26. Micallef, K., Sagaseta, J., Fernandez Ruiz, M., Muttoni, A. Assessing Punching Shear Failure in Reinforced Concrete Flat Slabs Subjected to Localized Impact Loading. *International Journal of Impact Engineering*. No. 71. 2014. Pp. 17-33.
27. Koyankin, A.A., Mitasov, V.M. Stress-strain state of precast and cast-in place building. *Magazine of Civil Engineering*. 2017. 74(6). Pp. 175-184. DOI: 10.18720/MCE.74.14.
28. Parashchenko, N.A., Gorshkov, A.S., Vatin, N.I. Partially rib precast and cast-in-situ floors with cellular-concrete blocks. *Magazine of Civil Engineering*. 2011. No. 6. Pp. 50-55. (rus)
29. Chepurnenko, A.S. Stress-strain state of three-layered shallow shells under conditions of nonlinear creep. *Magazine of Civil Engineering*. 2017. No. 8(74). Pp. 156-168. DOI: 10.18720/MCE.76.14
- ячеистобетонными блоками // Инженерно-строительный журнал. 2011. № 6. С. 50-55.
29. Чепурненко А.С. Расчет трехслойных пологих оболочек с учетом нелинейной ползучести // Инженерно-строительный журнал. 2017. № 8(76). С. 156-168. DOI: 10.18720/MCE.76.14

*Alexander Koyankin**,
+7(391)2934711; *KoyankinAA@mail.ru*

Valery Mitasov,
+7-913-912-23-64; *mitassovv@mail.ru*

Trofim Tskhay,
8-923-338-50-88; *vadershow@gmail.com*

*Александр Александрович Коянкин**,
+7(391)2934711;
эл. почта: *KoyankinAA@mail.ru*

Валерий Михайлович Митасов,
+7-913-912-23-64; эл. почта: *mitassovv@mail.ru*

Трофим Анатольевич Цхай,
8-923-338-50-88;
эл. почта: *vadershow@gmail.com*

© Koyankin, A.A., Mitasov, V.M., Tskhay, T.A., 2018

doi: 10.18720/MCE.84.17

Properties and thermal insulation performance of light-weight concrete

Свойства и теплоизоляционные эффективности легких бетонов

T.V. Lam,
D.T. Vu,
V.K. Dien,
B.I. Bulgakov,
E.A. Korol,*

*National Research Moscow State Civil
Engineering University, Moscow, Russia*

M.Sc., аспирант Т.В. Лам,
PhD, аспирант Д.Т. Ву,
M.Sc., аспирант В.К. Зиен,
канд. техн. наук, доцент Б.И. Булгаков,
д-р техн. наук, заведующая кафедрой
Е.А. Король,
Национальный исследовательский
Московский государственный строительный
университет, г. Москва, Россия*

Key words: expanded polystyrene bead; unprocessed fly ash; light-weight concrete; thermal insulation performance; temperature distribution; wall cover

Ключевые слова: пенополистирол; топливная зола-уноса; легкий бетон; теплоизоляционные свойства; температурное поле; стеновой материал

Abstract. The building energy performance is becoming increasingly important, because of environmental restrictions and rising costs of fuel end energy. Therefore, improve the thermal insulation performance of wall covers of buildings is crucial. The present study evaluated the combined effects of two types of materials of expanded polystyrene (EPS) beads and unprocessed fly ash (FA) in Vietnam on properties of light-weight concrete (LWC). The calculation of mixture proportions of LWC is applied in accordance with the absolute volume method. Twelve different concrete mixtures with a water to bind ratio of 0.3 and superplasticizer SR 5000F to Portland cement ratio of 0.02 were used. The EPS beads and FA were partially replaced with the volume of fresh concrete and cement, respectively. The engineering properties, including workability, density, compressive strength, tensile strength, modulus of elasticity and basic physical properties were investigated in 12 patterns of tested LWC and its correlations were made. In addition, the definition of temperature distribution over the thickness of the experimental wall cover was applied by the ANSYS 18 software. According to the experimental results, there is a decrease in dry density and mechanical properties with increasing these EPS beads and FA contents in LWC. The results by ANSYS 18 are shown that at the same thickness of 250 mm, a wall with the blocks LWC brick has better insulation than the wall made of other materials such as solid clay brick, clay hollow brick and solid brick with slag concrete.

Аннотация. Энергоэффективность здания становится все более важной из-за ограничений окружающей среды и роста стоимости энергии на топливо. Поэтому важно улучшить теплоизоляционные характеристики внешних стен высотных зданий. В настоящей статье приведены результаты исследования влияния концентрации гранул вспененного полистирола, а также разработанной органо-минеральной добавки, состоящей из водоредуцирующего поликарбоксилатного суперпластификатора и топливной зола-уноса, обладающей пуццолановой активностью, на плотность, прочность, модуль упругости и теплопроводность легкого бетона (ЛБ), пригодного для изготовления материалов, предназначенных для возведения внешних стен высотных зданий. Расчёт состава лёгкобетонной смеси был выполнен с помощью метода абсолютных объёмов. Расход суперпластификатора составил 2 % от массы цемента при водовяжущем отношении, равном 0,3. Для расчёта температурного поля в поперечном сечении стены из разработанного легкого бетона была использована компьютерная программа ANSYS 18. В результате проведённых исследований было установлено, что стена, состоящая из легких бетонных блоков толщиной 250 мм, обладает лучшими теплоизоляционными свойствами по сравнению со стенами аналогичной толщины из полнотелого и перфорированного глиняного кирпича, а также из кирпича на основе шлакопортландцемента.

1. Introduction

In recent years, buildings are large energy consumers in many countries in the world and energy demand is growing every day. The energy performance of a building is becoming increasingly important, because of environmental restrictions and rising costs of fuel end energy [1, 2]. The energy required in the building is mostly towards providing thermal comfort. To reduce the energy consumption in high-rise buildings, it is necessary to understand the thermal performance of the building envelope on the indoor environment. The studies [3, 4] the two parameters, which evaluate the thermal performance of walls are time lag and decrement factor. These are influenced by the external and internal surface temperatures of the enclosing structures of buildings.

In the climate of Hanoi – Vietnam in the summer, the outside temperature the building air is very high, sometimes up to 42 °C [5]. The temperature on the surface of the building's wall covers can be up to 50 °C when considering the effects of solar radiation factors [5, 6].

To ensure comfortable use in buildings, the temperature inside of the building is between 20÷25 °C, so the cover structure should ensure low heat transfer requirements

In order to reduce the transmission temperature from building outside to building's inside, some traditional methods have been introduced such as: Building solid brick wall and installing additional layer's insulation (layer of foam, insulating paint, or the use of hollow bricks, etc.) [7–11]. However, these solutions will increase labor, construction time, increase costs, etc. [12].

Many solutions have been proposed to increase the insulation of the walls [13–15]. One of those modern insulation solutions is using brick blocks from new material – light-weight concrete (LWC), which is capable of conducting low heat and withstanding the loads exerted on the walls of high-rise buildings.

Light-weight concretes have been successfully used in the buildings, thanks to its low dry density. LWC is an important material in reducing the dead-weight of concrete complying with special concrete structures of high-rise buildings [16–18]. To produce light-weight concrete, we can use several types of inorganic light-weight aggregates, like expanded clay, agropolite, or organic lightweight aggregates like expanded polystyrene (EPS) beads. When LWC base on inorganic light-weight aggregates has been widely used, LWC base on organic lightweight aggregates like EPS is now considered to be a new material in Vietnam [19, 20]. However, until now the structural LWC containing varying amounts of EPS beads is not specified in the standard in Vietnam.

The studies [21, 22] on EPS concretes have also revealed that mixtures produced using the normal vibration method will lead to a large number of EPS beads floating upward and serious concrete segregation, resulting in LWC while reducing its various engineering properties. This is due to the ultra-light EPS particles and being quite weak. It was found that the concrete is very prone to segregation and has low compressive strength. To improve the workability of the concrete mixtures containing EPS particles, a great deal of previous research [20, 23, 24] has used superplasticisers.

Some studies have reported the importance of using fly ash (FA) in concrete which can save a significant amount of energy and cost in cement manufacturing and also it can improve engineering properties of concrete by replacing with normal cement. For example, in these studies [25, 26] covers the use of EPS beads both in concrete and mortar, containing processed and unprocessed fly ash as the cementitious material. The concretes' dry densities were between 550 and 2185 kg/m³. The EPS replacements ranged from 0 % to 100 %. These studies are indicated that the EPS concrete mixes produced with processed fly ash show lower water absorption values and better chemical resistance compared to the normal concrete.

The purpose of this research was to determine the properties and thermal insulation performance of light-weight concrete for the production of the wall cover, which contains varying amounts of EPS beads and unprocessed FA (Vietnam).

The aim of the present study included four specific objectives to:

(1) Microstructural characterizations of unprocessed Fly Ash «Vung Ang» and Silica Fume was carried out by Scanning Electron Microscope (SEM) and X-ray diffraction (XRD).

(2) Apply in accordance with the absolute volume method to calculate the concrete mixture compositions.

(3) The American and Russian standard's requirements were used to determine the fresh concrete and light-weight concrete properties.

(4) Quantitatively describe the relationships between the various investigated light-weight concrete properties.

(5) Use the computer program ANSYS 18 to analyze the thermal insulation of the wall constructed from light-weight concrete brick blocks with walls constructed from some other materials.

2. Materials and Experimental works

2.1. Materials

1. The cement used was ordinary Portland cement (OPC) (40 Grade), manufactured at «Tam Diep» factory (Vietnam), specific weight of 3150 kg/m^3 . The experimental results of physical and mechanical properties of cement are presented in Table 1 and the results of the chemical compositions are presented in Table 2. The particle size distributions details of ordinary Portland cement is shown in Figure 1.

Table 1. Mineralogical Composition, physical and mechanical properties of «Tam Diep» Portland cement.

| Mineral composition (%) | | | | | Soundness Le Chatelier (mm) | Time of setting (min) | | Compressive strength (MPa) | | | Standard consistency (%) |
|-------------------------|------------------|------------------|-------------------|-------|-----------------------------------|--------------------------|-------|-------------------------------|--------|---------|--------------------------------|
| C ₃ S | C ₂ S | C ₃ A | C ₄ AF | Other | | Initial | Final | 3 days | 7 days | 28 days | |
| 56.3 | 23.4 | 4.7 | 12.4 | 3.2 | 3.2 | 142 | 235 | 35.1 | 40.4 | 47.3 | 29.5 |

2. Good quality river sand was used as a fine aggregate, which produced from the quartz sand (QS) of «Lo River» (Vietnam) with the size of $0.15 \div 5 \text{ mm}$. The fineness modulus $M_K = 3.1$, specific gravity and dry density are 2650 kg/m^3 and 1650 kg/m^3 . The particle size distributions details of fine aggregates is shown in Figure 1.

3. Unprocessed Fly Ash (FA) TPP «Vung Ang» (Vietnam) class F and Silica Fume SF-90 (SF90) (Vina Pacific). The chemical composition and physical properties of the FA TPP «Vung Ang» and silica Fume SF-90 are presented in Table 2 and their particle size distribution are presented in Figure 1.

Table 2. Chemical compositions and physical properties of Portland cement, FA TPP «Vung Ang» and Silica fume SF-90.

| Chemical components (wt. %) | FA TPP «Vung Ang» | Silica Fume SF-90 | Portland cement |
|---------------------------------------|-------------------|-------------------|-----------------|
| SiO ₂ | 54.62 | 91.65 | 20.4 |
| Al ₂ O ₃ | 24.17 | 2.25 | 4.4 |
| Fe ₂ O ₃ | 6.15 | 2.47 | 5.4 |
| SO ₃ | 2.81 | - | 3.4 |
| K ₂ O | 1.28 | - | 1.2 |
| Na ₂ O | 1.25 | 0.55 | 0.3 |
| MgO | 1.57 | - | 2.5 |
| CaO | 1.48 | 0.51 | 60.2 |
| P ₂ O ₅ | 1.63 | 0.03 | - |
| LOI ^(*) | 5.04 | 2.54 | 2.2 |
| Average particle size (μm) | 7.18 | 0.243 | 8.365 |
| Specific gravity (kg/m ³) | 2320 | 2150 | 3150 |
| Dry density (kg/m ³) | 575 | 760 | 1200 |
| Surface area (m ² /g) | 5.35 | 14.45 | 0.365 |

Note: ^(*)LOI – Loss on ignition.

4. Expanded polystyrene (EPS) beads were used as a light-weight aggregate with the size of $2 \div 5 \text{ mm}$. Its dry density is 18.1 kg/m^3 (Figure 5).

5. Superplasticizer SR 5000F «SilkRoad» (SR5000) (Korea). It is a new generation chemical additives based on polycarboxylate ethers with specific weight of 1100 kg/m^3 at $20 \pm 5 \text{ }^\circ\text{C}$.

6. Ordinary clean tap water (W) was used for both mixing concrete and curing of test concrete specimens.

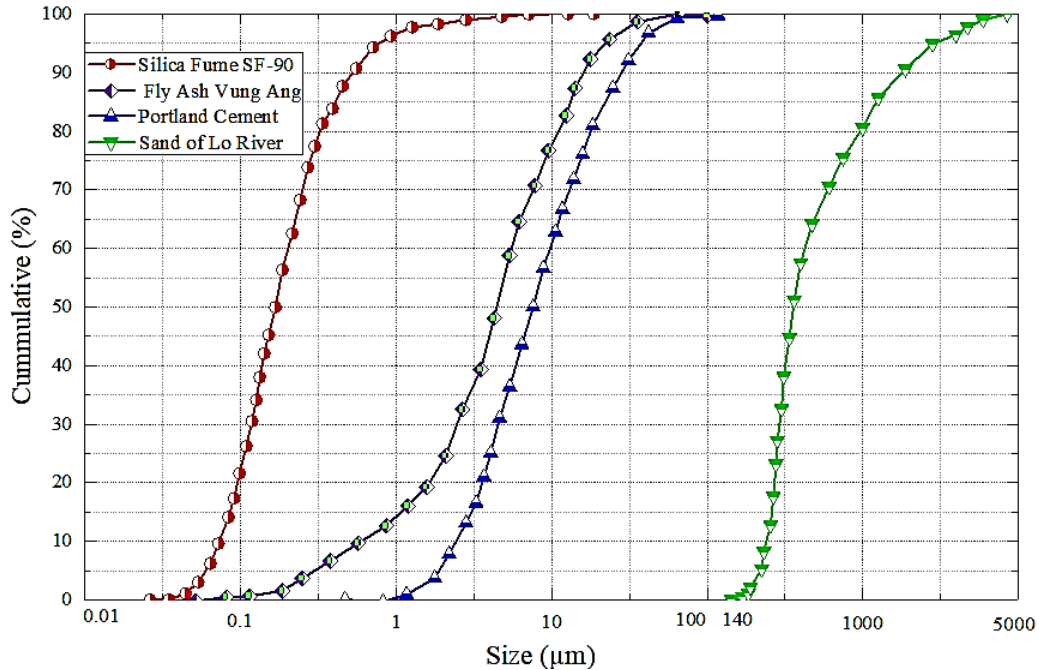


Figure 1. Sieving analysis of Silica Fume, Portland cement, Fly Ash and sand of river Lo.

2.2. Microstructural characterizations of Silica Fume and unprocessed Fly Ash «Vung Ang»

Scanning Electron Microscopy (SEM)

The morphology of dried active mineral additives was carried out by Scanning Electron Microscope (SEM, Quanta 450, USA) operated at 15 kV. Silica Fume and unprocessed Fly Ash particles were adhered on two side adhesive black tape and kept under high vacuum to get SEM images and is shown in Figure 2. SEM images show that Fly Ash «Vung Ang» exhibit larger spherical particles, irregular in shape and found to be more porous (Figure 2a) compared with Silica Fume SF-90 (Figure 2b). The particles of Silica Fume can be seen in proper arrangement and no agglomeration occurred. The spherical particle shape of these additives can give benefit for the workability of fresh concrete at the low water-cement ratio [27].

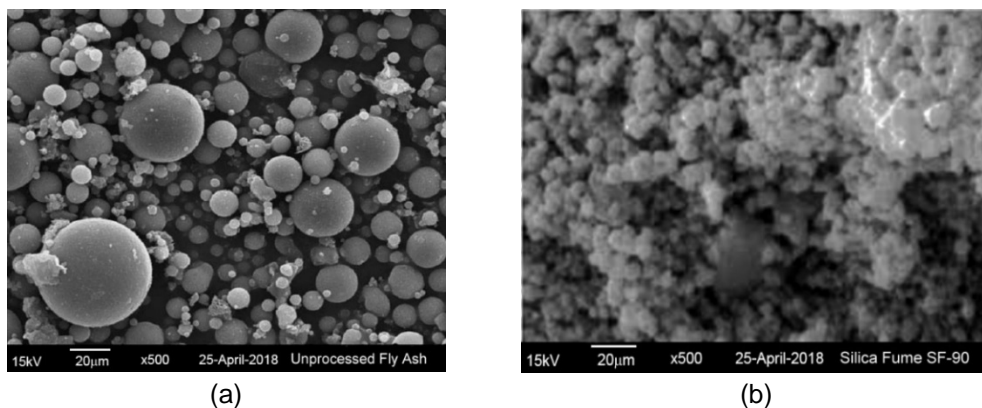


Figure 2. SEM images of (a) Unprocessed Fly Ash «Vung Ang» and (b) Silica Fume SF-90.

X-ray diffraction (XRD)

The XRD analysis provides the crystalline nature of the Unprocessed Fly Ash TPP «Vung Ang» and Silica Fume SF-90 used as the active mineral additives in mixture concrete on the device BT-9300Z. A peak with 26.5° (2θ) was observed as the highest intensity for Fly Ash, another peak with 18.5° (2θ) was observed as the highest intensity for Silica Fume SF-90 as are shown in Figure 3. The high peaks in both graphs corresponding to quartz silica. The rest of the peaks belonging to mineral Mullite presented in the graphs. The XRD results proved that both of the Fly Ash and Silica Fume consist of crystalline silica, which is the main important component in strength contribution. The other crystalline phase such as Mullite represent the minor phases.

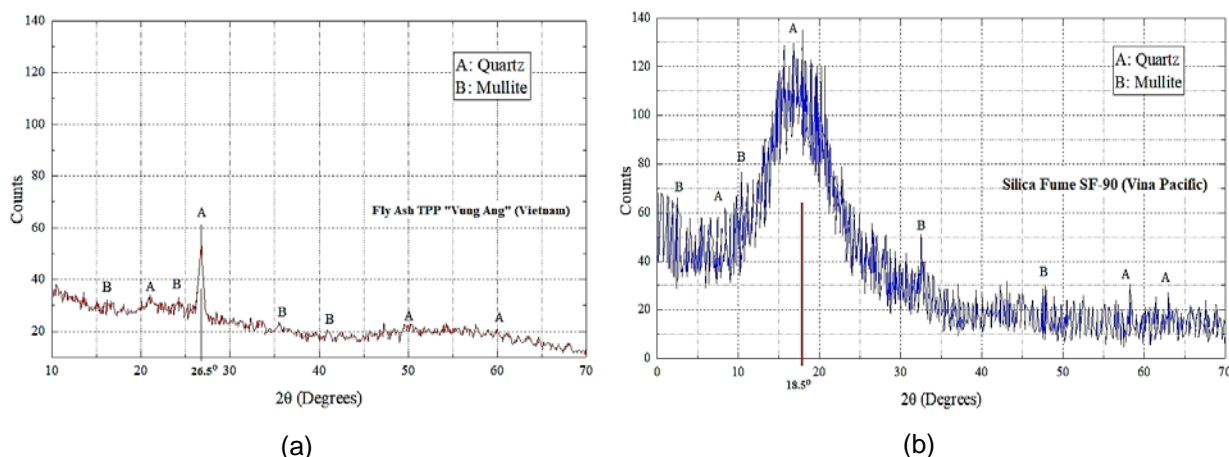


Figure 3. XRD analysis of (a) unprocessed fly ash «Vung Ang» and (b) Silica Fume SF-90.

2.3. Test methods

On the one hand, this paper will analyze the chemical composition and the grain composition of Unprocessed Fly Ash TPP «Vung Ang» by laser granulometry method on the device BT-9300Z. On the other hand, calculation method of compositions LWC is applied in accordance with absolute volume method. The flow ability of concrete mixture is determined by standard slump cone with dimensions of 100x200x300 mm in accordance with ASTM C143-15. Besides, the dry density of concrete is determined by standard ASTM C 138.

Compressive and Flexural Strengths of LWC specimens

The compressive strength of light-weight concrete is determined by a 70x70x70 mm cube specimen (Figure 6) by Russian standard GOST 10180-2012 at the ages of 3, 7, 14, 28 and 56 days. These cube samples are demolded after 24 hours later casting and placed in a 20 ± 5 °C water curing tank until the experiments.

The flexural strength of the LWC specimens was determined in accordance with ASTM C 78 on the 100x100x400 mm prismatic patterns and using the method of third point loading. The flexural strength of concrete was measured at 28 days.



Figure 4. Unprocessed fly ash TPP «Vung Ang».



Figure 5. Expanded polystyrene beads.

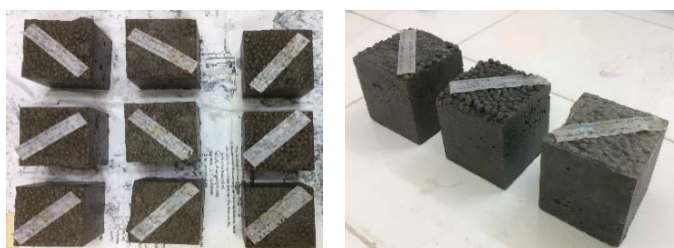


Figure 6. Specimens with the size of 70x70x70 mm of light-weight concrete.



Figure 7. Failure of concrete specimen under compression.

Modulus of elasticity

The static modulus of elasticity, which corresponds to the secant modulus, was determined for light-weight concrete in accordance with ASTM C 469-2002 at 28 days of age.

Thermal Conductivity of light-weight concrete

In order to understand the influence of the EPS beads and unprocessed FA on the improvement of thermal insulation properties of the developed light-weight concretes, their thermal conductivity λ [W/(m.°C)] was obtained using device ISOMET 2114 (Applied Precision, Ltd.). ISOMET 2114 is a multifunctional instrument for measuring thermal conductivity, thermal diffusivity, and volumetric heat capacity. The measurement is based on the analysis of the temperature response of the analyzed material to heat flow impulses. The heat flow is induced by electrical heating using a resistor heater having a direct thermal contact with the surface of the sample. LWC-samples with the side dimension of 70×70×70 mm were measured using a surface probe. Before the measurements, all specimens were dried at 100 ± 5 °C.

The measurements on both reference and pre-treated specimens were performed in the laboratory condition at 20 ± 5 °C and (30 ÷ 40) % relative humidity.

Testing procedures

In this study, uniaxial compressive tests on LWC samples (for each concrete sample) were performed with a constant loading rate of 500 N/s on system Controls Advantest 9 (Figure 7). The reason of choosing 500 N/s is to keep the loading rate to a minimum in the comparison of test LWC results.

2.4. Experimental Plan

Figure 8 shows the structure of the experimental plan. In this experimental program design, the determination of the concrete mixture compositions is according to the absolute volume method and the definition of temperature distribution over the thickness of the experimental wall structure is using the computer program ANSYS 18, which is the basis for comparison of thermal insulation performance in the structure of wall cover. The ANSYS computer program, based on the finite-element method, will analyze the thermal insulation performance of the object study.

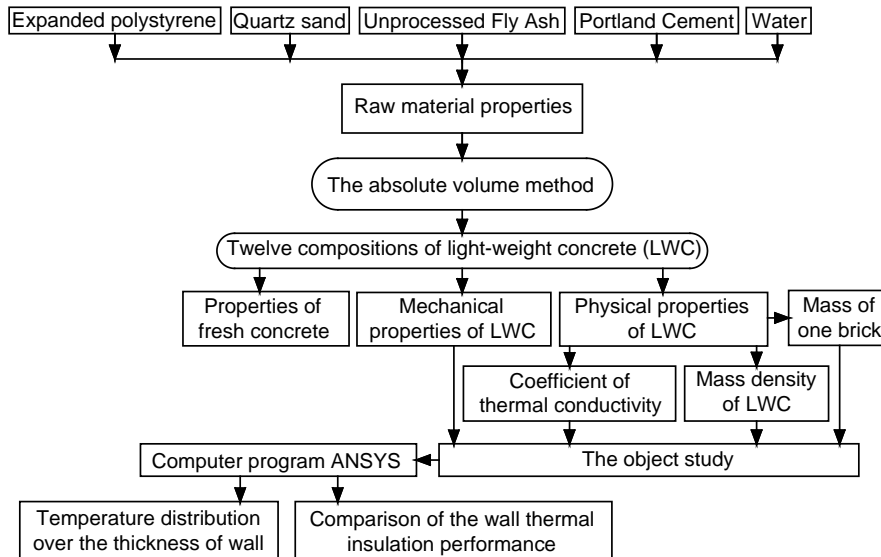


Figure 8. Experimental program

2.5. Fundamentals of the heat transfer theory in material and polystyrene concrete blocks

According to [28], the heat transfer equation in the wall is determined by formula (1):

$$\frac{\partial}{\partial x} \left(\lambda_x \frac{\partial T}{\partial x} \right) + \frac{\partial}{\partial y} \left(\lambda_y \frac{\partial T}{\partial y} \right) + \frac{\partial}{\partial z} \left(\lambda_z \frac{\partial T}{\partial z} \right) = \rho c \frac{\partial T}{\partial t}, \quad (1)$$

where $T(x, y$ and $z)$ is temperature in coordinates (x, y and z) (°C);

$\lambda_x, \lambda_y, \lambda_z$ are thermal conductivity coefficients of concrete along the x, y, z axes W/(m.°C);

c is specific heat (kJ/kg.°C);

ρ is density (kg/m³);

t is time (day).

To solve equation (1), it is necessary to know two main types of boundary conditions are Dirichlet and Cauchy boundary [29, 30], which can be written respectively as:

$$T = T_s; \quad (2)$$

$$\lambda \frac{\partial T}{\partial n} = \alpha_n (T_s - T_a), \quad (3)$$

where λ is thermal conductivity W/(m.°C);

n is the surface normal direction;

T_s is the temperature of cement mortar surface (°C);

T_a is atmospheric temperature (°C);

α_n is represented surface heat transfer coefficient (W/m².°C).

The problem of transfer heat through a wall structure, which is not a homogeneous material, is a complex problem. Therefore, appropriate methods often are used in the determination of heat transfer through the structure. In recent years, the most complete factor consideration for temperature problem solution possibly applies numerical methods, particularly, the finite element method through ANSYS, ADINA, ABAQUS, MIDAS CIVIL programs and others [30–33].

In this study analyze the thermal performance evaluation of the wall using complex computer program ANSYS 18, which is one of the modern programs, allowing users to put in necessary data, for example: thickness, physical and mechanical characteristics, etc. So that the results are approximate to the empirical results.

2.6. The object study

The objective of the current study was light-weight concrete for the production of the wall cover with size 1000x1000x250 mm, which is located at the cover of the High-Rise buildings and direct contact with the sun, considered at the time of June in North Vietnam. The basic properties of some types of materials are used in the analysis of heat transfer through the building wall coverings and are shown in Table 3. In this paper consider a block of this wall with two layers of mortar of thickness 15 mm (shown in Figure 9).

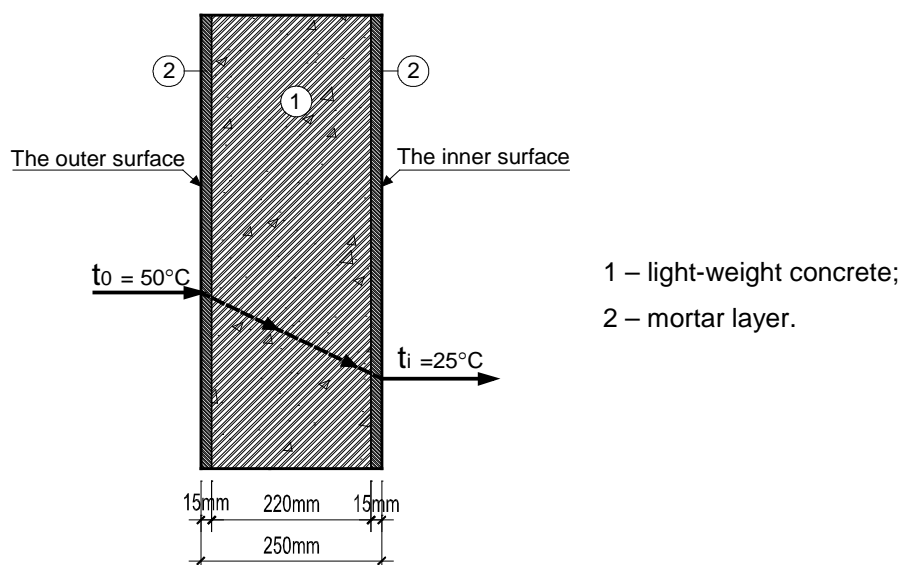
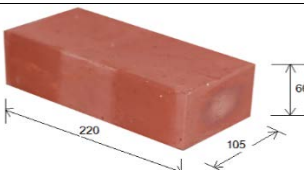
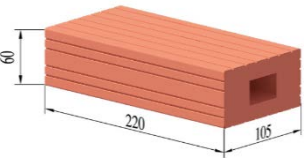
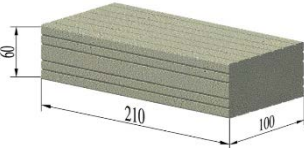


Figure 9. The wall cover, thickness 220 mm and two layers of mortar thickness 15 mm.

In standard TCVN 4605-1988 [6] «Heating techniques – Insulating component – Designs standard» is shown when considering solar radiation factors and other conditions, the estimated outdoor temperature is determined by: $t_0 = t_n + \varphi \cdot I_{tb} / \alpha_n = 49.64 \text{ }^\circ\text{C} \approx 50 \text{ }^\circ\text{C}$ with the outside temperature of the building $t_n = 40 \text{ }^\circ\text{C}$ in the summer, the heat transfer coefficient of the outer surface of the enclosing structure of the wall $\alpha_n = 25 \text{ (W/m}^2\cdot\text{}^\circ\text{C)}$; solar radiation intensity on average on the wall's surface $I_{tb} = 366 \text{ W/m}^2$ and absorption coefficient of outside surface (cement mortar) $\varphi = 0.65$.

The temperature of the outer (t_o) and inner (t_i) surfaces of the building's wall covering is $t_o = 50 \text{ }^\circ\text{C}$, $t_i = 25 \text{ }^\circ\text{C}$ and the heat transfer coefficient of the inner surface of the enclosing structure $\alpha_t = 5.9 \text{ W/m}^2\cdot\text{ }^\circ\text{C}$ (in Table 3 – TCVN 4605-1988 [1]). In this case, the moisture of the materials not is considered in numerical simulation of heat transfer in the walling structure.

Table 3. Material properties in thermal behavior analysis.

| No. | Materials | Figures | Physical properties of materials | | |
|-----|--|---|--|-----------------------------------|------------------------|
| | | | Coefficient of thermal conductivity λ (W/(m.°C)) | Mass density (kg/m ³) | Mass of one brick (kg) |
| 1 | Solid clay brick [6] |  | 0.81 | 1600 | 2.218 |
| 2 | Hollow clay brick [6] |  | 0.52 | 1350 | 1.6 |
| 3 | Solid unit with slag concrete [5, 6] |  | 0.7 | 1200 | 1.663 |
| 4 | Solid brick with light-weight concrete 400x220x60 mm [60 % EPS and 40 % FA in Table 8] |  | 0.275 | 785 | 4.145 |
| 5 | Cement mortar [6] | | 0.93 | 1800 | |

2.7. Calculation of the concrete mixture compositions

It is necessary to determine the concrete mixture compositions for the light-weight concrete production, which are intended for light-weight concrete blocks with low thermal conductivity in the High-Rise Construction in Northern of Vietnam. The initial ratios of raw materials by weight in concrete mixtures for the production of light-weight concrete are given in Table 4.

Table 4. Ratios of raw materials used in preliminary composition.

| Ratios | EPS (%volume fresh concrete) | $\frac{FA}{OPC}$ | $\frac{W}{BID}$ | $\frac{QS}{BID}$ | $\frac{SF}{OPC}$ | $\frac{SR5000}{OPC}$ | Volume of air in concrete |
|--------|------------------------------|------------------|-----------------|------------------|------------------|----------------------|---------------------------|
| Value | 30 ÷ 60 | 0.2 ÷ 0.4 | 0.3 | 1.2 | 0.1 | 0.02 | 2 % |

Note: BID – binder: $BID = OPC + FA + SF$.

Based on the characteristics of the raw materials and the ratios above, together with combined the Bolomey-Skrantsev equation, after solving the optimization problem and adjusting results experimentally in the laboratory, water-binder ratio of this light-weight concrete, with maximum compressive strength at 28-day of 30 MPa and dry unit weight of 800÷1500 kg/m³, was obtained $\frac{W}{BID} = 0.3$. Using the absolute volume method were obtained the compositions of specimens used in this work can be found in Table 5.

Table 5. Ingredient proportions for the preparation of concrete samples.

| Sample ID. | The rate of components | | | Concrete mixture compositions (kg/m ³) | | | | | | |
|-----------------|------------------------|---------|------------------|--|-----|------|-----|--------|-----|-------|
| | $\frac{W}{BID}$ | EPS (%) | $\frac{FA}{OPC}$ | OPC | FA | SF | QS | SR5000 | W | EPS |
| LWC-30EPS-0.2FA | 0.3 | 30 | 0.2 | 470 | 94 | 47.0 | 733 | 9.40 | 183 | 5.43 |
| LWC-30EPS-0.3FA | | | 0.3 | 434 | 130 | 43.4 | 730 | 8.69 | 182 | 5.43 |
| LWC-30EPS-0.4FA | | | 0.4 | 404 | 162 | 40.4 | 727 | 8.08 | 182 | 5.43 |
| LWC-40EPS-0.2FA | | 40 | 0.2 | 401 | 80 | 40.1 | 625 | 8.02 | 156 | 7.24 |
| LWC-40EPS-0.3FA | | | 0.3 | 371 | 111 | 37.1 | 622 | 7.41 | 156 | 7.24 |
| LWC-40EPS-0.4FA | | | 0.4 | 344 | 138 | 34.4 | 620 | 6.89 | 155 | 7.24 |
| LWC-50EPS-0.2FA | | 50 | 0.2 | 332 | 66 | 33.2 | 517 | 6.63 | 130 | 9.05 |
| LWC-50EPS-0.3FA | | | 0.3 | 307 | 92 | 30.7 | 515 | 6.13 | 129 | 9.05 |
| LWC-50EPS-0.4FA | | | 0.4 | 285 | 114 | 28.5 | 513 | 5.70 | 128 | 9.05 |
| LWC-60EPS-0.2FA | | 60 | 0.2 | 263 | 53 | 26.3 | 410 | 5.25 | 103 | 10.86 |
| LWC-60EPS-0.3FA | | | 0.3 | 243 | 73 | 24.3 | 408 | 4.85 | 102 | 10.86 |
| LWC-60EPS-0.4FA | | | 0.4 | 226 | 90 | 22.6 | 406 | 4.51 | 102 | 10.86 |

Note: $\frac{W}{BID}$ and $\frac{FA}{OPC}$ ratio by weight and the volume of air of 2 % volume of concrete.

Additionally, the twelve of the material compositions in the dry state of the light-weight concrete mixtures with varying amounts of EPS beads and unprocessed FA were made for this experiment as in Table 5. On the one hand, the volume of fresh concrete was replaced with 30 %, 40 %, 50 % and 60 % by volume of EPS beads [25, 34]. On the other hand, the ordinary Portland cement was replaced with 20 %, 30 % and 40 % by mass of FA TPP «Vung Ang» [35].

According to [23, 24], choosing lower substitutions of EPS in concrete mixture is within satisfactory limits. However, one of the main goals of the present work is to utilize as much EPS beads as possible, solving the disposal problem of waste expanded polystyrene foam and producing light-weight concrete blocks with low thermal conductivity in construction the High-Rise buildings.

In the case of this research, the ratios $\frac{W}{BID}$ and $\frac{SR5000}{OPC}$ of 0.3 and 0.02 respectively were kept constant for all mixtures and no adjustment to the water content was made for all mixtures. The superplasticizer SR 5000F «SilkRoad» has been used to reduce the $\frac{W}{BID}$ ratio and to increase workability of concrete mixtures.

3. Results and Discussion

3.1. Properties of fresh concrete

The average density of fresh concretes and the slump values for light-weight concretes containing varying amounts of EPS beads and Unprocessed FA are presented in Table 6 and Figure 10. The density values of concrete mixtures were in the range of 849÷1537 kg/m³. The slump values were between 14.5 and 20.5 cm.

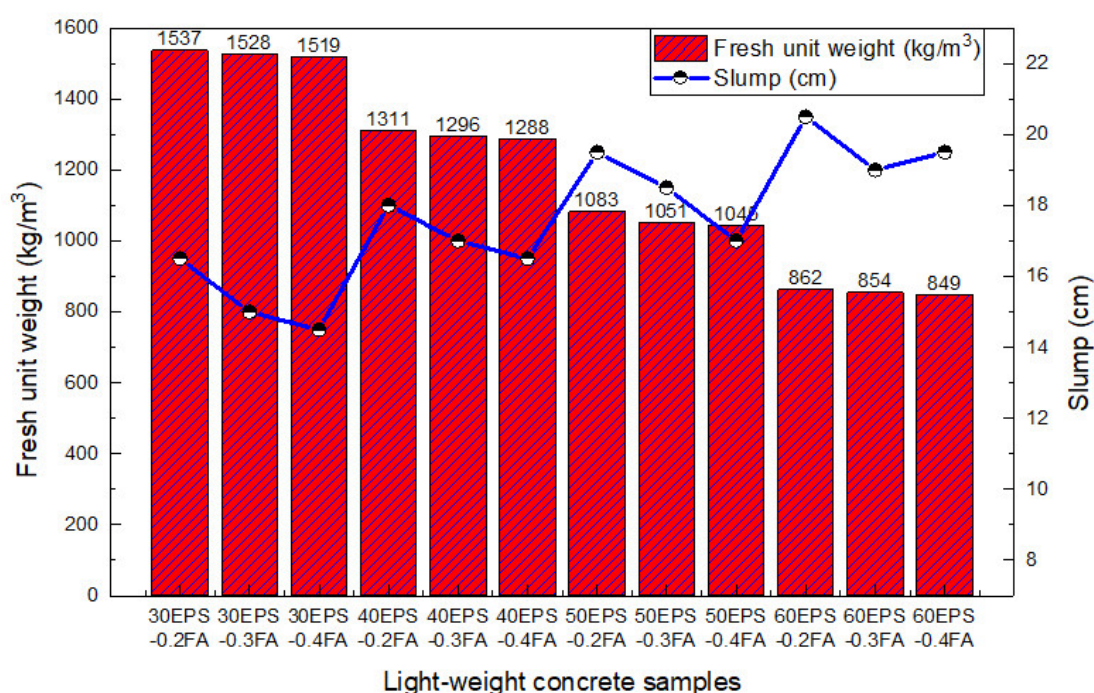
The consistency of the concretes containing (30 ÷ 60) % EPS beads was almost satisfying, and compaction and finish-ability processes were not easily achieved, but the consistency of all other mixtures were normal to work with, and casting, compaction, and finish-ability processes were performed easily. By increasing the EPS content, the slump values of the concrete mixtures increased but the average density of fresh concretes decreased. This was mainly due to the low water absorption of EPS compared with natural aggregate and the density value was much less than that of natural materials. In addition EPS beads are hydrophobic and resist absorption of the mixture's water.

3.2. Mechanical properties of light-weight concrete samples

The mechanical properties of light-weight concrete containing varying contents of EPS and unprocessed FA at different curing times are shown in Table 7. The compressive strength of the concrete sample was in the range of 4.08÷31.2 MPa at 28 days curing time. At this age, tensile strength and modulus of elasticity values were, respectively, in the range of 0.52÷2.45 MPa and 3266÷16855 MPa.

Table 6. Properties of fresh concrete mixtures.

| Sample ID. | $\frac{W}{BID}$ | EPS (%) | $\frac{FA}{OPC}$ | Fresh unit weight (kg/m ³) | Slump (cm) | |
|-----------------|-----------------|---------|------------------|--|------------|------|
| LWC-30EPS-0.2FA | 0.3 | 30 | 0.2 | 1537 | 16.5 | |
| LWC-30EPS-0.3FA | | | 0.3 | 1528 | 15.0 | |
| LWC-30EPS-0.4FA | | | 0.4 | 1519 | 14.5 | |
| LWC-40EPS-0.2FA | | 40 | 40 | 0.2 | 1311 | 18.0 |
| LWC-40EPS-0.3FA | | | | 0.3 | 1296 | 17.0 |
| LWC-40EPS-0.4FA | | | | 0.4 | 1288 | 16.5 |
| LWC-50EPS-0.2FA | | 50 | 50 | 0.2 | 1083 | 19.5 |
| LWC-50EPS-0.3FA | | | | 0.3 | 1051 | 18.5 |
| LWC-50EPS-0.4FA | | | | 0.4 | 1045 | 17.0 |
| LWC-60EPS-0.2FA | | 60 | 60 | 0.2 | 862 | 20.5 |
| LWC-60EPS-0.3FA | | | | 0.3 | 854 | 19.0 |
| LWC-60EPS-0.4FA | | | | 0.4 | 849 | 19.5 |


Figure 10. Effect of unprocessed Fly Ash and Expanded polystyrene on density and workability of mixtures concrete.
Table 7. Mechanical properties of light-weight concrete at different curing ages.

| Sample ID. | Compressive strength at different ages (MPa) | | | | | | Flexural strength at the age of 28 days (MPa) | Modulus of elasticity at 28 days (MPa) |
|-----------------|--|--------|--------|---------|---------|---------|---|--|
| | 1 days | 3 days | 7 days | 14 days | 28 days | 56 days | | |
| LWC-30EPS-0.2FA | 5 | 12.5 | 20.3 | 26.8 | 31.2 | 33.95 | 2.45 | 16855 |
| LWC-30EPS-0.3FA | 4.5 | 11.2 | 18.3 | 24.5 | 28.1 | 32.44 | 2.35 | 15811 |
| LWC-30EPS-0.4FA | 3.6 | 9 | 14.6 | 20.3 | 24.3 | 26.56 | 2.08 | 14135 |
| LWC-40EPS-0.2FA | 2.3 | 5.7 | 9.3 | 12.8 | 14.3 | 17.41 | 1.89 | 10548 |
| LWC-40EPS-0.3FA | 2.1 | 5.4 | 8.7 | 12.1 | 13.1 | 15.98 | 1.56 | 9224 |
| LWC-40EPS-0.4FA | 1.6 | 3.9 | 6.4 | 8.9 | 10.9 | 14.33 | 1.52 | 8272 |
| LWC-50EPS-0.2FA | 1.5 | 3.7 | 6 | 7.5 | 9.3 | 12.5 | 1.24 | 6295 |
| LWC-50EPS-0.3FA | 1.1 | 2.9 | 4.6 | 6.4 | 7.2 | 10.56 | 1.15 | 5135 |
| LWC-50EPS-0.4FA | 0.78 | 1.7 | 2.7 | 3.7 | 4.2 | 5.11 | 1.08 | 4387 |
| LWC-60EPS-0.2FA | 0.71 | 1.85 | 2.65 | 3.34 | 4.18 | 4.56 | 0.64 | 3900 |
| LWC-60EPS-0.3FA | 0.62 | 1.67 | 2.33 | 2.87 | 4.11 | 4.25 | 0.58 | 3606 |
| LWC-60EPS-0.4FA | 0.56 | 1.62 | 2.28 | 2.73 | 4.08 | 4.15 | 0.52 | 3266 |

Similar to the results presented in published studies [36-38], the strengths are decreased as the EPS beads and unprocessed FA contents in concrete samples are increased. For example, the compressive strength for the control concrete (30 % EPS + 20 % FA) was 31.2 MPa at 28 days of age and these decreased to 4.08 MPa for the concrete containing 60 % EPS + 40 % FA at the same age; the decrease in strength concrete was about 86.9 %.

The relationship between compressive strength and curing age for light-weight concrete shown in Figure 11.

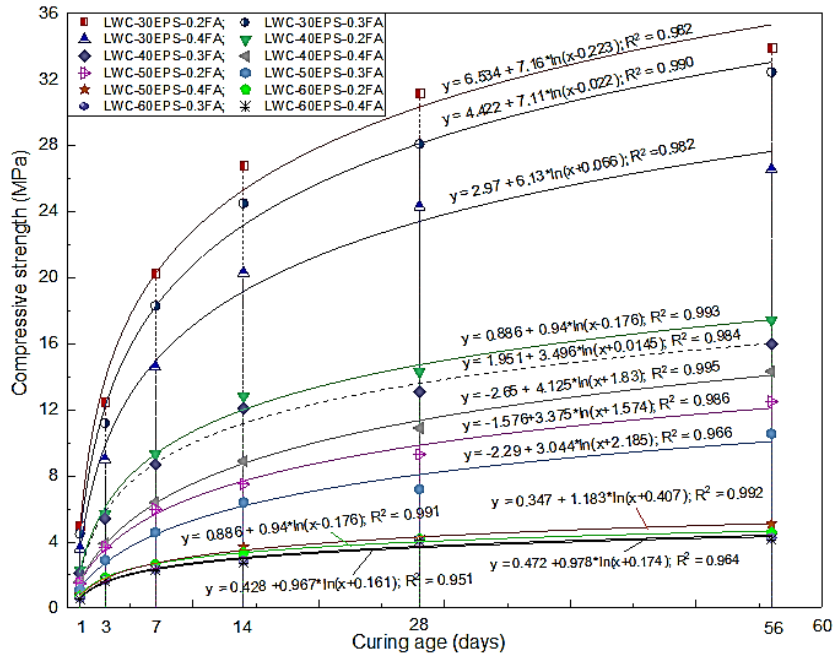


Figure 11. Compressive strength development of light-weight concrete at different ages.

The Portland cement concrete strength level and rate of gain are dependent on many factors. Hydration rate and percentage are two factors related to the used cement [39]. Besides the used cement, there are many factors contributing to both of strength level and its rate of gain at different ages. Mix composition, aggregate type and properties, temperature degree, curing time and method are some factors among the factors affecting both strength level and the gain rate at different ages of concrete [40].

According to experimental results, for all proportions of light-weight concrete, the relationship between age and the compressive strength could take the following shape:

$$y = A + B \cdot \ln(x + C) \tag{4}$$

where: y is the compressive strength of concrete (MPa) at age (x) days and (A), (B) and (C) are constants. These results, similar to the results presented in published studies [39–41].

It could be noticed that, for mixes of concrete containing 30 %, 40 %, 50 % and 60 % by volume of EPS beads and 20 %, 30 % and 40 % by mass of FA follow the proposed formula (4) with a correlation coefficient more than 95 % ($R^2 > 0.95$). The values of coefficients (A , B and C) for mixes containing EPS beads and FA seem to be different.

The relation between compressive strength (R_{cf} , MPa) and tensile strength (R_{ts} , MPa) of light-weight concrete is shown in Figure 12.

The empirical equation obtained for LWC with correlation coefficient ($R^2 = 0.9515$) is given as:

$$R_{cf} = 5.577R_{ts}^{1.886} \tag{5}$$

For light-weight concrete, the modulus of elasticity was determined from the empirical formula proposed by the ACI 318-14 [42, 43] commission, as specified below:

$$E_c = 43 \times \rho^{1.5} \sqrt{R_{cf}}, \tag{6}$$

where: E_c – modulus of elasticity (MPa); R_{cf} – compressive strength (MPa); ρ – dry density (kg/m^3).

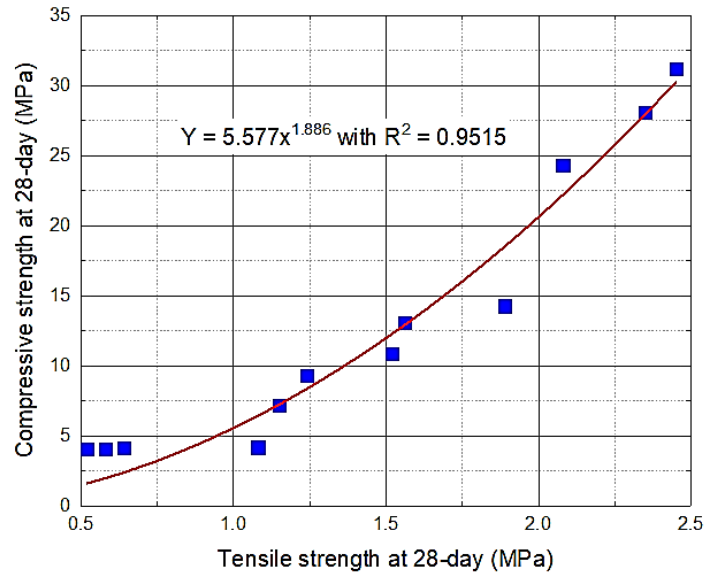


Figure 12. Correlation between compressive strength and tensile strength of light-weight concrete.

Equation (6), which relates the modulus of elasticity with the compressive strength of LWC was chosen because it also takes into account the density of the light-weight concrete. According to the results presented in study [44], the correlation between modulus of elasticity, compressive strength and density of LWC was determined from the empirical formula (7):

$$E_c = 70 \times \rho^{1.53} \times R_{cf}^{0.25} \text{ (MPa)}. \tag{7}$$

Based on the results of this study, the modulus of elasticity of the LWC at 28 days appears to increase with the increase in multiplier dry density and compressive strength of specimens. The relationship between modulus of elasticity, compressive strength and dry density of light-weight concrete made with different ESP beads and unprocessed FA contents is illustrated in Figure 13 and shown in formula (8):

$$E_c = 3.848\rho * \sqrt[3]{R_{cf}} - 1643.64 \text{ (MPa) with } R^2 = 0.993. \tag{8}$$

The value $R^2 = 0.993$ of Equation (8) represents a very strong negative correlation between the three compared parameters of the modulus of elasticity, compressive strength and dry density for the LWC incorporating different amounts of ESP beads and unprocessed FA.

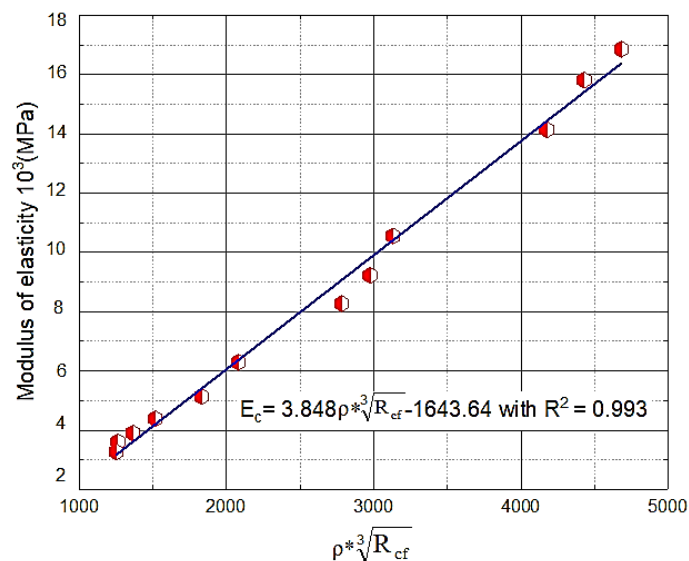


Figure 13. Correlation between modulus of elasticity, compressive strength and density of light-weight concrete.

3.3. Basic physical properties of tested light-weight concrete

The basic physical properties of light-weight concrete containing different contents of EPS beads and unprocessed FA is presented in Table 8. The density values were in the range of $782.42 \div 1487.1 \text{ kg/m}^3$, water absorption $10.5 \div 14.8 \%$ and thermal conductivity $0.275 \div 0.651 \text{ W/m}\cdot\text{°C}$.

Table 8. The basic physical properties of light-weight concrete specimens.

| Sample ID. | Dry density (kg/m^3) | Water absorption (%) | Thermal conductivity λ ($\text{W/m}\cdot\text{°C}$) |
|-----------------|---------------------------------|----------------------|---|
| LWC-30EPS-0.2FA | 1487.1 | 10.5 | 0.651 |
| LWC-30EPS-0.3FA | 1457 | 11.8 | 0.656 |
| LWC-30EPS-0.4FA | 1441.9 | 11.85 | 0.638 |
| LWC-40EPS-0.2FA | 1289.7 | 12.5 | 0.560 |
| LWC-40EPS-0.3FA | 1261.9 | 13.2 | 0.541 |
| LWC-40EPS-0.4FA | 1254.7 | 13.5 | 0.548 |
| LWC-50EPS-0.2FA | 989.5 | 13.8 | 0.402 |
| LWC-50EPS-0.3FA | 948 | 14 | 0.371 |
| LWC-50EPS-0.4FA | 940.2 | 14.2 | 0.387 |
| LWC-60EPS-0.2FA | 846.92 | 14.3 | 0.339 |
| LWC-60EPS-0.3FA | 787.38 | 14.5 | 0.298 |
| LWC-60EPS-0.4FA | 782.42 | 14.8 | 0.275 |

The relationship between the dry density and water absorption of light-weight concrete made with different ESP beads and unprocessed FA contents is illustrated in Figure 14. The dry density of the LWC appears to decrease with an increase in water absorption of specimens. A linear function appears to better describe the relationship between dry density and water absorption for all concretes made with different EPS beads and FA contents at 28 days and is shown in Equation (9):

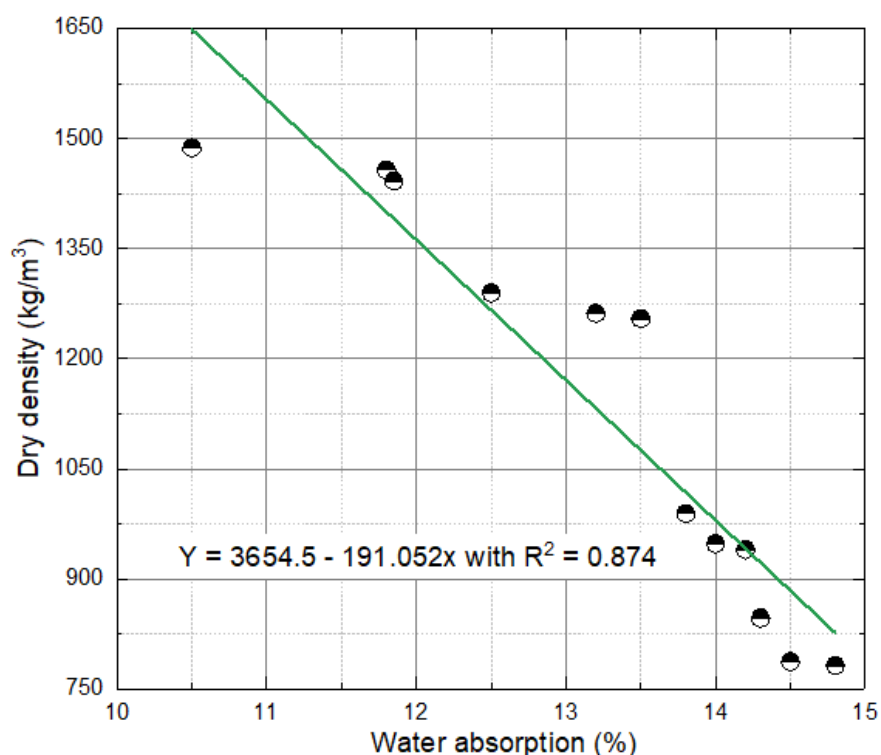


Figure 14. Relationship between dry density and water absorption of light-weight concrete.

$$Y = 3654.5 - 191.052x \text{ with } R^2 = 0.874. \quad (9)$$

In Equation (9), Y is the dry density (kg/m^3) and x is the water absorption (%). The value $R^2 = 0.874$ represents a relatively strong negative correlation between the two compared parameters of dry density and water absorption for the concrete incorporating different amounts of ESP beads and unprocessed FA.

The relationship between the thermal conductivity and dry density of LWC made with different ESP and FA contents are shown in Figure 15.

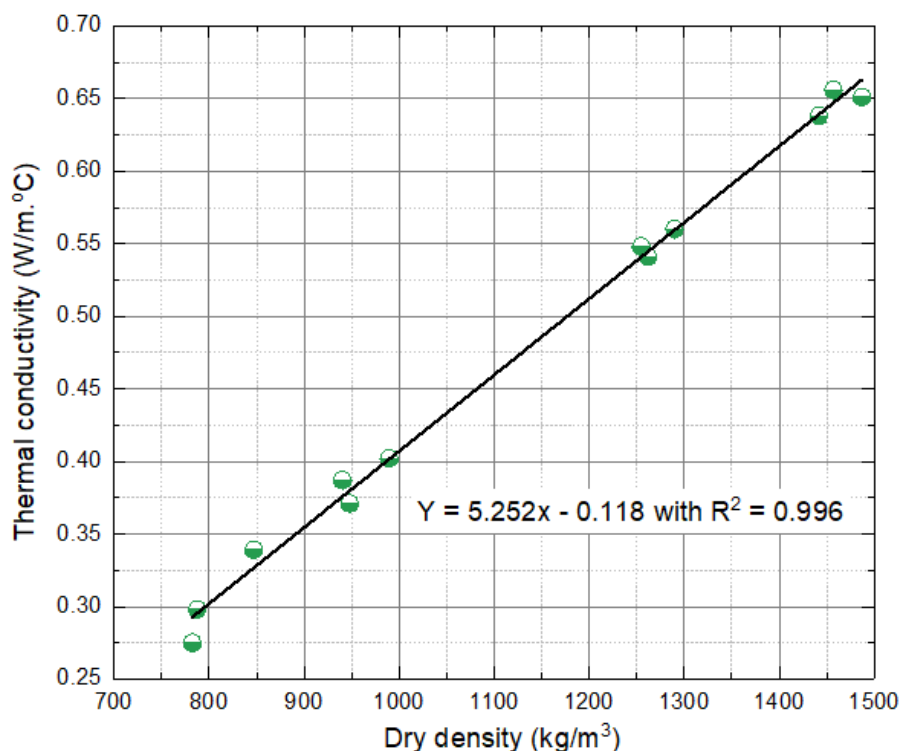


Figure 15. Relationship between thermal conductivity and dry density of light-weight concrete.

The dry density of the LWC appears to increase with an increase in thermal conductivity of LWC. Based on the results of the studies [45] for structural insulation of polystyrene concrete, a generalized dependence of thermal conductivity on dry density was proposed, which was approximated by a linear dependence according to the formula (10):

$$\lambda^{\text{LWC}} = 0.4228 \cdot \rho^{\text{LWC}} - 42.281 \text{ with } R^2 = 0.9515. \quad (10)$$

For this study, a linear function appears to better describe the relationship between thermal conductivity and dry density of light-weight concrete made with different EPS beads and FA contents at 28 days and is shown in Equation (11):

$$Y = 5.252x - 0.118 \text{ with } R^2 = 0.996. \quad (11)$$

The first (Y) and second (x) terms in equation (11) represent thermal conductivity (W/m.°C) and the dry density (kg/m³) of LWC, respectively. The value $R^2 = 0.996$ represents a very strong negative correlation between the two compared parameters of thermal conductivity and dry density for the LWC incorporating different amounts of ESP beads and unprocessed FA.

3.4. Definitions of temperature regime and comparison of thermal insulation performance of light-weight concrete block with the standard brick in enclosing structures

This study analyzes the heat transfer in the wall covering of buildings, which are built by block bricks light-weight concrete (which consist of 60 % EPS and 40 % FA, shown in Table 8), with the using a complex computer program ANSYS 18 (APDL). These analyzes allow for the assessment and comparison of the insulation of the wall covering made of light-weight concrete with wall coverings made from other materials.

The results of the analysis of the heat transfer through the wall coverings, which were constructed of solid clay brick, hollow clay brick, solid unit with slag concrete and solid brick with LWC, are shown in Figures 16, 17 and 18.

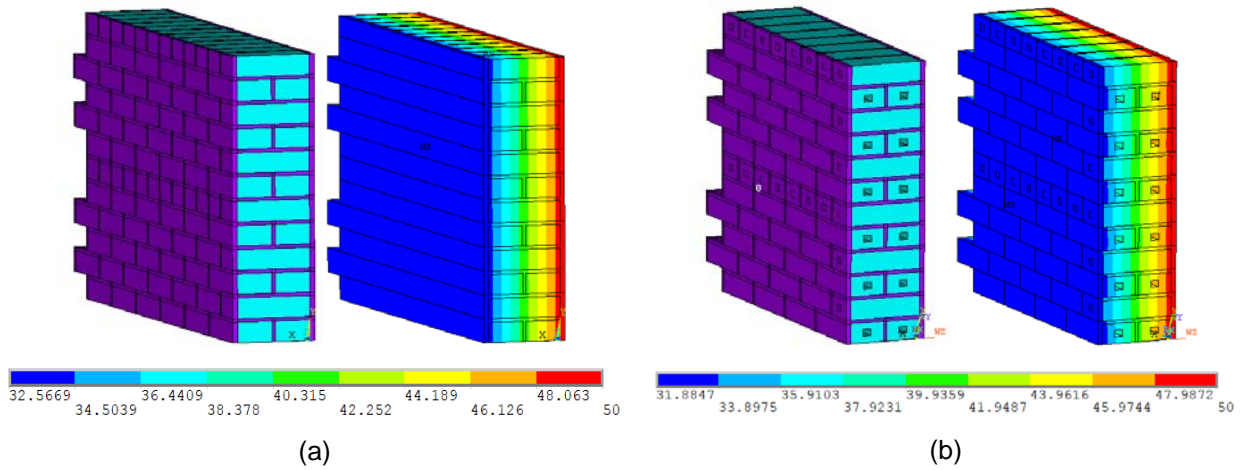


Figure 16. Temperature distribution over the thickness of wall: (a) by the solid clay brick and (b) by hollow clay brick.

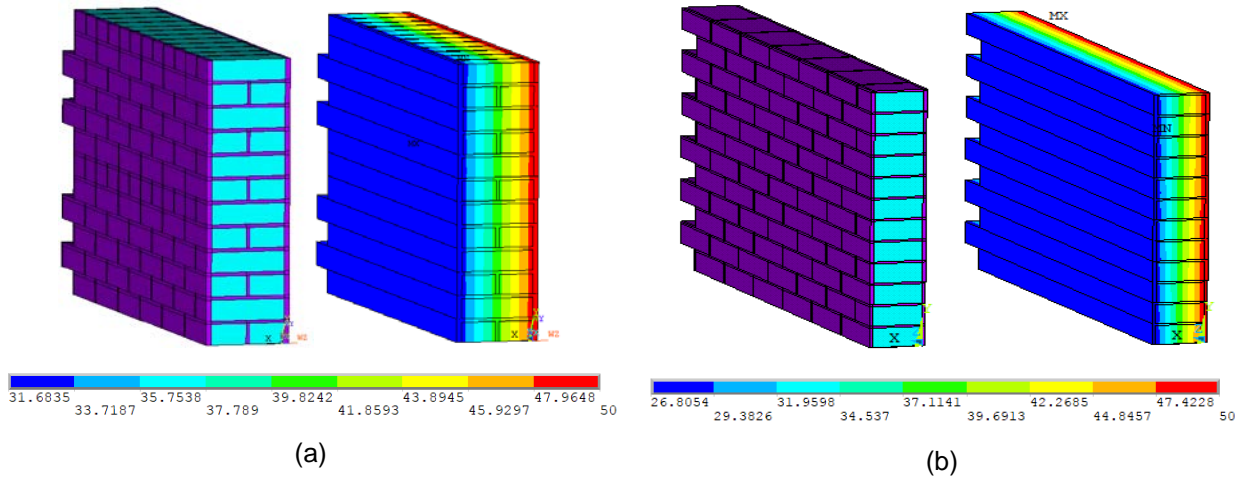


Figure 17. Temperature distribution over the thickness of wall: (a) by solid unit with slag concrete and (b) by solid brick with LWC.

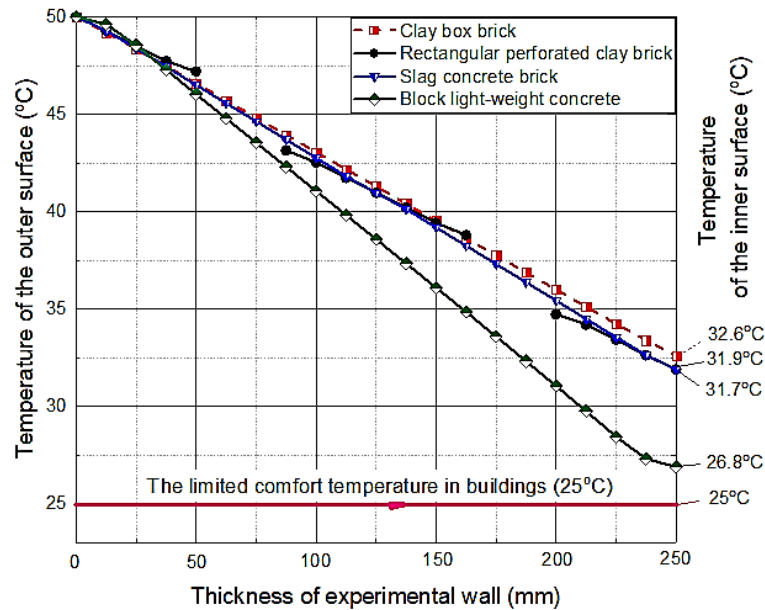


Figure 18. Comparison chart of heat distribution over the thickness of the experimental wall structure.

Based on the results, the analysis by ANSYS 18 software are shown that at the same thickness of 250 mm, a wall with the solid bricks with LWC has better insulation than the wall made of other materials such as: solid clay brick, hollow clay brick, solid unit with slag concrete.

By comparison, the comfort temperature in buildings (25 °C), the temperature of the inner surface of the experimental wall structure was increased 1.8 °C by solid brick with LWC; 7.6 °C by solid clay brick; 6.9 °C by clay hollow bricks and 6.7 °C by solid unit with slag concrete. Temperature of the inner surface of the experimental wall structure was increased not much, so the energy cost to reduce temperature in building will be lower than other wall solutions. In addition, the size of the block bricks from light-weight concrete is four times larger than that of the other bricks. The weight of a solid brick with LWC larger than 2 times the other bricks. The size of the large brick, while the weight of the brick is small. This will create favorable conditions and shorten construction time.

4. Conclusion

Based on the experimental results, the following conclusions may be drawn:

1. By increasing EPS beads and unprocessed FA in the twelve of compositions for light-weight concrete the strength, modulus of elasticity, dry density and thermal conductivity decreased, but its water absorption and thermal insulation performance increased. The level of decrease in the mechanical properties of LWC depends upon the replacement level of ESP and FA.

2. The concrete containing 60 % EPS and 40 % FA of contents can be used to produce light-weight bricks and concrete blocks with low thermal conductivity at the wall covers of the High-Rise buildings in Vietnam or may be used in low-strength concretes' applications for example footpaths, cycle paths, and noise reduction barriers in the music room and the study room.

3. The use of EPS beads and unprocessed FA (Vietnam) is an interesting way to extend its life in civil engineering applications providing light-weight concretes with enhanced thermal insulation properties and environmentally-friendly materials.

4. According to the results, the wall with block light-weight concrete bricks with low thermal conductivity is a rational, technological constructing solution under the climatic conditions of Vietnam, which allows providing the required parameters of the microclimate, creating a comfortable mode for indoor-life.

5. The advantages of the investigated block light-weight brick concrete design compared to traditional solutions are: increasing thermal uniformity due to the reduction of heat-conducting inclusions and increasing manufacturability by reducing the duration and complexity of work.

When EPS beads are manufactured correctly, with appropriate concrete mix design, the utilization of this novel fine, coarse and lightweight aggregate is made from EPS beads and unprocessed FA in light-weight concrete production is possible. However, more corrosion and mechanical experiments, resistivity, the specific heat of LWC and effect of the bond between the coating and waste EPS as future work needed to be done before this novel environmentally-friendly material could be used in different buildings and structures.

References

1. Lucolano, F., Liguori, B., Caputo, D., Colangelo, F., Cioffib, R. Recycled plastic aggregate in mortars composition: Effect on physical and mechanical properties. *Materials & Design*. Vol. 52. Pp. 916–922. DOI: 10.1016/j.matdes.2013.06.025.
2. Záleská, M., Pokorný, J., Pavlíková, M., Pavlík, Z. Thermal properties of light-weight concrete with waste polypropylene aggregate. In *AIP Conference Proceedings*. 2017. Vol. 1866(1). 040043. 5 p. DOI: 10.1063/1.4994523.
3. Jin, X., Zhang, X., Cao, Y., Wang, G. Thermal performance evaluation of the wall using heat flux time lag and decrement factor. *Energy and Buildings*. 2012. Vol. 47(0). Pp. 369–374. DOI: 10.1016/j.enbuild.2011.12.010
4. Korniyenko, S.V. The experimental analysis and calculative assessment of building energy efficiency. *Applied Mechanics and Materials*. 2014. No. 618. Pp. 509–513. DOI: 10.4028/www.scientific.net/AMM.618.509
5. QCVN 02-2009. Vietnam building code natural Physical & Climatic data for construction. Standard. Vietnam. 2009. 324 p.

Литература

1. Lucolano F., Liguori B., Caputo D., Colangelo F., Cioffib R. Recycled plastic aggregate in mortars composition: Effect on physical and mechanical properties // *Materials & Design*. Vol. 52. Pp. 916–922. DOI: 10.1016/j.matdes.2013.06.025.
2. Záleská M., Pokorný J., Pavlíková M., Pavlík Z. Thermal properties of light-weight concrete with waste polypropylene aggregate // In *AIP Conference Proceedings*. 2017. Vol. 1866(1). 040043. 5 p. DOI: 10.1063/1.4994523.
3. Jin X., Zhang X., Cao Y., Wang G. Thermal performance evaluation of the wall using heat flux time lag and decrement factor // *Energy and Buildings*. 2012. Vol. 47(0). Pp. 369–374. DOI: 10.1016/j.enb uild.2011.12.010
4. Korniyenko S.V. The experimental analysis and calculative assessment of building energy efficiency // *Applied Mechanics and Materials*. 2014. No. 618. Pp. 509–513. DOI: 10.4028/www.scientific.net/AM M.618.509
5. QCVN 02-2009. Vietnam building code natural Physical & Climatic data for construction, Standard. Vietnam, 2009. 324 p.
6. TCVN 4605-1988. Heating techniques – insulating component – Design standard. Standard. VietNam, 1988. 27 p.

Lam, T.V., Vu, D.T., Dien, V.K., Bulgakov, B.I., Korol, E.A. Properties and thermal insulation performance of light-weight concrete. *Magazine of Civil Engineering*. 2018. 84(8). Pp. 173–191. doi: 10.18720/MCE.84.17.

6. TCVN 4605-1988. Heating techniques – insulating component – Designs standard. Standard. VietNam. 1988. 27 p.
7. Vatin, N.I., Pestryakov, I.I., Sultanov, Sh.T., Ogidan, T., Yarusnischeva, Y.A., Kiryushina, A.P. Water vapour by diffusion and mineral wool thermal insulation materials. Magazine of Civil Engineering. 2018. 81(5). Pp. 184–193. DOI: 10.18720/MCE.81.18
8. QCVN 09-2013. National technical regulation on Energy efficiency building. Standard. Vietnam. 2013. 19 p.
9. Lam, N.S., Hanh, P.D. Thermal insulation for buildings. Journal of Science and Technology in Civil Engineering. 2015. No. 4. Pp. 36–41.
10. Michal, G., Eva, K. Impact Verification of Aerogel Insulation Paint on Historic Brick Facades. IOP Conf. Series: Materials Science and Engineering. 2017. No. 245. DOI: 10.1088/1757-899X/245/8/082021
11. Guo, W., Qiao, X., Huang, Y., Fang, M., Han, X. Study on energy saving effect of heat-reflective insulation coating on envelopes in the hot summer and cold winter zone. Energy and Buildings. 2012. Vol. 50. Pp. 196–203. URL: <https://doi.org/10.1016/j.enbuild.2012.03.040>
12. Korniyenko, S. Complex analysis of energy efficiency in operated high-rise residential building: Case study. E3S Web of Conferences. 2018. 33. 02005. DOI: 10.1051/e3sconf/20183302005
13. Zuginisov, M.T., Myrzahmetov, M.M., Sartayev, D.T., Orynbekov Ye. S. Heat-resistant ferrochrome slag based concrete. Magazine of Civil Engineering. 2014. 51(7). Pp. 38–45. DOI: 10.5862/MCE.51.5. (rus)
14. Bilous, I.Yu., Deshko, V.I., Sukhodub, I.O., Belous, I.Yu., Building inside air temperature parametric study. Magazine of Civil Engineering. 2016. 68(8). Pp. 65–75. DOI: 10.5862/MCE.68.7. (rus)
15. Leshchenko, M.V., Semko, V. Thermal characteristics of the external walling made of cold-formed steel studs and polystyrene concrete. Magazine of Civil Engineering. 2015. 60(8). Pp. 43–55. DOI: 10.5862/MCE.60.6. (rus)
16. Babu, K.G., Babu, D.S. Behaviour of lightweight expanded polystyrene concrete containing silica fume. Cem. Concr. Res. 2003. Vol. 33(5). Pp. 755–762. DOI: 10.1016/S0008-8846(02)01055-4.
17. Inozemtcev A.S. Average density and porosity of high-strength lightweight concrete. Magazine of Civil Engineering. 2014. 51(7). Pp. 31–37. DOI: 10.5862/MCE.51.4. (rus)
18. Korniyenko, S.V., Vatin, N.I., Gorshkov, A.S. Thermophysical field testing of residential buildings made of autoclaved aerated concrete blocks. Magazine of Civil Engineering. 2016. 64(4). Pp. 10–25. DOI: 10.5862/MCE.64.2. (rus)
19. Duc, H.M. Study on lightweight concrete structure insulation using expanded polystyrene beads. Journal of Science and Technology. 2017. No. 4. Pp. 39–47.
20. Hieu, D.N., Kim, X.T.T., Ngoc, M.N., Toan, T.D. Self – compacting lightweight aggregate concrete in Vietnam // IOP Conf. Series: Materials Science and Engineering 365 (2018) 032030. DOI: 10.1088/1757899X/365/3/032030.
21. Le Roy, R., Parant, E., Boulay, C. Taking into account the inclusions size in lightweight concrete compressive strength prediction // Cem. Concr. Res. 2005. Vol. 35 (4). Pp. 770–775. DOI: 10.1016/j.cemconres.2004.06.002
22. Chen, B., Liu, J. Mechanical properties of polymer-modified concretes containing expanded polystyrene beads. Constr. Build. Mater. 2007. Vol. 21(1). Pp. 7–11. DOI: 10.1016/j.conbuildmat.2005.08.001
23. Ganesh Babu, K., Saradhi Babu, D. Performance of fly ash concretes containing lightweight EPS aggregates. Cem. Concr. Compos. 2004. Vol. 26(6). Pp. 605–611. DOI: 10.1016/S0958-9465(03)00034-9
24. Babu D.S., Ganesh Babu K., Tiong-Huan W. Effect of polystyrene aggregate size on strength and moisture migration characteristics of lightweight concrete // Cem. Concr. Compos. 2004. Vol. 26(6). Pp. 605–611. DOI: 10.1016/S0958-9465(03)00034-9
7. Ватин Н.И., Пестряков И.И., Султанов Ш.Т., Огидан О.Т., Ярусничева Ю.А., Кирюшина А. Диффузионное влагопоглощение теплоизоляционных изделий и минеральной ваты // Инженерно-строительный журнал. 2018. № 5(81). С. 184–193. DOI: 10.18720/MCE.81.18.
8. QCVN 09-2013. National technical regulation on Energy efficiency building. Standard. Vietnam, 2013. 19 p.
9. Lam N.S., Hanh P.D. Thermal insulation for buildings // Journal of Science and Technology in Civil Engineering. 2015. № 4. Pp. 36–41.
10. Michal G., Eva K. Impact Verification of Aerogel Insulation Paint on Historic Brick Facades // IOP Conf. Series: Materials Science and Engineering. 2017. № 245. DOI: 10.1088/1757-899X/245/8/082021.
11. Guo W., Qiao X., Huang Y., Fang M., Han X. Study on energy saving effect of heat-reflective insulation coating on envelopes in the hot summer and cold winter zone // Energy and Buildings. 2012. Vol. 50. Pp 196–203. DOI: 10.1016/j.enbuild.2012.03.040
12. Korniyenko S. Complex analysis of energy efficiency in operated high-rise residential building: Case study // E3S Web of Conferences. 2018. 33. 02005. DOI: 10.1051/e3sconf/20183302005
13. Жугинисов М.Т., Мырзахметов М.М., Сартаев Д.Т., Орынбеков Е.С. Жаростойкий бетон на основе феррохромового шлака // Инженерно-строительный журнал. 2014. № 7(51). С. 38–45. DOI: 10.5862/MCE.51.5.
14. Белоус И.Ю., Дешко В.И., Суходуб И.О. Параметрический анализ внутренней температуры воздуха здания // Инженерно-строительный журнал. 2016. № 8(68). С. 65–75. DOI: 10.5862/MCE.68.7.
15. Лещенко М.В., Семко В.А., Теплотехнические свойства стеновых ограждающих конструкций из стальных тонкостенных профилей и полистиролбетона // Инженерно-строительный журнал. 2015. № 8(60). С. 43–55. DOI: 10.5862/MCE.60.6
16. Babu K.G., Babu D.S. Behaviour of lightweight expanded polystyrene concrete containing silica fume // Cem. Concr. Res. 2003. Vol. 33(5). Pp. 755–762. DOI: 10.1016/S0008-8846(02)01055-4.
17. Иноземцев А.С. Средняя плотность и пористость высокопрочных легких бетонов // Инженерно-строительный журнал. 2014. № 7(51). С. 31–37. DOI: 10.5862/MCE.51.4.
18. Корниенко С.В., Ватин Н.И., Горшков А.С. Натурные теплофизические испытания жилых зданий из газобетонных блоков // Инженерно-строительный журнал. 2014. № 4(64). С. 10–25. DOI: 10.5862/MCE.64.2.
19. Duc H.M. Study on lightweight concrete structure insulation using expanded polystyrene beads // Journal of Science and Technology. 2017. No.4. Pp. 39–47.
20. Hieu D.N., Kim X.T.T., Ngoc M.N., Toan T.D. Self – compacting lightweight aggregate concrete in Vietnam // IOP Conf. Series: Materials Science and Engineering 365 (2018) 032030. DOI:10.1088/1757899X/365/3/032030.
21. Le Roy R., Parant E., Boulay C. Taking into account the inclusions size in lightweight concrete compressive strength prediction // Cem. Concr. Res. 2005. Vol. 35 (4). Pp. 770–775. DOI: 10.1016/j.cemconres.2004.06.002.
22. Chen B., Liu J. Mechanical properties of polymer-modified concretes containing expanded polystyrene beads // Constr. Build. Mater. 2007. Vol. 21(1). Pp. 7–11. DOI: 10.1016/j.conbuildmat.2005.08.001.
23. Ganesh Babu K., Saradhi Babu D. Performance of fly ash concretes containing lightweight EPS aggregates // Cem. Concr. Compos. 2004. Vol. 26(6). Pp. 605–611. DOI: 10.1016/S0958-9465(03)00034-9.
24. Babu D.S., Ganesh Babu K., Tiong-Huan W. Effect of polystyrene aggregate size on strength and moisture migration characteristics of lightweight concrete // Cem. Concr. Compos. 2004. Vol. 26(6). Pp. 605–611. DOI: 10.1016/S0958-9465(03)00034-9.

Лам Т.В., Ву Д., Зиен В., Булгаков Б.И., Король Е.А. Свойства и теплоизоляционные эффективности легких бетонов // Инженерно-строительный журнал. 2018. № 8(84). С. 173–191.

24. Babu, D.S., Ganesh, Babu, K., Tiong-Huan, W. Effect of polystyrene aggregate size on strength and moisture migration characteristics of lightweight concrete. *Cem. Concr. Compos.* 2006. Vol. 28(6). Pp. 520–527. DOI: 10.1016/j.cemconcomp.2006.02.018
25. Lam Tang Van, Tho Vu Dinh, Dien Vu Kim, Bulgakov B.I., Aleksandrova O.V., Bazhenova S.I. Combined Effects of Bottom Ash and Expanded Polystyrene on Light-weight Concrete Properties. *MATEC Web of Conferences* 251, 01007. 2018. DOI: 10.1051/matecco nf/201825101007
26. Ganesh Babu D., Ganesh Babu K., Wee T.H. Properties of lightweight expanded polystyrene aggregate concretes containing fly ash. *Cem. Concr. Res.* 2005. Vol. 35(6). Pp. 1218–1223. DOI: 10.1016/j.cemconres.2004.11.015.
27. Burak, F., Kamile, T., Bülent, B., Akin, A., Bahadır, U. The effect of fly ash and limestone fillers on the viscosity and compressive strength of self-compacting repair mortars. *Cement and Concrete Research.* Vol. 36(9). 2006. Pp. 1719–1726. DOI: 10.1016/j.cemconres. 2006.04.002.
28. Moaveni, S. *Finite element analysis: Theory and application with ANSYS.* London. 2015. 861 p.
29. Shi, N., Zhang, R., Huang, D. Thermal stress analyses and reinforcement design of massive RC structures. *European Journal of Environmental and Civil Engineering.* 2015. Vol. 19(8). Pp. 901–916. DOI: 10.1080/19648189.2014.985849.
30. Lam, V.T., Chuc, T.N., Bulgakov, B., Anh, N.P. Composition and early-age temperature regime in massive concrete foundation. *MATEC Web of Conferences* 196, 04017. 2018. 8 p. DOI: 10.1051/mateconf/201819604017.
31. Bushmanova, A.V., Videnkov, N.V., Semenov, K.V., Barabanshchikov, Yu.G., Demakova, A.V., Korovina, V.K. The thermo – stressed state in massive concrete structures. *Magazine of Civil Engineering.* 2017. 71(3). Pp. 51–60. DOI: 10.18720/MCE.71.6.
32. Petr, K. *A Pragmatic Introduction To The Finite Element Method For Thermal And Stress Analysis.* World Scientific Publishing Co. Pte. Ltd. 2006. 292 p.
33. Ataei, H., Mamaghani, M. *Finite Element Analysis Applications and Solved Problems using ABAQUS.* USA. 2017. 372 p.
34. Kim, H.H., Kim, K., Truong, V.V., Bui, D.V., Nguyen, V.C. Survey optimal composition of lightweight concrete to create hollow beads EPS (Expanded Polystyrene) to produce the panel wall and panel floor used for the housing assembly. *Science & Technology Development,* Vol. 13. K3-2010. Pp. 14–28.
35. Lam, T.V., Hung, N.X., Bulgakov, B.I., Alexandrova, O.V., Larsen, O.A., Orekhova, A.Yu., Tyurina, A.A. Use of ash and slag waste as a supplementary cementing material. *Bulletin of BSTU named after V.G. Shukhov.* 2018. No. 8. Pp. 19-27. DOI: 10.12737/article_5b6d58455b5832.12667511. (rus)
36. Cui, H.Z., Lo, T.Y., Memon, S.A., Xu, W. Effect of lightweight aggregates on the mechanical properties and brittleness of lightweight aggregate concrete. *Constr. Build. Mater.* Vol. 35. 2012. Pp 149–158. DOI: 10.1016/j.conbuildmat.2012.02.053.
37. Sadrumontazi, A., Sobhani, J., Mirgozar, M.A., Najimi, M. Properties of multi-strength grade EPS concrete containing silica fume and rice husk ash. *Constr. Build. Mater.* 2012. Vol. 35. Pp. 211–219. DOI: 10.1016/j.conbuildmat.2012.02.049.
38. Demirboğa, R., Türkmen, I., Karakoç, M.B. Relationship between ultrasonic velocity and compressive strength for high-volume mineral-admixed concrete. *Cem. Concr. Res.* 2004. Vol. 34(12). Pp 2329–2336. DOI: 10.1016/j.cemconres.2004.04.017.
39. Abdelaty, M. Compressive strength prediction of Portland cement concrete with age using a new model. *HBRC journal.* 2014. Vol. 10(2). Pp. 145–155. DOI: 10.1016/j.hbrj.2013.09.005.
40. Hewlett P.C. *Lea's Chemistry of Cement and Concrete 4th Edition* // Elsevier Butterworth-Heinemann. New York. 2006. 1092 p.
41. Concr. Compos. 2006. Vol. 28(6). Pp. 520–527. DOI: 10.1016/j.cemconcomp.2006.02.018.
42. Lam Tang Van, Tho Vu Dinh, Dien Vu Kim, Bulgakov B.I., Aleksandrova O.V., Bazhenova S.I. Combined Effects of Bottom Ash and Expanded Polystyrene on Light-weight Concrete Properties. *MATEC Web of Conferences* 251, 01007. 2018. DOI: 10.1051/mateconf/201825101007.
43. Ganesh Babu D., Ganesh Babu K., Wee T.H. Properties of lightweight expanded polystyrene aggregate concretes containing fly ash // *Cem. Concr. Res.* 2005. Vol. 35(6). Pp. 1218–1223. DOI: 10.1016/j.cemconres.2004.11.015.
44. Burak F., Kamile T., Bülent B., Akin A., Bahadır U. The effect of fly ash and limestone fillers on the viscosity and compressive strength of self-compacting repair mortars // *Cement and Concrete Research.* Vol. 36(9). 2006. Pp. 1719–1726. DOI: 10.1016/j.cemconres.2006.04.002.
45. Moaveni S. *Finite element analysis: Theory and application with ANSYS.* London. 2015. 861 p.
46. Shi N., Zhang R., Huang D. Thermal stress analyses and reinforcement design of massive RC structures // *European Journal of Environmental and Civil Engineering.* 2015. Vol. 19(8). Pp. 901–916. DOI: 10.1080/19648189.2014.985849.
47. Lam V.T., Chuc T.N., Bulgakov B., Anh N.P. Composition and early-age temperature regime in massive concrete foundation // *MATEC Web of Conferences* 196, 04017. 2018. 8 p. DOI: 10.1051/mateconf/201819604017.
48. Бушманова А.В., Виденков Н.В., Семенов К.В., Барабанщиков Ю.Г., Дернакова А.В., Коровина В.К. Термонапряженное состояние массивных бетонных конструкций // *Инженерно-строительный журнал,* 2017, № 3(71). С. 51–60. DOI: 10.18720/MCE.71.6
49. Petr K. *A Pragmatic Introduction To The Finite Element Method For Thermal And Stress Analysis.* World Scientific Publishing Co. Pte. Ltd. 2006. 292 p.
50. Ataei H., Mamaghani M. *Finite Element Analysis Applications and Solved Problems using ABAQUS.* USA. 2017. 372 p.
51. Kim H.H., Kim K., Truong V.V., Bui D.V., Nguyen V.C. Survey optimal composition of lightweight concrete to create hollow beads EPS (Expanded Polystyrene) to produce the panel wall and panel floor used for the housing assembly // *Science & Technology Development,* Vol. 13. K3-2010. Pp. 14–28.
52. Лам Т.В., Хунг Н.С., Булгаков Б.И., Александрова О.В., Ларсен О.А., Орехова А.Ю., Тюрина А.А. Использование золошлаковых отходов в качестве дополнительного цементующего материала // *Вестник БГТУ им. В.Г. Шухова.* 2018. № 8. С. 19–27. DOI: 10.12737/article_5b6d58455b5832.12667511.
53. Cui H.Z., Lo T.Y., Memon S.A., Xu W. Effect of lightweight aggregates on the mechanical properties and brittleness of lightweight aggregate concrete // *Constr. Build. Mater.* 2012. Vol. 35. Pp 149–158. DOI: 10.1016/j.conbuildmat.2012.02.053.
54. Sadrumontazi A., Sobhani J., Mirgozar M.A., Najimi M. Properties of multi-strength grade EPS concrete containing silica fume and rice husk ash // *Constr. Build. Mater.* 2012. Vol. 35. Pp 211–219. DOI: 10.1016/j.conbuildmat.2012.02.049.
55. Demirboğa R., Türkmen I., Karakoç M.B. Relationship between ultrasonic velocity and compressive strength for high-volume mineral-admixed concrete. *Cem. Concr. Res.* 2004. Vol. 34(12). Pp 2329–2336. DOI: 10.1016/j.cemconres.2004.04.017.
56. Abdelaty M. Compressive strength prediction of Portland cement concrete with age using a new model // *HBRC journal.* 2014. Vol. 10(2). Pp. 145–155. DOI: 10.1016/j.hbrj.2013.09.005.
57. Hewlett P.C. *Lea's Chemistry of Cement and Concrete 4th Edition* // Elsevier Butterworth-Heinemann. New York. 2006. 1092 p.

Lam, T.V., Vu, D.T., Dien, V.K., Bulgakov, B.I., Korol, E.A. Properties and thermal insulation performance of light-weight concrete. *Magazine of Civil Engineering.* 2018. 84(8). Pp. 173–191. doi: 10.18720/MCE.84.17.

40. Hewlett, P.C. *Lea's Chemistry of Cement and Concrete* 4th Edition. Elsevier Butterworth – Heinemann. New York. 2006. 1092 p.
41. Colak, A. A new model for the estimation of compressive strength of Portland cement concrete. *Cement and Concrete Research*. 2006. Vol. 36(7). Pp. 1409–1413. DOI: 10.1016/j.cemconres.2006.03.002.
42. Moravia, W.G., Gumieri, A.G., Vasconcelos, W.L. Efficiency factor and modulus of elasticity of lightweight concrete with expanded clay aggregate // *Revista IBRACON de Estruturas e Materiais*, 2010, Vol. 3(2). Pp. 195–204. DOI: 10.1590/S1983-41952010000200005.
43. American Concrete Institute – ACI. *Manual of Concrete Practice, Part 3: «Building Code Requirements for Reinforced Concrete»*. Reported by ACI Committee 318-2014. Detroit. 2014. 524 p.
44. Saradhi Babua, D., Ganesh Babub, K., Weea, T.H. Properties of lightweight expanded polystyrene aggregate concretes containing fly ash. *Cement and Concrete Research*. 2005. Vol. 35(6). Pp. 1218–1223. DOI: 10.1016/j.cemconres.2004.11.015
45. Collet, F., Pretot, S. Thermal conductivity of hemp concretes: Variation with formulation, density and water content. *Construction and Building Materials*. 2014. Vol. 65(29). Pp. 612–619. DOI: 10.1016/j.conbuildmat.2014.05.039.
41. Colak A. A new model for the estimation of compressive strength of Portland cement concrete // *Cement and Concrete Research*. 2006. Vol. 36(7). Pp. 1409–1413. DOI: 10.1016/j.cemconres.2006.03.002.
42. Moravia W.G., Gumieri A.G., Vasconcelos W.L. Efficiency factor and modulus of elasticity of lightweight concrete with expanded clay aggregate // *Revista IBRACON de Estruturas e Materiais*, 2010, Vol. 3(2). Pp. 195–204. DOI: 10.1590/S1983-41952010000200005.
43. American Concrete Institute – ACI. *Manual of Concrete Practice, Part 3: «Building Code Requirements for Reinforced Concrete»*. Reported by ACI Committee 318-2014. Detroit. 2014. 524 p.
44. Saradhi Babua D., Ganesh Babub K., Weea T.H. Properties of lightweight expanded polystyrene aggregate concretes containing fly ash // *Cement and Concrete Research*. 2005. Vol. 35(6). Pp. 1218–1223. DOI: 10.1016/j.cemconres.2004.11.015.
45. Collet F., Pretot S. Thermal conductivity of hemp concretes: Variation with formulation, density and water content // *Construction and Building Materials*. 2014. Vol. 65(29). Pp. 612–619. DOI: 10.1016/j.conbuildmat.2014.05.039.

*Tang Vang Lam**,
+7(905)7581983; lamvantang@gmail.com

*Танг Ван Лам**,
+7(905)7581983;
эл. почта: lamvantang@gmail.com

Dinh Tho Vu,
+79654483924; vuthoks@gmail.com

Динь Тхо Ву,
+79654483924; эл. почта: vuthoks@gmail.com

Vu Kim Dien,
79685164689; kimdienxdb@gmail.com

Ву Ким Зиен,
79685164689; эл. почта:
kimdienxdb@gmail.com

Boris Igorevich Bulgakov,
+79104537985; fakultetst@mail.ru

Борис Игоревич Булгаков,
+79104537985; эл. почта: fakultetst@mail.ru

Elena Anatolyevna Korol,
+79857654780; korolea@mgsu.ru

Елена Анатольевна Король,
+79857654780; эл. почта: korolea@mgsu.ru

© Lam, T.V., Vu, D.T., Dien, V.K., Bulgakov, B.I., Korol, E.A., 2018

doi: 10.18720/MCE.84.18

Luminance distributions in the tropical sky conditions

Распределение яркости в условиях тропического неба

N.T.K. Phuong,
National Research Moscow State Civil
Engineering University, Moscow, Russia

М.С., аспирант Н.Т.Х. Фьюнг,
Национальный исследовательский
Московский государственный строительный
университет, г. Москва, Россия

Key words: daylight climate; firmament types;
sky luminance distributions; cloudiness
coefficient; daylighting calculations

Ключевые слова: световой климат; типа
небосвода; распределение яркости неба;
коэффициент облачности; расчет
естественного освещения

Abstract. Lighting engineering in construction is a complex scientific field, which requires the amalgamation of knowledge in the field of daylighting, construction and architecture, as well as other areas, including the humanities. Many studies have proven the benefits of natural light on health, activity, visual well-being and human productivity. Global environmental issues and the sustainable development movement require architectural design to achieve maximum energy efficiency. For all intents, daylighting calculations depend on the luminance distributions of the sky types. Currently, standard documents are used for the luminance distribution and daylighting calculations under overcast sky conditions in Vietnam, where the overcast sky and clear sky are not typically considered. For these reasons, an update of theoretical studies in the daylighting calculations and design the daylighting systems must be completed. Accordingly, this study offers the modern methods of analyzing the firmament luminance distributions when calculating Daylight Factor on the more realistic sky conditions. For this, the sky type have to be defined according to the location. Fifteen international standard types of the firmament with their descriptors are provided by Kittler et al. and a technique using a relation of diffuse and total solar illuminance levels named the cloudiness coefficient K_o are considered to define the sky condition in Hanoi and Ho Chi Minh City. As the results, the typical sky type for Hanoi is the partly cloudy sky no gradation towards zenith, slight brightening towards the Sun; when the sky type for Ho Chi Minh City is the partly cloudy, with brighter circumsolar region. From these results, the sky luminance distributions for daylighting calculations were proposed. A comparison shows the difference between these calculations can be allowed at the altitude angles γ of a point in the sky above 50° with the relative errors below 10 %. The method offered and verified in this study showed that, it has potential to be used for difference climate areas.

Аннотация. Светотехника в строительстве представляет собой сложную научную область, которая требует обобщения знаний в области естественного освещения, строительства и архитектуры, а также других областей, в том числе гуманитарных. Многие исследования доказали преимущества естественного освещения здоровья, активности, визуального благополучия и производительности человека. Глобальные экологические проблемы и движение за устойчивое развитие требуют архитектурного проектирования для достижения максимальной эффективности использования энергии. По этим причинам обновление теоретических исследований в расчетах естественного освещения и проектирования систем естественного освещения должно быть завершено. В настоящее время стандартные документы используются для расчетов естественного освещения в зависимости распределения яркости неба в условиях пасмурного неба во Вьетнаме, где особенность неба является не типично ясным и не типично пасмурным. Соответственно, это исследование предлагает современные методы анализа распределения яркости небосвода при расчете коэффициента естественного освещения на реальном небе местности. Для этого тип неба местности должен определяться. Пятнадцать международных стандартных типов небосвода с их дескрипторами, которые предоставляются Киттлером и др. и метод расчета по коэффициентам облачности K_o используются при определении реального неба в Ханое и Хошимин. Результаты показывают типичный тип неба для Ханоя - это облачное небо без градации к зениту, слабое осветление к Солнцу, когда тип неба для Хошимина является облачным, с более яркой окружной областью. Из этих результатов, значения распределения яркости неба предложены. Приведение сравнения показывает, что разница между этими методами расчета может быть разрешена при углах высоты расчетной точки в небе выше 50° с относительными погрешностями ниже 10 %. Метод

предложенный и подтвержденный в этом исследовании может использоваться для разных климатических зон.

1. Introduction

1.1 State of the art approach

Daylight is the sustainable source of lighting for buildings. Research has proven that it could provide energy saving, good color rendering, high work productivity, good visual comfort as well as human physiological and psychological needs. That natural light has always played a dominant role in human life [1–7]. To correctly calculate daylighting and accomplish energy simulations it is necessary to study daylight conditions during the whole year. There are several methods for defining daylight conditions in different climates and locations. The illuminance availability approach provides a direct view on illuminance changes, their levels and difference, because illuminance is calculated by the integration of luminance in the window solid angle, it is important to define luminance distribution on the sky under different situations [5, 8]. In most simulation programs, the models of the CIE overcast and CIE clear sky are applied. By now, in some simulation programs such as RADIANCE, Design-Builder..., intermediate skies are considered.

The luminance distributions of the sky is represented as a superposition of four standard CIE skies using the approach described in (Perez et al. 1990) [9]:

The general characteristics of the clear-sky luminance distributions are a large peak near the Sun: a minimum at a point on the other side of the zenith from the Sun, in the vertical plane containing the Sun, and an increase in luminance as the horizon is approached.

The Clear Skies luminance distributions has the form (Kittler, 1965, CIE, 1973) [10]

$$\beta_{cs} = \frac{L_{(\alpha,\gamma)}}{L_z} = \frac{(1 - e^{-\frac{0.32}{\sin \gamma}})(0.91 + 10e^{-3X} + 0.45 \cos^2 X)}{0.274 \cdot (0.91 + 10e^{-3Z_s} + 0.45 \cos^2 Z_s)} \quad (1)$$

$$X = \arccos(\cos Z_s \cdot \cos Z + \sin Z_s \cdot \sin Z \cdot \cos A_z) \quad (2)$$

Description of the Clear Turbid Skies luminance distributions (Matsuura, 1987) [11] by the expression:

$$\beta_{ts} = \frac{L_{(\alpha,\gamma)}}{L_z} = \frac{(1 - e^{-\frac{0.32}{\sin \gamma}})(0.856 + 16e^{-3X} + 0.3 \cos^2 X)}{0.274 \cdot (0.856 + 10e^{-3Z_s} + 0.3 \cos^2 Z_s)} \quad (3)$$

For the Intermediate Skies, formula describes the luminance distributions is [10]:

$$\beta_{is} = \frac{L_{(\alpha,\gamma)}}{L_z} = \frac{Z_1 Z_2}{Z_3 Z_4} \quad (4)$$

where:

$$Z_1 = \frac{[1.35(\sin 3.59\gamma - 0.009) + 2.31] \sin(2.6\gamma_s + 0.316) + \gamma + 4.799}{2.326} \quad (5)$$

$$Z_2 = \exp[-0.563\gamma(\gamma_s - 0.008)(\gamma + 1.059) + 0.812] \quad (6)$$

$$Z_3 = 0.99224 \cdot \sin(2.6\gamma_s + 0.316) + 2.73852 \quad (7)$$

$$Z_4 = \exp\left[-0.563\left(\frac{\pi}{2} - \gamma_s\right)(2.6298(\gamma_s - 0.008) + 0.812)\right] \quad (8)$$

The Overcast Sky luminance distribution has the form (Moon & Spencer, 1942) [12]:

$$\beta_{os} = \frac{L_\gamma}{L_z} = \frac{1 + 2 \sin \gamma}{3} \quad (9)$$

Unlike the clear sky case, the overcast sky distribution does not depend on the solar azimuth or the sky azimuth. Note that at fixed solar altitude the zenith ($\gamma = \pi/2$) is three times brighter than the horizon ($\gamma = 0$).

where β_{cs} : Clear sky luminance distributions (cd.m⁻²).

β_{ts} : Clear turbid sky luminance distributions (cd.m⁻²).

β_{is} : Intermediate sky luminance distributions (cd.m⁻²).

β_{os} : Overcast sky luminance distributions (cd.m⁻²).

α, γ : Azimuth and altitude angles of a point in the sky (radians).

L_z : Sky zenith luminance (cd.m⁻²).

γ_s : Altitude angle of the Sun (radians).

L_z : The zenith luminance (cd.m⁻²).

Z : The angular distance between a sky element and the zenith, $Z = 90^\circ - \gamma$.

$L_{\gamma\alpha}$: Luminance in any arbitrary sky element (cd.m⁻²).

X : The angular distance of the sky element from the Sun, defined by equation (2) (radians).

Z_s : The zenith distance of the Sun (radians).

A_z : The azimuth difference between the element and the solar meridian (radians) with $A_z = |\alpha - \alpha_s|$.

α and α_s are azimuthal angle of the vertical plane of the sky element and Sun position respectively (radians).

The definition sky type based on the concepts justifies the task to develop the new set of sky standards of Kittler et al., [13], which uses the ratio of diffuse sky illuminance to extraterrestrial horizontal illuminance D_v/E_v and the luminous turbidity factor T_v as the descriptors of sky types. A comparison with method assessment the luminance distribution for a particular location based on the cloudiness calculation proposed by A.K. Solovyov was conducted.

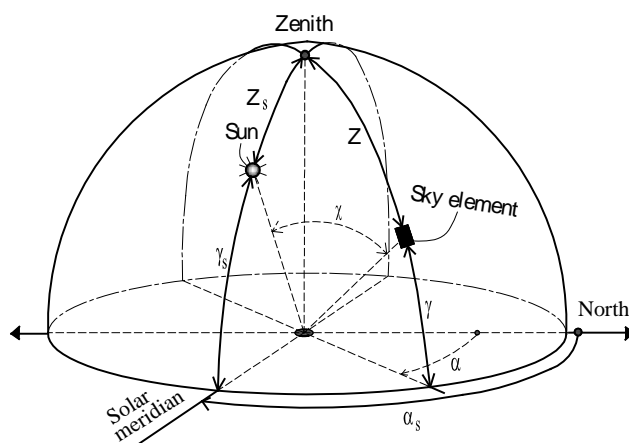


Figure 1. Angles defining the position of the Sun and sky element [4].

1.2. Aim and objectives

The aim of this research is to estimate the luminance distributions in real sky condition tropical Vietnam. Accordingly, this research is based on two main objectives:

- Define the sky types with two methods calculation: the first one using parameters of diffuse horizontal illuminance D_v to extraterrestrial horizontal illuminance E_v and the luminous turbidity factor T_v as descriptors of the sky types; the second one using the cloudiness coefficient K_0 to define real sky condition by statistic of cloudiness.

- Obtain the value illuminance distributions β from the real sky condition.

2. Methods

2.1. The research process flow

Figure 2 shows the flowchart of the research process, which was developed to determine the values of luminance distributions under a tropical climate in Vietnam with the representatives of Hanoi and Ho Chi Minh City.

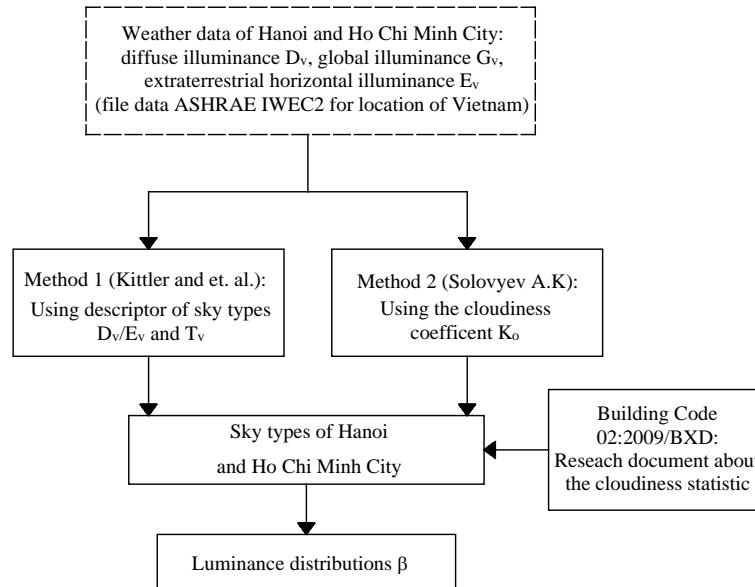


Figure 2. The research process.

2.2. A set of standard skies characterizing daylight conditions by Kittler et al.

To make a measurement ruler of relative luminance distributions in different sky types, a set of standard skies characterizing daylight conditions identified with three main purpose-conscious concepts [13]:

- The discrepancies and absence of standards to characterize unsteady-state daylight climates.
- The need of linking the whole spectrum of skies between the already standardized CIE Overcast and CIE Clear Skies covering the real conditions.
- The trend to evaluate and accept also cloudy and partly cloudy sky models which were seldom specified due to the complete absence of parameterization and measured sky luminance distributions.

Considering these concepts, fifteen sky types of relative luminance distributions by Kittler et al (1998) based on scan measured luminance data at Tokyo, Berkeley and Sydney were proposed at the same time. Five overcast, five clear and five transitional skies are modelled by the combination of graduation and indicatrix functions and the solution is proposed as a CIE code draft CIE (2001) [13, 14]. This determination of daylighting conditions is more detail and covers the whole occurrence spectrum considering different diffuse scattering by the atmosphere and effects of direct Sunlight [13, 15].

To identify the sky type at least two of the descriptors have to obtain: the relative of diffuse horizontal illuminance D_v to extraterrestrial horizontal illuminance E_v and the luminous turbidity factor T_v which approximates the number of ideally clean atmospheres representing an actual case [4, 16,17].

$$T_v = \frac{-\ln\left(\frac{P_v}{E_v}\right)}{av.m} \quad (10)$$

$$\frac{P_v}{E_v} = \frac{G_v}{E_v} - \frac{D_v}{E_v} \quad (11)$$

$$E_v = 133.8 \sin \gamma_s, \text{ lux} \quad (12)$$

$$m = \frac{1}{\sin \gamma_s + 0.50572(\gamma_s + 6.07995^0)^{-1.6364}} \quad (13)$$

$$A_v = \frac{1}{9.9 + 0.043.m} \quad (14)$$

where: T_v is the luminous turbidity factor.

P_v is direct solar horizontal exterior illuminance (Klux).

E_v is extraterrestrial horizontal illuminance (Klux).

D_v is diffuse sky illuminance (Klux).

G_v is global illuminance (Klux).

m is the air mass penetrated and A_v its ideal luminous extinction, dependent on solar altitude γ_s (degree) [18].

Calculation of the relative luminance distributions after the CIE general sky concept was provided with a functional formula. The position of the Sun and of the arbitrary sky element as well as parameters a, b, c, d and e which describe atmospheric conditions have to be taken as input calculation quantities.

$$\beta = \frac{L_{\gamma\alpha}}{L_z} = \frac{f(X)\phi(Z)}{f(Z_s)\phi(0^0)} \quad (15)$$

The luminance gradation function ϕ relates the luminance of a sky element to its zenith angle:

$$\phi(Z) = 1 + a \cdot \exp\left(\frac{b}{\cos Z}\right) \quad (16)$$

$$\phi(0^0) = 1 + a \cdot \exp b \quad (17)$$

$$f(X) = 1 + c \left[\exp(dX) - \exp\left(\frac{d\pi}{2}\right) \right] + e \cdot \cos^2 X \quad (18)$$

$$f(Z_s) = 1 + c \left[\exp(dZ_s) - \exp\left(\frac{d\pi}{2}\right) \right] + e \cdot \cos^2 Z_s \quad (19)$$

When $0 \leq Z \leq \pi/2$ and at the horizon is $\phi(\pi/2) = 1$.

Standard parameters a, b, c, d and e can be estimated after the definition of the sky type from Table 1.

Table 1. Standard parameters with various sky types.

| Type | Gradation indicatrix | a | b | c | d | e | Description of luminance distributions |
|------|----------------------|------|-------|----|------|------|---|
| 1 | I 1 | 4.0 | -0.7 | 0 | -1.0 | 0.00 | CIE Standard Overcast Sky, alternative form steep luminance gradation towards zenith, azimuthal uniformity |
| 2 | I 2 | 4.0 | -0.7 | 2 | -1.5 | 0.15 | Overcast, with steep luminance gradation and slight brightening towards the Sun |
| 3 | II 1 | 1.1 | -0.8 | 0 | -1.0 | 0.00 | Overcast, moderately graded with azimuthal uniformity |
| 4 | II 2 | 1.1 | -0.8 | 2 | -1.5 | 0.15 | Overcast, moderately graded and slight brightening towards the Sun |
| 5 | III 1 | 0.0 | -1.0 | 0 | -1.0 | 0.00 | Sky of uniform luminance |
| 6 | III 2 | 0.0 | -1.0 | 2 | -1.5 | 0.15 | Partly cloudy sky, no gradation towards zenith, slight brightening towards the Sun |
| 7 | III 3 | 0.0 | -1.0 | 5 | -2.5 | 0.30 | Partly cloudy sky, no gradation towards zenith, brighter circumsolar region |
| 8 | III 4 | 0.0 | -1.0 | 10 | -3.0 | 0.45 | Partly cloudy sky, no gradation towards zenith, distinct solar corona |
| 9 | IV 2 | -1.0 | -0.55 | 2 | -1.5 | 0.15 | Partly cloudy, with the obscured Sun |
| 10 | IV 3 | -1.0 | -0.55 | 5 | -2.5 | 0.30 | Partly cloudy, with brighter circumsolar region |
| 11 | IV 4 | -1.0 | -0.55 | 10 | -3.0 | 0.45 | White-blue sky with distinct solar corona |
| 12 | V 4 | -1.0 | -0.32 | 10 | -3.0 | 0.45 | CIE Standard Clear Sky, low illuminance turbidity |
| 13 | V 5 | -1.0 | -0.32 | 16 | -3.0 | 0.30 | CIE Standard Clear Sky, polluted atmosphere |
| 14 | VI 5 | -1.0 | -0.15 | 16 | -3.0 | 0.30 | Cloudless turbid sky with broad solar corona |
| 15 | VI 6 | -1.0 | -0.15 | 24 | -2.8 | 0.15 | White-blue turbid sky with broad solar corona |

Table 2. Typical value of descriptor linked with various sky types.

| Sky type | Sky code | T _v | Ratio D _v /E _v |
|----------|----------|----------------|--------------------------------------|
| 1 | I.1 | Over 45 | 0.10 |
| 2 | I.2 | Over 20 | 0.18 |
| 3 | II.1 | Over 45 | 0.15 |
| 4 | II.2 | Over 20 | 0.22 |
| 5 | III.1 | Over 45 | 0.20 |
| 6 | III.2 | Over 20 | 0.38 |
| 7 | III.3 | 12.0 | 0.42 |
| 8 | III.4 | 10.0 | 0.41 |
| 9 | IV.2 | 12.0 | 0.40 |
| 10 | IV.3 | 10.0 | 0.36 |
| 11 | IV.4 | 4.0 | 0.23 |
| 12 | V.4 | 2.5 | 0.10 |
| 13 | V.5 | 4.5 | 0.28 |
| 14 | VI.5 | 5.0 | 0.28 |
| 15 | VI.6 | 4.0 | 0.30 |

In Table 1 gave fifteen standard relative luminance distributions which are based on six groups of a and b values for the gradation function and six groups of c, d and e values for the indicatrix function. The resulting curves are illustrated in Figures 3 and 4 [4].

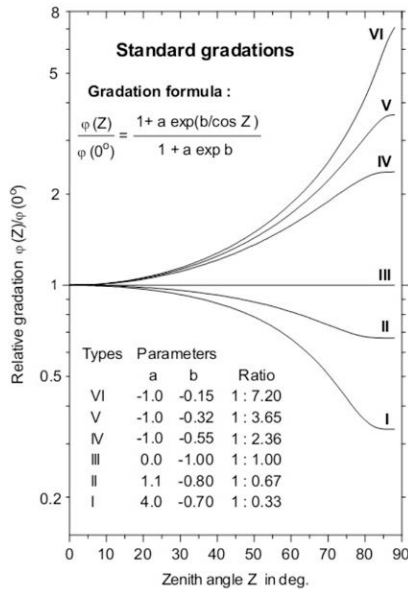


Figure 3. Standard gradations.

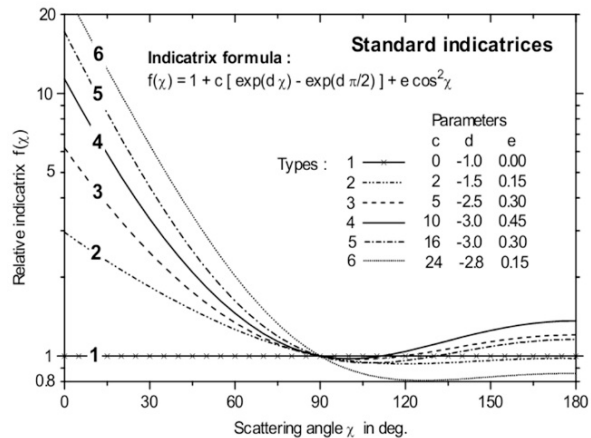


Figure 4. Standard indicatrices.

According to formulas from (10) to (19) after the sky type of the location has been defined, using standard parameters a, b, c, d and e for target sky types, the values luminance distributions of the real sky are obtained.

2.3. Assessment the light climate for a particular location based on the cloudiness calculation K₀

This is based on calculation the relative sky luminance distributions gap between two extreme CIE standard skies by using the cloudiness calculation and proposed by A.K. Solovyov. The method of determining the estimated positions of the Sun in the sky is described in document [19, 20]. In short:

The values of the elementary illumination of the sky sectors with angular dimensions in latitude 15° and on the meridian 70° (from 10° to 80°) were calculated. These values are the sum of the elementary illuminance by the sectors of the sky. In regions with the clear sky, luminance distributions depends on the Sun's position relative to the light opening. A position of the Sun is taken into account, where for a given orientation of the light opening, the value of Daylight Factor will be minimal, and the value of outdoor illumination will approach the critical E_{cr}. Then we have:

The condition of minimal Daylight Factor: From the articles [19, 20], the results show that the value of the angular distance of the sky element from the Sun X equals 105° and 225° are the most unfavorable orientation area of a light opening in relation to the solar meridian. In the calculations to definition sky luminance distributions, the position of the Sun has to be fixed as stated above as these formulas (1) and (2) can be suitable for practical calculations if X and Z_s values are used. It should be noted that in case of sky types 1, 3 and 5 (Table 1), when luminance azimuth uniformity takes place, sky luminance does not depend on the orientation of the light opening and in these cases, therefore, the Daylight Factor does not depend on the Sun's position.

The condition of critical illuminance E_{cr} : Method calculation for room natural illumination in the clear sky condition with proposing the adverse Sun's latitude at a given light opening orientation and external illuminance tends to critical (E_{cr}). The E_{cr} values were selected according to the follow expression for determining the Sun's latitude:

$$E_{cr} = 100 \frac{E_{art}^{norm}}{e^{norm}} \quad (20)$$

Where E_{art}^{norm} is normalized artificial illuminance and e^{norm} is normalized Daylight Factor values.

In the study [21], the analysis daylight assessment for Vietnam was taken with the represent of diffusue horizontal illuminances for Hanoi. It shows relative of Daylight Factor e (%), critical external illuminance E_{cr} (lux) and normalized artificial illuminance E_{art}^{norm} (target illuminance, lux) based on the analysis period of time from the working time using daylighting in a space (Table 3). For instance, Mardaljevic J. et al. [22] were evaluated some most probable daily activity hours e.g. 7:00 – 20:00, 8:00 – 17:00, 8:00 – 19:00 or 9:00 – 16:00. For Vietnam this period from 08h00 to 17h00 is represented as 100 % working time.

Table 3. Recommended average DF and E_{cr} for Vietnam

| E_{art}^{norm} (lux) | 50% of the analysis period | | 80% of the analysis period | | 100% of the analysis period | |
|------------------------|----------------------------|----------------|----------------------------|----------------|-----------------------------|----------------|
| | e (%) | E_{cr} (lux) | e (%) | E_{cr} (lux) | e (%) | E_{cr} (lux) |
| 500 | 1.5 | 33333 | 2.25 | 22222 | 3.5 | 14286 |
| 400 | 1.2 | 33333 | 1.8 | 22222 | 2.8 | 14286 |
| 300 | 0.9 | 33333 | 1.35 | 22222 | 2.1 | 14286 |
| 200 | 0.6 | 33333 | 0.9 | 22222 | 1.4 | 14286 |
| 100 | - | - | < 0.5 | - | 0.7 | 14286 |

Thus minimum critical external illuminance amounted approximately to 15000 lux, from which covers practically all E_{cr} value interval of the analysis period. From numerous studies, which carried out in the field study of outdoor illumination, the most reliable are measurements of Khrochitsky, Zeker and Littlefair, as well as P. Tregenza [20, 23], that confirm each other. As a result P. Tregenza suggests the following empirical formulas for horizontal diffuse illumination:

$$E_D = 10.5(\gamma_s + 5)^{2.5}, \text{ (with } -5^\circ < \gamma_s \leq 5^\circ) \quad (21)$$

$$E_D = 48800 \cdot \sin^{1.105} \gamma_s, \text{ (with } 5^\circ < \gamma_s \leq 60^\circ) \quad (22)$$

Using expressions (21) and (22) the angular heights of the Sun are obtained for various values of the critical illuminance.

Table 4. Calculation height distance of the Sun γ_s depend on critical illuminance E_{cr} .

| E_{cr} (lux) | γ_s (grad.) | E_{cr} (lux) | γ_s (grad.) |
|----------------|--------------------|----------------|--------------------|
| 15 000 | 20.1 | 25 000 | 33 |
| 17 500 | 23.3 | 27 500 | 36.5 |
| 20 000 | 26.5 | 30 000 | 40.1 |
| 22 500 | 29.8 | 32 500 | 44.4 |

If we assume that statistically, cloudiness ranges from overcast to clear sky conditions, a simple technique, which was proposed by G Gillette and S. Trido to account for local cloudiness can be used. The ratio of the diffuse to the global horizontal irradiances as well as the ratio of the diffuse to global

illuminances, which named the cloudiness coefficient $K_0 = E_D/E_Q$ provides a better information on cloudiness. This coefficient decreases from 1.0 under completely overcast skies to values around 0.2 under cloudless skies [19, 20, 24, 25]. Hence, the luminance of any point of the sky determined can be presented at a time as the weighted average of its two extreme value:

$$L(z, \alpha) = \xi \cdot L(z, \alpha)_{clear} + (1 - \xi) \cdot L(z)_{overcast} \tag{23}$$

Where: $L(z, \alpha)_{clear}$ is luminance of clear sky by R. Kittler's formula; $L(z)_{overcast}$ is luminance of overcast sky by Moon and Spencer's law; ξ is a phase function corresponding to the normal distribution law confirmed in work [25].

$$\xi = \frac{1 + \cos(K_0 \cdot \pi)}{2} \tag{24}$$

3. Results and Discussion

The weather data of diffuse horizontal illuminances, global horizontal illuminances and extraterrestrial horizontal illuminances are collected for Hanoi, Ho Chi Minh City cities from file ASHRAE IVEC2 – "White Box Technologies, weather data for energy calculations". This file was developed for ASHRAE by White Box Technologies, Inc. and based on the integrated hourly basis over the ISD surface for 3012 locations outside the US and Canada that have a minimum of 12 years of recording up to 25 years [26].

3.1. Define sky type with relative D_v/E_v and the luminous turbidity factor T_v based on a set of standard skies proposed by Kittler et al.

To obtain the relative of D_v/E_v , the data of diffuse horizontal illuminance and extraterrestrial horizontal illuminance were used in formulas (10) – (14). The result of calculations shown on Table 5.

Table 5. Descriptor D_v/E_v of Sky types.

| Month | January | February | March | April | May | June | July | August | September | October | November | December | Annual average |
|------------------------------|---------|----------|-------|-------|------|------|------|--------|-----------|---------|----------|----------|----------------|
| T_v | 17.8 | 17.3 | 13.4 | 22.6 | 30.2 | 23.5 | 26.1 | 17.1 | 18.6 | 6.5 | 6.5 | 12.5 | 17.7 |
| D_v/E_v | 0.36 | 0.31 | 0.38 | 0.35 | 0.37 | 0.37 | 0.35 | 0.36 | 0.36 | 0.33 | 0.33 | 0.34 | 0.35 |
| Sky type of Hanoi | VI | VI | VI | VI | VI | VI | VI | VI | VI | X | X | IX | VI |
| Sky type of Ho Chi Minh City | XIV | X | XIV | XIV | IX | X | X | X | X | X | X | X | X |

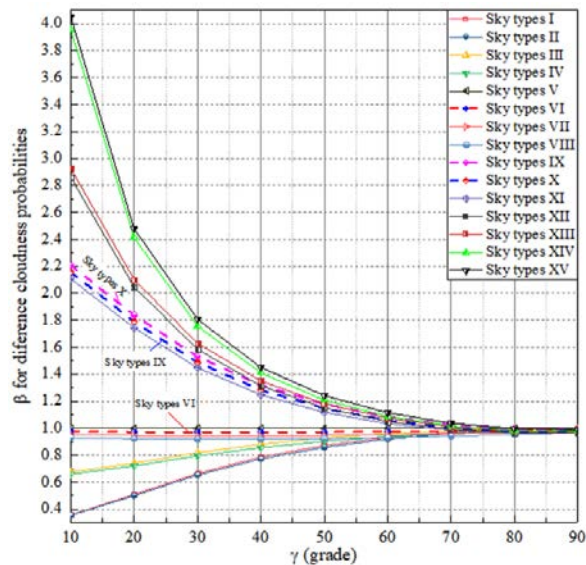


Figure 5. Distribution of relative luminance β in depending on sky types (sky type VI for Hanoi and X for Ho Chi Minh City).

In Hanoi, the sky types from October to December are partly cloudy with the obscured Sun and partly cloudy with the brighter circumsolar region, which describes sky types 9 and 10. From January to September, the typical sky type identifies partly cloudy sky, no gradation towards zenith, slight brightening towards the Sun with sky type 6. When the sky type 10 – partly cloudy, with brighter circumsolar region was represented for Ho Chi Minh City.

Figure 5 shows the graphic of relative luminance distributions β in depending on sky types, which was computed from the formulas from (15) to (19). For the calculations, standard parameters of sky types were used. The position of angular distance of the sky element from the Sun X estimated equals 105° (or 225°) is the most unfavorable orientation area. The angular distances between a sky element and the zenith, $Z = 90^\circ - \gamma$ were determined when γ changes from 10° to 90° .

3.2. Define sky type based on the cloudiness coefficient K_0

To estimate sky types for these cities with the cloudiness coefficient K_0 , the values of diffuse and global illuminances were obtained. The results have shown the values of K_0 average are 0.81 for Hanoi and 0.57 for Ho Chi Minh City (Table 6A and 6B).

Table 6A. Calculation cloudiness coefficient K_0 for Hanoi (21.03° N).

| Hours Month | 6.00 | 7.00 | 8.00 | 9.00 | 10.00 | 11.00 | 12.00 | 13.00 | 14.00 | 15.00 | 16.00 | 17.00 | 18.00 | 19.00 | Average K_0 |
|----------------|------|------|------|------|-------|-------|-------|-------|-------|-------|-------|-------|-------|-------|---------------|
| 1 | - | 1.09 | 0.90 | 0.79 | 0.93 | 0.40 | 0.72 | 0.73 | 0.65 | 0.69 | 0.86 | 0.84 | 0.72 | - | 0.78 |
| 2 | - | 0.91 | 0.80 | 0.90 | 0.88 | 0.49 | 0.79 | 0.87 | 0.83 | 0.89 | 0.92 | 0.84 | 0.94 | - | 0.84 |
| 3 | - | 1.02 | 0.98 | 0.93 | 0.93 | 0.56 | 0.89 | 0.90 | 0.90 | 0.89 | 0.93 | 0.95 | 0.96 | - | 0.90 |
| 4 | 1.08 | 1.27 | 0.97 | 0.87 | 1.02 | 0.52 | 0.79 | 0.88 | 0.82 | 0.78 | 0.86 | 0.72 | 0.89 | 0.80 | 0.88 |
| 5 | 0.78 | 0.91 | 0.78 | 0.74 | 0.74 | 0.50 | 0.73 | 0.70 | 0.70 | 0.71 | 0.72 | 0.77 | 0.92 | 0.93 | 0.76 |
| 6 | 0.91 | 0.92 | 0.89 | 0.82 | 0.81 | 0.53 | 0.82 | 0.84 | 0.86 | 0.87 | 0.89 | 0.94 | 0.92 | 0.87 | 0.85 |
| 7 | 0.92 | 0.96 | 0.92 | 0.88 | 0.82 | 0.56 | 0.81 | 0.82 | 0.83 | 0.85 | 0.81 | 0.87 | 0.90 | 0.95 | 0.85 |
| 8 | 1.15 | 1.05 | 0.89 | 0.83 | 0.85 | 0.57 | 0.79 | 0.85 | 0.80 | 0.78 | 0.91 | 0.96 | 1.02 | 1.15 | 0.90 |
| 9 | 0.85 | 0.95 | 0.80 | 0.74 | 0.71 | 0.44 | 0.64 | 0.64 | 0.67 | 0.69 | 0.71 | 0.83 | 0.96 | - | 0.74 |
| 10 | - | 1.26 | 0.77 | 0.71 | 0.69 | 0.45 | 0.64 | 0.69 | 0.65 | 0.71 | 0.84 | 0.91 | 0.95 | - | 0.77 |
| 11 | - | 0.95 | 0.81 | 0.72 | 0.71 | 0.39 | 0.60 | 0.62 | 0.60 | 0.63 | 0.75 | 0.88 | 0.83 | - | 0.71 |
| 12 | - | 0.82 | 0.86 | 0.68 | 0.71 | 0.38 | 0.66 | 0.65 | 0.64 | 0.68 | 0.77 | 0.90 | 0.90 | - | 0.72 |
| | | | | | | | | | | | | | | | 0.81 |

Table 6B. Calculation cloudiness coefficient K_0 for Ho Chi Minh City (10.82° N).

| Hours Month | 6.00 | 7.00 | 8.00 | 9.00 | 10.00 | 11.00 | 12.00 | 13.00 | 14.00 | 15.00 | 16.00 | 17.00 | 18.00 | 19.00 | Average K_0 |
|----------------|------|------|------|------|-------|-------|-------|-------|-------|-------|-------|-------|-------|-------|---------------|
| 1 | | 0.71 | 0.58 | 0.53 | 0.50 | 0.48 | 0.47 | 0.48 | 0.48 | 0.50 | 0.53 | 0.58 | 0.55 | | 0.53 |
| 2 | | 0.51 | 0.55 | 0.54 | 0.40 | 0.36 | 0.34 | 0.34 | 0.35 | 0.39 | 0.44 | 0.52 | 0.69 | | 0.45 |
| 3 | | 0.75 | 0.58 | 0.49 | 0.44 | 0.40 | 0.38 | 0.39 | 0.40 | 0.44 | 0.49 | 0.56 | 0.74 | | 0.51 |
| 4 | 0.72 | 0.68 | 0.53 | 0.46 | 0.42 | 0.39 | 0.38 | 0.39 | 0.41 | 0.44 | 0.50 | 0.58 | 0.74 | | 0.51 |
| 5 | 0.82 | 0.69 | 0.58 | 0.53 | 0.49 | 0.46 | 0.45 | 0.46 | 0.47 | 0.48 | 0.51 | 0.56 | 0.69 | | 0.55 |
| 6 | 0.82 | 0.68 | 0.58 | 0.55 | 0.52 | 0.48 | 0.47 | 0.47 | 0.47 | 0.49 | 0.53 | 0.57 | 0.66 | 0.60 | 0.56 |
| 7 | 0.77 | 0.72 | 0.63 | 0.60 | 0.58 | 0.54 | 0.53 | 0.53 | 0.53 | 0.57 | 0.60 | 0.64 | 0.70 | 0.69 | 0.62 |
| 8 | 0.68 | 0.73 | 0.62 | 0.58 | 0.56 | 0.53 | 0.51 | 0.52 | 0.53 | 0.55 | 0.59 | 0.61 | 0.69 | 0.57 | 0.59 |
| 9 | 0.74 | 0.74 | 0.65 | 0.60 | 0.58 | 0.57 | 0.54 | 0.55 | 0.56 | 0.60 | 0.62 | 0.67 | 0.70 | | 0.63 |
| 10 | 0.68 | 0.74 | 0.69 | 0.63 | 0.60 | 0.58 | 0.58 | 0.56 | 0.58 | 0.61 | 0.63 | 0.69 | 0.83 | | 0.64 |
| 11 | 0.62 | 0.75 | 0.64 | 0.58 | 0.57 | 0.54 | 0.54 | 0.56 | 0.57 | 0.60 | 0.62 | 0.66 | 0.81 | | 0.62 |
| 12 | | 0.71 | 0.62 | 0.57 | 0.55 | 0.54 | 0.53 | 0.52 | 0.54 | 0.56 | 0.59 | 0.65 | 0.82 | | 0.60 |
| | | | | | | | | | | | | | | | 0.57 |

Using formulas from (23) to (24), the luminance distributions β according to different cloudiness coefficient K_0 is determined by summing the values of illumination from the sky sectors. The results are obtained in Figure 6.

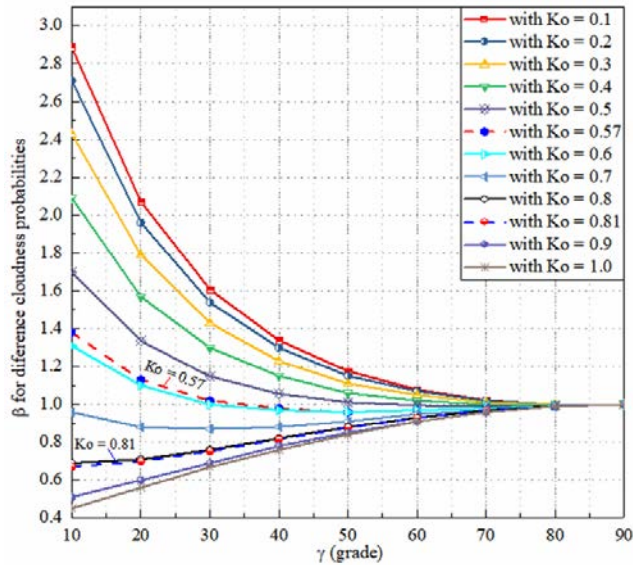


Figure 6. Distribution of relative luminance β with different cloudiness probabilities (for average cloudiness coefficient $K_0 = 0.81$ in Hanoi and $K_0 = 0.57$ in Ho Chi Minh City).

The study of Pham Ngoc Dang et al. about daylight climate in Vietnam [27–29], respectively with the document Building code [30] show that the cloudiness statistic has a great influence on daylight climate. The tropical sky of Vietnam is typically with high cloud covered of Cirrus (Ci) and Stratus (St), Cumulus (Cu) clouds. Statistic cloudiness Cirrus (Ci) and Stratus (St) is form at high altitude between 4 ÷ 12 km characterizes for the Sunny days. In this status, the sky characterizes of the high level of diffuse radiation and diffuse horizontal illuminance. Type of clouds Cumulus (Cu) and Cumulonimbus cloud (Cb) is form at low altitude (below 2 km and 0.6 ÷ 1 km) characterizes for the nasty days. The Cumulonimbus cloud is a dense, towering vertical cloud, forming from water vapour carried by powerful upward air currents. If observed during a storm, these clouds may be referred to as thunderheads. Besides, there are different types of cloud as Cirrostratus (Cs), Stratocumulus (Sc), which are formed at middle altitude.

For more specific sky conditions of Hanoi, the sky type VI - Partly cloudy sky, no gradation towards zenith, slight brightening towards the Sun. This sky type nearly approached to the Standard CIE Sky of uniform luminance. In consideration of the cloudiness coefficient $K_0 = 0.81$ was obtained for Hanoi; this is logical with the cloud covered of 7.8/10 from Code of Standard 02:2009/BXD. In the winter, the sky more clearly with sky type IX and X; or with K_0 value of 0.71 ÷ 0.74. In this period, statistic cloudiness from Code Standard show 6.4/10 ÷ 6.7/10 [30].

For Ho Chi Minh City, the sky is more clearly with statistics cloudiness average of value 6.3 [30], K_0 is 0.57 and sky type X was defined. Generally, the sky types in Hanoi and Ho Chi Minh City characterize by statistic cloud covered and Sunlight exposure as shown in Table 5-7.

Table 7. Statistic cloud covered and hours of Sunlight exposure for Hanoi and Ho Chi Minh City [30].

| | | January | February | March | April | May | June | July | August | September | October | November | December | Annual average |
|--|-----|---------|----------|-------|-------|-----|------|------|--------|-----------|---------|----------|----------|----------------|
| Hanoi | (1) | 8.2 | 9.1 | 9.2 | 8.7 | 7.7 | 8.2 | 8.0 | 7.9 | 6.8 | 6.4 | 6.5 | 6.7 | 7.8 |
| | (2) | 74 | 47 | 47 | 90 | 183 | 172 | 195 | 174 | 176 | 167 | 137 | 124 | 1585 |
| Ho Chi Minh | (1) | 4.6 | 4.4 | 4.4 | 5.6 | 6.9 | 7.5 | 7.3 | 7.4 | 7.7 | 7.3 | 6.6 | 5.7 | 6.3 |
| | (2) | 245 | 246 | 272 | 239 | 195 | 171 | 180 | 172 | 162 | 182 | 200 | 223 | 2489 |
| (1): Statistic cloudiness. (2): Hours of Sunlight exposure. | | | | | | | | | | | | | | |

For an overview, a comparison results defining luminance distributions for Hanoi and HCM by difference methods has shown on Table 8. As the results, it is seen that with altitude angles of a point in the sky γ above 50° , relative errors of the values luminance distributions β values less than 10 %. This means that under city building conditions, when the lower part of the horizon is blocked by an adjacent building, the results obtained by these two methods give a little difference.

Table 8. Comparison results defining luminance distributions for Hanoi and Ho Chi Minh City.

| γ (grade) | CIE overcast sky | Distribution luminance β | | | | | |
|---------------------|------------------|--------------------------------|----------------|--------------------|------------------|----------------|--------------------|
| | | Hanoi | | | Ho Chi Minh City | | |
| | | K_0 | $D_v/E_v, T_v$ | Relative error (%) | K_0 | $D_v/E_v, T_v$ | Relative error (%) |
| 10 | 0.45 | 0.67 | 0.98 | - 31.33 | 1.38 | 2.16 | - 36.1 |
| 20 | 0.56 | 0.70 | 0.97 | - 28.04 | 1.13 | 1.79 | - 36.9 |
| 30 | 0.67 | 0.75 | 0.97 | - 22.78 | 1.02 | 1.49 | - 31.5 |
| 40 | 0.76 | 0.82 | 0.97 | - 15.75 | 0.98 | 1.28 | - 23.4 |
| 50 | 0.84 | 0.88 | 0.97 | - 9.53 | 0.96 | 1.15 | - 16.5 |
| 60 | 0.91 | 0.93 | 0.98 | - 4.67 | 0.97 | 1.06 | - 8.5 |
| 70 | 0.96 | 0.97 | 0.98 | - 0.96 | 0.98 | 1.01 | - 3.0 |
| 80 | 0.99 | 0.99 | 0.98 | 0.67 | 0.99 | 0.98 | 1.0 |
| 90 | 1.00 | 1.00 | 0.99 | 1.14 | 1.00 | 0.99 | 1.0 |

4. Conclusion

1. To obtain the luminance distributions of real sky using in daylighting calculations, the sky types of tropical Hanoi and Ho Chi Minh City were defined based on the two extreme CIE Standard Skies: Overcast Sky (Moon & Spencer) and Standard Clear Sky (R. Kittler). In this research, the two methods of calculation were presented: method define luminance distributions based on a set of fifteen skies proposed by R. Kittler and et al.; the method using the cloudiness calculation K_0 to define the real sky luminance distributions gap between two extreme CIE Standard skies. This first method must begin with the definition the sky type with the parameter of descriptors D_v/E_v and T_v . As the results, sky types VI and X respectively were defined for Hanoi and Ho Chi Minh City.

2. Previous studies and standard documents confirm the result of calculation with the conclusion in the sky type of tropical Vietnam is neither overcast sky nor clear sky. The typical sky type is the partly cloudy sky with high cloud cover at high altitude Cirrus (Ci) and Stratus (St) in Sunny days, type of clouds Cumulus (Cu) and Cumulonimbus cloud (Cb) is form at low altitude characterizes for the nasty day.

3. The values of relative luminance distributions were presented. A comparison shows differences between results from the two methods respectively maximum equals 31.33 % ÷ 36.9 % for Hanoi and Ho Chi Minh City at the altitude angles γ of a point in the sky 10° . Minimum differences below 10 % at the altitude angles γ above 50° . This implies that under city building conditions when the lower part of the horizon is blocked by an adjacent building, the difference between these methods can be allowed.

References

- Solovyov, A.K. Research into illumination of buildings and construction, conducted in architectural and construction educational and scientific institutes: A review. *Light & Engineering*. 2017. 25(1). Pp. 23–30.
- Boyce, P.R. *Human Factors in Lighting*. CRC Press. 7 April 2014. London. 703 p.
- Tregenza, P., Mardaljevic, J. Daylighting buildings: Standards and the needs of the designer. *Lighting Research and Technology*. 2018. Vol. 50. Pp. 63–79. <https://doi.org/10.1177/1477153517740611>
- Darula, S., Kittler, R. CIE general sky standard defining luminance distributions. Proc. Conf. eSim 2002. The Canadian conference on building energy simulation. 2002. Montreal, Canada. 8 p.
- Solovyev, A.K., Tushina, O.A. A comparative thermal analysis of systems of the upper daylight (clerestory and daylight guidance system). *Magazine of Civil Engineering*. 2014. No. 2(46). Pp. 24–35. <https://doi.org/10.5862/MCE.46.4>

Литература

- Solovyov A.K. Research into illumination of buildings and construction, conducted in architectural and construction educational and scientific institutes: A review // *Light & Engineering*. 2017. Vol. 25(1). Pp. 23–30.
- Boyce P.R. *Human Factors in Lighting* // CRC Press. 7 April 2014. London. 703 p.
- Tregenza P., Mardaljevic J. Daylighting buildings: Standards and the needs of the designer // *Lighting Research and Technology*. 2018. Vol. 50. Pp. 63–79. <https://doi.org/10.1177/1477153517740611>
- Darula S., Kittler R. CIE general sky standard defining luminance distributions // Proc. Conf. eSim 2002. The Canadian conference on building energy simulation. 2002. Montreal, Canada. 8 p.
- Solovyev A.K., Tushina O.A. A comparative thermal analysis of systems of the upper daylight (clerestory and daylight guidance system) // *Magazine of Civil Engineering*. 2014. No. 2(46). Pp. 24–35. <https://doi.org/10.5862/MCE.46.4>

6. Popova, O.N., Glebova, Y.M. Energy sustainability of residential development as the assessment criterion of city energy-system. Construction of Unique Buildings and Structures. 2018. No. 3(66). Pp. 7–18. [https://doi: 10.18720/CUBS.66.1](https://doi.org/10.18720/CUBS.66.1)
7. Castro, J.C.L., Zaborova, D.D., Musorina, T.A., Arkhipov, I.E. Indoor environment of a building under the conditions of tropical climate. Magazine of Civil Engineering. 2017. No. 8. Pp. 50–57. [https://doi: 10.18720/MCE.76.5](https://doi.org/10.18720/MCE.76.5)
8. Dumortier, D., Fontynont, M., Avouac-Bastie, P. Daylight availability in Lyon. In: Proc. of the European Conference on Energy. Lyon: Ecole Nationale des Travaux de l'Etat Lyon. 1994. Pp. 1315–1320.
9. Perez, R., Ineichen, P., Seals, R. Modelling daylight availability and irradiance components from direct and global irradiance. Solar Energy. 1990. Pp. 271–289. [https://doi.org/10.1016/0038-092X\(90\)90055-H](https://doi.org/10.1016/0038-092X(90)90055-H)
10. CIE Technical Committee 4.2. Standardization of luminance distribution on clear skies. Publication No. 22, Commission Internationale d'Eclairage. CIE Pub. 1973. 33 p.
11. Matsuura, K. Luminance distributions of Various Reference Skies. CIE Technical Report of TC, CIE Pub. 1987. No. 3. Pp. 3–9.
12. Moon, P., Spencer, D. Illumination from a Nonuniform Sky. Illuminating Engineering. 1942. Vol. 37(12). Pp. 707–726.
13. Kittler, R., Perez, R., Darula, S. A set of standard skies characterizing daylight conditions for computer and energy conscious design. US SK 92 052 Final Report, ICA SAS Bratislava. 1998. Polygrafia Bratislava. 52 p.
14. Spatial distribution of daylight-CIE standard general sky. Draft standard CIE DS 011.0/E-2001. 2001. CIE Central Bureau, Vienna. 54 p.
15. Kittler, R., Darula, S. Parametric definition of the daylight climate. Renewable Energy. 2002. No. 26. Pp. 177–187. [https://doi: 10.1016/S0960-1481\(01\)00128-8](https://doi.org/10.1016/S0960-1481(01)00128-8)
16. Darula, S., Kittler, R., Wittkott, S.K. Outdoor Illuminance Levels in the Tropics and their Representation in Virtual Sky Domes. Architectural Science Review. 2006. Vol. 49(3). Pp. 301–313. <https://doi.org/10.3763/asre.2006.4940>
17. Darula, S., Kittler, R. Classification of daylight conditions in cloud cover situations. Light & Engineering. 2015. Vol. 23(1). Pp. 4–14.
18. Kasten, F., Young, A.T. Revised optical air mass tables and approximation formula. Applied Optics. 1989. No. 28. Pp. 4735–4738. <https://doi.org/10.1364/AO.28.004735>
19. Solovyov, A.K. Luminance distribution over the firmament: Taking it into account when designing natural illumination for building. Light & Engineering. 2009. Vol. 17(1). Pp. 59–64.
20. Zemtsov, V.A., Solovyov, A.K., Shmarov, I.A. Luminance parameters of the standard CIE sky within natural room illumination calculations and their application under various light climate conditions in Russia. Light & Engineering. 2017. No. 1. Pp.106–111.
21. Phuong, N.T.K., Solovyov, A.K. Potential daylight resources between tropical and temperate cities – a case study of Ho Chi Minh city and Moscow. Scientific journal Matec Web of Conferences 193, EDP Science Publishing. 2018. 8 p, <https://doi.org/10.1051/mateconf/201819304013>.
22. Mardaljevic, J., Christoffersen, J. Climate connectivity in the daylight factor basis of building standards. Building and Environment. 2017. Vol. 113. Pp. 200–209. <https://doi.org/10.1016/j.buildenv.2016.08.009>
23. Tregenza, P.R. Measured and calculated frequency distributions of daylight illuminance. Lighting Research & Technology. 1986. Vol. 18(2). Pp. 71–74. <https://doi.org/10.1177/096032718601800202>
24. Jeffrey, G.M. Solar energy: The State of Art. Earthscan. 2013. New York, USA, 724 p.
6. Попова О.Н., Глебова Ю.М. Энергетическая устойчивость жилой застройки как критерий комплексной оценки энергосистемы города // Строительство уникальных зданий и сооружений. 2018. № 3(66). С. 7–18. [https://doi: 10.18720/CUBS.66.1](https://doi.org/10.18720/CUBS.66.1)
7. Кастро Х., Заборова Д.Д., Мусорина Т.А., Архипов И.Е. Внутренняя среда жилых помещений в условиях тропического климата // Инженерно-строительный журнал. 2017. № 8(76). С. 50–57. [https://doi: 10.18720/MCE.76.5](https://doi.org/10.18720/MCE.76.5)
8. Dumortier D., Fontynont M., Avouac-Bastie P. Daylight availability in Lyon // In: Proc. of the European Conference on Energy. Lyon: Ecole Nationale des Travaux de l'Etat Lyon. 1994. Pp. 1315-1320.
9. Perez R., Ineichen P., Seals R. Modelling daylight availability and irradiance components from direct and global irradiance // Solar Energy. 1990. Pp. 271–289. [https://doi.org/10.1016/0038-092X\(90\)90055-H](https://doi.org/10.1016/0038-092X(90)90055-H)
10. CIE Technical Committee 4.2. Standardization of the Luminance distributions on Clear Skies // Publication No. 22, Commission Internationale d'Eclairage. CIE Pub. 1973. 33 p.
11. Matsuura K. Luminance distributions of Various Reference Skies // CIE Technical Report of TC, CIE Pub. 1987. No. 3. Pp. 3–9.
12. Moon P., Spencer D. Illumination from a Nonuniform Sky // Illuminating Engineering. 1942. Vol. 37(10). Pp. 707–726.
13. Kittler R., Perez R., Darula S. A set of standard skies characterizing daylight conditions for computer and energy conscious design // US SK 92 052 Final Report, ICA SAS Bratislava. 1998. Polygrafia Bratislava. 52 p.
14. Spatial distribution of daylight-CIE standard general sky // Draft standard CIE DS 011.0/E-2001. 2001. CIE Central Bureau, Vienna. 54 p.
15. Kittler R., Darula S. Parametric definition of the daylight climate // Renewable Energy. 2002. No. 26. Pp. 177–187. [https://doi: 10.1016/S0960-1481\(01\)00128-8](https://doi.org/10.1016/S0960-1481(01)00128-8)
16. Darula S., Kittler R., Wittkott S.K. Outdoor Illuminance Levels in the Tropics and their Representation in Virtual Sky Domes // Architectural Science Review. 2006. Vol. 49(3). Pp. 301–313. <https://doi.org/10.3763/asre.2006.4940>
17. Darula S., Kittler R. Classification of daylight conditions in cloud cover situations. Light & Engineering. 2015. Vol. 23(1). Pp. 4–14.
18. Kasten F., Young A.T. Revised optical air mass tables and approximation formula // Appl. Optics. 1989. No. 28. Pp. 4735–4738. <https://doi.org/10.1364/AO.28.004735>
19. Solovyov A.K. Luminance distribution over the firmament: Taking it into account when designing natural illumination for building // Light & Engineering. 2009. Vol. 17(1). Pp. 59–64.
20. Zemtsov V.A., Solovyov A.K., Shmarov I.A. Luminance parameters of the standard CIE sky within natural room illumination calculations and their application under various light climate conditions in Russia // Light & Engineering. 2017. No. 1. Pp.106–111.
21. Phuong N.T.K., Solovyov A. K. Potential daylight resources between tropical and temperate cities – a case study of Ho Chi Minh City and Moscow // Scientific journal Matec Web of Conferences 193, EDP Science Publishing. 2018. 8 p. <https://doi.org/10.1051/mateconf/201819304013>.
22. Mardaljevic J., Christoffersen J. Climate connectivity in the daylight factor basis of building standards // Building and Environment. 2017. Vol. 113. Pp. 200–209. <https://doi.org/10.1016/j.buildenv.2016.08.009>
23. Tregenza P.R. Measured and calculated frequency distributions of daylight illuminance // Lighting Research & Technology. 1986. Vol. 18(2). Pp. 71–74. <https://doi.org/10.1177/096032718601800202>
24. Jeffrey G.M. Solar energy: The State of Art // Earthscan. 2013. New York, USA, 724 p.

25. Gillete, G., Treado, S. The issue of sky conditions. Lighting Design & Application. March, 1985. 23(19). Pp. 22–27.
26. Joe Huang. ASHRAE Research Project 1477-RP Development of 3,012 typical year weather files for international locations. White Box Technologies. October 19, 2011. Moraga CA. 97 p.
27. Pham Ngoc Dang, Pham Duc Nguyen, Luong Minh. Architecture lighting, Building Physics (Part II and III). Construction Publishing. 1982. Hanoi. 53 p.
28. Ha, P.T.H. Energy efficiency façade design in high-rise apartment buildings using the calculation of solar heat transfer thorough windows with shading devise. IOP Conf. Series: Earth and Environmental Science 143 (2018) 012055. CUTE 2018. 14 p. <https://doi:10.1088/1755-1315/143/1/012055>.
29. Ha, P.T.H. A Concept for Energy-Efficient High-Rise Buildings in Hanoi and a Calculation Method for Building Energy Efficiency Factor. Procedia Engineering 142. 2016. Pp. 154–160. <https://doi: 10.1016/j.proeng.2016.02.026>
30. QCVN 02:2009/BXD Vietnam Building Code Natural Physical & Climatic Data for Construction. Ministry of Construction. 2009. Hanoi. 324 p.
25. Gillete G., Treado S. The issue of sky conditions. Lighting Design & Application. March, 1985. Vol. 23(19). Pp. 22–27.
26. Joe H. ASHRAE Research Project 1477-RP Development of 3,012 typical 2018 weather files for international locations // White Box Technologies. October 19, 2011. Moraga CA. 97 p.
27. Pham Ngoc Dang, Pham Duc Nguyen, Luong Minh. Architecture lighting, Building Physics (Part II and III) // Construction Publishing. 1982. Hanoi. 53 p.
28. Ha P.T.H. Energy efficiency façade design in high-rise apartment buildings using the calculation of solar heat transfer thorough windows with shading devise // IOP Conf. Series: Earth and Environmental Science 143 (2018) 012055. CUTE 2018. 14 p. <https://doi:10.1088/1755-1315/143/1/012055>.
29. Ha P.T.H. A Concept for Energy-Efficient High-Rise Buildings in Hanoi and a Calculation Method for Building Energy Efficiency Factor // Procedia Engineering 142. 2016. Pp. 154–160. <https://doi: 10.1016/j.proeng.2016.02.026>
30. QCVN 02:2009/BXD Vietnam Building Code Natural Physical & Climatic Data for Construction. Ministry of Construction. 2009. Hanoi. 324 p.

Nguyen Thi Khanh Phuong,
+7(968)8116209; phuongntk@nuce.edu.vn

Нгуен Тхи Хань Фьюнг,
89688116209;
эл. почта: phuongntk@nuce.edu.vn

© Phuong, N.T.K., 2018



ПОЛИТЕХ
Санкт-Петербургский
политехнический университет
Петра Великого

Инженерно-строительный институт
Центр дополнительных профессиональных программ

195251, г. Санкт-Петербург, Политехническая ул., 29,
тел/факс: 552-94-60, www.stroikursi.spbstu.ru,
stroikursi@mail.ru

Приглашает специалистов проектных и строительных организаций,
не имеющих базового профильного высшего образования
на курсы профессиональной переподготовки (от 500 часов)
по направлению «Строительство» по программам:

П-01 «Промышленное и гражданское строительство»

Программа включает учебные разделы:

- Основы строительного дела
- Инженерное оборудование зданий и сооружений
- Технология и контроль качества строительства
- Основы проектирования зданий и сооружений
- Автоматизация проектных работ с использованием AutoCAD
- Автоматизация сметного дела в строительстве
- Управление строительной организацией
- Управление инвестиционно-строительными проектами. Выполнение функций технического заказчика

П-02 «Экономика и управление в строительстве»

Программа включает учебные разделы:

- Основы строительного дела
- Инженерное оборудование зданий и сооружений
- Технология и контроль качества строительства
- Управление инвестиционно-строительными проектами. Выполнение функций технического заказчика и генерального подрядчика
- Управление строительной организацией
- Экономика и ценообразование в строительстве
- Управление строительной организацией
- Организация, управление и планирование в строительстве
- Автоматизация сметного дела в строительстве

П-03 «Инженерные системы зданий и сооружений»

Программа включает учебные разделы:

- Основы механики жидкости и газа
- Инженерное оборудование зданий и сооружений
- Проектирование, монтаж и эксплуатация систем вентиляции и кондиционирования
- Проектирование, монтаж и эксплуатация систем отопления и теплоснабжения
- Проектирование, монтаж и эксплуатация систем водоснабжения и водоотведения
- Автоматизация проектных работ с использованием AutoCAD
- Электроснабжение и электрооборудование объектов

П-04 «Проектирование и конструирование зданий и сооружений»

Программа включает учебные разделы:

- Основы сопротивления материалов и механики стержневых систем
- Проектирование и расчет оснований и фундаментов зданий и сооружений
- Проектирование и расчет железобетонных конструкций
- Проектирование и расчет металлических конструкций
- Проектирование зданий и сооружений с использованием AutoCAD
- Расчет строительных конструкций с использованием SCAD Office

П-05 «Контроль качества строительства»

Программа включает учебные разделы:

- Основы строительного дела
- Инженерное оборудование зданий и сооружений
- Технология и контроль качества строительства
- Проектирование и расчет железобетонных конструкций
- Проектирование и расчет металлических конструкций
- Обследование строительных конструкций зданий и сооружений
- Выполнение функций технического заказчика и генерального подрядчика

По окончании курса слушателю выдается диплом о профессиональной переподготовке
установленного образца, дающий право на ведение профессиональной деятельности

